

Carborane Containing Supramolecular Liquid Crystals

David Stewart

PhD

University of York

Chemistry

November 2013

Abstract

In this thesis several families of supermolecular liquid crystal which contain an *o*-carborane cluster are described. These materials were synthesized in order to explore any effect the cluster may have upon the liquid-crystalline properties generated, in particular to see whether the cluster would drive the formation of certain phase types over others. A number of different mesogens, morphologies and chemical groups used to link the cluster to the rest of the molecules were utilized.

It was found that the presence of the cluster induces smectogenic properties in the compounds produced. Through investigation of different linking functionalities it was possible to elucidate that this effect is independent of the chemical nature of the linking group. Furthermore, this effect is also present across materials with widely varying mesogenic moieties. Through use of model compounds it was possible to determine that the smectogenic properties of the carborane cluster are unlikely to be solely caused by a steric effect, but rather must have some electronic basis.

The compounds presented here are intimately linked to other supermolecular liquid crystals which contain a rigid three-dimensional cluster component such as fullerene or silsesquioxanes. Carborane is the smallest of this family of materials to be investigated thus far. Comparison of the thermal properties of this family of related materials appears to show a general trend: a maximum in phase stability is achieved when there is an approximate match between the diameter of the cluster and the area occupied by the appended mesogens. For materials presented here this maximum was achieved when between one and two mesogens were appended and as a result the first inorganic-cluster-containing supermolecular liquid crystal which displays appreciable enantiotropic mesomorphism with a single appended mesogen has been realized.

Table of Contents

Carborane Containing Supramolecular Liquid Crystals.....	1
Abstract.....	2
Table of Contents.....	3
Table of Figures.....	13
Table of Tables.....	22
Table of Graphs.....	23
Table of Schemes.....	24
Table of Equations.....	25
Acknowledgements.....	26
Declaration.....	27
1. Introduction.....	28
1.1 Liquid Crystals	29
1.1.1 Thermotropic Liquid Crystals.....	29
1.1.1.1 Melting of Thermotropic Liquid Crystals	30
1.1.1.2 The Nematic Phase	32
1.1.1.3 The Smectic A Phase	33
1.1.1.4 The Smectic C Phase	34
1.1.1.5 The Smectic B Phase (Hexatic B).....	35
1.1.1.6 The Chiral Nematic Phase	36
1.2 Microphase Segregation	37
1.3 Liquid Crystal Oligomers.....	41
1.3.1 Dimers.....	41
1.3.2 Higher Order Oligomers	42
1.4 Liquid Crystalline Polymers.....	43
1.4.1 Main-chain Liquid Crystal Polymers.....	43
1.4.2 Side-chain Liquid Crystal Polymers	44
1.5 Supramolecular Liquid Crystals.....	45
1.5.1 The Effect of the Core.....	47

Table of Contents

1.5.1.1	Soft Cores - Dendrimers.....	47
1.5.1.2	Hard Cores - Inorganic Clusters.....	50
1.5.2	The Effect of the Spacer.....	51
1.5.3	The Effect of the Periphery.....	52
1.5.3.1	Choice of Mesogen.....	52
1.5.3.2	Number of Mesogens.....	53
1.5.3.3	Mode of Attachment.....	53
1.6	Carboranes.....	54
1.6.1	High Molar Mass Carboranes.....	59
1.6.1.1	Carborane Containing Hyperbranched Network.....	59
1.6.1.2	Polyester Based Carborane Containing Dendrimers.....	60
1.6.1.3	Carborane Containing Carbosilane Dendrimers.....	61
1.6.2	Carboranes in Liquid Crystals.....	63
2.	Aims.....	69
3.	Siloxanes.....	73
3.1	Summary.....	74
3.2	Synthesis.....	74
3.2.1	Undesired Branching.....	78
3.2.2	The Origin of the Branched Isomers.....	79
3.3	Thermal Properties.....	80
3.3.1	Mesogens.....	81
3.3.2	Mono-substituted Carboranes.....	83
3.3.3	Di-substituted Carborane.....	85
3.3.4	Carborane Hexamer.....	89
3.3.4.1	X-ray Diffraction.....	92
3.3.4.2	Modelling.....	93
3.3.4.3	Neutron Diffraction.....	102
3.4	Concluding Remarks.....	103
4.	Mono-functional Silanes.....	105

Table of Contents

4.1	Summary	106
4.2	Synthesis.....	107
4.3	Thermal Properties	112
4.3.1	Two-ring Systems	112
4.3.2	Three-ring Systems	115
4.3.3	Four-ring Systems	121
4.3.3.1	End-On	122
4.3.3.2	Side-on	124
4.3.3.3	Comparison.....	127
4.4	Concluding Remarks	130
5.	Multi-functional Silanes.....	131
5.1	Summary	132
5.2	Synthesis.....	133
5.3	Thermal Properties	141
5.3.1	Two-Ring Systems.....	142
5.3.2	Three-Ring Systems.....	145
5.3.2.1	Phase Structure.....	148
5.3.2.2	Comparison.....	150
5.3.3	Four-Ring Systems.....	153
5.3.3.1	Comparison.....	157
5.4	Concluding Remarks	160
6.	Mono-functional Esters: The Effect of the Spacer.....	161
6.1	Summary	162
6.2	Synthesis.....	163
6.3	Thermal Properties	166
6.4	Concluding Remarks	177
7.	Mono-funtional Esters: The Effect of the Mesogen	179
7.1	Summary	180

Table of Contents

7.2	Synthesis.....	181
7.2.1	Octyloxy Biphenyl Benzoate	182
7.2.2	Biphenyl Cyanobenzoates and Biphenyl isothiocyanate Benzoates..	184
7.2.3	Cholesteryl Benzoates.....	186
7.3	Thermal Properties	188
7.3.1	Octyloxy Biphenyl Benzoates 35 – 37.....	190
7.3.1.1	Phase Structure.....	193
7.3.1.2	Comparisons	194
7.3.2	Biphenyl Cyanobenzoates.....	199
7.3.2.1	Phase Structure.....	202
7.3.2.2	Comparisons	202
7.3.3	Biphenyl Isothiocyanate Benzoates, 41, 42 and 43	204
7.3.3.1	Phase Structure.....	208
7.3.3.2	Comparisons	209
7.3.4	Cholesteryl Benzoates.....	213
7.3.4.1	Phase Structure.....	220
7.3.4.2	Comparisons	220
7.4	Concluding Remarks	221
8.	In Search of the Smectic C Phase	224
8.1	Summary	225
8.2	Synthesis.....	226
8.3	Thermal Properties	229
8.4	Concluding Remarks	238
9.	Conclusions.....	239
10.	Experimental	246
10.1	Experimental Methods.....	247
10.1.1	Starting Materials.....	247
10.1.2	Thin Layer Chromatography and Column Chromatography (TLC) .	247
10.1.3	Nuclear Magnetic Resonance (NMR) spectroscopy	248

Table of Contents

10.1.4	Mass Spectrometry (MS)	248
10.1.5	Infrared Spectroscopy (FT-IR)	249
10.1.6	Polarized Optical Microscopy (POM)	249
10.1.7	Differential Scanning Calorimetry (DSC)	249
10.1.8	CHN Microanalysis (CHN)	249
10.2	Synthetic Routes	250
10.2.1	2-((Pent-4-enyloxy)carbonyl)-1,4-phenylene bis(4-butoxybenzoate), 16 ¹⁴⁸	250
10.2.2	4'-Cyanobiphenyl-4-yl 4-(pent-4-enyloxy)benzoate, 17 ¹¹⁸	251
10.2.3	(S)-4-((4'-(Octyloxy)biphenyl-4-yloxy)carbonyl)phenyl 4-(2-methylbutoxy)-2-(pent-4-enyloxy)benzoate, 19 ¹²⁰	252
10.2.4	(S)-4-((4'-(octyloxy)biphenyl-4-yloxy)carbonyl)phenyl 2-(2-methylbutoxy)-4-(pent-4-enyloxy)benzoate, 18 ¹¹⁹	254
10.3	Experimental Details	256
10.3.1	4'-(Pent-4-enyloxy)biphenyl-4-carbonitrile, 5 ¹⁴⁹	256
10.3.2	4'-[5-(1,1,3,3-Tetramethyl-disiloxanyl)-pentyloxy]-biphenyl-4-carbonitrile, 7 ⁹⁷	257
10.3.3	1-Methyl, 2-(propyl-3-[4'-(5-[1,1,3,3-tetramethyl-disiloxy]-pentyloxy)biphenyl-4-carbonitrile])-dodecacarborane, 1	259
10.3.4	1-Phenyl, 2-(propyl-3-[4'-(5-[1,1,3,3-tetramethyl-disiloxy]-pentyloxy)biphenyl-4-carbonitrile])-dodecacarborane, 2	261
10.3.5	Bis 1,2-(propyl-3-[4'-(5-[1,1,3,3-tetramethyl-disiloxy]-pentyloxy)biphenyl-4-carbonitrile])-dodecacarborane, 3	263
10.3.6	Bis 1,2 (tri-ethyl-2-[4'-(5-[1,1,3,3-tetramethyl-disiloxy]-pentyloxy)biphenyl-4-carbonitrile])silyl-dodecacarborane, 4	265
10.3.7	1-Phenyl, 2-(3-(demethylsilyl)-propyl)dodecacaborane, 55	267
10.3.8	1-Methyl, 2-(3-(demethylsilyl)-propyl)dodecacarborane, 56	268
10.3.9	1-Methyl, 2-(propyl-3-[4'-(5-[dimethylsilyl]-pentyloxy)biphenyl-4-carbonitrile])-dodecacarborane, 8	269

Table of Contents

10.3.10	1-Phenyl, 2-[propyl-3-[4'-(5-(dimethylsilyl)-pentyloxy)biphenyl-4-carbonitrile]]-dodecacarborane, 9	271
10.3.11	2,5-Dihydroxy-benzoic acid pent-4-enyl ester, 57	272
10.3.12	Pent-4-enyl, 2-5 bis(4-butoxy benzoyl) bezoate, 16	274
10.3.13	1-Methyl, 2-(propyldimethylsilyl[5-pentyl, 2-5 bis(4-butoxy benzoyl) benzoate])dodecacarborane, 10.....	275
10.3.14	Methyl 4-hydroxybenzoate, 58	277
10.3.15	Methyl 4-(pent-4-enyloxy)benzoate, 59.....	277
10.3.16	4-(Pent-4-enyloxy)benzoic acid, 60	278
10.3.17	4'-Cyanobiphenyl-4-yl 4-(pent-4-enyloxy)benzoate, 17 ¹¹⁸	279
10.3.18	1-Methyl, 2-[propyl-3-dimethylsilyl-(4'-cyanobiphenyl-4-yl 4-(pentyloxy)benzoate)]dodecacarborane, 11	281
10.3.19	4'-(Octyloxy)-4-hydroxybiphenyl, 61 ¹⁵⁰	282
10.3.20	4'-(Octyloxy)biphenyl-4-yl 4-(benzyloxy)benzoate, 62	283
10.3.21	4'-(Octyloxy)biphenyl-4-yl 4-hydroxybenzoate, 63 ¹⁵¹	284
10.3.22	Methyl 2-hydroxy-4-(pent-4-enyloxy)benzoate, 64 ¹¹⁹	285
10.3.23	(<i>S</i>)-Methyl 2-(2-methylbutoxy)-4-(pent-4-enyloxy)benzoate, 65 ¹¹⁹ 286	
10.3.24	(<i>S</i>)-2-(2-Methylbutoxy)-4-(pent-4-enyloxy)benzoic acid, 66 ¹¹⁹	288
10.3.25	(<i>S</i>)-4-((4'-(Octyloxy)biphenyl-4-yloxy)carbonyl)phenyl 2-(2-methylbutoxy)-4-(pent-4-enyloxy)benzoate, 18 ¹¹⁹	289
10.3.26	1-Methyl ,2-[propyl-3-dimethylsilyl-((<i>S</i>)-4-((4'-(octyloxy)biphenyl-4-yloxy)carbonyl)phenyl 2-(2-methylbutoxy)-4-(pentyloxy)benzoate)]dodecacarborane, 12	291
10.3.27	1-Phenyl, 2-(propyl-3-dimethylsilyl)-((<i>S</i>)-4-((4'-(octyloxy)biphenyl-4-yloxy)carbonyl)phenyl 2-(2-methylbutoxy)-4-(pentyloxy)benzoate)dodecacarborane, 13	293
10.3.28	(<i>S</i>)-2-Hydroxy-4-(2-methyl-butoxy)-benzoic acid methyl ester, 67 295	

Table of Contents

10.3.29	(S)-4-(Methyl-butoxy)-2-pent-4-enyloxy-benzoic acid methyl ester,	68	296
10.3.30	(S)-4-(2-Methylbutoxy)-2-(pent-4-enyloxy)benzoic acid, 69	297
10.3.31	(S)-4-((4'-(Octyloxy)biphenyl-4-yloxy)carbonyl)phenyl	4-(2-methylbutoxy)-2-(pent-4-enyloxy)benzoate, 19 ¹²⁰ 298
10.3.32	1-Methyl, 2-(propyl-3-dimethylsilyl-((S)-4-((4'-(octyloxy)biphenyl-4-yloxy)carbonyl)phenyl	4-(2-methylbutoxy)-2-(pent-4-enyloxy)benzoate)dodecacarborane, 14 300
10.3.33	1-Phenyl, 2-(propyl-3-dimethylsilyl-((S)-4-((4'-(octyloxy)biphenyl-4-yloxy)carbonyl)phenyl	4-(2-methylbutoxy)-2-(pent-4-enyloxy)benzoate)dodecacarborane, 15 302
10.3.34	1,2 Di-(3-(dimethylsilyl)propyl)dodecacarborane, 70	304
10.3.35	1 Methyl, 2-(propyl-3-[silyl(methyl)bis(ethyl-2-[dimethylsilane])])dodecacarborane, 71	305
10.3.36	1,2 Di-(propyl-3-[4'-(5-[dimethylsilyl]-pent-4-enyloxy)biphenyl-4-carbonitrile])dodecacarborane, 20	306
10.3.37	1,2 Di-(propyl-3-dimethylsilyl-(4'-cyanobiphenyl-4-yl	4-(pent-4-enyloxy)benzoate)dodecacarborane, 21 308
10.3.38	1 Methyl, 2-(propyl-3-[silyl(methyl)bis(ethyl-2-[dimethylsilyl(4'-Cyanobiphenyl-4-yl 4-(pent-4-enyloxy)benzoate])])dodecacarborane, 22	309
10.3.39	Bis 1,2-(butyl-4-[silyl(methyl)bis(ethyl-2-[dimethylsilyl(4'-cyanobiphenyl-4-yl 4-(pent-4-enyloxy)benzoate])])dodecacarborane, 23	311
10.3.40	Bis 1,2-(propyl-3-dimethylsilyl-((S)-4-((4'-(octyloxy)biphenyl-4-yloxy)carbonyl)phenyl	4-(2-methylbutoxy)-2-(pent-4-enyloxy)benzoate)dodecacarborane, 24 313
10.3.41	1 Methyl, 2-(propyl-3-[silyl(methyl)bis(ethyl-2-[dimethylsilyl-[(S)-4-((4'-(octyloxy)biphenyl-4-yloxy)carbonyl)phenyl	4-(2-methylbutoxy)-2-(pent-4-enyloxy)benzoate)])dodecacarborane, 25 316
10.3.42	1 Methyl, 2-(propyl-3-[silyl(methyl)bis(ethyl-2-[dimethylsilyl-[(S)-4-((4'-(octyloxy)biphenyl-4-yloxy)carbonyl)phenyl	2-(2-methylbutoxy)-4-(pent-4-enyloxy)benzoate)])dodecacarborane, 27 318

Table of Contents

10.3.43	Ethyl undec-10-ynoate, 72	320
10.3.44	2-(Ethyl nonanoate)dodecacarborane, 73.....	321
10.3.45	1-Hydrido, 2-(nonanoic acid)dodecacarborane, 74.....	322
10.3.46	2-(Cyanobiphenyl nonanoate)dodecacarborane, 28.....	323
10.3.47	4' -Cyanobiphenyl-4-yl 4-(benzyloxy)benzoate, 75	324
10.3.48	4' -Cyanobiphenyl-4-yl 4-hydroxybenzoate, 76	325
10.3.49	1-Hydrido, 2-(4'-cyanobiphenyl-4-yl 4-[nonanoyloxy]benzoate)dodccacarborane, 29	326
10.3.50	4'-Cyanobiphenyl-4-yl 4-(nonanoyloxy)benzoate, 30.....	328
10.3.51	Benzyl pent-4-ynoate, 77	329
10.3.52	1-Hydrido, 2-(benzyl propanoate)dodecacarborane, 78.....	330
10.3.53	1-Hydrido, 2-(propanoic acid)dodecacarborane, 79.....	331
10.3.54	4'-Cyanobiphenyl-4-yl 4-(2-hydroxyethoxy)benzoate, 80.....	332
10.3.55	1-Hydrido, 2-(4'-cyanobiphenyl-4-yl 4-ethoxybenzoate propionate)dodecacarborane, 31	333
10.3.56	4'-Cyanobiphenyl-4-yl 4-(3-hydroxypropoxy)benzoate, 81	334
10.3.57	1-Hydrido, 2-(4'-cyanobiphenyl-4-yl 4-propoxybenzoate propionate)dodecacarborane, 32	335
10.3.58	4'-Cyanobiphenyl-4-yl 4-(3-hydroxypentoxy)benzoate, 82.....	337
10.3.59	1-Hydrido, 2-(4'-cyanobiphenyl-4-yl 4-pentoxybenzoate propionate)dodecacarborane, 33	338
10.3.60	4'-Cyanobiphenyl-4-yl 4-(6-hydroxyhexyloxy)benzoate, 83.....	339
10.3.61	1-Hydrido, 2-(4'-cyanobiphenyl-4-yl 4-hexyloxybenzoate propionate)dodecacarborane, 34	340
10.3.62	4'-(octyloxy)biphenyl-4-yl 4-(6-hydroxyhexyloxy)benzoate, 84... 342	
10.3.63	1-Hydrido, 2-(4'-(octyloxy)biphenyl-4-yl 4-(6-hydroxyhexyloxy)benzoate propionate)dodecacarborane, 35	343
10.3.64	4'-(Octyloxy)biphenyl-4-yl 4-(6-(3-phenylpropanoyloxy)hexyloxy)benzoate, 36.....	344

Table of Contents

10.3.65	4'-(Octyloxy)biphenyl-4-yl 4-(6-(propionyloxy)hexyloxy)benzoate,	
37	346	
10.3.66	4'-(Benzyloxy)biphenyl-4-ol, 85	347
10.3.67	6-(4'-(Benzyloxy)biphenyl-4-yloxy)hexan-1-ol, 86.....	348
10.3.68	6-(4'-(Benzyloxy)biphenyl-4-yloxy)hexyl 3-phenylpropanoate, 87	
	349	
10.3.69	6-(4'-Hydroxybiphenyl-4-yloxy)hexyl 3-phenylpropanoate, 88	350
10.3.70	1-Hydrido, 2-([6-(4'-(benzloxy)biphenyl-4-yloxy)hexyl]	
	propionate)dodecacarborane, 89	351
10.3.71	1-Hydrido, 2-([6-(4'-Hydroxybiphenyl-4-yloxy)hexyl]	
	propionate)dodecacarborane, 90	353
10.3.72	6-(4'-(Benzyloxy)biphenyl-4-yloxy)hexyl propionate, 91	354
10.3.73	6-(4'-Hydroxybiphenyl-4-yloxy)hexyl propionate, 92.....	355
10.3.74	1-Hydrido, 2-([6-(4'-(4-cyanobenzoyloxy)biphenyl-4-yloxy)hexyl]	
	propionate)dodecacarborane, 38	356
10.3.75	4'-(6-(3-Phenylpropanoyloxy)hexyloxy)biphenyl-4-yl 4-	
	cyanobenzoate, 39.....	357
10.3.76	4'-(6-(Propionyloxy)hexyloxy)biphenyl-4-yl 4-cyanobenzoate, 40	359
10.3.77	1-Hydrido, 2-([6-(4'-(4-isothiocyanatebenzoyloxy)biphenyl-4-	
	yloxy)hexyl] propionate)dodecacarborane, 41	360
10.3.78	4'-(6-(3-Phenylpropanoyloxy)hexyloxy)biphenyl-4-yl 4-	
	isothiocyanatobenzoate, 42	362
10.3.79	4'-(6-(Propionyloxy)hexyloxy)biphenyl-4-yl 4-	
	isothiocyanatobenzoate, 43	363
10.3.80	Benzyl 4-(benzyloxy)benzoate, 93.....	364
10.3.81	4-(Benzyloxy)benzoic acid, 94	365
10.3.82	4-Benzyloxy cholesterol benzoate, 95.....	366
10.3.83	4-Hydroxy cholesterol benzoate, 96.....	368
10.3.84	4-(6-Hydroxyhexyloxy) cholesterol benzoate, 97.....	369

Table of Contents

10.3.85	1-Hydrido, 2-([cholesterol phenyl-4-yl 4-(6-hexyloxy)benzoate] propionate) dodecacarborane, 44	370
10.3.86	Cholesteryl 4-(6-(3-phenylpropanoyloxy)hexyloxy)benzoate, 45	372
10.3.87	Cholesteryl 4-(6-(propanoyloxy)hexyloxy)benzoate, 46	374
10.3.88	1-Hydrido, 2-([(S)-4-((octan-2-yloxy)carbonyl)phenyl 4'-(11-undecyloxy)biphenyl-4-carboxylate] propionate) dodecacarborane, 47	375
10.3.89	1-Hydrido 2-(2,3-difluoro-4'-(4-propylcyclohexyl)biphenyl-4-yl nonanoate)dodecacarborane, 48	377
10.3.90	2,3-Difluoro-4'-(4-propylcyclohexyl)biphenyl-4-yl nonanoate, 49	378
10.3.91	6-(2,3-Difluoro-4'-(4-propylcyclohexyl)biphenyl-4-yloxy)hexan-1-ol, 98	380
10.3.92	1-Hydrido, 2-([6-(2,3-difluoro-4'-(4-propylcyclohexyl)biphenyl-4-yloxy)hexoyloxy] propionate) dodecacarborane, 50	381
10.3.93	6-(2,3-Difluoro-4'-(4-propylcyclohexyl)biphenyl-4-yloxy)hexyl 3-phenylpropanoate, 51	382
10.3.94	6-(2,3-Difluoro-4'-(4-propylcyclohexyl)biphenyl-4-yloxy)hexyl propionate, 52	384
Appendix: List of Final Compounds.....		386
Abbreviations.....		395
References.....		398

Table of Figures

Figure 1: Schematic diagram of typical mesogen molecular shapes	30
Figure 2: Melting behaviour of Liquid Crystals	31
Figure 3: Schematic diagram of the nematic phase	33
Figure 4: Schematic diagram of the smectic A phase.....	34
Figure 5: Schematic diagram of the smectic C phase	35
Figure 6: Schematic diagrams comparing the smectic A and smectic B phases	36
Figure 7: Schematic diagram of the chiral nematic phase	37
Figure 8: De-mixing and microphase segregation	38
Figure 9: Curvature in microphase segregation	39
Figure 10: Minimizing curvature through alternative packing arrangements	40
Figure 11: Cyanobiphenyl mesogens with different flexible chains ¹⁶⁻¹⁸	41
Figure 12: LC dimers	42
Figure 13: Liquid crystalline polymers.....	43
Figure 14: Lateral vs terminal attachment of mesogens in SCLCPs	45
Figure 15: Schematic diagram of a supermolecular liquid crystal.....	46
Figure 16: Schematic diagram of a 4x2 dendrimer of generation 1 - 3	48
Figure 17: G2 Carbosilane dendrimer functionalized with cyanobiphenyl mesogens	49
Figure 18: left) SMM manganese oxide cluster; right) gallate derivative functionalized with CB mesogens, reproduced from <i>Angew. Chem.-Int. Edit.</i> , 2008, 47 , 490-495 ³⁸	51
Figure 19: The effect of the mode of attachment of mesogens.....	54
Figure 20: Three centre 2 electron bonding in diborane	56
Figure 21: Linear combination of molecular orbitals diagram for 3D aromatic systems.....	57
Figure 22: Structure of Carboranes, each vertice equals a BH unit unless indicated	58
Figure 23: Left) 2,5-bis-(vinyl(tetramethyl disiloxane))dicarbadecaborane, Right) 1,3,5,7,9,11,13,15-Octakis-(dimethylsiloxane) substituted pentacyclo [9.5.1.1.1.1]octasiloxane	59

Table of Figures

Figure 24: Carborane containing polyester dendrimers, left, centre and right, generations 3, 4 and 5 respectively, reproduced from Langmuir, 2006, 22 , 5251-5255 ⁷⁶	60
Figure 25: Carborane functionalized carbosilane dendrimers, generations 1 and 2 left and right respectively, reproduced from Macromolecules, 2007, 40 , 5644-5652 ⁸⁰ ...	61
Figure 26: Siloxane core polypedes functionalized with 2, 3, 4 and 8 carboranes, top left, top right, bottom left bottom right respectively, reproduced from Macromolecules, 2008, 41 , 8458-84 ⁸¹	62
Figure 27: Polyanionic metallocarborane functionalized generation 2 carbosilane dendrimer (left) and cyclotetrasiloxane cored generation 1 carbosilane dendrimer (right), reproduced from Organometallics, 2009, 28 , 5550-5559 ⁸²	63
Figure 28: Diameter of the cylinder of rotation (top number in Å) and the HC··CH inter bridgehead distance (bottom number in Å) of p-dodecacarborane (top left), p-decacarborane (top right), a phenyl ring (bottom left) and bicyclooctyl ring (bottom right);calculated using HF/6-31G* method ⁸³	63
Figure 29: Physical dimensions of an o-carborane cluster (top) and a phenyl ring (bottom).....	64
Figure 30: Homostructural Series of 2-"ring" systems ⁸⁵	65
Figure 31: Comparison of partially fluorinated alky and alkyl structural homologues containing either p-dodecacarborane (left), phenyl ring (centre) or bicyclooctyl (right) groups ⁹⁰	66
Figure 32: Carborane containing bent-core liquid crystal ⁹⁶	67
Figure 33: Schematic diagram of possible carborane containing supermolecular liquid crystals in which the number of mesogens is being systematically increased	71
Figure 34: Schematic diagram of possible carborane containing supermolecular liquid crystals in which the mode of attachment at various points is systematically altered.....	71
Figure 35: Cyanobiphenyl Functionalized Carboranes with Siloxane linkages	74
Figure 36: The alkyl region of the DEPT 135° spectra of compound 2	78
Figure 37: The Chalk-Harrod mechanism of hydrosilylation with important side reactions	80
Figure 38: Left) photomicrograph of 5 at 70.0 °C cooled from the isotropic liquid at 0.1°C min ⁻¹ x100 magnification. Right) photomicrograph of 7 at 47.1 °C cooled from the isotropic at 2°C min ⁻¹ x100 magnification	82

Table of Figures

Figure 39: Alkoxy cyanobiphenyls ¹⁸	83
Figure 40: Molecular models of the branched and linear isomers of 2 (hydrogens omitted for clarity)	84
Figure 41: Phenyl biphenyl benzoate mesogens functionalized with bulky carbocycles units at the end of a flexible chain ¹⁰¹	85
Figure 42: Photomicrograph of 3 at -8.0 °C cooled at 0.1 °Cmin ⁻¹ from the isotropic liquid at x200 magnification a focal-conic defect has been circled in the enlargement on the right	86
Figure 43: The possible conformations of 3 within the smectic A phase	87
Figure 44: U-shaped mesogens ^{105, 106}	88
Figure 45: Photomicrograph of 4 focal-conic texture at 28.8 °C cooled from the isotropic at 5 °Cmin ⁻¹	89
Figure 46: DSC trace of 4	90
Figure 47: CB functionalized tetramers ¹⁰² (top and middle) and carbosilane dendrimer ¹⁰⁷ (bottom)	91
Figure 48: X-ray diffractograms of 4 A) RT cooled from Iso B) RT as received	92
Figure 49: A molecular model of 4 created using ChemDraw 3D 12.0 and minimized using MOPAC 2009 PM3 method/EF in the gas phase at 0 K; the hydrogens omitted for clarity	93
Figure 50: Cylindrical model of the hexamer 4	94
Figure 51: A bilayer SmA ₂ phase using the cylindrical model of the hexamer 4	95
Figure 52: Conic model of the hexamer 4	96
Figure 53: A SmA _d phase using the conic model of the hexamer 4 , the level of interdigitation of the cones shown assumes 4 Å of interdigitation of the CB mesogens at each layer interface	97
Figure 54: Hexagonal close-packing of the conic model of the hexamer 4	98
Figure 55: Square close-packing of the conic model of the hexamer 4	99
Figure 56: Fullerene containing supermolecular liquid crystal ¹¹⁰	100
Figure 57: The smectic A phases of LC fullerodendrimers ¹¹⁰	101
Figure 58: Neutron diffractogram of 4	102
Figure 59: Carboranes mono-functionalized via a silane linker with mesogens	107
Figure 60: The structures of the alkenyl mesogenic moieties 5 ¹¹⁷ , 16 , 17 ¹¹⁸ , 18 ¹¹⁹ and 19 ¹²⁰	108
Figure 61: The alkyl region of the DEPT 135° spectra of compound 9	111

Table of Figures

Figure 62: Siloxane and Silane terminated difluoroterphenyls ¹²²	114
Figure 63: DSC trace of compound 11 , heating/cooling rate of 10 °Cmin ⁻¹	117
Figure 64: POM of 11 at 100.7 °C cooled from the isotropic liquid at 0.5 °Cmin ⁻¹ after shearing.....	118
Figure 65: Cyclohexyldifluorobiphenyl mesogens with an internal silane linker ¹²⁴	119
Figure 66: Possible structures of the SmA phase of 11	120
Figure 67: Terminal halogen functionalized difluoroterphenyls ¹²²	121
Figure 68: POM micrograph of 12 at 79.3 °C upon cooling from the isotropic liquid at 0.5 °C min ⁻¹	122
Figure 69: DSC trace of compound 13 , heating/cooling rate 10 °Cmin ⁻¹	123
Figure 70: POM photomicrograph of 13 at 32.5 °C upon cooling rapidly from the isotropic liquid	124
Figure 71: POM photomicrograph of 14 at 38.9 °C cooling from the isotropic liquid at 1° Cmin ⁻¹	125
Figure 72: DSC trace of compound 15 , heating/cooling rate 10 °Cmin ⁻¹	125
Figure 73: POM photomicrograph of 15 at 29.5 °C upon cooling from the isotropic liquid at 1 °Cmin ⁻¹	126
Figure 74: Molecular models of 12 (top) and 14 (bottom), hydrogens omitted for clarity	127
Figure 75: Mesogens with a carbocyclic terminal group ¹⁰¹	129
Figure 76: Multipedal carboranes functionalized with pro-mesogenic moieties.....	133
Figure 77: The structures of the alkenyl mesogenic moieties 5 ¹¹⁷ , 17 ¹¹⁸ , 18 ¹¹⁹ and 19 ¹²⁰	134
Figure 78: Internal vs external CH ₂ Si protons	140
Figure 79: POM photomicrograph of 20 at 22.4 °C after cooling from the isotropic liquid at 1 °Cmin ⁻¹ and shearing.	142
Figure 80: U-shaped LC dimers based on phthalic acid ¹⁰⁶	143
Figure 81: Phenyl pyrimidine dimer ¹²⁷ and corresponding monomer ¹²⁸	144
Figure 82: Structures of compounds 21 , 22 and 23	146
Figure 83: The focal-conic texture of 21 at 187.7 °C after cooling from the isotropic liquid at 1 °Cmin ⁻¹	147
Figure 84: Focal-conic texture of 22 at 173.6° C after cooling from the isotropic liquid at 1° Cmin ⁻¹	147

Table of Figures

Figure 85: The focal-conic texture of 23 at 190.6° C after cooling from the isotropic liquid at 3 °Cmin ⁻¹	148
Figure 86: Schematic diagram of the possible smectic A phases of U-shaped LC dimers.....	149
Figure 87: Amphiphilic LC oligomers ¹²⁹	150
Figure 88: Structures of compounds 24 and 25	153
Figure 89: POM micrographs of: left) Grandjean plane texture of 25 at 50.0 °C upon cooling from the isotropic fluid at 1 °Cmin ⁻¹ and annealing for 1 week; right) the pseudo focal-conic texture of 25 at 50.0 °C after cooling from the isotropic fluid at 1 °Cmin ⁻¹ and annealing for 1 week.....	154
Figure 90: Structural models of 24 (right) and 25 (left), hydrogens omitted for clarity.....	155
Figure 91: Structure of compound 27	156
Figure 92: DSC trace of compound 27	156
Figure 93: POM micrographs of: left) the pseudo focal-conic texture of 27 at 50.2 °C upon cooling from the isotropic fluid at 1 °Cmin ⁻¹ and annealing for 2 days; right) the Grandjean plane texture of 27 at 55.4 °C upon cooling from the isotropic fluid at 2 °Cmin ⁻¹	157
Figure 94: Molecular models of 25 (far left and centre right) and 27 (far right and centre left), hydrogens omitted for clarity.....	158
Figure 95: Linear, H-shaped and T-shaped LC dimers ^{20, 21}	159
Figure 96: Mono-functional carboranes appended with mesogenic moieties via an ester linker and their non-carborane containing models.....	162
Figure 97: 4-Bromo-1-butanol cyclization.....	166
Figure 98: Photomicrographs of: left) the focal-conic texture of the SmA phase of 29 after shearing at 136.1 °C cooled from the isotropic liquid at 0.5 °Cmin ⁻¹ ; right) the schlieren texture of the N phase of 29 at 146.2 °C after cooling from the isotropic liquid at 5 °Cmin ⁻¹	168
Figure 99: Photomicrographs of: left) the schlieren texture of the N phase of 30 at 227.8° C upon cooling from the isotropic fluid at 1 °Cmin ⁻¹ ; right) the focal-conic texture of the SmA phase of 30 at 177.5 °C upon cooling from the isotropic fluid at 2 °Cmin ⁻¹	169
Figure 100: Mesogens with a carbocyclic terminal group ¹⁰¹	170

Table of Figures

Figure 101: Photomicrograph of 31 at 45.0 °C after annealing overnight and cooling from the isotropic fluid at 1 °Cmin ⁻¹ on a slide coated with ClSi(Me) ₃	171
Figure 102: Photomicrograph of 32 at 61.0 °C after cooling from the isotropic fluid at 0.5 Cmin ⁻¹	172
Figure 103: Photomicrograph of: left) the schlieren texture of the N phase of 33 at 115.3 °C after cooling from the isotropic liquid at 5 °Cmin ⁻¹ ; right) the focal-conic texture of the SmA phase of 33 at 94.2 °C after cooling from the isotropic fluid at 1 °Cmin ⁻¹ and subsequent shearing.....	173
Figure 104: Photomicrograph of: left) focal-conic texture of the SmA phase of 34 at 82.1 °C after cooling from the isotropic fluid at 5 °Cmin ⁻¹ ; right) the schlieren texture of the N phase of 34 at 99.3 °C after cooling from the isotropic fluid at 5 °Cmin ⁻¹	174
Figure 105: The mono-functional carboranes appened with mesogenic moieties via an ester linker and their phenyl and alkyl homologues.....	181
Figure 106: Structures of compounds 35 , 36 and 37	190
Figure 107: Photomicrograph of 35 at 94.6 °C after cooling from the isotropic liquid at 1 °Cmin ⁻¹	190
Figure 108: Photomicrograph of the schlieren texture of 36 at 131.3 °C upon cooling from the isotropic fluid at 1 °Cmin ⁻¹	191
Figure 109: A sequence of photomicrographs of the N-SmC transition of 36 starting at 106.5 °C upon cooling from the isotropic fluid at 1 °Cmin ⁻¹ and ending at 105.0 °C	192
Figure 110: POM micrographs of: left) the schlieren texture of the N phase of 37 at 168.4° C upon cooling from the isotropic liquid at 0.2° Cmin ⁻¹ ; right) the schlieren texture of the SmC of 37 with undulating instabilities at 138.1 °C upon cooling form the N at 1 °Cmin ⁻¹	193
Figure 111: Possible options for the phase structure of the smectic phases of the octyloxy biphenyl benzoates.....	194
Figure 112: The origin of the SmC phase in the octyloxy biphenyl benzoates, dipoles shown in red	197
Figure 113: Effect of polar end-group ¹²²	198
Figure 114: Dipole moment of o-carborane calculated by DFT (B3LYP/3-21G level of theory) methods	198
Figure 115: Coupling of carborane dipoles	199
Figure 116: Structures of compounds 38 , 39 and 40	200

Table of Figures

Figure 117: POM micrographs of: left) the schlieren texture of the N phase of 38 at 102.8 °C after cooling from the isotropic fluid at 1 °Cmin ⁻¹ ; right) the focal-conic texture of the SmA phase of 38 at 85.8 °C upon cooling from the N phase at 0.5 °Cmin ⁻¹	200
Figure 118: POM micrographs of: left) the schlieren texture of the N phase of 39 at 151.1 °C upon cooling from the isotropic liquid at 2 °Cmin ⁻¹ ; right) the focal-conic texture of the SmA phase of 39 at 96.5 °C upon cooling from the N phase at 2 °Cmin ⁻¹	201
Figure 119: POM photomicrographs of: left) the schlieren texture of the N phase of 40 at 182.4 °C upon cooling from the isotropic fluid at 2 °Cmin ⁻¹ ; right) the focal-conic texture of the SmA phase of 40 at 91.6° C upon cooling from the N phase at 1 °Cmin ⁻¹	202
Figure 120: Structures of compounds 41 , 42 and 43	204
Figure 121: POM photomicrograph of: left) the schlieren texture of the nematic phase of 41 at 123.9 °C upon cooling from the isotropic liquid at 1 °Cmin ⁻¹ ; right) the focal-conic texture of the SmA phase of 41 at 120.9 °C upon cooling from the N phase at 1 °Cmin ⁻¹	205
Figure 122: POM photomicrographs of: left) the focal-conic texture of the Hexactic B phase of 41 at 54.1 °C after rapid cooling from the SmA phase; right) the focal-conic texture of the SmA phase of 41 at 60.1 °C after rapid heating from the Hexactic B phase.....	206
Figure 123: POM photomicrographs of: left) the schlieren texture of the N phase of 42 at 159.4 °C upon cooling from the isotropic fluid at 1 °Cmin ⁻¹ ; right) the focal-conic texture of the SmA phase of 42 at 152.6 °C upon cooling from the N phase at 1 °Cmin ⁻¹	207
Figure 124: POM photomicrographs of: left) the parabolic texture of the hexatic B phase of 42 with herringbone defects at 64.4 °C upon rapid cooling from the SmA phase; right) the focal-conic texture of the SmA phase of 42 with herringbone defects at 67.6 °C upon rapid heating of the hexatic B phase	207
Figure 125: POM photomicrographs of: left) the schlieren texture of the N phase of 43 at 202.5 °C upon cooling from the isotropic fluid at 2 °Cmin ⁻¹ ; right) the focal-conic texture of 43 at 191.3 °C upon cooling from the N phase at 2 °Cmin ⁻¹	208

Table of Figures

Figure 126: POM photomicrograph of the focal-conic texture of the hexatic B phase of 43 with herringbone defects at 66.3 °C upon rapid cooling from the SmA phase	208
Figure 127: Associated dimers in the N phase.....	211
Figure 128: Molecular structure of a biphenyl 4-isothiocyanate (left) and biphenyl 4-cyano (right) benzoates	212
Figure 129: Phase transitions of 4-pentyl, 4'-cyanobiphenyl ¹³⁶ and 4-pentyl, 4'-isothiocyanatobiphenyl ¹⁴³	213
Figure 130: Structures of compounds 44 , 45 and 46	213
Figure 131: POM photomicrographs of: left) the Grandjean plane texture of the N* phase of 44 at 114.4 °C upon cooling from the isotropic fluid at 1 °Cmin ⁻¹ ; right) the focal-conic texture of the N* phase of 44 at 108.6 °C upon cooling from the isotropic fluid at 1 °Cmin ⁻¹	214
Figure 132: POM photomicrographs of: left) the N* to TGB phase transition from the focal-conic texture at 107.3 °C cooling at 1 °Cmin ⁻¹ ; right) the N* to TGB phase transition from the Grandjean planar texture at 100.3 °C cooling at 1 °Cmin ⁻¹	215
Figure 133: The paramorphic focal-conic texture of the SmA* phase of 44 at 98.0 °C upon cooling at 1 °Cmin ⁻¹	215
Figure 134: POM photomicrograph of the BP2 of 45 at 146.7 °C upon cooling from the isotropic fluid at 1 °Cmin ⁻¹	216
Figure 135: POM photomicrographs of: left) the Grandjean plane texture of the N* phase of 45 at 119.0 °C upon cooling from the isotropic liquid at 1 °Cmin ⁻¹ ; right) the focal-conic texture of the N* phase of 45 at 144.2 °C upon cooling from the isotropic liquid at 1 °Cmin ⁻¹	217
Figure 136: POM photomicrographs of 45 : left) the TGB to N* transition at 118.4 °C heating at 1 °Cmin ⁻¹ from the optically extinct texture of the SmA* phase; right) the N* to TGB phase transition at 117.8 °C upon cooling from the focal-conic texture of the N* phase at 1 °Cmin ⁻¹	217
Figure 137: Structure of the CrE phase.....	218
Figure 138: POM photomicrographs of: left) the focal-conic texture of the SmA* phase of 45 at 110.2 °C cooling at 1 °Cmin ⁻¹ ; right) the focal-conic texture of the CrE phase of 45 at 4.1 °C upon rapid cooling from the SmA*	218
Figure 139: POM photomicrographs of: left) the platelet texture of the BP2 of 46 at 183.1 °C upon cooling from the isotropic fluid at 1 °Cmin ⁻¹ ; right) the focal-conic	

Table of Figures

texture of the N* phase of 46 at 181.1 °C upon cooling from the BP2 phase at 1 °Cmin ⁻¹	219
Figure 140: POM photomicrographs of: left) the N* to TGB phase transition of 46 at 114.8 °C upon cooling at 1 °Cmin ⁻¹ ; right) the focal-conic texture of the SmA* phase of 46 at 127.5 °C upon cooling at 3 °Cmin ⁻¹ from the N* phase.....	219
Figure 141: Mono-functionalized carboranes appended with SmC promoting mesogenic moieties and their phenyl and alkyl analogues	225
Figure 142: SmC promoting mesogenic moieties.....	226
Figure 143: Structure of compound 47 and its carbocycle analogues with either a bicyclooctyl (O) or adamantly (P) end-group ¹⁴⁵	230
Figure 144: Space filling models of: left) bicyclooctyl; centre; adamantyl; right) and carboranyl end-groups (drawn to scale).....	230
Figure 145: Structures of compounds 48 and 49	231
Figure 146: POM photomicrograph of the schlieren texture of the N phase of 49 at 134.0 °C upon cooling from the isotropic fluid at 1 °Cmin ⁻¹	232
Figure 147: Possible intramolecular interactions in 49	233
Figure 148: Structures of compounds 50 , 51 and 52	233
Figure 149: POM photomicrographs of: left) the grainy texture of 50 at 21.2 °C upon cooling from the isotropic fluid at 5° Cmin ⁻¹ ; right) bâtonettes of the SmA phase of 50 at 24.2 °C upon heating at 0.5 °Cmin ⁻¹	234
Figure 150: POM photomicrograph of: left) the schlieren texture of the N phase of 51 at 38.8° C upon cooling from the isotropic fluid at 0.5 °Cmin ⁻¹ ; right) the focal-conic texture of the SmA phase of 51 at 37.0° C upon cooling from the N phase at 0.5 °Cmin ⁻¹	235
Figure 151: POM photomicrograph of: left) the schlieren texture of the N phase of 52 at 91.1° C upon cooling from the isotropic fluid at 1° Cmin ⁻¹ ; right) the focal-conic texture of the SmA phase of 52 at 48.9° C upon cooling from the N at 1 °Cmin ⁻¹ .	236

Table of Tables

Table 1: Wade's rules for predicting the structure of polyhedral clusters where n is the number of vertices.....	55
Table 2: Summary of transition temperatures of functionalized carboranes and cyanobiphenyl mesogens as recorded by DSC with a heating/cooling rate of 10 °Cmin ⁻¹ , values shown in brackets are for monotropic transitions	81
Table 3: The thermal behaviour of the carboranes mono-functionalized with mesogens, as recorded by DSC with a heating/cooling rate of 10 °Cmin ⁻¹ , values shown in brackets are for monotropic transitions	112
Table 4: The thermal properties of the alkenyl mesogens 5 ¹¹⁷ , 16 , 17 ¹¹⁸ , 18 ¹¹⁹ and 19 ¹²⁰ as measured by DSC, heating/cooling rate 10 °Cmin ⁻¹	112
Table 5: The thermal properties of the multipedal carboranes 20-27 , functionalized with mesogenic moieties, as recorded by DSC with a heat/cool rate of 10 °Cmin ⁻¹ , values in brackets indicate monotropic transitions	141
Table 6: The thermal properties of the alkenyl mesogens 5 ¹¹⁷ , 17 ¹¹⁸ , 18 ¹¹⁹ and 19 ¹²⁰ , as recorded by DSC with a heat/cool rate of 10 °Cmin ⁻¹	142
Table 7: The phase behaviour of the mono-functionalized carboranes appended with mesogenic moieties via an ester linker, values as measured by DSC with a heat/cool rate of 10 °min ⁻¹ , values in brackets are for monotropic transitions and the value marked with a * is taken from POM as it was not detectable by DSC	167
Table 8: Transitions temperatures of n-alkyl cyanobiphenyls ¹³⁵⁻¹⁴⁰	176
Table 9: The thermal properties of the mono-functionalized carboranes appended with mesogenic moieties via an ester linker and their phenyl and, values as measured by DSC except those marked * which are values determined by microscopy, values in brackets are for monotropic transitions.....	189
Table 10: The thermal properties of the mono-functionalized carboranes appended with SmC promoting mesogens: values taken from DSC with a heat/cool rate of 10 Cmin ⁻¹ except values marked with a * which are taken from POM, values in brackets are for monotropic transitions	229

Table of Graphs

Graph 1: The effect of the number of mesogens on phase stability (1 = 11 , 2 = 22 and 4 = 23).....	152
Graph 2: Transition temperatures verses spacer length for the series n = 2	175
Graph 3: The thermal properties of the octyloxy biphenyl benzoates and the carboranyl cyanobiphenyl benzoate 34 for comparison purposes, thermal behaviour shown in bars is that observed for cooling, the melting points shown are for the pristine sample	195
Graph 4: The thermal properties of the biphenyl cyanobenzoate series and the carboranyl cyanobiphenyl benzoate 34 included for comparison, thermal behaviour shown in bars is that observed for cooling cycles, the melting points shown are for the pristine sample	203
Graph 5: The thermal properties of the biphenyl cyanobenzoates; 38 , 39 and 40 and the biphenyl isothiocyanate benzoates; 41 , 42 and 43 , thermal behaviour shown in bars is that observed for cooling, the melting points shown are for the pristine sample	210
Graph 6: The phase behaviour of the cholesterol benzoates.....	221
Graph 7: The phase behaviour of the difluoro(propylcyclohexyl)biphenyls, thermal behaviour shown on the bars is for cooling and the meltings point are from pristine samples.....	237

Table of Schemes

Scheme 1: The synthesis of compound 7	76
Scheme 2: The Synthesis of compounds 1, 2, 3 and 4	77
Scheme 3: Branched and Linear Isomers.....	78
Scheme 4: The synthesis of carboranes mono-functionalized with mesogens	110
Scheme 5: Synthesis for the bifunctionalized carboranes 20, 21, 24 and 26 , functionalized with pro-mesogenic moieties using the structural motif I	135
Scheme 6: Synthesis of the bifunctionalized carboranes 22, 25 and 26 , functionalized with mesogenic moieties based on structural motif J	137
Scheme 7: Synthesis of carborane 23 functionalized with multiple mesogens based on structural motif C	139
Scheme 8: Synthesis of the carborane cores	164
Scheme 9: Synthesis of the cyanobiphenyl benzoate mesogen terminated with either a phenol or alkoxy alcohol.....	165
Scheme 10: Synthesis of the octyloxy biphenyl benzoate mesogen.....	183
Scheme 11: Synthesis of the biphenyl cyano and isothiocyanate benzoate mesogens	185
Scheme 12: The synthesis of the cholesterol benzoates	187
Scheme 13: The synthesis of compound 47	227
Scheme 14: The synthesis of materials 48 and 49 with a 2,3-difluoro-4'-(4-propylcyclohexyl)biphenyl mesogenic core with a direct ester linkage	227
Scheme 15: The synthesis of materials 50, 51 and 52 with a 2,3-difluoro-4'-(4-propylcyclohexyl)biphenyl mesogenic core with a central ester linkage	228
Scheme 16: The synthesis of compound 16	251
Scheme 17: Synthesis of compound 17	252
Scheme 18: Synthesis of 19	253
Scheme 19: Synthesis of 18	255

Table of Equations

Equation 1: The order parameter	33
Equation 2: Hückel's rule for 2D aromatics.....	56
Equation 3: Analogue of Hückel's rule for 3D aromatics.....	57

Acknowledgements

I would like to express my deep gratitude to Dr Isabel Saez for her constant guidance, encouragement and assistance in carrying out this work. I would also like to thank Dr Rosario Nuñez and Dr Albert Ferrer-Ugalde for kindly supplying numerous starting materials without which large parts of this project would not have been possible. My grateful thanks are also extended to Ms Heather Fish and Mr Karl Heaton for technical assistance with NMR and mass spectrometry respectively. In addition I would like to thank the whole Advance Materials group at The University of York in particular Professor John Goodby and Dr Stephen Cowling for much assistance with microscopy studies. My gratitude is also extended to The Department of Chemistry at the University of York and the EPSRC for funding and supporting my research. Finally I would like to thank my friends and family for supporting me through this difficult and testing endeavour in particular Charlie and Kirsty and my darling Jenny.

Declaration

I David Stewart declare that this thesis and the work contained within are my own and have been generated by myself as a result of my own original research. I confirm that this work was done wholly or mainly by me while a candidate for a research degree at the University of York. No parts of this thesis have been submitted for a degree at any institution. Where I have consulted the published literature this is always clearly attributed. The work presented in Chapters 2, 3 and 4 was carried out in collaboration with the research group of Dr Rosario Núñez, Institut de Ciència de Materials, CSIC, Campus U.A.B., 08193 Bellaterra, Spain, between October 2009 and October 2013. Within Chapters 2,3 and 4 the materials which were kindly provided by Dr Núñez are clearly referenced.

1. Introduction

1.1 Liquid Crystals

Liquid Crystals (LC) are often called the fourth state of matter, lying between three-dimensionally ordered crystalline solids and isotropic liquids, with no long-range directional or positional order. Due to LC phases being between the solid and liquid state they are often referred to as mesophases from the Greek *mesos* meaning middle. LCs all have a degree of orientational order and in some cases positional order. This order is often short-range or considered to be only quasi long-range order.

There are two main types of LC. The first are lyotropic LCs; at the molecular level they are generally composed of amphiphiles with specific regions of hydrophobicity and hydrophilicity within each molecule. The key feature of lyotropics is that they form mesophases in the presence of a solvent, usually water. The phases generated are controlled by the concentration of the solution and the nature of the amphiphile¹. Lyotropics typically form smectic, columnar or cubic phases. The second main type of liquid crystal are thermotropics. These materials form mesophases upon melting from the solid or cooling from the isotropic liquid. They can form mesophases when pure or in mixtures. The phases generated are determined by various factors relating to the molecular structure of the material which define the molecular interactions.

1.1.1 Thermotropic Liquid Crystals

There are two common varieties of molecules/moieties which promote the formation of thermotropic liquid crystalline mesophases. These molecules/moieties are often called mesogens because they exhibit mesomorphic behaviour; this behaviour results from a combination of the molecular shape and polarizability of the mesogens. The two most common molecular shapes which result in mesomorphic behaviour are rod-like (calamitic) mesogens and disc-like (discotic) mesogens (Figure 1). Calamitic mesogens have a long thin molecular core which is rigid and usually polarizable. In general, flexible aliphatic regions are incorporated terminally to the molecular long axis in order to lower the melting point.

Discotic mesogens are formed from rigid planar discs often of aromatic nature. Again flexible (usually aliphatic) groups are often attached to the periphery and in plane with the rigid disk. Different mesogens will promote different mesophases due to their structural properties. Typically calamitics will result in nematic or smectic phases and discotics will result in columnar or nematic phases.

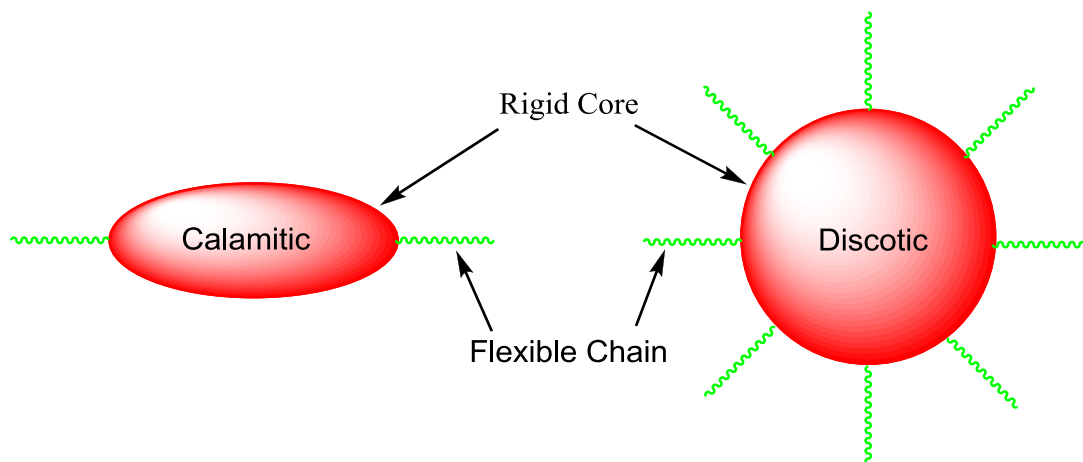


Figure 1: Schematic diagram of typical mesogen molecular shapes

1.1.1.1 Melting of Thermotropic Liquid Crystals

In an organic crystal the molecules are arranged in a three-dimensional lattice with long-range positional and often orientational order. Furthermore the molecules are not free to rotate within their lattice positions. Upon heating, a non-mesogenic molecule will begin to increase its vibrational motions until eventually the molecules gain enough energy to overcome the intermolecular forces holding them in their lattice positions. These forces are essentially equal in all directions and thus are broken in all directions simultaneously, resulting in melting into a typical isotropic liquid which exhibits no directional or positional order (T_1 Figure 2).

However when a mesogen is heated from a crystalline state something quite different occurs. Like non-mesogenic materials the mesogens will have both positional and directional order within the crystal lattice and will similarly not be free to rotate. Upon heating the mesogens initially begin to vibrate like their isotropic counterparts. However, because of the anisotropic shape and polarizability of the mesogens, the

Chapter 1: Introduction

intermolecular forces holding them in their lattice positions are not equal in all directions. At thermal energy T_2 (Figure 2) in a calamitic system, the terminal intermolecular forces acting on the mesogen are overcome more rapidly than that of the lateral intermolecular forces. This results in a situation where layers of mesogens are able to flow over one another while still maintaining a degree of positional and orientational order. The mesogens are now in a liquid crystalline state.

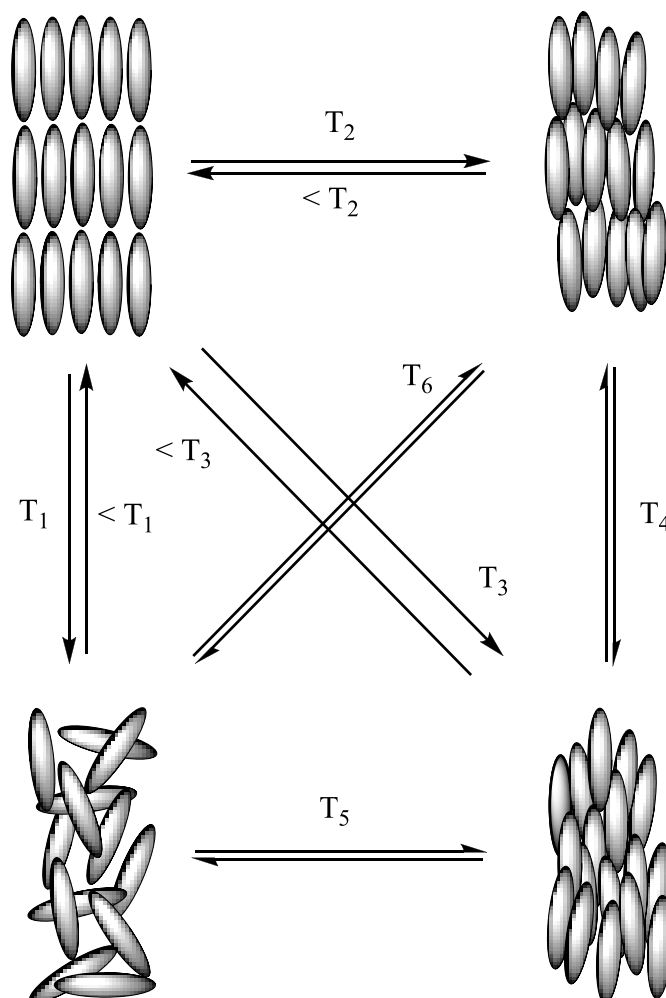


Figure 2: Melting behaviour of Liquid Crystals

Upon continued heating, the lateral attractions of the mesogens are overcome further. This results in the loss of the layers as the mesogens begin to diffuse more randomly, as such positional order is lost. However, orientational order may still be maintained (T_4 Figure 2). This is an example of a LC to LC phase transition. Continued heating will eventually give the mesogens enough energy to overcome the intermolecular

Chapter 1: Introduction

interactions in all directions resulting in the material transitioning to an isotropic liquid state (T_5 Figure 2).

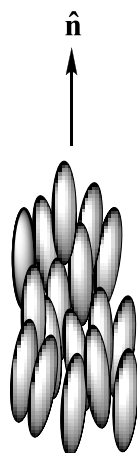
Not all mesogens exhibit the same mesophases or phase sequences. Depending on the mesogen situations can arise in which the lateral and terminal intermolecular forces break down simultaneously resulting in a phase which has only orientation order (T_3 Figure 2). Likewise a LC phase which exhibits both orientational and positional order may overcome all anisotropic intermolecular forces simultaneously rather than stepwise, resulting in a transition to an isotropic liquid (T_6 Figure 2).

When a mesogen displays more than one mesophase we describe this as polymorphism. Furthermore the phase sequence observed is not necessarily the same upon heating and cooling. Phases which are observed on both heating and cooling are referred to as enantiotropic, whereas phases which are only observed upon cooling are referred to as monotropic².

For the purposes of brevity and relevance we shall now only discuss calamitic mesogens and their phases.

1.1.1.2 The Nematic Phase

The Nematic (N) phase is the most disordered of the LC phases. The molecules in the N phase only exhibit long-range directional order. This directional order arises from the alignment of the calamitic mesogens along their long molecular axis, this orientational preference occurs along a vector known as the director (\hat{n}). In reality the molecules are moving as a fluid, diffusing randomly and rotating about all three axes. However, for calamitic mesogens rotation around the short molecular axis is more hindered than that around the long axis, meaning that rotation around the long axis is much faster. As a result calamitic mesogens tend to spend on average slightly more time with their long molecular axis aligned with the director than not³. Different mesophases have various degrees of order both positional and directional, but in all cases the preference for the molecules to be in their ordered position/orientation is very small.



Nematic

Figure 3: Schematic diagram of the nematic phase

The nematic phase is characterized by the mesogens having a slight orientational preference along the director (orientational order) but with no positional order. In other words the ends of the molecules do not align in layers but are distributed randomly (Figure 3). The degree to which the molecular long axis of the mesogens aligns with the director can be quantified by the order parameter (S). The order parameter is defined in Equation 1⁴, where θ is the average angle between the director and the long axis of each molecule. If $S = 0$ there is no order in the phase, which can be described as an isotropic liquid. If $S = 1$ then all the molecular long axes would be perfectly aligned with the director. Typical order parameters for nematics are between $S = 0.3$ and $S = 0.7$.

$$S = \frac{1}{2} \langle 3\cos^2\theta - 1 \rangle$$

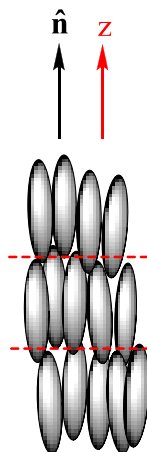
Equation 1: The order parameter

1.1.1.3 The Smectic A Phase

In smectic phases calamitic mesogens also exhibit a slight orientational preference along the director (\hat{n}), as is in the N phase. However, in smectic phases calamitic mesogens also exhibit a slight positional order, forming layers (Figure 4). We define a direction perpendicular to the plane of the layers and call this the layer normal (\hat{z}).

Chapter 1: Introduction

In the smectic A (SmA) phase this is parallel to the director ($\hat{\mathbf{n}}$). Smectic phases in which the director is parallel with the layer normal are described as orthogonal phases.



Smectic A

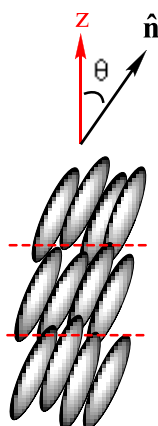
Figure 4: Schematic diagram of the smectic A phase

The layers form due to increased lateral attractions between the mesogens in comparison to the N phase. In the SmA phase this results in the mesogens forming fluid layers in which they are able to freely move in two dimensions within the layer plane but with more hindered motion in the third dimension between the layers⁵. This results in a system that displays a density wave function as one moves through the layers rather than well defined “hard” layers. These “soft” layers are characteristic of smectic phases.

1.1.1.4 The Smectic C Phase

In the smectic C (SmC) phase, like in the N and SmA phases, calamitic mesogens orient along a director ($\hat{\mathbf{n}}$). The SmC phase also exhibits a lamellar structure like the SmA phase, with the formation of soft fluid layers (Figure 5). However the director is tilted with respect to the layer normal (z) with the tilt angle (θ) being dependent upon the mesogen and the temperature. It is important to note that in the SmC phase the direction of tilt is locally uniform within any domain⁶. Smectic phases where

there is a tilt angle between the director and the layer normal are referred to as tilted phases.



Smectic C

Figure 5: Schematic diagram of the smectic C phase

The reasons why the mesogens tilt in the SmC phase, while extensively studied are not yet fully understood. There are two broad theories, one citing steric factors⁷ for the origin of the tilt and the other dipole considerations⁸. However it now appears that it is a combination of these factors which interplay in a rather complex manner to result in the formation of tilted smectic phases.

1.1.1.5 The Smectic B Phase (Hexatic B)

The smectic B (SmB) phase, also known as the hexatic B (HexB) phase is another orthogonal smectic phase displaying orientational order as well as a lamella structure similar to that of the SmA phase. However, the SmB displays short-range in plane positional order⁹. The mesogens form a hexagonal packing arrangement which breaks down over long distances (approximately 150 to 600 Å), Figure 6. In all other respects it is very similar to the SmA phase.

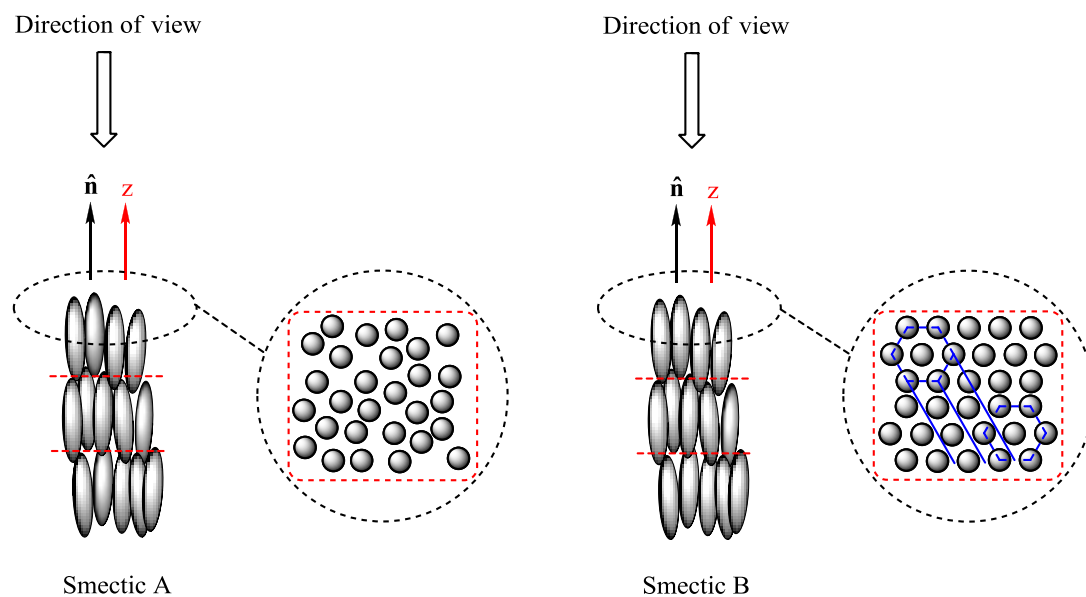
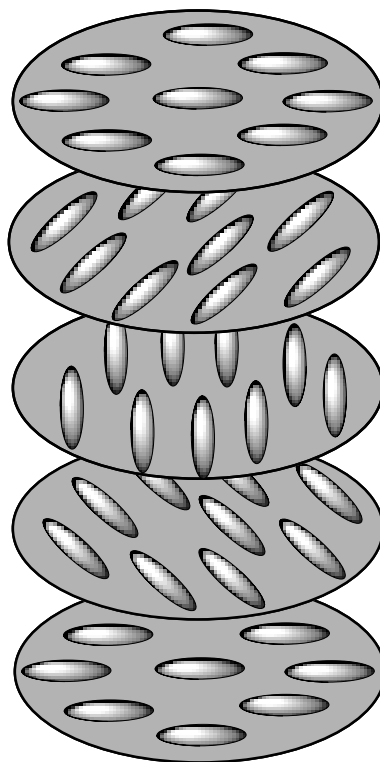


Figure 6: Schematic diagrams comparing the smectic A and smectic B phases

1.1.1.6 The Chiral Nematic Phase

The chiral nematic phase (N^*) is a variation of the N phase. It is formed by mesogens which are themselves chiral and enantiomerically pure (or have an enantiomeric excess of one of the isomers) or from achiral mesogens doped with a small amount of an enantiomerically pure chiral material. This can result in a nematic phase where the calamitic mesogens form a helical macrostructure perpendicular to the director¹⁰ (Figure 7). It is important to remember that although in Figure 7 there are planes drawn for clarity, in reality there is no layered structure and there is no long-range positional order.



Chiral Nematic (N*)

Figure 7: Schematic diagram of the chiral nematic phase

The pitch of the helix in a N* phase is temperature dependent. At higher temperatures the mesogens have more energy and thus are able to sustain a larger angle change in the director, resulting in a tighter pitch. As the material cools the angle becomes smaller and the pitch lengthens. However, this is not always the case and there are rare examples where this behaviour is reversed¹¹. The pitch length can vary from approximately 0.1 μm towards infinity.

1.2 Microphase Segregation

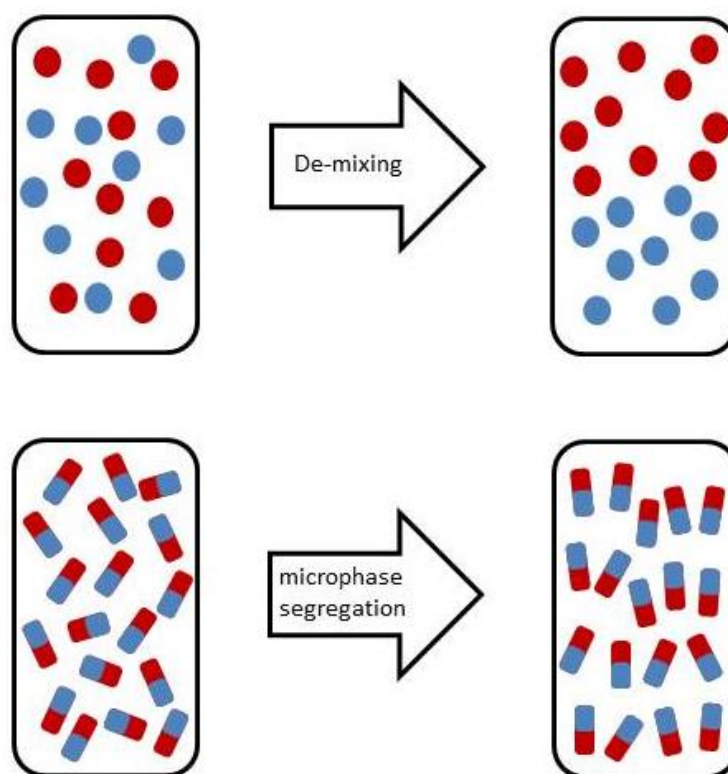


Figure 8: De-mixing and microphase segregation

If one divides up a mesogen into chemically distinct regions and considers the different intermolecular attractive forces between similar regions and dissimilar regions it becomes evident that the attractive forces between dissimilar regions can be quite different to those between similar regions. When this occurs the molecules self-assemble in such a way as to minimize the unfavourable interactions between dissimilar regions by forming layers within the phase which separate the incompatible regions¹². This effect is known as microphase segregation and is analogous to the de-mixing of mixtures of non-compatible fluids such as water and hexane (Figure 8).

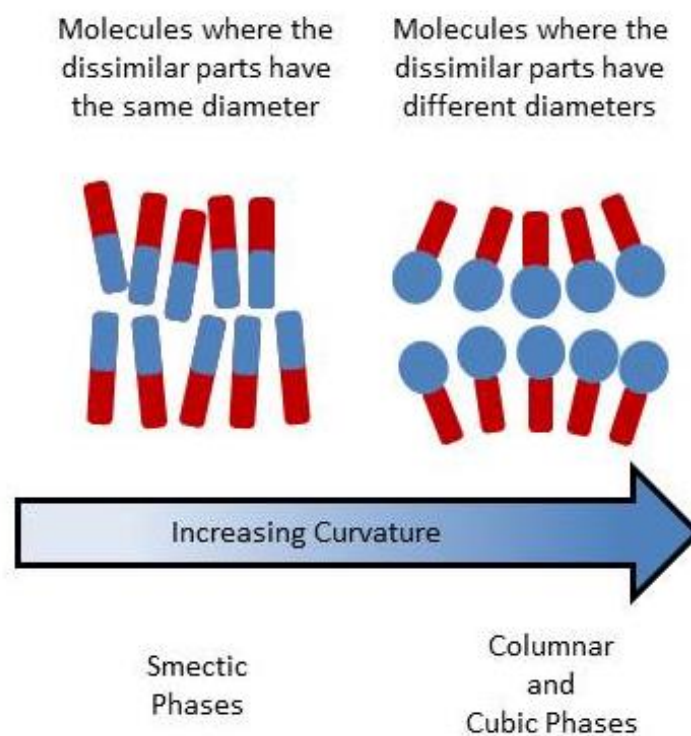


Figure 9: Curvature in microphase segregation

Furthermore, if the different regions which the mesogen is divided up into have roughly the same rotational volume then smectic phases form due to the effect of microphase segregation (Figure 9). Sometimes however the different regions of the mesogen do not have similar rotational volumes. When this occurs layers still form due to microphase segregation, but rather than having flat interfaces, curvature occurs in order to satisfy space filling requirements^{13, 14}. This can lead to the formation of columnar and cubic phases akin to those formed by some lyotropic systems. The steric forces driving curvature are often in competition with the self-assembly caused by the anisometric shapes of the mesogens. As such increasing the steric bulk of one end of a mesogen does not guarantee columnar or cubic phases. Sometimes the molecules will pack antiparallel, mixing the different regions of the mesogens in order to minimise curvature which is disfavoured in rod-like molecules¹⁵ (Figure 10 top). Alternatively curvature can be minimized by local segregation leading to undulating smectic phases (Figure 10 bottom).

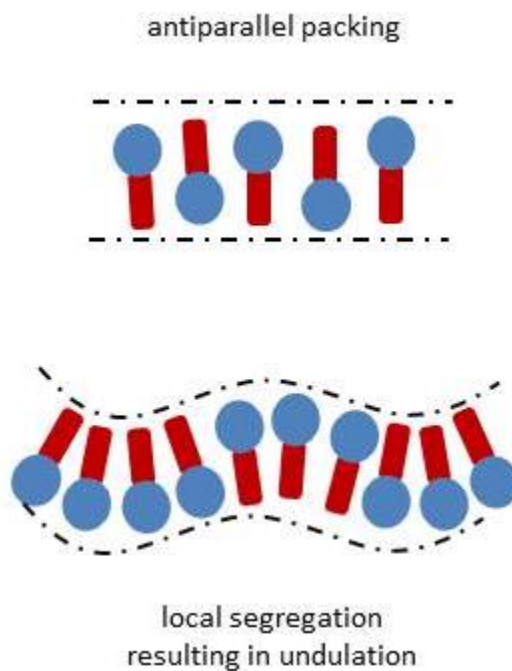
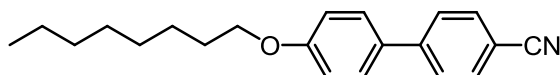
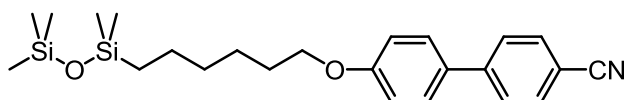


Figure 10: Minimizing curvature through alternative packing arrangements

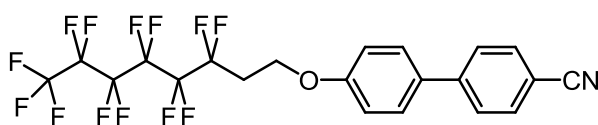
A good example of the effect of microphase segregation within calamitic systems is provided by comparing the phase behaviour of a cyanobiphenyl mesogen with an alkoxy chain to that of the same mesogen bearing an alkoxy chain with a pentamethyl disiloxane unit at the terminal end (Figure 11). Upon addition of the chemically dissimilar siloxane unit the N phase of the cyanobiphenyl mesogen is completely lost in favour of a broader SmA phase. This can be explained by the unfavourable interactions between the siloxy and aromatic/aliphatic areas of the molecules destabilizing the N phase, microphase segregation of the siloxy units minimizes these interactions and thus only a smectic phase is observed. Another example of this effect is provided by the alkoxy perfluoro cyanobiphenyl shown in Figure 11.



Cr 54.5 SmA 67.0 N 80.0 I



Cr 46.0 SmA 53.8 I



CrK 89.4 SmC 162.0 SmA 162.7 I

Figure 11: Cyanobiphenyl mesogens with different flexible chains¹⁶⁻¹⁸

1.3 Liquid Crystal Oligomers

Low molar mass mesogens have been linked together *via* flexible spacers to form liquid crystal oligomers. These oligomers vary in the number of mesogens linked together, from simple dimers through to materials containing many tens of mesogenic moieties¹⁹. These materials are discrete molecular entities and do not display any polydispersity. The properties depend on a number of factors including; the manner in which the mesogens are linked to one another and the number and nature of the mesogenic moieties.

1.3.1 Dimers

Liquid crystal dimers can display dramatically different phase behaviour depending on how the mesogens are attached to one another. The mesogens may both be attached terminally to each other to create a linear LC dimer, however they may also both be attached laterally to one another creating an H-shaped LC dimer,

alternatively one mesogen may be attached terminally and the other laterally resulting in a T-shaped LC dimer²⁰.

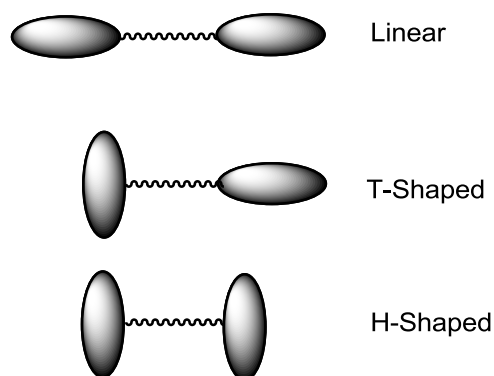


Figure 12: LC dimers

It has been shown that linear dimers generally display the highest melting points and clearing points, and from the higher thermodynamic values such as ΔH_{N-I} and ΔS_{N-I} that they also show the highest molecular order within the phases. H-shaped mesogens display the poorest phase stability but show a tendency towards smectic phases. This observation can be explained by the lower degree of freedom which the mesogens in the H-shaped dimer exhibit. The mesogens are less able to move freely resulting in higher order smectic phases. Finally the T-shaped mesogens display the opposite dependence of ΔH_{N-I} and ΔS_{N-I} on the length of the flexible spacer than that of the linear and H-shaped dimers. The T-shaped dimers display more stable mesophases with increasing spacer length, while the linear and H-shaped dimers display the opposite. This is accounted for by the increasing ability of the mesogens to be able to adopt a parallel alignment with increasing spacer length in the T-shaped dimers. While in the linear and H-shaped dimers an increasing spacer length increases the conformational freedom of the mesogens and thus destabilizes the mesophases.

1.3.2 Higher Order Oligomers

There is a broad selection of higher order LC oligomers which display a diversity of structure property relationships^{19, 21}. These however are outside the scope of this work and shall not be discussed further except to say that generally as the number of

mesogens increases in oligomeric systems the materials begin to behave more and more like liquid crystal polymers.

1.4 Liquid Crystalline Polymers

Thermotropic liquid crystalline properties have been generated in polymeric systems generally using one of two main approaches (Figure 13). The first is by appending low molar mass mesogenic moieties to side chains attached to a polymer backbone. This results in what are known as side chain liquid crystal polymers²² (SCLCP). The second method is to incorporate rigid mesogenic moieties into the polymer backbone itself, thus creating main chain liquid crystal polymers²³ (MCLCP).

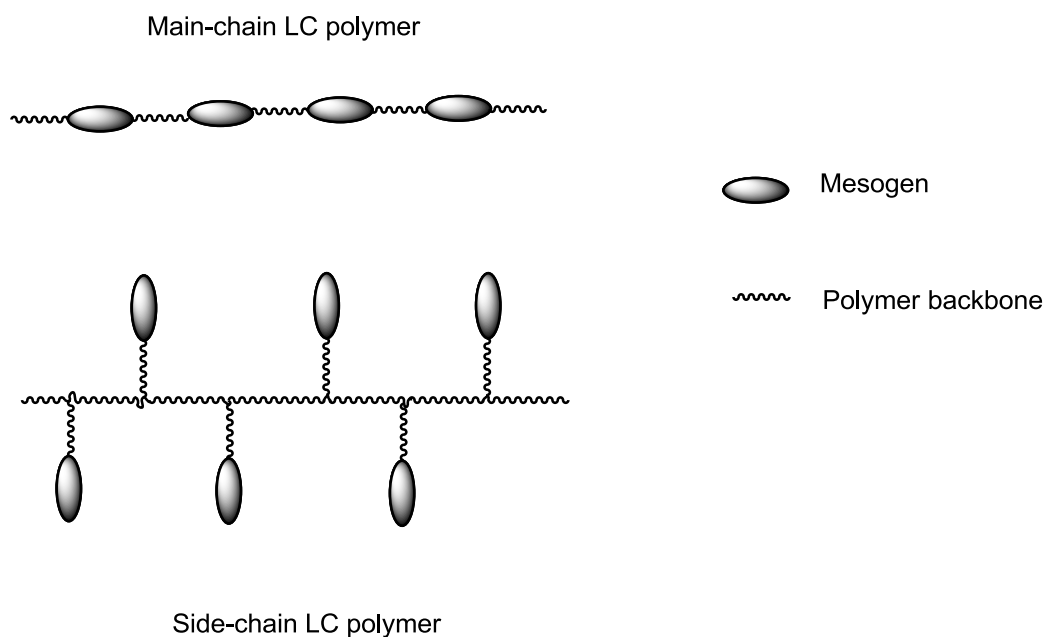


Figure 13: Liquid crystalline polymers

1.4.1 Main-chain Liquid Crystal Polymers

In main chain LC polymers the polymer backbone can be rigid due to the direct coupling of mesogenic cores together. In this case the polymers as a whole form long rigid rod-like structures which can align like low molecular weight LCs and form mesophases²³⁻²⁵. Alternatively the MCLCP can have flexible spacers between the rigid mesogenic cores, which act much like the flexible moieties used as end groups

on low molecular weight calamitic mesogens, thus allowing the individual mesogenic cores to align independently of the polymer backbone and form LC phases.

1.4.2 Side-chain Liquid Crystal Polymers

Side-chain LC polymers exhibit a competition between the flexible polymer backbone's preference to form an isotropic randomly coiled conformation and the mesogens' preference to form an ordered anisotropic mesophase²³⁻²⁵. If the mesogen is directly attached to the polymer backbone then usually the preference of the polymer backbone dominates and an isotropic conformation is preferred. As such flexible spacer moieties have been employed to decouple the movement of the polymer backbone from the mesogens. This helps minimise the inhibition of mesomorphic behaviour caused by the polymer backbone resulting in polymers which exhibit liquid crystalline behaviour. However, decoupling can never be perfect thus reducing the degrees of freedom of the tethered mesogens in comparison to that of the free mesogens. As a result there is a tendency for more ordered smectic mesophases to be formed in preference of the less ordered nematic mesophase.

The way in which the mesogens are attached to the flexible spacer in SCLCPs has an effect on the types of phases which are exhibited (Figure 14). When calamitic mesogens are attached terminally to the flexible spacer smectic phases are favoured, as the polymer backbone tends to segregate leading to lamellar type packing. When appended laterally the mesogens are simply unable to form layers. Thus laterally appended mesogens in SCLCPs result in nematic phases.

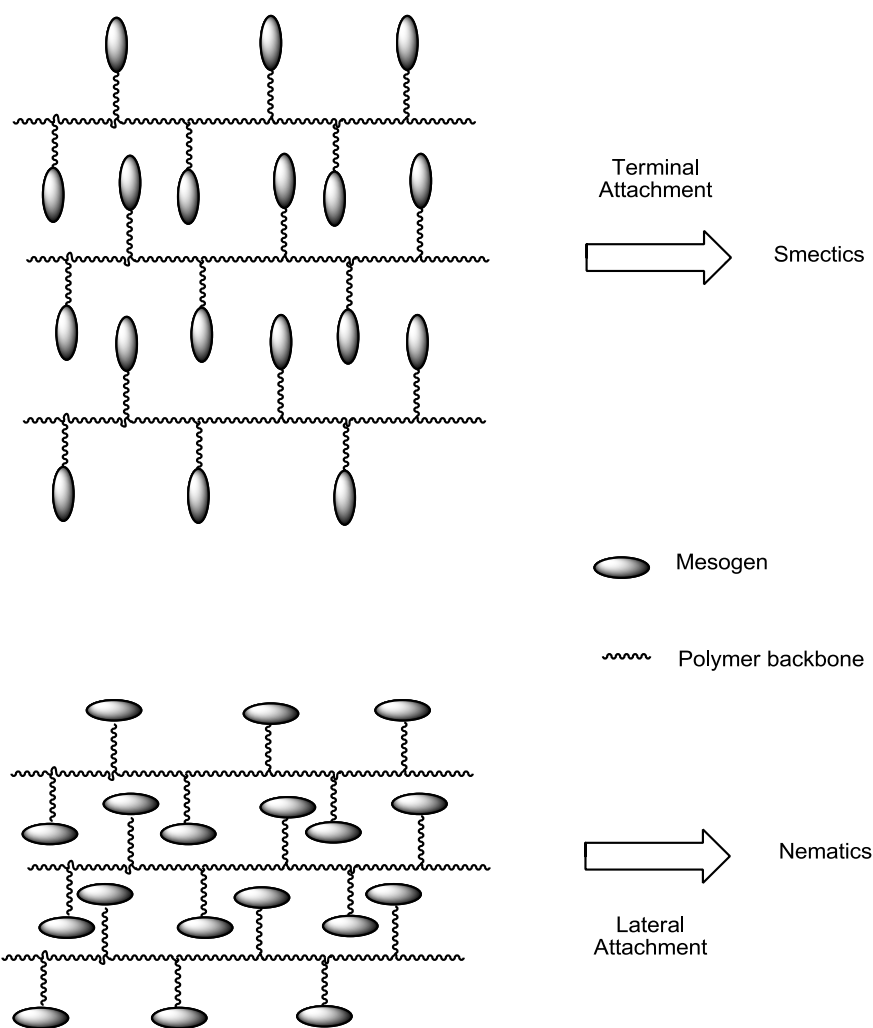


Figure 14: Lateral vs terminal attachment of mesogens in SCLCPs

1.5 Supermolecular Liquid Crystals

Supermolecular liquid crystals are giant molecular substances comprising of many smaller identifiable-parts, which as a whole exhibit liquid-crystalline properties²⁶. The liquid-crystalline properties usually arise as a result of low molar mass mesogens being incorporated onto the periphery of the supermolecular structure. Typically, but not exclusively, these low molar mass mesogens are attached to some form of scaffold *via* flexible spacers (Figure 15). The liquid crystalline behaviour exhibited is often altered by the supermolecular scaffold they are attached to²⁷. The nature of all of these components can be widely varied resulting in materials exhibiting a whole host of different mesophases and material properties.

Chapter 1: Introduction

Supramolecular LCs can be considered in many respects to have behaviour which is intermediate to that of LC oligomers and LC polymers.

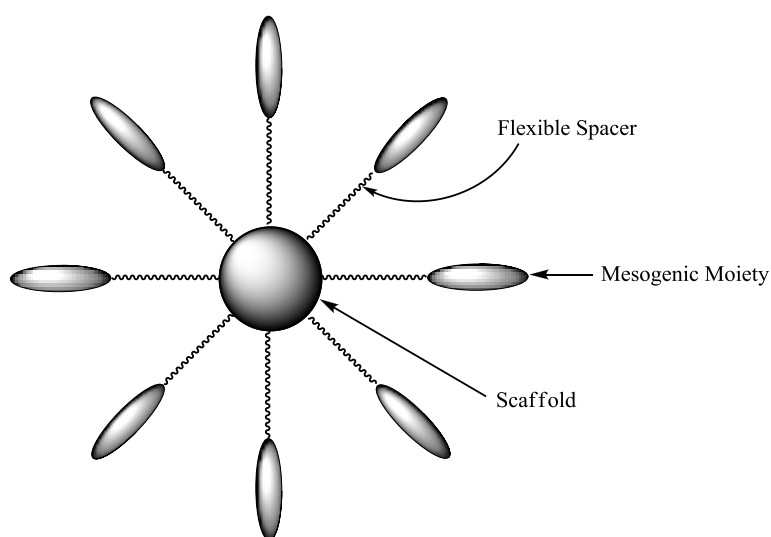


Figure 15: Schematic diagram of a supermolecular liquid crystal

One of the critical factors in defining the LC properties of this class of materials is the topology of the supermolecular LC as a whole²⁶. This is defined by a number of factors including: the nature of the core, be it rigid or soft; the level of decoupling of the mesogenic units, generally defined by the length and nature of the spacer; the density of the mesogens on the periphery, which is affected by the nature and number of mesogens and their mode of attachment (lateral or terminal). Broadly speaking the overall shapes of supermolecular LCs range from loosely rod-like through a disc-like configuration to a spherulitic shape.

If the supermolecule has an overall shape which is rod-like it is typical to expect LC properties similar to that of low molar mass calamitic mesogens (smectic and nematic phases). If the material has a gross shape which can broadly be described as disc-like then it is often observed that columnar mesophases are supported. Whereas if the material has a spherulitic aspect then often cubic phases are formed, similar to those expected for lyotropic materials²⁸.

1.5.1 The Effect of the Core

As previously mentioned the core of supermolecular LCs can affect the overall molecular topology of the materials and thus the liquid-crystalline properties exhibited. There are two basic categories of scaffold, either a soft deformable core or a hard rigid core. Examples of soft cores are dendrimers and hyperbranched polymers. Examples of hard core systems are inorganic clusters and nanoparticles.

1.5.1.1 Soft Cores - Dendrimers

Dendrimers are a class of regularly branched polymer formed from a core surrounded by layer upon layer of branching units (monomers) with each successive layer being referred to as a generation (Figure 16) and the degree of branching precisely controlled²⁹. Figure 16 depicts various generations of a dendrimer with a tetra-functional core and a bifunctional repeat unit.

Mesogens may be incorporated into dendrimers in order to form dendritic liquid crystals in a similar manner to how mesogens may be incorporated into polymers in order to form liquid crystal polymers. Like LC polymers, mesogens may be included in LC dendrimers in two different ways. The first, which is analogous to MCLCPs involves using a mesogenic moiety as a repeat unit in the dendritic scaffold³⁰. This typically results in discotic, columnar or cubic type phases, we shall not discuss these types of materials further. Mesogenic moieties may also be grafted onto the periphery of a dendrimer, before, during or after its formation. This results in LC dendrimers which are analogues of SCLCPs³¹. These materials have a tendency towards forming mesophases more akin to those of calamitic LCs.

Due to the fact that the dendrimer scaffold is usually made of flexible organic constituents, it is deformable. In the dendritic LC system this means that the core can deform in order to accommodate the packing of the mesogens into a mesophase, allowing the mesogens to dominate the phase behaviour observed³¹. As a result the supermolecular core has little effect upon the phase behaviour of the material.

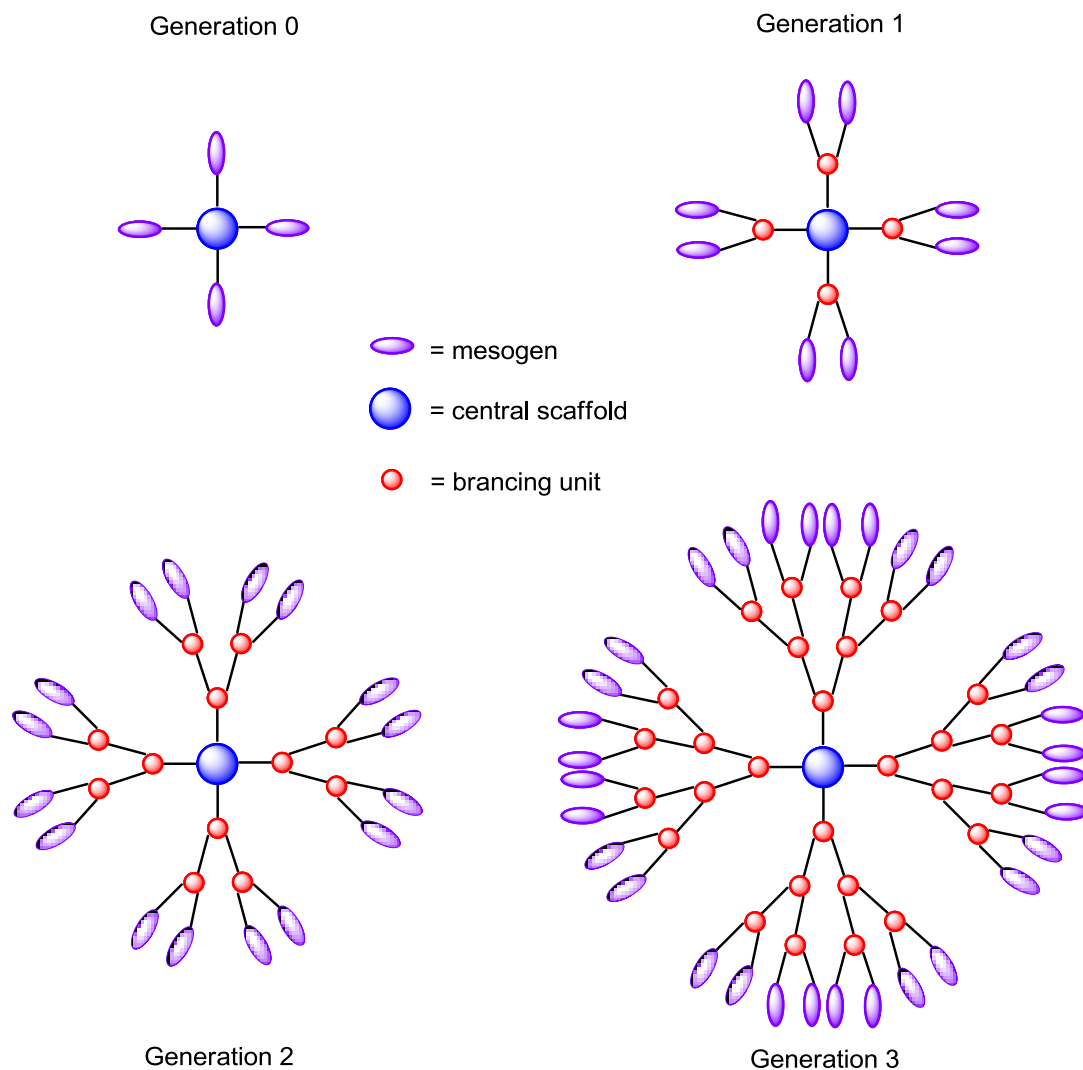


Figure 16: Schematic diagram of a 4x2 dendrimer of generation 1 - 3

This is not always the case however; dendritic LCs of high generation can reach the packing limit of mesogens on the periphery. This is a steric consideration in which there is simply no room for any more mesogens to fit on the periphery and in these situations the gross shape of the supermolecule is likely to be globular or spherulitic³². In such cases the supermolecular core will dominate the resulting phase behaviour likely to be observed because it forces a particular gross molecular shape upon the supermolecule³³.

An example of soft-cored LC dendrimers are the carbosilane dendrimers functionalized with cyanobiphenyl mesogenic moieties presented by Frey *et al*^{34, 35} (Figure 17) which display broad enantiotropic LC phases. Typically the higher the generation the more stable the phase. Interestingly the ΔH_{N-I} of these materials when

Chapter 1: Introduction

taken on a per mesogen basis is much lower than that of the free low molar mass mesogens, 1.2 kJmol^{-1} for the G2 dendrimer versus around $4\text{-}6 \text{ kJmol}^{-1}$ for the free mesogens. This is caused by the presence of the dendritic core which has a tendency towards an isotropic phase competing with the mesogens tendency towards ordered mesophases. This results in a less ordered mesophase and thus a lower ΔH_{N-I} per mesogen. This is a very similar effect to that observed for LC polymers.

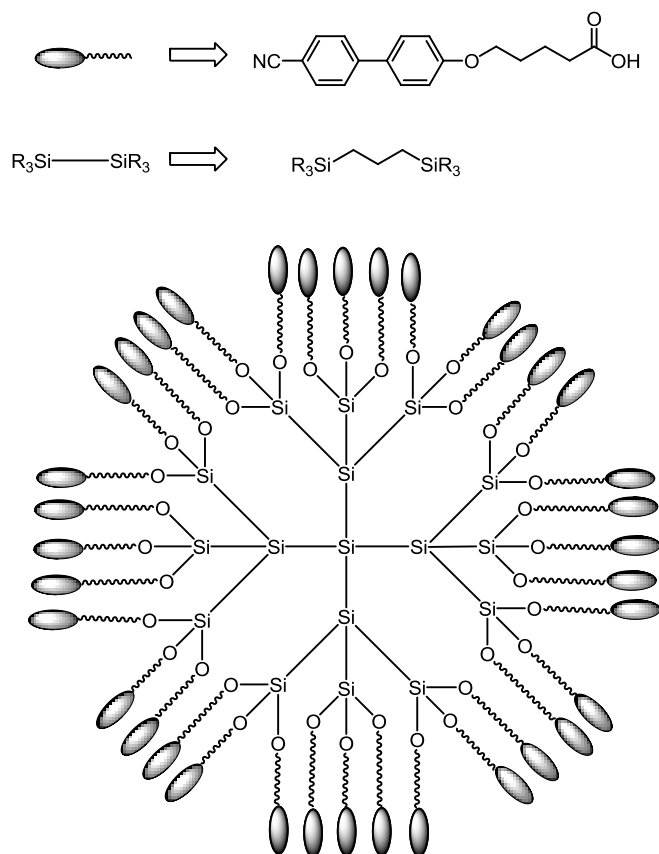


Figure 17: G2 Carbosilane dendrimer functionalized with cyanobiphenyl mesogens

Furthermore these LC dendrimers did not crystallize upon continued cooling, but the smectic phases froze as a result of the mesogens not being able to adopt a close packed crystal structure resulting from the limited degree of freedom caused by attachment to the dendritic scaffold. Again this is similar to the behaviour observed for LC polymers. However, at odds with LC polymers these materials showed lower viscosities than their polymeric analogues. The high viscosities associated with LC polymers is due to entanglement of the polymer backbones which is absent in LC dendrimers.

1.5.1.2 Hard Cores - Inorganic Clusters

There have been several reports of inorganic clusters being used as the core of LC supermolecules^{33, 36, 37}. Generally, the cores have some functional property which would be enhanced or altered for practical application by the addition of mesomorphic behaviour, which is introduced into the systems using mesogens on the periphery of the supermolecules.

An example of this is the functionalization of single-molecule magnets (SMM's) with cyanobiphenyl mesogens (CB) as described by Donnio *et al*³⁸ (Figure 18). Manganese oxide ($\text{Mn}_{12}\text{O}_{12}(\text{OAc})_{16}(\text{H}_2\text{O})_4$) clusters, one of the most well-known and intensively studied SMMs were functionalised by ligand exchange with gallate derivatives with R terminal groups to generate three new materials. One simply with methyl ethers (R = 48), which was used as a model compound to get detailed structural information about the inorganic core; the second with C_{12} alky ethers (R = 48) and the third with C_{11} alkyl ethers terminated with CB (R = 48) mesogenic moieties attached *via* an ether linkage.

The first compound was found to be non-mesomorphic. The second however displays a cubic phase as determined by X-ray experiments. This is interesting as the LC behaviour is not generated by a mesogenic moiety but rather the close packing of spherulitic supermolecules into a body centred cubic arrangement, similar to that of self-assembling LC dendrimers described by Percec³⁹. This type of phase is usually observed in lyotropic systems. The material melts from a crystal into the cubic phase and then decomposes before clearing into the isotropic liquid. This material is a good example of how the overall topology of a supermolecular material can lead to LC behaviour. The third compound also shows mesomorphic behaviour and displays a SmA phase upon melting from a glass and decomposes before clearing to the isotropic liquid. This phase was also identified by X-ray studies. This third material is an example of the mesogenic moieties imparting liquid crystallinity onto a system and the mesogens can be said to be dominating the phase behaviour of the system. All three materials retain the magnetic properties of the cluster despite the functionalization.

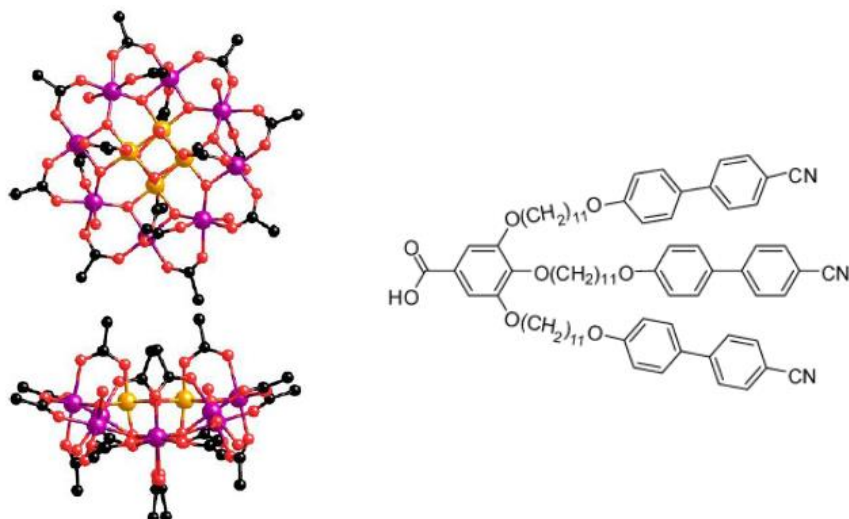


Figure 18: left) SMM manganese oxide cluster; right) gallate derivative functionalized with CB mesogens, reproduced from *Angew. Chem.-Int. Edit.*, 2008, **47**, 490-495³⁸

1.5.2 The Effect of the Spacer

The spacer in supermolecular LCs can influence which part of a particular supermolecular LC dominates the behaviour⁴⁰. In general, if the spacer is short then the core of the material will have a strong effect on the overall behaviour and if the spacer is long then the mesogenic moiety will dominate. This trend is also observed in LC polymer systems, which share similarities with LC supermolecules in terms of the factors that determine their behaviour⁴¹.

It can be considered that the core and the periphery of a supermolecular LC are in competition to dictate the behaviour of the material as a whole. If the spacer is long and flexible, the mesogenic moieties are able to move more freely and behave like low molar mass mesogens of the same type⁴². This is known as decoupling the motions of the mesogen from the core, allowing them to overcome the constraints of the core and dictate the behaviour of the material. If the spacer is short or rigid, the topology of the core will be transferred to the periphery and force the mesogenic moieties to adopt specific conformations. This often results in behaviour which deviates dramatically from that of the related low molar mass mesogens⁴³.

1.5.3 The Effect of the Periphery

The periphery of supermolecular LCs is often where mesomorphic behaviour is generated in these systems by the incorporation of low molar mass mesogens⁴⁴. The phases observed are often determined by the choice of mesogen, the number of mesogens and their mode of attachment. By carefully designing materials the properties can be tuned in order to generate substances with specific material properties, for specific applications^{45, 46}.

1.5.3.1 Choice of Mesogen

Typically the types of phases exhibited by a supermolecular LC will be similar to those observed for the low molar mass mesogen that is attached. As such low molar mass mesogens which exhibit N phases will likely provide nematic phases in a supermolecular environment⁴⁷, likewise with smectic phases⁴⁸. In SCLCPs the mesogens are typically more ordered than in unimolecular systems as a result of the spacer precluding complete decoupling of the mesogenic motions from the backbone²². A similar effect is also observed for supermolecular LCs such as dendrimers. This results in a more ordered structure which leads to more ordered phases⁴⁹. Furthermore chiral mesogens which form chiral phases in a low molar mass environment will normally form chiral phases when incorporated into supermolecular systems⁵⁰.

However, the situation can be greatly complicated in a supermolecular system where more than one type of mesogen may be incorporated into one supermolecule. This can be done randomly over the surface⁵¹ or in a very controlled manner⁵². Synthetic challenges exist in both cases. Both also display different behaviours, which are often very complex in explaining as the overall behaviour depends on many competing factors, such as the relative ratio of mesogens, spacer length, chemical nature of the linking group and the multiplicity of the core.

1.5.3.2 Number of Mesogens

The number of mesogenic moieties attached to a supermolecular framework has a significant effect on the thermal stability of any phases formed by the material. In general a greater number of mesogens will result in an increase in phase stability³¹ in analogy with the effect of the degree of polymerization observed in SCLCPs⁵³. If one considers the stability of a given material's LC phases as a function of the competition between the isotropic parts of the material (the core and spacers) and the anisotropic parts (the mesogenic moieties) then it is logical to expect that increasing the ratio of anisotropic to isotropic regions will increase the stability of the phases. This relationship however is not linear, and upon further increasing the number of mesogens incorporated into the supermolecule, a plateau is reached²⁶. However, at difference with traditional SCLCPs, supermolecular LCs are monodisperse, composed of a single molecular entity, which eliminates the dependency of mesomorphic properties such as transition temperatures, with the degree of substitution and molecular weight^{26, 27, 30, 31}.

1.5.3.3 Mode of Attachment

The way in which the mesogens are attached to the supermolecular scaffold or spacers has a significant impact on the types of phases observed in a similar manner to that of LC polymers. Namely, when a calamitic mesogen is attached terminally to the backbone, scaffold or spacer, smectic and/or nematic phases are formed, however when attached laterally the tendency to form lamellar phases is suppressed and generally only N phases are observed^{39, 40, 54, 55} (Figure 15).

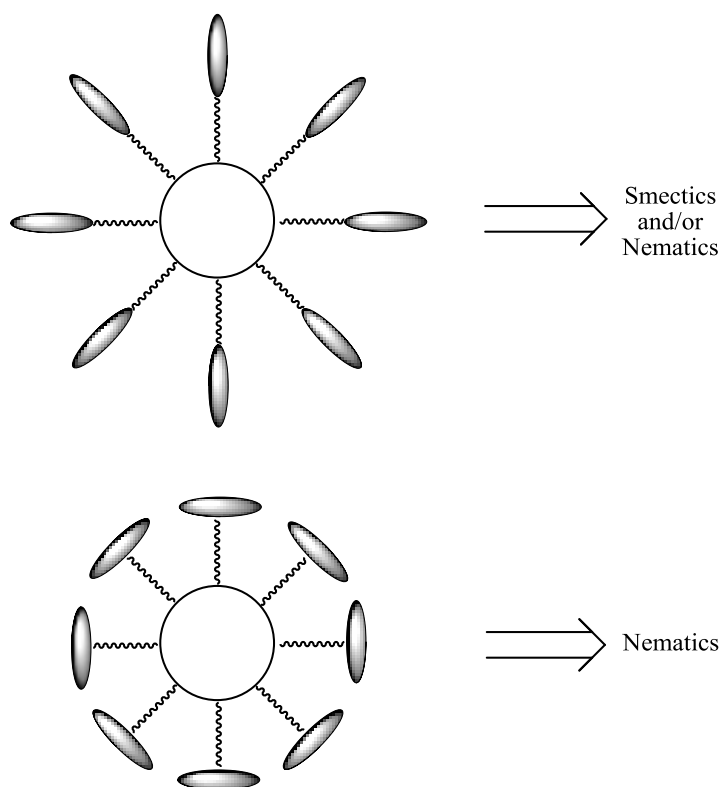


Figure 19: The effect of the mode of attachment of mesogens

1.6 Carboranes

Carboranes are a family of deltahedral inorganic-organic hybrid clusters made from BH and CH fragments with the general formula $C_2B_{x-2}H_x$. The bonding properties of these materials determine their structures and this is best described by Wade's rules^{56, 57}. By counting the number of electrons in the valence band of all the components of a particular cage and then adding them together then depending upon the number of vertices (n) the structure likely to be adopted can be predicted (Table 1). A deltahedron is a polyhedron which has no non-triangular faces connecting the vertices. This is the parent structure and occurs when the the electron count is $4n+2$ and is referred to as the *closo* structure. The other related structures are generated by either adding or removing vertices as shown in Table 1.

Electron Count	Name	Predicted Structure
$4n-2$	Bicapped <i>closo</i>	$n-2$ vertex <i>closo</i> deltahedron with 2 capped faces
$4n$	Capped <i>closo</i>	$n-1$ vertex <i>closo</i> deltahedron with 1 capped face
$4n+2$	<i>Closo</i>	<i>Closo</i> deltahedron with n vertices
$4n+4$	<i>Nido</i>	$n+1$ vertex <i>closo</i> deltahedron with 1 vertex missing
$4n+6$	<i>Arachno</i>	$n+2$ vertex <i>closo</i> deltahedron with 2 vertices missing
$4n+8$	<i>Hypho</i>	$n+3$ vertex <i>closo</i> deltahedron with 3 missing vertices

Table 1: Wade's rules for predicting the structure of polyhedral clusters where n is the number of vertices

Carboranes are characterised by electron deficient 3 centre 2 electron bonding, such as in diborane (Figure 20), delocalised over the entire cage, sometimes known as sigma aromaticity⁵⁸ or superaromaticity. This is due to the fact that the delocalised bonds are of anodal sp hybrid orbitals and thus have sigma character. In contrast, two-dimensional aromaticity (e.g. benzene) is constructed of uninodal p-orbitals. Hückel's rule⁵⁹ (Equation 2) infers that molecules must have a specific number of delocalised electrons and be planar to display aromaticity.

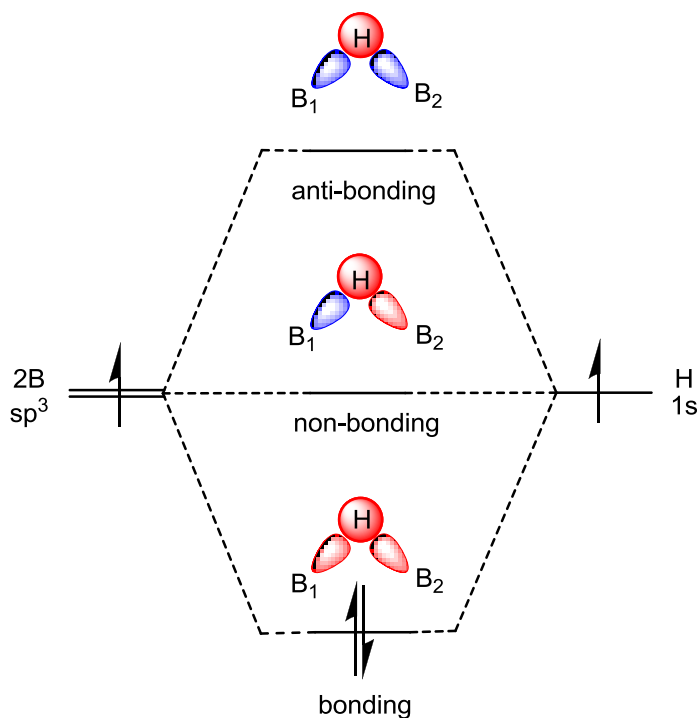


Figure 20: Three centre 2 electron bonding in diborane

However, in three-dimensional systems Hückel's rule does not apply. Sigma aromaticity by necessity cannot be planar. To understand three-dimensional (3D) aromaticity it is necessary to consider the linear combination of atomic orbitals. Each vertex in the system contributes three internal orbitals with the fourth being used to form a sigma bond to an external group e.g. BH units contribute one atomic orbital to form an external B-H bond. Two of these internal orbitals are termed tangential orbitals⁶⁰ which combine to form the framework of the material (Figure 21), be it a two-dimensional (2D) ring as for planar aromatics or a 3D cage structure for 3D aromatics. The third internal orbital is termed a radial orbital⁶⁰; overlap of these and filling of the subsequent molecular orbitals (MOs) is what results in aromaticity⁵⁸ and is termed core bonding (Figure 21).

$$4k + 2 = d$$

k is a non-negative integer and d is the number of π electrons

Equation 2: Hückel's rule for 2D aromatics

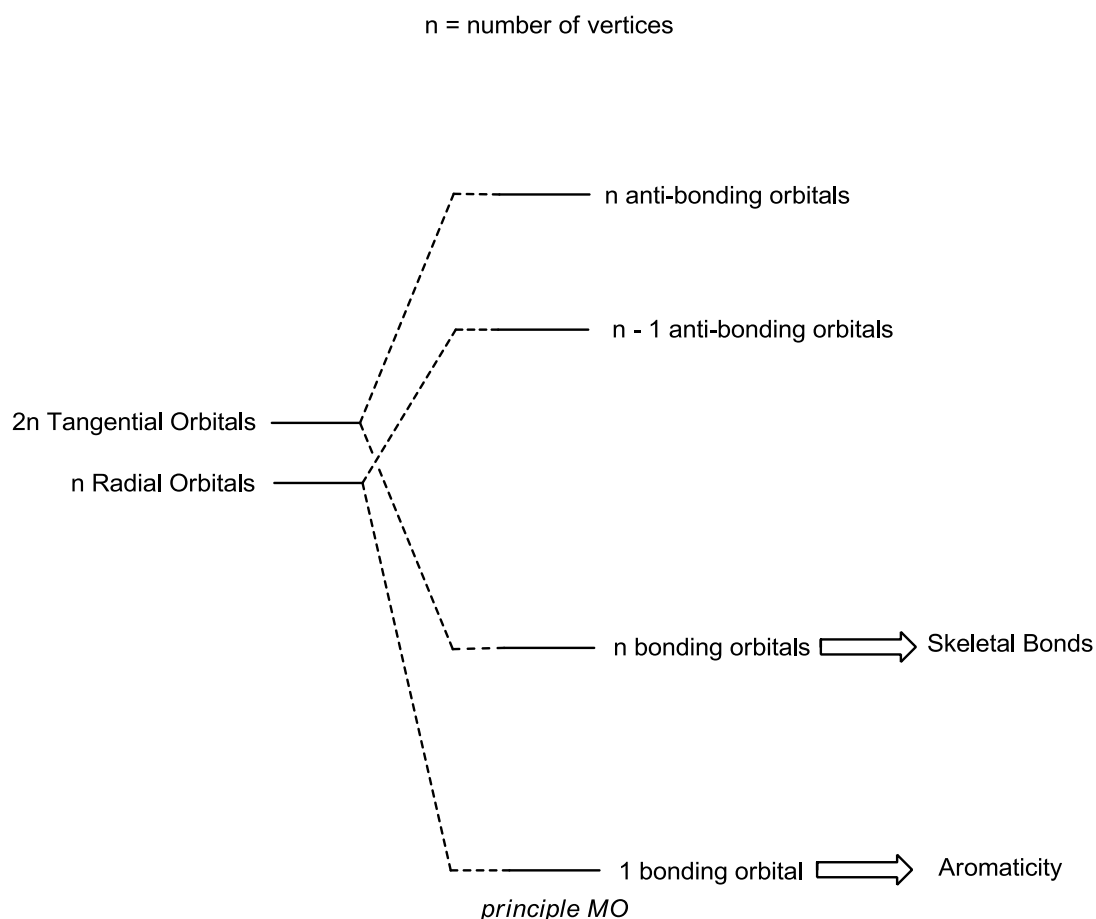


Figure 21: Linear combination of molecular orbitals diagram for 3D aromatic systems

Each system therefore has $2n$ tangential and n radial atomic orbitals; where n is the number of vertices. Combination of the $2n$ tangential orbitals results in n bonding and n anti-bonding MOs. In the case of benzene with $n = 6$, this results in 6 bonding and 6 anti-bonding orbitals corresponding to the σ -bond network making up the ring.

$$4k + 2 = c$$

k is any non-negative integer and c is the number of core bonding electrons

Equation 3: Analogue of Hukel's rule for 3D aromatics

For the case of $B_xH_x^{2-}$ boranes and the isoelectronic $C_2B_{x-2}H_x$ carboranes, regardless of how the remaining n radial atomic orbitals are combined there is always an eigenvalue which is more positive than any of the other eigenvalues called the *principle eigenvalue*⁵⁸. The MO which corresponds to this eigenvalue is known as

Chapter 1: Introduction

the *principle core orbital*. From Wade's rules⁶⁰ $B_nH_n^{2-}$ boranes and $C_2B_{n-2}H_n$ carboranes have $2n + 2$ skeletal electrons of which $2n$ are used to fill the surface bonding orbitals derived from combination of the $2n$ tangential orbitals. This leaves two electrons to fill the *principle core orbital*. Thus carboranes can be considered 3D aromatic systems with $4k + 2 = 2$ core bonding electrons, where $k = 0$ (Equation 3); which is analogous to $4k + 2 \pi$ electrons for planar aromatics (Equation 2).

Aihara⁶¹ applied a similar methodology to Hückel and used a linear combination of atomic orbitals as described above to calculate the resonance stabilization energies of deltahedral polyborane anions ($B_xH_x^{2-}$), which are isoelectronic with carboranes, finding that they also exhibit a significant stabilization due to aromaticity.

This σ -aromaticity makes carboranes extraordinarily stable, both thermally and chemically. 1,2-dicarba-*closo*-dodecaborane, more commonly known as *o*-carborane, is thermally stable up to 400 °C, and under inert atmosphere it isomerizes, to 1,7-dicarba-*closo*-dodecaborane between 500 and 600 °C and then to 1,12-dicarba-*closo*-dodecaborane between 600 and 700 °C⁶². These isomers are otherwise known as *m*-carborane and *p*-carborane respectively as an analogue to di-substituted benzene derivatives (Figure 22). Furthermore, all three are highly resistant to oxidising agents, alcohols and strong acids⁶³. Additionally they also exhibit a relatively high polarizability⁶⁴. A combination of these factors has resulted in carboranes being of intense research interest in the field of materials science, with studies into high temperature stable hybrid polymers⁶⁵, non-linear optical materials⁶⁶ and ion-selective electrodes⁶⁷, among others.

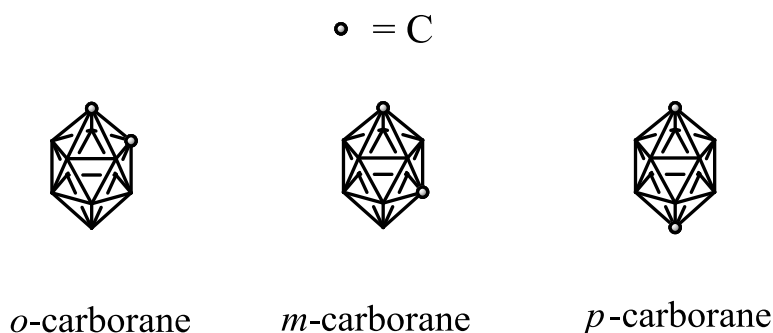


Figure 22: Structure of Carboranes, each vertice equals a BH unit unless indicated

1.6.1 High Molar Mass Carboranes

Carboranes have been incorporated into supermolecules in a number of different ways in order to utilize their material properties. Apart from being incorporated into polymers^{68, 69}, most reports of such materials have been dendrimers, perhaps because of their perfectly defined structures as well as allowing synthetic flexibility and control. However, there are examples of carborane containing supermolecules that are not dendritic.

1.6.1.1 Carborane Containing Hyperbranched Network

An example of a carborane containing hyperbranched network has been described by Kolel-Veetil⁷⁰ in which a vinyl terminated disiloxane derivative of *m*-carborane, is used as a spacer unit and a silane terminated polyhedral oligomeric silsesquioxane (POSS) derivative (Figure 23) as the branching unit. These were polymerized *via* a hydrosilylation reaction using Karstedt's catalyst to generate a hyperbranched network. These materials exhibited extraordinary thermal and thermo-oxidative properties which far exceeded those of other reported POSS derived organic/inorganic polymers. This example shows how carboranes can be used in conjunction with other inorganic building blocks to generate high performance functional materials.

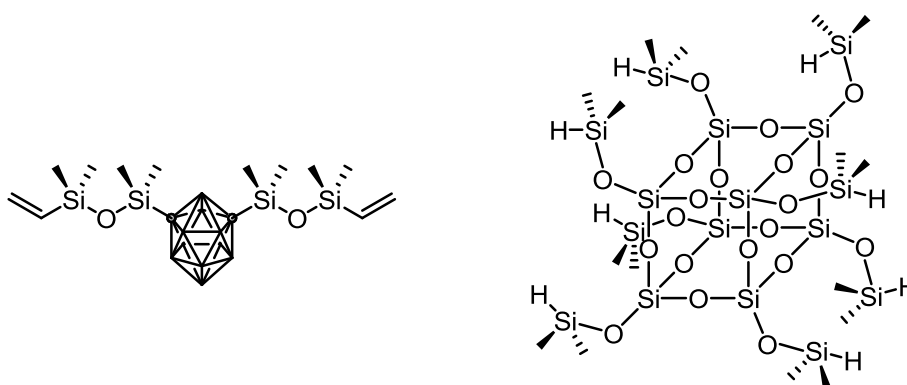


Figure 23: Left) 2,5-bis-(vinyl(tetramethyl disiloxane))dicarbodecaborane, Right)
1,3,5,7,9,11,13,15-Octakis-(dimethylsiloxane) substituted pentacyclo
[9.5.1.1.1.1]octasiloxane

1.6.1.2 Polyester Based Carborane Containing Dendrimers

There are numerous examples of carboranes being incorporated into dendrimers⁷¹⁻⁷⁴ using a wide variety of dendritic scaffolds including polyesters, polyaryl ethers and carbosilanes. There are two reported ways of incorporating the carborane moiety into dendrimers. The vast majority append the carborane to the periphery. However, Valliant *et al* describe the synthesis of a series of multi-part polyester dendrimers that incorporate carboranes into the dendritic scaffold of the materials⁷⁵ as part of the flexible spacer, leaving the periphery functionalized with hydroxyl groups making the material water soluble.

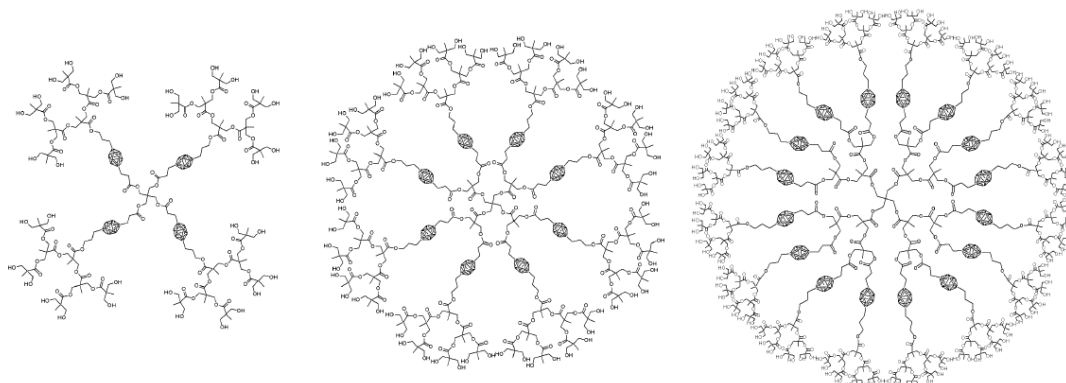


Figure 24: Carborane containing polyester dendrimers, left, centre and right, generations 3, 4 and 5 respectively, reproduced from Langmuir, 2006, 22, 5251-5255⁷⁶

Valliant also describes the curious behaviour of these materials when heating them in an aqueous solution⁷⁶. Upon heating a critical temperature is reached at which point the materials precipitated out of solution. This counterintuitive behaviour is explained by the changing shape of the dendrimer; as more thermal fluctuations occur, the hydrophobic carboranes become more “visible” to the surface of the dendrimers. Once a critical point is reached the solubility drops and the material precipitates. This behaviour has been observed before in other dendrimers⁷⁷, and is also observed in some polymer systems^{78,79}.

1.6.1.3 Carborane Containing Carbosilane Dendrimers

Nuñez *et al* have synthesized a series of carborane containing dendrimers that provide excellent examples of the incorporation of carboranes onto the periphery of dendritic systems. Initially both convergent and divergent methods of generating carbosilane dendrimers of generations 1 and 2 were explored, with carborane moieties appended to the periphery using the hydrosilylation reaction⁸⁰ (Figure 25). De-boronation of the peripheral carborane clusters generated polyanionic carbosilane dendrimers functionalized with either 4 or 8 *nido*-carboranes, depending on generation. This was done as a stepping stone towards generating dendrimers with multiple metallocarborane clusters attached to the periphery. The rationale for designing boron rich anionic supermolecules was to develop new low-nucleophilic anionic bioactive molecules for uses in medicine i.e. the extraction of radionuclides.

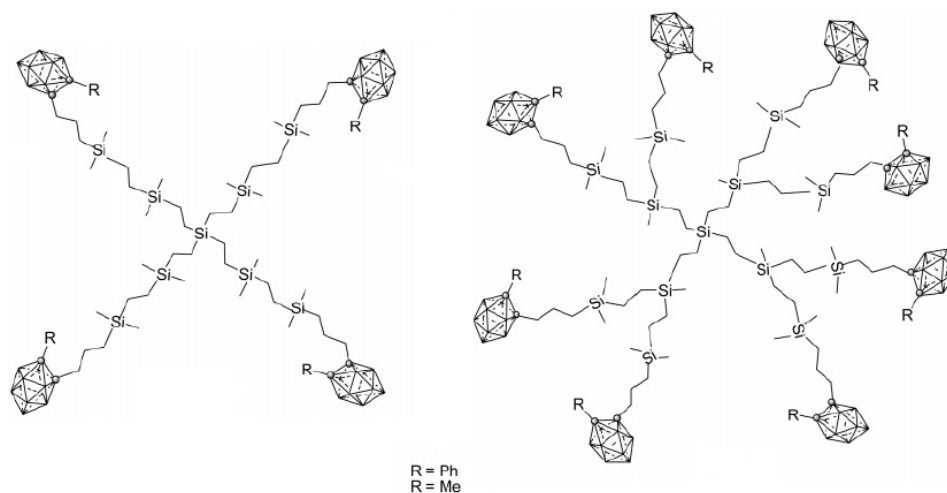


Figure 25: Carborane functionalized carbosilane dendrimers, generations 1 and 2 left and right respectively, reproduced from *Macromolecules*, 2007, **40**, 5644-5652⁸⁰

Nuñez *et al* have also investigated using polysiloxanes rather than silanes as the core of their carborane functionalized polypedes⁸¹. These materials are also synthesized using hydrosilylation, but rather than reducing the chlorosilane products to Si-H, as is typical for hydrosilylation coupling between alkenes, they employed a hydrolysis reaction in order to generate cyclic polysiloxane cores in a convergent process. In this way they generated carborane functionalised polypedes with siloxane cores with

Chapter 1: Introduction

2, 3, and 4 carborane clusters appended to the periphery. In order to increase the number of carborane moieties attached to their materials a POSS core was used, made using a similar hydrolysis reaction as the polysiloxanes. This resulted in eight carborane moieties being incorporated onto the periphery (Figure 26). This method enabled them to incorporate a similar number of carboranes into the molecular structure as they achieved with the silane dendrimers, but with a shorter synthetic route. Finally, again towards their aims of polymetallocarborane materials, the carborane clusters were deboronated to generate polyanionic materials.

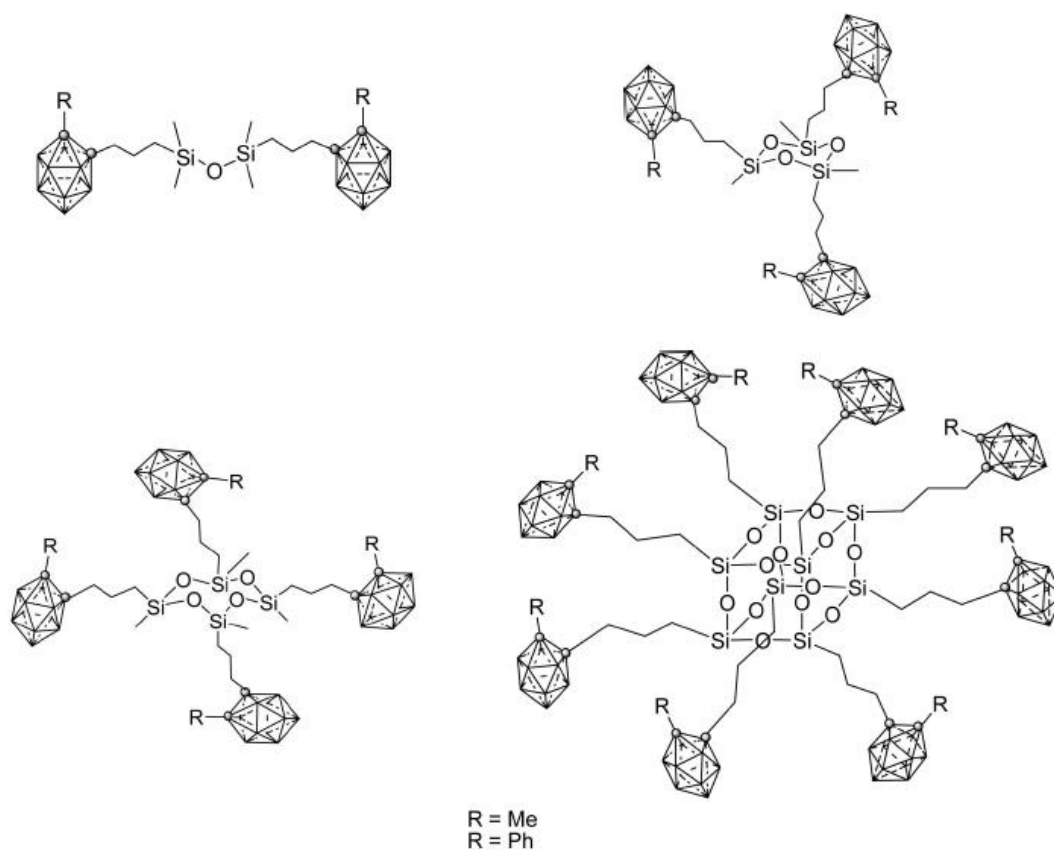


Figure 26: Siloxane core polypedes functionalized with 2, 3, 4 and 8 carboranes, top left, top right, bottom left bottom right respectively, reproduced from *Macromolecules*, 2008, **41**, 8458-84⁸¹

Nuñez *et al* eventually realised their goal of synthesising polyanionic metallocarborane functionalized dendrimers⁸² (Figure 27). Using a divergent method they synthesised generations 1 and 2 carbosilane dendrimers functionalised with either 4 or 8 metallocarborane moieties on the periphery. Furthermore they also

Chapter 1: Introduction

describe the synthesis of polyanionic cyclotetrasiloxane cored metallocarborane functionalised polypedes also with either 4 or 8 carborane moieties on the surface.

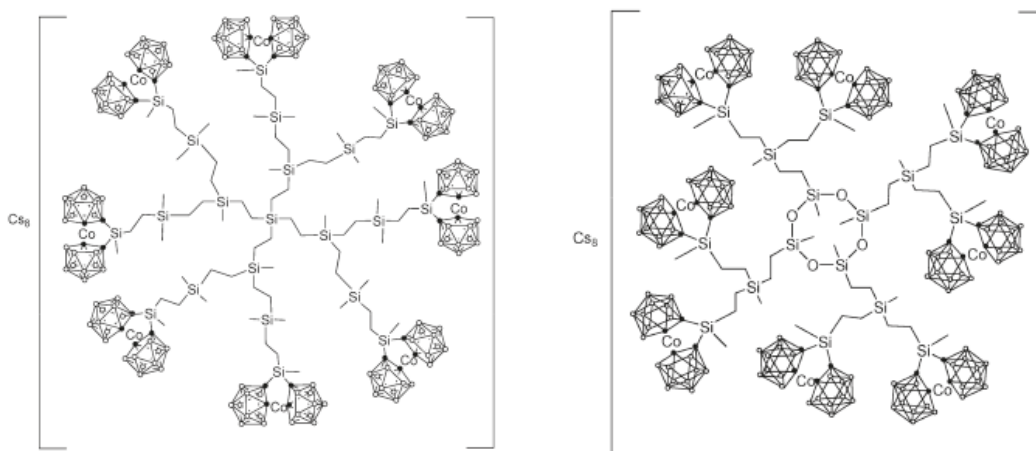


Figure 27: Polyanionic metallocarborane functionalized generation 2 carbosilane dendrimer (left) and cyclotetrasiloxane cored generation 1 carbosilane dendrimer (right), reproduced from *Organometallics*, 2009, **28**, 5550-5559⁸²

1.6.2 Carboranes in Liquid Crystals

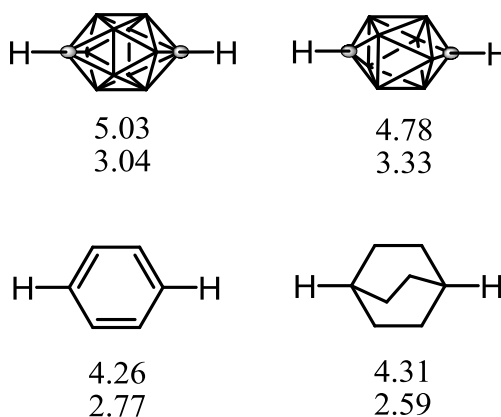


Figure 28: Diameter of the cylinder of rotation (top number in Å) and the HC...CH inter bridgehead distance (bottom number in Å) of *p*-dodecacarborane (top left), *p*-decacarborane (top right), a phenyl ring (bottom left) and bicyclooctyl ring (bottom right); calculated using HF/6-31G* method⁸³

To date there has only been one approach to incorporating carboranes into LCs. That is to replace phenyl rings in typical LC molecular structures with carborane clusters.

Chapter 1: Introduction

The reason for this is that the *p*-decarborane ($B_8C_2H_{10}$, a ten vertex analogue of dodecacborane) and *p*-dodecacborane clusters both have similar space filling properties to phenyl rings and bicyclooctyl groups, which are commonly used in LC synthesis (Figure 28)⁸³ but with very different polarizability.

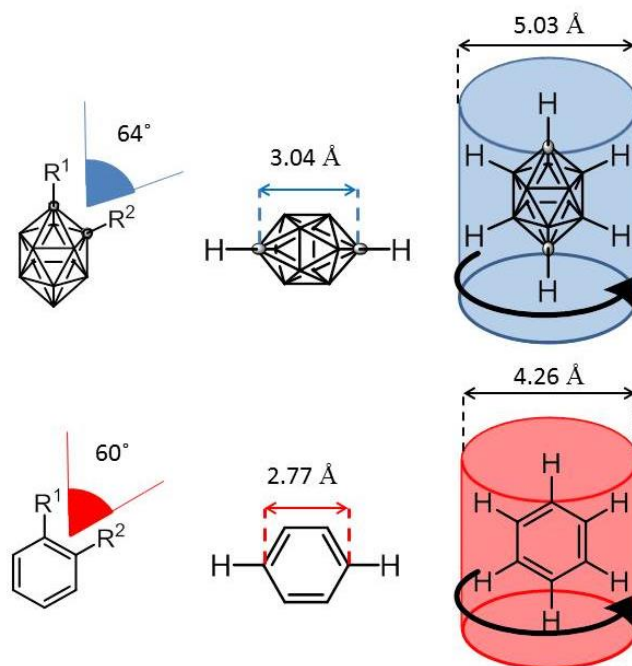


Figure 29: Physical dimensions of an *o*-carborane cluster (top) and a phenyl ring (bottom)

Kaszynski and co-workers have produced a whole series of materials which incorporate carboranes into the mesogenic cores in various typical LC molecular structures and have investigated their properties extensively. A series of homostructural two-ring systems was synthesized, in which the rigid core of the mesogens consisted of two dodecacborane, decacarborane, phenyl rings or bicyclooctyl rings (Figure 30). Any conformational bias caused by the interactions of alkyl chains and the cores was controlled by making another homostructural series in which the alkyl chains were separated from the cores by alkynyl groups in order to decouple the movement of the chains completely from the cores. A comparison of the stability of virtual mesophases for these materials in a nematic host showed that carboranes of both the 12 and 10-vertex variety are effective substituents in LC cores⁸⁴, although they did find that 12-vertex dodecacborane results in higher mesophase stabilities⁸⁵.

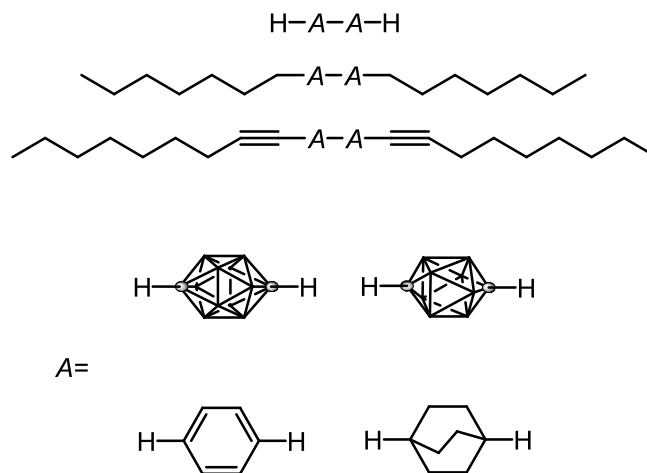


Figure 30: Homostructural Series of 2-"ring" systems⁸⁵

In a later study Kaszynski and co-workers compared the electronic properties of 10-vertex *p*-carboranes and 12 vertex *p*-carboranes functionalized with either alkynyl or alkyl substituents⁸⁶. Using a combination of *ab initio* calculations, UV-adsorption spectroscopy, substituent effects in ¹³C NMR and crystallographic data they probed the extent of electronic coupling of the C_{cage} to the C_{substituents}. They found that there are strong interactions between the cage and substituents in the 10-vertex carboranes, while the 12-vertex carboranes are largely electronically isolated; this is despite both C_{cluster} carbons being in very similar hybridization states.

The bridgehead carbons of the 10-vertex clusters showed behaviour which would be expected of a sp² hybridized carbon, while the 12-vertex carborane clusters bridgehead carbons appeared to behave as if sp³ hybridized; when substituted with an acetylene group the UV adsorption band of the 10-vertex carborane at 200 nm was red shifted to 232 nm, whereas the adsorption band of the 12-vertex carborane at 193 nm was unaffected. Furthermore the effect of substituting an alkyne with a 10-vertex carborane causes a similar change in chemical shift observed for the alkyne carbon in ¹³C NMR to that of substitution with a phenyl ring. Whereas substitution with a 12-vertex carborane caused a comparable change in the chemical shift observed for the alkyne carbon to that of substitution with a methyl group. Finally the crystallographic data showed that the average C_{cage}-alkyl bond distance and C_{cage}-alkyne bond distance for the 10-vertex cages are close to the bond distances expected if the cage

Chapter 1: Introduction

were an alkene and for the 12-vertex cluster if the cage were an alkyl substituent respectively.

Kaszynski has also noted that carborane containing liquid crystals, which are structural homologs of traditional liquid-crystalline materials, are almost exclusively nematogenic even when the phenyl homologues display smectic polymorphism⁸⁷. This behaviour is similar to that observed in bicyclooctyl and cyclohexyl containing homologues first reported by Dewar⁸⁸. In light of the electronically isolated nature of 12-vertex carboranes this is not surprising. If the clusters do not interact with the rest of the mesogenic core electronically then the anisotropic polarizability is likely to be lower. This will lead to less chance of intermolecular quadrupolar interactions and interactions *via* dispersion forces, which will result in decreased lateral attractive forces between the mesogens and thus materials which are less likely to form smectic phases. Furthermore Kaszynski has also found that for *p*-substituted carboranes there is a large degree of substituent conformational mobility, with an energy difference of approximately 2 kJmol⁻¹ between the eclipsed and staggered conformations⁸⁹. This conformational freedom disrupts packing and therefore destabilizes smectic phases.

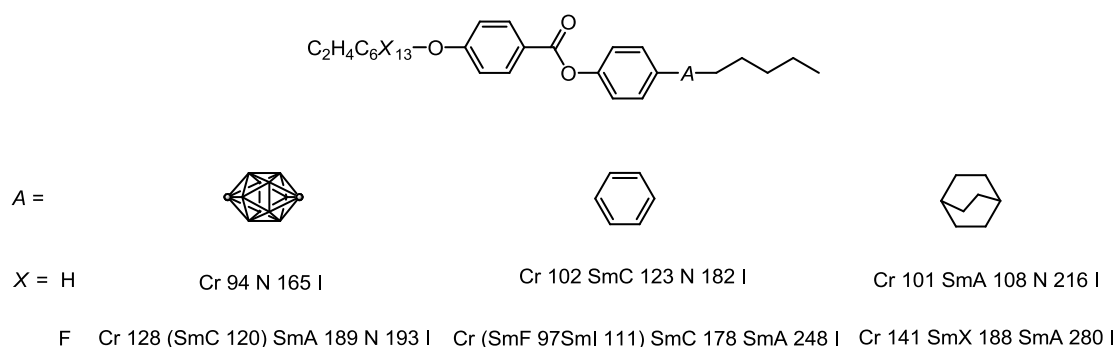


Figure 31: Comparison of partially fluorinated alky and alkyl structural homologues containing either p-dodecacarborane (left), phenyl ring (centre) or bicyclooctyl (right) groups⁹⁰

However, Kaszynski and co-workers have generated a number of carborane containing materials that do form smectic phases⁹¹⁻⁹⁴. Figure 31 shows a series of compounds which demonstrate many of the previous points⁹⁰. In order to generate stable smectic phases in the carborane containing LC, fluorination of a terminal chain

was used. This is a well-tested method of generating smectic phases⁹⁵. A comparison of the non-fluorinated materials shows that the carborane containing material alone exhibits only nematic behaviour, whereas the phenyl and bicyclooctyl homologues both show smectic behaviour, with the phenyl homologue showing the greatest smectic stability. Upon fluorination all the materials exhibit smectic polymorphism; however the carborane derivative is unique in retaining its nematic phase, with the phenyl homologue displaying the greatest smectic polymorphism and a range of smectic and soft crystal phases. These series taken together demonstrate the order of smectic stability to be phenyl > bicyclooctyl > carboranyl which was first rationalized by Kaszynski⁹⁰. Based on the arguments previously put forward, this can be explained by the fact that the carborane moiety is electronically isolated from the rest of the core and has a high degree of substituent conformational mobility. The bicyclooctyl moiety is also electronically isolated from the rest of the core but does not have as high a degree of substituent conformational mobility and thus is better at promoting smectic phases than the carborane. Finally the phenyl ring is neither electronically isolated nor does it have a high degree of substituent conformational mobility, making it the most suitable core component for promoting smectic phases.

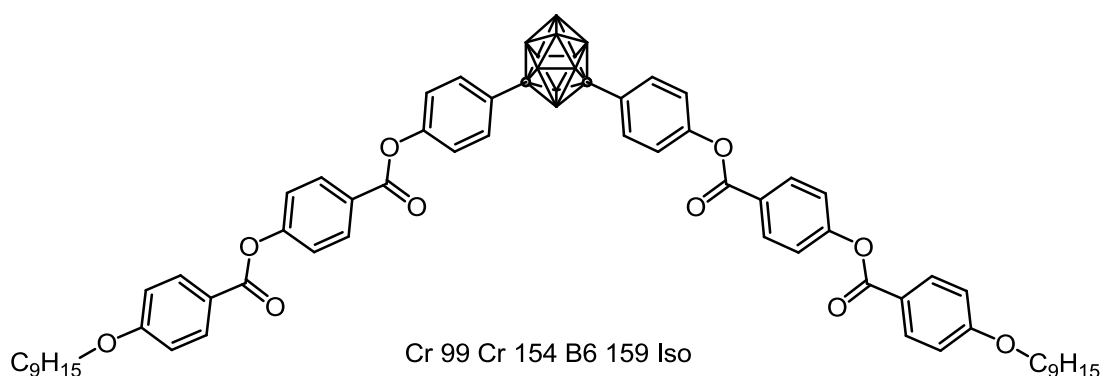


Figure 32: Carborane containing bent-core liquid crystal⁹⁶

There is one example in which a carborane cluster has been incorporated into a non-calamitic LC system. Kaszynski and co-workers utilized a *m*-carborane cluster as the central inflexion point of a banana-shaped liquid crystal (Figure 32), also called a bent-core mesogen⁹⁶. The aim of this work was to determine whether replacing a planar aromatic ring system as the bent unit with a non-planar moiety, such as *m*-carborane or adamantane, would have any effect on the phase behaviour of this class

Chapter 1: Introduction

of materials. *m*-Carborane is ideally suited for this as it has an inter-substituent bond angle of around 120 °, comparable to *m*-substituted phenyl rings, and is a non-planar aromatic. It was shown that both the adamantane and carborane homologues formed non-polar banana phases which are in contrast to the significantly more stable polar banana phases formed by the phenyl derivatives. This observation is rationalised by considering the greater conformational freedom of the substituents in the carborane analogues in comparison to the phenyl derivatives, as was discussed earlier for calamitic mesogens. The greater the substituents conformational freedom the more flexible the molecule is, which can disrupt the formation of LC phases and in particular lamellar phases.

2. **Aims**

Chapter 2: Aims

The aims of this work are to investigate the effects of incorporating carborane clusters into supermolecular liquid crystals, more specifically as the central scaffold. This will enable a comparison between the observed behaviour of these carborane containing supermolecular liquid crystals and those of other previously described cluster containing supermolecular liquid crystals. It is hoped that the results of this study will help to begin to identify any underlying trends that may be present which may describe the behaviour of this class of material more generally.

The synthesis of a range of different carborane containing supermolecular liquid crystals, in which several important components of the supermolecular structure are varied, is planned. This should allow a broad understanding of the structure property relationships within these systems to be established. Once this is achieved it is expected that it will be possible to begin to identify similarities and differences between the general behaviour of the target materials and previously published related materials.

A variety of different mesophases will be targeted in order to see any effect the inclusion of carborane clusters may have on the phase behaviour. Including but not limited to; the nature of the phases generated and the stability of these phases, both in absolute terms as measured by phase ranges and isotropization points, and relative to the free mesogens as well as model compounds, which do not contain carborane clusters. This will provide the opportunity to gain an overall assessment of the effect of the carborane cluster on phase behaviour in as general a scope as possible.

The variation of the number of mesogens attached to the clusters (Figure 33) is also planned. This will enable the determination of the number of mesogens required for mesomorphic properties to occur in the target systems. Given this information it will be possible to take it into account when designing materials for study and during comparisons between the target materials as well as published materials.

Chapter 2: Aims

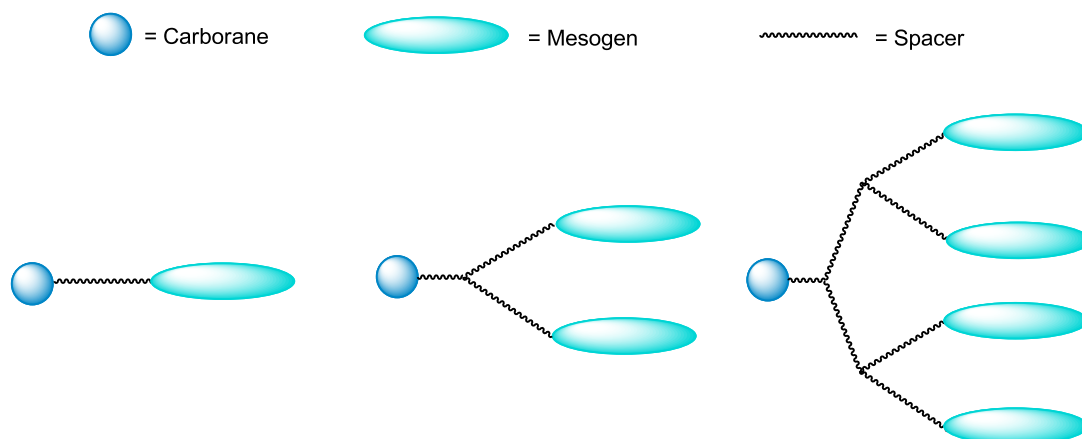


Figure 33: Schematic diagram of possible carborane containing supermolecular liquid crystals in which the number of mesogens is being systematically increased

In addition to controlling the number of mesogens attached to the clusters, the mode of attachment of both the mesogens to the flexible spacers as well as the flexible spacers to the clusters (Figure 34) will be investigated. This will allow the identification of any effects caused by these modes of attachment. As such it will be possible to avoid attributing effects caused by these various modes of attachment erroneously to the presence of the carborane cluster.

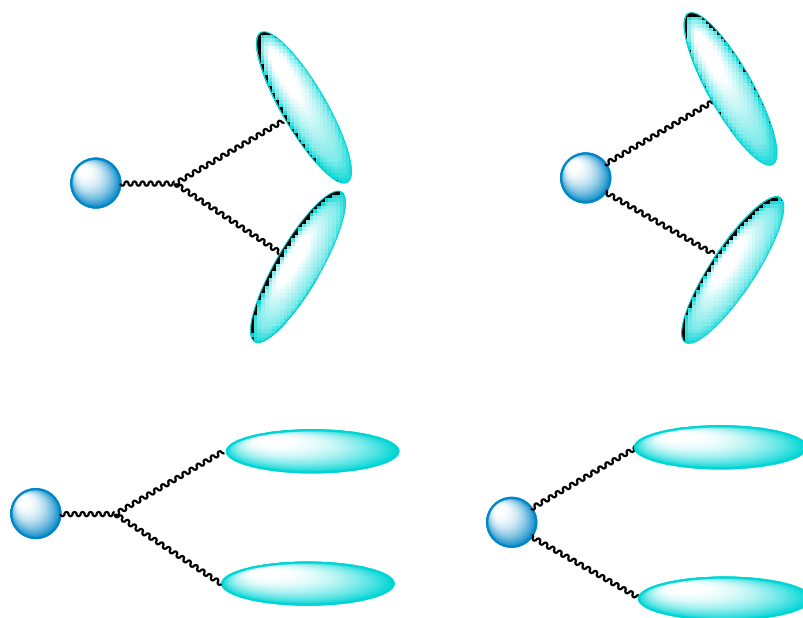


Figure 34: Schematic diagram of possible carborane containing supermolecular liquid crystals in which the mode of attachment at various points is systematically altered

Chapter 2: Aims

Finally a number of different chemical moieties will be utilized to link the mesogens to the carborane clusters. This will be done in order to identify potential effects on phase behaviour caused by the linker and as such avoid attributing it to the cluster.

3. Siloxanes

3.1 Summary

In this chapter the synthesis and analysis of a series of compounds containing a carborane cluster which is functionalised with pro-mesogenic moieties attached *via* a siloxane linkage will be described.

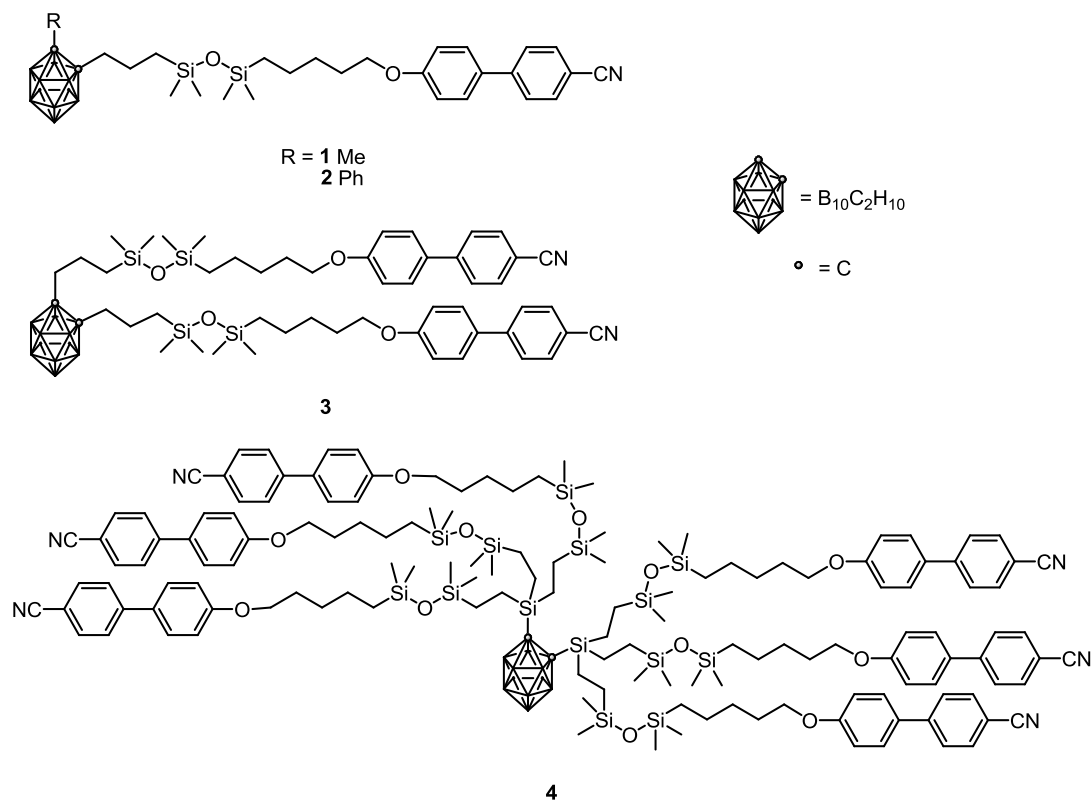


Figure 35: Cyanobiphenyl Functionalized Carboranes with Siloxane linkages

3.2 Synthesis

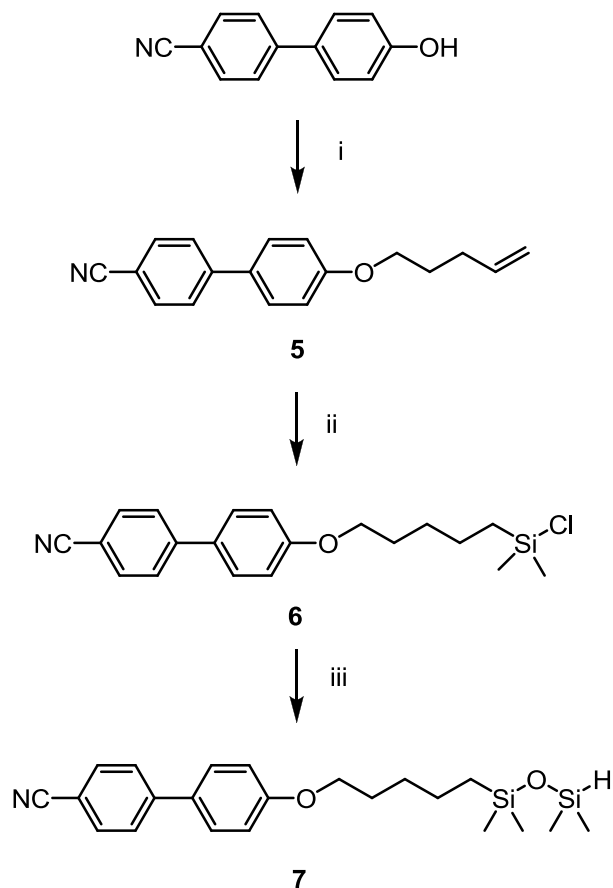
The focus in this chapter was on the synthesis of cyanobiphenyl functionalized carboranes due to the large number of materials previously published utilizing this mesogen, giving a good starting point for comparison with other work. The carborane precursors used as scaffolds contain either allyl or vinyl silane end units. The strategy followed is the hydrosilylation of the carborane olefinic bonds with a mesogen containing a hydrosiloxane functional group at the end of the flexible spacer. In all cases the spacer separating the cyanobiphenyl core and the

Chapter 3: Siloxanes

tetramethyldisiloxane linking unit has been kept constant (pentamethylene spacer) so meaningful structure property correlations can be established.

The hydridosiloxane terminated mesogen **7**⁹⁷ was synthesised according to Scheme 1 following the procedure previously described for the undecyloxy analogue⁴⁸. The Williamson etherification of 4-hydroxy-4'-cyanobiphenyl with 5-bromo-1-pentene was undertaken followed by the stepwise addition of the dimethyldisiloxy unit resulting in compound **7**. This synthetic approach was chosen in order to guarantee the purity of the mesogen which was assessed by ²⁹Si NMR. The usual one step synthesis of **7**⁹⁸ using tetramethyl disiloxane results in the noticeable presence of hexamethyltrisiloxane as an impurity, due to impurities found in 1,1,3,3-tetramethyldisiloxane provided by many chemical suppliers. This is a significant problem for this application as it will result in a mixture of materials with different parity spacers which are virtually inseparable by chromatography and often difficult to detect.

Hydrosilylation of **5** with dimethylchlorosilane using Karstedt's catalyst (Platinum(0)-1,3-divinyl-1,1,3,3-tetramethyldisiloxane complex solution) yields compound **6**, which was used *in situ*. The co-hydrolysis of **6** with a large excess of dimethylchlorosilane in the presence of pyridine and water yields **7** in good purity.

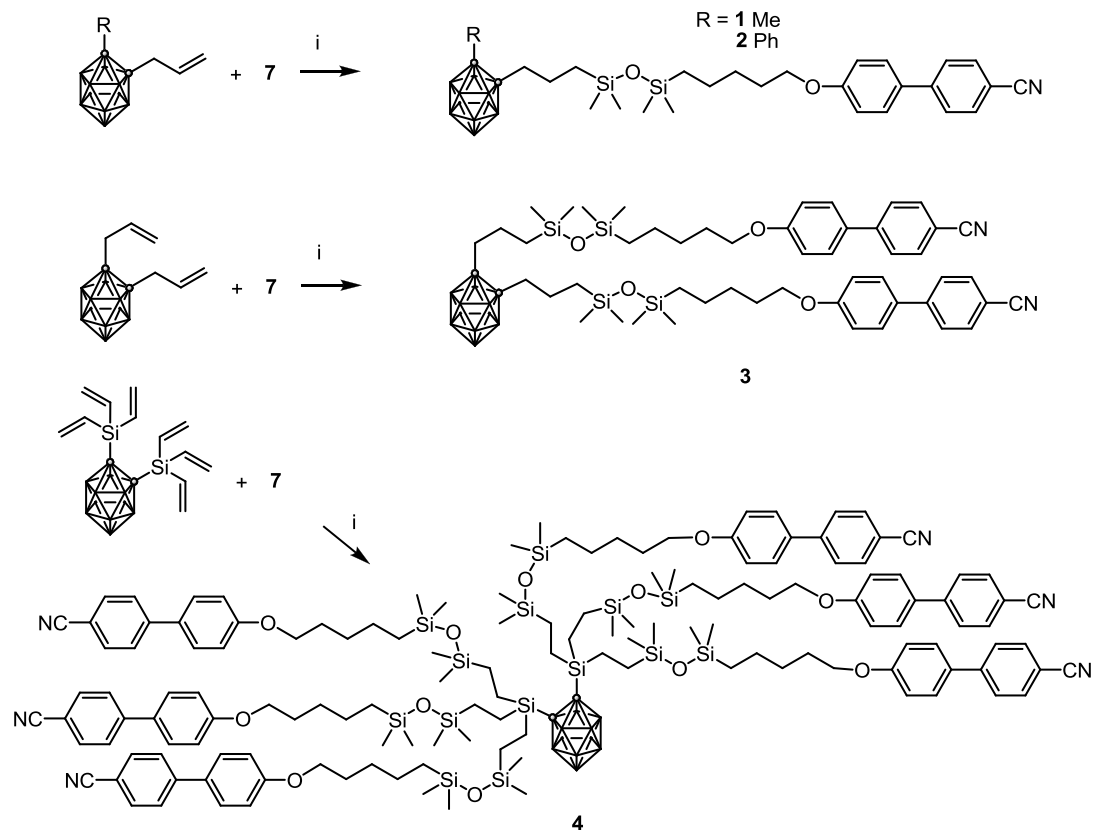


- i) K_2CO_3 , KI, 5-bromopentene in butanone
 ii) Dimethylchlorosilane, Karstedt's catalyst in dry toluene
 iii) Dimethylchlorosilane, pyridine, water in THF

Scheme 1: The synthesis of compound 7

In order to prepare the carborane containing supermolecules, **7** was attached to a variety of carborane cores carrying allyl or vinyl substituents amenable to hydrosilylation (provided by collaborators) *via* a standard hydrosilylation reaction using Karstedt's catalyst (Scheme 2). The reactions were monitored by ^1H NMR following the disappearance of the resonances associated with the alkene group at between 5 and 6 ppm. The only exception to this was in the synthesis of **4** which took two runs of the hydrosilylation reaction to fully convert all of the vinyl groups.

Chapter 3: Siloxanes



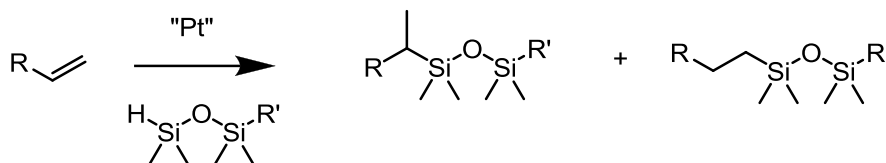
i) Karstedt's catalyst in dry low sulphur toluene under Ar at room temperature

The catalyst was used until variance in results were observed, at which point a new batch of catalyst was used

Scheme 2: The Synthesis of compounds 1, 2, 3 and 4

The successful hydrosilylation reaction was confirmed by ^1H NMR by the absence of alkene resonances and the appearance of a new multiplet in the region 0.5 ppm associated with the SiCH_2 moiety and the corresponding singlets at 0.0 ppm associated with the CH_3Si of the disiloxane unit. The B-H resonances appear as a broad unresolved feature spanning from 1.3 to 3.3 ppm, which overlaps with some of the resonances due to the mesogen. This is caused by coupling of the B-H protons to the B-H boron nuclei. As such boron decoupled ^1H NMR was carried out and three broad singlets at 2.7, 2.4 and 2.3 ppm with intergrations equal to 2, 4 and 2 respectively were observed in addition to the resonances which had previously been observed in non-decoupled NMR. These resonances are associated with the BH protons of the cluster. The intergration does not account for all of the protons as decoupling is not complete and thus some intensity is lost.

3.2.1 Undesired Branching



Scheme 3: Branched and Linear Isomers

In the final hydrosilylation steps it was found that a significant amount of the undesired branched isomers of compounds **1**, **2**, **3** and **4** were formed (Scheme 3). The branched isomers were initially identified by the presence of unexpected resonances in ^1H NMR spectra at 0.95 and 0.90 ppm and in ^{13}C NMR spectra at 13.9 and 21.6 ppm associated with the CH_3 and CHSi of the branched isomer respectively. Upon further investigation with the use of DEPT 135° experiments, the nature of these resonances was elucidated and the presence of the branched isomers confirmed.

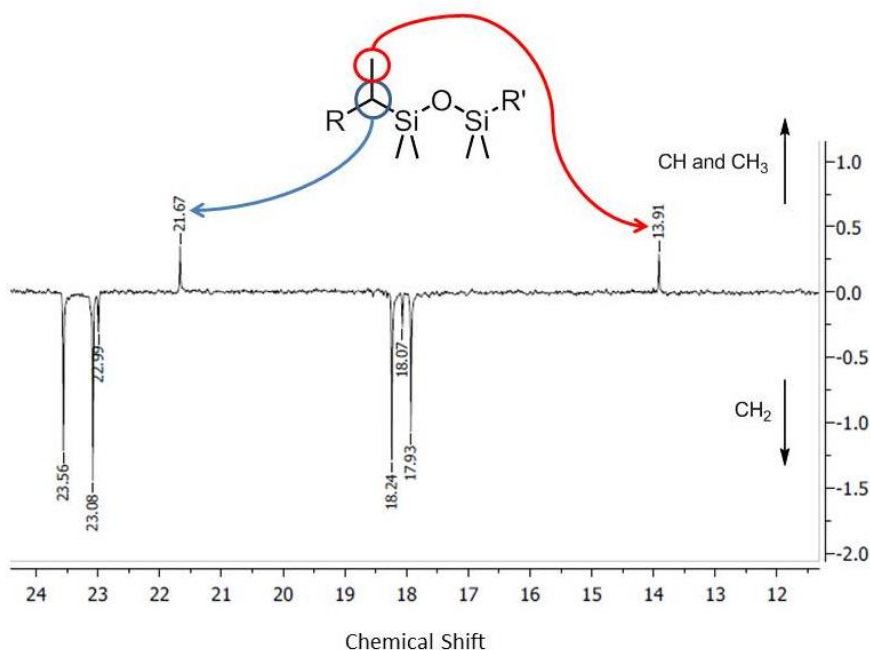


Figure 36: The alkyl region of the DEPT 135° spectra of compound **2**

Figure 36 shows an excerpt of the DEPT 135° spectra of **2**, which is typical of all the final compounds presented in this chapter. In the linear isomer of **2**, all of the alkyl carbons have two protons attached and thus it would be expected that all of the

resonances would be of negative phase. However, the branched isomer of **2** has a CH and CH₃ unit at the branching point. These carbons, owing to the odd number of protons attached, would be expected to have resonances of positive phase in the DEPT 135° experiment and this is what is observed in Figure 36, thus confirming the presence of the branched isomers.

Further evidence of the branched isomers was also obtained from ²⁹Si NMR. Four resonances were observed in the spectra; one pair corresponding to the linear isomer at 8.4 and 7.0 ppm and a second pair corresponding to the branched isomer at 8.9 and 7.8 ppm. The resonances associated with the branched isomer had significantly less intensity than those of the linear isomer. However due to the slow relaxation time of the ²⁹Si nucleus, integration of the peaks would not give relative ratios of the linear to branched isomers.

The comparison of the integration of the pseudo-triplet associated with the SiCH₂ at around 0.5 ppm in the ¹H NMR spectra of the linear isomer and that of the doublet associated with the SiCHCH₃ at around 0.9 ppm of the branched isomer allowed the amount of branched arms present in each material to be estimated. It was found that in compounds **1**, **2**, **3** and **4** there was approximately 25 %, 20%, 25 % and 33 % branching respectively.

For compounds **1** and **2**, there are only two possible isomers within the mixture. However, for compounds **3** and **4** the situation is further complicated by the fact that there are multiple combinations of isomers which can be formed from this side reaction. Compound **3** has a possible four isomers which can be formed and **4** has a possible sixty four. It is not possible to identify how many of these different isomers are present, only the overall amount of branching in the sample as a whole.

3.2.2 The Origin of the Branched Isomers

The origin of the branched isomers can be explained mechanistically with the Chalk-Harrod mechanism⁹⁹ (Figure 37). The important step for the generation of the unwanted branched isomer is the hydrogen insertion step. If the hydrogen inserts

onto the β carbon then the desired linear product will be generated as shown on the cycle to the left (Figure 37). However, if the hydrogen inserts onto the α carbon, either β -hydride elimination or reductive elimination will occur as competing processes, which is described by the cycle on the right (Figure 37). If β -hydride elimination occurs then the alkene will be internalised and if reductive elimination occurs then the branched isomer will be generated.

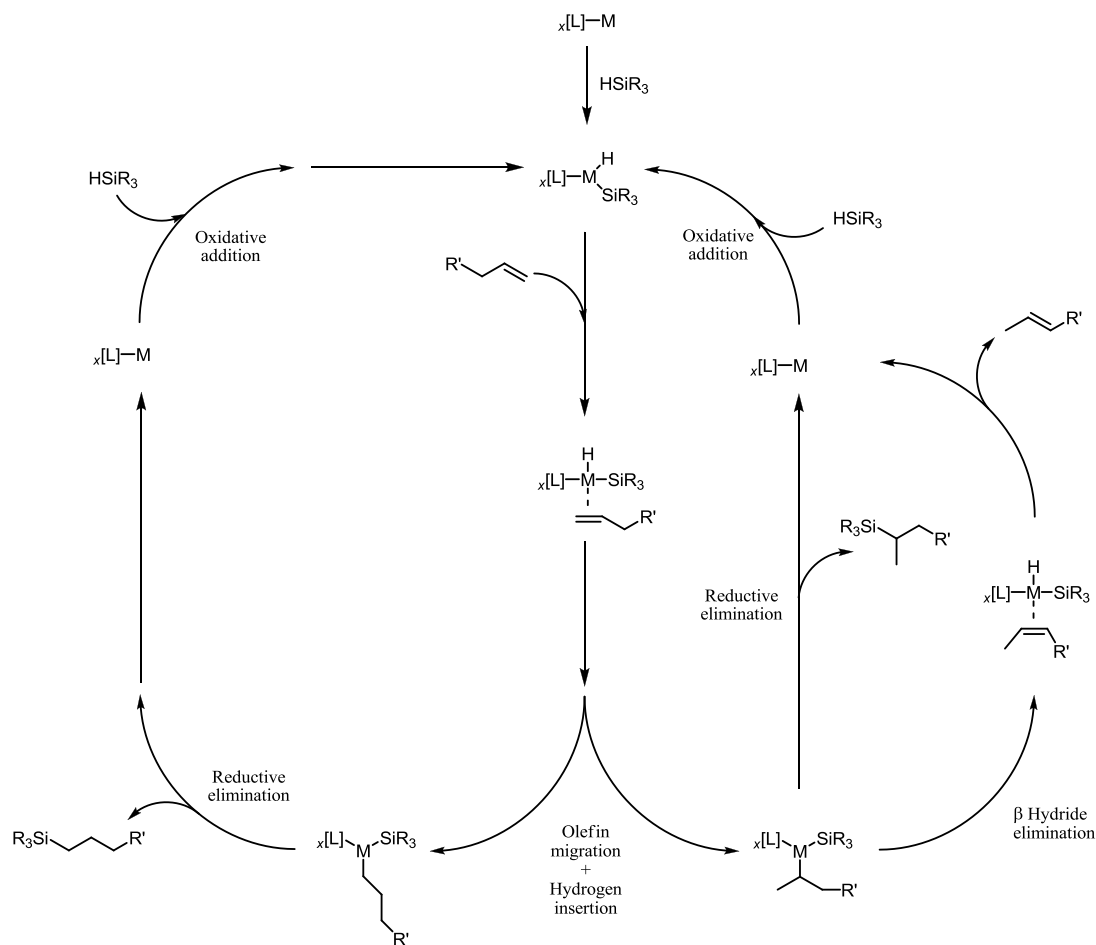


Figure 37: The Chalk-Harrod mechanism of hydrosilylation with important side reactions

3.3 Thermal Properties

The thermal properties and any subsequently observed phase behaviour of all of the functionalized carboranes were investigated using polarised optical microscopy (POM) and differential scanning calorimetry (DSC). The results are summarized in

Table 2. The transition temperatures of the siloxane mesogen **7** and its alkenyl precursor **5** have been included for comparison.

Compound	Glass	Crystal	SmA	N	Iso	
1	•			-28.3	•	
2	•			-22.8	•	
3		• (-7.6	•)	29.9	•	
4		• -45.3	•	56.8	•	
5		•	75.8	•	88.2	•
7		• -1.9	•	52.5	•	

Table 2: Summary of transition temperatures of functionalized carboranes and cyanobiphenyl mesogens as recorded by DSC with a heating/cooling rate of 10 °Cmin⁻¹, values shown in brackets are for monotropic transitions

3.3.1 Mesogens

Compound **7** and its alkenyl precursor **5** are both liquid-crystalline. The precursor **5** displays a short range enantiotropic nematic phase. The DSC trace showed that there are two reproducible thermal events. One with onset at 75.8 °C and an enthalpy of 30.4 kJmol⁻¹, which is associated with the melting point. The second has onset at 88.2 °C and an enthalpy of 0.98 kJmol⁻¹ corresponding to the isotropization. Both the crystallization and clearing temperatures show supercooling of around 15 °C. The phase was identified *via* POM by the appearance of a *schlieren* texture displaying both four brush and two brush defects upon cooling from the isotropic liquid (Figure 38 left). When homeotropically aligned the sample displayed no birefringence. This allows the assignment of this phase as nematic.

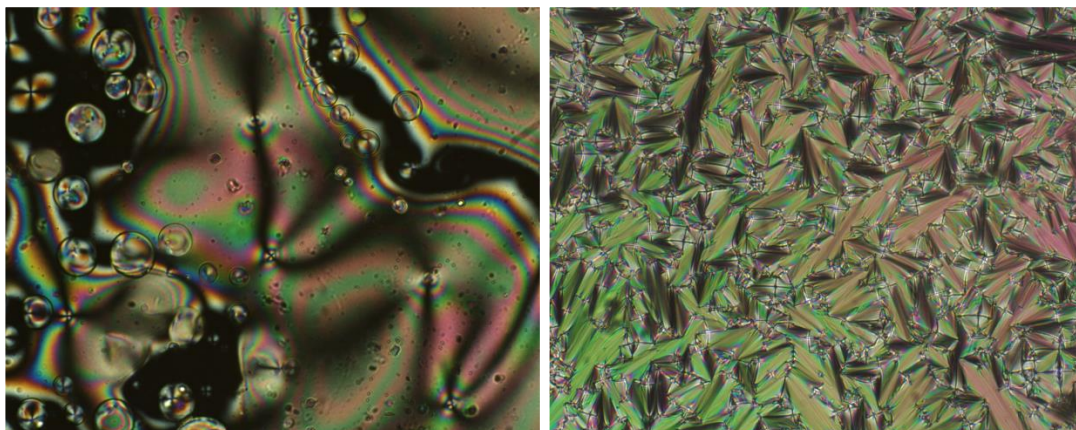
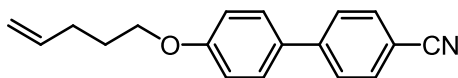


Figure 38: Left) photomicrograph of **5** at 70.0 °C cooled from the isotropic liquid at 0.1 °C min⁻¹ x100 magnification. Right) photomicrograph of **7** at 47.1 °C cooled from the isotropic at 2 °C min⁻¹ x100 magnification

The DSC trace of compound **7** showed two reproducible endotherms upon heating. The first, due to melting with onset at -1.9 °C had an enthalpy of 0.2 kJmol⁻¹. The second, associated with isotropization with onset at 52.5 °C and an enthalpy of 3.3 kJmol⁻¹. The phase was identified by POM. Upon cooling from the isotropic liquid the sample formed a focal-conic defect texture displaying ellipses and hyperbolae of optical discontinuity (Figure 38 right). Areas of homeotropic alignment appeared optically extinct with no sign of a *schlieren* texture. Combined these observations allow for the assignment of this phase as smectic A.

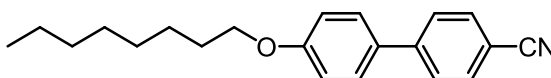
Compound **5** shows only a very short N phase whereas compound **7** shows a broad SmA phase. Compound **5** has a relatively short mesophase in comparison to other alkoxy cyanobiphenyls¹⁰⁰ with longer chains (Figure 39). This is because increasing the chain length lowers the melting point due to increased molecular flexibility, this may also be associated with microphase segregation. A general increase in isotropization temperature is also observed with increasing chain length, giving a net result of increasing phase stability upon increasing the chain length. Upon moving from **5** to **7** the chain length is increased by three atoms, furthermore the disiloxane functional group has a propensity to be highly disordered. This lowers the melting point of **7** in comparison to **5** more dramatically than if the chain had been lengthened by addition of methylene groups instead (Figure 39). The additional disruption of the disiloxane unit does lower the clearing point of **7** in comparison to

5, however when coupled with the large drop in melting point, **7** displays a significantly broader mesophase than **5**.

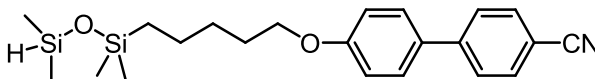


5

Cr 75.8 N 88.2 I



Cr 54.5 SmA 67.0 N 80.0 I



7

Cr -1.9 SmA 52.5 I

Figure 39: Alkoxy cyanobiphenyls¹⁸

Compound **7** only displays a broad SmA phase as a result of the addition of the disiloxane unit. The siloxane moiety is bulky and displays stronger intermolecular interactions with other siloxane groups in comparison to the aliphatic or aromatic parts of the molecules. This results in the microphase segregation of the siloxane units and the suppression of the N phase.

3.3.2 Mono-substituted Carboranes

Both of the mono-substituted carboranes **1** and **2** were found not to be mesogenic. Both were found to be glasses with glass transitions at the fastest rate of change in heat capacity at -28.3 and -22.8 °C respectively. It appears that upon adding the carborane cluster to the mesogen the melting point is lowered significantly. Furthermore, the fact that both **1** and **2** are glasses implies that the systems are much more disordered than the mesogen itself and are unable to pack efficiently.

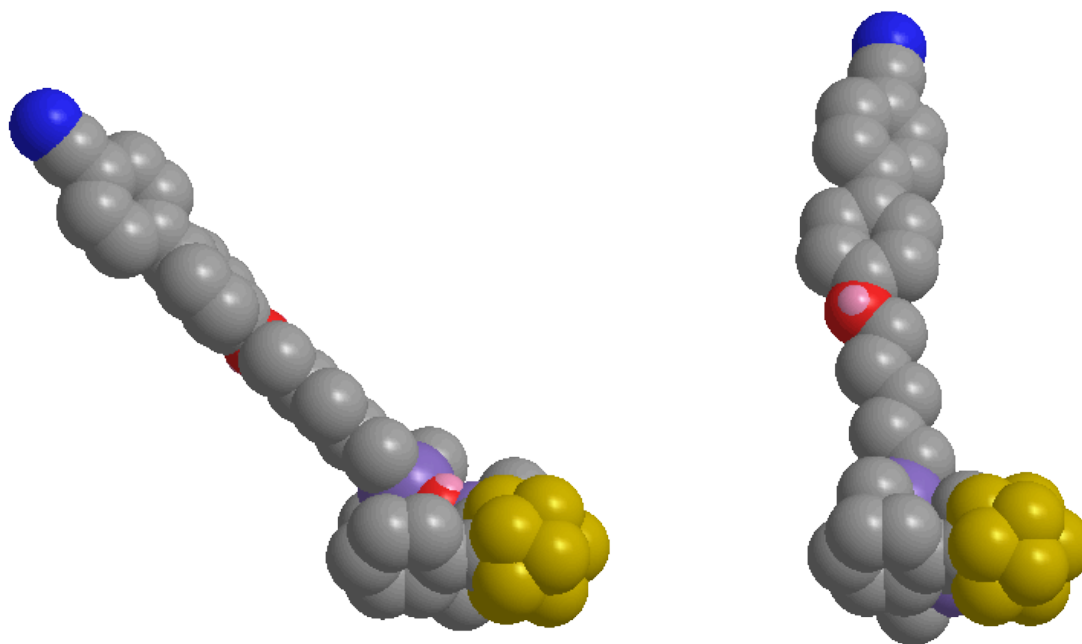
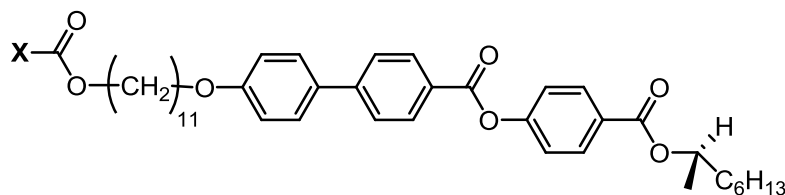


Figure 40: Molecular models of the branched and linear isomers of **2** (hydrogens omitted for clarity)

There are several ways to explain these observations. The presence of the bulky clusters may disrupt the core-core interactions of the cyanobiphenyls which are critical for the stability of the phase. Figure 40 illustrates how large the cluster is in comparison to the mesogenic core. Goodby *et al* have shown that bulky end-groups such as carbocycles destabilize liquid-crystalline properties¹⁰¹ (Figure 41), reducing the clearing point with increasing size of carbocycle. It therefore stands to reason that a similar effect would be observed for carborane clusters attached in a similar manner as they have similar space filling properties.

Secondly, the presence of the branched isomers in **1** and **2** could further confound the chances of generating liquid-crystalline behaviour. Figure 40 shows molecular models of the isomers of **2**. It can clearly be seen that in the all *trans* configuration they have rather dissimilar molecular shapes. This will result in a poor ability to pack, reducing the likelihood of mesomorphism and also explaining why both form glasses, rather than crystallize.



X =

Transition Temperatures

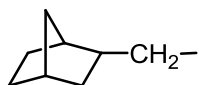
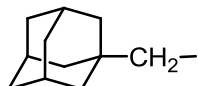
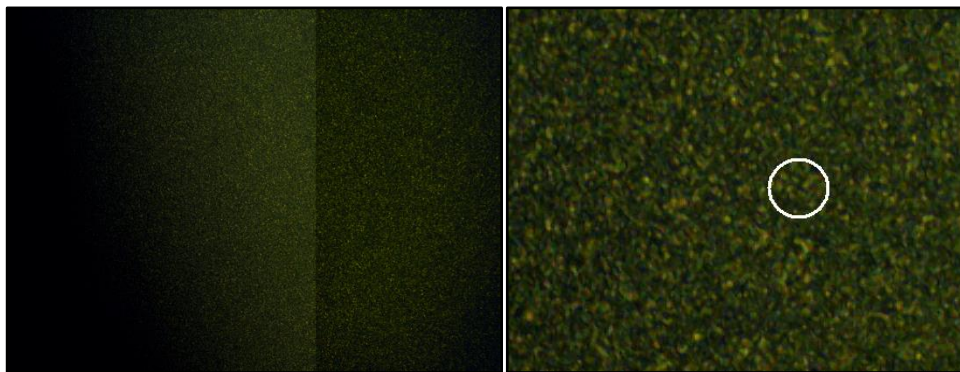
Cr 48.1 SmC_A* 77.8 SmC* 91.1 SmA* 95.6 ICr 53.9 SmX* 59.7 SmC_A* 71.5 ICr 45.7 (SmC_A* 40.0) SmC* 57.4 I

Figure 41: Phenyl biphenyl benzoate mesogens functionalized with bulky carbocycles units at the end of a flexible chain¹⁰¹

3.3.3 Di-substituted Carborane

The di-substituted carborane **3** shows a monotropic smectic A phase. The DSC trace of **3** shows an endotherm upon the first heat with onset at 29.9 °C ($\Delta H = 14.3 \text{ kJmol}^{-1}$) due to melting to the isotropic fluid. Upon subsequent heat/cool cycles, a reproducible glass transition with the fastest rate of change of the heat capacity at -24.5 °C and a broad exotherm with an onset at -7.8 °C ($\Delta H = 2.5 \text{ kJmol}^{-1}$ which corresponds to 1.2 kJmol^{-1} per mesogen appended to the carborane) are evident, indicating that the crystallization of this material is highly hindered. The POM of **4** proved difficult to obtain a clear texture to identify the phase, owing to the low temperature. Only grainy textures were achievable and even with 200 x magnification it was extremely difficult to find focal-conic defects, although areas of optically extinct homeotropic alignment were not difficult to obtain. Further evidence for this being a smectic phase was offered by the observation of oily streaks upon shearing the sample.



*Figure 42: Photomicrograph of **3** at $-8.0\text{ }^{\circ}\text{C}$ cooled at $0.1\text{ }^{\circ}\text{Cmin}^{-1}$ from the isotropic liquid at $\times 200$ magnification a focal-conic defect has been circled in the enlargement on the right*

The appearance of a liquid-crystalline phase upon the addition of a second mesogen to the carborane core is not unexpected, owing to the increased molecular anisotropy. It can be argued that two CB mesogens are able to overcome the destabilizing effect of the clusters steric bulk, thus allowing the formation of a mesophase. The fact that the phase is monotropic and is only observed over $\sim 17\text{ }^{\circ}\text{C}$, in comparison to the mesogens $\sim 54\text{ }^{\circ}\text{C}$, suggests that the cluster still causes a degree of destabilization within the phase as discussed previously in regards to the mono-substituted carboranes. The nature of the mesophase, namely smectic A, was not unexpected. Siloxane CB mesogens have a strong tendency to form smectic phases, owing to the microphase separation of the chemically distinct regions of the molecules within the phase¹⁰²⁻¹⁰⁴. The addition of the cluster should not greatly affect this propensity.

Unlike previously reported siloxane dimers²¹ which are linear, **3** is forced to adopt a hairpin conformation folded at the carborane-siloxane junction. As such, the most probable arrangement of **3** in the mesophase would be for the CB mesogens to aggregate together leaving the aromatic and siloxy regions in close proximity to themselves. Three possible phases can be formed from such an arrangement. The different regions of the molecules can microphase segregate and a smectic A bilayer (SmA_2) or an interdigitated smectic A (SmA_d) phase is formed⁹, in which the clusters would likely show some degree of ordering within the phase and each molecule would be confined to the same layer (Figure 43 top). Alternatively microphase segregation does not occur and the carborane clusters are randomly distributed throughout the phase and the mesogens form a simple smectic A monolayer (SmA_1)

phase, in which the individual molecules would be randomly distributed amongst different layers (Figure 43 bottom). The fourth possibility is that two or three of these arrangements occur in different regions and the phase is incommensurate. In reality these phases would be much more disordered than those shown in Figure 43, they are drawn in this way to help easily distinguish them from one another.

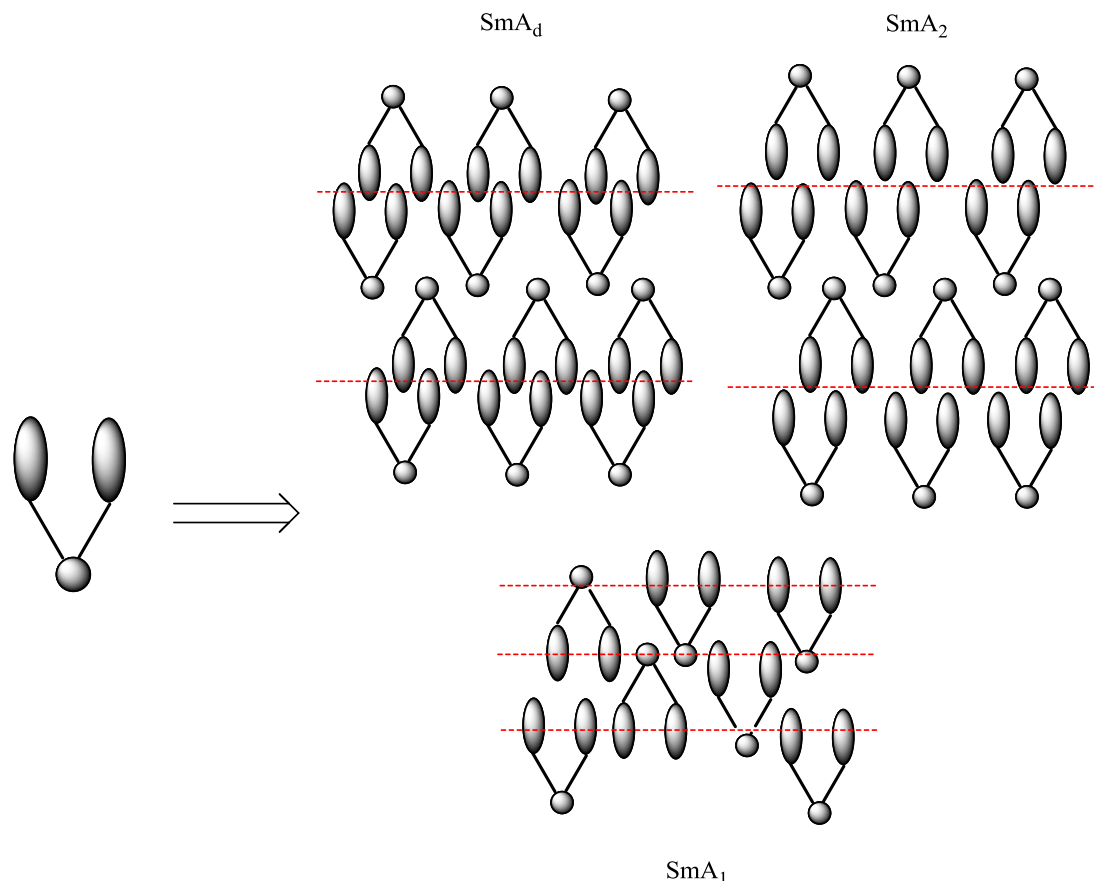
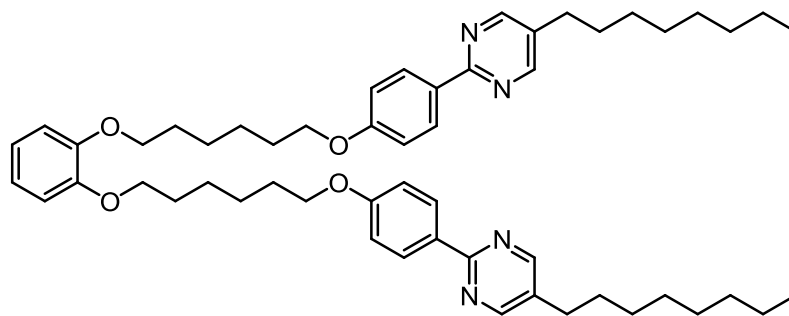


Figure 43: The possible conformations of **3** within the smectic A phase

The only way to distinguish between these phases usually would be with an X-ray diffraction experiment. Typically for a low molar mass mesogen, it would be expected that the layer spacing would be found to be somewhere around two times the molecular length for a SmA₂ phase, around one molecular length for the monolayer SmA₁ phase, and around 1.7 for the SmA_d phase, thus making it possible to differentiate them. For compound **3** the molecular length used would be that of the most likely bent conformation of the molecule. Unfortunately it was not possible to determine whether a SmA₁, SmA₂ or SmA_d phase was formed due to being unable to obtain X-ray data for this phase.

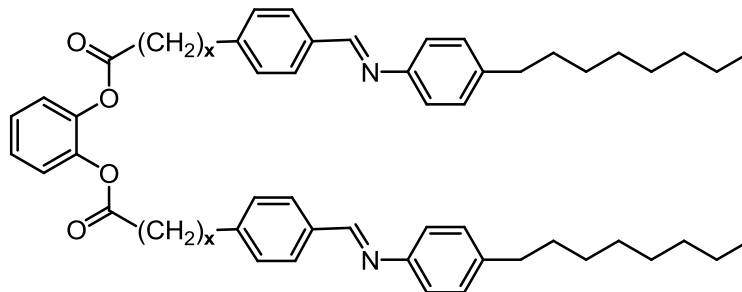
Chapter 3: Siloxanes

The bent topology of compound **3** has much in common with the U-shaped bi-mesogens presented by Yoshizawa^{44, 105} and Attard¹⁰⁶ (**A** and **B** respectively Figure 44). Typically such materials exhibit SmA₂ bilayer phases as is the case with the family of catechol benzoates **B** in Figure 44. As such it also seems likely that **3** will adopt a similar SmA₂ phase. However the presence of the terminal cyano group in the CB mesogen may result in a SmA_d phase instead.



Cr (SmC 43.4) 76.0 N 83.3 I

A



X = Transition Temperatures

B3 Cr (SmF 72 SmB 78 SmA 105) 111 I

B4 Cr (SmF 65 SmB 74) 82 SmA 94 I

B5 Cr (SmF 62 SmB 69 SmA 89) 103 I

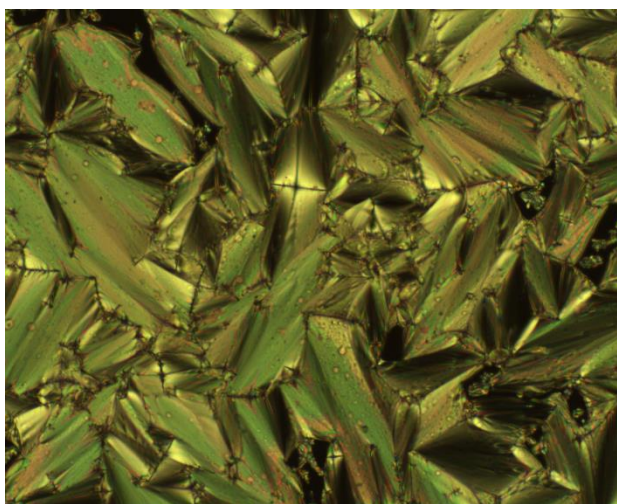
B6 Cr (SmF 59 SmB 65) 79 SmA 80 I

Figure 44: U-shaped mesogens^{105, 106}

There is an important difference between **3** and the U-shaped mesogens **A** and **Bx**. The bending unit is a phenyl ring in **A** and **Bx** whereas it is a carborane cluster with one face surrounded by tetramethyldisiloxane units in **3**. The phenyl rings would

exhibit π -stacking behaviour within the SmA₂ bilayer and thus help stabilize the smectic phases. The cluster-cluster interactions of the carboranes are still unclear. As such it is not obvious whether the cluster-cluster interactions would be net attractive or net repulsive. However, given that upon addition of the carborane cluster to the CB mesogen in compounds **1** and **2** mesomorphism was lost, it seems reasonable to assume that the net contribution of the carborane is to lower phase stability, whether this is an electronic cluster-cluster effect or simply a steric effect is also still unclear.

3.3.4 Carborane Hexamer



*Figure 45: Photomicrograph of **4** focal-conic texture at 28.8 °C cooled from the isotropic at 5 °Cmin⁻¹*

Compound **4**, the hexa-substituted carborane displays an enantiotropic SmA phase. The DSC trace (Figure 46) shows an endotherm at -45.3 °C ($\Delta H = 4.1 \text{ kJmol}^{-1}$) and a very broad endotherm with onset at 56.8 °C ($\Delta H = 16.3 \text{ kJmol}^{-1}$ or 2.7 kJmol^{-1} per mesogen). The phase was identified as SmA from the focal-conic fan texture, which it exhibited showing clear focal-conic defects (Figure 45) and areas of homeotropic alignment which were optically extinct.

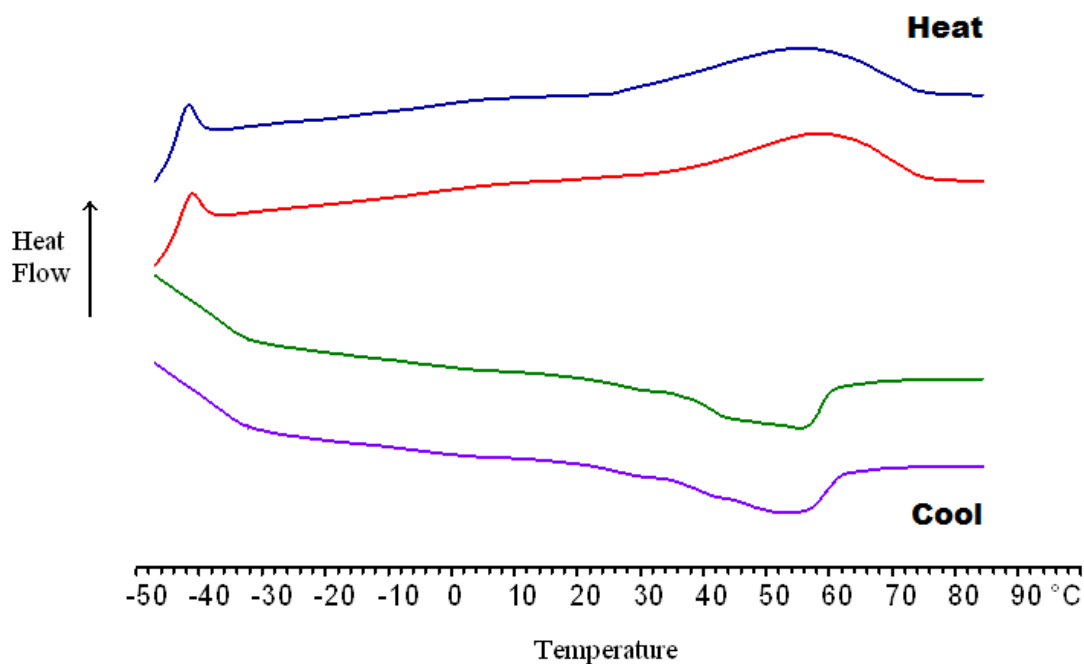


Figure 46: DSC trace of **4**

The uneven transition to and from the isotropic liquid, shown in Figure 46, appears to suggest there may be multiple transitions which overlap, with the lowest temperature transitions being comparatively weaker. This is entirely consistent with a mixture of geometric isomers with different clearing points in which the minor components in the mixture have lower clearing points than the major component. These branched isomers will have a less favourable arrangement of the CB cores in the mesophase resulting in lower transition temperatures as was discussed previously in relation to compounds **1**, and **2**. Furthermore the effect is likely cumulative, thus with increasing content of branching within the molecules, it is also likely that the isotropization temperature would fall. The net result of this is to broaden the transition to the isotropic fluid and move it to lower temperature.

It is also interesting to note that **4** displays a significantly lower clearing point than the siloxane cored supermolecules which contain four CB mesogens described by Goodby and Mehl¹⁰² (Figure 47 top and middle). These tetrapedes with similar flexible spacer lengths (6 methylene units for **C** and **D** in Figure 47 compared to 5 in **4**) displayed clearing points no lower than 118 °C. Typically it is expected that with an increase in the number of mesogens the clearing point would increase. Therefore

Chapter 3: Siloxanes

it was expected that **4** would have a higher clearing point tetrapedes. However, **4** also bears resemblance to siloxane dendrimers with eight mesogens reported by Shibaev¹⁰⁷ (Figure 47 bottom), which have a clearing point of 92 °C. Clearly **4** does not fit into either of these systems well.

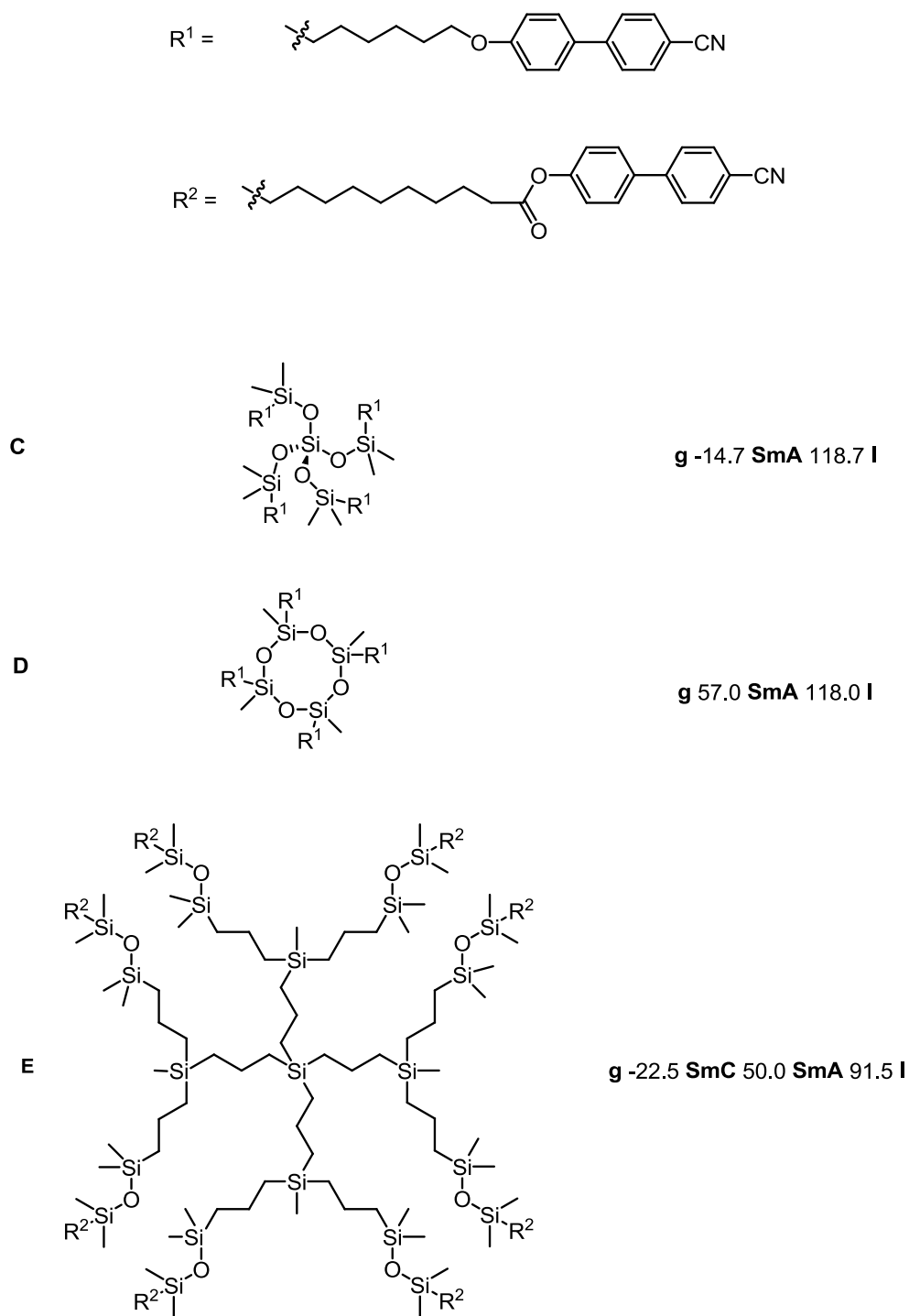


Figure 47: CB functionalized tetramers¹⁰² (top and middle) and carbosilane dendrimer¹⁰⁷ (bottom)

The transition into the isotropic fluid is completely over at 80 °C for compound **4**. This is significantly lower than either the carbosilane dendrimers or the siloxane tetramers. This is not entirely explained by the mixture of geometric isomers present in the material, as the transition into the isotropic fluid is completely finished at 80 °C. The carborane cluster, due to its steric bulk, is likely to disrupt close packing in the mesophase and thus lower the clearing point as discussed previously for compounds **1**, **2** and **3**. The phase behaviour, or lack thereof, of compounds **1** to **4** all support the suggestion that the presence of the carborane cluster causes a significant destabilization of the mesophase.

3.3.4.1 X-ray Diffraction

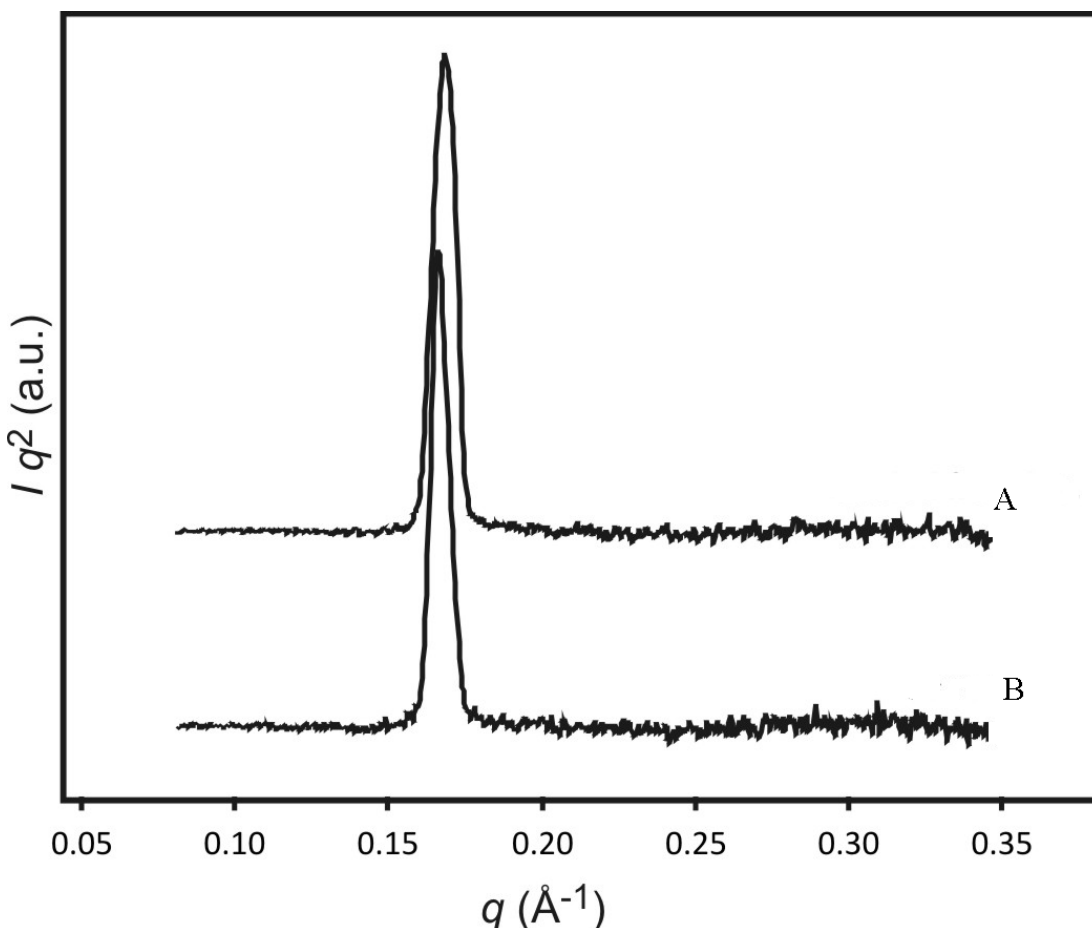
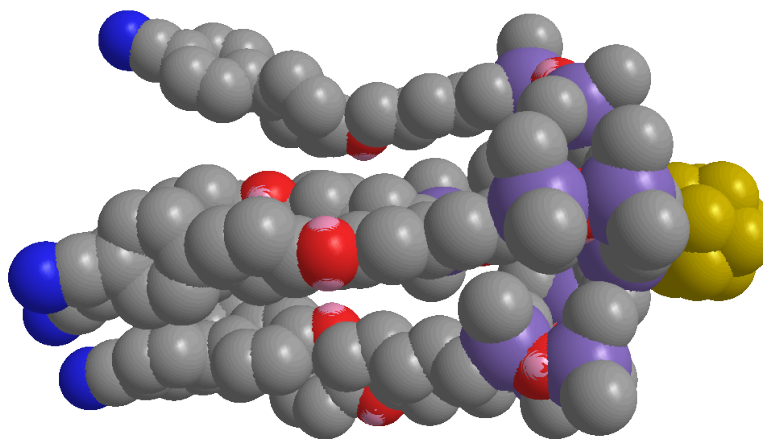


Figure 48: X-ray diffractograms of **4** A) RT cooled from Iso B) RT as received

The SmA phase of **4** was further investigated by small angle X-ray diffraction in order to determine the layer periodicity and help elucidate the structure of the phase. Only one diffraction peak was observed at $37.6 \pm 0.2 \text{ \AA}$ which corresponds to the

layer spacing of the SmA phase (Figure 48). The lack of additional higher order diffraction peaks suggests that the layers are not well defined, possibly due to high thermal fluctuation around the equilibrium points of many moieties. This is not unexpected due to the presence of many flexible siloxane groups and such a high number of different geometric isomers. The bent isomers will each have a slightly different geometry which when combined in a mixture will create a great deal of disorder as the many slightly different shaped molecules attempt to close-pack together within the mesophase.

3.3.4.2 Modelling



*Figure 49: A molecular model of **4** created using ChemDraw 3D 12.0 and minimized using MOPAC 2009 PM3 method/EF in the gas phase at 0 K; the hydrogens omitted for clarity.*

In order to better understand how the hexamer **4** sits in the mesophase a series of geometric models based on the dimensions gleaned from the calculated minimized structure (Figure 49) were constructed. This method has been employed to understand the phases of other cluster containing supermolecular liquid crystals¹⁰⁸. Initially it was assumed that there is no interdigitation of the CB mesogens. This results in a model of the molecule as a cylinder (Figure 50).

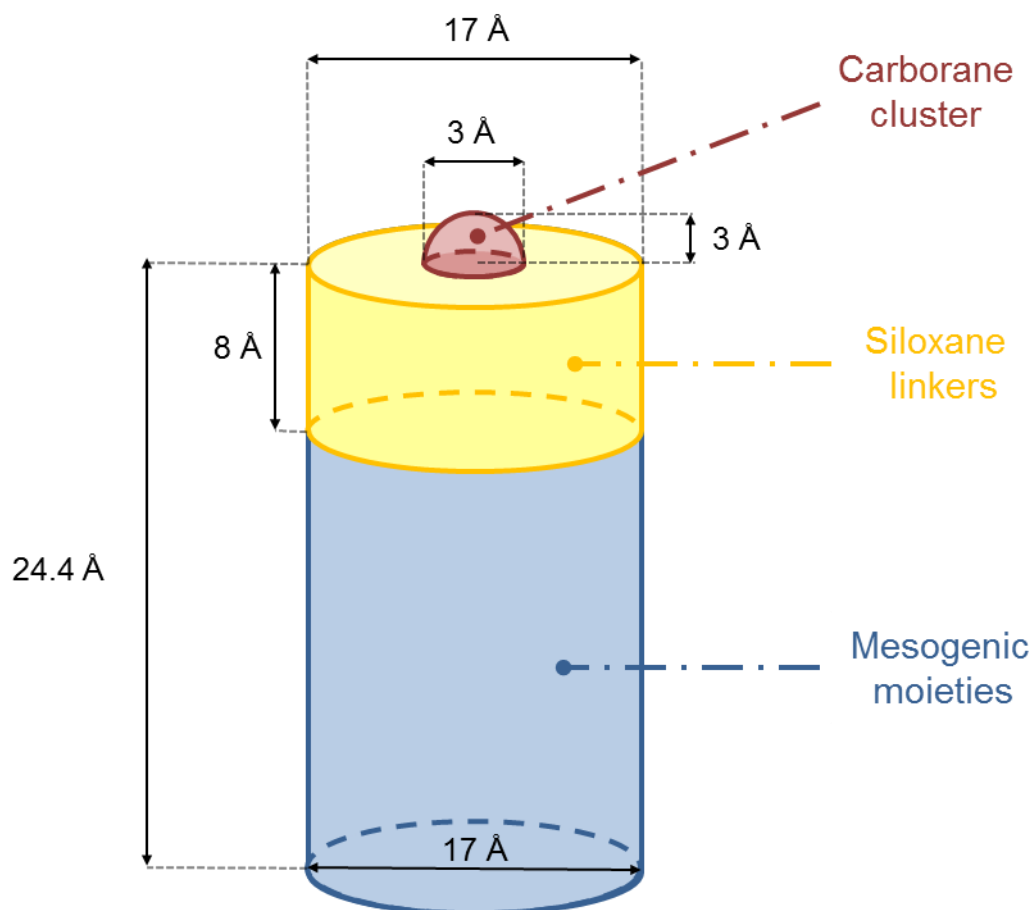


Figure 50: Cylindrical model of the hexamer 4

The total molecular length of 27.4 Å however is much smaller than the layer spacing as measured by X-ray diffraction. Therefore the material cannot adopt a simple monolayer SmA_1 phase. Therefore the phase must be either a SmA_2 or SmA_d as these both possess a bilayer structure (Figure 51). As can be seen, even when allowing for the complete interdigitation of the carborane clusters, a bilayer SmA_2 phase using this cylindrical model results in a layer spacing much larger than the measured layer spacing. Thus it is likely that a greater degree of interdigitation must be present within the phase, most likely including the CB mesogens resulting in a SmA_d phase.

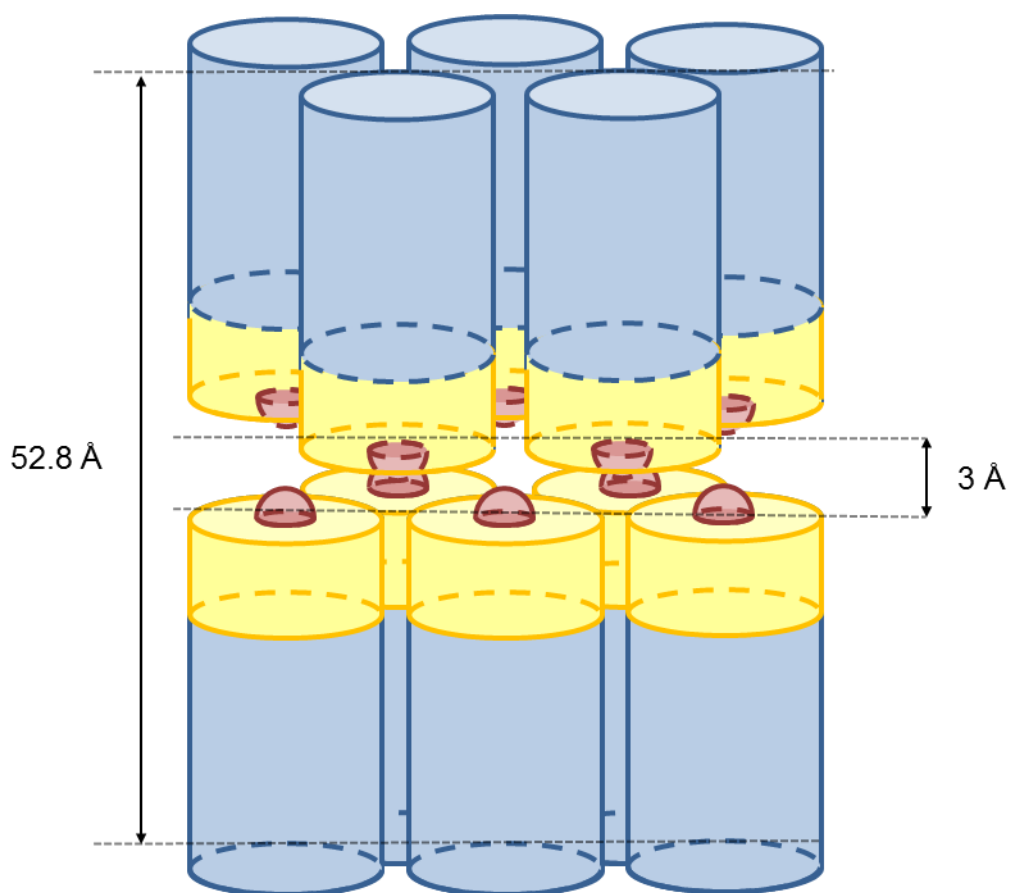


Figure 51: A bilayer SmA_2 phase using the cylindrical model of the hexamer 4

Given this the assumptions by which the initial model was created were changed. Firstly, it was now assumed that there is interdigitation of the CB mesogens and that this interdigitation is complete at each layer interface. Meaning that for each mesogen from one layer at the interface there is another mesogen from the second layer. Therefore the model needs to accommodate twice as many mesogens at the layer interface. To do this the area of the bottom face of the cylinder was doubled resulting in a truncated cone (Figure 52). Furthermore if the truncated cone is projected to its full length it is found to be 96 Å in height. As such in any close-packing arrangement of the cones it can be assumed that the carborane can be ignored as it is completely contained within the volume of the full cone.

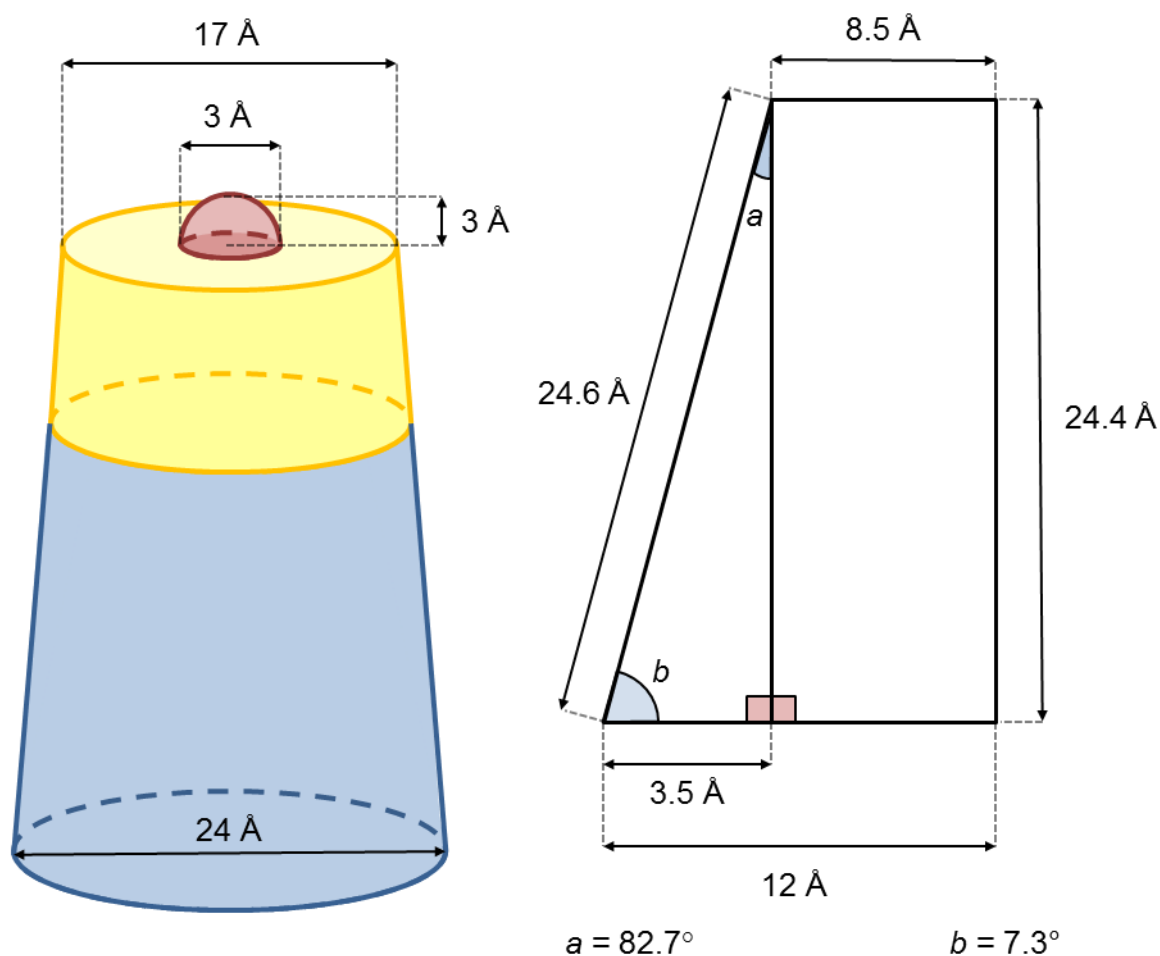
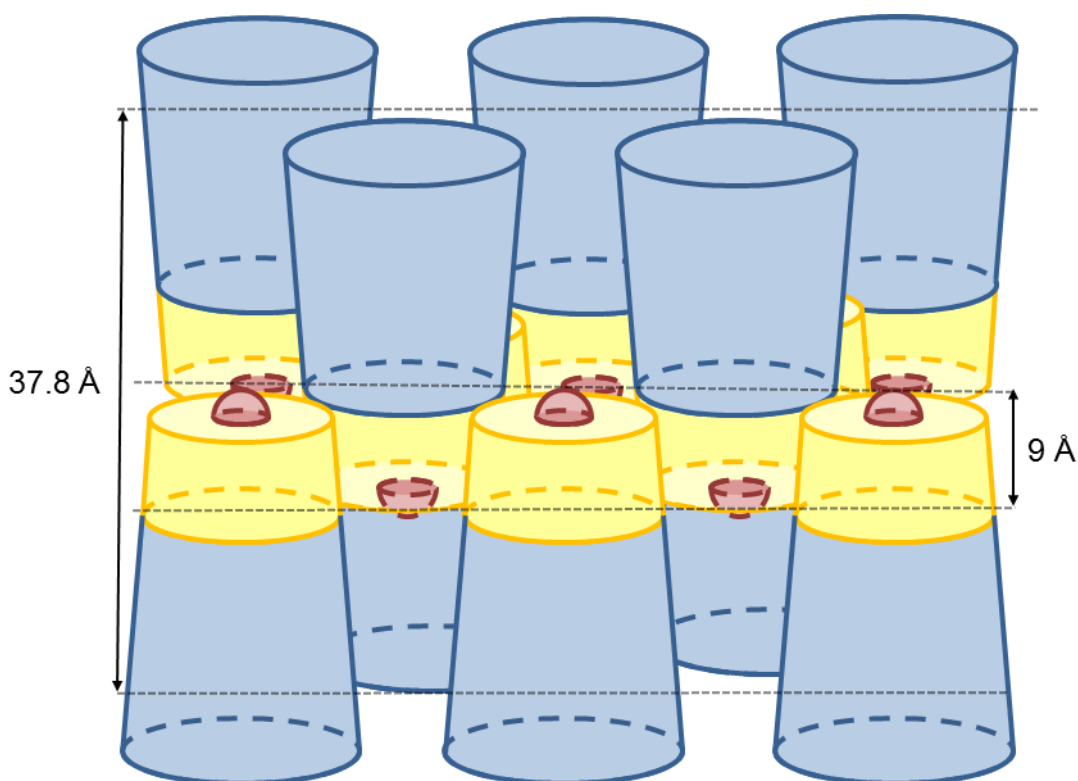


Figure 52: Conic model of the hexamer 4

As the conic model has the same height as the cylindrical model a SmA_1 type phase also does not correlate with the measured layer spacing. As the CB mesogens are interdigitated a SmA_d phase is proposed, however unlike the cylinders the cones are able to interdigitate allowing the model of the phase to be made to fit the measured layer spacing (Figure 53). In this new model the amount of interdigitation of the cones is dependent on the level of interdigitation assumed for the CB mesogens. In Figure 53 this is assumed to be 4 Å of interdigitation of the CB mesogens at each layer interface. This value was chosen as it is reasonably typical of CB mesogens¹⁰⁹. This leaves 9 Å above the measured layer spacing which must be accounted for by the interdigitation of the cones.



*Figure 53: A SmA_d phase using the conic model of the hexamer **4**, the level of interdigitation of the cones shown assumes 4 Å of interdigitation of the CB mesogens at each layer interface*

The resulting model appears to be fairly sensible. The level of interdigitation of the cones is almost exactly equal to the amount of the cones made up of the siloxane linker. The segregation of this part of the cone is entirely consistent with other similar systems¹⁴. Once a functional model of the phase had been constructed possible close-packing arrangements of the cones was considered in order to see whether there is any possibility of further ordering of the carborane clusters within the phase.

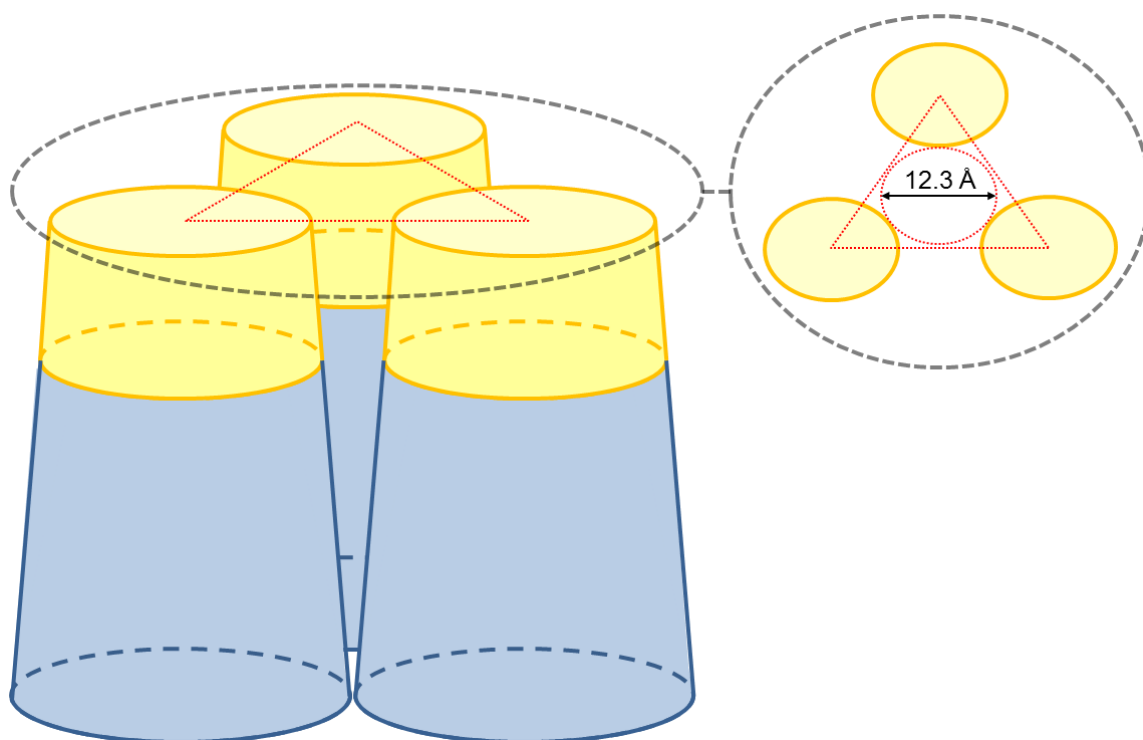


Figure 54: Hexagonal close-packing of the conic model of the hexamer 4

Initially hexagonal close-packing of the largest face of the cones (Figure 54) was considered as this would result in the minimization of free space within the model. However, as the cones have a very steep gradient when the bases are close-packed into a hexagonal lattice there is not enough room between the smaller faces of the cones for another cone to fit between them in a SmA_d phase as we have proposed. As such the model cannot possibly show hexagonal close-packing of this type.

Next the large faces of the cones were close-packed onto a square grid (Figure 55). Although this arrangement is not as efficient as hexagonal packing in minimizing the amount of free space, it should allow for larger interstitial gaps in which the cones can interdigitate. However, as can be seen even with this less demanding packing regime there is still not enough space for the cones to interdigitate, although this packing system is much closer to allowing the interdigitation necessary for the model.

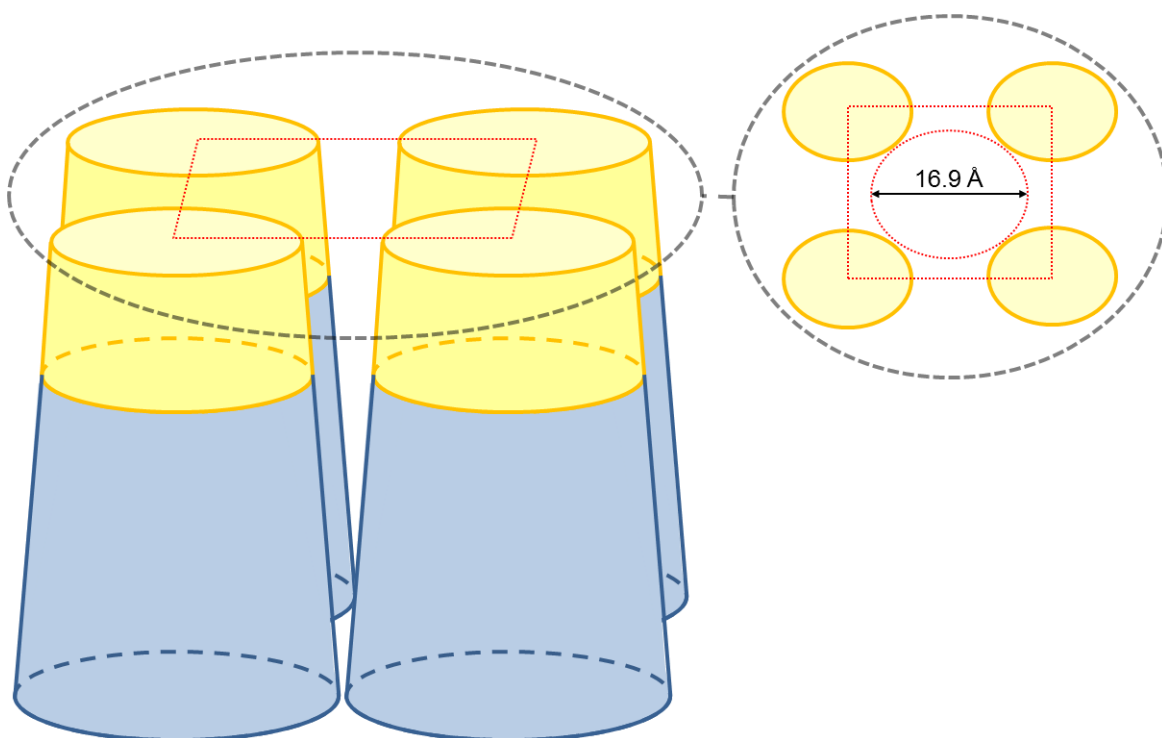


Figure 55: Square close-packing of the conic model of the hexamer 4

As the small face of the cones cannot become smaller, the bottom face must increase in area in order to allow for the interdigitation of the cones necessary for the model to fit the measured layer spacing in a close-packing regime. This would either mean: that the assumption that the fully interdigitated CB mesogens require twice the volume of the cylindrical model is wrong; and/or there is no close-packing of the large cone faces and they are disordered within the plane.

Although this model is a useful aid in understanding the possible arrangement of molecules within the observed phase it is worth noting that there are a number of limitations associated with it. Firstly and most importantly the dimensions used for all the models were taken from a minimization of just one isomer of compound **4** at 0 K in the gas phase. This minimization although useful is unlikely to be particularly representative of the isomer within the actual phase. In addition to this there is a distribution of a possible sixty four different isomers present in the sample which are likely to have different dimensions thus adding confusion to the model.

Following on from this it is assumed that it is possible to model the actual material behaviour using the simple packing of hard cones. In reality the molecules and layers

in which they sit in are fluid and deformable. As such the model is unable to account for these properties. Having noted the limitations and simplicity of the model it does however still get a reasonably good fit to the observed layer spacing with a phase structure which appears feasible.

The LC fullerodendrimers described by Deschenaux et al¹¹⁰ (Figure 56) share many structural features with **4**. In both cases there is an aromatic spherical (or close to) cluster attached to a branching unit and the branching unit then connects to mesogenic moieties by a flexible spacer. Finally in both systems cyanobiphenyl based mesogens are employed.

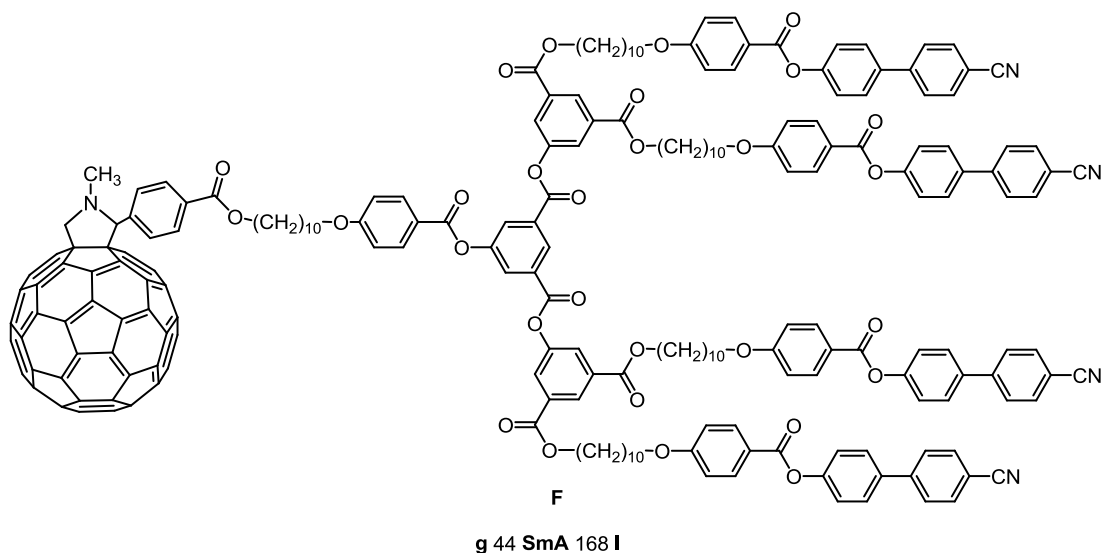


Figure 56: Fullerene containing supermolecular liquid crystal¹¹⁰

Deschenaux and co-workers found that the LC fullerodendrimers, of which compound **F** (Figure 56) is the second generation, display purely SmA phases and that clearing points increased with generation. It was also found that at low generation (G1 to G2) the dendrimers adopted a head to tail packing arrangement, resulting in a SmA₂ phase with a distinct layer of fullerene moieties in between each layer of mesogens (Figure 57 left). The mesogens themselves showed interdigitation of the cyano groups and the mesogens attached to each dendrimer were confined to one layer. This description is practically identical to that of the SmA phase of compound **4** which we have proposed.

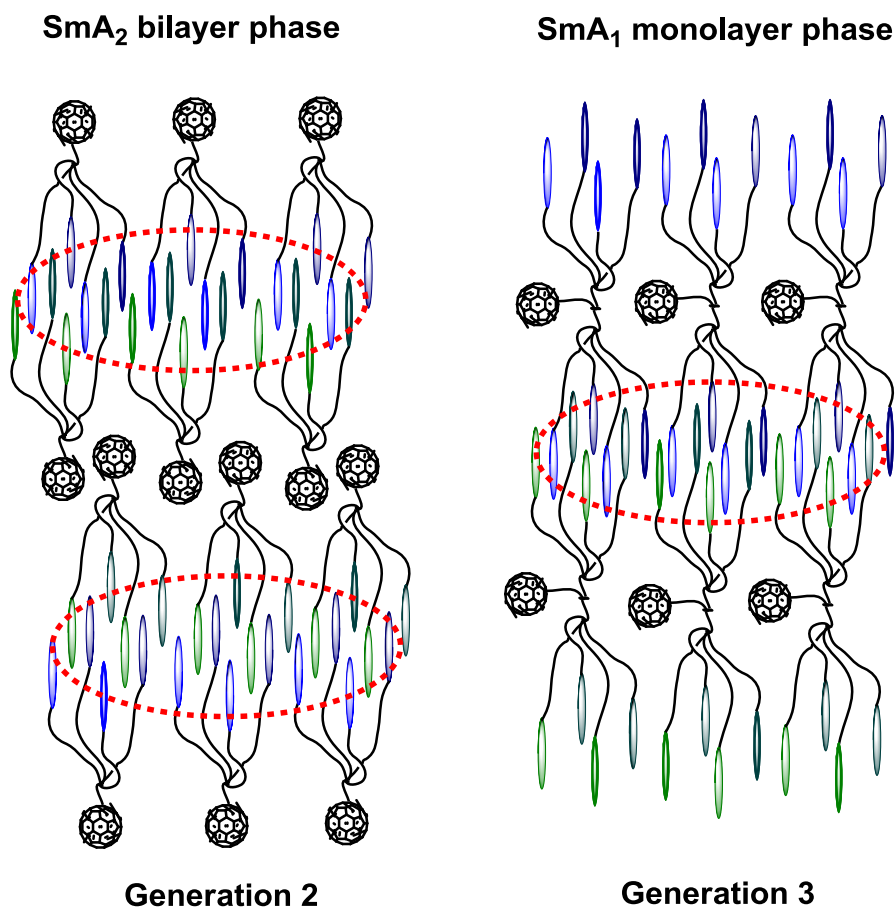


Figure 57: The smectic A phases of LC fullerodendrimers¹¹⁰

However, interestingly it was shown that when going from the second generation dendrimer with four mesogens to the third generation dendrimer with eight mesogens the nature of the SmA phase changed. Rather than packing in a head-to-tail manner and forming a bilayer SmA₂ phase the dendrimers formed a monolayer SmA₁ phase in which the mesogens of each molecule could belong to different layers of mesogens (Figure 57 right).

Compound **4** is mid-way between the G2 and G3 dendrimers in terms of the number of mesogens. As such it would be difficult to predict which conformation would be adopted. However, **4** differs from the fullerodendrimers in an important way. There is a flexible chain which separates the cluster from the branching units in the fullerodendrimers, which gives the mesogens more conformational freedom and allows the formation of the monolayer SmA₁ phase. As there is no flexible chain separating the cluster from the branching unit in **4**, the mesogens are forced to

populate the same side of the cluster, thus precluding any chance of the formation of a SmA₁ phase in a similar manner as the G3 dendrimer.

3.3.4.3 Neutron Diffraction

The X-ray experiments calculated the distance between the areas of high electron density in the phase, namely the aromatic regions. This however does not allow for the location of the boron clusters as they are not electron rich. The clusters do have a high mass density though, and therefore should show up well in neutron diffraction which is sensitive to areas of high mass density. In order to further investigate the SmA phase of **4** and to attempt to locate the boron clusters within the phase, neutron diffraction experiments were carried out.

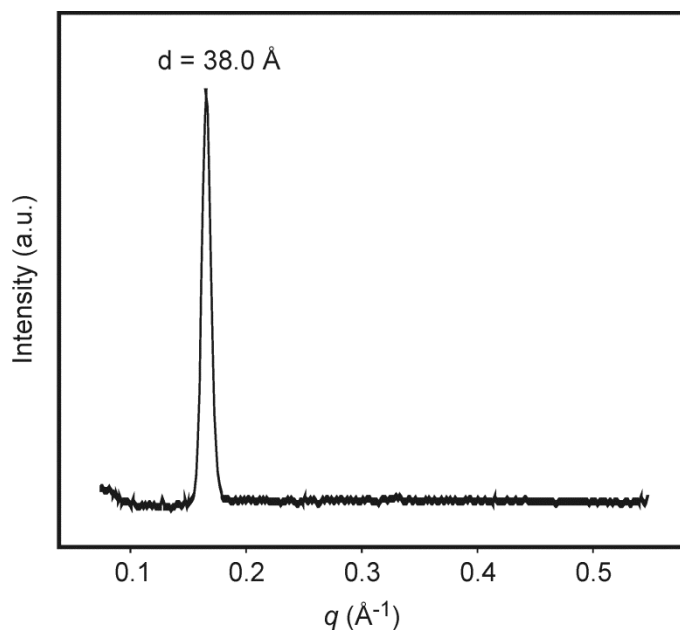


*Figure 58: Neutron diffractogram of **4***

Only one diffraction peak was observed in the neutron experiment (Figure 58) at 38.0 \AA , which corresponds well to the peak measured by X-ray. It is most likely due to the layer spacing of the SmA phase. The neutron diffraction experiment revealed that there is no additional ordering of the carborane cluster within the phase.

3.4 Concluding Remarks

This chapter has detailed the synthesis and thermal properties of a series of cyanobiphenyl functionalized carboranes with a siloxane spacer. It has been shown that one CB moiety is not a powerful enough mesogen to generate liquid-crystalline materials in these systems. By increasing the number of mesogens to two, liquid-crystalline properties have been introduced into the system, albeit weakly. Further increasing the number of mesogens to six generated a broad liquid-crystalline phase.

It appears that the carborane cluster has a destabilizing effect on mesophases. This could be from disruption of the core-core interactions of the CB mesogens by the presence of the bulky carborane cluster. However, as is consistent with other supermolecular liquid crystals, upon addition of more mesogenic moieties the mesophase stability increased. This allows for the formation of a monotropic phase with two mesogens and a broad enantiotropic phase with six mesogens.

The nature of the mesophases generated, namely smectic A is also within expectations given the nature of the mesogen employed and the siloxy linker, which is prone to microphase segregation. The SmA₂ or SmA_d phase which we have proposed for **3** are broadly consistent with other U-shaped mesogens reported in the literature, which often have smectogenic character resulting from the restricted degrees of freedom of the mesogens. In addition, the model of the SmA_d phase of **4** which was developed in order to make sense of the layer spacing, as measured by XRD and neutron diffraction, suggests that **4** behaves in a similar manner to that of low generation LC fullerodendrimers. These dendrimers also adopt a head-to-tail packing arrangement with interdigitation of the CB mesogens to form a SmA_d phase. The model also showed that the carborane cluster is disordered within the phase. This may be due to the relative size of the cluster in comparison to the supermolecule as a whole.

The generation of branched isomers in the final hydrosilylation step has proved to be an unresolvable issue. There is no synthetic way to avoid their generation, and separation of the branched and linear isomers is not a practical solution. These

Chapter 3: Siloxanes

unwanted isomers must have an effect upon the thermal properties of the materials investigated. While it is possible to rationalise the effect of the branched isomers it is not possible to measure it. As such a new synthetic method which can produce similar materials was needed in order to eliminate this problem.

4. Mono-functional Silanes

4.1 Summary

Given the structural problems associated with the presence of the branched siloxane isomers in the hydrosilylation reaction described in Chapter 3, this issue was addressed by the replacement of the tetramethyldisiloxane unit with a dimethylsilane unit. The silane linkage was chosen as its synthetic route is similar to the siloxane materials described in the previous chapter; however the problem of unwanted branched isomers should be eliminated¹¹¹. As such in this chapter a series of mono-functionalized carboranes are described in which the mesogenic moieties are attached by a silane linkage.

Unlike the previous chapter a range of different mesogens are employed here, in order to target different mesophases. This is done with the aim of assessing the effect of the carborane cluster in these different mesophases and also to see whether the carborane cluster has any effect on the type of phase which is exhibited. A number of different mesogenic cores are employed and the topology of connection between the mesogenic core and the flexible spacer is varied.

The cyanobiphenyl mesogen will continue to be employed as there is a large body of literature which utilises these mesogens thereby aiding comparison. However, a cyanobiphenyl benzoate core because it has a broader mesophase range thus allowing the generation of more stable mesophases to study. This mesogenic core has been used extensively in other supermolecular systems¹¹²⁻¹¹⁶ thus making for easier comparisons to be made. Both of these mesogens have a propensity for the formation of smectic phases. As side-on mesogens often favour the formation of the nematic phase²⁶ a second three-ring mesogenic core, an alkoxy 1,4-bis-phenylene benzoate, will be employed and attached in a side-on fashion. This allows for the targeting of different phases as well as the comparison of the effect of a having a larger three-ring mesogen replacing the two-ring system used previously.

Finally we also used an octyloxybiphenylcarbonyl phenyl benzoate mesogen with the chiral (*S*)-2-methylbutoxy chain attached either terminally or laterally on the final ring. This mesogen has a tendency to form the chiral nematic phase when attached

Chapter 4: Mono-functional Silanes

laterally⁵⁵. Typically when mesogens are attached terminally in supermolecular LC systems, nematic and smectic phases are promoted²⁶. Both chiral smectic and nematic phases were targeted so it would be possible to assess if there is any effect on chiral phases by the presence of the carborane cluster. Furthermore, extension of the mesogenic core to a four-ring system should also aid in mesophase stability.

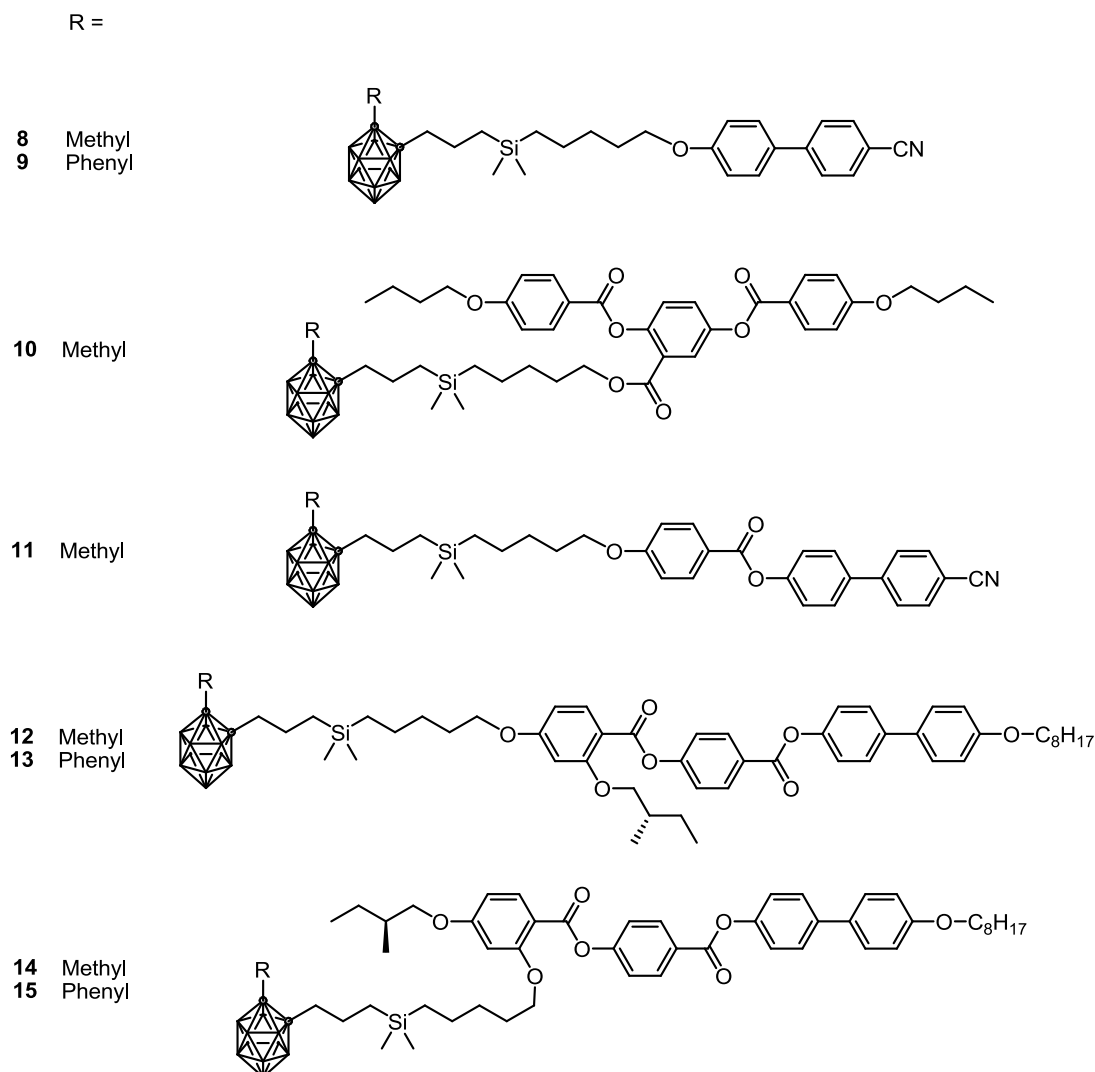


Figure 59: Carboranes mono-functionalized via a silane linker with mesogens

4.2 Synthesis

The functionalized carboranes in this chapter were synthesized using the general procedure described in Scheme 4. The synthesis of the alkenyl mesogenic cores used

Chapter 4: Mono-functional Silanes

in this chapter (Figure 60) were produced by literature procedures and are described in the Experimental section.

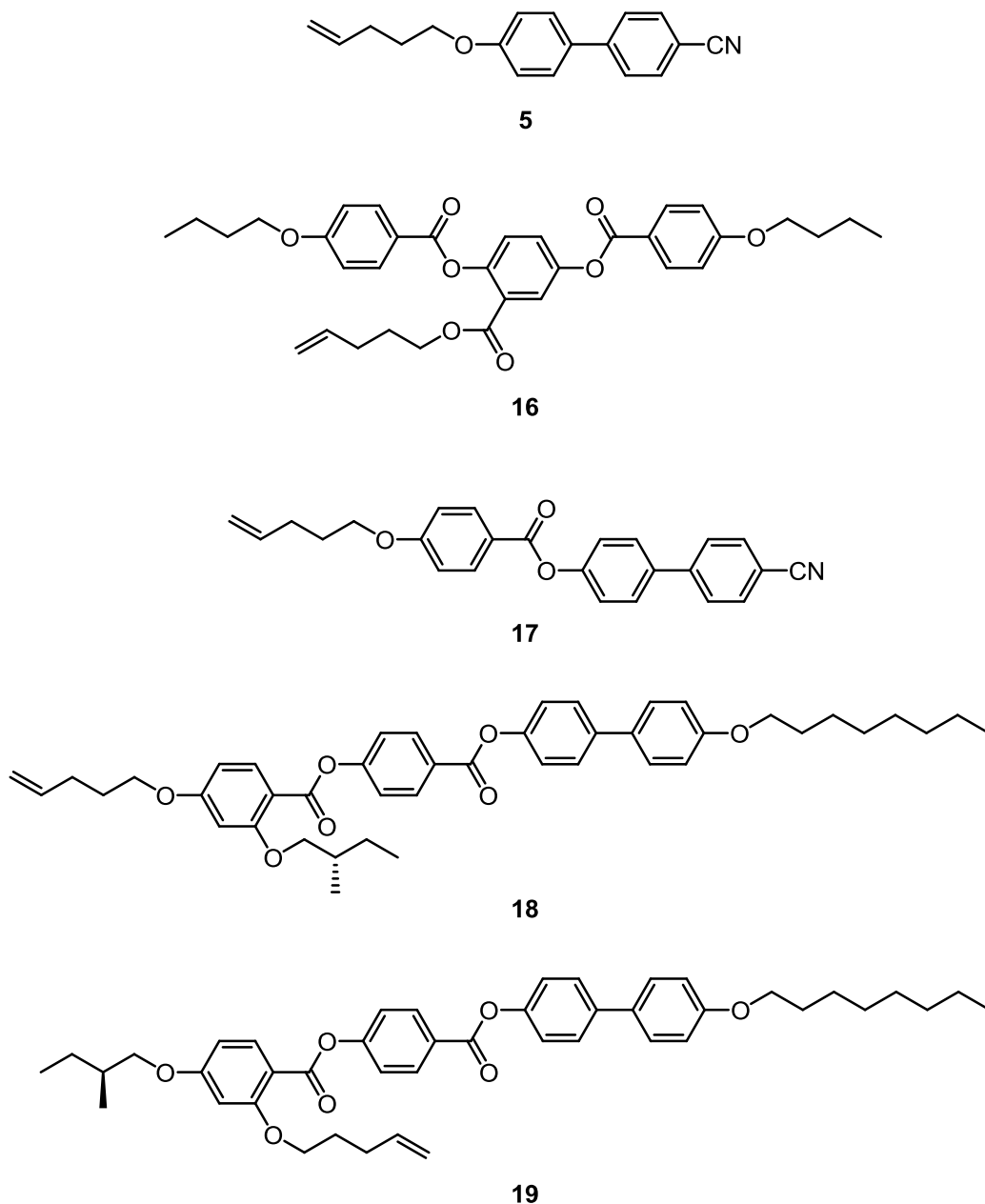


Figure 60: The structures of the alkenyl mesogenic moieties **5**¹¹⁷, **16**, **17**¹¹⁸, **18**¹¹⁹ and **19**¹²⁰

Considering the available allyl carborane derivatives, the functionalization with mesogenic moieties could be accomplished either by hydrosilylation of the allyl carborane with a mesogenic hydrosilane; or alternatively by generating a carborane carrying the Si-H functionality and subsequent hydrosilylation with a mesomogenic

Chapter 4: Mono-functional Silanes

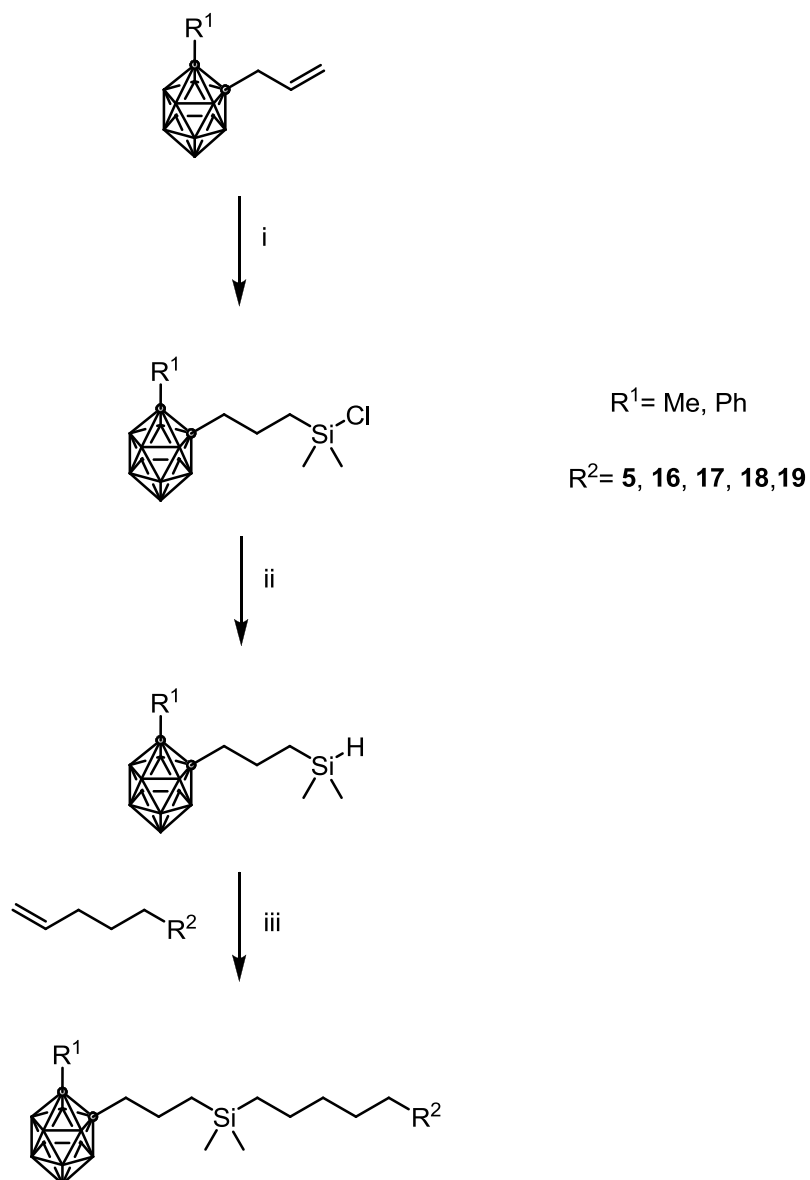
alkene. The second approach was chosen since it is easier to accomplish synthetically.

In all cases described in this chapter the allyl carborane precursors were converted to the corresponding carboranyl silanes. The relevant 4-pentenyl mesogenic derivatives were used in order to keep the overall spacer chain length between the cluster and the mesogen constant so that appropriate comparisons could be established.

The initial step is the hydrosilylation using Karstedt's catalyst and dimethylchlorosilane in dry low sulphur toluene to generate the chlorosilane terminated functionalized carborane. This reaction was monitored by ^1H NMR and was stopped upon the disappearance of the resonances at ~ 5.6 , 5.0 and 4.7 ppm associated with the CH and CH_2 of the alkene functional group. This material was used without further purification *in situ*. The reduction of the chlorosilane to the silane functionalities was accomplished by reaction with LiAlH_4 in THF. The final step of the synthesis involves the hydrosilylation of the silane functionalized carborane with the alkenyl functionalized mesogenic cores, again using Karstedt's catalyst in dry low sulphur toluene at room temperature.

The successful final hydrosilylation reaction was confirmed by ^1H NMR by the disappearance of the resonances between 5 and 6 ppm associated with alkenyl protons of the unreacted mesogen. In addition to this new resonances, a multiplet at 0.5 ppm and a singlet at 0.0 ppm, appear in the ^1H NMR spectra associated with the CH_2Si and the CH_3Si respectively. Furthermore, in the boron decoupled ^1H NMR spectra the three broad singlets at 2.7 , 2.4 and 2.3 ppm associated with the BH protons, as observed in the previous chapter, were also present. Finally ^{29}Si NMR confirmed the presence of just one silicon environment in the final compounds with a singlet at around 2.9 ppm.

Chapter 4: Mono-functional Silanes



- i) dimethylchlorosilane, Karstedt's catalyst and dry low sulphur toluene
- ii) LiAlH_4 and THF
- iii) Karstedt's catalyst and dry low sulphur toluene

Scheme 4: The synthesis of carboranes mono-functionalized with mesogens

A major problem with the synthesis of the siloxane linked functionalized carboranes described in the previous chapter was the undesired side reaction resulting in the presence of branched isomers in the desired materials. In this chapter a silane linkage was used instead in an effort to eliminate this problem. Therefore it was imperative to determine whether this branching had been eliminated using NMR studies.

Chapter 4: Mono-functional Silanes

Inspection of the ^1H , ^{13}C and ^{29}Si NMR spectra did not show any resonances associated with branched products in any of the silanes synthesized. Furthermore, ^{13}C DEPT 135° experiments were carried out in order to confirm that within the detection limits of the methods employed there is no branched isomer in any of these materials.

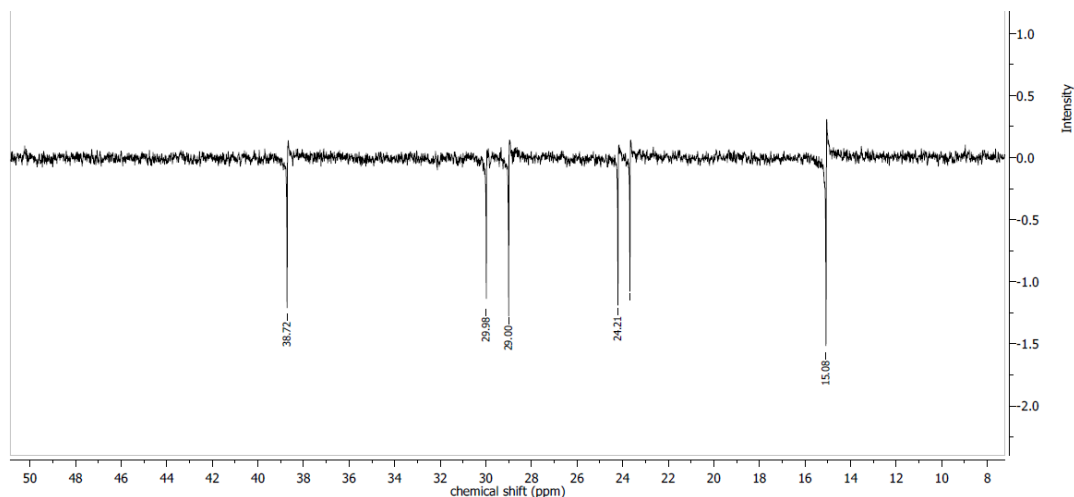


*Figure 61: The alkyl region of the DEPT 135° spectra of compound **9***

As with the siloxanes in the previous chapter the linear isomers of the silanes contain only CH_2 units in the linkage between the carborane and the mesogen, therefore all resonances in the alkyl region associated with the linkage should show negative phase in the DEPT 135° experiment. Figure 61 shows an excerpt from the DEPT 135° spectra of compound **9** and is typical of all the compounds in this series; **9** was chosen as there are no other signals except for the linking chain in the alkyl region. The absence of resonances with positive phase, associated with CH or CH_3 , indicate that the branched isomer was not generated.

Therefore it can be concluded that the use of a silane linkage has eliminated the problem of the branched isomers encountered in the previous chapter. This allows for the study of the thermal properties of these new materials without the added structural isomerism resulting in the complex mixtures generated previously.

4.3 Thermal Properties

The thermal properties and any subsequently observed phase behaviour of the carboranes mono-functionalized with mesogens was investigated with DSC and POM. Table 3 shows a summary of the materials thermal behaviour.

Compound	Cr1	Cr2	Cr3	SmA	N*	Iso
8	• 51.4	•			117.1	•
9	•				63.0	•
10	•				51.9	•
11	•		102.6	•	103.3	•
12	• 33.0	•		(87.4 •)	89.0	•
13	• 18.0	• 36.9	•	(37.3 •)	64.0	•
14	•			(38.3 •)	56.2	•
15	•			(35.9 •)	46.3	•

Table 3: The thermal behaviour of the carboranes mono-functionalized with mesogens, as recorded by DSC with a heating/cooling rate of $10\text{ }^{\circ}\text{Cmin}^{-1}$, values shown in brackets are for monotropic transitions

For the purposes of comparison the thermal properties of the alkenyl mesogens is summarized in Table 4 and their structures are shown in Figure 60.

Compound	Cr	N	N*	Iso
5	• 75.8	•	88.2	•
16	• 85.7	•	110.4	•
17	• 108.0	•	264.0	•
18	•	128.9	• 167.5	•
19	•	110.3	• 151.4	•

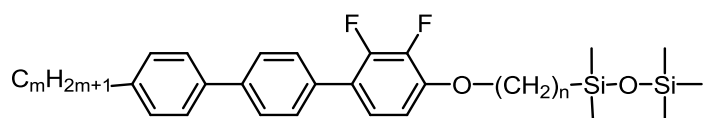
Table 4: The thermal properties of the alkenyl mesogens 5^{117} , 16 , 17^{118} , 18^{119} and 19^{120} as measured by DSC, heating/cooling rate $10\text{ }^{\circ}\text{Cmin}^{-1}$

4.3.1 Two-ring Systems

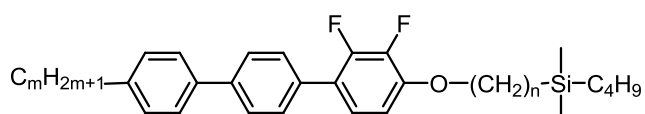
The initial focus was on systems functionalized with mesogens consisting of two rings, namely cyanobiphenyls. Neither compounds **8** or **9** proved to be mesogomorphic. However, unlike compounds **1** and **2** from the previous chapter,

both **8** and **9** crystallize rather than form glasses, and melt at higher temperatures. This can be explained by the absence of any branched isomers within the sample. Mixtures of materials always show a depression of the melting point¹²¹ so it is reasonable to expect that by removing the branched isomers that the melting points would increase. In addition to this the silane group is both less conformationally flexible and sterically demanding than the siloxy group. Both of these factors would also raise the melting point and increase the possibility of crystallization of the silane linked materials in comparison to the siloxy linked materials.

The difluoroterphenyls reported by Goodby *et al*¹²², in which a terminal pentamethyl disiloxane unit is replaced by an internal dimethyl silyl unit while keeping the overall chain length the same (Figure 62), illustrate the rather small change in behaviour typically observed when moving from a siloxane to a silane functionality. As can be seen from the absence of any N phases, silanes also cause microphase segregation resulting in the suppression of N phases in preference for smectic phases. Furthermore, there is only a minimal change in the transition temperatures observed when moving from the siloxy to the silyl materials, with the siloxy materials exhibiting slightly higher isotropization temperatures to the silanes.



m	n	Cr	SmC	Iso
5	5	•	57.4	•
5	7	•	70.0	•
7	5	•	76.3	•
7	7	•	62.7	•



m	n	Cr	SmC	SmA	Iso
5	5	•	61.0	•	•
5	7	•	60.0	•	•
7	5	•	60.0	•	•
7	7	•	65.0	•	•

Figure 62: Siloxane and Silane terminated difluoroterphenyls¹²²

Given the trends observed for the difluoroterphenyls described above when moving from siloxy to silyl substituents, it is likely that compounds **1** and **2** from the previous chapter would not have been liquid-crystalline even had they not been a mixture of the linear and bent isomers. It would be expected that the melting behaviour of the siloxy materials would be similar to their silyl analogues **8** and **9**, with transition temperatures only slightly different. Therefore it can be concluded that a single two-ring mesogen is not able to overcome the destabilizing effect upon mesophases caused by the attachment of the carborane cluster.

Comparing the melting points of **8** and **9** to those of the mesogen **5** it can be seen that there is an increase of the melting point upon the addition of the methyl-substituted carborane cluster, whereas the addition of the phenyl-substituted carborane cluster lowers the melting point. The methyl-substituted compound **1** also had a higher glass transition temperature than the phenyl-substituted **2** from Chapter 3. It is logical to expect that the larger phenyl substituent is more sterically demanding and thus lowers the melting point in comparison to the smaller methyl substituent.

4.3.2 Three-ring Systems

As compounds **8** and **9** illustrate, mesogenic groups comprising of two-ring systems do not provide enough molecular anisotropy to generate liquid-crystalline behaviour in the mono-functionalized materials as they cannot counteract the steric destabilization introduced by the carborane cluster. As such mesogens comprising of three-ring systems were investigated. The mode of attachment, either terminal or lateral, was also investigated to see whether it would have an effect on the mesogenic properties of the materials formed.

Compound **10** is functionalized with a 2,5-(4-butoxybenzoyloxy)benzoate mesogen, **16**, which is connected laterally. Similar mesogens have been widely used in liquid crystal research as a laterally attached mesogen¹²³. The material was found to be non-mesomorphic, melting to the isotropic liquid at 55.2 °C. As with the two-ring systems the side-on three-ring mesogen, **16**, does not impart a high enough degree of anisotropy to the cluster in order to generate mesomorphic behaviour. As with compounds **1**, **2**, **8** and **9** it is suggested that this is caused by the steric destabilization imparted by the bulky carborane cluster interfering with the core-core interactions between the mesogenic moieties.

Upon addition of the carborane cluster to the mesogen, **16**, thus generating **10**, the melting point decreases by around 30 °C. This depression is most likely caused by the non-linear molecular shape of **10**. Compound **10** has a bulky carborane cluster attached to the side chain of the mesogen, which is less able to pack efficiently into a crystal lattice in comparison to **16** and thus has a lower melting point.

It is also noteworthy that **10** crystallizes rather than forms a glass upon cooling. As was discussed for compounds **8** and **9**, this is likely due to the removal of the branched isomers and the replacement of the siloxy linking group with the silane linking group.

Compound **11**, like **10**, has a three-ring mesogen appended, this time a cyanobiphenyl benzoate, **17**. Cyanobiphenyl benzoates have been used

successfully before in supermolecular materials with the fullerene core¹¹². Compound **11** displayed a very short enantiotropic SmA phase. The DSC trace (Figure 63) showed three reproducible thermal events upon heating. A glass transition where the fastest rate of change in the enthalpy was at -3.4 °C followed by an exotherm with onset at 66.0 °C and an enthalpy of -5.5 kJmol⁻¹. This exotherm is associated with a cold crystallization event. Finally there is an endotherm, with onset at 102.6 °C and an enthalpy of 8.0 kJmol⁻¹, which is associated with the melting point. However upon cooling there are only two reproducible thermal events, firstly, an endotherm with onset at 103.6 °C and an enthalpy of -1.1 kJmol⁻¹, corresponding to a transition into a LC phase. The second is the glass transition where the fastest rate of change in the enthalpy was at -2.5 °C.

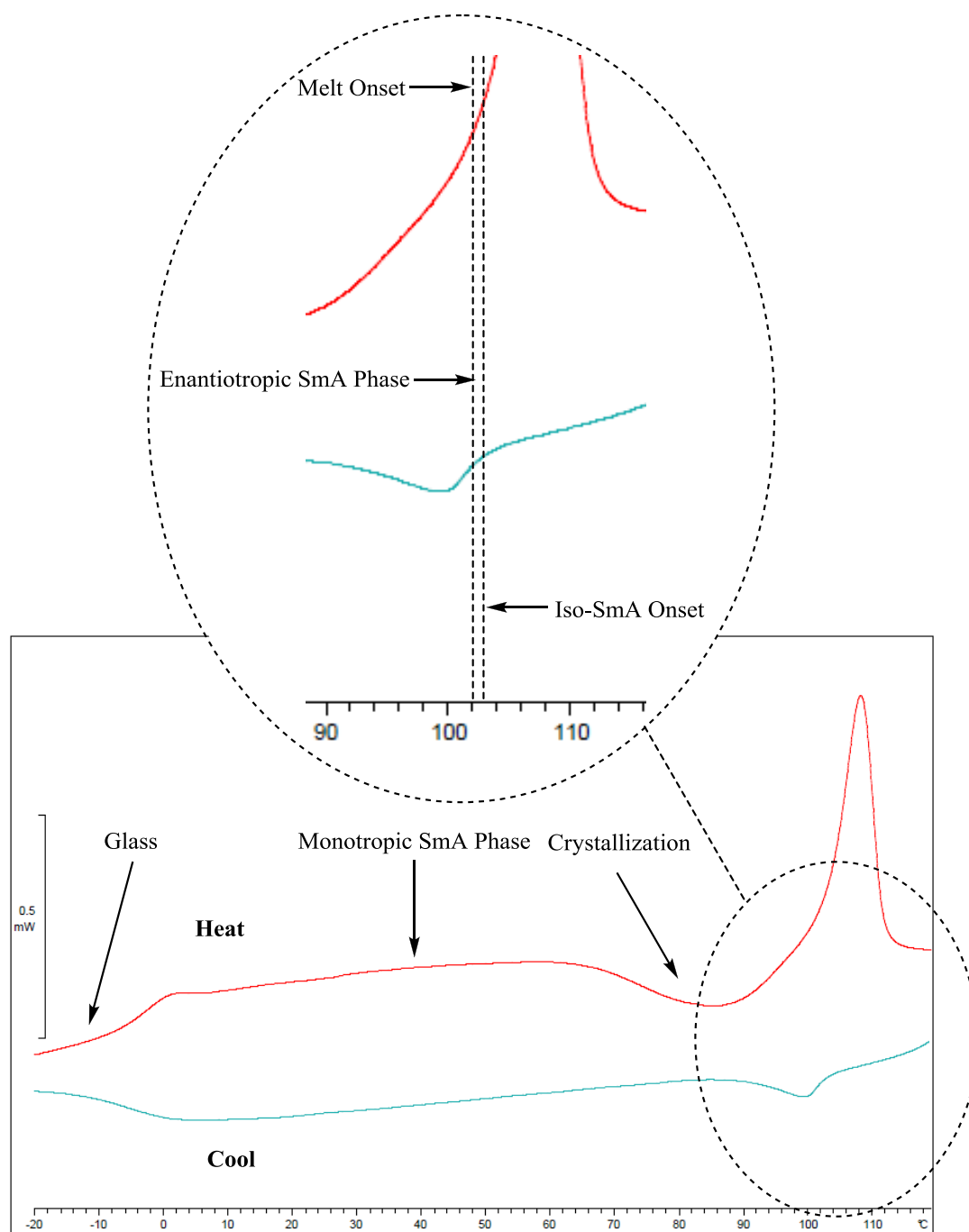


Figure 63: DSC trace of compound **11**, heating/cooling rate of $10\text{ }^{\circ}\text{Cmin}^{-1}$

Figure 64 shows the focal-conic texture of **11** which was generated upon cooling from the isotropic liquid. The material had a very strong tendency to homeotropic alignment and required mechanical shearing in order to form any discernible texture. However, the material relaxed extremely quickly to homeotropic alignment making acquiring an image very difficult. The presence of the focal-conic texture and optically extinct homeotropic regions allow this phase to be identified as SmA.

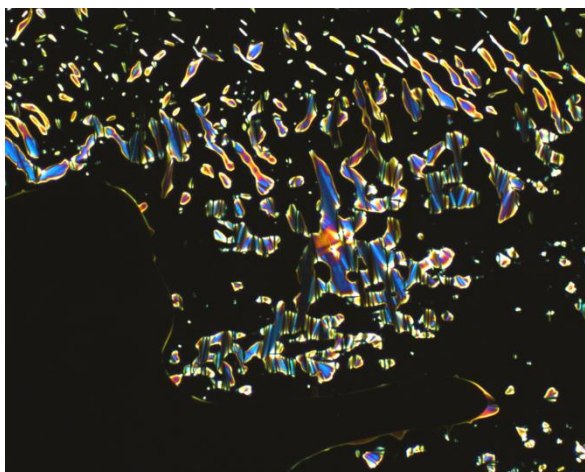


Figure 64: POM of 11 at 100.7 °C cooled from the isotropic liquid at 0.5 °Cmin⁻¹ after shearing

The SmA phase remained metastable far below the melting point of the material until it eventually froze into a glass, which retains the smectic A texture, as seen in the DSC (Figure 63). Upon heating, this glass transforms back into the SmA phase until it reaches 66.0 °C at which point it nucleates kinetically to form a thermodynamically stable crystal. The enantiotropic SmA phase is not observed in either the POM or DSC on heating as the isotropization is concurrent with the melting. Theoretically the onset of the Iso to SmA transition should be the same upon heating and cooling. Therefore it can be inferred that the transition is lost in the endotherm of the melt (Figure 63 inset). Thus allowing the assignment of the SmA phase as enantiotropic, albeit very weakly.

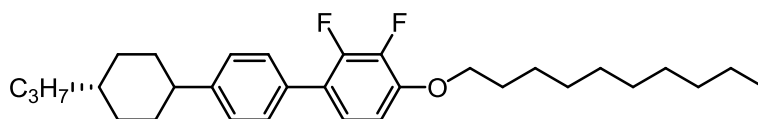
Compound **11** demonstrates that a three-ring mesogenic moiety is enough to impart LC behaviour upon the mono-functionalized carboranes. Although **10** is non-mesomorphic it is not possible to ascertain whether the mode of attachment is the cause of the lack of mesomorphism as the mesogens used are too dissimilar to draw conclusions.

The addition of the carborane cluster to the mesogen **17** results in a very slight decrease in melting point, which is caused by the carboranes steric bulk. However, more interestingly the nature of the mesophase formed is entirely different for **11** than for **17**, going from the N phase to the SmA phase upon the addition of the

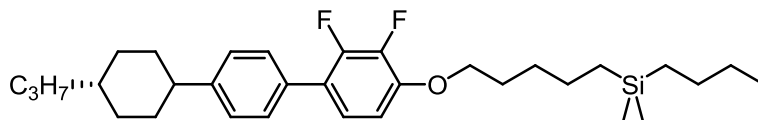
Chapter 4: Mono-functional Silanes

carborane cluster. Furthermore the stability of this phase is greatly reduced in the carborane containing material and the majority of the phase behaviour was monotropic.

The suppression of the N phase is likely the result of the silane linker. The cyclohexyldifluorobiphenyls shown in Figure 65 reported by Davis¹²⁴, demonstrate the change in phase behaviour observed when a methylene unit in the centre of a flexible chain is replaced by a dimethylsilyl unit. Incorporation of the silyl unit completely suppresses the N phase and there is a depression of the melting point and phase stability.



Cr 49.7 SmC 62.9 SmA 95.8 N 129.4 I



Cr 31.5 SmC 44.7 SmA 89.3 I

Figure 65: Cyclohexyldifluorobiphenyl mesogens with an internal silane linker¹²⁴

Without X-ray analysis it is not possible to determine whether this effect is caused by the microphase segregation of the silyl unit; or steric disruptions caused by the bulky dimethylsilyl unit which may operate more prominently in the N phase. However, it is not possible to know whether the carborane cluster contributed to either of these effects from the available information.

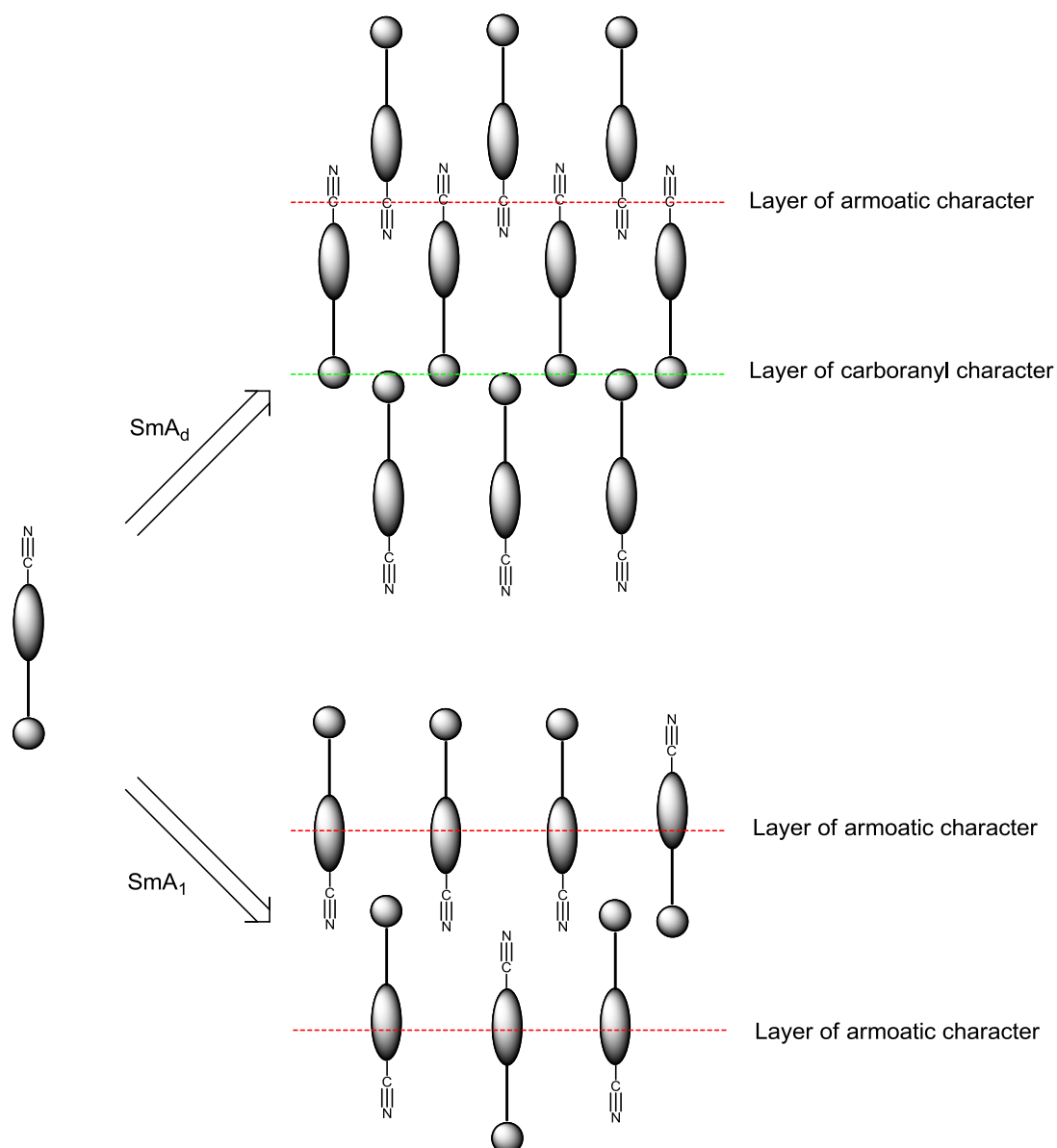
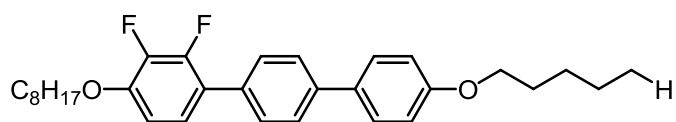


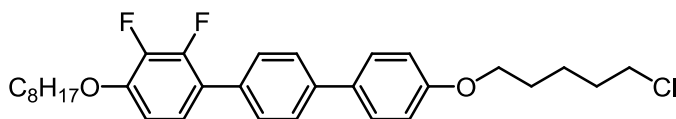
Figure 66: Possible structures of the SmA phase of **11**

The structure of the SmA phase of **11** can be one of two possibilities. If microphase segregation of the carborane clusters occurs as was shown to be the case for compound **4** then a SmA_d phase would be expected, with strong interdigitation of the cyano groups into the aromatic layers (Figure 66 top). This would result in a layer spacing slightly less than twice the molecular length. However, if no segregation of the carborane occurs then a monolayer SmA₁ phase will result (Figure 66 bottom) with a layer spacing of approximately the molecular length.



Cr 93.5 SmC 144 SmA 148 N 159 Iso

G



Cr 80.2 SmA 154.9 Iso

H

Figure 67: Terminal halogen functionalized difluoroterphenyls¹²²

The addition of substituents to the terminus of flexible alkyl chains attached to mesogenic cores has been shown to favour smectic phases over nematic ones (Figure 67). As can be seen by comparing **G** and **H**, addition of a polar end-substituent, in this case a halogen atom decreases the melting point but does not greatly affect the mesophase stability as measured by phase range. Furthermore, it can be seen that the addition of this end-group suppresses the N phase, similar to that of the behaviour observed for our materials. However, at difference with our materials the chlorine end-group used in **H** is much smaller than the carborane cluster and highly polar. It is the polar interactions at the layer interfaces which suppress smectic polymorphism and particularly the formation of the SmC phase¹²². Upon addition of non-polar end-groups such as carbocycles, tilted smectic phase are not suppressed¹⁰¹.

4.3.3 Four-ring Systems

Although Compound **11** showed that a three-ring mesogenic moiety is adequate to generate LC behaviour the material was still only weakly enantiotropic. Therefore a four-ring mesogen was investigated. In addition the mode of attachment of the four-ring mesogenic core varied in order to probe the effect of lateral versus terminal attachment. The substituent on the carborane cluster was also varied, either a methyl or phenyl substituent.

An (*S*)-4-((4'-(octyloxy)biphenyl-4-yloxy)carbonyl)phenyl 2-(2-methylbutoxy)-4-(pent-4-enyloxy)benzoate, **18** was used as the terminally attached four-ring mesogen and (*S*)-4-((4'-(octyloxy)biphenyl-4-yloxy)carbonyl)phenyl 4-(2-methylbutoxy)-2-(pent-4-enyloxy)benzoate, **19** as the laterally attached mesogen. The core structure of both materials is identical except for the mode of attachment to allow for a true comparison of the effect of lateral versus terminal attachment. Additionally, both materials have been used to functionalize other cage-containing supermolecular liquid crystals^{26,55} thus allowing for meaningful comparisons.

4.3.3.1 End-On

Compounds **12** and **13** are both functionalized in an end-on fashion, with **12** having a methyl substituted carborane cluster and **13** having a phenyl substituted carborane cluster. The DSC trace of **12** shows two reproducible thermal events upon heating. The first is an exotherm, with onset at 33.0 °C and an enthalpy of -6.3 kJmol⁻¹, which is related to a cold crystallization. The second is an endotherm, with onset at 89.0 °C and an enthalpy of 36.7 kJmol⁻¹, is due to the melting into the isotropic liquid. Upon cooling there are two more reproducible thermal events, an exotherm with onset at 87.4 °C with $\Delta H = -0.6$ kJmol⁻¹ which can be ascribed to a monotropic Iso-LC phase transition. The second with onset at 54.2 °C and a ΔH of -10.3 kJmol⁻¹ is crystallization.

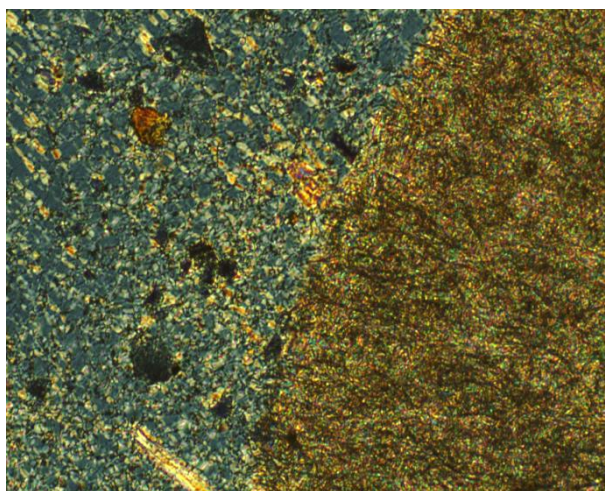


Figure 68: POM micrograph of 12 at 79.3 °C upon cooling from the isotropic liquid at 0.5 °C min⁻¹

Upon cooling from the isotropic liquid, **12** formed the Grandjean plane texture (Figure 68). This allows us to assign this phase as a monotropic N* phase. As can be seen in Figure 68 the material readily crystallizes below the melting.

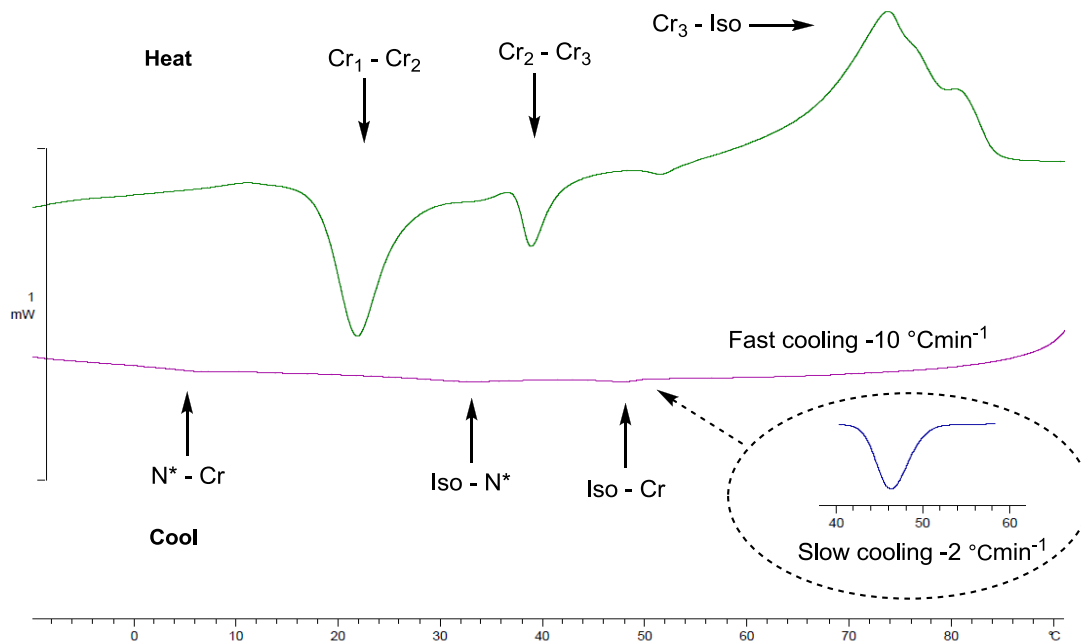


Figure 69: DSC trace of compound **13**, heating/cooling rate 10 °Cmin⁻¹

The DSC trace of **13** (Figure 69) showed three reproducible thermal events upon heating: two cold crystallizations, one at 18.0 °C with $\Delta H = -15.4 \text{ kJmol}^{-1}$ and the other at 36.9 °C with $\Delta H = -3.1 \text{ kJmol}^{-1}$; and a melting event into the isotropic liquid with onset at 64.0 °C and associated ΔH of 30.7 kJmol^{-1} . Upon cooling there were three reproducible exotherms, one at 50.1 °C ($\Delta H = -0.2 \text{ kJmol}^{-1}$), 37.8 °C ($\Delta H = -0.3 \text{ kJmol}^{-1}$) and 9.5 °C ($\Delta H = -0.3 \text{ kJmol}^{-1}$).

Upon rapid cooling of the sample from the isotropic liquid at approximately 37 °C the Grandjean plane texture of the N* phase develops (Figure 70). As can be seen in Figure 70 crystallites had already begun to form as would be expected from a monotropic phase. Upon further cooling to lower temperatures the sample completely crystallized. However, this leaves the thermal event at 50 °C unaccounted for. Microscopy also showed that crystallization of the sample often began at around 50 °C suggesting the exotherm was due to crystallization. To confirm this, a second DSC experiment was run with a cooling rate of -2 °Cmin⁻¹. As would be expected

from a crystallization event the energy of this exotherm greatly increased thus confirming this to be a crystallization which is kinetically hindered.

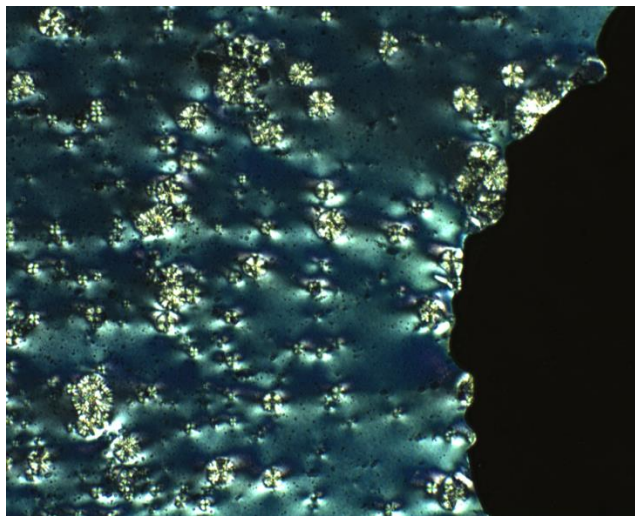


Figure 70: POM photomicrograph of 13 at 32.5 °C upon cooling rapidly from the isotropic liquid

4.3.3.2 Side-on

Compounds **14** and **15** are side-on homologues of **12** and **13**. Both have the same side-on mesogen but vary with either a methyl or phenyl group attached to the carborane cage respectively. The DSC trace of **14** shows three reproducible thermal events upon heating. The first is a glass transition where the greatest rate of change in the heat capacity was at -2.3 °C followed by an exotherm with onset at 36.9 °C ($\Delta H = -17.9 \text{ kJmol}^{-1}$) and finally an endotherm at 56.2 °C ($\Delta H = 18.5 \text{ kJmol}^{-1}$). The exotherm at 36.9 °C is associated with a cold crystallization and the endotherm at 56.2 °C the melt into the isotropic fluid. Upon cooling the DSC trace shows only two reproducible events an exotherm, with onset at 38.3 °C and an enthalpy of -0.2 kJmol^{-1} related to a Iso-LC phase transition, and a glass transition where the greatest rate of change of the heat capacity was at -0.3 °C. The glass transition indicates the freezing of the metastable LC phase similar to that observed for **11**, complete with the corresponding glass transition back into the metastable LC on the heating cycle.

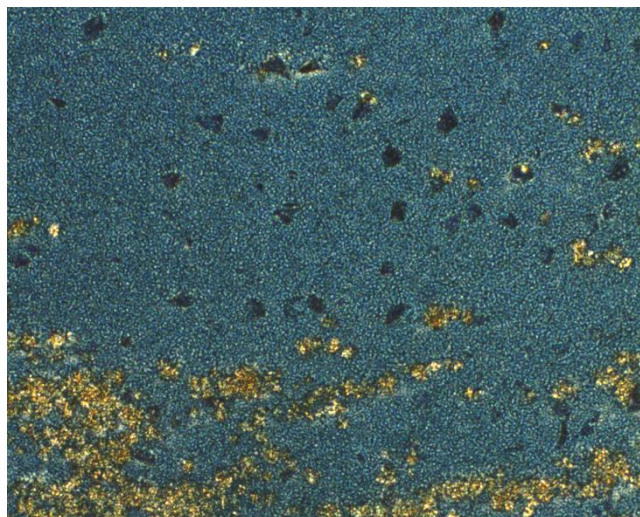


Figure 71: POM photomicrograph of **14** at 38.9 °C cooling from the isotropic liquid at 1° Cmin⁻¹

Upon cooling **14** from the isotropic liquid the Grandjean plane texture of the N* phase developed (Figure 71). While the texture obtained does not show the usual defect pattern of the Grandjean plane texture upon rotating the microscope stage the birefringence colour changed dramatically indicating a chiral structure. Given the lack of focal conic defects the phase cannot be the chiral smectic phase; therefore it has to be assigned as the chiral nematic phase.

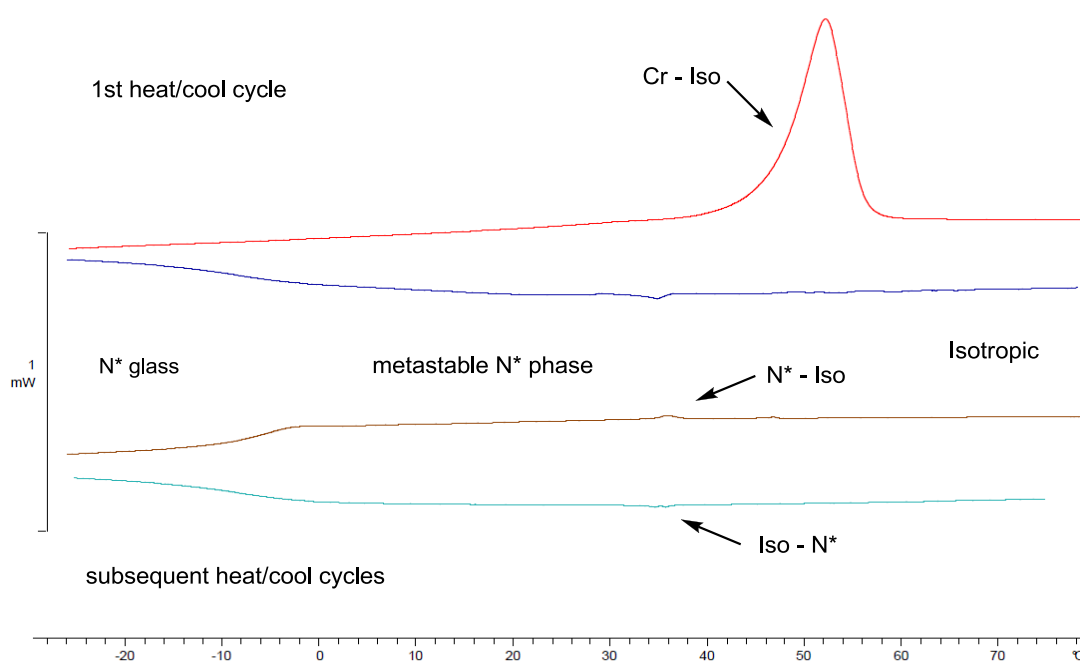


Figure 72: DSC trace of compound **15**, heating/cooling rate 10 °Cmin⁻¹

Chapter 4: Mono-functional Silanes

The DSC trace of **15** (Figure 72) shows two reproducible events on the heating cycle. However, only in the first heat is the melt from the crystal observed with onset at 46.3 °C and enthalpy of 45.9 kJmol⁻¹. Upon cooling there are two thermal events, an Iso-LC transition at 35.9 °C with an enthalpy of approximately 90 Jmol⁻¹, followed by a glass transition with a maximum rate of change in the heat capacity at -2.3 °C. Both thermal events are reproducible upon further cycles of heating and cooling. If annealed for long enough however, the metastable LC phase crystallized.

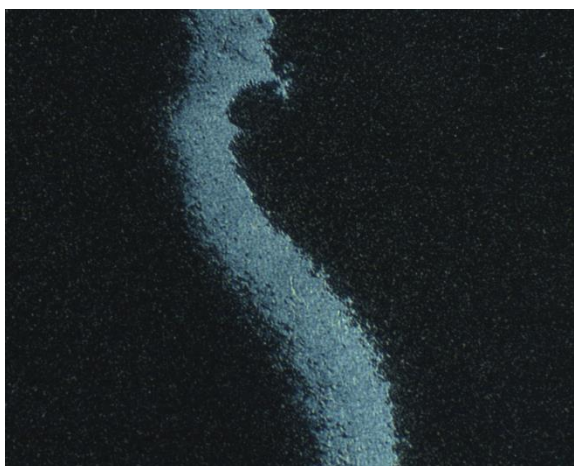
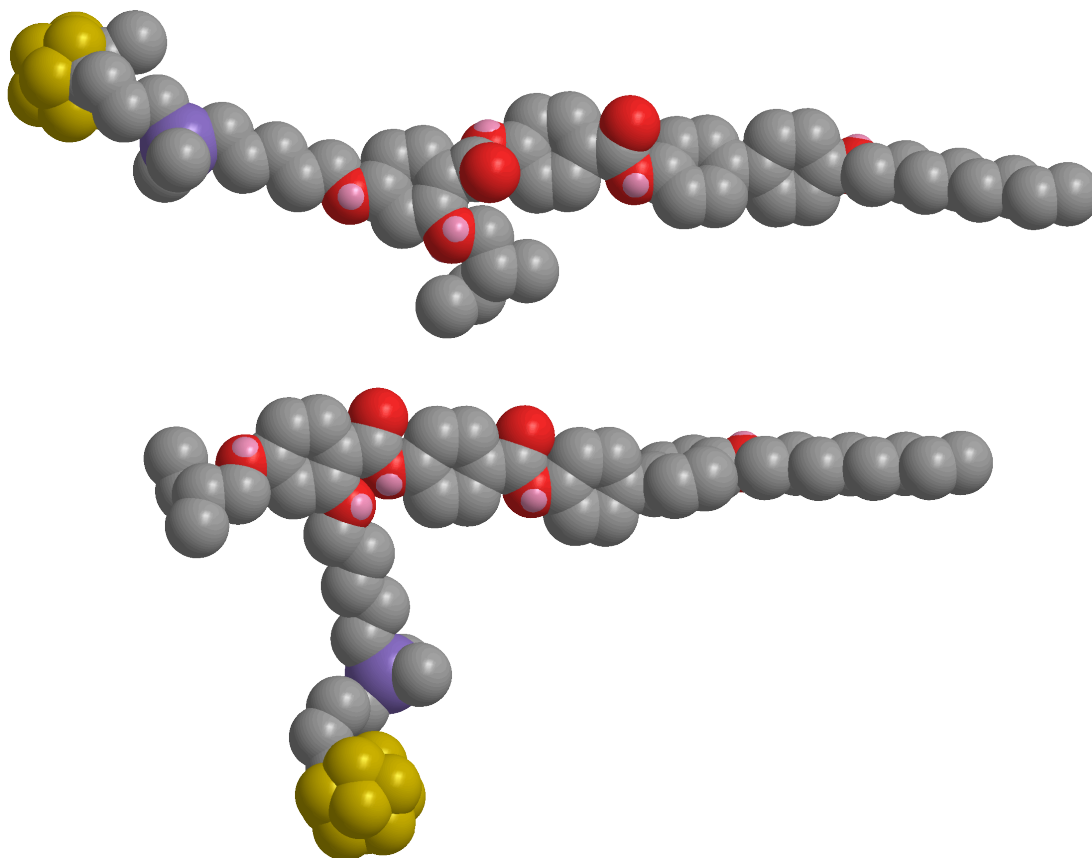


Figure 73: POM photomicrograph of 15 at 29.5 °C upon cooling from the isotropic liquid at 1 °Cmin⁻¹

Upon cooling **15** from the isotropic liquid a grainy birefringent texture develops (Figure 73). This texture does not immediately identify the phase, although upon rotation of the microscope stage the birefringence colour changes dramatically. This indicates that the phase must be chiral and the change of colour due to the selective reflection of light by the chiral phase. Given that the phase shows no signs of developing a focal-conic texture and upon shearing no oily streaks are visible it is likely the phase is not smectic in nature. As such the phase can be tentatively assigned as a N* phase. A similar texture has been observed in polyhedral octasilsesquioxanes substituted with this mesogen¹²⁵.

4.3.3.3 Comparison

Compounds **12**, **13**, **14** and **15** allow us to directly compare the effect of lateral versus terminal attachment of the mesogenic moiety and the effect of either a methyl or phenyl substituted carborane cage. Upon inspection of the thermal properties of the end-on materials, **12** and **13** with the side-on materials **14** and **15**, one obvious difference stands out, the end-on materials more readily crystallize. Upon cooling at $10\text{ }^{\circ}\text{Cmin}^{-1}$ both **12** and **13** crystallize whereas **14** and **15** eventually freeze their monotropic N* phases into a glass. Further evidence of the end-on materials having more stable crystalline forms is given by the melting points, which are consistently higher for the end-on versus side-on materials.



*Figure 74: Molecular models of **12** (top) and **14** (bottom), hydrogens omitted for clarity*

This behaviour can be easily explained. The end-on materials present a molecular shape with the carborane in plane with the mesogenic core (Figure 74 top), better fitting to the traditional calamitic shape, thus allowing for easier close-packing and

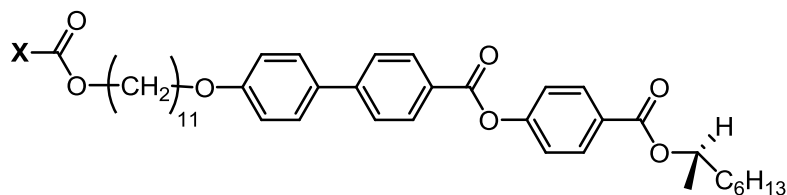
crystallization. In contrast, the side-on materials have a relatively large bulky group which is perpendicular with the mesogenic core (Figure 74 bottom) resulting in it being more difficult for them to close-pack and crystallize.

On comparison of the methyl-substituted **12** and **14** with the phenyl-substituted **13** and **15** another trend stands out. Firstly both methyl-substituted materials have higher melting points than their phenyl-substituted counterparts, which is in agreement with the trend observed for other mono-substituted carboranes presented thus far. Also the Iso-N* phase transition for methyl-substituted materials is higher than that of the corresponding phenyl-substituted materials. This suggests, as was presented in Chapter 3, that the phenyl-substitution of the carborane cluster has a greater destabilizing effect upon the mesomorphic properties of the mesogen than that of methyl-substitution.

This behaviour appears logical, the greater the steric bulk included outside of the longitudinal rotational volume of the mesogenic core the greater the destabilization to any mesomorphic properties displayed. This is in keeping with the trend observed for mesogens with a terminal carbocyclic unit¹⁰¹ (Figure 75), albeit with a mesogenic core different to that used in this work. This effect is likely caused by bulky terminal groups interfering with core-core interactions between the mesogenic moieties. As the steric bulk increases, so does the disruption caused to these intermolecular forces and so phase stability falls.

Upon addition of the carborane cluster to mesogens **18** and **19** the melting point both cases is depressed. This is broadly in agreement with the trend observed for both the two-ring and three-ring systems presented in this chapter. It can also be noted that the side-on mesogen **19** has a lower melting point than the end-on mesogen **18** and that this is still the case after attachment of either of the carborane clusters. This suggests that the factors resulting in this pattern of behaviour are not altered by the presence of the carborane but rather are accentuated by it, namely the deviation from a rod-like molecular shape resulting in a lower melting point. This lowering of the melting point is again likely due to the greater steric bulk of the carborane hindering the formation of ordered crystalline phases.

Chapter 4: Mono-functional Silanes

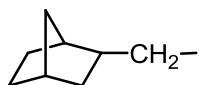


X =

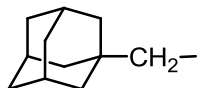
Transition Temperatures



Cr 48.1 SmC_A* 77.8 SmC* 91.1 SmA* 95.6 I



Cr 53.9 SmX* 59.7 SmC_A* 71.5 I



Cr 45.7 (SmC_A* 40.0) SmC* 57.4 I

Figure 75: Mesogens with a carbocyclic terminal group¹⁰¹

Finally it is interesting to note that compounds **12** - **15** display the nematic phase. Until this point we had only observed SmA phases once a carborane cluster had been attached to the mesogen. Given that the mesogens **18** and **19** are strongly nematogenic this is an expected result and in fact was an intentional aim of the use of this mesogen. That being said the fact that the N phase is still formed means that the microphase segregation caused by either the silane, cluster or both is not so strong as to completely suppress all N phases.

Other than the phase stability, which is decreased, it appears as if the presence of the carborane has little effect on the N phase or on its chiral modification. If one separates the cluster-cluster interactions and the cluster-mesogen interactions the reason for this appears intuitive. The cluster-mesogen interactions seem to be destabilizing, possibly as a result of the clusters steric hindrance perturbing core-core interactions between the mesogens. The cluster-cluster interactions however, are still not well understood and as such we are unable to say whether they are positive in terms of mesophase stability or negative. On the other hand, as there are no layer interfaces where the clusters are likely to interact with one another in the N* phase

the contributions to phase stability resulting from cluster-cluster interactions are likely to be minimal. Therefore the only effect the carborane cluster has on the N* phase is to destabilize it.

4.4 Concluding Remarks

In this chapter the synthesis and thermal properties of a series of carboranes mono-functionalized with mesogenic moieties comprising of two-, three- or four-ring systems attached in either a lateral or terminal mode has been detailed. It has been shown that the mesogenic moiety must comprise at least three rings in order for mono-functionalized carboranes to form mesophases. Additionally it has been demonstrated that terminally attached mesogens are more likely to result in mesomorphism and that any phases generated by terminally attached mesogens are likely to be more stable than their laterally attached counterparts.

The fact that all of the phases generated were monotropic or very weakly enantiotropic suggests that even with the increased molecular anisotropy of larger four-ring mesogens the carborane cluster still has a significant destabilizing effect on mesomorphic properties. However, this was expected as other work involving the functionalization of different clusters with mesogens typically shows that at least two mesogens are required if not more^{112, 126} to generate LC properties. The fact any mesomorphism is displayed at all with a single mesogen is notable in functionalized cluster systems, although not outside of expectations given the relative size of the clusters involved. To our knowledge compound **11** is the first inorganic cluster containing supermolecular liquid crystal which displays an enantiotropic LC phase with just one mesogen attached.

The change of siloxane linkage between the cluster and the mesogen to a silane linkage has eliminated the problem of branching in the final hydrosilylation step. This has allowed the synthesis of materials which, unlike in Chapter 3, do not contain a mixture of isomers. This means that the conclusions drawn are based upon the thermal properties of the materials presented and any resulting trends only on the effects of the carboranes and mesogens employed.

5. Multi-functional Silanes

5.1 Summary

In this chapter a series of carboranes functionalized with multiple mesogenic moieties which employ a silane linker will be presented. As in the previous chapter the silane linker was chosen to eliminate the problem of branched isomers encountered in Chapter 3. Furthermore the use of the same linker as the mono-functional silanes described previously facilitates comparison of properties.

In this chapter the same mesogenic units were used as in the mono-functionalized carborane silanes in order to aid comparison. The mode of attachment of the mesogen is varied, lateral versus terminal attachment in order to modulate the mesophase type encountered. Additionally in this chapter the effect of the mode of attachment at the carborane itself is investigated. The mesogens are attached either directly to the cluster at two different points resulting in materials akin to LC dimers (structural motif **I** Figure 76), or joined to the focal point of dendron-type structures, where the branching units are used to control the number of mesogens incorporated (structural motif **J** and **K**), Figure 76).

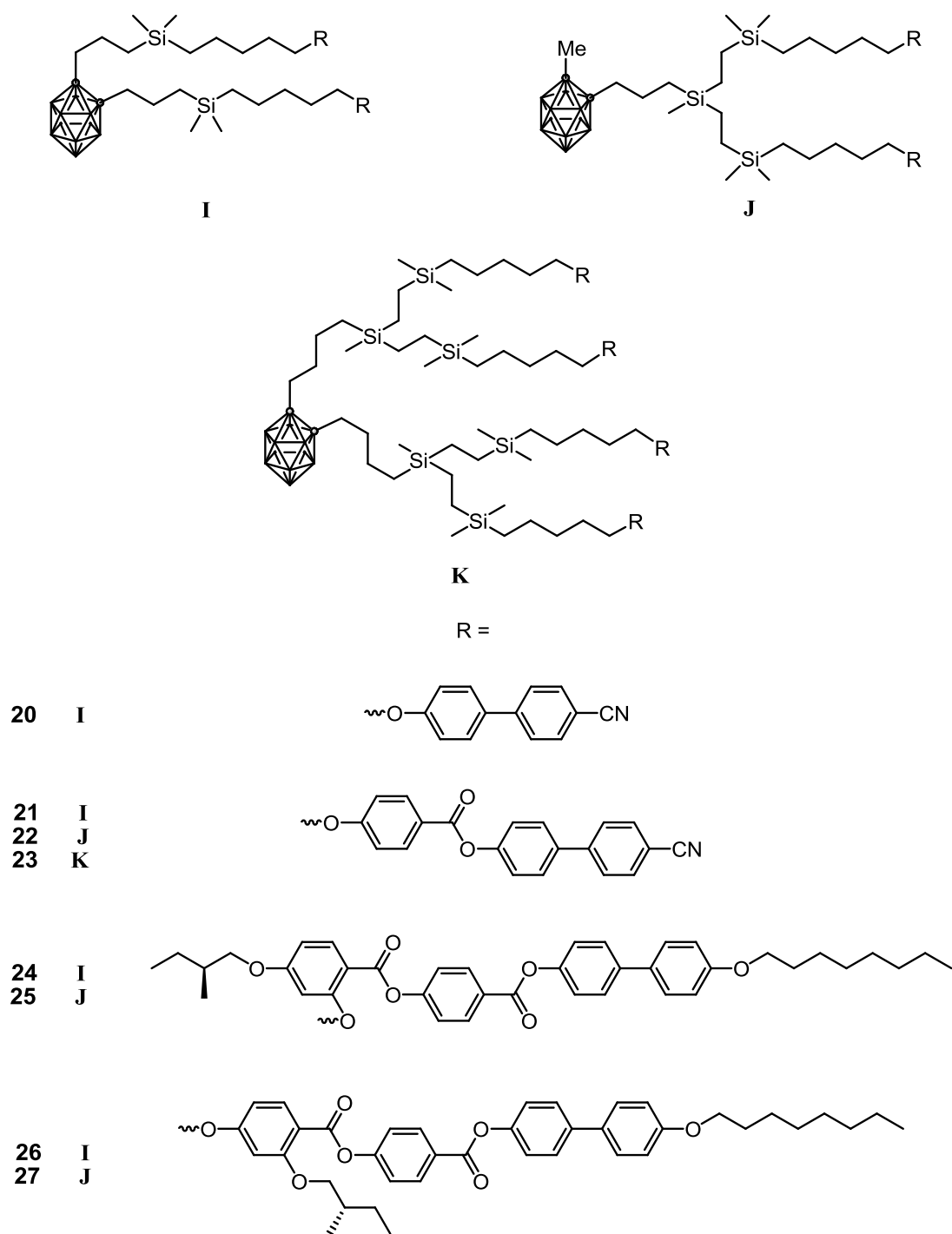


Figure 76: Multipedal carboranes functionalized with pro-mesogenic moieties

5.2 Synthesis

The functionalized multipedal carboranes were synthesized using procedures similar to those described for the monomeric carboranes presented in the previous chapter.

Chapter 5: Multi-functional Silanes

The mesogens used in this chapter are the same as those utilized in Chapter 4 and will not be discussed further (Figure 77).

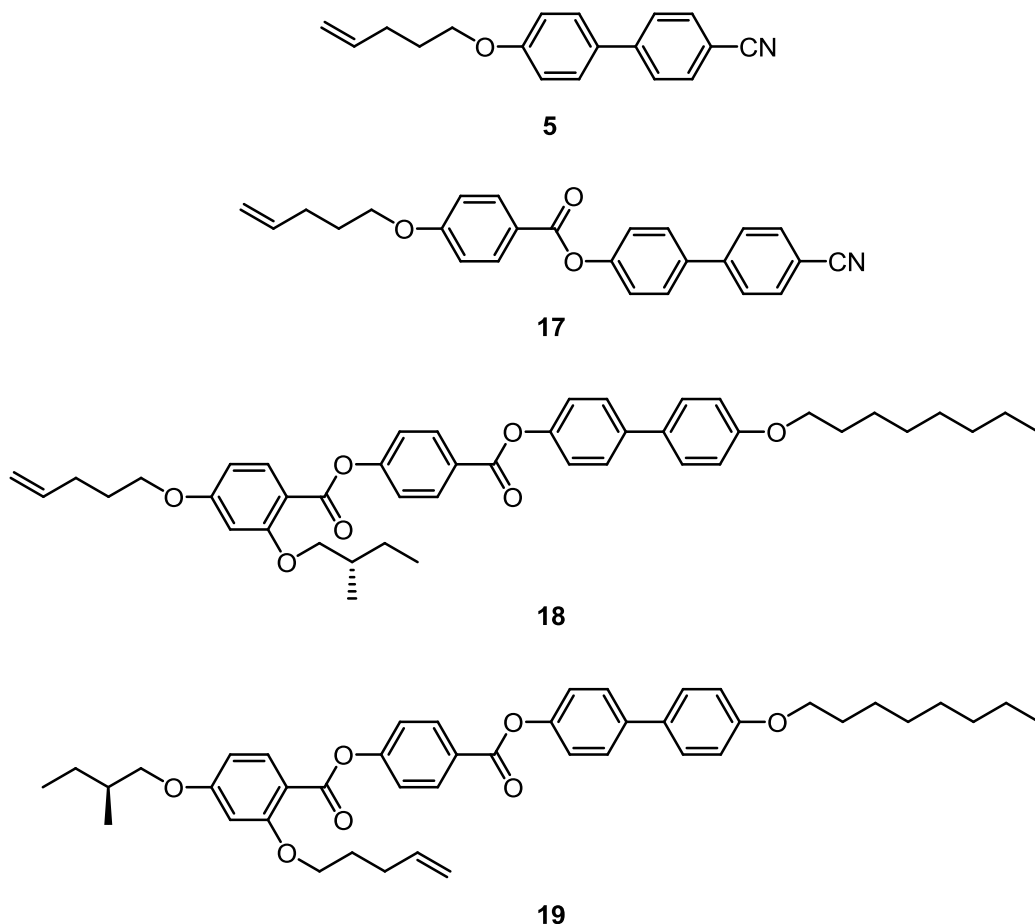
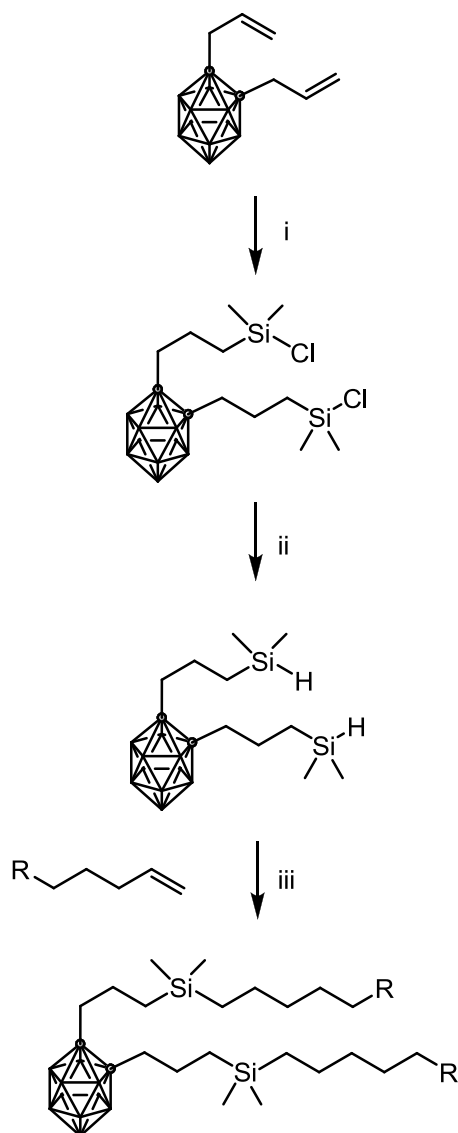


Figure 77: The structures of the alkenyl mesogenic moieties **5**¹¹⁷, **17**¹¹⁸, **18**¹¹⁹ and **19**¹²⁰

The bifunctionalized carboranes, **20**, **21**, **24** and **26**, with the structural motif, **I** (Figure 76), were synthesized according to Scheme 5. This is a similar synthetic procedure to that used to synthesize the mono-functionalized carboranes in the previous chapter, except that two equivalents of all the reagents were used to functionalize both allyl arms of the starting carborane.



20, 21, 24 and 26

- i) Dimethylchlorosilane, Karstedt's catalyst and dry low sulphur toluene
- ii) LiAlH_4 and THF
- iii) Karstedt's catalyst and dry low sulphur toluene

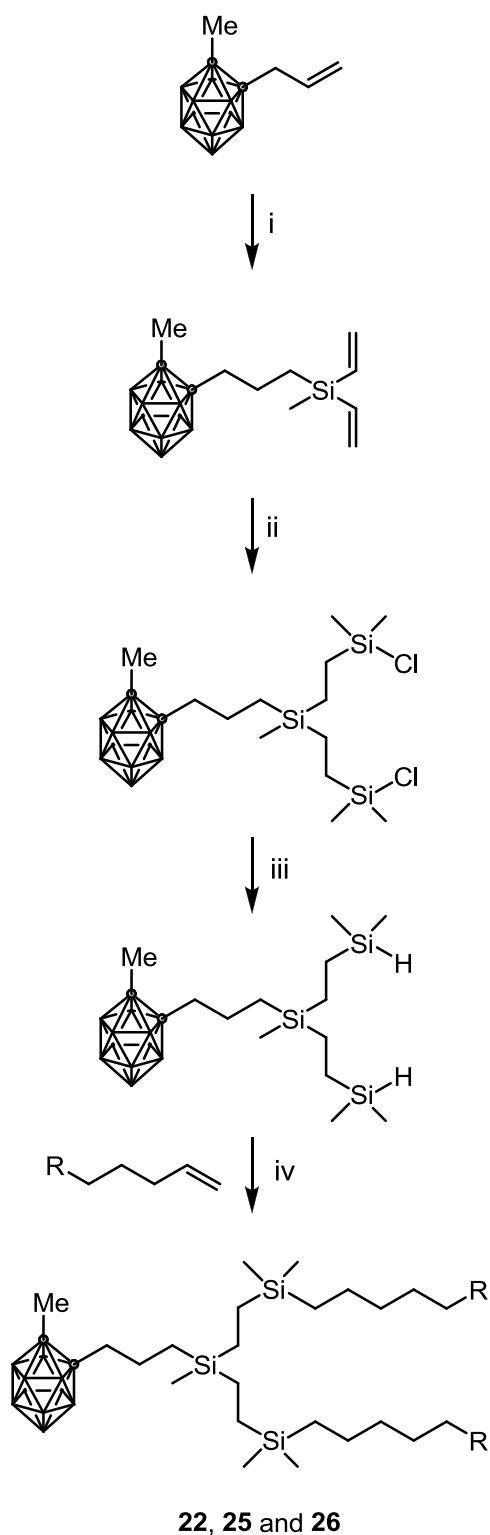
Scheme 5: Synthesis for the bifunctionalized carboranes 20, 21, 24 and 26, functionalized with pro-mesogenic moieties using the structural motif I

As with the mono-functionalized carboranes from Chapter 4 the first step of the reaction was monitored by ^1H NMR. When the resonances associated with the alkene moiety at ~ 5.6 , 5.0 and 4.7 ppm disappeared the reaction was deemed to be over. The presence of a quintet at 3.8 ppm in the ^1H NMR spectrum related to the SiH proton confirmed the successful reduction to the hydrosilane in step two. Furthermore the integration of this quintet, which was equal to two also provides

evidence for the reduction to the silane occurring completely on both arms of the molecule.

^1H NMR confirmed the successful completion of the final reaction in Scheme 5 by the disappearance of the resonances between 5 and 6 ppm associated with alkenyl protons of the unreacted mesogen. Additionally new resonances, a multiplet at 0.5 ppm and a singlet at 0.0 ppm, appear in the ^1H NMR spectra, associated with the CH_2Si and the CH_3Si respectively. Furthermore, in the boron decoupled ^1H NMR spectra there are three broad singlets at 2.7, 2.4 and 2.3 ppm associated with the BH protons similar to as observed for the clusters described in previous chapters. Finally the ^{29}Si NMR spectra confirmed the presence of just one silicon environment in the final compounds with a singlet at around 2.9 ppm.

The synthesis of compound **26** was carried out. However, owing to the small amount of starting material available and difficulties during purification it was not possible to obtain a sample for further analysis. Furthermore, owing to time limitations it was not possible to obtain or synthesize more starting material in order to re-attempt the synthesis. As such **26** will not be discussed further.



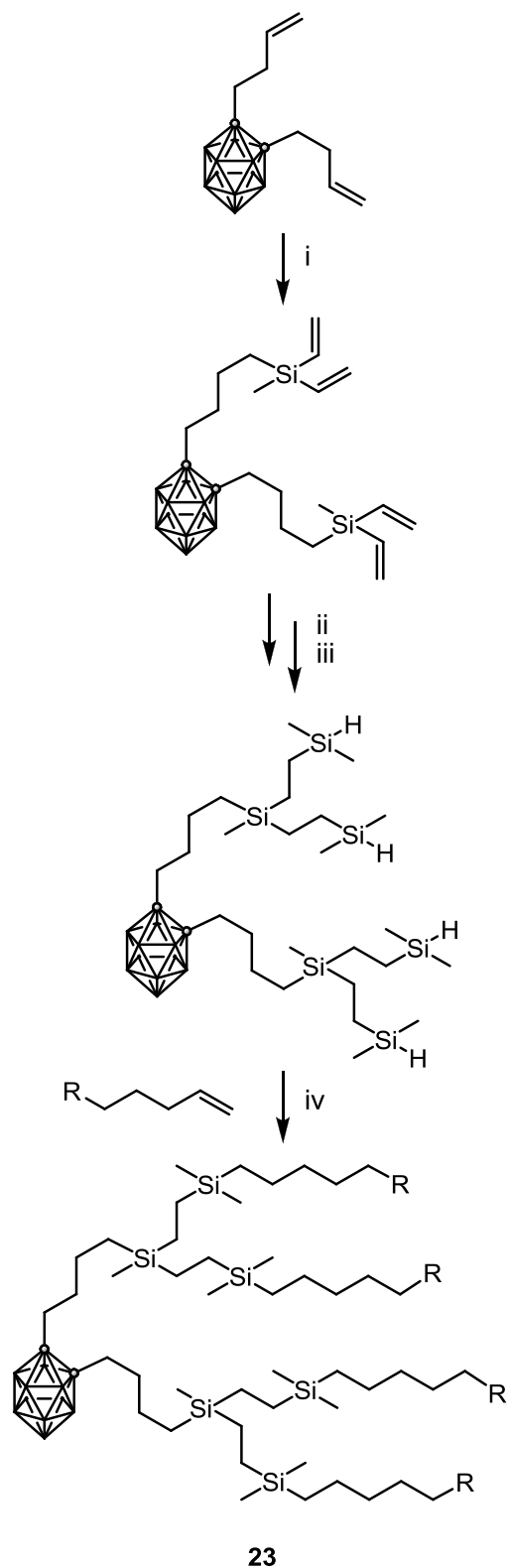
- i) Divinylmethylsilane, Karstedt's catalyst and dry low sulphur toluene
- ii) Dimethylchlorosilane, Karstedt's catalyst and dry low sulphur toluene
- iii) LiAlH_4 and THF
- iv) Karstedt's catalyst and dry low sulphur toluene

Scheme 6: Synthesis of the bifunctionalized carboranes 22, 25 and 26, functionalized with mesogenic moieties based on structural motif J

Chapter 5: Multi-functional Silanes

The bifunctionalized carboranes based on structural motif **J** (Figure 76) were synthesized according to Scheme 6. The first step, as in Scheme 5, is the hydrosilylation with Karstedt's catalyst. However in Scheme 6 divinylmethylsilane is used instead of dimethylchlorosilane, this allows the bifurcation of the arm and thus provides the basis of the branching unit. Steps ii and iii are similar to those utilizing motif **I**, with hydrosilylation with dimethylchlorosilane, followed by reduction and then finally another hydrosilylation to adjoin the mesogenic moieties. In all cases, the substituent on the *o*-carborane is the methyl group since the methyl-substituted materials in Chapter 4 had better mesomorphic properties than the phenyl-substituted derivatives.

The synthesis of the materials based on structural motif **J** up to step iii of Scheme 6 was carried out by Nuñez *et al* and the materials passed on to us for the final functionalization step. This steps completion was confirmed by a combination of ^1H , ^{13}C and ^{29}Si NMR in a similar manner to that of the materials based on structural motif **I**.



- i) Divinylmethylsilane, Karstedt's catalyst and dry low sulphur toluene
- ii) Dimethylchlorosilane, Karstedt's catalyst and dry low sulphur toluene
- iii) LiAlH_4 and THF
- iv) Karstedt's catalyst and dry low sulphur toluene

Scheme 7: Synthesis of carborane 23 functionalized with multiple mesogens based on structural motif C

The carborane **23**, tetra-functionalized with mesogenic moieties based on structural motif **K** (Figure 76), was prepared as shown in Scheme 7 which synthetically is a combination of those for structural motifs **I** and **J**. The carborane core supports a dendritic structure grown from the bis(3-butenyl) derivative by the hydrosilylation with methyldivinylsilane followed by reduction protocol as described for structural motifs **I** and **J**. Finally the hydrosilylation of **17** with the carborane core affords **23**.

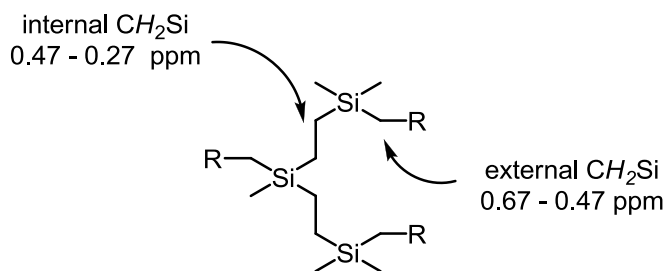


Figure 78: Internal vs external CH₂Si protons

The synthesis of **23**, based on structural motif **K**, up to step iii of Scheme 7 was carried out by Nuñez *et al* and the materials passed on to us for the final functionalization step. The successful completion of this step was confirmed by a combination of ¹H, ¹³C and ²⁹Si NMR. The ¹H NMR spectrum for **23** shows two separate environments for the CH₂Si protons (Figure 78). The protons which are inbetween the two silicon atoms show a multiplet between 0.47 and 0.27 ppm whereas the protons external to the two silicon atoms show a multiplet between 0.67 to 0.47 ppm. The order of these multiplets was deduced from the integrations, with the external signal integrating to twelve protons and the internal integrating to sixteen protons. In addition the ¹H NMR spectrum also showed a new resonance, a multiplet between 0.16 to -0.16 ppm which is associated with the CH₃Si protons.

The ¹³C NMR spectrum interestingly only showed two environments for the CH₃Si carbons. The first at -3.75 ppm which we attribute to the CH₃Si carbons attached to the silicon atoms closest to the mesogens. The second resonance at -6.0 ppm is related to the CH₃Si carbons closest to the cluster. It was possible to differentiate which of the resonances was associated with which carbons based on the relative intensities of the resonances. Although the ¹³C NMR experiments which were carried out are not able to provide quantitative analysis based on integrations, the significantly

more intense (roughly three times as intense) resonance was almost certainly from the environment containing eight carbon atoms rather than the one containing just two.

Silicon NMR provided a similar picture, with two separate environments, one associated with silicon atoms closest to the cluster which displayed a resonance at 6.7 ppm and another associated with silicon atoms closest to the mesogens with a resonance at 4.5 ppm. Like in the ^{13}C NMR spectrum the resonance associated with the silicon atoms closest the cluster was significantly less intense than the other. Finally MALDI mass spectrometry confirmed the molecular weight as 2262.15 $(\text{M}+\text{K})^+$, compared to a theoretical value of 2262.12 $(\text{M}+\text{K})^+$.

5.3 Thermal Properties

The thermal properties and phase behaviour of all the materials described were investigated with a combination of DSC and POM and are summarized in Table 5. The thermal properties and phase behaviour of the alkenyl mesogens (Figure 77) are summarized in Table 6 for the purposes of comparison.

Compound	Glass	Crystal	SmA	N	N*	Iso
20		•		(15.8 •)		79.7 •
21	•		21.9 •			182.8 •
22	•		18.0 •			180.8 •
23	•		21.2 •			164.7 •
24		•				48.2 •
25		•		54.8	•	61.1 •
27		•		63.2	•	63.5 •

Table 5: The thermal properties of the multipedal carboranes 20-27, functionalized with mesogenic moieties, as recorded by DSC with a heat/cool rate of $10\text{ }^{\circ}\text{Cmin}^{-1}$, values in brackets indicate monotropic transitions

Compound	Cr	N	N*	Iso
5	• 75.8	•	88.2	•
17	• 108.0	•	264.0	•
18	•	128.9	• 167.5	•
19	•	110.3	• 151.4	•

Table 6: The thermal properties of the alkenyl mesogens **5**¹¹⁷, **17**¹¹⁸, **18**¹¹⁹ and **19**¹²⁰, as recorded by DSC with a heat/cool rate of 10 °Cmin⁻¹

5.3.1 Two-Ring Systems

As in previous chapters the initial focus was on materials incorporating mesogens with a two-ring system, namely cyanobiphenyls. Compound **20**, unlike its mono-functionalized counterparts **8** and **9**, was found to be mesomorphic, albeit with a monotropic phase. The DSC trace of **20** shows an endotherm upon the first heat with onset at 79.7 °C ($\Delta H = 31.6 \text{ kJmol}^{-1}$) which corresponds to the melt into the isotropic fluid. Upon further heat/cool cycles the material showed two reproducible thermal events: the glass transition where the greatest rate of change in the heat capacity was at -1.6 °C and an endotherm with onset at 15.8 °C ($\Delta H = -2.3 \text{ kJmol}^{-1}$) associated with a LC – Iso liq. transition.

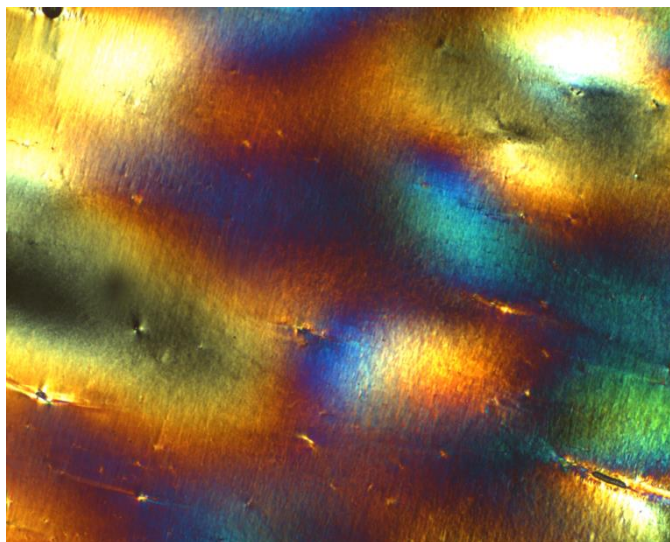


Figure 79: POM photomicrograph of **20** at 22.4 °C after cooling from the isotropic liquid at 1 °Cmin⁻¹ and shearing.

POM of **20** proved difficult owing to the nature of the monotropic phase near room temperature and the high viscosity of the material. This resulted in optically extinct homeotropically aligned or grainy textures which did not shear easily. However, upon shearing the grainy birefringent texture flashed and formed the texture shown in Figure 79. Upon further annealing the texture returned to the optically extinct homeotropically aligned texture. The absence of focal-conic defects and oily streaks upon shearing combined with the optically extinct homeotropic texture allows this phase to be assigned as a nematic phase.

The mono-functionalized carboranes **8** and **9**, with mesogen **5**, proved to be non-mesomorphic. Compound **20** with two mesogens of the same type illustrates that by increasing the number of mesogenic units LC properties can be introduced into the system. This is the same pattern of behaviour as observed in Chapter 3. A comparison of bifunctional siloxane, **3**, with **20** shows that both materials form monotropic LC phases of approximately the same range (~ 17 °C) and both occur near or below room temperature. However, the similarity ends there. Compound **3** shows the SmA phase whereas **20** shows the N phase, also **20** has a higher glass transition temperature and clearing point.

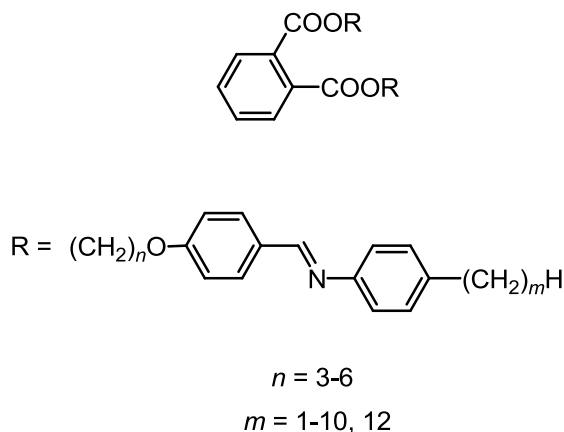


Figure 80: U-shaped LC dimers based on phthalic acid¹⁰⁶

Given that both materials have the same carborane core and the same mesogen the only cause for these differences has to be the nature of the linker and the absence of any branched isomers. Compound **3** has a tetramethyldisiloxane linker whereas compound **20** has a dimethylsilane linker. Siloxanes are bulkier and more polar than

silanes and are usually considered to promote microphase segregation more strongly. However, the tetramethyldisiloxane unit also results in a total spacer length which is two atoms longer. Typically increasing spacer chain-lengths stabilizes smectic phases. Thus, simply by increasing the spacer chain-length from compound **3** to compound **20**, the likelihood of a smectic phase is increased. Furthermore Douglass and Attard¹⁰⁶ noted that members of their U-shaped LC dimers family (Figure 80) with short spacers between the mesogen and focal point ($n = 3$) display the N phase so long as the terminal chains were not too long. Thus **20** displaying the N phase in comparison to **3**, which displays a smectic phase, is in keeping with these observations.

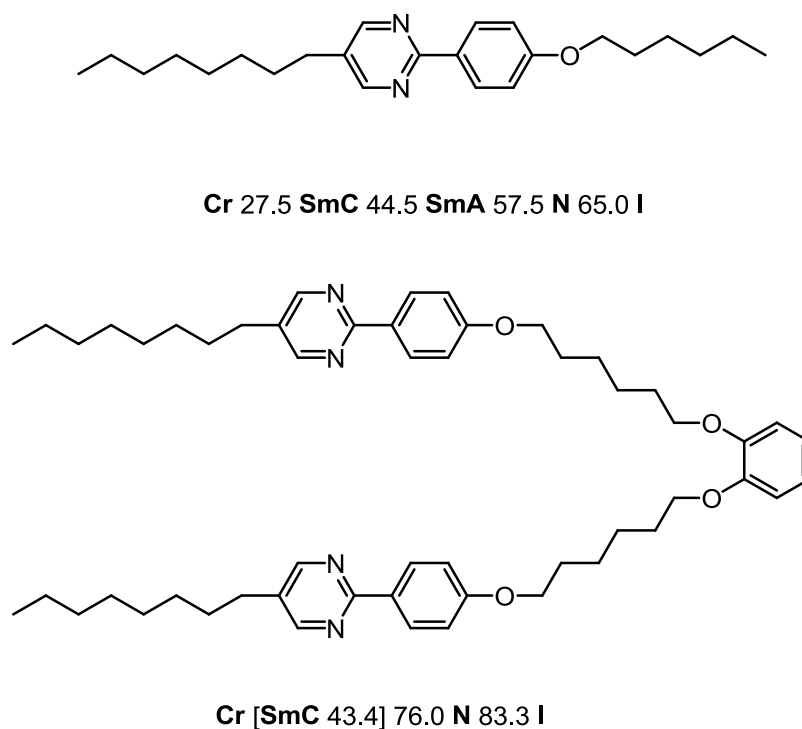


Figure 81: Phenyl pyrimidine dimer¹²⁷ and corresponding monomer¹²⁸

Figure 81 shows the thermal behaviour of a phenyl pyrimidine dimer based on catechol reported by Yamaguchi *et al*¹²⁷, with a topology related to that of materials derived from structural motif **I**, and the corresponding monomer¹²⁸. Comparison of their thermal properties and phase behaviour shows two effects upon tethering two mesogens together into a U-shaped dimer. Firstly the clearing point is increased by 18.3 °C and secondly the melting point is increased by 48.5 °C. The raising of the

clearing point can be explained by the mesogens behaving co-operatively thus stabilizing the mesophase in comparison to the monomer. The increase in the melting point however, is likely the result of the larger molecular mass. Finally the loss of the SmA phase is attributed to the greater excluded volume caused by packing of the dimers in the smectic layers. This results in the molecules tilting to minimize this excluded volume and thus the suppression of the SmA phase.

However, the clearing point of the dimer **20** is 8.5 °C lower than the monomer **5** implying that the *o*-carborane cluster causes more disruption to the mesophase than an *ortho*-substituted phenyl ring. Although as the change in isotropization temperatures is so small in both cases it is hard to draw any firm conclusions from this. The observation can be rationalized given that the phenyl focal point will likely display π -stacking behaviour with other phenyl focal points and the mesogenic cores which may help stabilize the phase and minimize the effect of tethering the mesogens together. The carborane cluster on the other hand lacks these stabilizing interactions, which coupled to its non-planar nature, results in a drop in phase stability. Finally, a comparison of the melting points of **20** and **5** shows that there is a slight increase when moving from the mesogen to the dimer. This is in keeping with the trend observed by Yamaguchi, although the effect observed in the carborane derivative is much smaller.

5.3.2 Three-Ring Systems

As in the previous chapter materials incorporating three-ring mesogenic systems were investigated next with the aim of generating enantiotropic phases. Furthermore the effect of the mode of attachment of the mesogens at the carborane was studied, rather than at the mesogen, by anchoring the same mesogenic units to the structural motifs **I**, **J** and **K**.

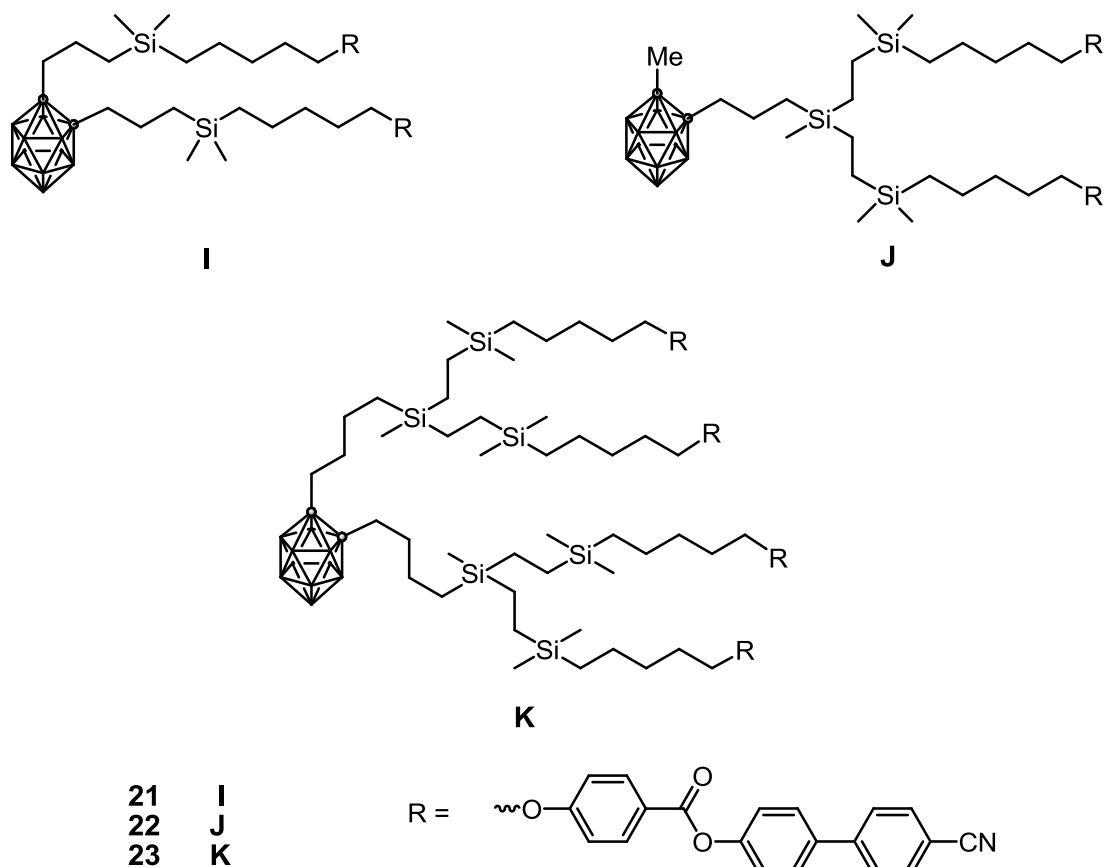


Figure 82: Structures of compounds 21, 22 and 23

Compound **21** incorporates two mesogens attached at two different points to the cluster and can be described as a generation 0 dendrimer with a di-functional focal point (Figure 82).

Compound **21** showed an enantiotropic SmA phase. The DSC trace of **21** shows two reproducible thermal events upon heating and cooling. The first is a glass transition where the greatest rate of change of the heat capacity was at 21.9 °C and the second an endotherm at 182.8 °C with ΔH of 6.8 kJmol⁻¹ (3.4 kJmol⁻¹ per mesogen). The POM of **21** upon cooling from the isotropic liquid showed the focal-conic texture (Figure 83) with clear sets of ellipses and hyperbolae of optical discontinuity and areas of homeotropic alignment which were optically extinct. Thus allowing this phase to be assigned as an enantiotropic SmA phase.



*Figure 83: The focal-conic texture of **21** at 187.7 °C after cooling from the isotropic liquid at 1 °Cmin⁻¹*

Compound **22** incorporates two mesogenic moieties which are attached to the cluster via a branching unit and can be described as derived from the 1st generation vinyl carborane dendrimer with a mono-functional focal point (Figure 82).

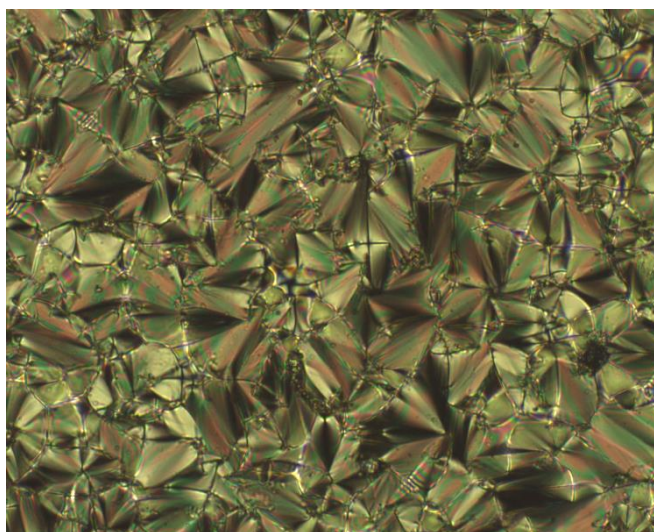


*Figure 84: Focal-conic texture of **22** at 173.6° C after cooling from the isotropic liquid at 1° Cmin⁻¹*

Compound **22** also showed an enantiotropic SmA phase. The DSC trace shows two reproducible thermal events. One being a glass transition where the fastest rate of change of the heat capacity was at 18.0 °C and the other an endotherm with onset at 180.8 °C and $\Delta H = 9.7 \text{ kJmol}^{-1}$ (4.9 kJmol^{-1} per mesogen). Upon cooling from the

isotropic liquid the material displayed a focal-conic texture (Figure 84) with clear sets of ellipses and hyperbole of optical discontinuity allowing this phase to be assigned as SmA.

In compound **23** we increased the number of mesogens incorporated from two to four. The material employs elements of both structural motifs **I** and **J** and can be described as a generation 1 dendrimer with a di-functional focal point (Figure 82).

The DSC trace of **23** showed two reproducible thermal events. The first is a glass transition where the greatest rate of change of the heat capacity is at 21.2 °C and the second is a broad endotherm with onset at 164.7 °C and $\Delta H = 14.7 \text{ kJmol}^{-1}$ (3.7 kJmol^{-1} per mesogen). POM showed that upon cooling from the isotropic liquid a focal-conic texture developed (Figure 85) showing clear sets of ellipses and hyperbolae of optical discontinuity and areas of homeotropic alignment which were optically extinct. This allows this phase to be assigned as an enantiotropic SmA phase.

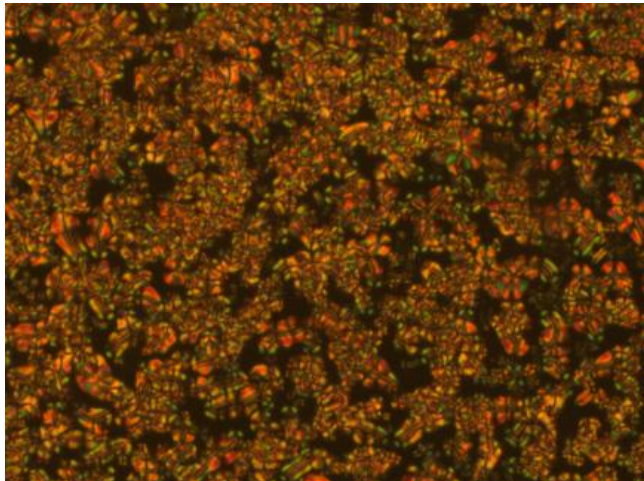


*Figure 85: The focal-conic texture of **23** at 190.6° C after cooling from the isotropic liquid at 3 °Cmin⁻¹*

5.3.2.1 Phase Structure

The structure of the SmA phases of compounds **21**, **22** and **23** are likely to be very similar both to each other and to those of compounds **3** and **4**. The two options are microphase segregation occurs, in which case either a SmA_d or SmA₂ phase (Figure

86 top) will be formed, or it does not and a SmA_1 phase is formed (Figure 86 bottom). As was discussed in Chapter 3 X-ray diffraction experiments would confirm which phase is formed. On balance however, given what was learned from the X-ray and neutron experiments carried out on **4** and from other similar systems within the literature; such as Deschenaux *et al*'s fullerodendrimers¹¹⁰ (discussed in Chapter 3) and Douglass and Attard's U-shaped mesogens (Figure 80)¹⁰⁶, the most likely phase is the SmA_d . In reality these phases would be much more disordered than those shown in Figure 86, they are drawn in this way for clarity.

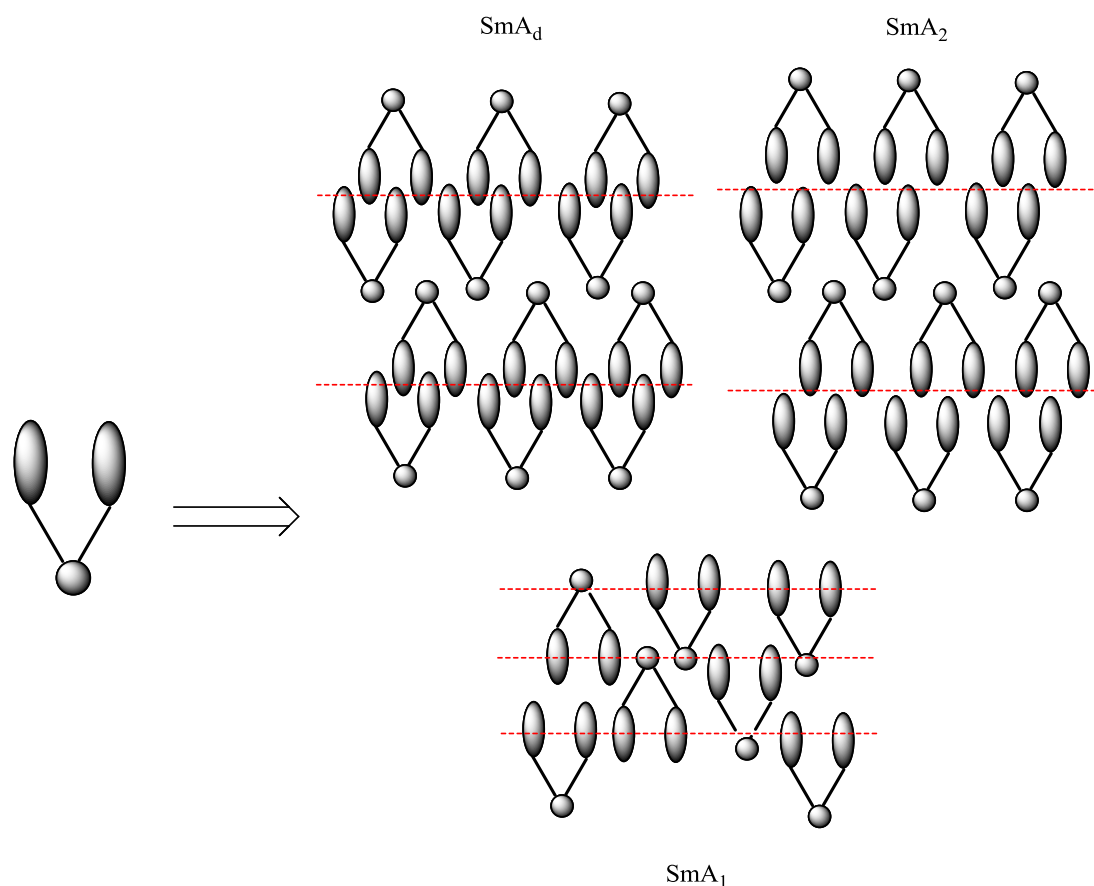


Figure 86: Schematic diagram of the possible smectic A phases of U-shaped LC dimers

There may however be another possibility. If microphase segregation does occur and the dimers are also effectively confined to one layer and not freely able to move between layers, as is the case in smectic phases, the system may be described as a 1D crystal. Such a material would be characterized by a periodic lattice in only one dimension, in this case the alternating layers of aromatic and carboranyl/alkyl

density. If a 1D crystal is formed it would be expected that there would be many higher order diffractions peaks associated with the layer spacing observable in the XRD pattern of this phase.

5.3.2.2 Comparison

Firstly, it is worth noting that none of the materials retained the same type of mesophase as the mesogenic moiety. This can be explained by the molecular topology. The cluster forces the mesogens to nanosegregate, as discussed in Chapter 3 in regards to compound **3**, which aids in the formation of layers. This is also in keeping with the other materials presented thus far. Furthermore it suggests that the cluster greatly affects the phase behaviour of the material as a whole by enforcing a specific molecular shape and by reducing the conformational freedom of the mesogens.

Yoshizawa produced a series of LC oligomers with cyanobiphenyl terminated arms connected to a focal point with a perfluorinated chain¹²⁹ (Figure 87). This system bears some resemblance to **20**, **21** and **22**, in particular the oligomer functionalized with two mesogens, as all these materials have two CB based mesogens which are held in a U-shaped topology connected to an incompatible molecular component. Yoshizawa found that the dimer formed a columnar phase followed by a SmA phase. The SmA phase reported was investigated with X-ray diffraction and was found to have a very similar structure to that which we have proposed for the SmA phases of the three-ring mesogen systems, namely a SmA_d in which there is segregation of the incompatible molecular unit between layers of interdigitated mesogens.

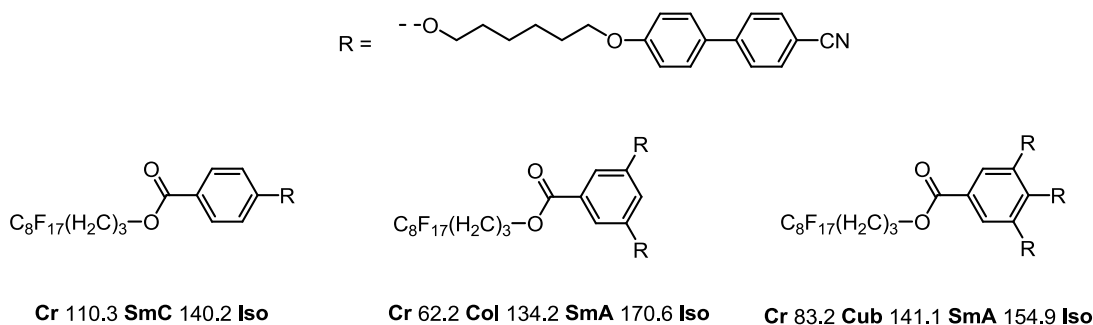


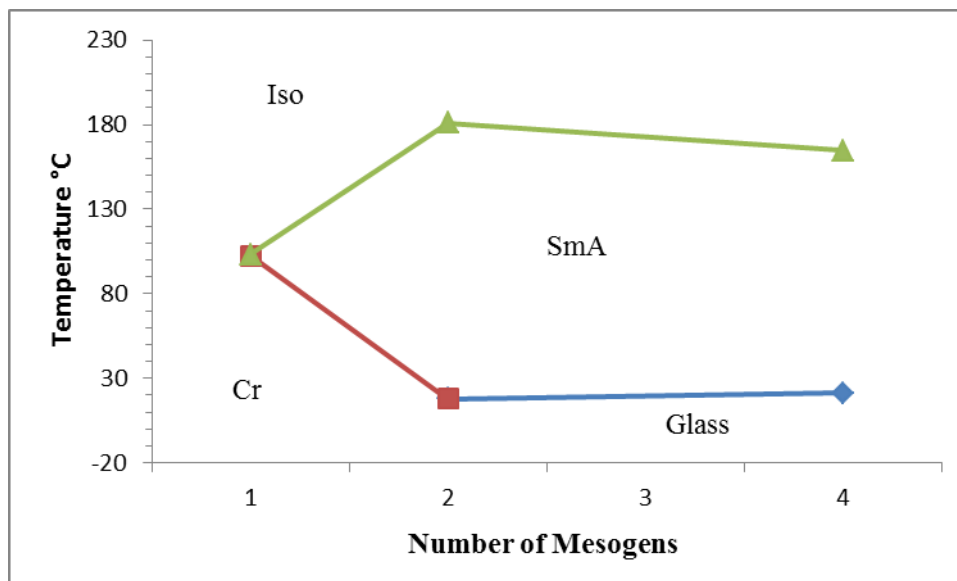
Figure 87: Amphiphilic LC oligomers¹²⁹

However there were no observed columnar phases in the materials presented thus far. A simple explanation can be made for this based on how deformable the segregating aspect of the molecule is and how strong the segregation is. In the Yoshizawa system the perfluorinated chains are far more deformable than that of the carborane/silane linkers and impose stronger segregation. This allows them to deform and form the interior of the columns in the low temperature columnar phase. It is simply not possible for the carborane to do this and as such only the smectic behaviour is observed.

Furthermore, it is also worth noting that compound **20**, which is the most similar to Yoshizawa's dimer (Figure 87 centre) of the materials presented so far given that it also has CB mesogens, displays only a monotropic N phase. This suggests that the smectogenic properties of the three-ring dimers **21** and **22** are more likely the result of the change in mesogen. The carborane and silane linkers cannot be as powerful a driver of microphase segregation as the perfluoro chain. This may be due to the relative sizes of the carborane versus perfluoro moieties and the relative differences in polarity.

Upon moving from the two-ring mesogenic system **20**, to the three-ring systems **21** and **22**, the materials' LC behaviour went from being monotropic to enantiotropic. This is exactly as expected and as was observed in previous chapters. A simple argument can be made to explain this. The three-ring mesogen imparts a higher degree of molecular anisotropy to the system than the two-ring mesogen resulting in more stable mesophases.

By attaching two mesogens to the carborane cluster, as in materials **21** and **22**, an increase in the phase stability is achieved with an increase in the isotropization point of around 80 °C in comparison to the mono-functionalized carborane **11** (Graph 1). This can be explained by the increasing number of mesogens being more able to compensate for the destabilizing effect of the carborane cluster. This observation is in keeping with the other carborane dimers presented.



Graph 1: The effect of the number of mesogens on phase stability (1 = **11**, 2 = **22** and 4 = **23**)

Compound **23** shows a large increase in phase stability, as measured by isotropization temperature, in comparison to the mono-functional carborane **11** (~60 °C), and a small decrease in comparison to **21** and **22** (~15 °C). This shows that the increase in phase stability is not linear with the number of mesogens (Graph 1). The mesogens must still be working cooperatively to generate the large increase in phase stability in comparison to **11**; however the cumulative effect for **23** must be smaller than that for **21** and **22**. This indicates that there is an optimal amount of dendritic branching that can be accommodated, related to the relative cross-sectional area of the carborane and silane branching moieties and the cross-sectional area of the mesogens. Too many mesogens and the molecule will develop a distinct tapered shape which would not pack efficiently and thus result in a less stable phase. Too few mesogens and there is not enough molecular anisotropy to counteract the destabilizing effect of the carborane cluster, again resulting in a less stable phase.

The bifunctionalized materials presented in this chapter so far can be described as U-shaped mesogens⁴⁴. They are in fact very similar to materials reported by Attard and Douglass¹⁰⁶ (Figure 80) which were based on an *ortho*-substituted phenyl ring as the focal point. However the phenyl ring, unlike the carborane, would be able to mix with the mesogenic units thus resulting in a less segregated system. Therefore the phase behaviour in Douglass and Attard's materials is not likely to be affected by

microphase segregation as much as the dimers presented here. Interestingly though the parity and length of the spacer had a strong effect upon the polymorphism of Douglass and Attard's materials. This is an avenue to be explored in further work on these systems.

5.3.3 Four-Ring Systems

As in the previous chapter, materials incorporating mesogens comprising of four-rings were investigated next. Furthermore both the mode of attachment was studied both at the carborane using structural motifs **I** and **J**, and also at the mesogen *via* lateral or terminal attachment. Again the same mesogens as in Chapter 4 were chosen for ease of comparison.

Compound **24** based on structural motif **I** with two laterally attached mesogens was found to be non-mesomorphic (Figure 88). The DSC trace upon the first heat showed a broad endotherm with onset at 48.2 °C and $\Delta H = 37.3 \text{ kJmol}^{-1}$. Upon further heating and cooling cycles the DSC trace showed a glass transition where the greatest rate of change in the heat capacity was at -2.2 °C. POM showed no traces of birefringent textures typical of mesomorphic behaviour.

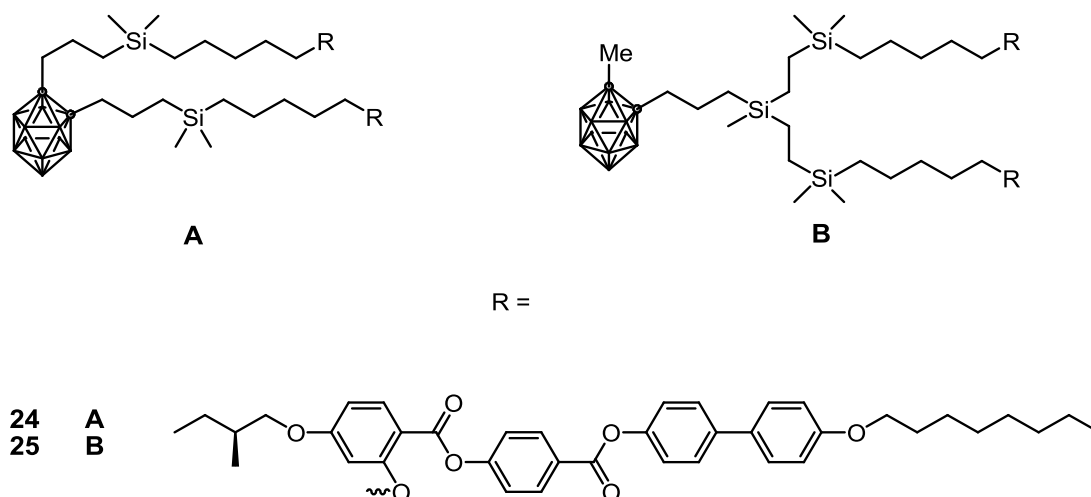
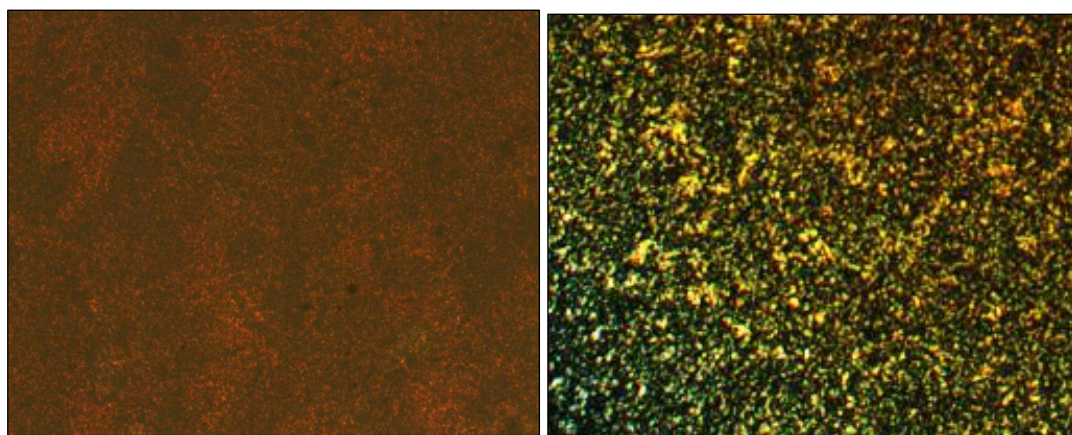


Figure 88: Structures of compounds **24** and **25**

Compound **25** was found to be mesomorphic. It is based on structural motif **J** and has two laterally attached mesogens (Figure 88). The DSC trace shows a large endotherm upon the first heating with onset at 54.8 °C ($\Delta H = 39.5 \text{ kJmol}^{-1}$), which is associated with the melting of the material. Upon subsequent heat/cool cycles there were two reproducible thermal events: a glass transition where the greatest rate of change in the heat capacity was at 9.0 °C followed by a small endotherm with onset at 61.1 °C ($\Delta H = 0.9 \text{ kJmol}^{-1}$) associated with a LC-Iso liq. transition.



*Figure 89: POM micrographs of: left) Grandjean plane texture of **25** at 50.0 °C upon cooling from the isotropic fluid at 1 °Cmin⁻¹ and annealing for 1 week; right) the pseudo focal-conic texture of **25** at 50.0 °C after cooling from the isotropic fluid at 1 °Cmin⁻¹ and annealing for 1 week*

As with the other four-ring systems the POM of **25** proved challenging; the material is highly viscous, resulting in grainy textures which had to be annealed for a week. Upon cooling from the isotropic liquid it was possible to generate both the Grandjean plane and pseudo focal-conic textures of the N* phase (Figure 89). The materials non-symmetrical molecular shape hinders the crystallization process, which is reflected in the ability to anneal it in the chiral nematic phase below its melting point for long periods of time without sign of crystallization.

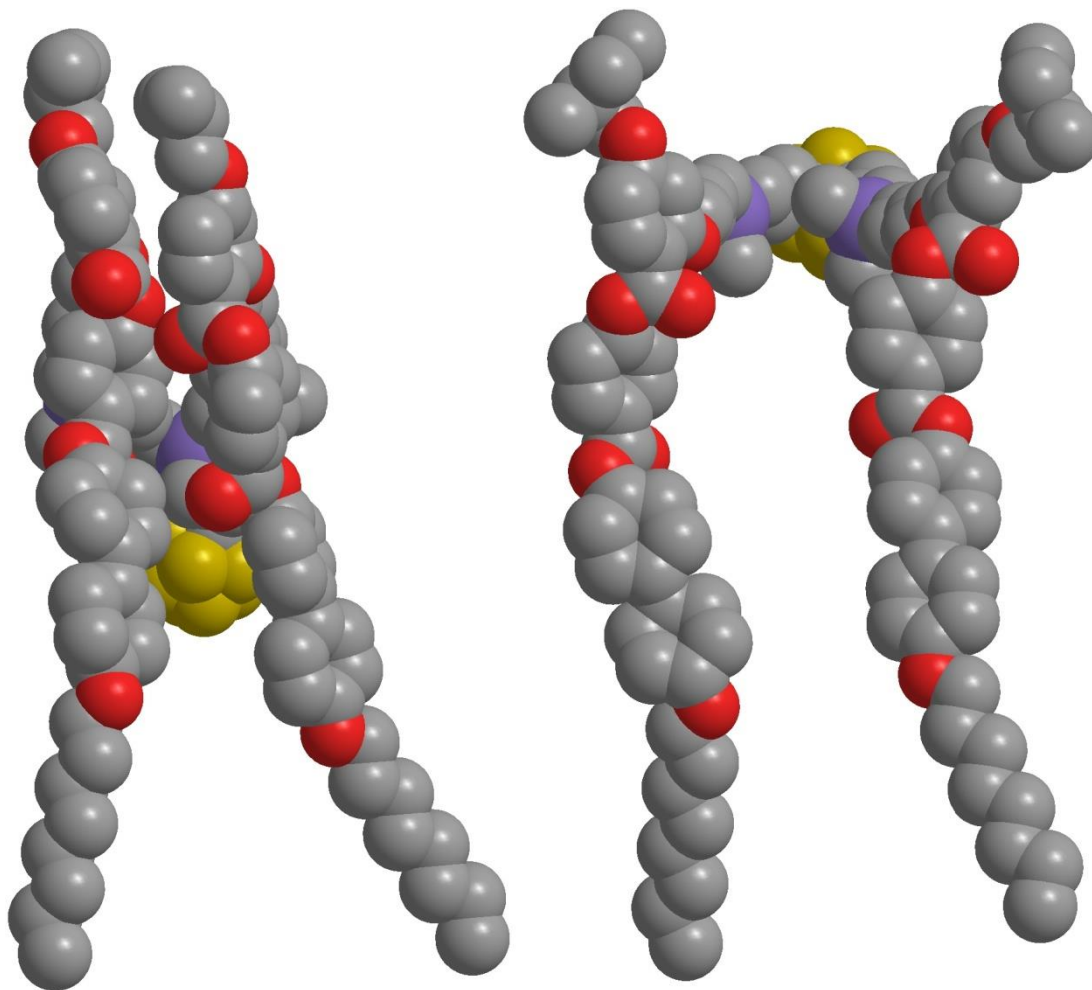


Figure 90: Structural models of **24** (right) and **25** (left), hydrogens omitted for clarity

It is interesting to note that **24** using structural motif **I** is non-mesomorphic whereas **25** using structural motif **J** is. Very little difference in mesomorphic behaviour was found between the two structural motifs when using terminally attached mesogens, **21** and **22**. It could be speculated that because of the larger size of the mesogen and its lateral attachment a greater frustration is caused when trying to pack and/or align to form the mesophase. Thus changes to the mode of attachment at the core cause a greater destabilizing effect upon the materials phase behaviour. As can be seen in Figure 90, **24** with structural motif **I**, results in poorer packing of the mesogens than **25** with structural motif **J**, and demonstrates the effect of the mode of attachment at the core to the overall molecular shape which has a great impact on mesomorphic behaviour.

It could also be argued that the overall spacer length between the carborane core and the mesogen is longer (twelve units) in **25** than in **24** (nine units) which may allow better decoupling of the mesogens motions from the core, allowing mesomorphic behaviour to appear.

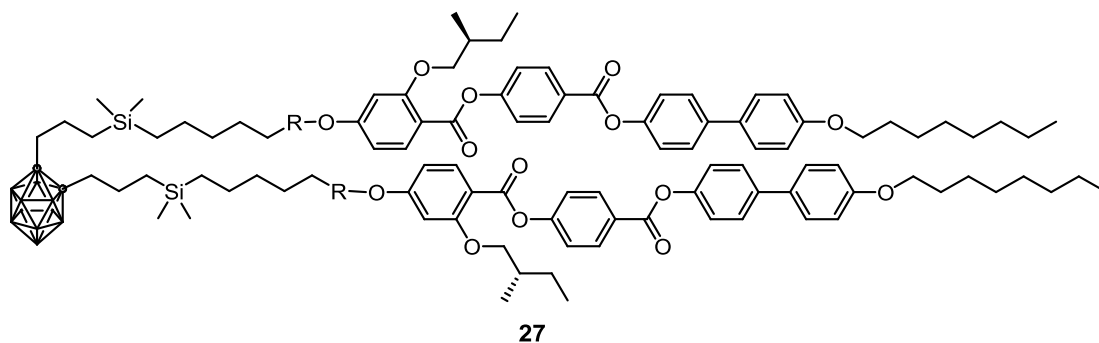


Figure 91: Structure of compound **27**

Compound **27** using structural motif **J**, has two terminally attached four-ring chiral mesogens (Figure 91). The DSC trace (Figure 92) shows two reproducible thermal events on heating, the first is a large endotherm with onset at 63.2 °C ($\Delta H = 24.5 \text{ kJmol}^{-1}$) due to melting and a smaller endotherm with onset at 63.5 °C ($\Delta H = 6.7 \text{ kJmol}^{-1}$) due to a LC-Iso liq transition. Upon cooling only one thermal event occurs, a large exotherm with onset at 58.3 °C ($\Delta H = -29.6 \text{ kJmol}^{-1}$) due to a supercooled crystallization. The lack of an Iso-LC transition on cooling in the DSC trace of **27** suggests that the transition must be very weakly first order.

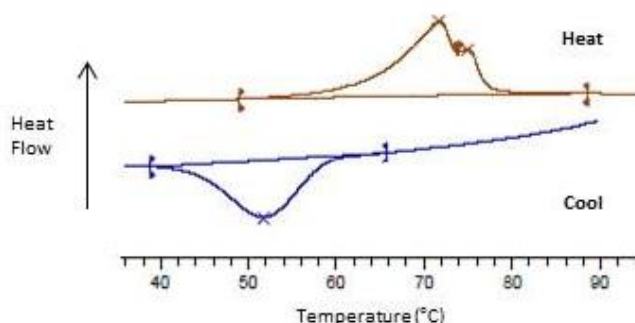
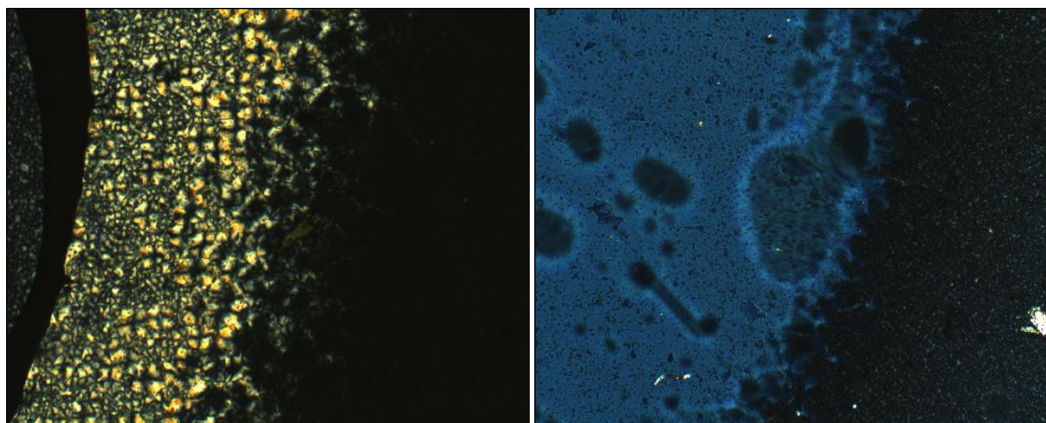


Figure 92: DSC trace of compound **27**



*Figure 93: POM micrographs of: left) the pseudo focal-conic texture of **27** at 50.2 °C upon cooling from the isotropic fluid at 1 °Cmin⁻¹ and annealing for 2 days; right) the Grandjean plane texture of **27** at 55.4 °C upon cooling from the isotropic fluid at 2 °Cmin⁻¹*

Upon cooling **27** from the isotropic liquid POM showed the Grandjean plane texture develop (Figure 93 right). After annealing for two days the pseudo focal-conic texture was evident (Figure 93 left). These facts combined allow this phase to be assigned as the as N* phase.

5.3.3.1 Comparison

As in the previous chapter the effect that lateral versus terminal attachment of the mesogen has on the materials mesomorphic behaviour was investigated. Comparison of **25** (lateral attachment, motif **J**) and **27** (terminal attachment, motif **J**) shows that there is very little difference in the behaviour of the materials, they both have similar melting and clearing points and both have short temperature range enantiotropic N* phases. Figure 94 shows that in both **25** and **27** the mesogens are able to pack to a similar efficiency in both materials resulting in similar thermodynamic behaviour with the materials having similar clearing points.

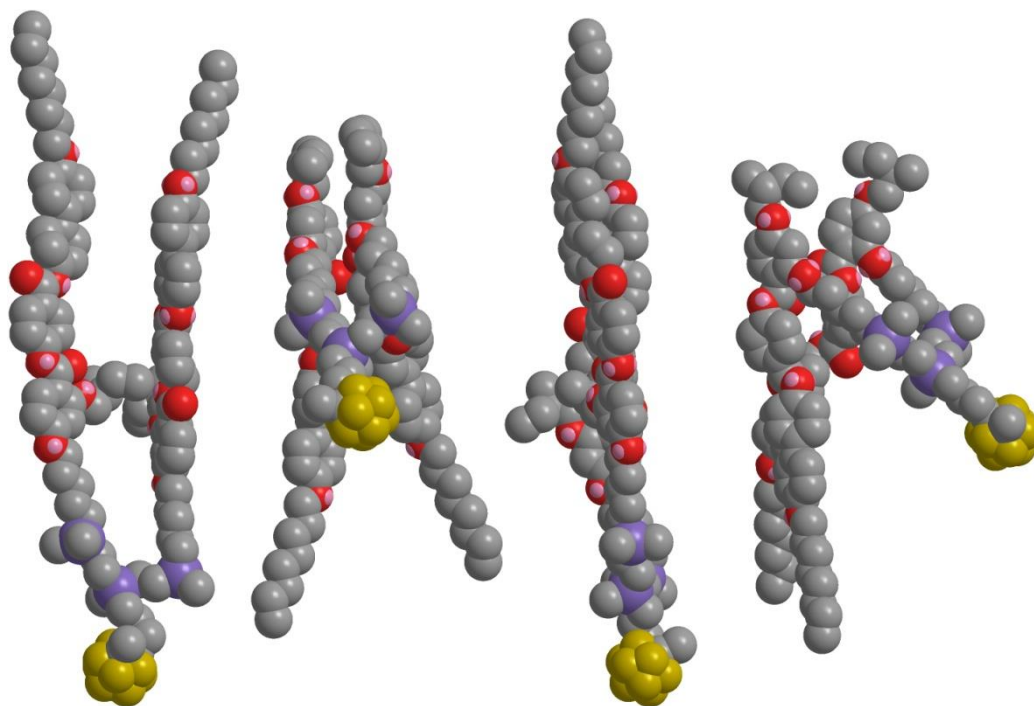


*Figure 94: Molecular models of **25** (far left and centre right) and **27** (far right and centre left), hydrogens omitted for clarity*

The difference in molecular shape however makes itself known in the kinetic behaviour of the materials phases, **25** forms a broad monotropic N* phase which eventually forms a glass. Compound **27** on the other hand, readily crystallizes upon cooling. The most likely reason for this is that **27** has a more symmetrical and easily close-packed shape aiding crystallization, whereas **25** is less symmetrical and less easy to close-pack into a crystal lattice (Figure 94).

The terminally attached materials, as in the two- and three-ring systems, have molecular structures which can be described as U-shaped⁴⁴. However, unlike the materials discussed so far, the four-ring mesogen is strongly nematogenic and despite the anchoring to the carborane, the nematic behaviour is retained.

Likewise the laterally attached materials **24** and **25** are akin to H-shaped mesogens²¹. Jin et al²⁰ made a series of LC dimers attaching the mesogens in a linear, H-shaped and T-shaped fashion (Figure 95). They found that the H-shaped materials had the lowest tendency for mesomorphism but the highest tendency towards smectic behaviour. However, when the flexible spacer was increased to twelve methylene units the smectic phase was lost. This is explained by the reduced conformational

5.4 Concluding Remarks

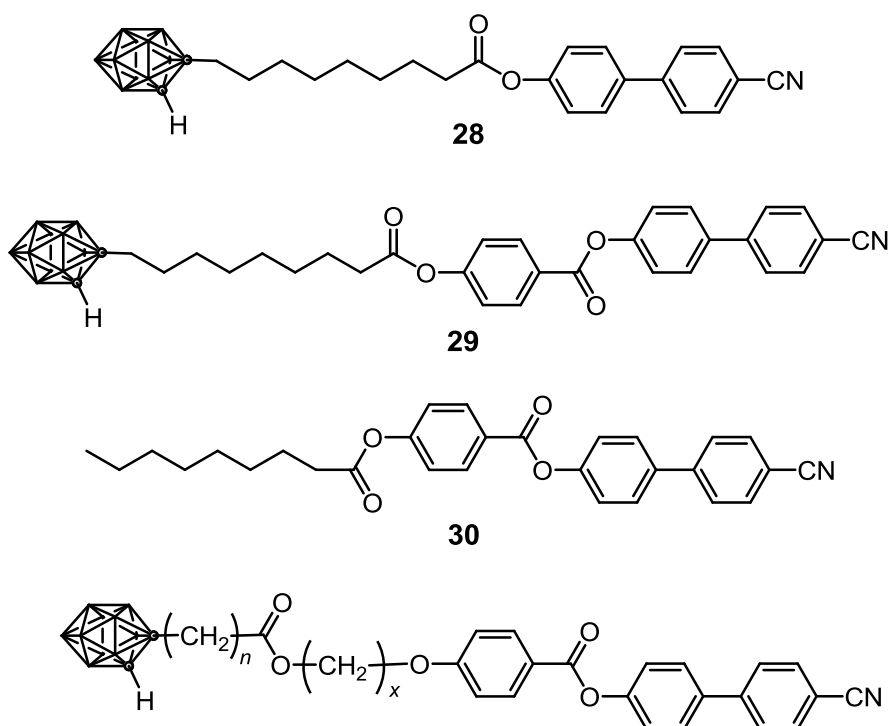
Increasing the number of mesogens from one to two has resulted, as expected, in more stable mesophases (higher clearing points and broader phase ranges) for all the mesogenic cores studied. Increasing to four mesogens continues this trend, although it does show that the relationship between phase stability and number of mesogens is not linear, as would be expected when moving into a more dendritic system³¹. Furthermore, as was also shown in the previous chapter, using mesogens with larger rigid cores results in a higher propensity for enantiotropic phases. However, upon moving to the four-ring systems, the added stability expected by the presence of multiple mesogens is reduced, most likely due to steric constraints. This is particularly noticeable in the laterally attached systems.

It has also been demonstrated that the mode of attachment at the carborane core (linear versus dendritic) makes little difference to the mesomorphic properties, although it has still not been possible to directly assess the impact of the carborane itself on the properties observed. It would also be useful to eliminate dimethylsilane as a linking group owing to its bulkiness and segregating properties. Doing this would enable the better assessment of the effect of the carborane on phase behaviour. Furthermore it can be concluded that the mesogenic moiety dominates the nature of the phases exhibited hinting that the carborane may not be as strongly segregating as initially thought.

6. Mono-functional Esters: The Effect of the Spacer

6.1 Summary

In this chapter a series of mono-functionalized carboranes appended with mesogenic moieties *via* an ester linker are presented. An ester linker was chosen in order to eliminate silicon from the materials and hopefully better understand the nanophase segregating properties of the *o*-carborane itself. The materials presented in this chapter are derived from tailor-made carborane clusters, which were synthesized in order to establish meaningful structure property relationships.



Compound	$n =$	$x =$	Spacer
31	2	2	7
32	2	3	8
33	2	5	10
34	2	6	11

Figure 96: Mono-functional carboranes appended with mesogenic moieties via an ester linker and their non-carborane containing models

Herein a carborane cluster is used which is mono-substituted with an alkyl chain terminated with a carboxylic acid, and the length of the alkyl chain is varied to assess its effect on the mesomorphic properties of the materials. Furthermore, the mesogen

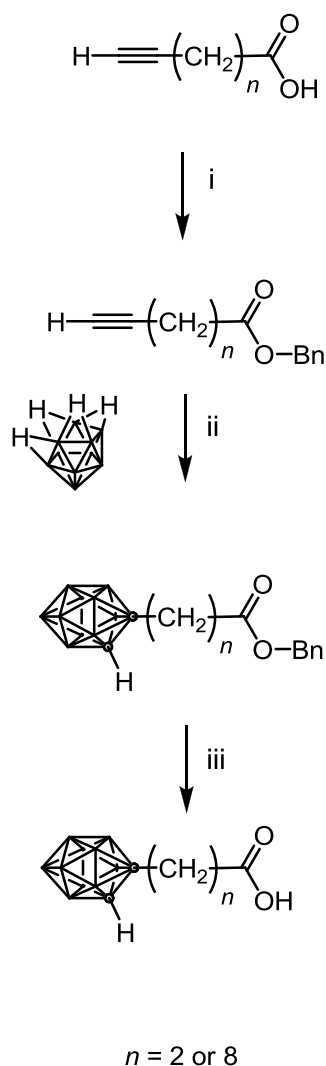
employed is also varied, using two- and three-ring systems based on cyanobiphenyl. In addition the spacer between the mesogen and the linking group is varied again to assess its impact on phase behaviour.

6.2 Synthesis

The mono-substituted carborane cores terminated with the carboxylic acid functionality were synthesized according to Scheme 8. The Steglich esterification¹³⁰ of a ω -alkynyl carboxylic acid with benzyl alcohol was carried out to install the benzyl protecting group on the acid. This is followed by capping the decaborane with the protected alkyne¹³¹ (step ii Scheme 8). This procedure entails the reaction of decaborane with acetonitrile in toluene to generate an acetonitrile-decaborane complex¹³², followed by the addition of the alkyne to the complex. The reaction was followed by ¹¹B NMR where the depletion of signals below -20 ppm and the emergence of signals at between -3 and -15 ppm with a characteristic relative intensity of 1:1:2:2:2:2 indicated the reaction had gone to completion. Typically this took between two and three days.

The final step of the synthesis was the hydrogenolysis of the benzyl protecting group catalysed by Pd on carbon (step iii Scheme 8) to yield the corresponding ω -carboranyl carboxylic acids. This reaction was followed by the elimination of the CH_2Bn signal at around 5 ppm in ¹H NMR. The deprotected acids readily crystallized into white needles in high purity.

Once the ω -carboranyl carboxylic acids were in hand, the synthetic protocol for the mesogenic moieties with either a phenol or a terminal alcohol group were established. For the materials **28**, **29** and **30** phenolic mesogenic cores were required. The cyanobiphenyl benzoate derivatives were synthesized as described in Scheme 9.



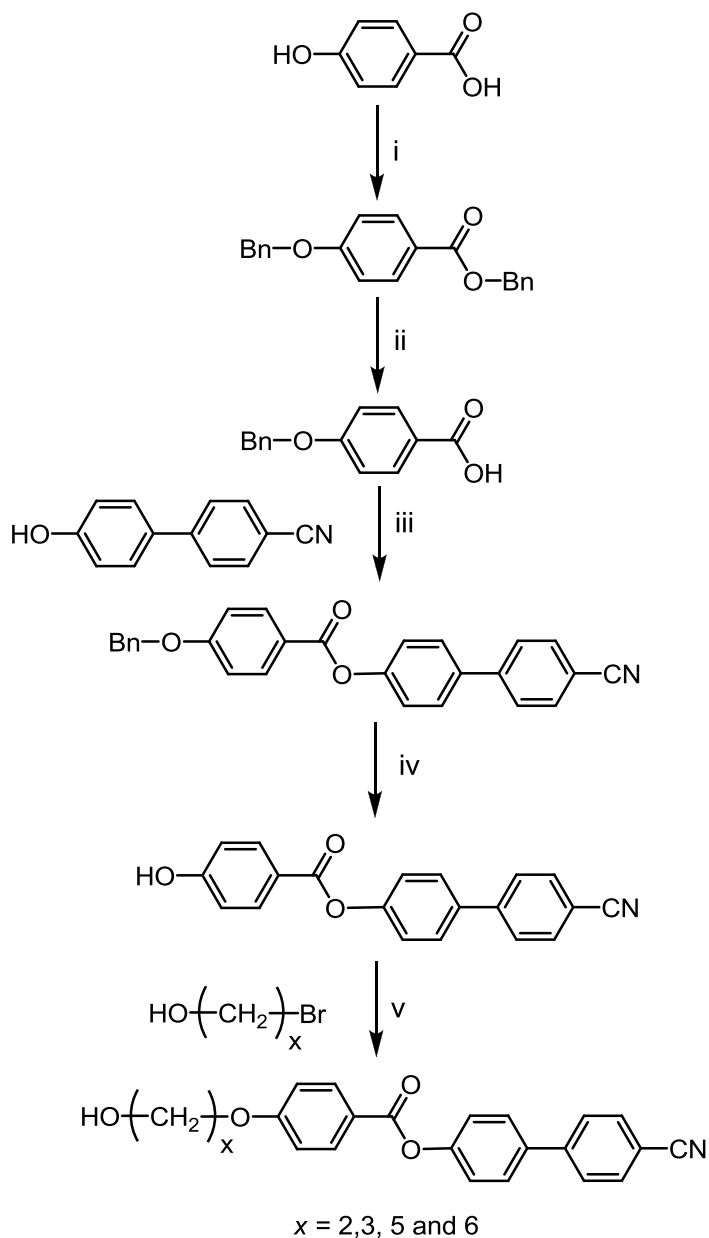
- i) Benzyl alcohol, DMAP and EDAC in DCM
- ii) Acetonitrile and dry toluene
- iii) H_2 and Pd on carbon in THF

Scheme 8: Synthesis of the carborane cores

Williamson etherification with benzyl bromide to protect the phenol as a benzyl ether also protects the acid as a benzyl ester (step i Scheme 9). Deprotection of the acid with NaOH in ethanol and water yields the benzyloxy protected benzoic acid (step ii Scheme 9). Following on from this a Steglich esterification with cyanobiphenol was used to form the benzyl protected mesogenic core (step iii Scheme 9). Finally, to generate the phenolic mesogenic core the benzyl ether was deprotected using H_2 and Pd on carbon (step iv Scheme 9).

Chapter 6: Mono-functional Esters: The Effect of the Spacer

For materials **31** to **34**, the alcohol-terminated spacer was installed by Williamson etherification with commercial ω -bromo-alcohols with different chain lengths (step v Scheme 9).



- i) Benzyl bromide, K_2CO_3 and KI in butanone
- ii) NaOH in water and ethanol
- iii) DMAP and EDAC in DCM
- iv) H_2 and Pd on carbon in THF
- v) K_2CO_3 and KI in butanone

Scheme 9: Synthesis of the cyanobiphenyl benzoate mesogen terminated with either a phenol or alkoxy alcohol

However, despite multiple attempts, step v (Scheme 9) failed for $x = 4$, probably through decomposition of the 4-bromobutanol under the reaction conditions.

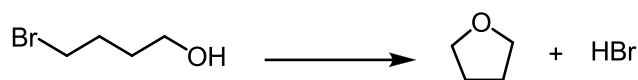


Figure 97: 4-Bromo-1-butanol cyclization

It was later discovered through a search of the literature that 4-chloro-1-butanol cyclizes to form THF and HCl particularly when heated¹³³. Therefore it is likely that a similar reaction occurs with 4-bromo-1-butanol. This explains why it was not possible to successfully use the Williamson etherification using bromo-4-butanol as upon heating the bromo-alcohol cyclized (Figure 97) rather than reacting with the phenol. A suitable reaction scheme could be devised starting from 1,4-butanediol, however due to time constraints it was not pursued further.

The final step in the synthesis of the mono-functionalized carboranes is the esterification of the carboranyl carboxylic acids with the phenolic mesogenic cores or the alkoxy alcohol terminated mesogens using the Steglich protocol which typically resulted in relatively low yields. The successful esterification was determined by a shift in the COO resonance in ¹³C NMR spectra from 177.19 ppm in the acid to ~171 ppm in the esters. Further evidence for the successful reaction is provided by the ¹H NMR spectra which show a shift in the resonance for the CH₂O protons from ~3.6 ppm in the alcohols to ~4.0 ppm in the esters. In addition the ¹³C NMR spectra show a shift in the ArC-OH resonance from ~162 ppm in the phenols to 155 ppm in the ester.

6.3 Thermal Properties

The thermal properties and phase behaviours of the mono-functionalized carboranes appended with mesogenic moieties *via* an ester linker were investigated by POM and DSC and are summarized in Table 7.

Compound	Crystal 1	Crystal 2	SmA	N	Iso
28	• 46.8	•		88.2	•
29	• 59.4	• 101.8	• 139.8	• 149.0	•
30	• 68.9	• 83.0	• 178.7*	• 234.9	•
31	•		(48.2 •)	122.9	•
32	• 35.8	•	(76.5 •)	94.3	•
33	•	(99.6 •)	(119.0 •)	145.8	•
34	•	(92.5 •)	(108.5 •)	158.4	•

Table 7: The phase behaviour of the mono-functionalized carboranes appended with mesogenic moieties via an ester linker, values as measured by DSC with a heat/cool rate of $10\text{ }^{\circ}\text{min}^{-1}$, values in brackets are for monotropic transitions and the value marked with a * is taken from POM as it was not detectable by DSC

Compound **28** has the CB aromatic core connected to the *o*-carborane via a spacer of 10 atoms. The material was found to be non-mesogenic. DSC shows two reproducible thermal events upon heating, a cold crystallization with onset at $46.8\text{ }^{\circ}\text{C}$ ($\Delta H = -18.8\text{ kJmol}^{-1}$) and the melt to the isotropic liquid with onset at $88.2\text{ }^{\circ}\text{C}$ ($\Delta H = 42.1\text{ kJmol}^{-1}$). The lack of mesomorphism for **28** is in agreement what has been learned in previous chapters. One cyanobiphenyl mesogen simply does not impart enough molecular anisotropy for a mono-functionalized carborane to display LC behaviour even after removing the dimethylsilane linking group altogether. This is most likely due to a strong destbalizing effect caused by the presence of the carborane.

Compound **29** has a cyanobiphenyl benzoate mesogen connected to the carborane cluster via a spacer of 10 atoms. The DSC trace of **29** shows four reproducible thermal events upon heating. The first is a broad exotherm with onset at $59.4\text{ }^{\circ}\text{C}$ ($\Delta H = -0.6\text{ kJmol}^{-1}$) corresponding to a cold crystallization, followed by a broad endotherm with onset at $101.8\text{ }^{\circ}\text{C}$ ($\Delta H = 25.6\text{ kJmol}^{-1}$) which is related to a melting event. This is followed by a small endotherm with onset at $139.8\text{ }^{\circ}\text{C}$ ($\Delta H = 0.3\text{ kJmol}^{-1}$) caused by a LC - LC transition and finally a second small endotherm with onset at $149.0\text{ }^{\circ}\text{C}$ ($\Delta H = 0.3\text{ kJmol}^{-1}$) due to the clearing point.

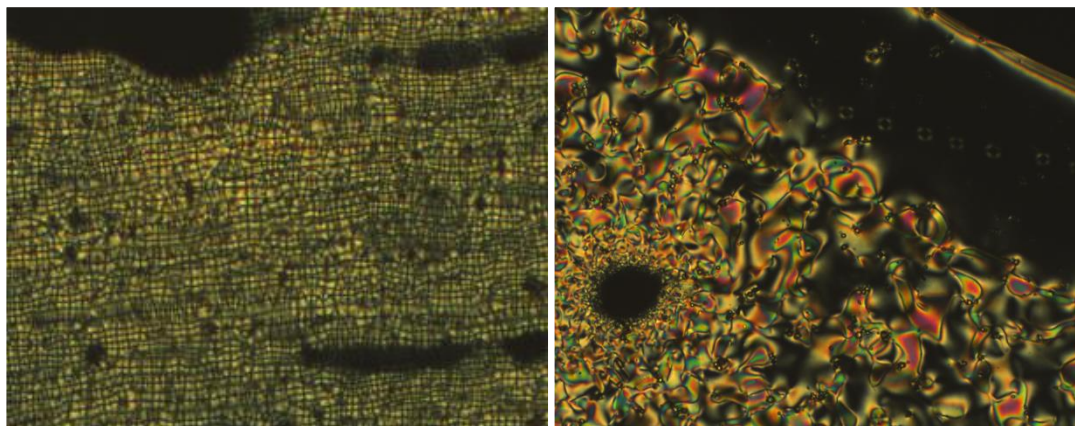


Figure 98: Photomicrographs of: left) the focal-conic texture of the SmA phase of **29** after shearing at 136.1 °C cooled from the isotropic liquid at 0.5 °Cmin⁻¹; right) the schlieren texture of the N phase of **29** at 146.2 °C after cooling from the isotropic liquid at 5 °Cmin⁻¹

Upon cooling **29** from the isotropic liquid POM showed that a *schlieren* texture with both two and four brush defects formed. In addition the material was optically extinct in areas of homeotropic alignment (Figure 98 right). This allows this phase to be assigned as a nematic phase. Upon further cooling the whole texture became optically extinct. However upon shearing the sample exhibited oily streaks which rapidly developed into the focal-conic texture (Figure 98 left). This combined allows this phase to be assigned as a SmA phase.

For comparison, and to help understand the effect of the carborane cluster on phase behaviour the model compound **30** was synthesized. This material is identical to **29** except that at the end of the flexible spacer chain there is no carborane. The DSC trace of **30** shows three reproducible thermal events on heating and cooling. The first is a Cr – Cr transition with onset at 68.9 °C ($\Delta H = 2.7 \text{ kJmol}^{-1}$) followed by a melting event starting at 83.0 °C ($\Delta H = 32.8 \text{ kJmol}^{-1}$) and finally a LC – Iso liq. transition with onset at 234.9 °C ($\Delta H = 0.9 \text{ kJmol}^{-1}$).

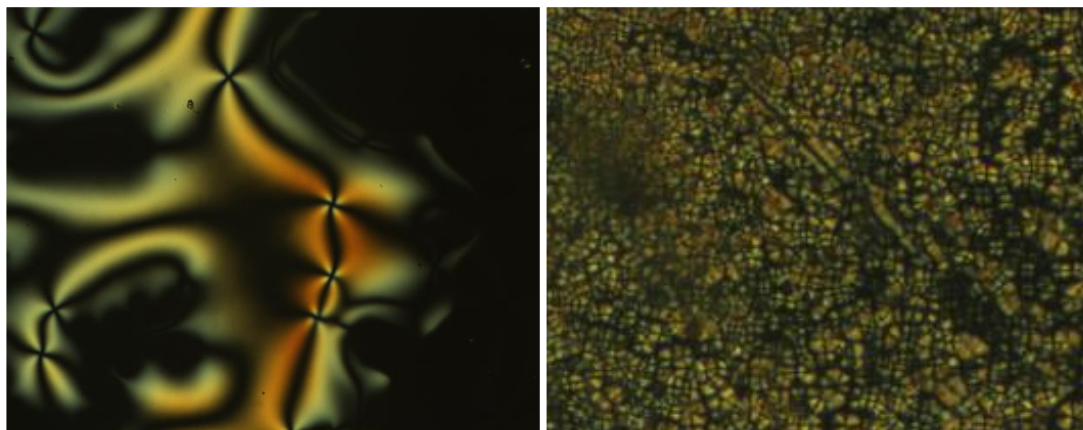


Figure 99: Photomicrographs of: left) the schlieren texture of the N phase of **30** at 227.8° C upon cooling from the isotropic fluid at 1 °Cmin⁻¹; right) the focal-conic texture of the SmA phase of **30** at 177.5 °C upon cooling from the isotropic fluid at 2 °Cmin⁻¹

The *schlieren* texture of the N phase with two and four brush defects, and areas of homeotropic alignment which were optically extinct was evident upon cooling **30** from the isotropic fluid (Figure 99 left). Upon further cooling, despite the DSC not showing a transition, at 178.7 °C a focal-conic texture began to develop indicating that a transition to the SmA phase had occurred. The fact that the transition was not observed by DSC shows that it must have had a very low enthalpy and was most likely weakly first order.

Comparing the behaviour of **29** and **30** reveals that the mesomorphic properties of the cyanobiphenyl benzoate mesogen is severely disrupted, although not completely destroyed, upon addition of the carborane to the end of the flexible chain. the mesomorphic phase range decreased from 151.9 °C in **30** to 47.2 °C in **29**. This is a clear demonstration of the destabilizing effect of the *o*-carborane cluster on mesomorphic properties as was discussed in previous chapters. However, now it is possible to quantify the effect of just the addition of the carborane by itself and decouple it from any other effects associated with the linking groups as well. The decrease in mesophase stability caused by the carborane cluster is a much larger disruption than that caused by the addition of either an adamantyl or bicyclooctyl group to the end of a flexible spacer reported by Goodby *et al*¹⁰¹ (Figure 100), although on a different aromatic core. This suggests that the carborane causes a

Chapter 6: Mono-functional Esters: The Effect of the Spacer

greater disruption to mesophase stability than either the adamantane or the bicyclooctyl moieties despite being of similar dimensions and topology, which points out that the effect is not entirely steric and that there also must be some electronic effects at play.

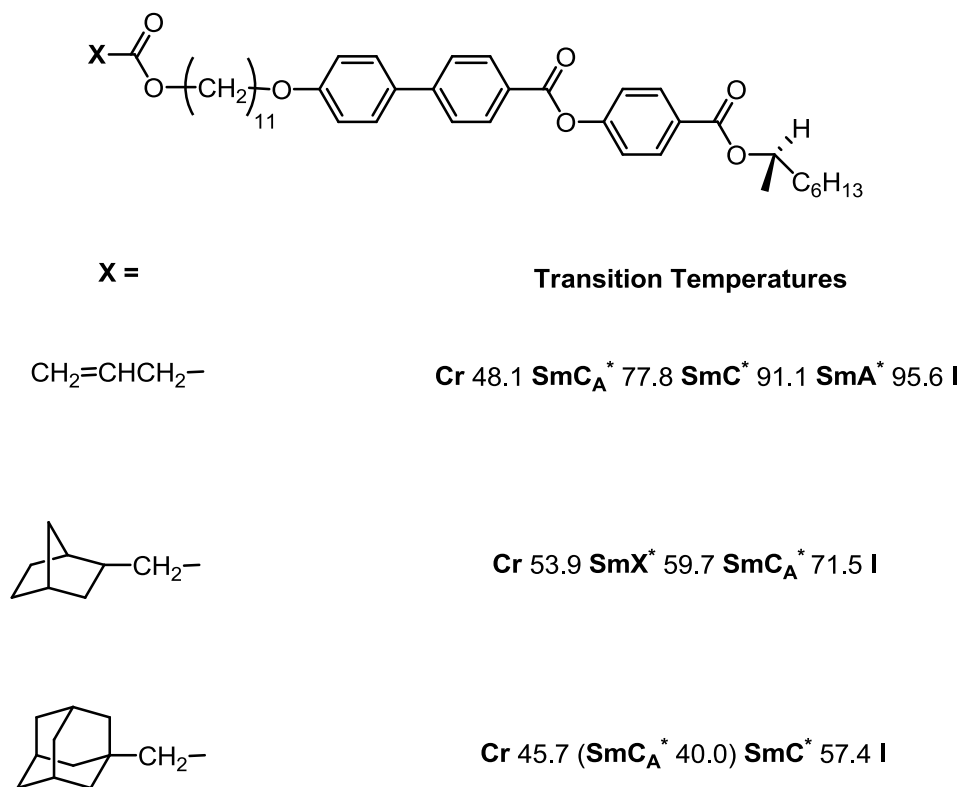


Figure 100: Mesogens with a carbocyclic terminal group¹⁰¹

Compound **29** is also noteworthy by the fact that it is the first mono-substituted carborane functionalized with only one mesogenic moiety which displays an appreciable enantiotropic mesophase range. Consequently it is also the first example of an inorganic cluster, functionalized with only one mesogen, to display a broad enantiotropic LC phase. However, this is not as unprecedented as it seems. Typically inorganic clusters are much larger than carborane and as such naturally require a stronger driving force to generate LC properties. This material might be associated more appropriately with liquid crystals with pendant groups where various carbocycles of similar sizes as the carborane have been attached to the end of the mesogens flexible tail¹⁰¹, although the comparison is only a topological one because electronically the carborane is very different to carbocycles.

Chapter 6: Mono-functional Esters: The Effect of the Spacer

Having established that mesomorphic behaviour can be achieved in mono-substituted cyanobiphenyl benzoates, the effect of the position of the ester linking group in the alkyl spacer in this family of materials was investigated next. Compounds **31** – **34** ($n = 2$, $x = 2, 3, 5$, and 6 respectively) all have an n chain equal to 2 (derived from 1-hydrido, 2-(propanoic acid)dodecacarborane) and a CB benzoate mesogen attached *via* an x chain of varying length.

The DSC trace of compound **31** ($x = 2$, spacer = 7) shows one thermal transition on the first heat, an endotherm at 122.9 °C ($\Delta H = 43.2 \text{ kJmol}^{-1}$) due to melting to the isotropic fluid. On subsequent heat/cool cycles two thermal events were evident: one a glass transition where the greatest rate of change in the heat capacity was at 28.9 °C; the other a weak endotherm with onset at 48.2 °C ($\Delta H = 0.1 \text{ kJmol}^{-1}$) resulting from a LC to Iso liq. transition.

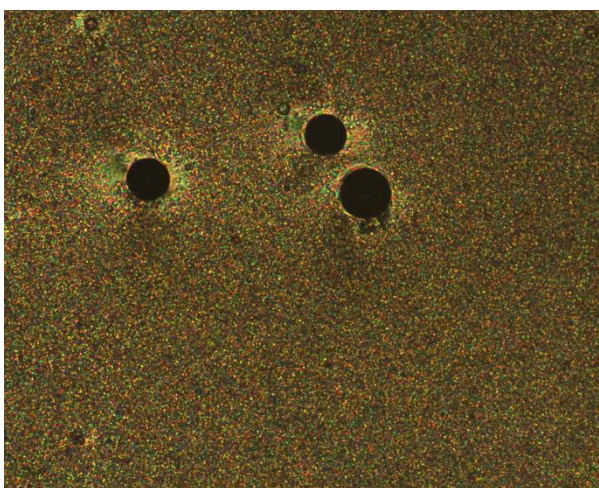


*Figure 101: Photomicrograph of **31** at 45.0 °C after annealing overnight and cooling from the isotropic fluid at 1 °Cmin⁻¹ on a slide coated with ClSi(Me)₃*

Upon cooling **31** from the isotropic liquid the material initially formed a grainy birefringent texture which rapidly became homeotropically aligned and optically extinct. In order to form a more informative texture a slide coated with ClSi(Me)₃ (Figure 101) was used. This again resulted in a grainy birefringent texture however it did not rapidly become homeotropic. Upon shearing the material flashed and did not show any signs of oily streaks. Therefore this phase can be assigned as a monotropic N phase.

The DSC trace of compound **32** ($x = 3$, spacer = 8) showed two thermal events upon the first heat. One was a cold crystallization at 35.8 °C ($\Delta H = -13.3 \text{ kJmol}^{-1}$) and the second was the melting to the isotropic liquid with onset at 94.3 °C ($\Delta H = 24.5 \text{ kJmol}^{-1}$). Upon further heat/cool cycles two reversible thermal events were present. The first a glass transition where the greatest rate of change in the heat capacity was at 20.1 °C and the second a LC-Iso liq. transition at 76.5 °C ($\Delta H = 0.1 \text{ kJmol}^{-1}$).

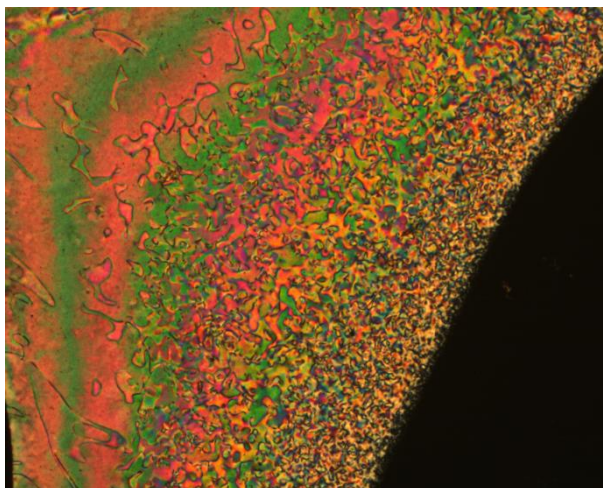


Figure 102: Photomicrograph of **32** at 61.0 °C after cooling from the isotropic fluid at 0.5 Cmin^{-1}

When cooled from the isotropic fluid **32** formed a *schlieren* texture (Figure 102) which flashed upon shearing and showed areas of homeotropic alignment which were optically extinct. This allows the phase to be assigned as a monotropic N phase. This material also exhibited the same strong affinity for homeotropic alignment as compound **31**.

The DSC trace of **33** ($x = 5$, spacer = 10) showed on the first heat a large endotherm with onset at 145.8 °C ($\Delta H = 42.6 \text{ kJmol}^{-1}$) associated with the melting to the isotropic liquid. Upon further heat/cool cycles three reproducible thermal events were detected. The first, a glass transition where the greatest rate of change of the heat capacity was at 17.1 °C, the second a weak endotherm with onset at 99.6 °C ($\Delta H = 0.1 \text{ kJmol}^{-1}$) due to a LC-LC transition and finally the LC-Iso liq. transition with onset at 119.0 °C ($\Delta H = 0.4 \text{ kJmol}^{-1}$).

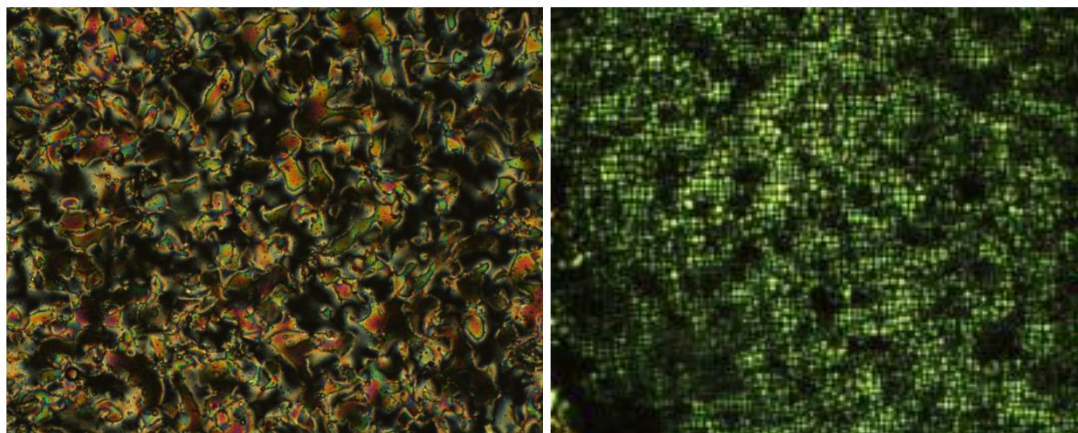


Figure 103: Photomicrograph of: left) the schlieren texture of the N phase of **33** at 115.3 °C after cooling from the isotropic liquid at 5 °Cmin⁻¹; right) the focal-conic texture of the SmA phase of **33** at 94.2 °C after cooling from the isotropic fluid at 1 °Cmin⁻¹ and subsequent shearing

Upon cooling **33** from the isotropic liquid a *schlieren* texture formed (Figure 103 left) which flashed upon shearing and rapidly changed to a homeotropic alignment which was optically extinct. This allows the phase to be assigned as a N phase. Upon further cooling the material remained optically extinct, however upon shearing smectic like streaks were observed which rapidly formed into a focal-conic texture (Figure 103 right) although this again quickly became homeotropic and optically extinct. This allows us to assign this phase as SmA. Both phases exhibited are monotropic as with the others in this series and also are similarly metastable.

The DSC trace of **34** ($x = 6$, spacer = 11) showed one event upon the first heat, a large endotherm with onset at 158.4 °C ($\Delta H = 59.8 \text{ kJmol}^{-1}$) associated with the melt to the isotropic liquid. Upon subsequent heat/cool cycles three reproducible thermal events were evident. The first is a glass transition centred at 13.2 °C. The second a LC-LC transition with onset at 92.5 °C ($\Delta H = 0.1 \text{ kJmol}^{-1}$) and the final a LC-Iso liq. transition at 108.5 °C ($\Delta H = 0.2 \text{ kJmol}^{-1}$).

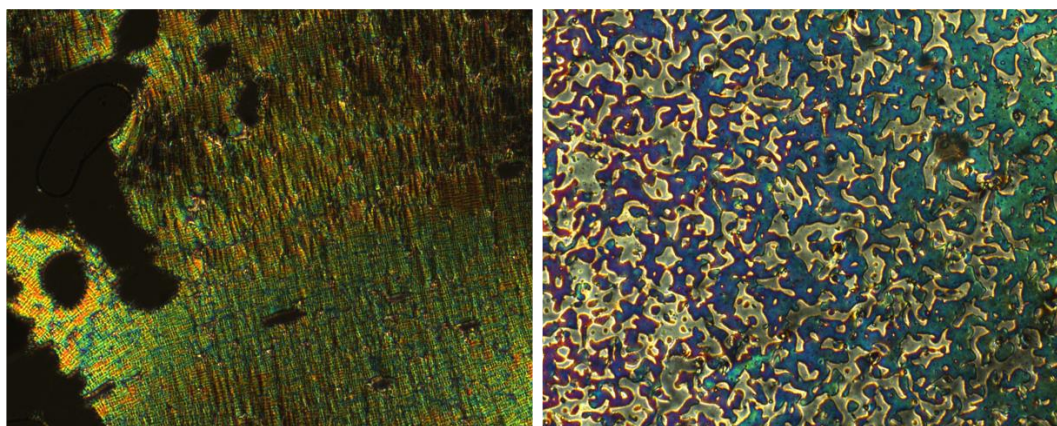
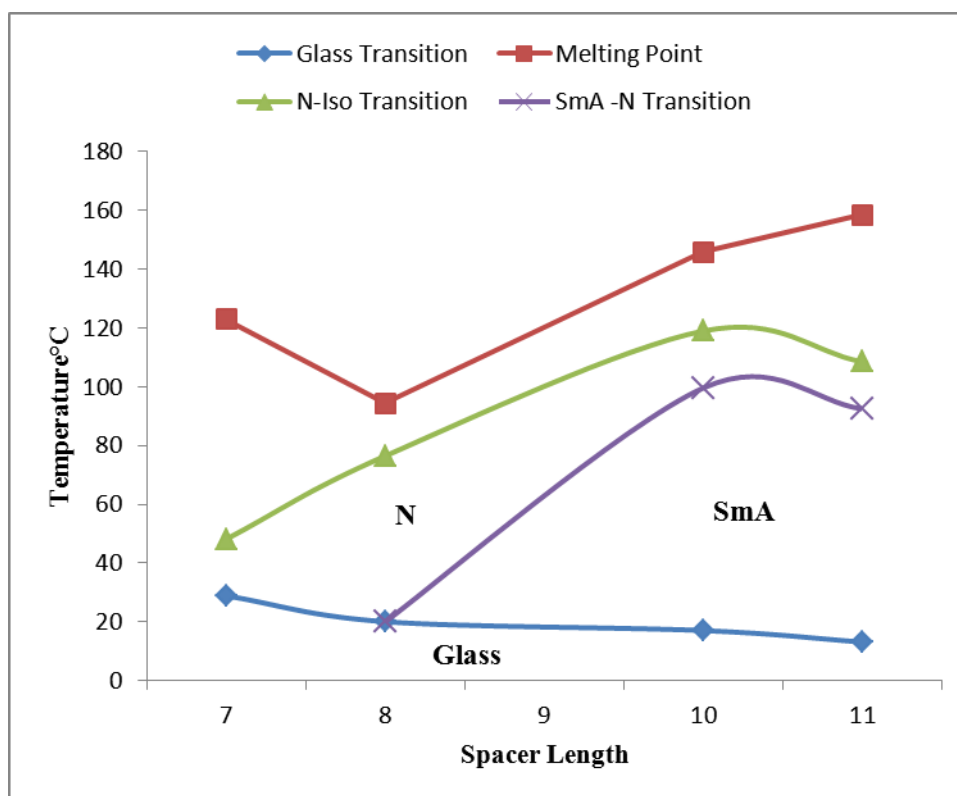


Figure 104: Photomicrograph of: left) focal-conic texture of the SmA phase of **34** at 82.1 °C after cooling from the isotropic fluid at 5 °Cmin⁻¹; right) the schlieren texture of the N phase of **34** at 99.3 °C after cooling from the isotropic fluid at 5 °Cmin⁻¹

Upon cooling **34** from the isotropic liquid a *schlieren* texture forms (Figure 104 right) which flashed upon shearing and rapidly changed to an optically extinct homeotropic alignment. Further cooling resulted in a focal-conic defect texture (Figure 104 left) which also rapidly formed areas of homeotropic alignment which were optically extinct. Therefore the phase sequence can be assigned as Iso-N-SmA. As with the other materials of this series the phases must be metastable due to the very slow crystallization process.

Graph 2 shows the plots of the phase transitions of the series $n = 2$ versus total spacer length. As described earlier, all the materials proved to be monotropic. Their melting points increase with spacer length and shows a possible odd-even affect although as there is no data for the material with spacer = 9, it is not possible to confirm this. Generally, the phase stability also increases with spacer length except for the spacer = 11, in which case there is a slight reduction.



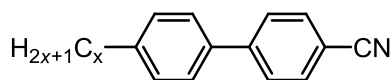
Graph 2: Transition temperatures versus spacer length for the series $n = 2$

This behaviour is typical of low molar mass mesogens as evidenced by the *n*-alkyl cyanobiphenyls series in Table 8¹³⁴. As can be seen from Table 7, there is a distinct odd-even effect in which melting points and transition temperatures are depressed for even members of the homologous series in comparison to the odd members of the series. This is explained by the relative linearity of the alkyl chain in all-*trans* conformation. The odd members of the series have a more symmetrical shape in all-*trans* conformation and as such melting points and transition temperatures increase accordingly.

In addition the *n*-alkyl cyanobiphenyl series also display a rapid fall in melting point to a minimum at $x = 6$ and then there is a general increase in the melting afterwards. The series of mono-functional carboranes appears to display similar behaviour in which a melting point minimum is reached at a spacer length of eight and then begins to increase again for longer spacers. It is also interesting to note that both series display solely nematic behaviour at short chain lengths followed by the onset of smectic phases at longer chain lengths, although the materials continue to display

Chapter 6: Mono-functional Esters: The Effect of the Spacer

nematic phases even at longer chain lengths. This could be a result of the more strongly nematogenic mesogen.



x	Cr	SmA	N	Iso
1	•		110	•
2	•		76	•
3	•		68	•
4	•		48	•
5	•	24	• 35	•
6	•	15	• 29	•
7	•	29	• 42	•
8	•	21	• 34	• 40
9	•	42	• 48	• 49
10	•	43	•	51
11	•	53	•	57

Table 8: Transitions temperatures of *n*-alkyl cyanobiphenyls¹³⁵⁻¹⁴⁰

The *n*-alkyl cyanobiphenyls display a continuing increase in the clearing point with longer chain length when the odd-even effect is account for. At difference with the *n*-alkyl cyanobiphenyl derivatives, the carborane series shows a maximum of the clearing point at a spacer length of ten. Furthermore, when the spacer is equal to ten there is also a maximum of phase range. This could be due to the carborane cluster gaining enough conformational freedom so that it can interfere with the core-core interactions of the CB mesogen it is attached to when the spacer reaches a critical length, in this case ten. All of these observations combined point towards these materials behaving in much the same way as low molar mass liquid crystals.

Looking at the stability of the N phase against that of the SmA phase in this series of mono-functionalized carboranes, we can see that a dramatic shift occurs with respect to which phase is favoured. This shift appears to occur when the spacer = 9 (which is unfortunately the material that was not possible to synthesize). However, this behaviour can be explained in terms of microphase segregation and molecular topology. In the shorter chain materials the spacer will have very little flexibility lending a rigid rod-like aspect to the molecule. This leads to the formation of the N phase. As the spacer length increases the chain becomes more flexible and more able

to microphase segregate resulting in the emergence of a SmA phase at the expense of the N phase.

It is also interesting to note that at short spacer length the ΔS_{N-Iso} of the transition is very low in the members of the series presented with a short spacer length (2.1 Jmol⁻¹K⁻¹ and 1.3 Jmol⁻¹K⁻¹ for compounds **31** and **32** respectively) which suggests that these phases have low order. This is likely the result of the disruption caused by the carborane cluster. However, when the spacer is equal to ten there is a maxima in the ΔS_{N-Iso} of 3.4 Jmol⁻¹K⁻¹ for compound **33**. This indicates that this N phase is the most ordered of our series and also coincides with the phase range maximum. After this point the ΔS_{N-Iso} begins to fall again much as the clearing point and phase range do. This indicates that there may be a balance in terms of the spacer length: too short and the phase is not stable, however if the spacer becomes too long then the carborane may be able to interfere with the core-core interactions on the CB benzoate mesogen it is attached to and thus the phase stability and order fall.

Finally the consistent tendency for the carborane containing materials to favour homeotropic alignment suggests that there is some strong affinity between the materials and the glass slides. It is suggested that this is most likely due to some electrostatic attraction between the cluster and the borosilicate glass. However, more non-carborane containing analogues would need to be studied in order to ascertain this point.

6.4 Concluding Remarks

A series of mono-functionalized carboranes appended with mesogenic moieties in which the effect of the spacer's nature and length on the phase properties of the materials was investigated. It was found that by removing the dimethylsilane linkage in the chain and replacing it with an ester it was possible to increase the phase stability of the materials produced. Furthermore, by removing the linker group altogether, the first inorganic cluster appended with only one mesogenic moiety which displays broad enantiotropic mesophases could be realized.

Chapter 6: Mono-functional Esters: The Effect of the Spacer

It has been demonstrated that the effect of the length of the spacer on phase behaviour is analogous to that of the terminal flexible chain in low molar mass calamitic mesogens. Additionally it was possible to quantify the effect of the carborane cluster by itself on phase stability and found, as suspected, that it greatly disrupts mesomorphism most likely due to its steric bulk. However the carborane does drive the formation of smectic phases over nematics, possibly due to microphase segregation.

7. Mono-functional Esters: The Effect of the Mesogen

7.1 Summary

In this chapter four series of mono-functional carboranes appended with various mesogens *via* an ester linker and their phenyl and alkyl homologues will be presented. The ester linkage was utilized again as it proved to be a more synthetically flexible method than either the silanes or siloxanes. Four different mesogenic cores were used in order to probe the structure property relationships and the structure of the smectic phases generated. Analogues of all the carborane materials were made, replacing the cluster with either a phenyl ring or an alkyl group (Figure 105), in order to better understand the effect of the carborane cluster on the mesomorphic properties of the materials.

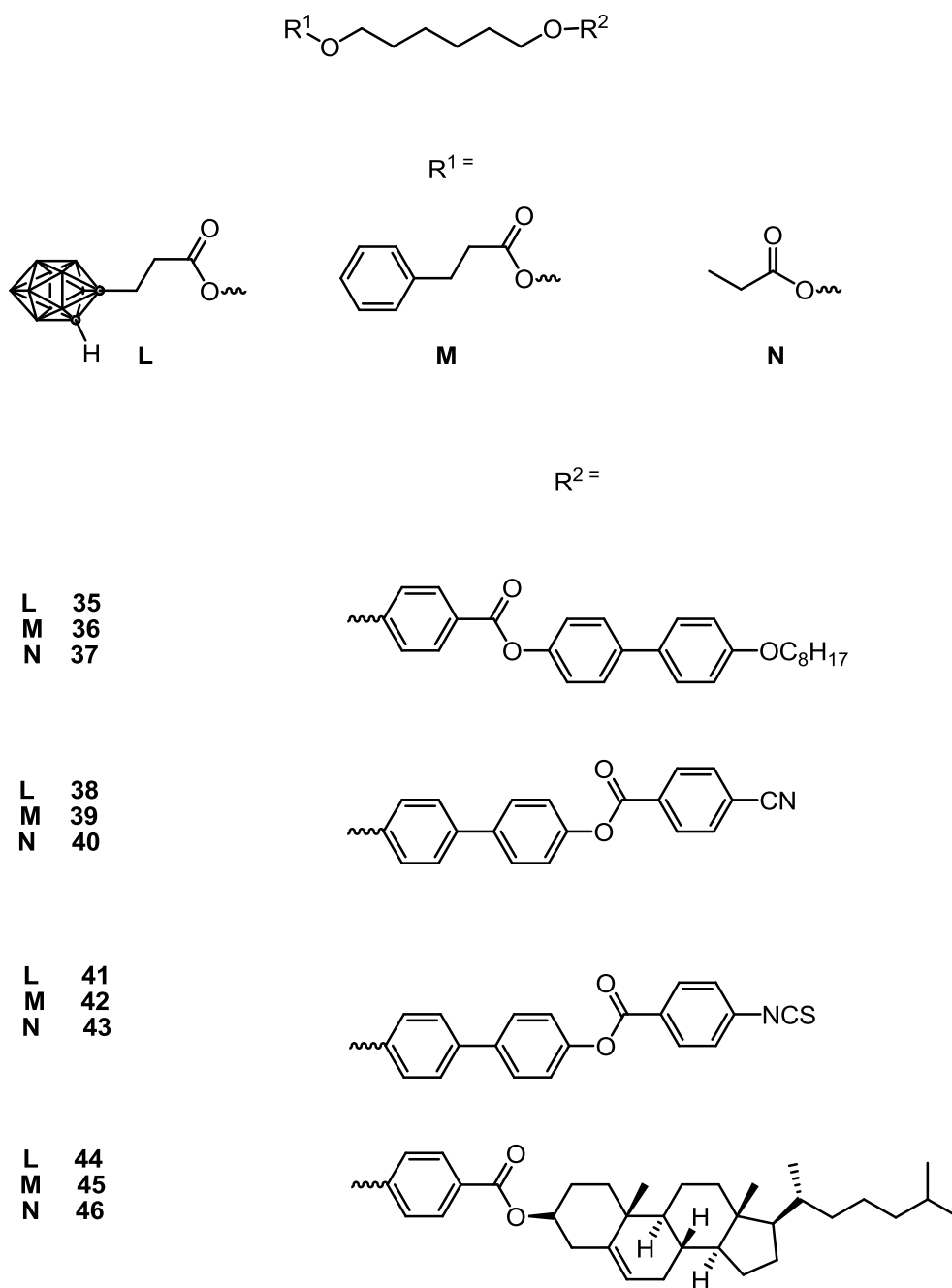


Figure 105: The mono-functional carboranes appended with mesogenic moieties via an ester linker and their phenyl and alkyl homologues

7.2 Synthesis

Four phenolic mesogenic cores were synthesized in order to link them to the carborane cluster in the same manner as in the previous chapter. The carborane cluster employed in this chapter was the same as that in Chapter 6 and was linked to

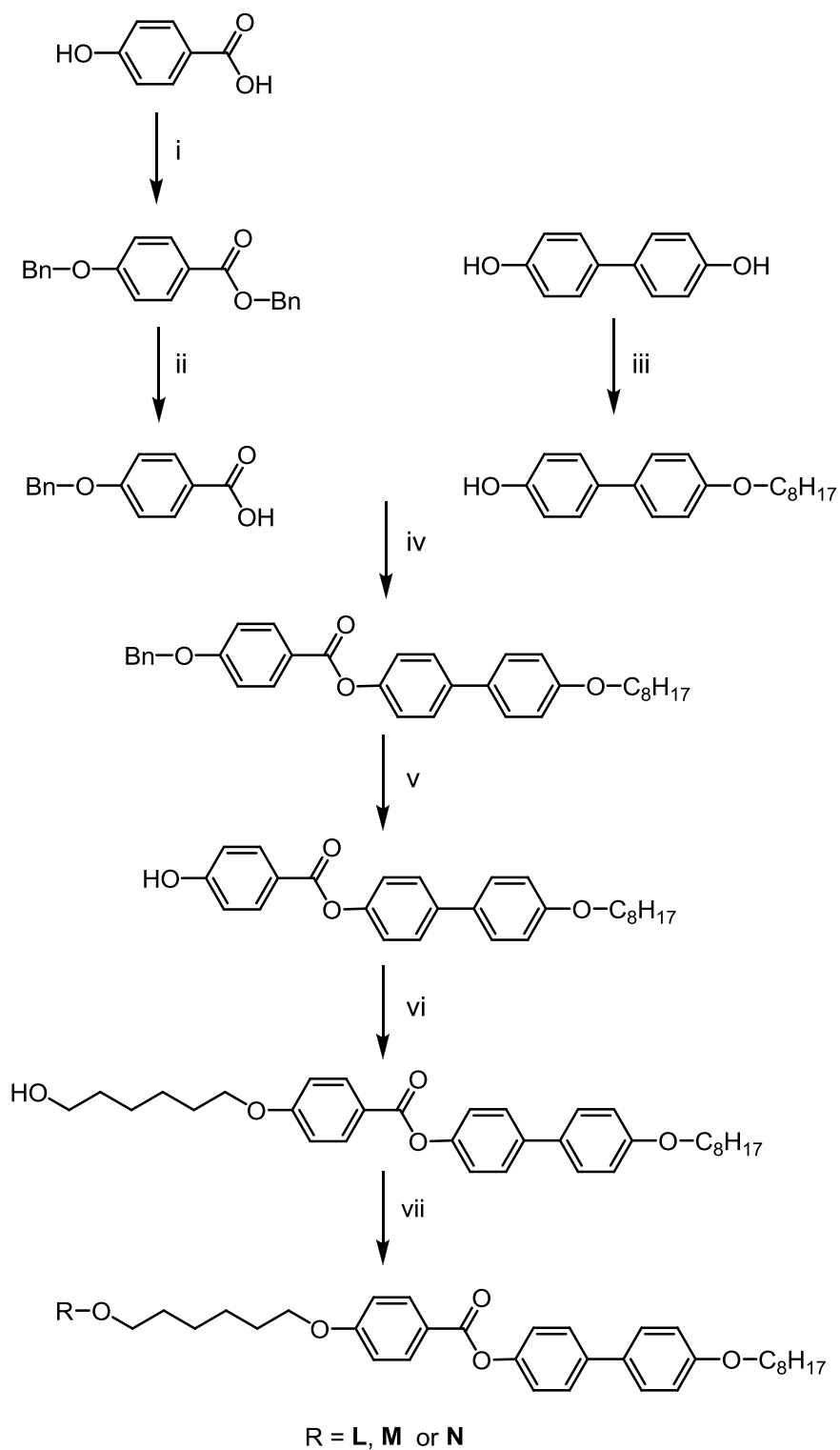
the phenolic cores by Steglich esterification as described earlier. Thus these steps will not be discussed here.

7.2.1 Octyloxy Biphenyl Benzoate

The synthesis starts with the benzyl protection of 4-hydroxy benzoic acid using benzyl bromide *via* a Williamson etherification (step i Scheme 10), this was followed by TLC. As the benzyl protection is not selective the acid must next be deprotected using NaOH to give 4-benzyloxy benzoic acid (step ii Scheme 10). In parallel with this the biphenyl unit is mono-functionalized using 8-bromooctane *via* another Williamson etherification in high dilution (step iii). These two materials are then coupled together using a Steglich esterification (step iv Scheme 10). The last step in the synthesis of the core is the deprotection of the benzyl ether *via* hydrogenation to give the phenolic octyloxy biphenyl benzoate core.

The next step, as in the previous chapter, is a final Williamson etherification of the phenolic core with a ω -bromoalcohol. In this chapter the chain was kept to C6 as the previous chapter showed that these materials were most likely to display a range of mesomorphic phases. Once this step is complete the final reaction coupling either 1-hydroxy-2-propanoic acid (**L**), hydrocinnamic acid (**M**) or propionic acid (**N**) with the free alcohol *via* a Steglich esterification was carried out to yield the final monopodal carborane functionalized with an octyloxy biphenyl benzoate mesogen, **35**, and its phenyl, **36**, and alkyl, **37**, models respectively (step vii Scheme 10).

Chapter 7: Mono-functional Esters: The Effect of the Mesogen



- i) Benzyl bromide, K_2CO_3 , KI in butanone
- ii) NaOH in H_2O /ethanol
- iii) 1-Bromooctane, K_2CO_3 , KI in butanone
- iv) DMAP, EDAC in DCM
- v) H_2 and Pd on carbon in THF
- vi) 6-Bromo-hexan-1-ol, K_2CO_3 , KI in butanone
- vii) 1-Hydrido-2-propanoic acid dicarba-closo-dodecacarborane (**L**)
or hydrocinnamic acid (**M**) or propionic acid (**N**), DMAP and EDAC in DCM

Scheme 10: Synthesis of the octyloxy biphenyl benzoate mesogen

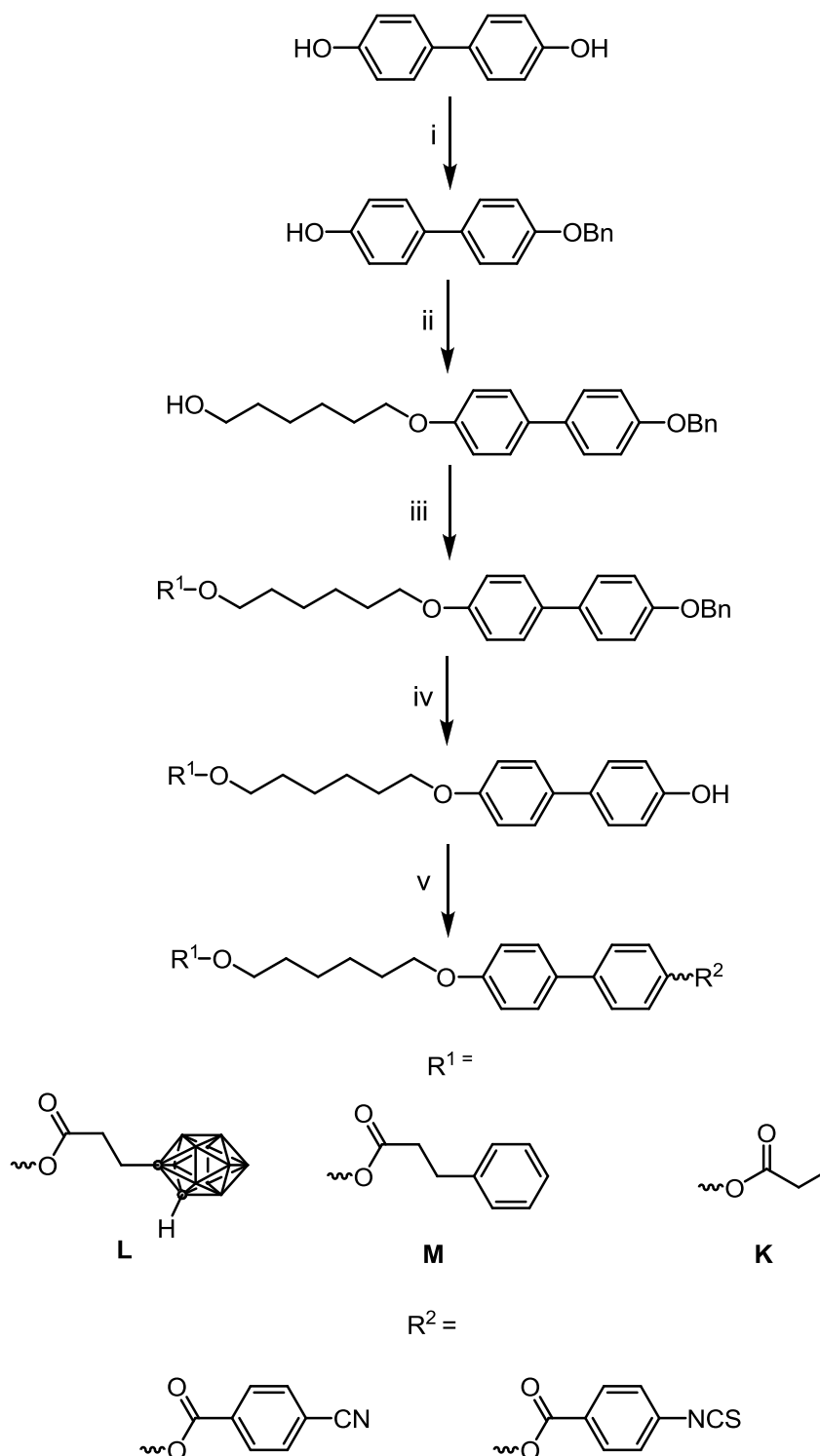
7.2.2 Biphenyl Cyanobenzoates and Biphenyl isothiocyanate Benzoates

The synthesis of the biphenyl cyano and isothiocyanate benzoate mesogens both start with the same partial synthesis of the mesogenic core which is then coupled with either a carborane, phenyl ring or alkyl group. The mesogenic core is then completed in the last step installing either a cyano benzoate or an isothiocyanate benzoate. This method was chosen as it allowed the sharing of the largest number of intermediates for all of the final compounds, thereby reducing the amount of synthesis required overall.

Scheme 11 starts the synthesis with the mono benzyl protection of biphenol in high dilution conditions using a small excess of the biphenol in comparison to the bromide in order to maximize the mono-substituted yield. The next step was a Williamson etherification of the mono-protected biphenol with 6-bromohexan-1-ol (step ii Scheme 11). Again the C6 chain was chosen as it was shown in the previous chapter to be most likely to generate a number of LC phases in the final materials. Step ii had a low yield due to the poor solubility of the benzyl protected biphenol.

Incorporation of the carborane cluster (**L**), step iii, was carried out by Steglich esterification, and the corresponding materials subjected to Pd/C catalysed hydrogenolysis to yield the phenolic derivatives (step iv Scheme 11). Finally Steglich esterification with either 4-cyano benzoic acid or 4-isothiocyanate benzoic acid to yield the carboranyl, phenyl and alkyl analogues substituted with either biphenyl cyanobenzoates (**38**, **39** and **40** respectively) or biphenyl isothiocyanate benzoates (**41**, **42** and **43** respectively).

Chapter 7: Mono-functional Esters: The Effect of the Mesogen



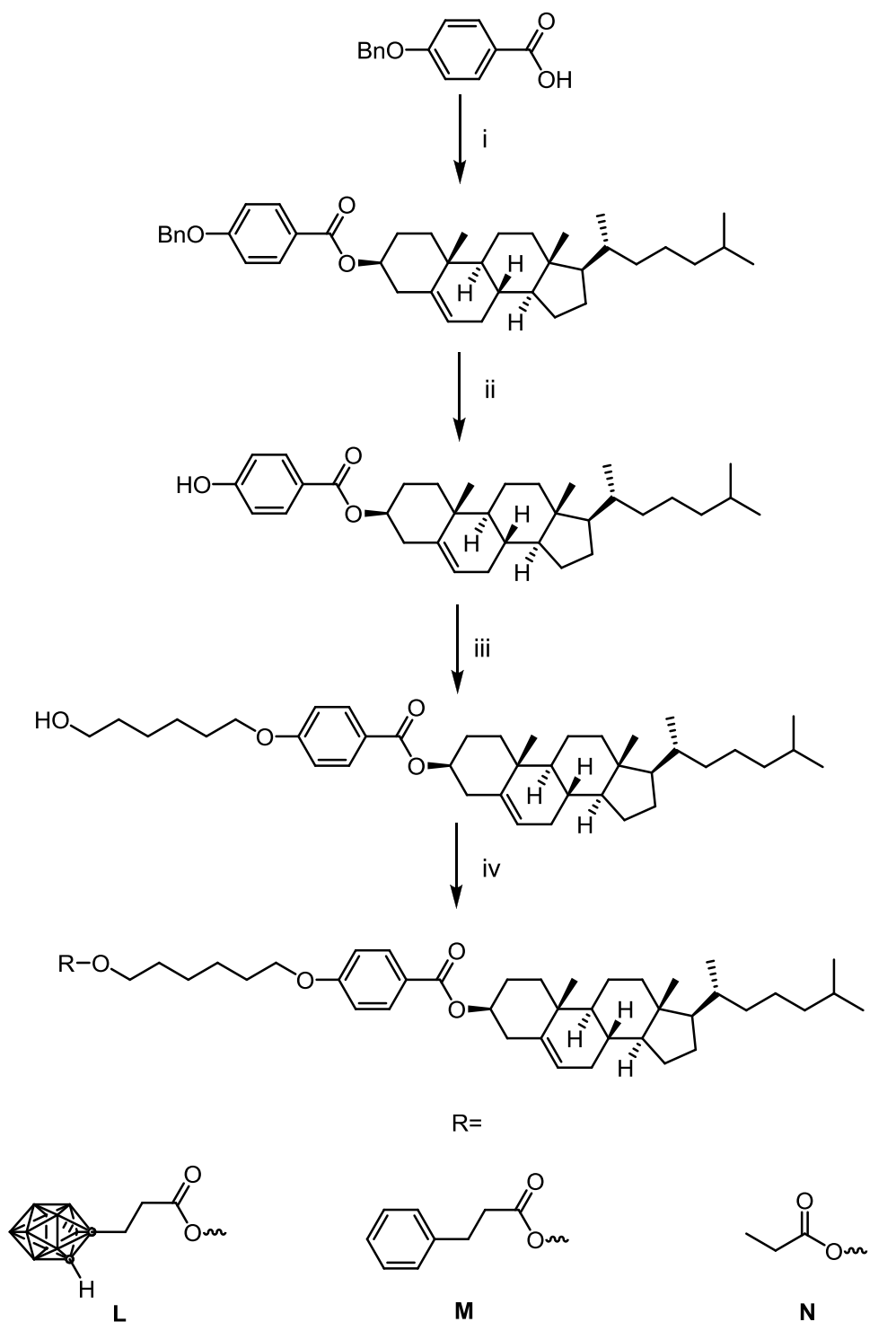
- i) Benzyl bromide, K_2CO_3 , KI in butanone
- ii) 1-Bromo-hexan-1-ol, K_2CO_3 , KI in butanone
- iii) 1-Hydrido-2-propanoic acid dicarba-closo-dodecacarborane (**L**) or hydrocinnamic acid (**M**) or propionic acid (**K**), DMAP and EDAC in DCM
- iv) H_2 and Pd on carbon in THF
- v) 4-Cyano benzoic acid or 4-isothiocyanate benzoic acid, DMAP, EDAC in DCM

Scheme 11: Synthesis of the biphenyl cyano and isothiocyanate benzoate mesogens

7.2.3 Cholesteryl Benzoates

The mono-functionalized carborane and its phenyl and alkyl analogues appened with a cholesteryl benzoate mesogen were synthesized according to Scheme 12. The method employed is similar to that as used for the octyloxy biphenyl benzoates with the first two steps being identical, as such they will not be discussed again. Step i (Scheme 12) involves the coupling of 4-benzyloxy benzoic acid with cholesterol *via* Steglich esterification which is then followed, again similar to Scheme 10, with the deprotection of the benzyl protected phenol using hydrogenation. This is then followed by the installation of the alcohol terminated alkoxy chain using the Williamson etherification just as in Scheme 10.

The final step, the introduction of the carborane or its phenyl and alkyl analogues is again achieved using Steglich esterification with either 1-hydrido-2-propanoic acid dicarba-closo-dodecacarborane (**L**), hydrocinnamic acid (**M**) or propionic acid (**N**) to yield the final mono-functionalized carborane appened with a cholesterol benzoate mesogen, **44**, and its phenyl, **45**, and alkyl, **46**, models respectively (step vi Scheme 12).



- i) Cholesterol, DMAP, EDAC in DCM
 ii) H₂ and Pd on carbon in THF
 iii) 6-Bromo-hexan-1-ol, K₂CO₃, KI in butanone
 iv) 1-Hydrido-2-propanoic acid dicarba-closo-dodecacborane (**L**)
 or hydrocinnamic acid (**M**) or propionic acid (**N**), DMAP, EDAC in DCM

Scheme 12: The synthesis of the cholesterol benzoates

7.3 Thermal Properties

The thermal properties and any subsequent mesophase behaviour of the mono-functionalized carborane clusters with an ester linker were investigated *via* POM and DSC. In addition the thermal behaviour of the phenyl and alkyl model analogues was also investigated. All the thermal data for the compounds presented in this chapter are summarised in Table 9.

Chapter 7: Mono-functional Esters: The Effect of the Mesogen

Compound	Crystal 1	Crystal 2	CrE	Hexatic B	SmC	SmA	SmA*	TGB	N	N*	BP2	Iso				
35	•	72.2	•			84.1	•				93.0	•				
36	•	63.1	•		85.4	•		109.9	•		136.6	•				
37	•	80.4	•		95.8	•	142.0	•	145.8	•	168.4	•				
38	•					(89.0	•)	106.6	•		107.9	•				
39	•	73.1	•			77.6	•	119.0	•		151.7	•				
40	•					92.9	•	99.2	•		187.0	•				
41	•			(55.4	•)	(125.8	•)	(127.0	•)		130.1	•				
42	•	55.6	•	(66.3	•)	66.9	•	154.3	•		162.0	•				
43	•			62.0	•	89.7	•	191.2	•		203.5	•				
44	•						(113.2	•)	(107.3*	•)	(131.7	•)	143.2	•		
45	•	35.7	•	(16.0	•)		49.2	•	116.9*	•	118.0	•	148.7*	•	148.9	•
46	•						101.4	•	142.0*	•	152.2	•	182.2*	•	185.3	•

Table 9: The thermal properties of the mono-functionalized carboranes appended with mesogenic moieties via an ester linker and their phenyl and, values as measured by DSC except those marked * which are values determined by microscopy, values in brackets are for monotropic transitions

7.3.1 Octyloxy Biphenyl Benzoates 35 – 37



Figure 106: Structures of compounds 35, 36 and 37

The first series of compounds investigated were functionalized with an octyloxy biphenyl benzoate mesogen with either a carboranyl, phenyl or alkyl end-group (Figure 106), in order to test whether removing the cyano group of the mesogen and replacing it with an octyloxy chain would remove any quadrupolar interactions of the cyano group and reduce the tendency for smectic phases.

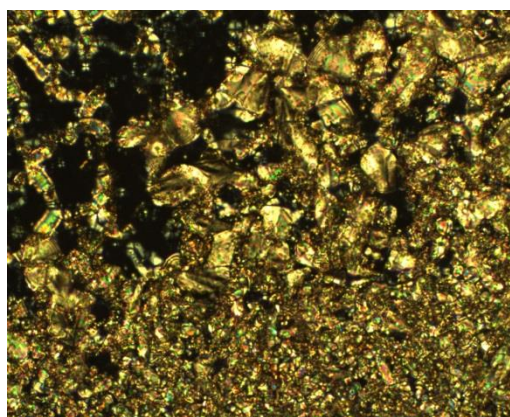
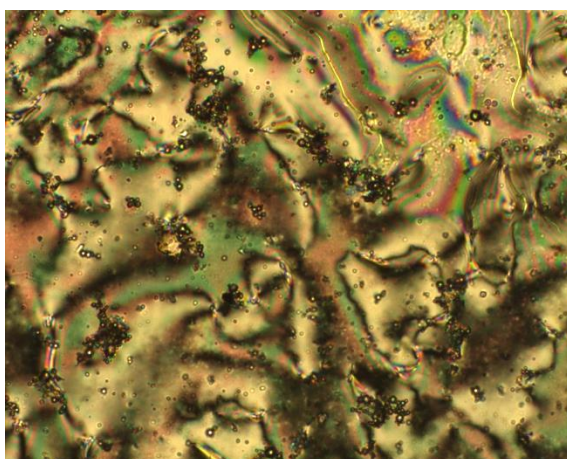


Figure 107: Photomicrograph of 35 at 94.6 °C after cooling from the isotropic liquid at 1 °Cmin⁻¹

The DSC trace of compound 35 showed three reproducible thermal events upon heating, a Cr-Cr transition with onset at 72.2 °C ($\Delta H = 6.0 \text{ kJmol}^{-1}$), followed by an

event at 84.1 °C ($\Delta H = 16.3 \text{ kJmol}^{-1}$) which is a melt into a LC phase and finally an event starting at 93.0 °C ($\Delta H = 1.5 \text{ kJmol}^{-1}$) which corresponds to the clearing point. Upon cooling the crystallization supercools by around 20 °C. Figure 107 shows the focal-conic texture of compound **35** after cooling from the isotropic fluid. Pairs of ellipses and hyperbolae of optical discontinuity were present along with areas of homeotropic alignment which were optically extinct. This allows the phase to be assigned as an enantiotropic SmA phase.

The DSC trace of compound **36** showed four reproducible events on heating and cooling cycles. The first is a Cr-Cr transition with onset at 63.1 °C ($\Delta H = 16.3 \text{ kJmol}^{-1}$). The second transition corresponds to a melt with onset at 85.4 °C ($\Delta H = 24.1 \text{ kJmol}^{-1}$), following this there is a LC-LC transition at 109.9 °C ($\Delta H = 0.6 \text{ kJmol}^{-1}$). The final thermal event corresponds to the clearing point and starts at 136.6 °C ($\Delta H = 0.7 \text{ kJmol}^{-1}$).



*Figure 108: Photomicrograph of the schlieren texture of **36** at 131.3 °C upon cooling from the isotropic fluid at 1 °Cmin⁻¹*

Upon cooling from the isotropic liquid compound **36** forms the *schlieren* texture (Figure 108) with both two and four brush defects and areas of homeotropic alignment which are optically extinct, this allows the phase to be assigned as N. Further cooling of the N phase of compound **36** results in the emergence of a SmC phase. Figure 109 shows a sequence of photomicrographs taken over the transition of the N to SmC phases centred on an area of homeotropic alignment in the N phase. As the material is cooled further the *schlieren* texture develops in the area of

homeotropic alignment. This new texture does not show two brush defects indicating that this is a tilted smectic phase. The crosshatched texture which then envelops the *schlieren* texture is caused by undulation instabilities which arise as a result of layer contraction caused by an increase of the tilt angle¹⁴¹. The tilt angle presumably is highly temperature dependent near the transition thus resulting in a large enough change in tilt angle to cause the undulating instabilities.

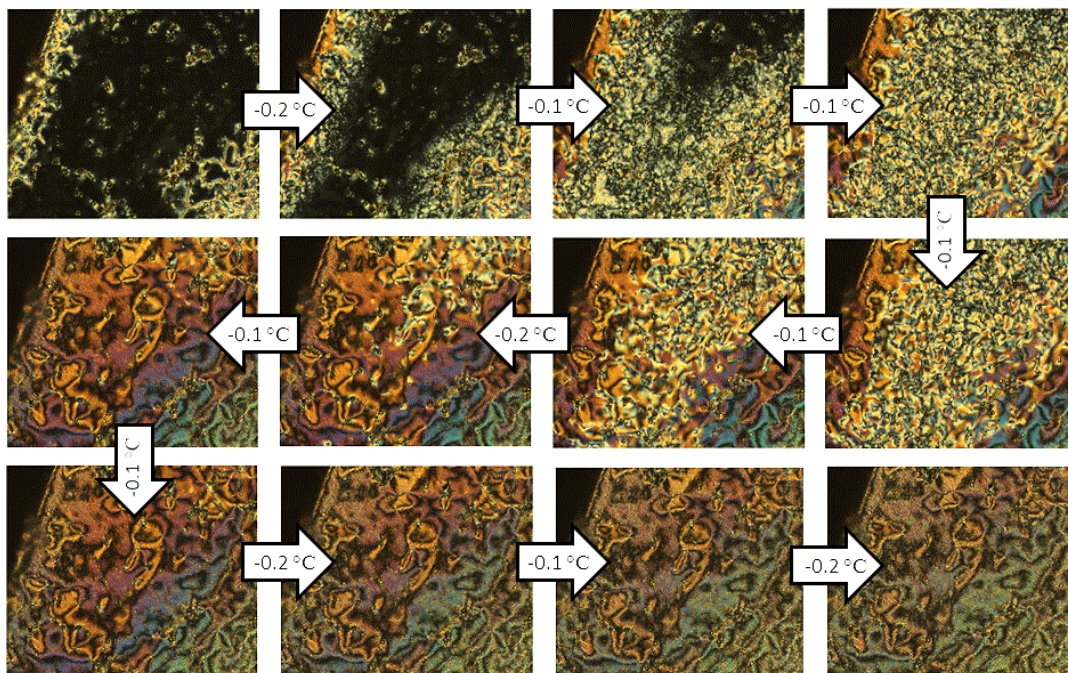


Figure 109: A sequence of photomicrographs of the N-SmC transition of **36** starting at 106.5 °C upon cooling from the isotropic fluid at 1 °Cmin⁻¹ and ending at 105.0 °C

Compound **37** showed the phase sequence Cr₁ 80.4 Cr₂ 95.8 SmC 142.0 SmA 145.8 N 168.4 Iso as determined by combination of DSC and POM (Figure 110) as described for the carboranyl **35**. Assignment of the SmA phase proved more challenging as a result of the material having a strong tendency towards homeotropic alignment. This resulted in the N phase always being homeotropically aligned when passing into the SmA phase. As such the sample remained optically extinct. Upon moving to the SmC phase the *schlieren* texture rapidly developed and immediately showed the same SmC undulation instabilities as **36** (Figure 110 right). The fact that the intermediary phase between the N and SmC remained optically extinct indicates that the phase is orthogonal. As such the only likely phase was the SmA.

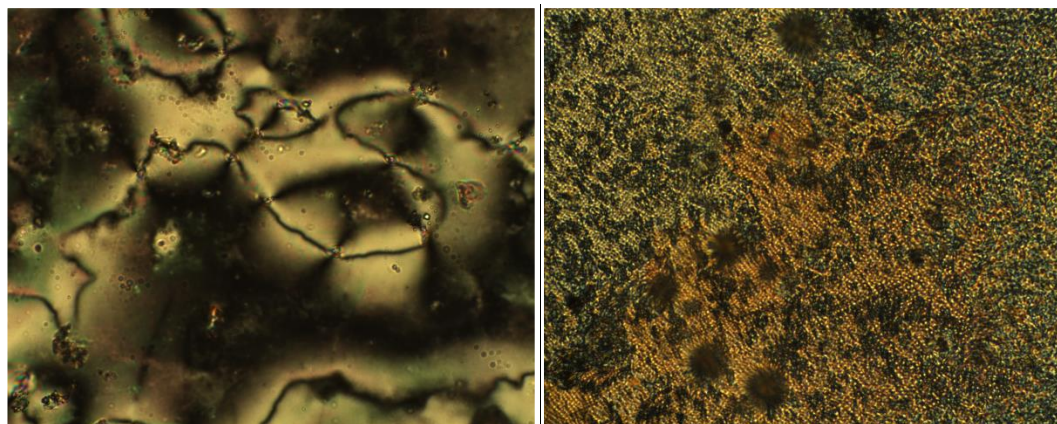


Figure 110: POM micrographs of: left) the schlieren texture of the N phase of 37 at 168.4° C upon cooling from the isotropic liquid at 0.2° Cmin⁻¹; right) the schlieren texture of the SmC of 37 with undulating instabilities at 138.1 °C upon cooling from the N at 1 °Cmin⁻¹

7.3.1.1 Phase Structure

There are again two options for the phase structure of the SmA phases of the octyloxy biphenyl benzoates (Figure 111). For **35**, either the carborane group segregates resulting in a SmA₂ or SmA_d phase, as discussed previously for other materials, or they mix with the alkoxy chains and a SmA₁ phase is formed. For **37** there is no reason why the alkyl end-group would segregate and so it would be expected to see a SmA₁ phase form. The SmA phase of **36** is also likely to be a SmA₁ as there is no driving force for the formation of the SmA₂ or SmA_d type phase due to the lack of quadrupolar interactions.

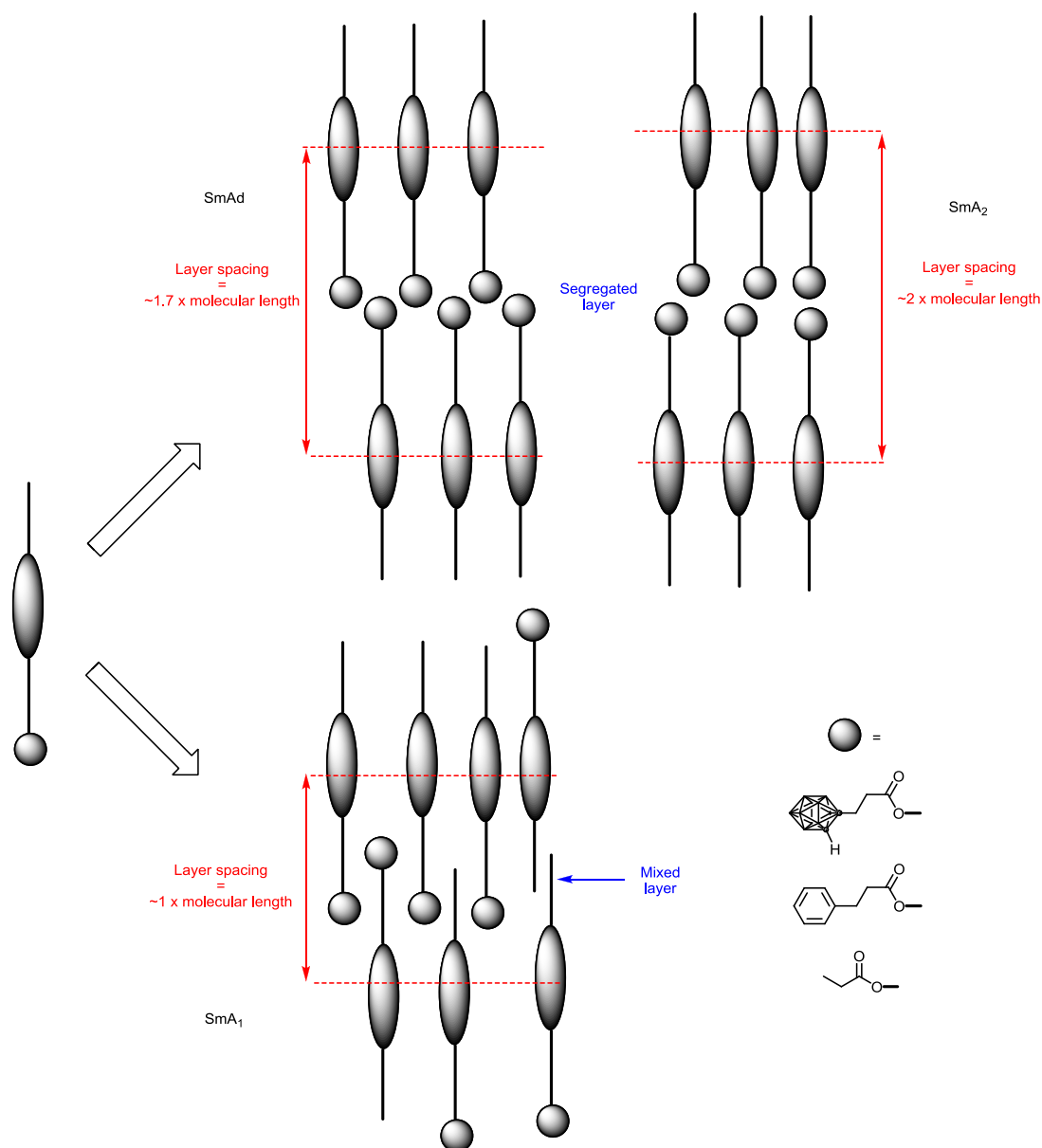
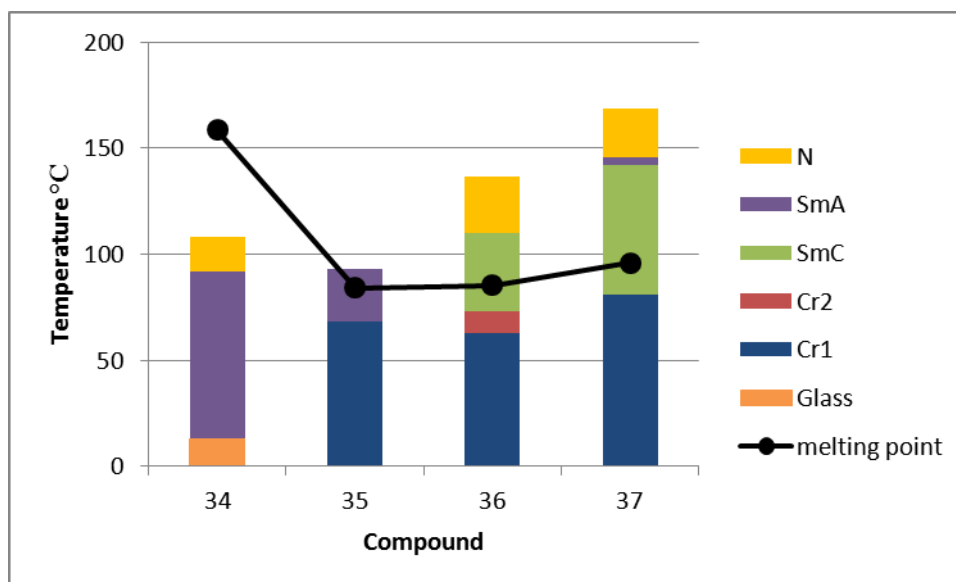


Figure 111: Possible options for the phase structure of the smectic phases of the octyloxy biphenyl benzoates

7.3.1.2 Comparisons

Graph 3 summarises the thermal properties of the carborane **35** functionalized with an octyloxy biphenyl benzoate mesogen and its phenyl, **36**, and alkyl, **37**, analogues. As can be seen all the materials form crystalline solids and a smectic phase. However, carborane **35** only shows a short range enantiotropic SmA phase, whereas both **36** and **37** show relatively broad SmC and N phases, with compound **37** also showing a very short range intermediary SmA phase. Upon addition of a phenyl

ring and then subsequently replacing that with the slightly larger carborane the isotropization temperature and phase range drops away rapidly. This is unsurprising as it would be expected that the bulky end-group would destabilize mesomorphism, with a larger group likely to destabilize it more. This is in keeping with the general trend observed so far for the destabilizing effect of the carborane.



*Graph 3: The thermal properties of the octyloxy biphenyl benzoates and the carboranyl cyanobiphenyl benzoate **34** for comparison purposes, thermal behaviour shown in bars is that observed for cooling, the melting points shown are for the pristine sample*

The complete lack of the N phase in the carboranyl material suggests that the carborane may, as has previously been suggested, microphase segregate resulting in the suppression of nematic behaviour in favour of smectic phases. However, it is also possible that the destabilization caused by the steric bulk of the cluster may be more prominent in the N phase and in this case suppresses it completely. Without X-ray analysis to determine whether the phase is SmA₁, SmA₂ or SmA_d it is not possible to say which of these explanations is correct. Although, given what was observed for compound **4** and other similar materials in the literature such as Deschenaux *et al*'s LC fullerodendrimers¹¹⁰ discussed in Chapter 3, it is plausible that the phase will be SmA₂ or SmA_d.

If comparing **35** with compound **34**, which has a terminal cyano rather than a terminal octyloxy group, the first thing of note is that by addition of the octyloxy chain the melting point is lowered dramatically. This is typical behaviour for low molar mass mesogens² with the alkoxy group disrupting crystal lattice packing resulting in a lower melting point. However, the cost of a lower melting point is a greatly reduced phase stability for the SmA phase and a complete loss of the N phase. It is likely that this loss in stability is due to the loss of the quadrupolar interactions of the cyano groups coupled with a long flexible chain which favour smectic phases as was discussed for the *n*-alkyl cyanobipenyls in Chapter 6.

The presence of the SmC phase in the phenyl and alkyl analogues of the octyloxy biphenyl benzoates and its absence in the carboranyl octyloxy biphenyl benzoate and the cyanobiphenyl benzoate is interesting. Figure 112 shows the outboard terminal dipoles in both the octyloxy biphenyl benzoate (left) and cyanobiphenyl benzoate (right) systems. As can be seen the octyloxy biphenyl benzoates have terminal outboard dipole moments at both ends of the mesogenic core which are a requirement for the formation of the SmC phase in the McMillan model⁸ and indeed they do show SmC behaviour. The cyanobiphenyl benzoate however has a strong terminal dipole moment along the long molecular axis in the form of a cyano group. This breaks the requirements of the McMillan model and no SmC behaviour is observed.

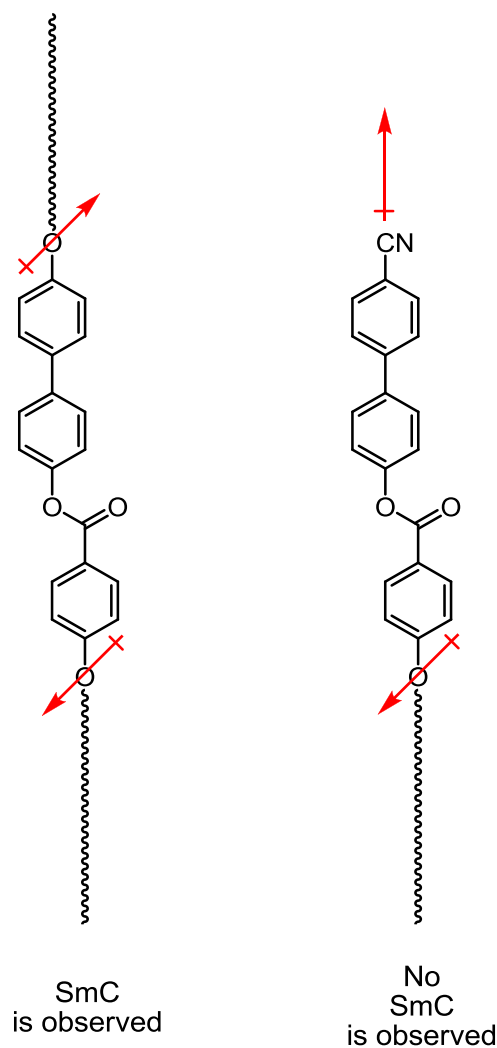
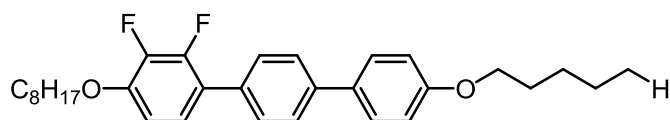
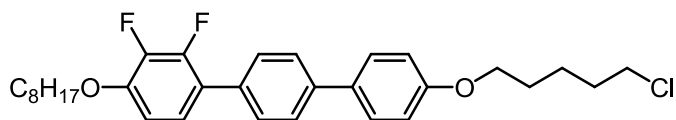


Figure 112: The origin of the SmC phase in the octyloxy biphenyl benzoates, dipoles shown in red

The lack of a SmC phase in the carboranyl material is interesting as it is present in both of its analogues, both of which show a very strong temperature dependence on the tilt angle as indicated by the undulating instabilities in their respective SmC phases. However, it is not possible to determine whether this is a direct result of the presence of the carborane or that the SmC phase is not observed due to the the greatly reduced phase range caused by the carborane.



Cr 93.5 SmC 144 SmA 148 N 159 Iso



Cr 80.2 SmA 154.9 Iso

Figure 113: Effect of polar end-group¹²²

It is possible however that the smectic C phase is being suppressed for another reason. Liquid crystals with polar end-groups tend to show strong anchoring at the layer interface caused by coupling of dipoles between different layers. This has the effect of suppressing tilted phases and is demonstrated by the suppression of the SmC phase upon the addition of a chlorine end-group in the difluoroterphenyls shown in Figure 113¹²².

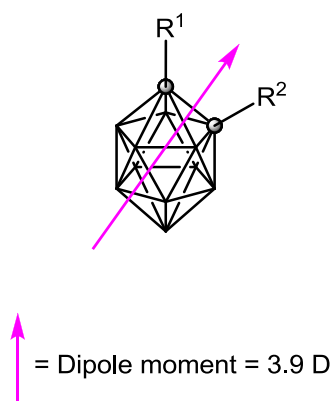


Figure 114: Dipole moment of o-carborane calculated by DFT (B3LYP/3-21G level of theory) methods

It has been shown by Laubengayer and Rysz that *o*-carborane displays a dipole moment of 4.5 D¹⁴². Furthermore, DFT calculations indicate that the dipole is directed towards the substituted carbon atoms (Figure 114), although there is a difference in the magnitude of the dipole moment calculated compared to the experimental value. As such, it is possible that these dipoles couple within the

microphase segregated part of a possible SmA_2 or SmA_d phase containing the carborane clusters as shown in Figure 115. This could result in strong anchoring as seen for other mesogens with polar end-groups and thus suppression of the SmC phase.

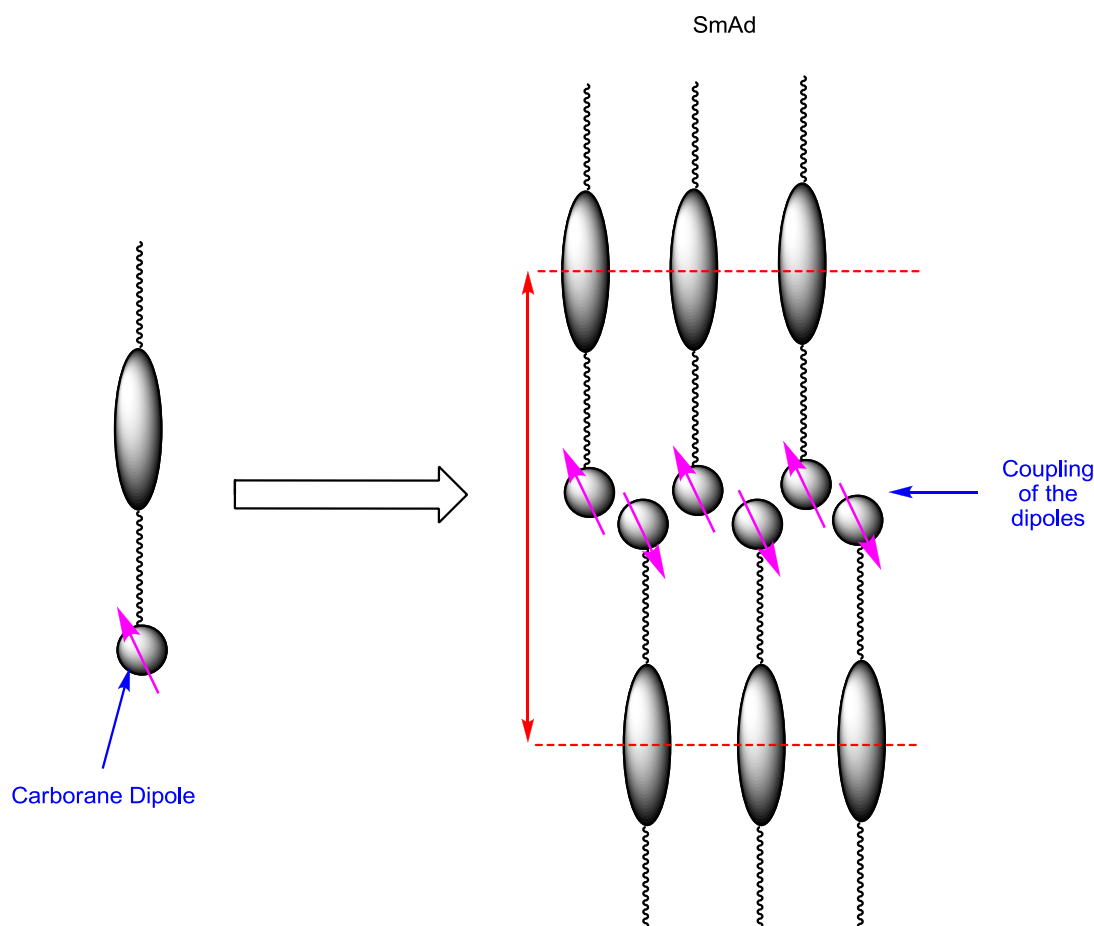


Figure 115: Coupling of carborane dipoles

7.3.2 Biphenyl Cyanobenzoates

This series of compounds comprises of mono-substituted carboranes functionalized with a biphenyl cyanobenzoate mesogen and its phenyl and alkyl analogues (Figure 116). This mesogen was chosen in conjunction with a biphenyl isothiocyanate benzoate mesogen in order to probe the effect of the cyano mediated quadrupolar interactions and also as a comparison with the cyanobiphenyl derivatives **29** and **30** - **34**. In this series quadrupolar interactions are expected to be present causing strong smectogenic behaviour as observed for the cyanobiphenyl mesogens.

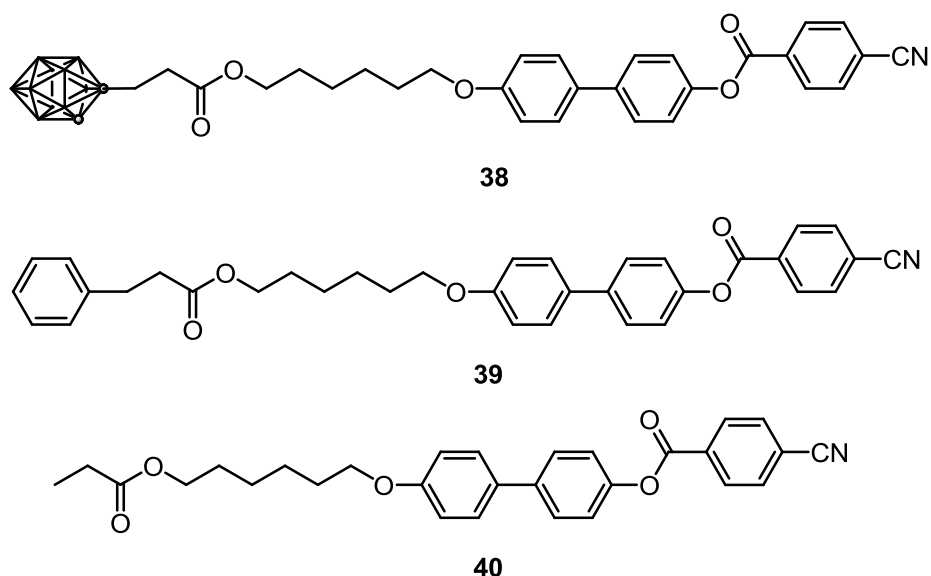


Figure 116: Structures of compounds **38**, **39** and **40**

The DSC trace of **38** shows a melt to the isotropic liquid on the first heat with onset at 106.6 °C ($\Delta H = 33.0 \text{ kJmol}^{-1}$). Upon subsequent heat cycles there were three reproducible thermal events, a glass transition with a maximum in the rate of change of the heat capacity at 20.2 °C, a cold crystallization starting at 84.3 °C ($\Delta H = -8.3 \text{ kJmol}^{-1}$) and an endotherm at 108.2 °C ($\Delta H = 10.7 \text{ kJmol}^{-1}$) corresponding to a melt into the isotropic fluid. Upon cooling **38** also shows three reproducible transitions, an Iso liq. - LC transition at 107.9 °C ($\Delta H = -0.4 \text{ kJmol}^{-1}$), a LC-LC transition at 89.0 °C ($\Delta H = -0.3 \text{ kJmol}^{-1}$) and the glass transition, as on heating, at 20.2 °C.

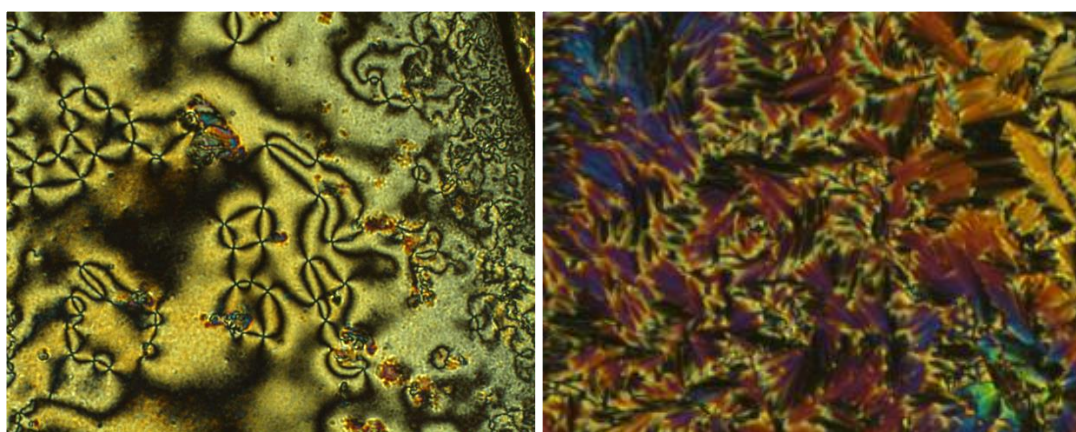


Figure 117: POM micrographs of: left) the schlieren texture of the N phase of **38** at 102.8 °C after cooling from the isotropic fluid at 1°Cmin^{-1} ; right) the focal-conic texture of the SmA phase of **38** at 85.8 °C upon cooling from the N phase at $0.5^\circ \text{Cmin}^{-1}$

Chapter 7: Mono-functional Esters: The Effect of the Mesogen

Upon cooling **38** from the isotropic liquid a *schlieren* texture (Figure 117 left) showing both two and four brush defects and areas of homeotropic alignment which are optically extinct develop. This allows the phase to be assigned as N. Further cooling results in the formation of a focal-conic texture (Figure 117 right) and areas of homeotropic alignment which were optically. This allows the phase to be assigned as a SmA phase which is monotropic in nature.

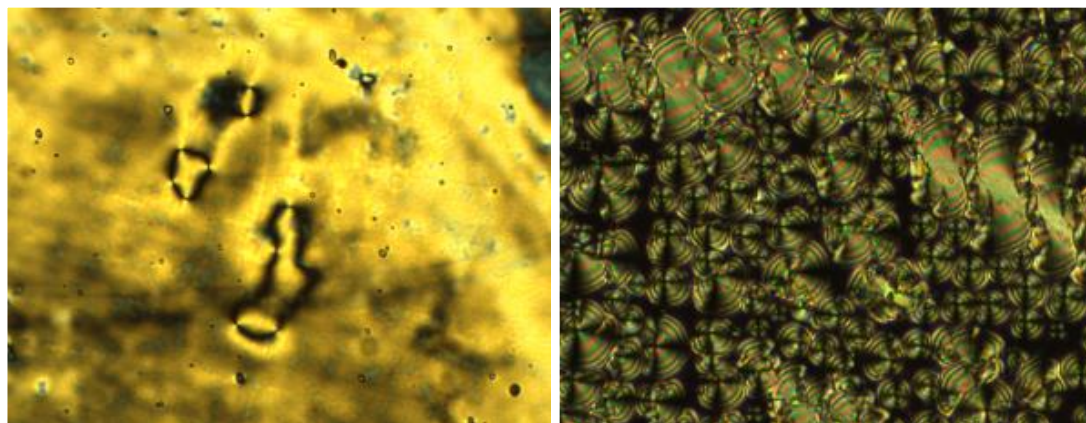


Figure 118: POM micrographs of: left) the schlieren texture of the N phase of 39 at 151.1 °C upon cooling from the isotropic liquid at 2 °Cmin⁻¹; right) the focal-conic texture of the SmA phase of 39 at 96.5 °C upon cooling from the N phase at 2 °Cmin⁻¹

1

The phase sequence of **39** was found to be Cr₁ 73.1 Cr₂ 77.6 SmA 119.0 N 151.7 Iso liq. as determined by DSC and POM (Figure 118) in the same manner as that for compound **38**.

Likewise the phase sequence of **40** was found to be Cr 92.9 SmA 99.2 N 187.0 Iso liq. as determined by DSC and POM (Figure 119).

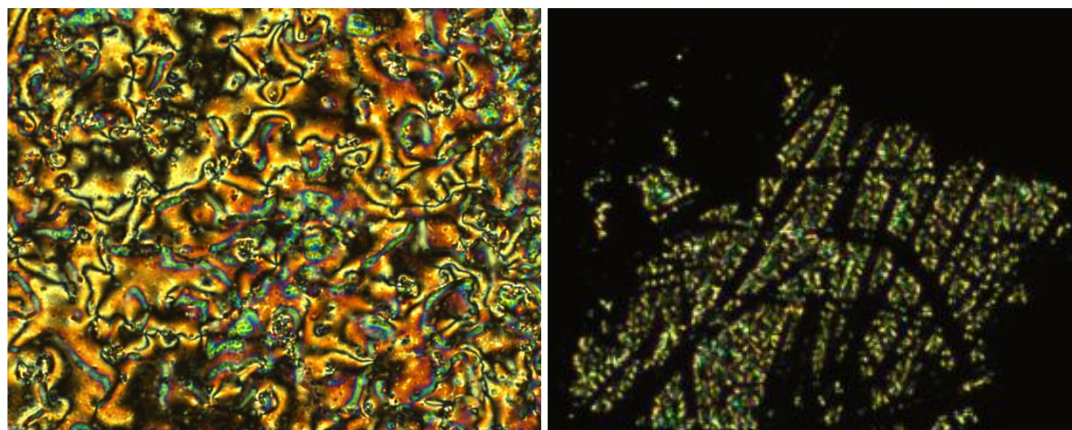


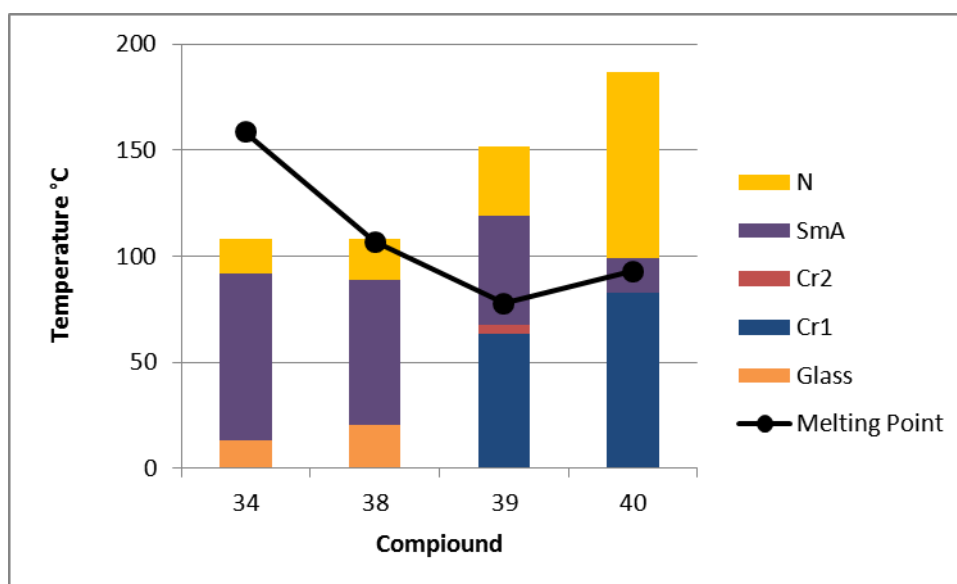
Figure 119: POM photomicrographs of: left) the schlieren texture of the N phase of 40 at 182.4 °C upon cooling from the isotropic fluid at 2 °Cmin⁻¹; right) the focal-conic texture of the SmA phase of 40 at 91.6° C upon cooling from the N phase at 1 °Cmin⁻¹

7.3.2.1 Phase Structure

As with the octyloxy biphenyl benzoates there are two options for the structure of the smectic phases in this series. Either, the carboranes do not microphase segregate and form a SmA₁ phase or they do and either a SmA₂ or SmA₄ phase is formed. It would be expected that the SmA_d phase would be favoured by all three materials in this series owing to the cyano group interdigitating in the same manner as has been described for the cyanobiphenyl based mesogens from previous chapters.

7.3.2.2 Comparisons

Graph 4 summarises the phase behaviour and thermal properties of the biphenyl cyanobenzoate series, **38**, **39** and **40**. As observed in the octyloxy series, moving from ethyl to phenyl to carboranyl end-group results in a consistent decrease in clearing points. This can be attributed to the bulkier groups creating a larger destabilization of the mesophases resulting from the greater steric hindrance they lend to the molecule.



*Graph 4: The thermal properties of the biphenyl cyanobenzoate series and the carboranyl cyanobiphenyl benzoate **34** included for comparison, thermal behaviour shown in bars is that observed for cooling cycles, the melting points shown are for the pristine sample*

The stability of the N and smectic phases in this series also correlate strongly to the size of the end-group, with the carboranyl having the broadest SmA phase followed by phenyl and alkyl. The behaviour observed can be explained by a stronger tendency to segregate when going from an alkyl, to phenyl and then to a carboranyl thus resulting in a broader SmA phase at the expense of the N phase. Currently it is not possible to ascertain whether this is a purely steric effect or whether the different electronic natures of the end-groups play a role.

Compounds **34** and **38** differ on the position of one phenyl ring and direction of the ester group. In **34** it is on the terminal side of the ester giving a cyanobiphenyl terminal group and in **38** it is on the internal side of the ester giving a cyanophenyl terminal group. These changes however have a dramatic effect on the melting point which is reduced by 50.5 °C on going from **34** to **38**, but otherwise the mesomorphic properties are very similar, both showing the SmA phase and a short range N phase.

7.3.3 Biphenyl Isothiocyanate Benzoates, 41, 42 and 43

The third series of compounds chosen for investigation in this chapter were a mono-functionalized carborane appended with a biphenyl isothiocyanate benzoate mesogen and its phenyl and alkyl analogues (Figure 120). This series in conjunction with the previous one was chosen in order to examine the effect of the quadrupolar interactions between the cyano groups of the mesogens and whether this helps to establish the smectogenic properties in them.

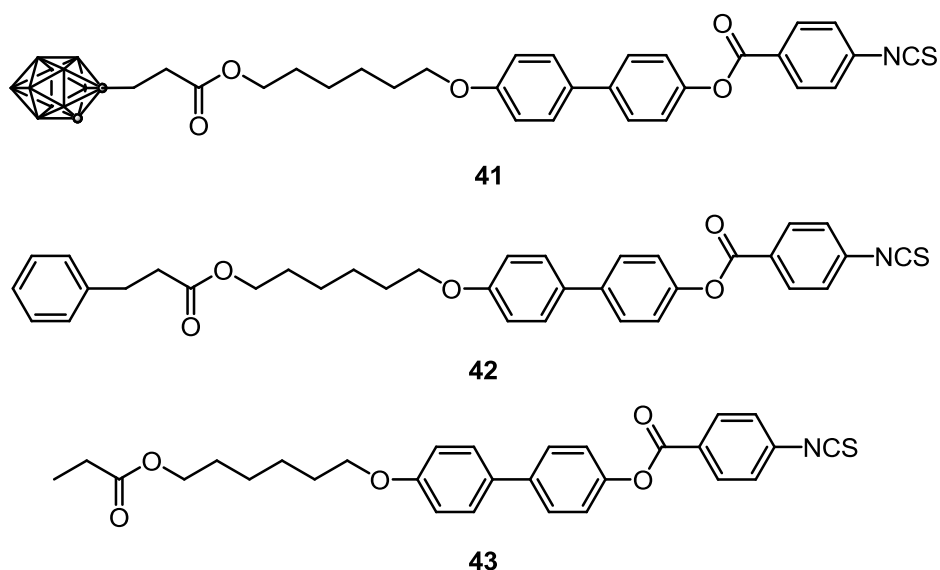
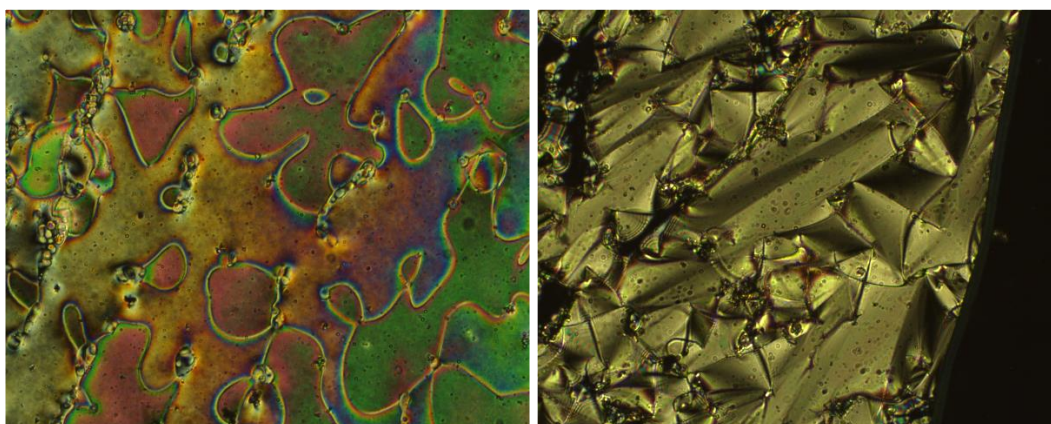


Figure 120: Structures of compounds 41, 42 and 43

Compound **41** shows a large endotherm upon the first heat associated with the melt into the isotropic liquid with onset at 130.1 °C and a $\Delta H = 44.4 \text{ kJmol}^{-1}$. Upon cooling there are four reproducible thermal events, the first at 127.0 °C ($\Delta H = -0.5 \text{ kJmol}^{-1}$) attributed to an Iso liq. to LC transition. Immediately following this there is another small exotherm at 125.8 °C ($\Delta H = -1.9 \text{ kJmol}^{-1}$) associated with a LC-LC transition, another LC-LC transition at 55.4 °C ($\Delta H = -1.3 \text{ kJmol}^{-1}$) is followed by a glass transition with a maximum in the rate of change in the heat capacity at 12.8 °C.

Upon subsequent heat cycles the material displayed the same glass transition as on cooling at 12.8 °C. This is followed by a LC-LC transition with onset at 47.8 °C ($\Delta H = 1.3 \text{ kJmol}^{-1}$), upon further heating to 89.0 °C there is a cold crystallization event ($\Delta H = -4.5 \text{ kJmol}^{-1}$). Finally there are two more endotherms with onsets at 121.5 °C

and 132.6 °C and ΔH s of 3.2 kJmol⁻¹ and 9.7 kJmol⁻¹ respectively. These are ascribed to a Cr-Cr transition followed by a melt into the isotropic fluid.



*Figure 121: POM photomicrograph of: left) the schlieren texture of the nematic phase of **41** at 123.9 °C upon cooling from the isotropic liquid at 1 °Cmin⁻¹; right) the focal-conic texture of the SmA phase of **41** at 120.9 °C upon cooling from the N phase at 1° Cmin⁻¹*

Upon cooling the material from the isotropic liquid the *schlieren* texture formed (Figure 121 left). As this phase was very narrow the material did not have time to develop defects although upon shearing the material flashed and there were areas of homeotropic alignment which were optically extinct. This evidence combined is enough to assign this phase as a monotropic N phase. Further cooling results in the development of a focal-conic texture (Figure 121 right) which displayed clear sets of ellipses and hyperbolae of optical discontinuity and areas of homeotropic alignment which are optically extinct, as such it was possible to assign this phase as a monotropic SmA phase.

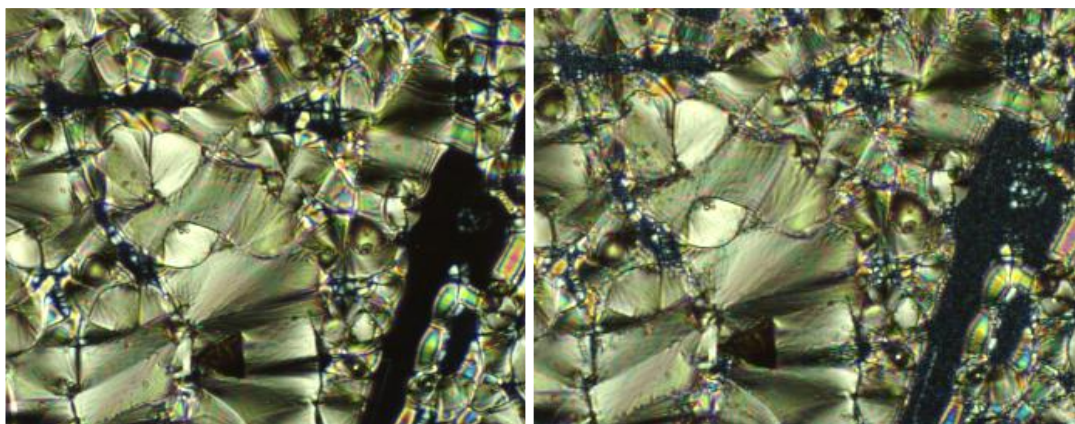


*Figure 122: POM photomicrographs of: left) the focal-conic texture of the Hexactic B phase of **41** at 54.1 °C after rapid cooling from the SmA phase; right) the focal-conic texture of the SmA phase of **41** at 60.1 °C after rapid heating from the Hexactic B phase*

Identification of the lowest lying mesophase was more challenging. Initially the phase transition was not obvious by microscopy with slow heat/cool rates. However, when scanned across the phase transition rapidly, herringbone defects developed on the fan backs (Figure 122) which after time would anneal out. There was no evidence of the fans becoming broken when entering the lower lying phase; this indicates that there were no long-range in plane correlations ruling out a soft crystal phase. This behaviour was observed both for heating and cooling. Furthermore, upon heating some of the homeotropically aligned domains formed a mosaic like texture (Figure 122 right); this combined with the other evidence allows this phase to be assigned as a hexactic B phase^{6,9}.

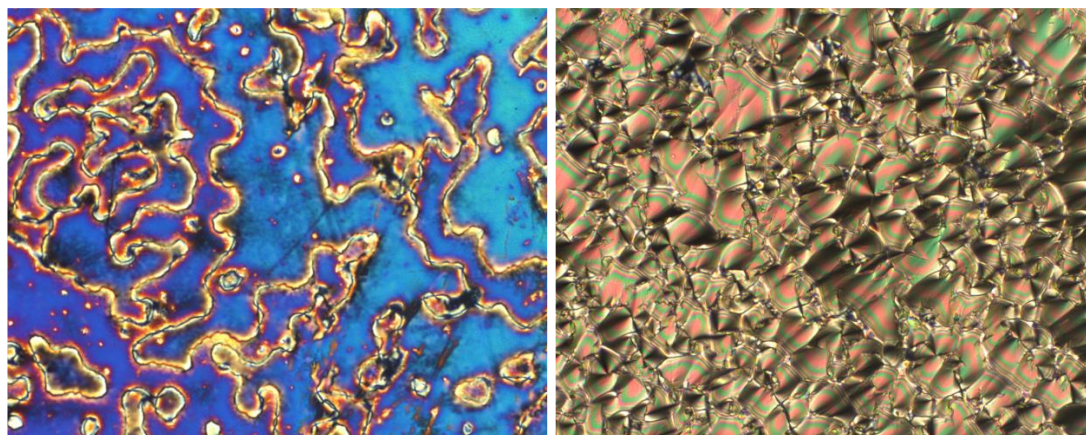


*Figure 123: POM photomicrographs of: left) the schlieren texture of the N phase of **42** at 159.4 °C upon cooling from the isotropic fluid at 1 °Cmin⁻¹; right) the focal-conic texture of the SmA phase of **42** at 152.6 °C upon cooling from the N phase at 1 °Cmin⁻¹*

The phase sequence for compound **42** was determined to be Cr₁ 55.6 Cr₂ (66.3 HexB) 66.9 SmA 154.3 N 162.0 Iso liq. by a combination of DSC and POM (Figure 123 and Figure 124) in a similar manner to compound **41**.

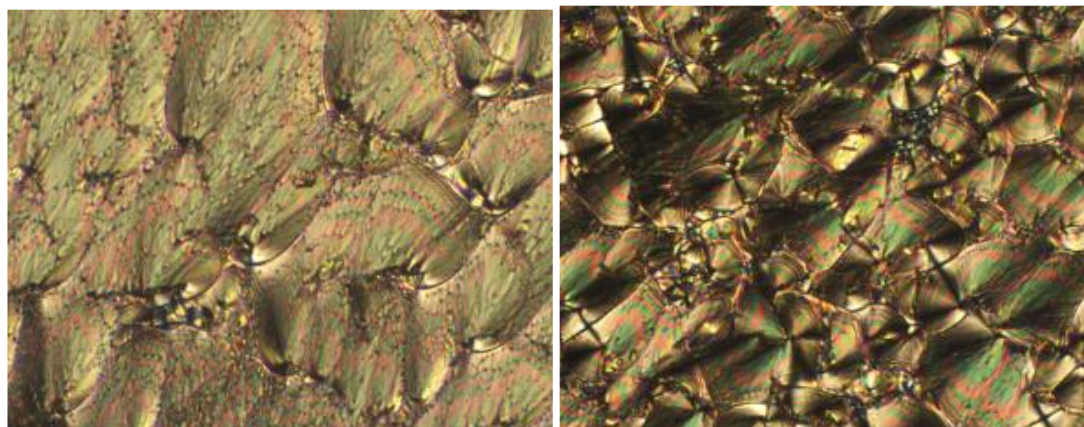


*Figure 124: POM photomicrographs of: left) the parabolic texture of the hexatic B phase of **42** with herringbone defects at 64.4 °C upon rapid cooling from the SmA phase; right) the focal-conic texture of the SmA phase of **42** with herringbone defects at 67.6 °C upon rapid heating of the hexatic B phase*

The phase sequence of compound **43** was found to be Cr 62.0 HexB 89.7 SmA 191.2 N 203.5 Iso liq. by a combination of DSC and POM (Figure 125 and Figure 126).

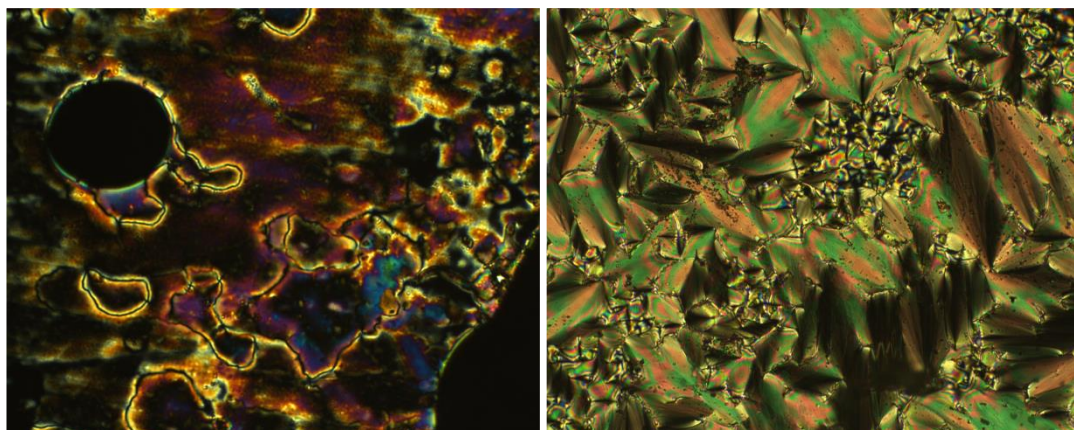


*Figure 125: POM photomicrographs of: left) the schlieren texture of the N phase of **43** at 202.5 °C upon cooling from the isotropic fluid at 2 °Cmin⁻¹; right) the focal-conic texture of **43** at 191.3 °C upon cooling from the N phase at 2 °Cmin⁻¹*

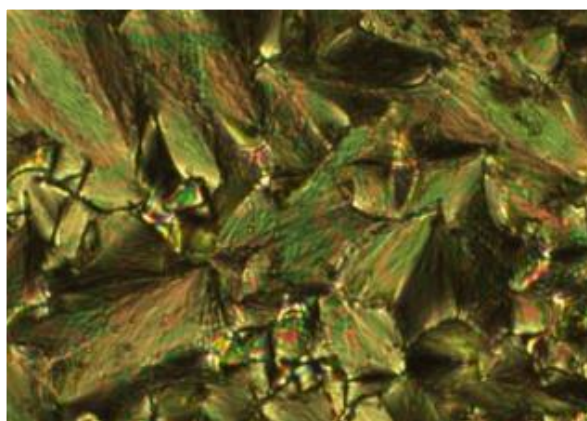


*Figure 126: POM photomicrograph of the focal-conic texture of the hexatic B phase of **43** with herringbone defects at 66.3 °C upon rapid cooling from the SmA phase*

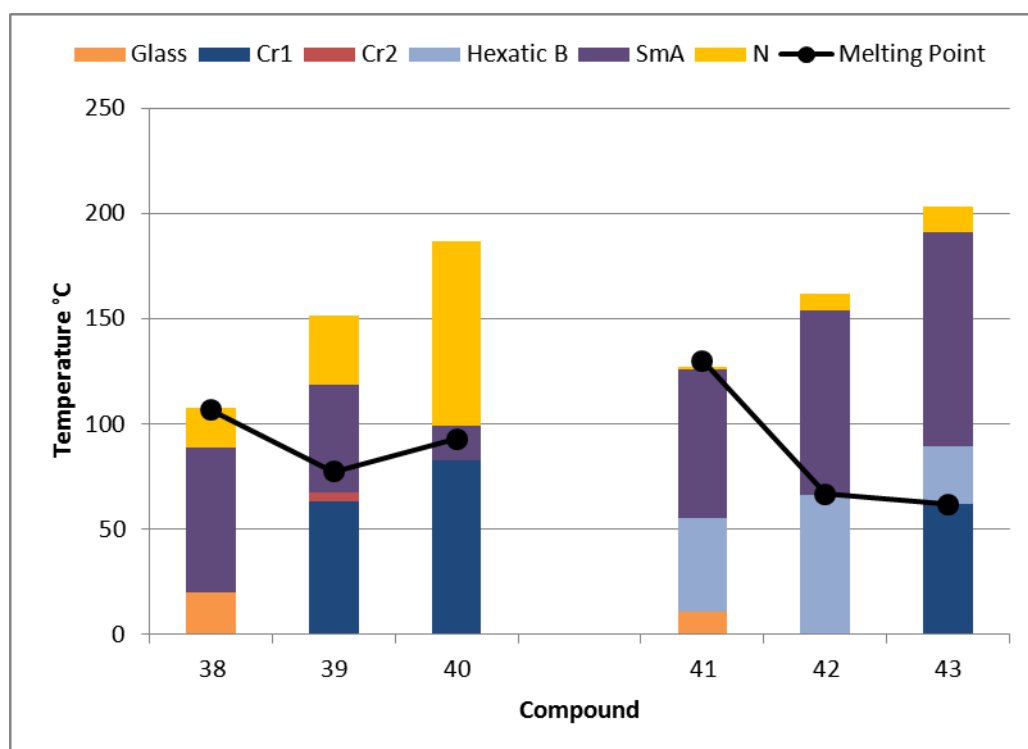
7.3.3.1 Phase Structure

It is proposed that the structure of the SmA phases of the biphenyl isothiocyanate benzoate series is likely to be very similar to that of the octyloxy biphenyl benzoates. While either a SmA₁ or SmA₂ phase is possible for all three materials it is unlikely that the phenyl or alkyl analogues will display a SmA_d phase. This is because without the cyano group there is no driving force for interdigitation and therefore if a bilayer type phase were to form it would be SmA₂. However it is possible that the carboranyl material may display interdigitation of the carborane clusters and thus form a SmA_d phase.

The hexatic B phases of the biphenyl isothiocyanate benzoate series would be expected to be very similar to those of the SmA phases with the exception of short-range in plane hexatic order. The optical texture which indicated the hexatic B phase is a by-product of the ordering of the birefringent part of the materials, namely the mesogens. This hexatic ordering however does not necessarily transfer to the end-groups, but most importantly to the carboranes.

7.3.3.2 Comparisons

Graph 5 summarizes the phase behaviour of the biphenyl cyanobenzoate series (**38**, **39** and **40**) and its sister series the biphenyl isothiocyanate benzoates (**41**, **42** and **43**). In analogy to the other series presented in this chapter the carboranyl derivatives **38** and **41** showed the highest melting points and the lowest clearing points, again with their phase behaviour being entirely monotropic. In contrast, the phenyl and alkyl analogues show enantiotropic behaviour. Although, despite being monotropic in nature, the type of mesophase(s) observed is the same: the phases present in the model compounds are preserved. Again, similar to the other series the phenyl and alkyl members have similar melting points and the alkyl biphenyl isothiocyanate benzoate has the highest clearing point. This series again shows phase stability being greatest when the end-group is not present and smallest when the end-group is largest and the same arguments can be made to explain this.



Graph 5: The thermal properties of the biphenyl cyanobenzoates; 38, 39 and 40 and the biphenyl isothiocyanate benzoates; 41, 42 and 43, thermal behaviour shown in bars is that observed for cooling, the melting points shown are for the pristine sample

The first thing to notice when moving from a cyano group to an isothiocyanate group is the loss of the N phase in favour of broader smectic phases. This can be explained by the N phase being stabilized by associated dimers acting as single rod-like units increasing the anisotropy of the system. These dimers are facilitated by dipolar interactions of the cyano groups (Figure 127). As isothiocyanate moieties are not linear (Figure 128) replacing the terminal cyano with a terminal isothiocyanate will result in a loss of this terminal outboard dipole similar to that seen for the octyloxy biphenyl benzoates. This in turn will preclude the formation of associated dimers which would otherwise have stabilized the N phase.

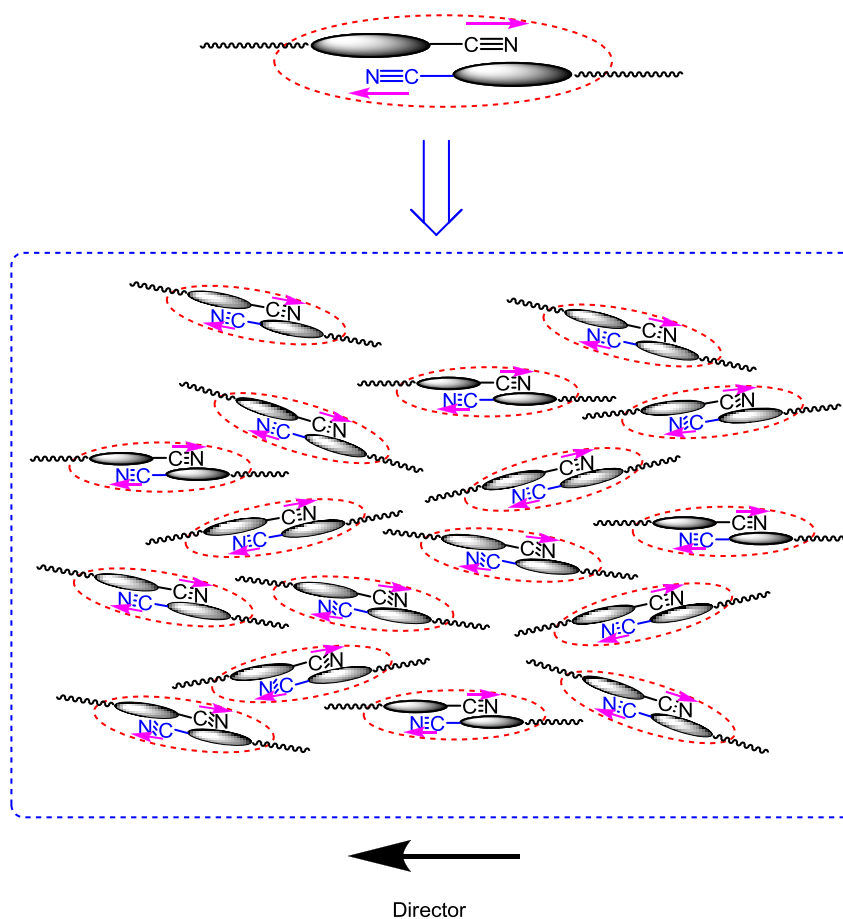


Figure 127: Associated dimers in the N phase

Figure 129 shows the phase transitions of 4-pentyl, 4'-cyanobiphenyl¹³⁶ and its isothiocyanate¹⁴³ analogue. It can be seen that by replacing the cyano group with an isothiocyanate group the mesophase range is increased and the N phase of the cyano compound is completely suppressed in favour of a SmA phase in the isothiocyanate material. The behaviour of the cyano and isothiocyanate compounds presented in this chapter mirrors that observed for simple cyanobiphenyl and isothiocyanate biphenyl derivatives (Figure 129). These series of compounds suggest that the smectogenic properties of the carborane clusters functionalized with cyano terminated mesogens are not due to the interactions of the cyano groups, in fact this group seems to be enhancing nematic tendency.

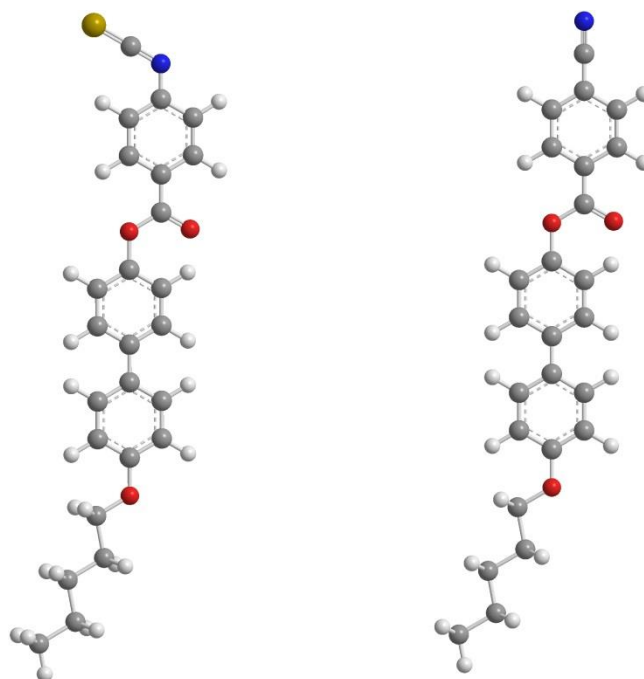
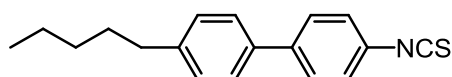


Figure 128: Molecular structure of a biphenyl 4-isothiocyanate (left) and biphenyl 4-cyano (right) benzoates

The presence of the hexatic B phase in the isothiocyanate series and not the cyano series can be explained in terms of crystallization. Upon cooling of the SmA phase in the isothiocyanate series the mesogens start to become more ordered within the plane of the smectic layers resulting in the formation of the hexatic B phase. Whereas in the cyano series as the SmA phase is cooled the mesogens simply crystallize owing to stronger quadrupolar interactions in the solid state. Further evidence of this can be seen in the difference in phase behaviour within the isothiocyanate series. Compounds **41** and **42** both have bulky end-groups which would be expected to disrupt packing and preclude crystallization, both show monotropic hexatic B behaviour. Whereas compound **43**, which has no such hindrance crystallizes readily and shows no monotropic hexatic B phase.



Cr 53 SmA 74 Iso



Cr 24 N 35 Iso

Figure 129: Phase transitions of 4-pentyl, 4'-cyanobiphenyl¹³⁶ and 4-pentyl, 4'-isothiocyanatobiphenyl¹⁴³

7.3.4 Cholesteryl Benzoates

The final series of compounds investigated in this chapter were mono-functionalized carboranes appended with a cholesteryl benzoate mesogen attached *via* an ester (**44**) linker and its phenyl (**45**) and alkyl (**46**) analogues (Figure 130) since cholesteryl benzoates promote chiral nematic behaviour. Furthermore, they serve as comparison to materials **12** – **15** derived from mesogen **18**, a four-ring chiral mesogen employed in previous chapters.

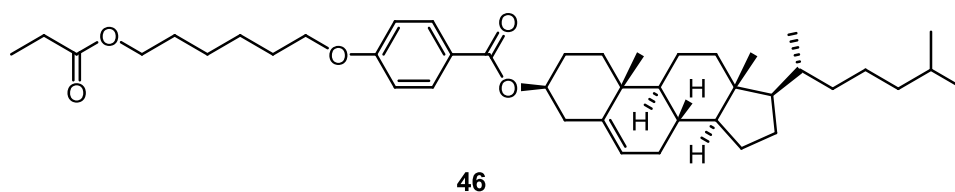
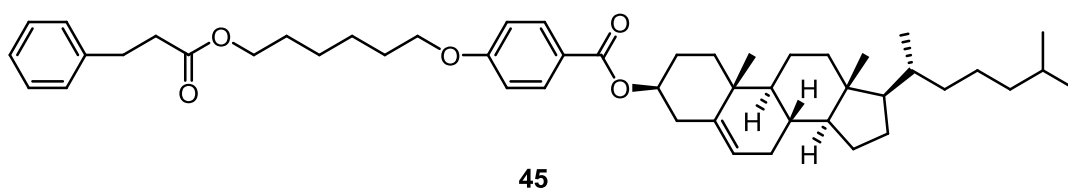
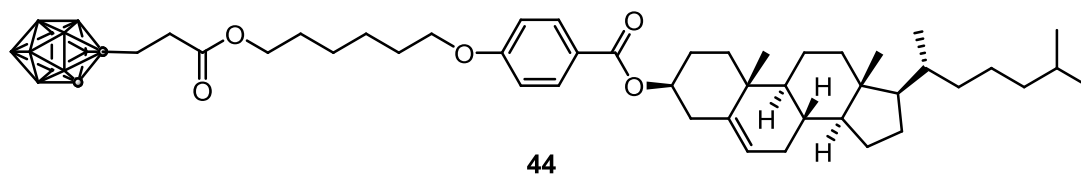


Figure 130: Structures of compounds **44**, **45** and **46**

The DSC trace of **44** shows a large endotherm upon the first heat with onset at 143.2 °C ($\Delta H = 25.4 \text{ kJmol}^{-1}$) which is caused by melting into the isotropic liquid. Upon cooling there were three reproducible thermal events, the first is an Iso liq. - LC transition at 131.7 °C ($\Delta H = -0.8 \text{ kJmol}^{-1}$), followed by a LC - LC transition with onset at 113.2 °C ($\Delta H = -0.6 \text{ kJmol}^{-1}$) and finally a glass transition where the greatest rate of change in the heat capacity was at 27.4 °C. Upon subsequent heating cycles there were four reproducible thermal events. The first three corresponded to the transitions observed upon cooling, however the final transition with onset at 143.2 °C is caused by the melting of partially recrystallized sample. It was possible to determine that this was the case as the enthalpy of this transition varied widely due to a varying amount of crystallization occurring on different heat/cool cycles.

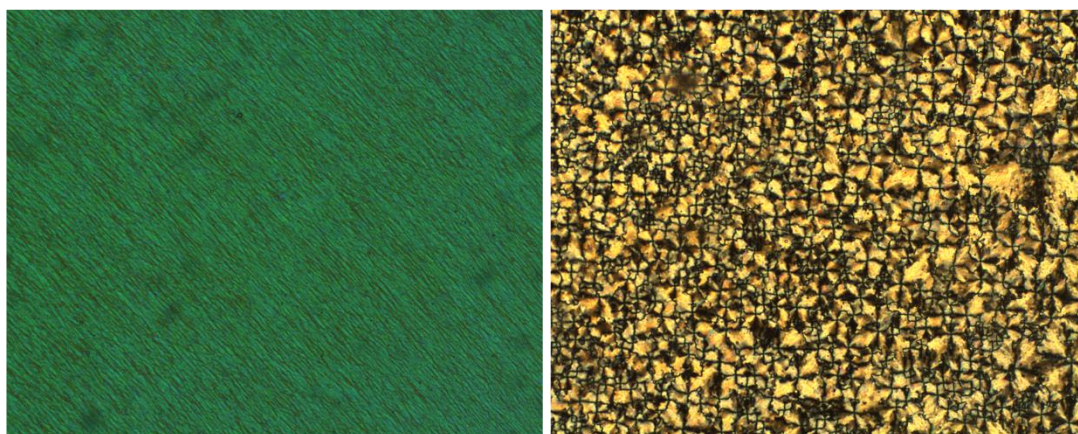


Figure 131: POM photomicrographs of: left) the Grandjean plane texture of the N phase of **44** at 114.4 °C upon cooling from the isotropic fluid at 1 °Cmin⁻¹; right) the focal-conic texture of the N* phase of **44** at 108.6 °C upon cooling from the isotropic fluid at 1 °Cmin⁻¹*

Upon cooling from the isotropic fluid compound **44** forms either the Grandjean plane texture (Figure 131 left) or a focal-conic texture (Figure 131 right) which allows us to assign this phase as a monotropic N* phase. It is worth noting that although this material was not particularly viscous (qualitative observation) the texture is very slow to respond to thermal changes thus allowing the capture photomicrographs of the N* phase below the phase transition as measured by DSC (Figure 131 right).

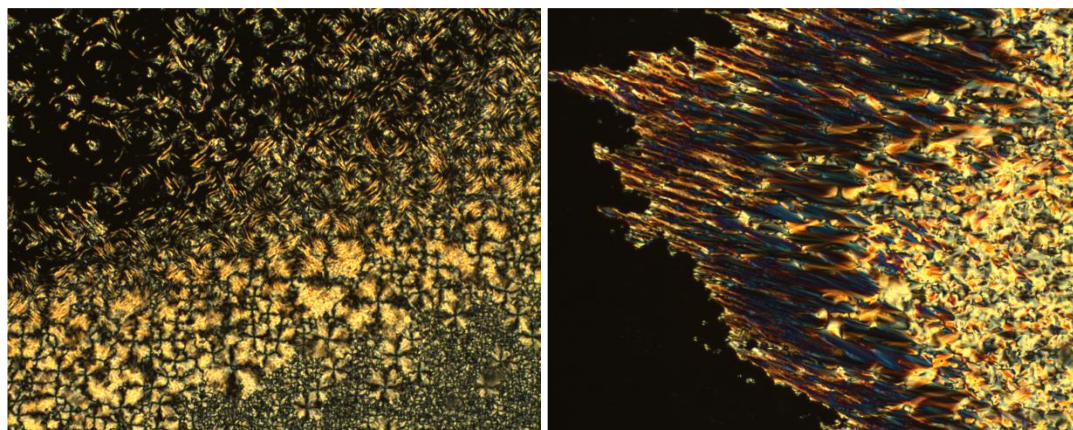


Figure 132: POM photomicrographs of: left) the N to TGB phase transition from the focal-conic texture at 107.3 °C cooling at 1 °Cmin⁻¹; right) the N* to TGB phase transition from the Grandjean planar texture at 100.3° C cooling at 1 °Cmin⁻¹*

Further cooling of the N* phase results in the formation of a transient twist grain boundary (TGB) phase which was identified primarily from the degradation of the focal-conic texture into fibrils (Figure 132 left). If cooling from the Grandjean plane texture however these fibrils were not observed, instead a broken focal-conic-like texture formed (Figure 132 right) which demonstrates the necessity for careful microscopy and the effect of paramorphosis on the observed texture of a phase. Owing to the transient nature of this phase it was not observed by DSC. The phase was only observed for around 1 °C by POM.

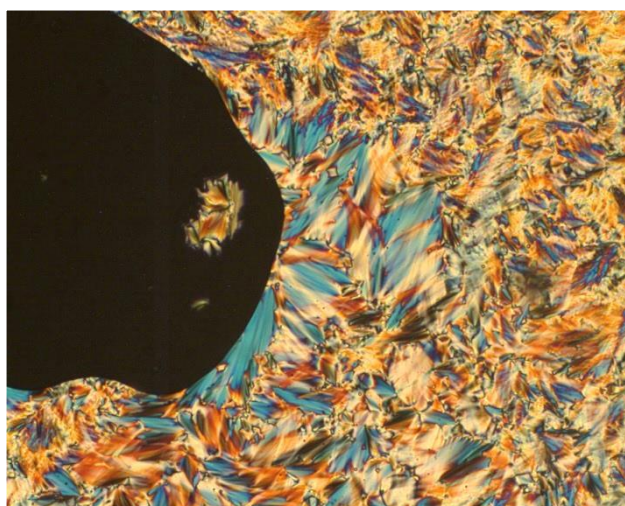
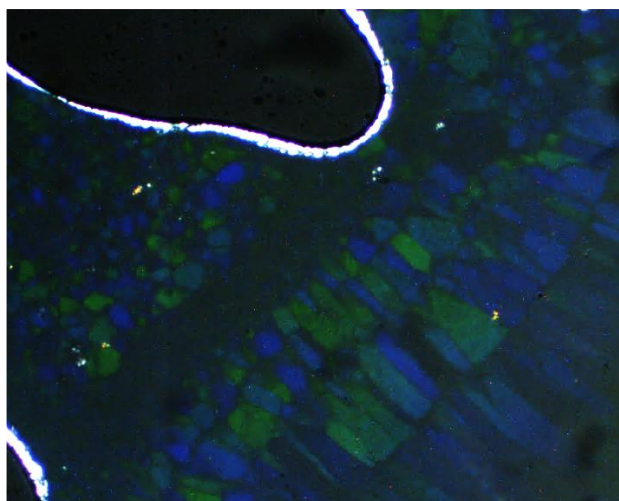


Figure 133: The paramorphic focal-conic texture of the SmA phase of **44** at 98.0 °C upon cooling at 1 °Cmin⁻¹*

At temperatures below the observed TGB phase of **44**, either an optically extinct texture was observed if cooled from the focal-conic texture of the N* phase or a strongly paramorphic focal-conic texture was observed when cooling from the Grandjean plane texture of the N* phase. The optically extinct texture is caused by the homeotropic alignment of the material indicating that the phase is orthogonal. The focal-conic texture although highly distorted points to a SmA* phase, in addition to this shearing of the sample results in oily streaks, in combination this allows the phase to be assigned as a monotropic SmA* phase.



*Figure 134: POM photomicrograph of the BP2 of **45** at 146.7 °C upon cooling from the isotropic fluid at 1 °Cmin⁻¹*

The phase sequence of compound **45** was determined by DSC and POM (Figure 134 to Figure 138) and was found to be Cr₁ 35.7 Cr₂ (16.0 CrE) 49.2 SmA* 116.9 TGB 118.0 N* 148.7 BP2 148.9 Iso liq. The blue phase II (BP2) was identified by the characteristic blue and green platelet texture observed when cooling from the isotropic liquid (Figure 134). Both the TGB and BP2 phases were only observed by POM.

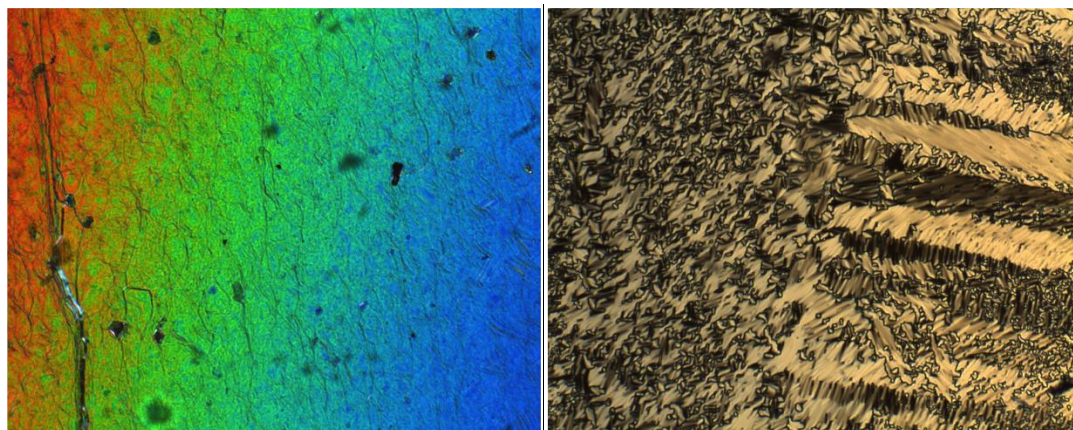
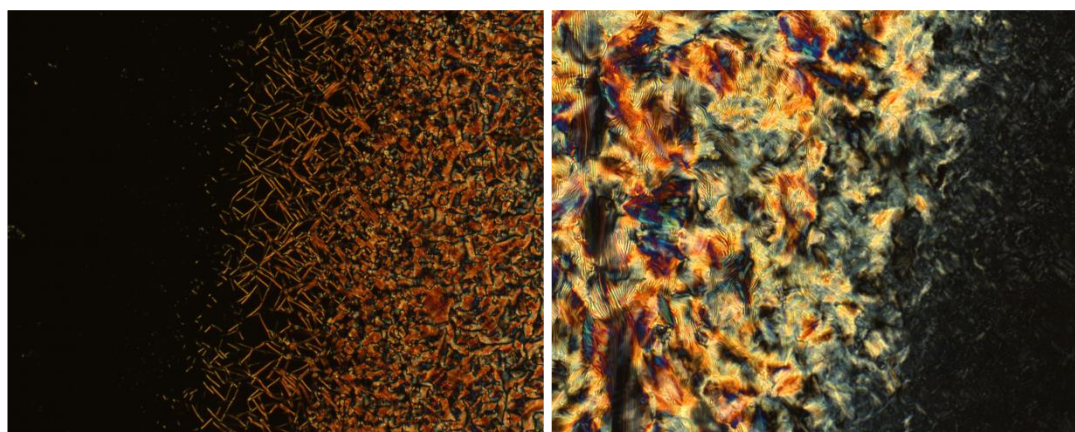


Figure 135: POM photomicrographs of: left) the Grandjean plane texture of the N^ phase of **45** at $119.0\text{ }^\circ\text{C}$ upon cooling from the isotropic liquid at $1\text{ }^\circ\text{Cmin}^{-1}$; right) the focal-conic texture of the N^* phase of **45** at $144.2\text{ }^\circ\text{C}$ upon cooling from the isotropic liquid at $1\text{ }^\circ\text{Cmin}^{-1}$*



*Figure 136: POM photomicrographs of **45**: left) the TGB to N^* transition at $118.4\text{ }^\circ\text{C}$ heating at $1\text{ }^\circ\text{Cmin}^{-1}$ from the optically extinct texture of the SmA^* phase; right) the N^* to TGB phase transition at $117.8\text{ }^\circ\text{C}$ upon cooling from the focal-conic texture of the N^* phase at $1\text{ }^\circ\text{Cmin}^{-1}$*

Compound **45** displays a monotropic crystal E (CrE) phase. This was identified by striations forming across the fan backs upon cooling from the SmA^* phase, which would disappear again upon heating back into the SmA^* phase. These striations are caused by the formation of a monoclinic lattice in the CrE phase and are related to the a and b lattice parameters (Figure 137). In addition the phase transition to and from the CrE phase was followed by strong transition lines caused by stressing of the

fans resulting from a change in volume of the smectic layers. This behaviour is characteristic of the CrE phase¹⁴⁴ thus allowing this phase to be assigned as a monotropic CrE phase.

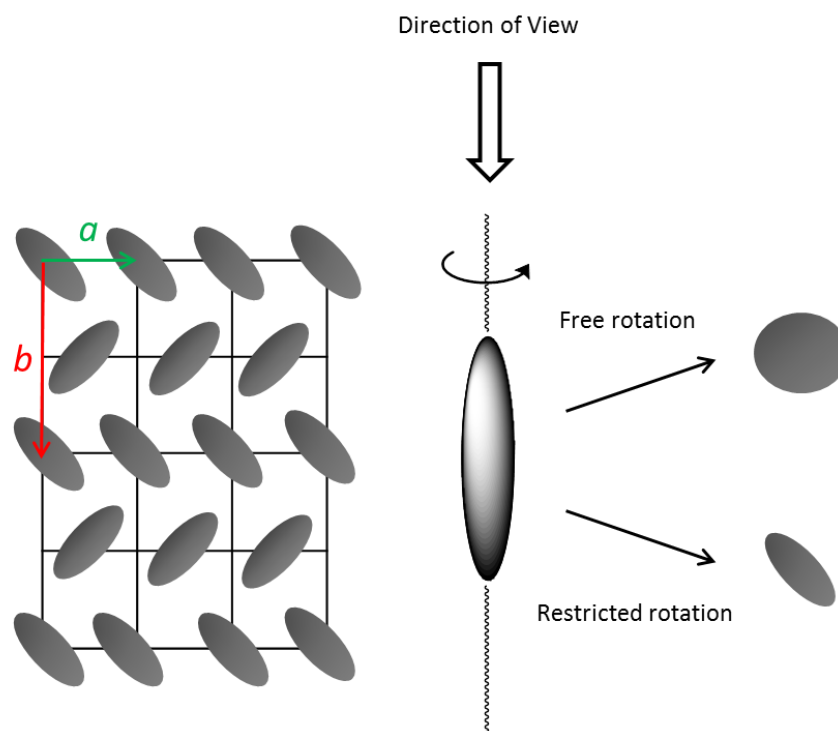


Figure 137: Structure of the CrE phase

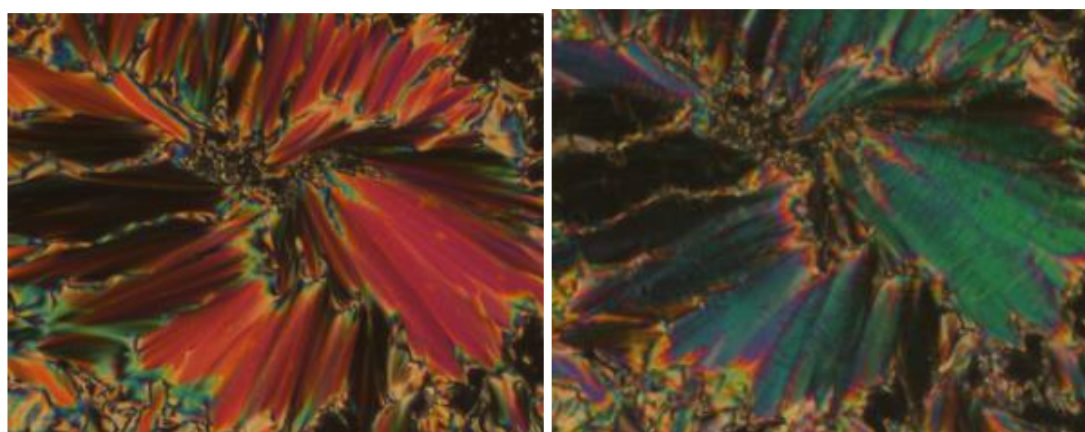
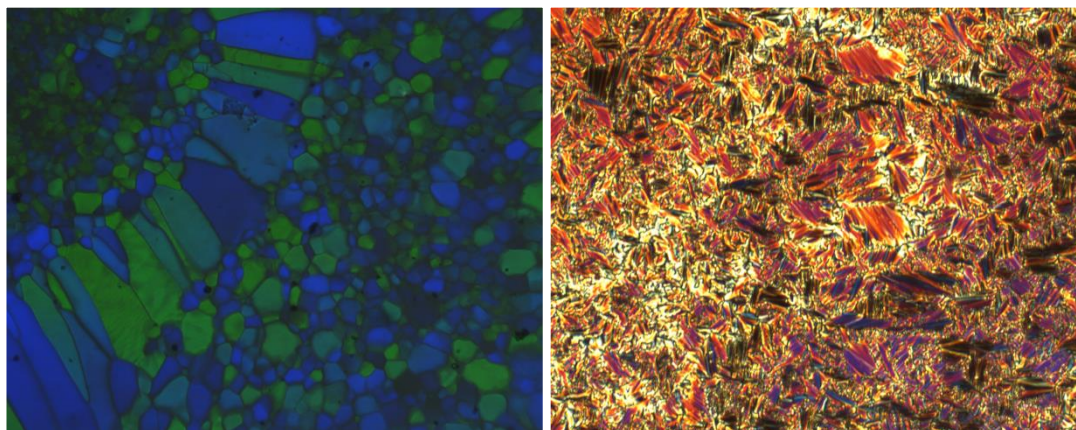


Figure 138: POM photomicrographs of: left) the focal-conic texture of the SmA* phase of **45** at 110.2 °C cooling at 1° Cmin⁻¹; right) the focal-conic texture of the CrE phase of **45** at 4.1 °C upon rapid cooling from the SmA*

The phase sequence of **46** was found to be Cr 101.4 SmA* 142.0 TGB 152.2 N* 182.2 BP2 185.3 Iso liq. and was determined by a combination of DSC and POM

(Figure 139 and Figure 140). Both the TGB and BP2 phases were only observed by microscopy. It is also worth noting that the material, despite not being particularly viscous (qualitative assessment), was very sluggish to react to thermal changes. As such the TGB phase appears to be far broader than it actually is when taken in conjunction with other values from DSC. POM showed that this phase only existed over ~ 1 °C.



*Figure 139: POM photomicrographs of: left) the platelet texture of the BP2 of **46** at 183.1 °C upon cooling from the isotropic fluid at 1 °Cmin⁻¹; right) the focal-conic texture of the N* phase of **46** at 181.1 °C upon cooling from the BP2 phase at 1 °Cmin⁻¹*

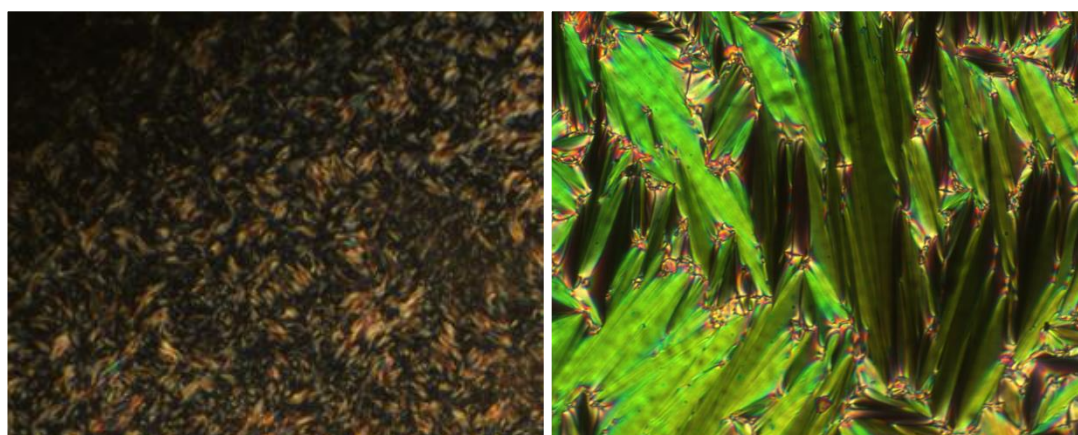


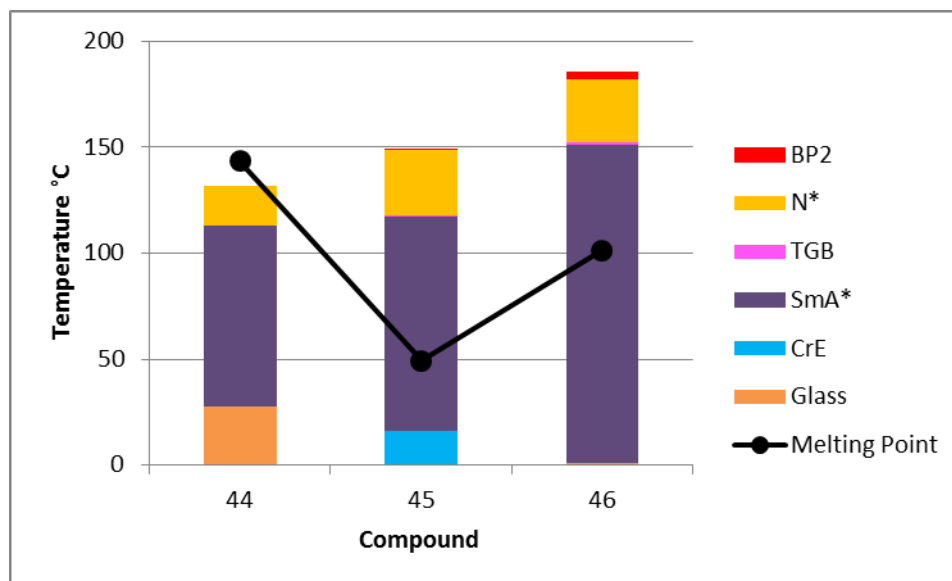
Figure 140: POM photomicrographs of: left) the N to TGB phase transition of **46** at 114.8 °C upon cooling at 1 °Cmin⁻¹; right) the focal-conic texture of the SmA* phase of **46** at 127.5 °C upon cooling at 3 °Cmin⁻¹ from the N* phase*

7.3.4.1 Phase Structure

The structure of the SmA* phase presented by the carboranyl derivative in this series is likely to resemble the SmA phase of the octyloxy biphenyl benzoates. The arguments for which type of structure is formed are also similar to those of the octyloxy biphenyl benzoates, either the materials can adopt a bilayer SmA₂ or SmA_d phase, or a simple monolayer SmA₁ type phase. The carboranyl material, **44** is most likely to form the SmA₂ or SmA_d type phase due to microphase segregation of the carborane clusters, as discussed for **38** and **41**.

7.3.4.2 Comparisons

Graph 6 summarises the phase behaviour of the cholesteryl benzoate series. Again, in this series the clearing points decrease steadily from **46** upon introduction of the phenyl (**45**) and then carboranyl (**44**) end-groups, which is consistent with behaviour observed for the other materials in this chapter. The carboranyl derivative has the lowest mesophase stability. In addition to this the carboranyl member of this series, **44**, has the highest melting point, therefore the lowest combined mesophase range, and only exhibits monotropic phase behaviour. However, in this series the melting points of the phenyl and alkyl members, **45** and **46**, are markedly different, with the phenyl material having the lowest melting point. This difference in behaviour is attributed to the nature of the mesogenic core. In all the other series presented the mesogenic core is poly-aromatic. However, in this series the mesogenic core is an unsaturated poly-alicyclic. It is argued that the phenyl end-group is less able to closely pack with the unsaturated poly-alicyclic and as such has a depressed melting point.



Graph 6: The phase behaviour of the cholesterol benzoates

Initially, it is worth noting that the smaller the end-group the more stable the BP2 becomes. The BP2 is a frustrated phase and the disturbance of a bulky end-group would almost certainly destabilize it. In addition, **44** has the smallest range for the TGB phase. Given that the TGB phase is also a frustrated phase it is unsurprising that the largest end-group causes the greatest disruption.

This series also shows the apparent stabilization of the SmA* phase at the expense of the N* upon addition of the carborane. This is in full agreement with what has been observed throughout this and previous chapters. Overall there is strong evidence to support the notion that the carborane cluster is imparting strong smectogenic properties upon the materials produced. This behaviour can only be attributed to micro-phase segregation of the carborane clusters.

7.4 Concluding Remarks

Through this chapter the emergence of a number of trends which bridge across all of the different mesogenic cores and therefore they are likely trends caused by the carborane end-group have become evident. In the four series presented here, the mesophase types present in the model compounds are preserved in the carboranyl

derivatives. However, the transition temperatures are lowered significantly and the lowering is not uniform across them- each phase type is affected differently.

The carborane cluster also causes a significant lowering of the clearing point. Furthermore, this lowering of the clearing point is not entirely a steric effect, as the phenyl end-group, which is only marginally smaller than the carborane showed a much smaller depression in the clearing point.

The reason for this seems to be twofold: firstly, the steric hindrance caused by the cluster is bigger than that of a phenyl ring. A bulky end-group makes space filling and close packing more difficult and thus lowers the clearing point, but this effect is much bigger for the carborane than for the phenyl. Secondly there is an electronic component, the carborane contains no π -electrons therefore is unable to stabilize π -stacking with the mesogenic cores. The phenyl end-group however, does have delocalized π -electrons and therefore the phase can be stabilized by π -stacking between the phenyl end-group and the mesogenic core or between end-groups. Further proof for this can be seen in the greater destabilization caused by the phenyl end-group in the cholesterol benzoate series owing to the reduced amount of delocalized π -electrons in the mesogenic core.

It has also been shown that the carborane cluster is strongly smectogenic regardless of the nature of the mesogenic core employed. Initially it was thought that the use of mesogens with cyano terminal end-groups was helping to drive smectogenic behaviour in the materials presented (Chapters 3 – 6). In this chapter it has been shown that the terminal cyano groups in fact stabilize the N phase, in effect helping to mask the strong smectogenic tendencies of the carborane end-group.

It is proposed that smectogenic behaviour is most probably due to a tendency of the carborane clusters to microphase segregate. The phenyl analogues also show a tendency towards smectic phases. Therefore, there is likely a steric effect at play in regards to both end-groups. If the carborane clusters segregate in the smectic phase, they do not cause a destabilization of the close packing of the mesogens. In addition to this, end-groups can interpenetrate the close packing of the mesogens thus lowering the destabilization as demonstrated by the phenyl end-group. In the N phase

neither of these options are possible. As such materials with end-groups are more likely to form smectic phases and from the series presented so far, the likely segregation of the carboranes causes a stronger tendency towards smectic phases than that of the interdigitation of the phenyl end-groups. X-ray diffraction of any of the phases in this chapter would enable more a confident assertion that the carboranes are microphase segregating and thus causing the formation of SmA₂ or SmA_d type phases.

In this chapter the first example of a carborane liquid crystal material which displays a higher order smectic phase has been observed, **41** displays a hexatic B phase. However this hexatic order is not necessarily passed on to the carborane clusters.

None of the carborane containing materials exhibit a tilted smectic phase. The model compounds **36** and **37** of the octyloxy biphenyl benzoate series both show the SmC phase, whereas the carboranyl member **35** only shows an orthogonal SmA phase. It is still unclear whether this lack of tilted phases is due to the depression of the phase range caused by the bulky end-group or whether it is a direct effect of the carborane such as polar anchoring.

8. In Search of the Smectic C Phase

8.1 Summary

Up to this point a tilted smectic phase has not been observed in compounds containing a carborane cluster. One possibility for the cause of this observation is a strong anchoring at the layer interface caused by dipole-dipole interactions between the carborane clusters which has been observed for other liquid crystals with terminal polar groups¹²² and was discussed in Chapter 7. In this chapter a series carboranes mono-functionalized with mesogens shown to support SmC phase formation in non-carborane-containing systems (Figure 141) is presented with the aim of generating tilted smectic phases.

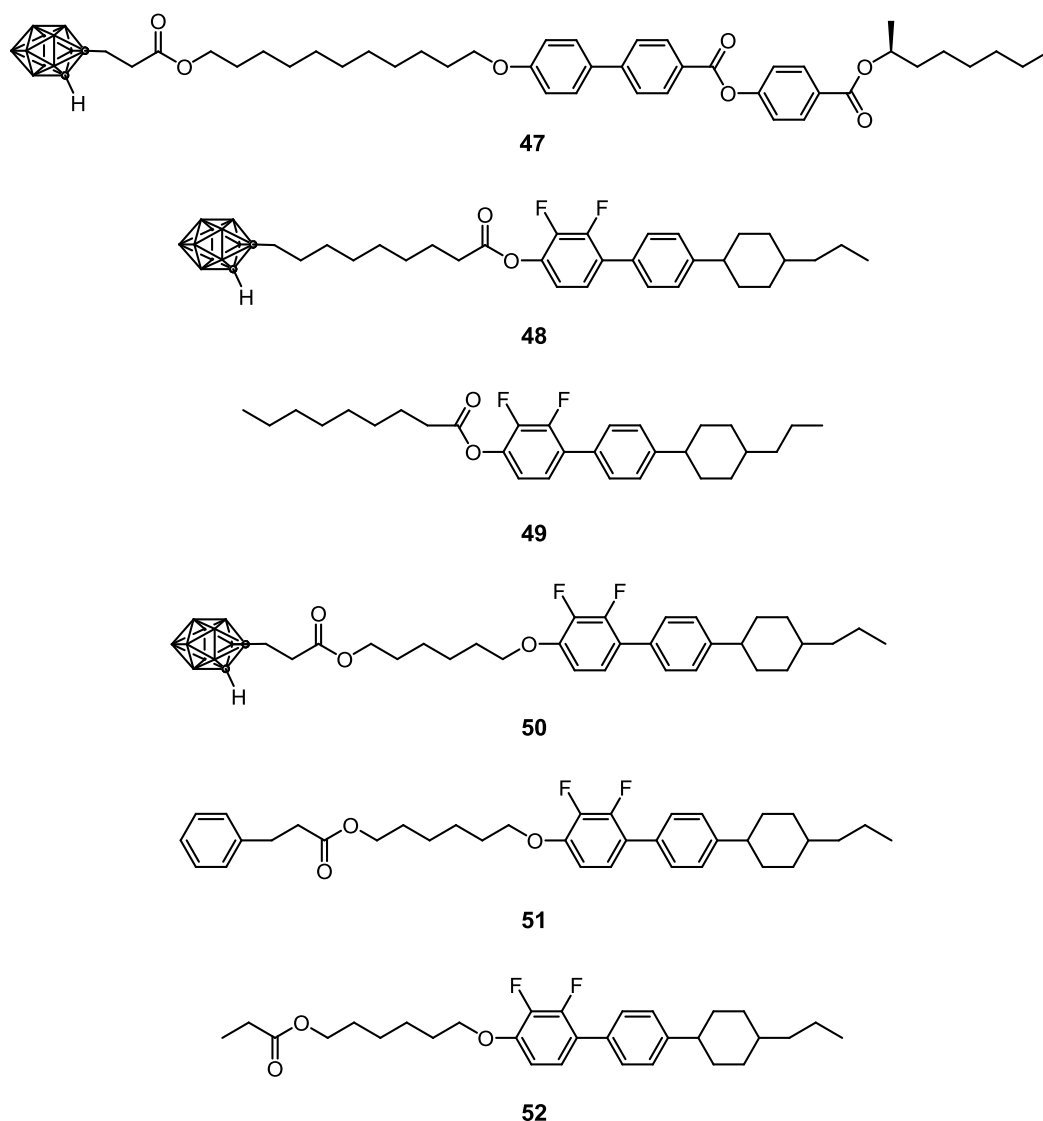


Figure 141: Mono-functionalized carboranes appended with SmC promoting mesogenic moieties and their phenyl and alkyl analogues

Chapter 8: In Search of the Smectic C Phase

In this chapter a material which is analogous to previously reported compounds which have a tilted smectic phase with carbocyclic pendant groups¹⁰¹ is described. In addition, carborane containing compounds appended with the difluorobiphenylcyclohexyl mesogenic moiety which has been shown to support SmC phases in non-carborane-containing systems¹²⁴ and their alkyl and phenyl analogues as model compounds in the same manner as previous chapters are also presented.

8.2 Synthesis

The SmC-promoting mesogens, **53** and **54**, were kindly provided by Dr Stephen Cowling¹⁰¹ and Dr Edward Davis¹²⁴ respectively. As such their synthesis will not be discussed here.

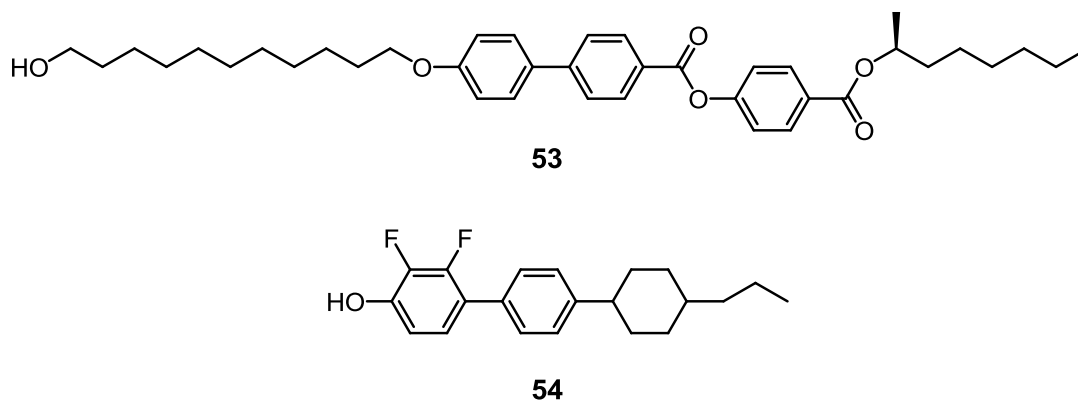
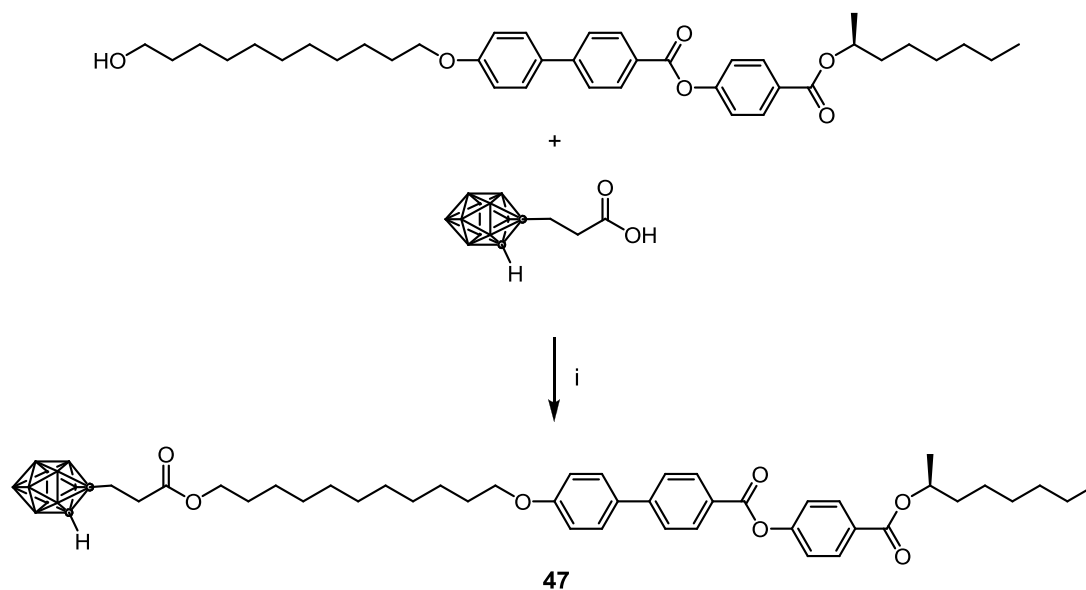


Figure 142: SmC supporting mesogenic moieties

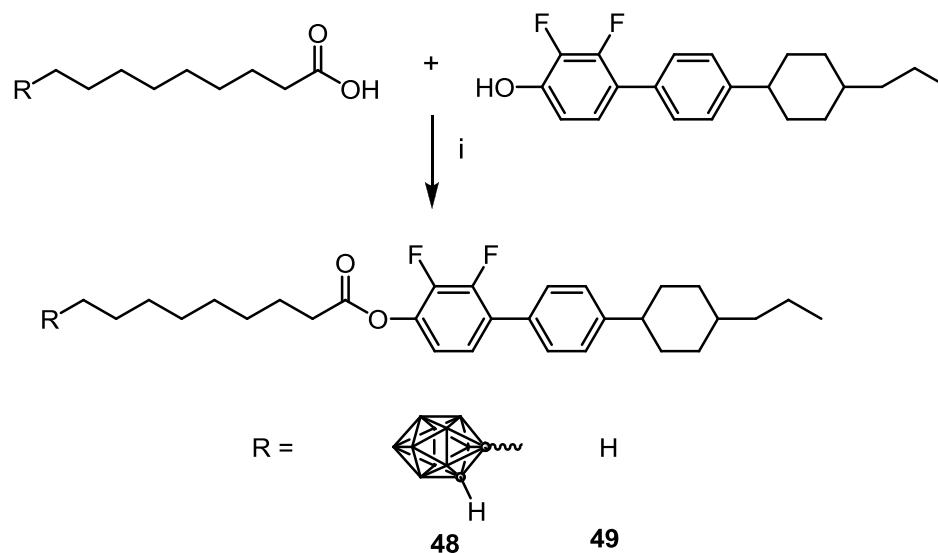
Compound **47** uses 1-hydroxy-2-propanoic acid dicarba-*closo*-dodecacarborane described in Chapter 6 and its synthesis will not be discussed here. The final compound **47** was obtained by a simple Steglich esterification between the mesogen **53** and 1-hydroxy-2-propanoic acid dicarba-*closo*-dodecacarborane (Scheme 13).



i) DMAP and EDAC in DCM

Scheme 13: The synthesis of compound 47

Scheme 14 shows the synthesis of the mono-functionalized carborane with a 2,3-difluoro-4'-(4-propylcyclohexyl)biphenyl mesogenic core connected *via* a direct ester linkage to the core (compound **48**) and its alkyl analogue (compound **49**), using the same synthetic protocol described for **47** (Scheme 13).



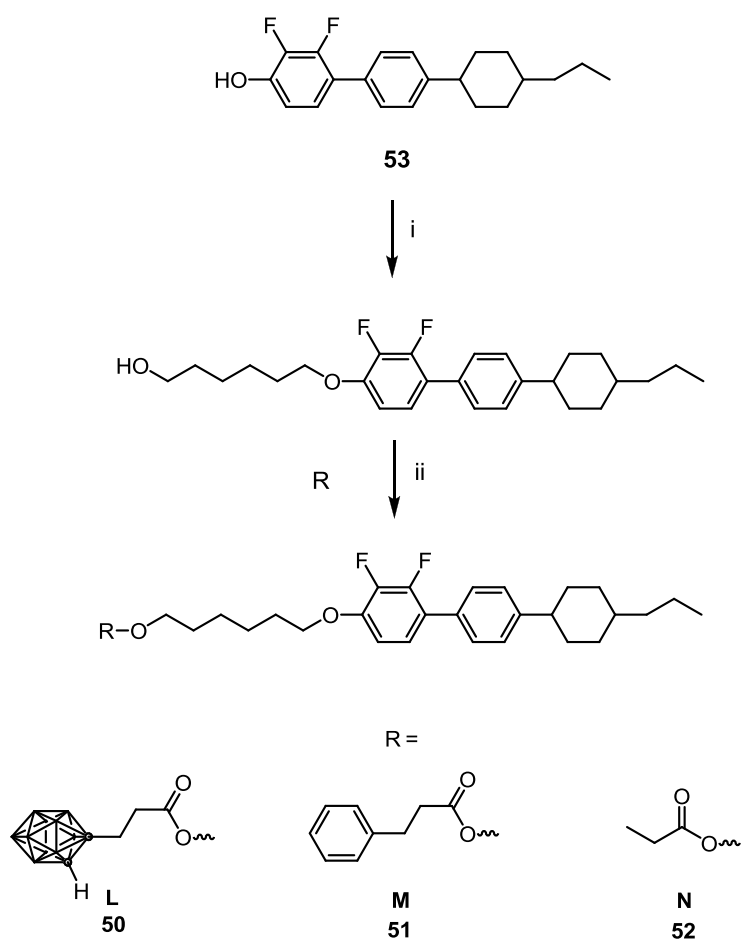
i) DMAP and EDAC in DCM

Scheme 14: The synthesis of materials 48 and 49 with a 2,3-difluoro-4'-(4-propylcyclohexyl)biphenyl mesogenic core with a direct ester linkage

Chapter 8: In Search of the Smectic C Phase

Scheme 15 summarises the synthesis of the mono-functionalized carborane with a 2,3-difluoro-4'-(4-propylcyclohexyl)biphenyl mesogenic core attached *via* a central ester linkage (**50**) and its phenyl (**51**) and alkyl (**52**) analogues. This synthesis follows the same general procedure as that of the octyloxy biphenyl benzoate functionalized materials from the previous chapter.

Williamson etherification of the phenolic mesogenic core with 6-bromohexan-1-ol installs the flexible spacer between the mesogenic core and the ester linking group. Finally a Steglich esterification with either 1-hydro-2-propanoic acid dicarbocloso-dodecacarborane, hydrocinnamic acid or propionic acid installs the end-group yielding **50**, **51** and **52** respectively.



i) 6-Bromohexan-1-ol, K_2CO_3 and KI in butanone
ii) DMAP and EDAC in DCM

*Scheme 15: The synthesis of materials **50**, **51** and **52** with a 2,3-difluoro-4'-(4-propylcyclohexyl)biphenyl mesogenic core with a central ester linkage*

8.3 Thermal Properties

The thermal properties and any subsequent phase behaviour of the mono-functionalized carboranes appended with SmC promoting mesogens and their phenyl and alkyl analogues were investigated using DSC and POM and is summarised in Table 10.

Compound	Glass	Crystal 1	Crystal 2	SmA	N	Iso		
47		•			101.2	•		
48		•			123.3	•		
49		•		92.9	•	138.7		
50		•	78.4	• (20.1* •)	97.9	•		
51	•			-28.0	•	34.8	•	
52		•	7.8	•	28.9	•	55.0	•

Table 10: The thermal properties of the mono-functionalized carboranes appended with SmC promoting mesogens: values taken from DSC with a heat/cool rate of 10 Cmin⁻¹ except values marked with a * which are taken from POM, values in brackets are for monotropic transitions

Compound **47**, the mono-functionalized carborane appended with an (*S*)-4-((octan-2-yloxy)carbonyl)phenyl biphenylcarboxylate *via* an ester linkage (Figure 143) was found to be non-mesogenic. The DSC trace showed one reproducible thermal event upon heating, the melt into the isotropic fluid with onset at 101.2 °C ($\Delta H = 71.3$ kJmol⁻¹). Upon cooling the crystallization supercools by 42 °C to 59.0 °C ($\Delta H = -48.0$ kJmol⁻¹).

The previously reported series of compounds with bulky alicyclic end-groups using the same mesogenic core all display liquid-crystalline behaviour¹⁴⁵ (Figure 143). The general rule found was that with increasing size of the end-group the clearing point fell and orthogonal phases were suppressed, whereas the melting point stayed around 50 +/- 10 °C. The carboranyl derivative **47**, which although not identical to the motif used previously, having one additional methylene group between the cluster and the ester, is similar enough that the completely different behaviour observed in this material is significant.

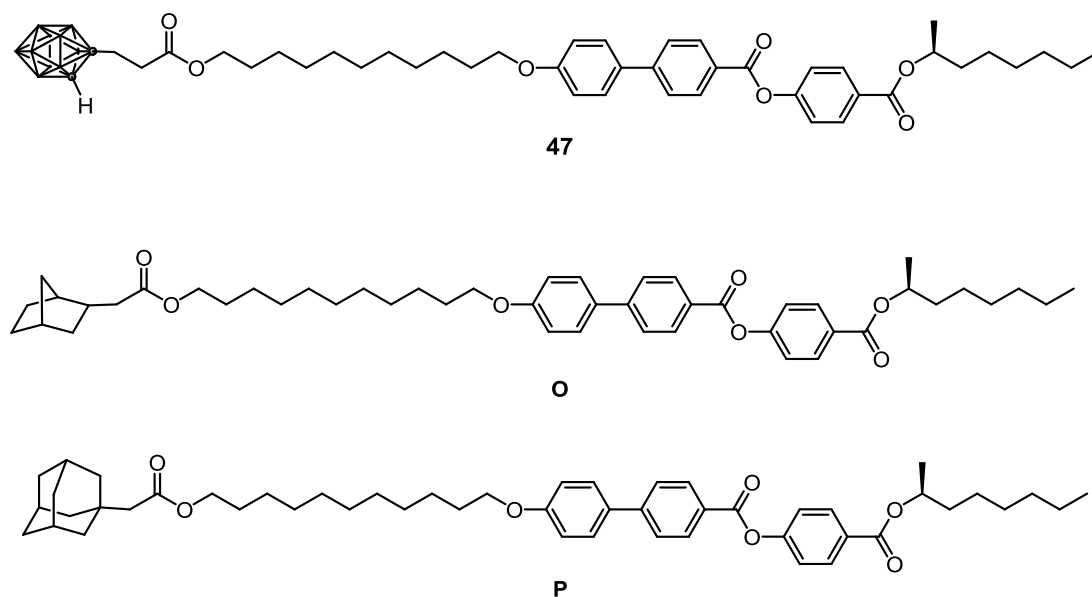


Figure 143: Structure of compound **47** and its carbocycle analogues with either a bicyclooctyl (**O**) or adamantly (**P**) end-group¹⁴⁵

Figure 144 shows space filling models of the two largest end-groups used previously and the carboranyl end-group which was employed in this chapter. The carboranyl group is slightly larger than the adamantane with a cross-section of around 5.7 Å compared to 5.0 Å respectively. Furthermore, both the carborane cluster and the adamantane are rigid spherical structures. If only sterics and conformational flexibility affect the observed phase behaviour, it would be expected that the carboranyl material **47** would exhibit similar phase properties except a likely lower isotropization point.

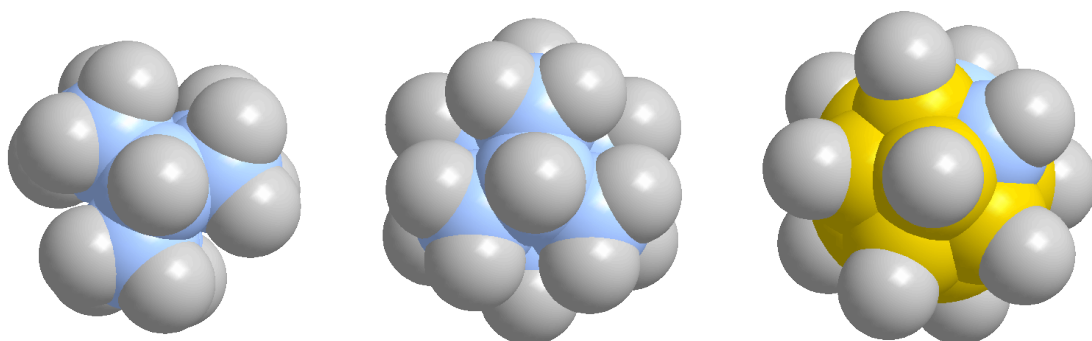


Figure 144: Space filling models of: left) bicyclooctyl; centre; adamantyl; right) and carboranyl end-groups (drawn to scale)

Chapter 8: In Search of the Smectic C Phase

Compound **47** however is entirely non-mesogenic whereas the adamantane terminated material previously reported (Figure 143 **P**) showed an enantiotropic chiral smectic C (SmC*) phase of around 12 °C and a monotropic SmC* anticlinic phase. The carboranyl material also displays a significantly higher melting point, far more so than would be expected from an odd even effect caused by the additional methylene group. This increase in melting point is consistent with the other mono-functionalized carboranes appended with mesogenic moieties from Chapters 6 and 7. It is likely that any mesophase which may have been observed is lost owing to the high melting point and strong crystalline nature of the material. As such we are it is not possible to infer anything about the observed suppression of tilted phases caused by the carborane cluster from this material.

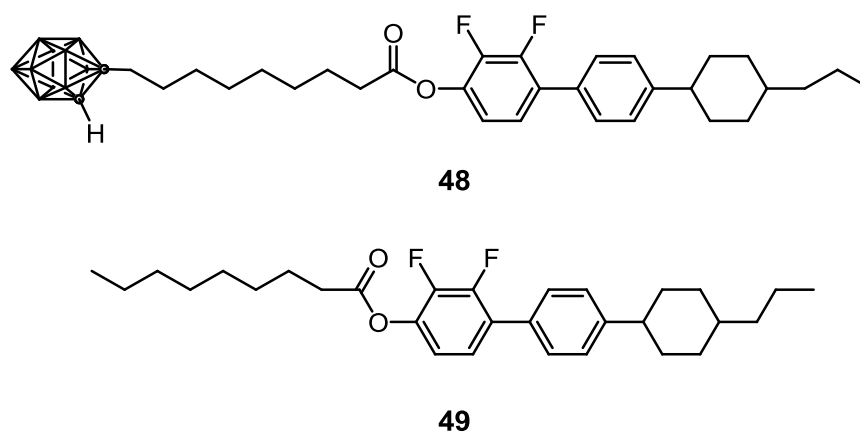
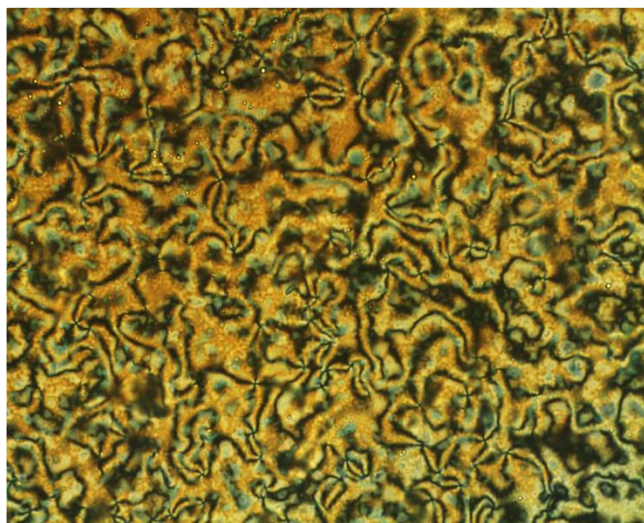


Figure 145: Structures of compounds **48** and **49**

Compound **48**, the mono-functionalized carborane appended with a 2,3-difluoro-4'-(4-propylcyclohexyl)biphenyl mesogenic core connected *via* a direct ester linkage (Figure 145) showed one reproducible thermal event upon heating, a large endotherm with onset at 123.3 °C ($\Delta H = 14.7 \text{ kJmol}^{-1}$) associated with a melt into the isotropic liquid. Upon cooling the crystallization supercools by 26.1 °C to 97.3 °C ($\Delta H = -15.9 \text{ kJmol}^{-1}$). POM failed to show any birefringent textures associated with LC phases. As such this material is non-mesogenic.

Compound **49** (Figure 145) however showed two reproducible thermal events upon heating. The first is a large endotherm with onset at 92.9 °C ($\Delta H = 28.4 \text{ kJmol}^{-1}$) which is attributed to a melt into a LC phase. The second is a weak endotherm at

138.7 °C ($\Delta H = 0.6 \text{ kJmol}^{-1}$) caused by a transition into the isotropic fluid. The crystallization supercools by around 8 °C.



*Figure 146: POM photomicrograph of the schlieren texture of the N phase of **49** at 134.0 °C upon cooling from the isotropic fluid at 1 °Cmin⁻¹*

When **49** is cooled from the isotropic fluid the *schlieren* texture develops (Figure 146) showing both two and four brush defects and areas of homeotropic alignment which are optically extinct. Furthermore, upon mechanical shearing the material flashes. This combined indicates that this is an enantiotropic N phase.

The lack of a mesophase in the carboranyl **48** is not that surprising given the limited mesogenic properties of the alkyl member **49**. In previous chapters it has been seen that the inclusion of the carborane moiety tends to increase the melting point and depress the clearing point of any mesophases present. This is exactly the behaviour which observed here. The melting point of the carboranyl material is around 30 °C higher, bringing the melting point close to the original clearing point. As the clearing point is also likely depressed it is to be expected that it would fall below the melting point. Compound **48** however does not display any monotropic phases most likely due to a strong tendency to crystallize.

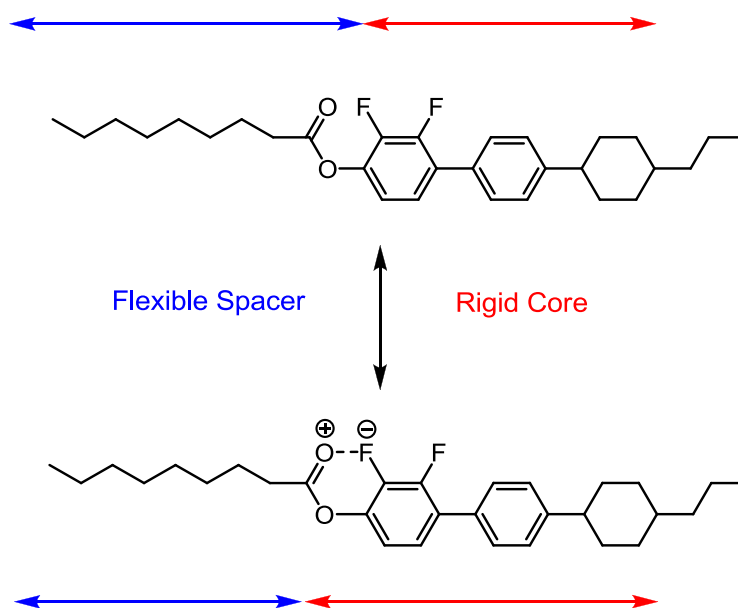


Figure 147: Possible intramolecular interactions in **49**

The absence of smectic phases at all let alone a SmC phase in compound **49** is interesting. However, it can be explained by a simple examination of likely intramolecular interactions between different substituents. It is possible that the COO of the ester interacts with the fluorine on the 2 position of the external phenyl ring via a halogen bond (Figure 147). This would effectively incorporate the ester into the rigid core of the mesogen lengthening it and shortening the flexible terminal chain. This would destabilize smectic phases in favour of the N phase.

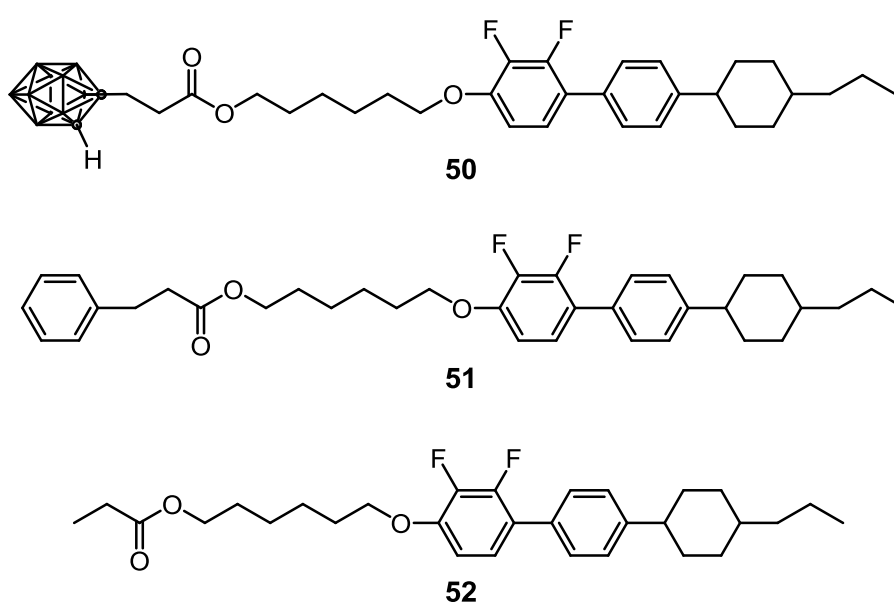
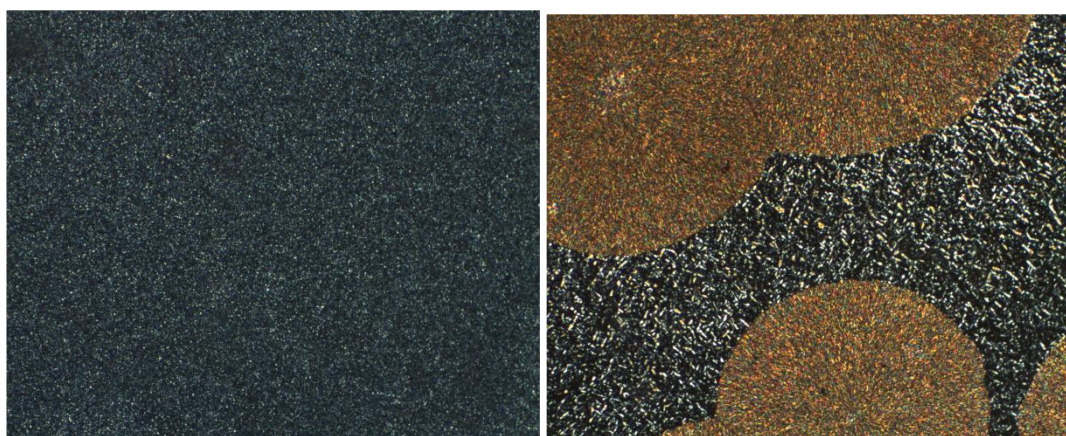


Figure 148: Structures of compounds **50**, **51** and **52**

Compound **50** (Figure 148) shows two thermal events upon the first heat. The first is a crystal to crystal transition with onset at 78.4 °C ($\Delta H = 6.5 \text{ kJmol}^{-1}$) which is followed by a melt into the isotropic fluid at 97.9 °C ($\Delta H = 35.3 \text{ kJmol}^{-1}$). On cooling there are two reproducible thermal events. A partial crystallization at around 35 °C which had a variable enthalpy and a glass transition which displayed a maximum in the change of the heat capacity at -13.8 °C. Upon subsequent heat cycles there is a corresponding glass transition followed by a cold crystallization at 19.5 °C ($\Delta H = -8.9 \text{ kJmol}^{-1}$). Finally there is a melt to the isotropic liquid at 78.8 °C ($\Delta H = 26.8 \text{ kJmol}^{-1}$).



*Figure 149: POM photomicrographs of: left) the grainy texture of **50** at 21.2 °C upon cooling from the isotropic fluid at 5 °Cmin⁻¹; right) bâtonettes of the SmA phase of **50** at 24.2 °C upon heating at 0.5 °Cmin⁻¹*

Upon cooling **50** from the isotropic liquid the material initially begins to crystallize at around 35 °C, further cooling to 20.1 °C results in the formation of a grainy birefringent texture (Figure 149 left) in the areas which had yet to crystallize. Reheating the sample resulted in the isotropization of this birefringent fluid again at around 20 °C however reheating triggered a cold crystallization which required the sample to be melted again. The grainy texture of this phase was gently annealed up to directly below the isotropization point which resulted in the formation of a bâtonette-like texture (Figure 149 right) indicative of a smectic phase⁵. As there were areas of homeotropic alignment which were optically extinct this phase must be orthogonal. Therefore it can be tentatively assigned as a monotropic SmA phase.

Chapter 8: In Search of the Smectic C Phase

Compound **51** (Figure 148) showed three reproducible thermal events. A glass transition which showed a maximum in the rate of change of the heat capacity at $-28.0\text{ }^{\circ}\text{C}$ followed by a LC-LC transition with onset at $34.8\text{ }^{\circ}\text{C}$ ($\Delta H = 0.3\text{ kJmol}^{-1}$). Finally the isotropization occurs with onset at $46.9\text{ }^{\circ}\text{C}$ ($\Delta H = 0.3\text{ kJmol}^{-1}$).

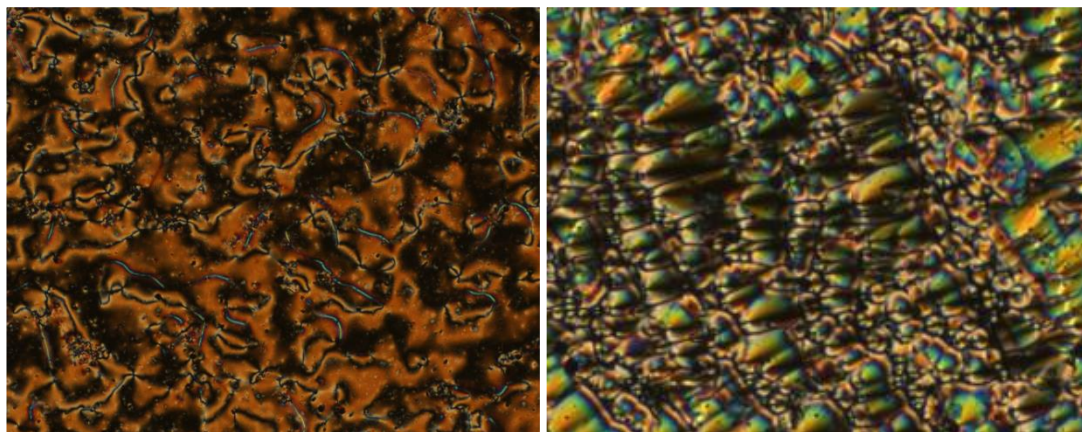


*Figure 150: POM photomicrograph of: left) the schlieren texture of the N phase of **51** at 38.8°C upon cooling from the isotropic fluid at $0.5\text{ }^{\circ}\text{Cmin}^{-1}$; right) the focal-conic texture of the SmA phase of **51** at 37.0°C upon cooling from the N phase at $0.5\text{ }^{\circ}\text{Cmin}^{-1}$*

When **51** is cooled from the isotropic liquid the *schlieren* texture is formed (Figure 150 left) which displays both two and four brush defects and rapidly adopts homeotropic alignment which is optically extinct. This allows this phase to be assigned as an enantiotropic N phase. After further cooling a focal-conic texture (Figure 150 right) is formed which shows clear sets of ellipses and hyperbolae of optical discontinuity. Furthermore, when homeotropically aligned the phase is optically extinct allowing this phase to be assigned as an enantiotropic SmA phase.

Compound **52** (Figure 148) shows four reproducible thermal events in DSC. The first is a Cr-Cr transition with onset at $7.8\text{ }^{\circ}\text{C}$ ($\Delta H = 1.1\text{ kJmol}^{-1}$). This is immediately followed by a Cr-LC transition at $28.9\text{ }^{\circ}\text{C}$ ($\Delta H = 24.3\text{ kJmol}^{-1}$). Next there is a weak endotherm with onset at $55.0\text{ }^{\circ}\text{C}$ ($\Delta H = 0.2\text{ kJmol}^{-1}$) associated with a LC-LC transition. Finally there is another weak endotherm at $94.6\text{ }^{\circ}\text{C}$ ($\Delta H = 0.5\text{ kJmol}^{-1}$) which is attributed to the isotropization point.

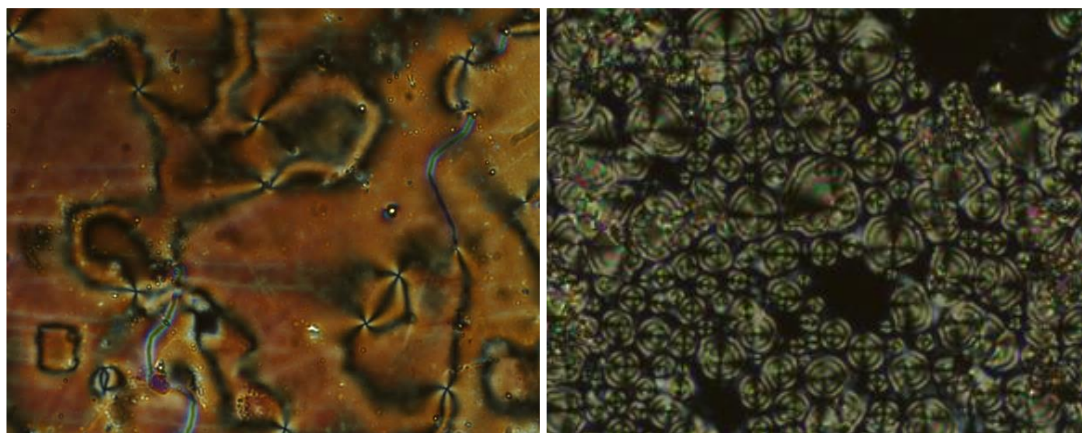
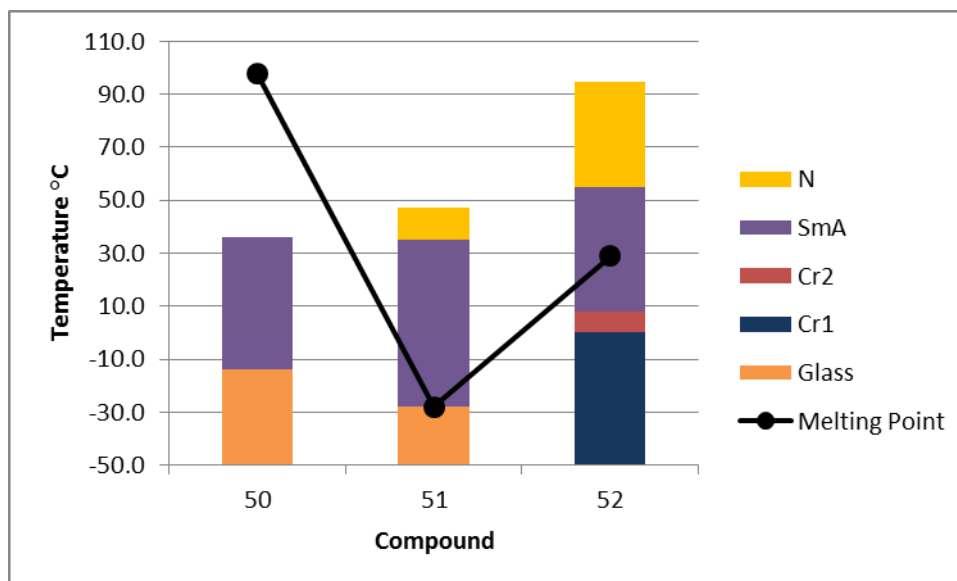


Figure 151: POM photomicrograph of: left) the schlieren texture of the N phase of **52** at 91.1° C upon cooling from the isotropic fluid at 1° Cmin⁻¹; right) the focal-conic texture of the SmA phase of **52** at 48.9° C upon cooling from the N at 1 °Cmin⁻¹

When compound **52** was cooled from the isotropic liquid the *schlieren* texture formed (Figure 151 left) which displayed both two and four brush defects and areas of homeotropic alignment which were optically extinct. This allows this phase to be assigned as an enantiotropic N phase. Further cooling results in the formation of a focal-conic texture (Figure 151 right) which displayed regions of homeotropic alignment that were optically extinct. This allows the assignment of this phase to be made as an enantiotropic SmA phase.

In absence of X-ray data it is tentatively proposed that the phase structure of the SmA phases in this series is again likely to be consistent with the smectic A phases of the octyloxy biphenyl benzoate series reported in Chapter 7.

Graph 7 summarises the phase behaviour of the mono-functionalized carborane appended with a difluoro(propylcyclohexyl)biphenyl mesogen *via* a central ester linkage (**50**) and its phenyl (**51**) and alkyl (**52**) analogues. This series of compounds also follow the general rule observed before in previous chapters of decreasing clearing point with increasing size of end-group, with the carboranyl member of the series having the highest melting point and the phenyl having the lowest.



Graph 7: The phase behaviour of the difluoro(propylcyclohexyl)biphenyls, thermal behaviour shown on the bars is for cooling and the meltings point are from pristine samples

Again as is the trend for previous compounds it can be seen that the carboranyl member of the series only displays smectic phases and with increasing size of end-group the nematic phase becomes increasingly destabilized. The likely cause of this might be the microphase segregation of the carborane clusters within a bilayer phase. In addition to this in the N phase either end-group, carboranyl or phenyl, would disrupt the packing of mesogenic cores and therefore the phase. This would result in a greater propensity for smectic phases. It is also interesting that in this series the phenyl end-group material **51** displays the lowest melting point. This is similar to the cholesteryl benzoate series from Chapter 7 and the same arguments for the cause of this can be made, namely that as the mesogenic core is not entirely polyaromatic π -stacking interactions between the mesogen and the end-group are not as prevalent resulting in a less stable crystal form and a lower melting point.

A tilted smectic phase was not observed even in the alkyl variant, and therefore it is not possible to make any inferences about the lack of a titled phase within the carboranyl member. The lack of a tilted phase in the alkyl material can be explained by the mesogenic cores non-conformity to either the McMillan or Wulf models⁶ of the SmC phase.

8.4 Concluding Remarks

Although it has not been possible to generate a carborane containing supermolecular liquid crystal which displays tilted phases in the attempt to do so the effect of the carborane cluster upon the phase behaviour of liquid crystals has been further reinforced. Unfortunately none of the model compounds presented which do not contain a carborane cluster also did not display any titled smectic phases, and therefore it is not possible to come to any conclusions about the lack of them within the carborane containing materials.

The comparison of compound **47** with similar literature compounds proved to be illuminating. It has shown that the increased melting points of the carborane containing materials presented are unlikely due to the steric effect of the cluster and therefore must be electronic. As carborane clusters are highly polarizable and as polarizability increases so do does the strength of associated London dispersion forces this could in an increase in melting point in the carboranyl materials.

9. **Conclusions**

Chapter 9: Conclusions

Throughout this body of work the synthesis and behaviour of several series of related materials that can be described as supermolecular liquid crystals which contain a carborane cluster has been detailed. These materials are intimately related to other supermolecular liquid crystals which also contain inorganic clusters of various types. It was the aim of this work to investigate the effect of the carborane cluster on the phase behaviour of these materials and to compare any trends observed with those of other inorganic cluster-containing supermolecular liquid crystals in order to identify any global patterns in behaviour amongst these materials.

A number of related series of carborane-containing supermolecular liquid crystals using a variety of different mesogens, linkers and topologies have been synthesized and characterized. A large variety of different mesogens were employed in order to generate a large number of different types of phases in order to see whether any patterns which developed were general across different phase types. Furthermore it was desirable to ascertain whether the cluster itself would have any effect on the types of phases observed or whether the cluster played an entirely passive role in respect to the formation of any liquid-crystalline phases.

It was found that the carborane cluster played a significant role and had an effect upon the phases which were observed. Typically the carborane cluster promoted smectic phases in preference to nematic phases. This can be tentatively explained by a tendency of the cluster to microphase segregate thus forcing the materials to adopt layered phases. Nematic phases were obtained in some instances, most likely due to the strongly nematogenic tendencies of the relevant mesogen as exemplified by the N* phases displayed by the materials functionalized with the (S)-4-((4'-(octyloxy)biphenyl-4-yloxy)carbonyl)phenyl 2-(2-methylbutoxy)-4-(pent-4-enyloxy)benzoate mesogen **18**.

It is also worthy of note that it was not possible to generate any liquid crystals containing a carborane cluster which displayed a tilted smectic phase. This is particularly noticeable in compound **47**, of which there exist hydrocarbon based cluster containing analogues in the literature which do display tilted smectic phases¹⁰¹. This has led to the idea that this effect cannot simply be steric but must have some electronic basis. In addition to this the octyloxy biphenyl benzoate

Chapter 9: Conclusions

family of compounds: **35**, **36** and **37**; also demonstrate pointedly that the presence of the carborane cluster clearly disrupts the formation of tilted smectic phases. However, it was not possible to conduct a thorough enough study of this effect to come to any definitive explanations as this result proved to be unexpected and there was not time to fully investigate this observation.

Comparison of the carborane-containing supermolecular liquid crystals with the alky and phenyl model analogues presented predominantly in Chapter 7 also showed that the inclusion of the carborane cluster typically increased the melting point of the materials. This result initially could have been attributed to an artefact of the extra steric bulk and additional mass associated with the cluster. However, compound **47** when compared to published analogues containing carbocyclic end-groups of similar mass, proportions and conformational flexibility was still found to have a significantly raised melting point. This result indicates strongly that the origin of the observed effect is more complicated than simple size and steric shape, and suggests some electronic effect. Logically this makes sense as it would be expected that the delocalized electrons of the aromatic cluster would be far more susceptible to dispersion forces resulting in a greater attraction between the carborane clusters thus increasing the melting point.

In addition to the different mesogens employed in this work, a number of analogous materials which differed in the number of mesogens attached to the carborane cluster were studied in order to determine the number of mesogens required to generate liquid-crystalline properties. This was done to compare carborane-containing supermolecular liquid crystals with other inorganic-cluster-containing liquid crystals to ascertain whether a general pattern was observable.

It was found that typically at least two mesogens were required in order to generate any enantiotropic mesomorphism within the systems presented. However, one material displayed an appreciable enantiotropic mesophase; compound **35** displayed an enantiotropic smectic A phase. This currently appears to be the only inorganic-cluster-containing supermolecular liquid crystal to display an enantiotropic phase with only one mesogen. As was explored in Chapter 4 the increase in phase stability

Chapter 9: Conclusions

associated with attaching another mesogen showed a maximum when going from one to two mesogens.

When comparing the carboranyl derivatives with other inorganic-cluster-containing supermolecular liquid crystals a pattern is beginning to emerge. It appears that the onset of mesomorphism occurs when there is an approximate match between the cross-sectional area occupied by the mesogens and that of the cluster. The *o*-carborane cluster, which is the smallest of the related materials, required between one and two mesogens to display enantiotropic mesomorphism. The larger silsesquioxane cluster however has been shown to require at least either two large four-ring type mesogens or more typically three mesogens¹¹⁹. Moving to yet a larger cluster, fullerene requires at least four mesogens¹¹², while going to the extreme of this series is the manganese oxide single molecule magnet functionalized with cyanobiphenyl³⁸ which required eight mesogens to display enantiotropic mesophase behaviour.

This trend appears to be sterically driven, given that one factor which drives it is the ratio between the size of the cluster and the area occupied by the mesogens. However, there is clearly an interplay between this steric effect and possible electronic cluster-cluster interactions, which is demonstrated by the increased melting point for compound **47** in comparison to its carbocyclic analogues.

Should this trend hold true for inorganic clusters in general, it has potentially useful implications for the design of new functional materials. Knowledge of this trend would enable the more effective design of materials which include an inorganic cluster as a functional unit while also displaying mesomorphic behaviour. However, there currently lacks a broad enough base of evidence to generalize this trend to all inorganic clusters. As such it is recommend further research into other inorganic cluster containing systems, particularly ones which may display electronic interactions between the clusters be carried out. This would enable both, further probing of any interactions between the clusters and, provide a broader evidence base in order to make firmer assertions in regards to this trend and its generalization.

Chapter 9: Conclusions

The mode of attachment at two different points in the molecules was also investigated to see whether this would have an effect on the phase behaviour displayed. This facet of the research was mostly conducted with di-functionalized carboranes appended with two mesogens, although mono-functionalized carboranes were also employed. Either the mode of attachment of the mesogen to the linker was varied or the mode of attachment of the linker to the cluster. This enabled the probing of the effect of molecular topology on the properties of the materials presented.

In general, it was found that materials in which the mesogens are attached in an end-on manner show slightly broader mesophases than those which are attached in a side-on manner. However, it is also worth noting that the materials whose molecular topology deviated most from a rod-like shape typically showed monotropic mesophases, whereas those which were rod-like tended to crystallize easily. This can be explained by the ability of the materials to close pack. The more rod-like a material, the easier it is for it to close pack both in a mesophase, resulting in better phase stability, and in a crystal lattice resulting in a strong propensity to crystallize.

In addition to this the mode of attachment of the linker to the carborane cluster was investigated in disubstituted carboranyl materials and showed that changes to the core of the molecule can be propagated to the periphery resulting in the destabilization of a mesophase, as in the case of di-functionalized **24** and **25**. However this effect is mitigated by the ability of the molecules to adopt the most favourable conformations as demonstrated by the minor effect of this variation of this mode of attachment observed in di-functionalized **21** and **22**.

Combined these studies show that the ability of these materials to form stable mesophases is intimately linked to their molecular topology. The gross shape of these supermolecules appears to, to a large extent dictate the phase behaviour they exhibit. This ties in well with the previous observation that the area occupied by the inorganic cluster must be equal to or smaller than the cross-sectional area occupied by the mesogens in order to display enantiotropic mesophase behaviour.

Chapter 9: Conclusions

This observation is reasonably intuitive, given that for low molar mass mesogens many of the explanations for their self-assembly rely on arguments based on shape, for instance the Wulf model of the SmC phase⁷. Therefore it is not a great leap of logic to expect something similar for supermolecular liquid crystals. In fact this notion ties in well with work carried out by Percec on self-assembling dendrons¹⁴.

Finally the effect of the linker on the phase behaviour observed was also investigated. This would enable allowances for any effect observed from the linker to be taken into account when making comparisons to other families of inorganic-cluster-containing supermolecular liquid crystals.

This study initially used siloxane linkers. However, the generation of unwanted branched isomers as side-products in the hydrosilylation reaction impacted negatively on the mesomorphic properties. Therefore, silane linkers were used which did not exhibit this issue. In both cases predominantly smectic A phases were observed. Silane and siloxane moieties are well known promoters of smectic phases, as such this observation is not surprising. To test whether the propensity for smectic phases was caused solely by the use of silane and siloxane linkers a number of materials employing ester linkages were prepared. These materials also showed a strong tendency towards smectic phases, and therefore it is likely that the carborane cluster was contributing to the smectogenic properties of the materials.

The cause of this enhancement of smectogenic properties as a result of the presence of the carborane cluster can be rationalized in a similar way to that of the same effect observed for silanes and siloxanes. The carborane, like the silane or siloxane presents a region of the molecule which is chemically distinct from that of the rest of the molecule. As more favourable interactions occur between molecules in areas which are chemically similar, these areas segregate and display microphase segregation. This results in a strong tendency towards the formation of layers and thus smectic phases.

Another contributing factor which may have enhanced the smectogenic properties of these materials, excluding mono-functionalized materials, is the enforced proximity of mesogens to one another caused by tethering to the cluster. As all of the multi-

Chapter 9: Conclusions

functionalized carboranes were based on *o*-carborane, the mesogens were always held in close proximity to each other as a result of the molecular structure. This lack of translational freedom may destabilize the nematic phase and thus result in the enhanced smectogenic behaviour observed. It would be interesting to compare the phase behaviour of analogous materials synthesized from *m* and *p*-carborane. If this argument holds true then a greater affinity for the nematic phase should be observed as the isomers became more linear.

10. Experimental

10.1 Experimental Methods

10.1.1 Starting Materials

All starting materials and reagents were acquired from either Sigma-Aldrich, Apollo Scientific or Alfa Aesar and used without purification unless otherwise stated. Solvents were obtained from Fisher Scientific except for anhydrous solvents which were procured from Sigma-Aldrich and all were used without further purification. The coupling agent *N*-(3-dimethylaminopropyl)-*N'*-ethylcarbodiimide hydrochloride (EDAC) was purchased from CarboSynth and used without purification. Decaborane (14) was obtained from KatChem and used without further purification. All carborane starting materials whose synthesis is not detailed here were kindly provided to us by the research group of Dr Rosario Nuñez, Institut de Ciències de Materials de Barcelona and used without further purification. (*S*)-4-((octan-2-yloxy)carbonyl)phenyl 4'-(11-hydroxyundecyloxy)biphenyl-4-carboxylate, compound **53** and 2,3-difluoro-4'-(4-propylcyclohexyl)biphenyl-4-ol, compound **54** were kindly provided by Dr Stephen Cowling and Dr Edward Davis respectively and were used without further purification.

10.1.2 Thin Layer Chromatography and Column Chromatography (TLC)

Where possible the progress of reactions was followed by thin layer chromatography (TLC) with appropriate solvent mixtures. Silica coated aluminum plates (Kieselgel 60 F-254) were purchased from Merck and were visualized by UV light (254 nm or 365 nm) or by oxidation with potassium permanganate solution. Separations achieved by column chromatography were carried out using flash grade silica gel (Fluka, 70-230 mesh, 63 μm – 200 μm particle size). When required, increased flow rate was achieved by the use of flash techniques¹⁴⁶.

10.1.3 Nuclear Magnetic Resonance (NMR) spectroscopy

Proton (^1H) and Carbon (^{13}C) NMR were carried out on either a JEOL ECX or JEOL ECS spectrometer. Silicon (^{29}Si) and Boron (^{11}B) NMR were carried out on a JEOL ECS spectrometer. Proton Boron decoupled NMR (^1H { ^{11}B }) was carried out on a Bruker AV500 spectrometer. The acquisition frequency, solvent and internal reference is stated before the listing of all chemical shifts presented. Typically ^1H and ^{13}C internal references were residual protic solvents. ^{11}B and ^{29}Si NMR were recorded with external references. All experiments were carried out at 25 °C unless otherwise stated. Integrations given for non-proton spectra are estimates based on visual appraisal of the intensity of the signals. These integrations are not quantitative due to the varied relaxation times of different species and complications caused by the nuclear overhauser effect. They are provided only as an aid to assigning spectra. Abbreviations used to describe multiplicity are listed below.

s-	singlet
d-	doublet
t-	triplet
q-	quartet
dd-	double doublet
ddd-	double double doublet
dt-	double triplet
ddt-	double double triplet
m-	multiplet

10.1.4 Mass Spectrometry (MS)

Mass spectra were recorded using Bruker micrOTOF MS-Agilent series 1200LC spectrometer for electrospray ionisation (ESI), a Waters GCT Premier Agilent 7890A GC for liquid introduction field desorption ionisation (LIFDI) and a Bruker Solarix FT-ICR for matrix assisted laser desorption ionisation (MALDI). High resolution mass spectrometry was carried out for a number of compounds and where this is the

case the observed mass is given to four decimal places and a theoretical mass is also provided for comparison.

10.1.5 Infrared Spectroscopy (FT-IR)

Infrared spectroscopy was performed using a Shimadzu IR prestige-21 with a Specac diamond ATR IR insert.

10.1.6 Polarized Optical Microscopy (POM)

Polarized optical microscopy was performed on a Zeiss Axioskop 40 Pol microscope using a Mettler FP82HT temperature control unit, which was controlled by a Mettler FP90 control unit. An Infinity X-21 digital camera was used to record photomicrographs.

10.1.7 Differential Scanning Calorimetry (DSC)

The transition temperatures and associated enthalpies were determined using DSC. Thermograms were obtained using a Mettler DSC822_e unit operating with the Star_e software package. In each case the scan rate was 10 °C min⁻¹. The results obtained were normalized relative to an indium standard (onset = 156.55 ± 0.2 °C, ΔH = 28.45 ± 0.40 J g⁻¹). Monotropic phase transitions are noted within brackets. Enthalpies are given after transition temperatures within square brackets in kJmol⁻¹ in the format: Transition temperature [enthalpy kJmol⁻¹].

10.1.8 CHN Microanalysis (CHN)

CHN microanalyses were carried out using a Exeter Analytical Inc. CE440 analyser on samples of between 1.6 and 1.8 mg weighed on a Sartorius SE2 analytical balance. The instrument was calibrated against Acetanilide with an S-Benzythioronium Chloride internal standard. It is commonly observed that materials which have high boron or silicon content do not combust well and typically show elemental analyses which deviate noticeably from their calculated composition¹⁴⁷.

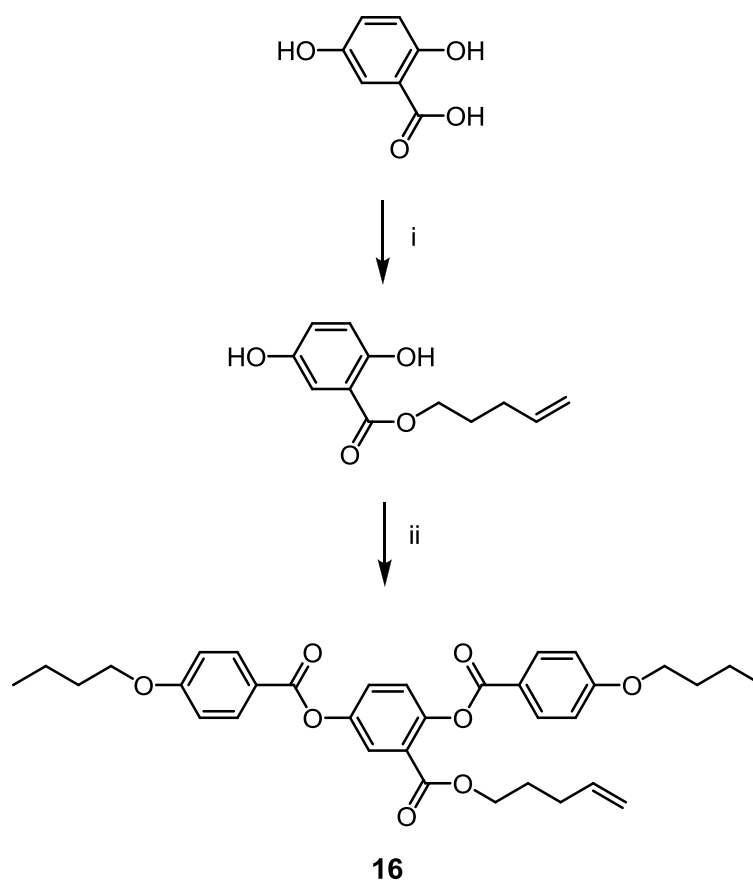
Samples which did not combust completely were run with a vanadium pentoxide combustion aid and this is noted where necessary in the experimental procedure.

10.2 Synthetic Routes

Schemes 1 - 4 detail the synthetic routes used to synthesize mesogens **16**, **17**, **18** and **19** which were utilized in Chapters 4 and 5 which are based on procedures reported in the literature and as such were not presented or discussed within the main body of work.

10.2.1 2-((Pent-4-enyloxy)carbonyl)-1,4-phenylene bis(4-butoxybenzoate), **16**¹⁴⁸

The synthesis of **16** (Scheme 16) involves the direct alkylation of 2,4-dihydroxybenzoic acid with 5-bromo-pent-1-ene using KHCO_3 in DMF, and finally the Steglich esterification using DCC and DMAP to install the two arms of the mesogen¹⁴⁸ to yield **16** in approximate overall yield of 52 %.

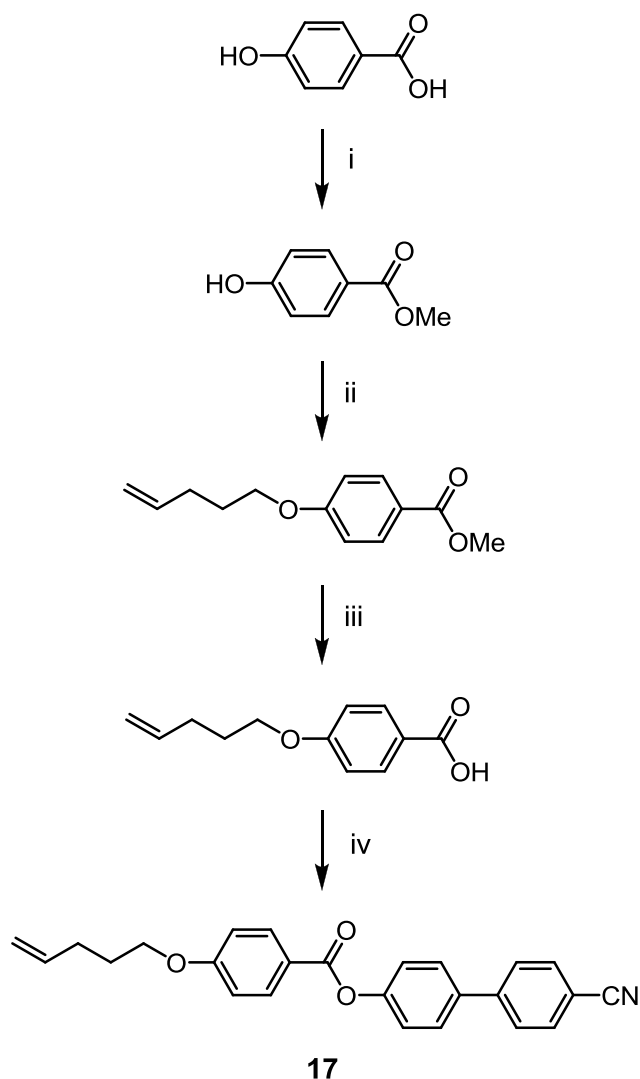


- i) 5-Bromopent-1-ene, KHCO_3 in DMF
 ii) 4-Butoxybenzoic acid, DCC, DMAP in DCM

Scheme 16: The synthesis of compound 16

10.2.2 4'-Cyanobiphenyl-4-yl 4-(pent-4-enyloxy)benzoate, **17**¹¹⁸

The synthesis of **17** (Scheme 17) involves the methyl ester protection of 4-hydroxy benzoic acid using acidic conditions, followed by the installation of the alkenyl spacer *via* a Williamson etherification. The acid was deprotected under basic conditions and finally coupled with cyanobiphenol using the Steglich esterification¹¹⁸ to yield **17** in approximately 72 % overall yield.

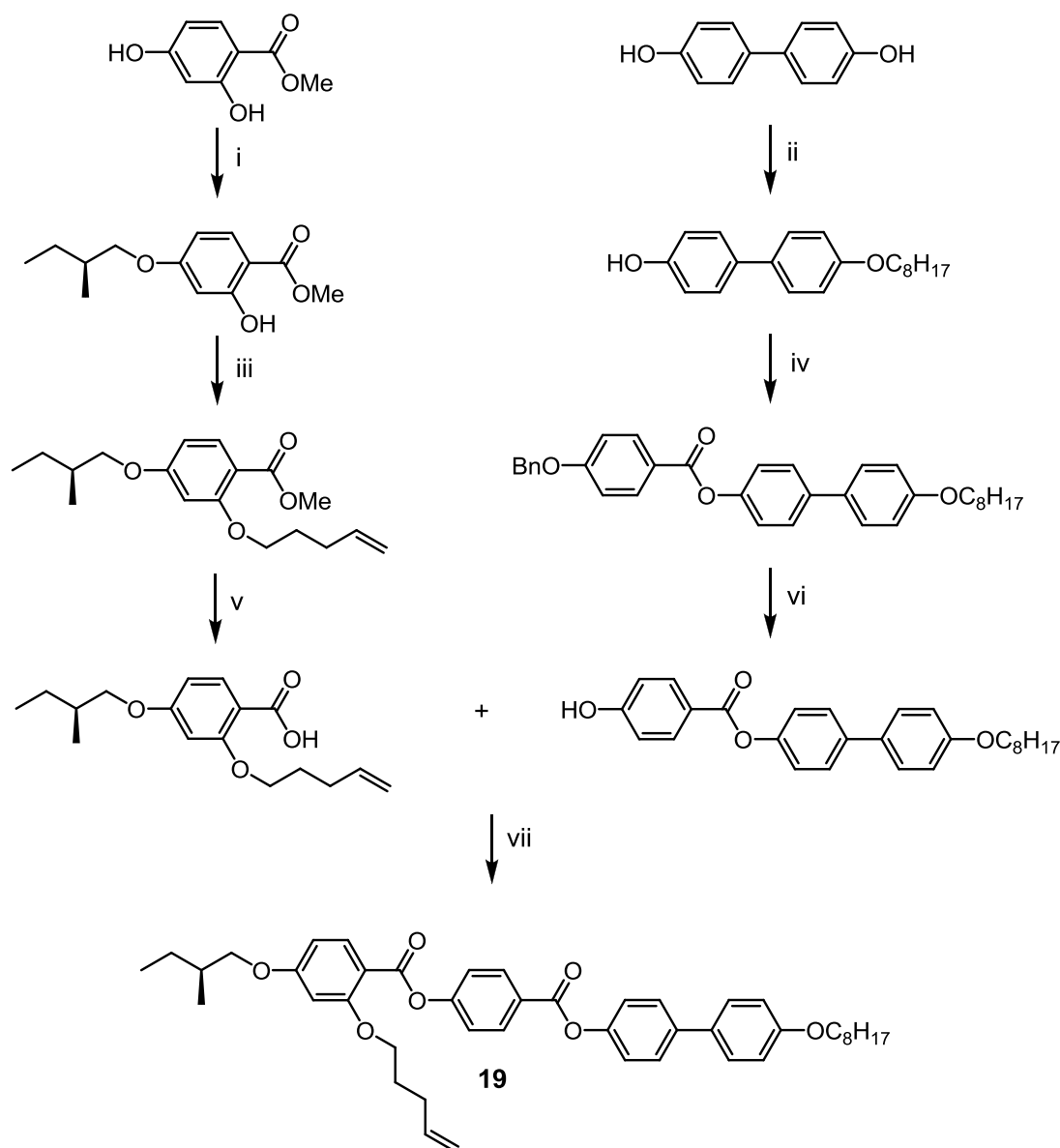


- i) MeOH, H₂SO₄
 ii) 5-Bromo-pent-1-ene, K₂CO₃, KI, butanone
 iii) NaOH, MeOH/H₂O
 iv) 4'-Hydroxy-4-cyanobiphenyl, DMAP, EDAC, DCM

Scheme 17: Synthesis of compound 17

10.2.3 (*S*)-4-((4'-(Octyloxy)biphenyl-4-yloxy)carbonyl)phenyl 4-(2-methylbutoxy)-2-(pent-4-enyloxy)benzoate, **19**¹²⁰

The synthesis of compound **19**¹²⁰ (Scheme 18) begins with the installation of the (*S*)-2-methylpropyl group onto 2,4-dihydroxy methyl benzoate *via* a Williamson etherification (step i Scheme 18). This reaction is directed by the favourable electronic activation at the four position caused by the presence of the ester, (although some of the undesired isomer which is functionalized at the two position was also generated).



- i) (S)-1-Bromo-2-methylbutane, K_2CO_3 , KI, butanone
- ii) 1-Bromo-octane, KOH, EtOH/ H_2O
- iii) 5-Bromo-pent-1-ene, K_2CO_3 , butanone
- iv) 4-Benzyloxybenzoic acid, DMAP, EDAC, DCM
- v) NaOH, MeOH/ H_2O
- vi) H_2 Pd/C, THF
- vii) DMAP, EDAC, DCM

Scheme 18: Synthesis of 19

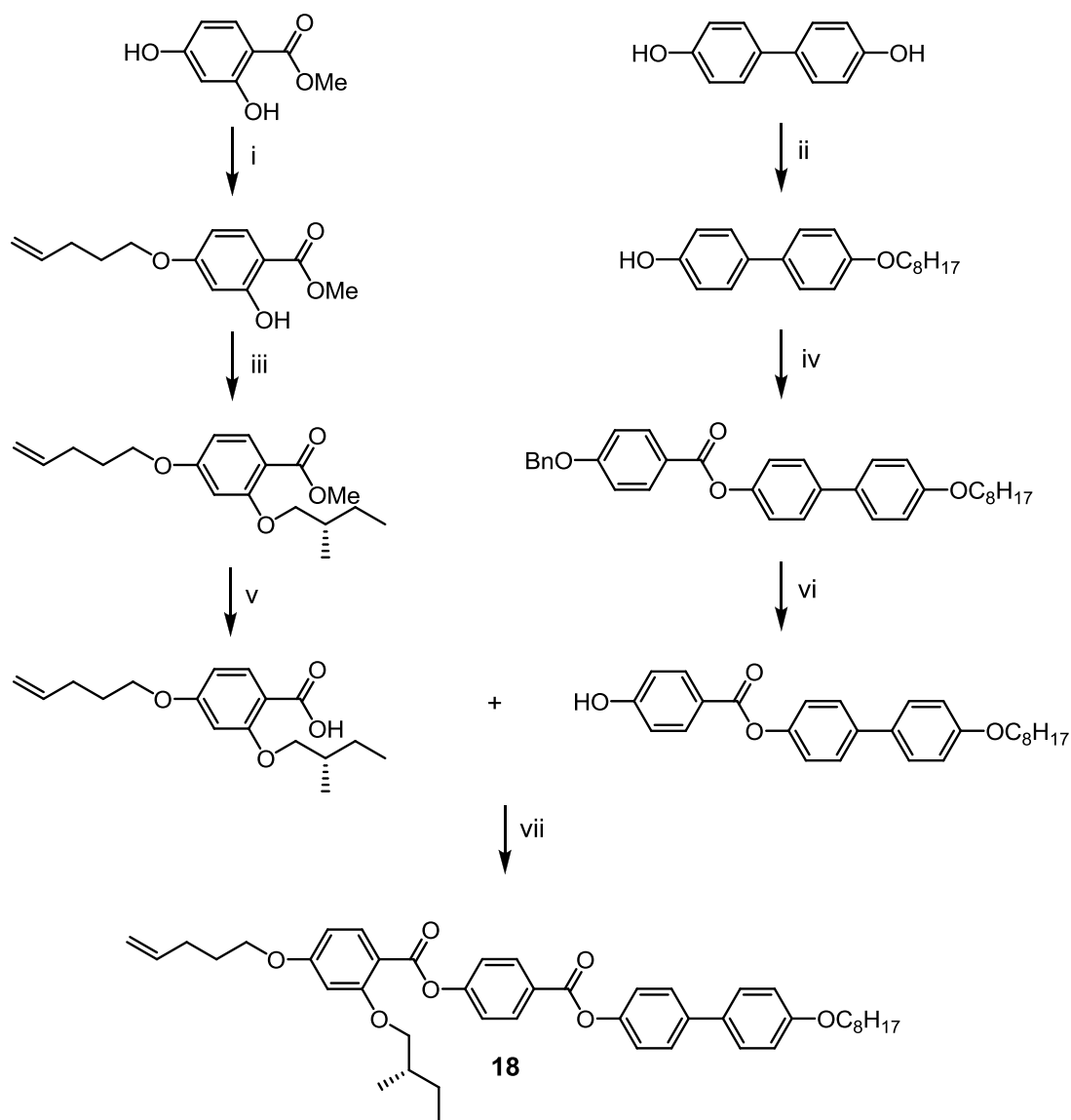
However this was removed by column chromatography. Concomitantly another Williamson etherification, this time of 4,4'-dihydroxybiphenyl with 8-bromooctane, is used to install the flexible spacer which ends up at the other end of the mesogen. This reaction was done under high dilution conditions with an excess of the 4,4'-dihydroxybiphenyl to maximise the yield of the desired mono-substituted product.

The next step in the synthesis is another Williamson etherification this time with 5-bromo-pent-1-ene on the two position of the alkenyl functionalized benzoate. As there was no competing reaction here we were able to use a small excess of the bromide and force the reaction to completion thus maximising yield. Again concomitantly a Steglich esterification was carried out using 4-benzyloxybenzoic acid with the 4-octyloxy-4'-hydroxybiphenyl.

The final step of the left hand fragment (Scheme 18) is the deprotection of the acid using NaOH. The right hand fragment is also deprotected at this point; however this is achieved via hydrogenation of the benzyl protecting group. Finally both fragments are combined via another Steglich esterification reaction to give the final product **19** in approximately 19 % overall yield.

10.2.4 (S)-4-((4'-(octyloxy)biphenyl-4-yloxy)carbonyl)phenyl 2-(2-methylbutoxy)-4-(pent-4-enyloxy)benzoate, **18¹¹⁹**

The synthesis of **18** (Scheme 19) is based on that of compound **19**¹²⁰ except that the initial Williamson etherification of the left hand fragment (step i, Scheme 19) takes place between 5-bromopent-1-ene in order to install the linking group onto the terminal position. Again this reaction is directed by the electronic effect of the ester group thus minimizing the occurrence of the undesired 2-substituted product. This is followed by the installation of the chiral group onto the 2 position of the phenyl ring again via Williamson etherification by the same method as used for the alkenyl substituent for compound **19**. The remaining steps of the synthesis are identical and will not be discussed again and resulted in an approximate overall yield of 5 %.

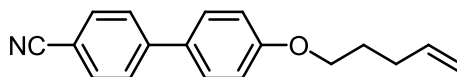


- 5-Bromo-pent-1-ene, K_2CO_3 , KI, butanone
- 1-Bromo-octane, KOH, EtOH/ H_2O
- (S)-1-Bromo-2-methylbutane, K_2CO_3 , KI, butanone
- 4-Benzyloxybenzoic acid, DMAP, EDAC, DCM
- NaOH, MeOH/ H_2O
- H_2 , Pd/C, THF
- DMAP, EDAC, DCM

Scheme 19: Synthesis of 18

10.3 Experimental Details

10.3.1 4'-(Pent-4-enyloxy)biphenyl-4-carbonitrile, **5**¹⁴⁹



4'-Hydroxy-biphenyl-4-carbonitrile (8.24 g, 42.2 mmol), K_2CO_3 (23.3 g, 168.8 mmol) and KI (0.35 g, 2.11 mmol) were added to dry butanone (400 mL). The suspension was brought to a gentle reflux and then 5-bromopentene (5.0 mL, 42.2 mmol) was added. The solution was stirred vigorously overnight and allowed to cool to room temperature. The suspension was poured onto water (300 mL), the aqueous phase washed with diethyl ether (2x 100 mL), the organic phases combined and washed with 5 % w/w NaOH in water (300 mL), 5 % w/w NaCl in water (300 mL) and finally water (2 x 200 mL). The solution was dried over $MgSO_4$ and the solvent removed *in vacuo*. The product was recrystallised from ethanol yielding **5** as pale yellow needles (10.34 g, 93.4%).

1H NMR: (CDCl₃, 400 MHz, CDCl₃ internal standard)

δ (ppm)= 7.69 (d ($J = 8.3$ Hz), 2H, ArH), 7.64 (d ($J = 8.3$ Hz), 2H, ArH), 7.53 (d ($J = 8.7$ Hz), 2H, ArH), 6.99 (d ($J = 8.7$ Hz), 2H, ArH), 5.87 (ddt ($J = 16.9$ (*trans*), 10.2 (*cis*), 6.6 (*gem*) Hz), 1H, CH=CH₂), 5.08 (dd ($J = 17.1, 1.6$ Hz), 1H, CH_{*trans*}H=CH), 5.02 (dd ($J = 10.2, 1.3$ Hz), 1H, CH_{*cis*}H=CH), 4.03 (t ($J = 6.4$ Hz), 2H, CH₂O), 2.26 (m, 2H, CH₂CH=CH₂), 1.91 (m, 2H, CH₂CH₂O)

^{13}C NMR: (CDCl₃, 100.4 MHz, CDCl₃ internal standard)

δ (ppm)= 159.67 (1C, ArC-O), 145.23 (1C, ArC-CN), 137.65 (1C, ArC), 132.54 (2C, ArC), 131.31 (1C, ArC), 128.31 (2C, ArC), 127.05 (2C, ArC), 119.11 (1C, CH=CH₂), 115.31 (1C, C≡N), 115.05 (2C, ArC), 110.01 (1C, CH₂=CH), 67.26 (1C, CH₂O), 30.05 (1C, CH₂CH=CH₂), 28.31 (1C, CH₂CH₂CH₂)

Chapter 10: Experimental

IR (cm⁻¹): 2924 (m, ArH), 2222 (m, C≡N), 1597 (s, C-O), 810 (vs)

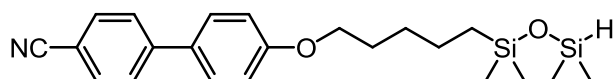
Mass (ESI):

m/z = 263.1310 (M)⁺, 264.1 (M+H)⁺, 195.1, 166.1, 140.1, 41.0

calculated = 263.1310 (M)⁺

DSC/POM: Cr 75.8 [30.4] N 88.2 [1.0] Iso

10.3.2 4'-[5-(1,1,3,3-Tetramethyl-disiloxanyl)-pentyloxy]-biphenyl-4-carbonitrile, **7**⁹⁷



Dimethylchlorosilane (6.2 mL, 57 mmol) was added to a solution of 4'-(Pent-4-enyloxy)biphenyl-4-carbonitrile, (6.0 g, 22.8 mmol) in low sulfur toluene (30 mL) in a dry Schlenk tube under Ar. This solution was degassed and placed under Ar. Karstedt's catalyst (20 μL) was added and the solution stirred over night. The solvent was evaporated *in situ* under vacuum. The residue was dissolved in dry THF (10mL). Dimethylchlorosilane (29.8 mL, 0.27 mol) was added and a solution of pyridine (40.6 mL, 0.50 mol) in water (9.0 mL 0.50 mol) was added drop-wise at 0 °C over 1 h. The solution was stirred over night resulting in a two layer system. The mixture was diluted with diethyl ether (200 mL) and washed with water (5x 100 mL). The organic phase was collected, dried over MgSO₄ and the solvent removed *in vacuo* to yield **7**, a waxy white solid (9.08 g, >95%) which was used without further purification.

¹H NMR: (CDCl₃, 400 MHz, CDCl₃ internal standard)

δ (ppm)= 7.69 (d (*J* = 8.6Hz), 2H, ArH), 7.64 (d (*J* = 8.6Hz), 2H, ArH), 7.53 (d (*J* = 8.9Hz), 2H, ArH), 6.99 (d (*J* = 8.9Hz), 2H, ArH), 4.68 (m, 1H, SiH), 4.00 (t (*J* = 6.6Hz), 2H, CH₂O), 1.80 (m, 2H, CH₂CH₂O), 1.49 (m, 2H, CH₂CH₂CH₂), 1.42 (m, 2H, CH₂CH₂CH₂), 0.57 (m, 2H

Chapter 10: Experimental

CH_2Si , 0.15 (d ($J = 2.8$ Hz), 6H, $O(CH_3)_2SiH$), 0.07 Hz (s, 6H, $O(CH_3)_2SiCH_2$)

^{13}C NMR: (CDCl₃, 100.4 MHz, CDCl₃ internal standard)

δ (ppm)= 159.69 (1C, ArC-O), 145.09 (1C, ArC-CN), 132.39 (2C, ArC), 131.02 (1C, ArC), 128.16 (2C, ArC), 126.88 (2C, ArC), 118.95 (1C, ArC), 114.95 (2C, ArC), 109.86 (1C, C \equiv N), 67.97 (1C, CH₂O), 29.54 (1C, CH₂CH₂O), 28.82 (1C, CH₂CH₂CH₂), 22.91 (1C, CH₂CH₂CH₂), 17.94 (1C, CH₂Si), 0.81 (2C, CH₃Si), -0.04 (2C, CH₃SiH)

^{29}Si NMR: (CDCl₃, 79.0MHz)

δ (ppm)= 10.39 (1Si, SiH), -6.21 (1Si, SiCH₂)

IR (cm⁻¹): 2954 (m, ArH), 2222 (m, CN), 2098 (m, Si-H), 1604 (s, C-O), 1049 (vs), 817 (vs)

Mass (ESI):

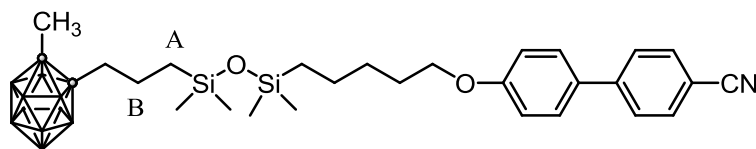
m/z = 397.1893 (M)⁺, 326.1, 195.1, 133.0, 73.0

calculated = 397.1893 (M)⁺

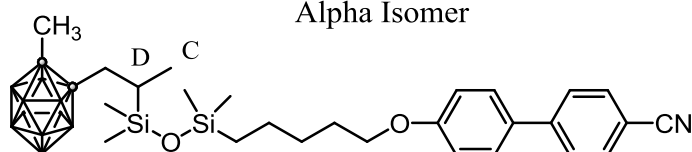
DSC/POM: Cr -1.9 [0.2] SmA 52.5 [3.3] Iso

10.3.3 1-Methyl, 2-(propyl-3-[4'-(5-[1,1,3,3-tetramethyl-disiloxy]-pentyloxy)biphenyl-4-carbonitrile])-dodecacarborane, 1

Beta Isomer



Alpha Isomer



A solution of 4'-[5-(1,1,3,3-Tetramethyl-disiloxanyl)-pentyloxy]-biphenyl-4-carbonitrile, **7**, (69.2 mg, 0.173 mmol) in dry, low sulfur toluene (2 mL) and a solution of 1-methyl, 2-(prop-2-ene)-dodecacarborane, (34.3 mg, 0.173 mmol) in dry, low sulfur toluene (2 mL) were placed in a dry Schlenk tube under Ar. The resulting solution was degassed and purged with Ar. Karstedt's catalyst (10 μ L) was added at 0 °C, the solution was left to reach room temperature and stirred for 18 h. The solvent was removed *in vacuo* and the product purified *via* flash column chromatography (DCM/Hex 50:50, flash grade silica, R_f 0.27) yielding **1** as a clear viscous oil (66.2 mg, 64.2%).

Note: The integrations given for the nuclei which appear at different chemical shifts in each isomer are reported to reflect their abundance in relation to their own isomer and not the mixture as a whole.

^1H { ^{11}B } NMR: (CDCl₃, 500 Mhz, CHCl₃ internal standard)

δ (ppm)= 7.68 (AA'BB' (J = 8.3 Hz, 2H, ArH), 7.64 (AA'BB' (J = 8.6 Hz), 2H, ArH), 7.53 (AA'XX' (J = 8.6 Hz), 2H, ArH), 7.00 (AA'XX' (J = 8.6 Hz), 2H, ArH), 4.02 (t (J = 6.5 Hz), 2H, CH₂O), 2.27 (s, 2H, BH), 2.24 (s, 2H, BH), 2.18 (inverted t (J = 10.0 Hz), 2H, CH₂Cluster),

Chapter 10: Experimental

2.17 (s, 2H, BH), 2.11 (s, 2H, BH), 2.00 (m, 3H, CH₃Cluster), 1.83 (m, 2H, CH₂CH₂O), 1.59 (m, 2H, C_BH₂ β isomer), 1.52 (m, 2H, CH₂), 1.41 (m, 2H, CH₂), 1.06 (d (*J* = 7.0 Hz), 3H, C_CH₃CHSi), 0.95 (m, 1H, C_DH₂Si α isomer), 0.58 (m, 2H, CH₂Si α and β isomers), 0.52 (m, 2H, C_AH₂Si β isomer), 0.08 (s, 6H, CH₃Si β isomer), 0.07 (s, 6H, CH₃Si β + α isomer), 0.05 (s, 6H, CH₃Si α isomer)

¹³C NMR: (CDCl₃, 100.4 MHz, CHCl₃ internal standard)
δ (ppm)= 159.89 (1C, ArCO), 145.38 (1C, ArC), 132.66 (2C, ArC), 131.37 (1C, ArC), 128.43 (2C, ArC), 127.17 (2C, ArC), 119.24 (1C, ArC), 115.18 (2C, ArC), 110.10 (1C, CN), 79.77 (1C, CCluster), 78.31 (1C, CCluster), 68.22 (1C, CH₂O β isomer), 68.15 (1C, CH₂O α isomer), 38.76 (1C, CH₂Cluster), 36.98 (1C, CH₂CH₂O), 29.86 (1C, CH₂), 29.08 (1C, CH₂), 23.92 (1C, C_BH₂ β isomer), 23.45 (1C, C_DH₂ α isomer), 23.25 (1C, C_AH₂Si β isomer), 21.96 (1C, CH₃Cluster), 18.43 (1C, CH₂Si), 14.36 (1C, C_CH₃ α isomer), 0.52 (2C, CH₃Si β isomer), 0.49 (2C, CH₃Si β isomer), -1.39 (2C, CH₃Si C_CH₃ α isomer), -2.04 (2C, CH₃Si C_CH₃ α isomer)

²⁹Si NMR: (CDCl₃, 79.0 MHz, CHCl₃ internal standard)
δ (ppm)= 9.58 (1Si, α), 8.69 (1Si, β), 8.09 (1Si, α), 7.13 (1Si, β)

¹¹B NMR: (CDCl₃, 160.0 MHz)
δ (ppm)= -4.98 (t (*J* = 176.6 MHz), 2B), -9.84 (t (*J* = 199.4 Hz), 8B)

IR (cm⁻¹): 2931 (m, ArH), 2576 (vs, br, BH), 2222 (m, CN), 1604 (s, C-O)

Mass (ESI):

m/z = 597.4370 (M)⁺, 582.2, 554.2, 536.2

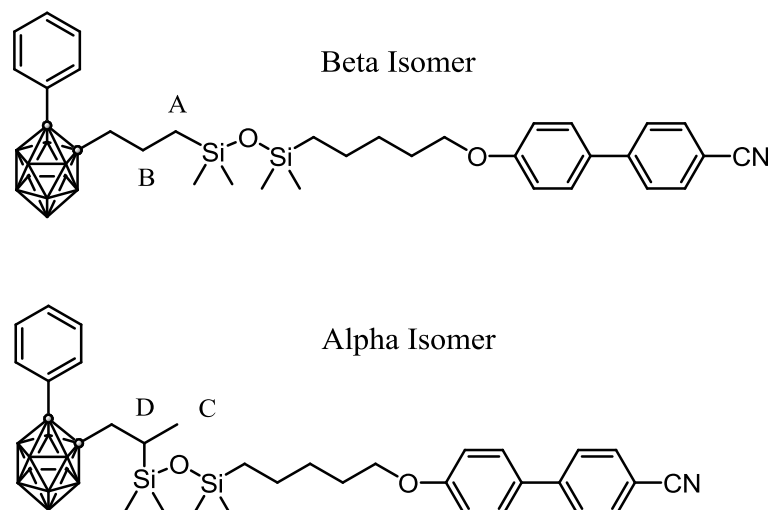
Calculated: 597.4232 (M)⁺

CHN Microanalysis:

Observed: C 57.34 %, H 8.36 %, N 2.38 %

Calculated: C 56.43 %, H 8.29 %, N 2.35 %

10.3.4 1-Phenyl, 2-(propyl-3-[4'-(5-[1,1,3,3-tetramethyl-disiloxy]- pentyloxy)biphenyl-4-carbonitrile])-dodecacarborane, 2



A solution of 4'-[5-(1,1,3,3-Tetramethyl-disiloxanyl)-pentyloxy]-biphenyl-4-carbonitrile, **7**, (63.8 mg, 0.17 mmol) in dry, low sulfur toluene (1 mL) and a solution of 1-phenyl, 2-(prop-2-ene)-dodecacarborane, (32.5 mg, 0.13 mmol) in dry, low sulfur toluene (2 mL) were placed in a dry Schlenk tube under Ar. The solution was degassed, purged with Ar and cooled to 0 °C. Karstedt's catalyst (10 μ L) was added, the solution allowed to reach room temperature and stirred overnight. The product was purified by flash column chromatography (Hexane initially with slowly increasing volume of DCM up to 50%, flash grade silica, R_f 0.19 (in DCM:Hex 50:50)) to yield **2** as a clear low melting point glassy solid (55.6 mg, 64.9%).

Note: The integrations given for the nuclei which appear at different chemical shifts in each isomer are reported to reflect their abundance in relation to their own isomer and not the mixture as a whole.

^1H { ^{11}B } NMR: (CDCl₃, 500 MHz, CHCl₃ internal standard)

δ (ppm)= 7.69 (AA'BB' (J = 8.4Hz), 2H, ArH), 7.64 (AA'BB' (J = 8.1Hz), ArH), 7.63 (AA'XX' (J = 7.6Hz), 2H, ArH), 7.53 (AA'XX' (J = 8.8Hz), 2H, ArH), 7.41 (m, 3H, ArH), 7.00 (AA'XX' (J = 8.8Hz), 2H,

Chapter 10: Experimental

ArH), 4.02 (t ($J = 6.5\text{Hz}$), 2H, OCH₂), 2.73 (s, 2H, BH), 2.37 (s, 4H, BH), 2.25 (s, 2H, BH), 1.82 (m, 2H, OCH₂CH₂), 1.77 (m, 2H, CH₂Cluster), 1.51 (m, 2H, CH₂), 1.41 (m, 2H, CH₂), 1.31 (m, 2H, C_BH₂), 0.96 (d ($J = 7.1\text{Hz}$), 3H, C_CH₃CHSi α isomer), 0.90 (m, 1H, C_DH₂Si α isomer), 0.53 (m, 2H, CH₂Si β isomer), 0.45 (m, 1H, CH₂Si α isomer), 0.27 (m, 2H, C_AH₂Si β isomer), 0.02 (s, 6H, CH₃Si β isomer), -0.05 (s, 6H, CH₃Si β isomer), -0.08 (s, 6H, CH₃Si α isomer), -0.20 (s, 3H, CH₃Si α isomer), -0.22 (s, 3H, CH₃Si α isomer)

¹³C NMR: (CDCl₃, 100.4 MHz, CHCl₃ internal standard)

δ (ppm)= 159.75 (1C, ArC-O), 145.24 (1C, ArC-CN), 132.52 (2C, ArC CB), 131.28 (1C, ArC Ph), 131.19 (1C, ArC Ph), 131.07 (1C, ArC CB), 130.87 (1C, ArC Ph), 130.51 (2C, ArC Ph), 128.81 (2C, ArC CB), 128.29 (2C, ArC CB), 127.03 (2C, ArC CB), 119.10 (1C, ArC, CB), 115.04 (2C, ArC CB), 109.64 (1C, C \equiv N), 84.27 (1C, C-B₁₀H₁₀), 82.88 (d ($J = 94.1\text{Hz}$), 1C, C-B₁₀H₁₀), 68.08 (1C, CH₂O), 39.33 (1C, CH₂C-B₁₀H₁₀ β), 36.85 (1C, CH₂C-B₁₀H₁₀ α), 29.69 (1C, CH₂CH₂O β), 29.65 (1C, CH₂CH₂O α), 28.94 (1C, CH₂), 23.56 (1C, CH₂ β), 23.08 (1C, CH₂ labelled B β), 22.99 (1C, CH₂ α), 21.67 (1C, CHSi labelled D α), 18.25 (1C, CH₂ β), 18.07 (1C, CH₂ α), 17.93 (1C, CH₂ labelled A β), 13.91 (1C, CH₃CH labelled C α), 0.33 (2C, CH₃Si β), 0.23 (2C, CH₃Si β), -1.92 (2C, CH₃Si α), -1.94 (2C, CH₃Si α)

²⁹Si NMR: (CDCl₃, 79.0 MHz)

δ (ppm)= 8.97 (1Si, α), 8.44 (1Si, β), 7.85 (1 Si, α), 7.04 (1Si, β)

¹¹B NMR: (CDCl₃, 160 MHz)

δ (ppm)= -3.38 (d ($J = 3.2\text{Hz}$), 2B), -10.25 (d ($J = 131.2\text{Hz}$), 8B)

IR (cm⁻¹): 2931 (m, ArH), 2576 (br, vs, BH), 2222 (m, CN), 1604 (m, C-O),

Mass (ESI):

$m/z =$ 659.4446 (M)⁺, 410.7, 390.2, 349.2, 322.2

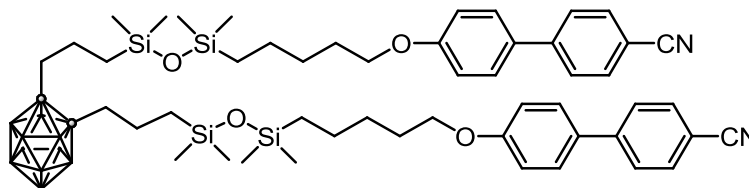
calculated = 659.4389 (M)⁺

CHN Microanalysis:

Observed: C 60.85 %, H 7.90 %, N 2.40 %

Calculated: C 60.23 %, H 7.81 %, N 2.13 %

**10.3.5 Bis 1,2-(propyl-3-[4'-(5-[1,1,3,3-tetramethyl-disiloxy]-
 pentyloxy)biphenyl-4-carbonitrile])-dodecacarborane, 3**



Solutions of bis 1,2-(prop-1-enyl)-dodecacarborane, (33.5 mg, 0.15 mmol) and 4'-[5-(1,1,3,3-Tetramethyl-disiloxanyl)-pentyloxy]-biphenyl-4-carbonitrile, **7** (118.9 mg, 0.30 mmol) in dry low sulfur toluene (2 mL each) were degassed by bubbling with Ar for 10 mins, transferred to a dry Schlenk tube under Ar and cooled to 0 °C. Karstedt's catalyst (10 μ L) was added; the solution allowed to warm to room temperature and stirred overnight. The solvent was removed *in vacuo* and the product purified by flash column chromatography (eluting with DCM, flash grade silica, R_f 0.44) to yield **3** as a glassy clear solid (52.3 mg, 34.2%).

Note: The integrations given for the nuclei which appear at different chemical shifts in each isomer are reported to reflect their abundance in relation to their own isomer and not the mixture as a whole.

^1H { ^{11}B } NMR: (CDCl₃, 500 MHz, CHCl₃ internal standard)

δ (ppm)= 7.68 (AA'BB' (J = 8.3 Hz), 4H, ArH), 7.63 (AA'BB' (J = 8.3 Hz), 4H, ArH), 7.52 (AA'XX' (J = 8.6 Hz), 4H, ArH), 6.99 (AA'XX' (J = 8.6 Hz), 4H, ArH), 4.01 (t (J = 6.4 Hz), 4H, CH₂O), 2.25 (s, 2H, BH), 2.22 (s, 4H, BH), 2.15 (t (J = 7.5 Hz), 4H, CH₂Cluster), 2.12 (s, 2H, BH), 1.83 (m, 4H, CH₂CH₂O), 1.55 (m, 8H, CH₂), 1.40 (m, 4H, CH₂), 1.06 (d (J = 7.1 Hz), 3H, CH₃CHSi α addition), 0.90 (m, 1H, CHSi α addition), 0.57 (m, 4H, CH₂Si α + β addition), 0.51 (m, 2H, CH₂Si β addition)

Chapter 10: Experimental

addition), 0.07 (s, 6H, SiCH₃ β addition), 0.07 (s, 6H, SiCH₃ β addition), 0.06 (s, 6H, SiCH₃ α addition), 0.05 (s, 6H, SiCH₃ α addition)

¹³C NMR: (CDCl₃, 400 MHz, CHCl₃ internal standard)

δ (ppm)= 159.91 (2C, ArC-O), 145.38 (2C, ArC), 132.67 (4C, ArC), 131.36 (2C, ArC), 128.43 (4C, ArC), 127.17 (4C, ArC), 119.23 (2C, ArC), 115.19 (4C, ArC), 110.14 (2C, CN), 79.84 (2C, CCluster), 68.23 (2C, CH₂O β addition), 68.17 (1/2C, CH₂O α isomer), 38.68 (1/2C, CH₂ α addition), 38.53 (2C, CH₂ β addition), 36.71 (2C, CH₂), 29.87 (2C, CH₂ β addition), 29.84 (1/2C, CH₂ α addition), 29.11 (2C, CH₂), 23.96 (2C, CH₂), 23.27 (2C, CH₂CH₂Si β addition), 21.95 (1/2C, CHSi α addition), 18.45 (2C, CH₂ β addition), 18.39 (1/2C, CH₂ α addition), 14.42 (1/2C, CH₃CHSi α addition), 9.82 (2C, CH₂), 0.54 (4C, CH₃Si β only), -0.21 (4C, CH₃Si β+α), -1.40 (4C, CH₃Si α+β), -1.90 (4C, CH₃Si α only)

²⁹Si NMR: (CDCl₃, 79.0 MHz)

δ (ppm)= 9.53 (1Si α), 8.71 (1Si β), 8.02 (1Si α), 7.09 (1Si β)

¹¹B NMR: (CDCl₃, 160.0 MHz)

δ (ppm)= -4.64 (d (J= 119.6 Hz), 2B), -10.46 (d (J= 114.7 Hz), 8B)

IR (cm⁻¹): 2933 (m, ArH), 2574 (br, vs, BH), 2214 (m, CN), 1600 (s, C-O)

Mass (ESI):

m/z = 1020.6293 (M)⁺, 906.3, 832.2, 758.2, 684.2, 610.2, 536.2, 507.4, 413.3, 352.3, 311.3

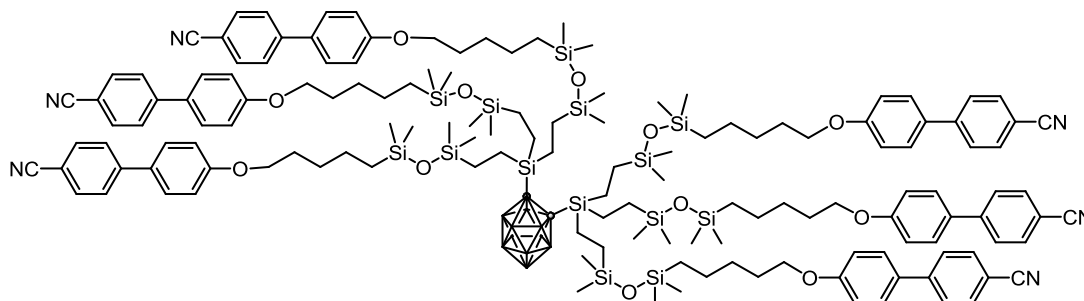
calculated = 1020.6282 (M)⁺

CHN Microanalysis:

Observed: C 61.54 %, H 8.09 %, N 2.79 %

Calculated: C 61.25 %, H 8.11 %, N 2.75 %

10.3.6 Bis 1,2 (tri-ethyl-2-[4'-(5-[1,1,3,3-tetramethyl-disiloxy]-pentyloxy)biphenyl-4-carbonitrile])silyl-dodecacarborane, **4**



Solutions of 4'-[5-(1,1,3,3-Tetramethyl-disiloxanyl)-pentyloxy]-biphenyl-4-carbonitrile, **7** (355.9 mg, 0.905 mmol) and bis 1,2 (trivinylsilyl)dodecacarborane (54.3 mg, 0.151 mmol) in low sulphur, dry degassed toluene (2 mL) were placed in a Schlenk tube under Ar and cooled to 0 °C. Karstedt's catalyst (20 µL) was added and the solution allowed to warm to room temperature. The pale yellow solution was stirred overnight, the solvent removed *in vacuo* and the product purified by flash column chromatography (eluting with Hexane/DCM 1:1, flash grade silica gel). Four different fractions were isolated with varying amounts of substitution ranging from 65 % to 80 % as measured by NMR. The fractions were combined and dissolved in low sulphur, dry, degassed toluene (2 mL) and placed in a schlenk tube under Ar with a solution of 4'-[5-(1,1,3,3-Tetramethyl-disiloxanyl)-pentyloxy]-biphenyl-4-carbonitrile, **7** (478.7 mg, 1.2 mmol) in low sulphur, dry, degassed toluene (2 mL). Karstedt's catalyst (20 µL) was added and the solution stirred for 48 h. The resulting solution was passed through a silica pad eluting with DCM to remove Pt black residue and dried *in vacuo*. The product was purified *via* flash column chromatography (eluting with DCM/Hexane 4:1, flash grade silica gel, R_f 0.24 in DCM). The residue was recrystallized with DCM/Ethanol yielding **4** as a white viscous room temperature liquid crystal (147.2 mg, 35.5%).

Note: The integrations given for the nuclei which appear at different chemical shifts in each isomer are reported to reflect their abundance in relation to their own isomer and not the mixture as a whole.

Chapter 10: Experimental

^1H NMR: (CDCl₃, 400 MHz, CHCl₃ internal standard)

δ (ppm) = 7.67 (AA'BB' (J = 8.4 Hz), 12H, ArH), 7.62 (AA'BB' (J = 8.4 Hz, 12H, ArH), 7.52 (AA'XX' (J = 8.7 Hz, 12H, ArH), 6.99 (AA'XX' (J = 8.7 Hz, 12H, ArH), 4.01 (t (J = 6.5 Hz), 12H, CH₂O), 1.83 (m, 12H, CH₂), 1.52 (m, 12H, CH₂), 1.43 (m, 12H, CH₂), 1.27 (s, 9H, CH₂SiB), 1.10 – 0.85 (m, 6H, CHSi alpha isomer), 0.59 (m, 12H, CH₂Si), 0.45 (d (J = 7.0 Hz), 9H, CH₃CHSi alpha isomer), 0.14 – 0.02 (m, 72H, CH₃Si)

^{13}C NMR: (CDCl₃, 100.4 MHz, CHCl₃ internal standard)

δ (ppm) = 159.94 (6C, ArC-O), 145.42 (6C, ArC), 132.71 (12C, ArC), 131.39 (6C, ArC), 128.45 (12C, ArC), 127.21 (12C, ArC), 119.26 (6C, ArC-CN), 115.21 (12C, ArC), 110.18 (6C, C \equiv N), 68.30 (6C, CH₂O), 29.87 (6C, CH₂), 29.13 (6C, CH₂), 23.31 (6C, CH₂), 18.51 (6C, CH₂), 9.85 (6C, CH₂), 0.57 (12C, CH₃Si), -0.19 (12C, CH₃Si)

^{10}B NMR: (CDCl₃, 160.0 MHz)

δ (ppm) = 23.57 (br, BH), -4.71 (br, BH)

^{29}Si NMR: (CDCl₃, 79.0 MHz)

δ (ppm) = 8.84 (s, 2Si, B-Si), 7.69 (s, 3Si, Si(CH₃)₂), 7.67 (s, 3Si, Si(CH₃)₂)

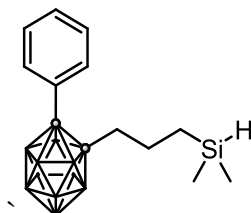
IR (cm⁻¹): 2924 (m, ArH), 2569 (w, br, BH), 2222 (m, CN), 1604 (s, C-O)

DSC/POM: Cr -45.3 [4.1] SmA 56.8 [16.3] Iso

CHN Microanalysis:

Observed: C 63.07 %, H 8.00 %, N 3.01 %

Calculated: C 63.84 %, H 7.85 %, N 3.06 %

10.3.7 1-Phenyl, 2-(3-(dimethylsilyl)-propyl)dodecacaborane, **55**

1-Phenyl, 2-(prop-2-enyl)dodecacaborane (87.1 mg, 0.335 mmol) and dimethyl chlorosilane (5 mL) were placed in a dry schlenk tube under Ar and the solution was purged with Ar. Karstedt's catalyst (50 μL) was added and the solution stirred over night. The solvent was removed *in vacuo*, residue dissolved in dry THF (10 mL) *in situ* and cooled to 0 °C. A solution of LiAlH_4 in dry THF (11 mL, 0.09 mol dm^{-3}) was added dropwise over 1 h. The resulting solution was allowed to warm to room temperature and stirred overnight. Ethyl acetate (50 mL) was added to destroy the excess LiAlH_4 and the solution dried *in vacuo*. The product was extracted with DCM and the solution was passed through a celite pad to yield **55** as a pale yellow oil (100.2 mg, 93.3 %).

^1H NMR: (CDCl₃, 400.0 MHz, CHCl₃ internal standard)
 δ (ppm) = 7.63 (d (J = 7.4 Hz), 2H, ArH), 7.42 (m, 3H, ArH), 3.68 (septet (J = 3.6 Hz), 1H, SiH), 1.90 – 1.71 (m, 2H, CH₂cluster), 1.51 – 1.33 (m, 2H, CH₂), 0.42 – 0.27 (m, 2H, CH₂Si), -0.05 (d (J = 3.7 Hz), 6H, CH₃Si)

^{13}C NMR: (CDCl₃, 100.4 MHz, CHCl₃ internal standard)
 δ (ppm) = 131.24 (2C, ArC), 130.92 (1C, ArC), 130.70 (1C, ArC), 128.99 (2C, ArC), 83.58 (1C, C_{cluster}), 82.47 (1C, C_{cluster}), 38.22 (1C, CH₂), 24.65 (1C, CH₂), 13.91 (1C, CH₂), -4.54 (2C, CH₃Si)

^{10}B NMR: (CDCl₃, 160.0 MHz)
 δ (ppm) = -4.61 (s, 2B), -11.32 (s, 6B)

Chapter 10: Experimental

^{29}Si NMR: (CDCl_3 , 79.0 MHz)

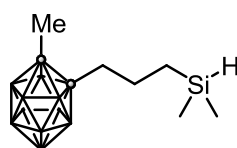
δ (ppm) = 12.98 (s, 1Si, SiH)

Mass (ESI):

m/z = 345.2032 ($\text{M}+\text{Na}$)⁺, 329.21, 301.14, 283.11, 256.14, 235.17, 213.07,
180.95, 167.01, 141.96, 125.99, 110.01, 81.52, 61.01

Calculated = 345.2789 ($\text{M}+\text{Na}$)⁺

10.3.8 1-Methyl, 2-(3-(demethylsilyl)-propyl)dodecacarborane, **56**



A solution of 1-methyl, 2-(prop-3-enyl)dodecacarborane (111.8 mg, 0.565 mmol) and dimethylchlorosilane (5 mL) in dry, low sulphur toluene (1 mL) was placed in a dry schlenk tube under Ar and purged with Ar. Karstedt's catalyst (20 μL) was added and the solution stirred overnight. The toluene solvent and excess dimethylchlorosilane were evaporated *in situ*. The residue was dissolved in dry THF (10 mL) and purged with Ar. A solution of LiAlH_4 (11.7 mL, 0.15 mol dm^{-3}) was added drop wise at 0 °C over 1 h. The resultant solution was allowed to warm to room temperature and stirred over night. Ethyl acetate (10 mL) was added to destroy excess LiAlH_4 and the solution was dried *in vacuo*. The product was extracted with DCM, filtered through a celite pad and the solvent removed *in vacuo* to yield **56** as a straw coloured oil (121.3 mg, 83.1 %).

^1H NMR: (CDCl_3 , 400.0 MHz, CHCl_3 internal standard)

δ (ppm) = 3.88 (sept ($J = 7.1$ Hz), 1H, SiH), 2.26 – 2.13 (m, 2H, CH_2 cluster),
2.00 (s, 3H, CH_3 cluster), 1.71 – 1.49 (m, 2H, CH_2), 0.68 – 0.53 (m,
2H, CH_2Si), 0.10 (d ($J = 3.7$ Hz), 6H, CH_3Si)

Chapter 10: Experimental

^{13}C NMR: (CDCl_3 , 100.4 MHz, CHCl_3 internal standard)

δ (ppm) = 78.24 (1C, Ccluster), 74.77 (1C, Ccluster), 38.57 (1C, CH_2), 24.89 (1C, CH_2), 23.24 (1C, CH_2), 14.17 (1C, CH_3 cluster), -4.44 (2C, CH_3Si)

^{10}B NMR: (CDCl_3 , 128.0 MHz)

δ (ppm) = -1.55 – -8.33 (m, 2B), -8.29 – -15.40 (m, 8B)

^{29}Si NMR: (CDCl_3 , 79.0 MHz)

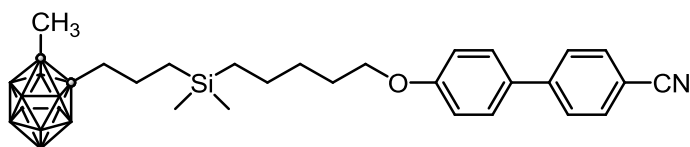
δ (ppm) = -12.78 (1Si, SiH)

Mass (ESI):

m/z = 299.2948 ($\text{M}+\text{K}$) $^+$, 288.92, 256.14, 226.95, 193.97, 158.96, 141.96, 125.99, 101.00, 90.98, 81.52

calculated = 299.2371 ($\text{M}+\text{K}$) $^+$

10.3.9 1-Methyl, 2-(propyl-3-[4'-(5-[dimethylsilyl]- pentyloxy)biphenyl-4-carbonitrile])-dodecacarborane, **8**



1-Methyl, 2-(3-(dimethylsilyl)-propyl)dodecacarborane, **56** (98.9 mg, 0.38 mmol) and 4'-(pent-4-enyloxy)biphenyl-4-carbonitrile, **5** (120.0 mg, 0.46 mmol) were dissolved in dry, low sulphur toluene (1 mL) in a schlenk tube, placed under Ar and purged with Ar. Karstedt's catalyst (20 μL) was added and the solution stirred overnight; the solution was dried *in vacuo* and the residue purified by flash column chromatography (eluting with DCM, flash grade silica gel, R_f - 0.56) yielding **8** as a white solid (106.6 mg, 53.8%).

Chapter 10: Experimental

^1H $\{^{10}\text{B}\}$ NMR: (CDCl₃, 500.0 MHz, CHCl₃ internal standard)

δ (ppm) = 7.69 (AA'BB' (J = 8.4 Hz), 2H, ArH), 7.64 (AA'BB' (J = 8.3 Hz), 2H, ArH), 7.53 (AA'XX' (J = 8.7 Hz), 2H, ArH), 6.99 (AA'XX' (J = 8.7 Hz), 2H, ArH), 4.01 (t (J = 6.5 Hz), 2H, CH₂O), 2.36 – 2.05 (m, 10H, BH), 1.99 (s, 3H, CH₃cluster), 1.81 (m, 2H, CH₂CH₂Cluster), 1.54 (m, 4H, CH₂), 1.44 – 1.33 (m, 2H, CH₂), 0.62 – 0.53 (m, 2H, CH₂), 0.53 – 0.46 (m, 2H, CH₂Si), 0.00 (s, 6H, CH₃Si)

^{13}C NMR: (CDCl₃, 100.4 MHz, CHCl₃ internal standard)

δ (ppm) = 159.86 (1C, ArC-O), 145.36 (1C, ArC), 132.66 (2C, ArC), 131.34 (1C, ArC), 128.43 (2C, ArC), 127.16 (2C, ArC), 119.23 (1C, ArC-CN), 115.17 (2C, ArC), 110.08 (1C, CN), 78.24 (1C, ClusterC), 74.70 (1C, ClusterC), 68.16 (1C, CH₂O), 39.09 (1C, CH₂CH₂O), 30.01 (1C, CH₂), 29.02 (1C, CH₂), 24.44 (1C, CH₂), 23.76 (1C, CH₂), 23.23 (1C, CH₃Cluster), 15.41 (1C, CH₂Si), 15.17 (1C, CH₂Si), -3.32 (2C, CH₃Si)

^{10}B NMR: (CDCl₃, 160.0 MHz)

δ (ppm) = -5.38 (s, 1B), -6.65 (s, 1B), -10.05 (s, 2B), -10.75 (s, 2B), -11.57 (s, 4B)

^{29}Si NMR: (CDCl₃, 79.0 MHz)

δ (ppm) = 2.99 (s, 1Si, SiCH₂)

IR (cm⁻¹): 2916 (m, ArH), 2576 (s, B-H), 2229 (m, C-N), 1604 (s, C-O)

Mass (ESI):

m/z = 524.4146 (M+H)⁺, 485.11

calculated = 524.4123 (M+H)⁺

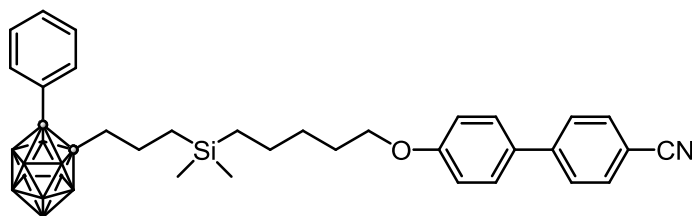
DSC/POM: Cr1 51.4 [-23.0] Cr2 117.1 [26.1] Iso

CHN Microanalysis:

Observed: C 59.44 %, H 8.43 %, N 2.56 %

Calculated: C 59.84 %, H 8.31 %, N 2.68 %

10.3.10 1-Phenyl, 2-[propyl-3-[4'-(5-(dimethylsilyl)-pentyloxy)biphenyl-4-carbonitrile)]-dodecacarborane, **9**



1-Phenyl, 2-(3-(dimethylsilyl)propyl)dodecacarborane, **55** (32.8 mg, 0.102 mmol) and 4'-(5-(dimethylsilyl)pentyloxy)biphenyl-4-carbonitrile, **5** (33.6 mg, 0.128 mmol) were dissolved in dry, low sulphur toluene (1 mL) in a Schlenk tube, placed under Ar and purged with Ar. Karstedt's catalyst (20 μ L) was added and the solution stirred overnight, the solvent was evaporated and the residue purified by flash column chromatography (eluting with DCM, flash grade silica gel, R_f 0.67) yielding **9** as a viscous oil (26.4 mg, 44.1 %).

^1H $\{^{10}\text{B}\}$ NMR: (CDCl₃, 500.0 MHz, CHCl₃ internal standard)

δ (ppm) = 7.69 (AA'BB' (J = 8.3 Hz), 2H, ArH), 7.64 (AA'BB' (J = 7.9 Hz), 2H), 7.63 (d (J = 7.1 Hz), 2H, ArH), 7.53 (AA'XX' (J = 8.7 Hz), 2H, ArH), 7.41 (m, 3H, ArH), 6.99 (AA'XX' (J = 8.7 Hz), 2H, ArH), 4.00 (t (J = 6.5 Hz), 2H, CH₂O), 2.43 (m, 10H, BH), 1.78 (m, 4H, CH₂), 1.52 – 1.42 (m, 2H, CH₂), 1.42 – 1.33 (m, 2H, CH₂), 1.33 – 1.21 (m, 2H, CH₂), 0.49 – 0.35 (m, 2H, CH₂Si), 0.32 – 0.20 (m, 2H, CH₂Si), -0.14 (s, 6H, CH₃Si)

^{13}C NMR: (CDCl₃, 100.4 MHz, CHCl₃ internal standard)

δ (ppm) = 159.89 (1C, ArC-O), 145.40 (1C, ArC), 132.71 (2C, ArC), 131.44 (1C, ArC), 131.25 (2C, ArC), 130.99 (1C, ArC), 130.68 (1C, ArC), 128.97 (2C, ArC), 128.48 (2C, ArC), 127.21 (2C, ArC), 119.25 (1C, ArC-CN), 115.20 (2C, ArC), 110.19 (1C, CN), 83.47 (1C, CCluster), 82.53 (1C, CCluster), 68.20 (1C, CH₂O), 38.77 (1C, OCH₂CH₂),

Chapter 10: Experimental

30.03 (1C, CH₂), 29.05 (1C, CH₂), 24.25 (1C, CH₂), 23.73 (1C, CH₂),
15.13 (2C, CH₂Si), -3.39 (2C, CH₃Si)

¹⁰B NMR: (CDCl₃, 160.0 MHz)
δ (ppm)= -4.57 (s, 2B), -11.34 (s, 8B)

²⁹Si NMR: (CDCl₃, 79.0 MHz)
δ (ppm)= 2.84 (s, Si)

IR (cm⁻¹): 3348 (m, br, B-H), 2924 (s, ArH), 2584 (m, B-H), 2229 (w, CN),
1712 (s, C-O stretch)

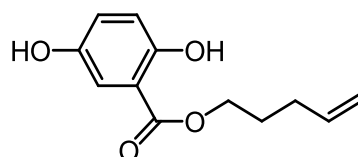
Mass (ESI):
m/z = 586.4324 (M+H)⁺, 564.25, 536.17, 529.18
calculated = 586.4279 (M+H)⁺

POM/DSC: Cr 63.0 [24.7] Iso

CHN Microanalysis:

Observed: C 65.40 %, H 7.67 %, N 1.94 %
Calculated: C 63.77 %, H 7.77 %, N 2.40 %

10.3.11 2,5-Dihydroxy-benzoic acid pent-4-enyl ester, 57



2,5-Dihydroxy benzoic acid (2.3 g, 14.92 mmol) and KHCO₃ (1.8 g, 17.9 mmol) were dissolved in dry DMF (25 mL) and stirred for 10 mins under Ar. 4-Bromopentene (2 mL, 17.9 mmol) was added, the solution brought to 40 °C and stirred for 4 h. The solution was allowed to cool to room temperature and poured onto a mixture of ethylacetate/H₂O 1:1 (60 mL). The organic phase was separated, washed with 5 % w/w NaHCO₃ in water (30 mL), followed by a 5 % w/w NaCl in water (30 mL) and

Chapter 10: Experimental

finally with water (30 mL). The organic phase was dried over MgSO_4 , the solvent removed *in vacuo* and the residue purified by flash column chromatography (DCM 5% ethyl acetate, flash grade silica, $R_f = 0.37$) to yield **57** as a white crystalline solid (1.95 g, 58.8 %).

^1H NMR: (400 MHz, CDCl_3 , CDCl_3 internal standard)

δ (ppm)= 10.44 (s, 2H, OH), 7.29 (d ($J = 3.2\text{Hz}$), 1H, ArH), 7.01 (dd ($J = 3.1\text{Hz}$, 8.9Hz), 1H, ArH), 6.87 (d ($J = 8.9\text{Hz}$), 1H, ArH), 5.83 (dd ($J = 16.9$ (*trans*), 10.2 (*cis*), 6.6 (*gem*) Hz), 1H, $\text{CH}=\text{CH}_2$), 5.07 (dd ($J = 17.1$, 1.7 Hz), 1H, $\text{CH}_{\text{trans}}\text{H}=\text{CH}$), 5.02 (dd ($J = 10.2$, 1.7 Hz), 1H, $\text{CH}_{\text{cis}}\text{H}=\text{CH}$), 4.34 (t ($J = 6.5\text{Hz}$), 2H, CH_2O), 2.19 (m, 2H, OCH_2CH_2), 1.87 (m, 2H, $\text{CH}_2=\text{CHCH}_2$)

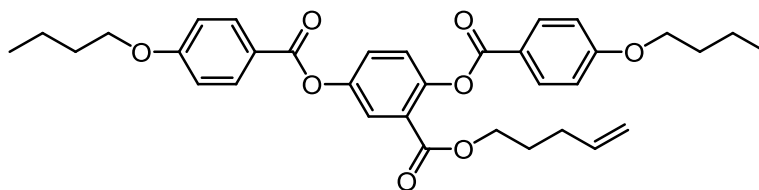
^{13}C NMR: (100.4 MHz, CDCl_3 , CDCl_3 internal standard)

δ (ppm)= 169.75 (1C, COO), 155.72 (1C, Ar), 147.70 (1C, Ar), 137.08 (1C, $\text{CH}_2\text{CH}=\text{CH}_2$), 123.97 (1C, Ar), 118.44 (1C, Ar), 115.62 (1C, Ar), 114.70 (1C, $\text{CH}_2=\text{CH}$), 112.33 (1C, Ar), 64.82 (1C, CH_2OCO), 29.97 (1C, CH_2), 27.61 (1C, CH_2)

IR (cm^{-1}): 3340 (s, br, OH), 2916 (w, ArH), 1666 (s, C=O), 1442 (m), 1195 (s), 786 (vs)

Mass (ESI):

$m/z = 221.08$ ($\text{M}+\text{H}$) $^+$

10.3.12 Pent-4-enyl, 2-5 bis(4-butoxy benzoyl) bezoate, **16**

4-*n*-Butoxy benzoic acid (3.76 g, 19.36 mmol), 2,5-dihydroxy-benzoic acid pent-4-enyl ester, **57** (1.95 g, 8.8 mmol), DCC (4.36 g, 21.12 mmol) and DMAP (2.2 g, 8.8 mmol) were dissolved in DCM (250 mL) and the solution stirred overnight. A white precipitate formed which was filtered off and the filtrate dried *in vacuo*. The residue was purified by flash column chromatography (DCM/Hexane 3:1, flash grade silica, R_f 0.42) to yield **16** as a white crystalline solid (4.35 g, 96.7 %).

^1H NMR: (400 MHz, CDCl_3 , CDCl_3 internal standard)

δ (ppm) = 8.16 (m, 4H, ArH), 7.89 (d ($J = 2.7\text{Hz}$), 1H, ArH), 7.45 (dd ($J = 2.9\text{Hz}$, 8.8Hz), 1H, ArH), 7.26 (d ($J = 8.7\text{Hz}$), 1H, ArH), 6.98 (m, 4H, ArH), 5.67 (ddt ($J = 16.9$ (*trans*), 10.3 (*cis*), 6.5 (*gem*) Hz), 1H, $\text{CH}=\text{CH}_2$), 4.94 (dd ($J = 9.7$, 1.8 Hz), 1H, $\text{CH}_{\text{cis}}\text{H}=\text{CH}$), 4.91 (m, 1H, $\text{CH}_{\text{trans}}\text{H}=\text{CH}$), 4.17 (t ($J = 6.7\text{Hz}$), 2H, CH_2OCO), 4.06 (m, 4H, CH_2OPh), 2.01 (m, 2H, $\text{CH}_2\text{CH}_2\text{OCO}$), 1.82 (m, 4H, $\text{CH}_2\text{CH}_2\text{OPh}$), 1.52 (m, 6H, $\text{CH}_2\text{CH}=\text{CH}_2 + \text{CH}_2\text{CH}_3$), 1.00 (t ($J = 7.4\text{Hz}$), 6H, CH_3)

^{13}C NMR: (100.4 MHz, CDCl_3 , CDCl_3 internal standard)

δ (ppm) = 165.07 (1C, COO), 164.73 (1C, COO), 164.19 (1C, COO), 163.88 (1C, ArC-O), 163.74 (1C, ArC-O), 148.45 (1C, ArC-O), 148.25 (1C, ArC-O), 137.46 (1C, $\text{HC}=\text{CH}_2$), 132.59 (2C, ArC), 132.52 (2C, ArC), 127.26 (1C, ArC), 125.15 (1C, ArC), 125.12 (1C, ArC), 125.01 (1C, ArC), 121.53 (1C, ArC), 121.14 (1C, ArC), 115.31 (1C, $\text{HC}=\text{CH}_2$), 114.51 (2C, ArC), 114.48 (2C, ArC), 68.17 (1C, CH_2O), 68.13 (1C, CH_2O), 65.03 (1C, CH_2O), 31.25 (2C, CH_2), 30.02 (1C, CH_2), 27.62 (1C, CH_2), 19.33 (2C, CH_2), 13.96 (2C, CH_3)

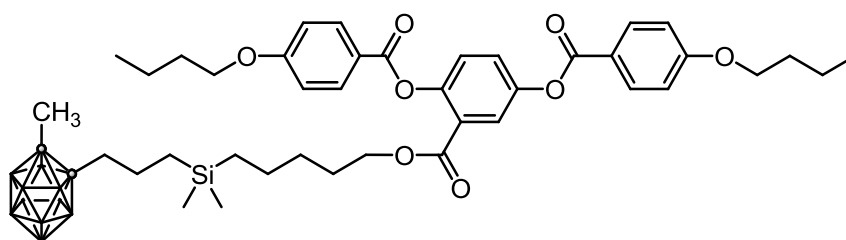
IR (cm^{-1}): 2954 (m, ArH), 1720 (vs, C=O), 1249 (vs), 1072 (s)

Mass (ESI):

 $m/z = 597.24 (M+Na)^+$

DSC/POM: Cr 85.7 [41.0] N 110.4 [1.4] Iso

10.3.13 1-Methyl, 2-(propyltrimethylsilyl[5-pentyl, 2-5 bis(4-butoxy benzoyl) benzoate])dodecacarborane, **10**



A solution of 1-methyl, 2-(prop-3-dimethylsilyl)dodecacarborane, **56** (60.0 mg, 0.23 mmol) and pent-4-enyl, 2-5 bis(4-butoxy benzoyl) benzoate, **16** (160.0 mg, 0.28 mmol) in dry, low sulphur toluene (4 mL) was placed in a dry Schlenk tube under Ar and purged with Ar. Karstedt's catalyst (40 μ L) was added and the solution stirred overnight. The solution was dried *in vacuo* and the product isolated by flash column chromatography (eluting with DCM, flash grade silica, R_f 0.53) yielding **10** as a viscous colourless oil (89.2 mg, 46.5 %).

$^1\text{H} \{^{10}\text{B}\}$ NMR: (CDCl₃, 500.0 MHz, CHCl₃ internal standard)

δ (ppm) = 8.16 (d ($J = 8.5$ Hz), 2H, ArH), 8.15 (d ($J = 8.6$ Hz), 2H, ArH), 7.89 (d ($J = 2.8$ Hz), 1H, ArH), 7.45 (dd ($J = 8.7, 2.9$ Hz), 1H, ArH), 7.26 (d ($J = 8.7$ Hz), 1H, ArH), 6.99 (d ($J = 3.5$ Hz), 2H, ArH), 6.98 (d ($J = 3.4$ Hz), 2H, ArH), 4.16 (t ($J = 6.7$ Hz), 2H, CH₂O), 4.07 (t ($J = 6.4$ Hz), 2H, CH₂O), 4.06 (t ($J = 6.4$ Hz), 2H, CH₂O), 2.23 (s, br, 5H, BH), 2.19 – 2.10 (m, 2H, CH₂Cluster), 2.14 (s, br, 3H, BH), 2.09 (s, br, 2H, BH), 1.98 (s, 3H, CH₃Cluster), 1.88 – 1.78 (m, 4H, CH₂), 1.59 – 1.44 (m, 8H, CH₂), 1.38 – 1.12 (m, 4H, CH₂), 1.01 (t ($J = 7.4$ Hz), 6H, CH₃), 0.49 – 0.44 (m, 2H, CH₂Si), 0.46 – 0.38 (m, 2H, CH₂Si), -0.04 (s, 6H, CH₃Si)

^{13}C NMR: (CDCl₃, 400.0 MHz, CHCl₃ internal standard)

Chapter 10: Experimental

δ (ppm) = 165.02 (1C, COO), 164.70 (1C, COO), 164.18 (1C, COO), 163.88 (1C, ArC-O), 163.69 (1C, ArC-O), 148.41 (1C, ArC-O), 148.23 (1C, ArC-O), 132.55 (2C, ArCH), 132.47 (2C, ArCH), 127.21 (1C, ArCH), 125.12 (1C, ArCH), 125.04 (1C, ArCH), 125.02 (1C, ArC), 121.54 (1C, ArC), 121.08 (1C, ArC), 114.50 (2C, ArCH), 114.41 (2C, ArCH), 78.26 (1C, Ccluster), 74.70 (1C, Ccluster), 68.15 (1C, CH₂O), 68.11 (1C, CH₂O), 65.59 (1C, CH₂O), 39.07 (1C, CH₂), 31.24 (1C, CH₂), 31.22 (1C, CH₂), 29.73 (1C, CH₂), 28.17 (1C, CH₂), 24.40 (1C, CH₂), 23.49 (1C, CH₂), 23.21 (1C, CH₃cluster), 19.30 (2C, CH₂), 15.32 (1C, CH₂), 15.04 (1C, CH₂), 13.94 (2C, CH₃CH₂), -3.41 (2C, CH₃Si)

¹⁰B NMR: (CDCl₃, 160.0 MHz)

δ (ppm) = -5.05 (t (J = 170.8 Hz), 2B), -9.74 (dd (J = 256.9, 140.9 Hz), 8B)

²⁹Si NMR: (CDCl₃, 79.0 MHz)

δ (ppm) = 2.93 (1Si, Si(CH₃)₂)

IR (cm⁻¹): 2931 (m, ArH), 2870 (m, ArH), 2576 (s, br, BH), 1728 (s, C=O stretch), 1604 (s, C-O stretch)

Mass (ESI):

m/z = 856.5228 (M+Na)⁺, 781.17, 684.20, 610.18, 541.12, 485.11

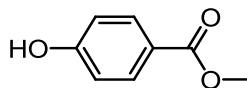
calculated = 856.5235 (M+Na)⁺

POM/DSC: Cr 51.9 [26.7] Iso

CHN Microanalysis:

Observed: C 59.31 %, H 7.74 %, N 0.00 %

Predicted: C 60.55 %, H 7.74 %, N 0.00 %

10.3.14 Methyl 4-hydroxybenzoate, 58

4-Hydroxybenzoic acid, (10.0 g, 72.4 mmol) was dissolved in methanol (250 mL), the solution acidified with conc. H_2SO_4 and heated to reflux for 2 h. The solution was allowed to cool, extracted into DCM (250 mL) and washed with water (3 x 100 mL). The solution was dried over MgSO_4 and the solvent removed *in vacuo*. The product was recrystallized from toluene to yield **58** as a white crystalline solid (10.41 g, 94.5 %).

^1H NMR: (CDCl₃, 400.0 MHz, CHCl₃ internal standard)

δ (ppm): 7.95 (d (J = 8.7 Hz), 2H, ArH), 7.04 (s, 1H, OH), 6.91 (d (J = 8.7 Hz), 2H, ArH), 3.91 (s, 3H, CH₃)

^{13}C NMR: (CDCl₃, 100.4 MHz, CHCl₃ internal standard)

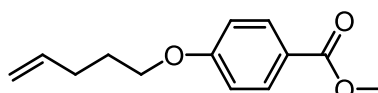
δ (ppm) = 167.95 (1C, COO), 160.70 (1C, ArC-O), 132.13 (2C, ArC), 122.09 (1C, ArC), 115.50 (2C, ArC), 52.35 (1C, CH₃)

IR (cm⁻¹): 3278 (vs, br, O-H), 1674 (s, C=O), 1589 (C-O)

Mass (ESI):

m/z = 153.0539 (M+H)⁺, 137.03, 125.99, 101.00, 81.52

calculated = 153.0552 (M+H)⁺

10.3.15 Methyl 4-(pent-4-enyloxy)benzoate, 59

Methyl 4-hydroxybenzoate, **58** (10.41 g, 68.4 mmol), K_2CO_3 (37.09 g, 268.4 mmol) and KI (1.11 g, 6.71 mmol) were suspended in butanone (400 mL). The suspension

Chapter 10: Experimental

was brought to reflux, 5-bromopent-1-ene (12.23 g, 82.1 mmol) was added and the resultant solution stirred overnight. The solution was allowed to cool, was extracted with DCM (400 mL), washed with water (3 x 200 mL), dried over MgSO₄ and the solvent removed *in vacuo*. The residue was dissolved in DCM and passed through a silica pad to yield **59** as a colourless oil (14.74 g, 97.8 %).

¹H NMR: (CDCl₃, 400.0 MHz, CHCl₃ internal standard)
δ (ppm) = 7.97 (d (*J* = 8.9 Hz), 2H, ArH), 6.89 (d (*J* = 9.0 Hz), 2H, ArH), 5.84 (ddt (*J* = 16.9 (*trans*), 10.2 (*cis*), 6.6 (*gem*) Hz), 1H, CH=CH₂), 5.06 (dd (*J* = 17.1, 1.8 Hz), 1H CH=CH_{*trans*}H), 5.01 (dd (*J* = 10.2, 1.9 Hz), 1H, CH=CH_{*cis*}H), 4.00 (t (*J* = 6.4 Hz), 2H, CH₂O), 3.87 (s, 3H, CH₃O), 2.26 – 2.21 (m, 2H, CH₂), 1.96 – 1.84 (m, 2H, CH₂)

¹³C NMR: (CDCl₃, 100.4 MHz, CHCl₃ internal standard)
δ (ppm) = 166.97 (1C, COO), 162.94 (1C, ArC-O), 137.66 (1C, CH=CH₂), 131.66 (2C, ArC), 122.49 (1C, ArC), 115.49 (1C, CH=CH₂), 114.15 (2C, ArC), 67.40 (1C, CH₂O), 51.92 (1C, CH₃O), 30.11 (1C, CH₂), 28.34 (1C, CH₂)

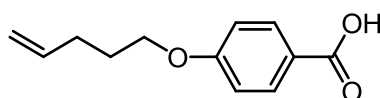
IR (cm⁻¹): 2947 (w, ArH), 1712 (vs, C=O stretch), 1604 (s, C-O stretch)

Mass (ESI):

m/z = 221.1173 (M+H)⁺, 189.09, 171.06, 150.55, 125.99, 90.98

calculated = 221.1178 (M+H)⁺

10.3.16 4-(Pent-4-enyloxy)benzoic acid, **60**



Methyl 4-(pent-4-enyloxy)benzoate, **59** (14.74 g, 66.9 mmol) was dissolved in MeOH (200 mL) and placed under Ar. A solution of NaOH (10.70 g, 267.6 mmol) in

Chapter 10: Experimental

water (50 mL) was added and the solution refluxed for 1 h. The solution was allowed to cool, acidified with conc. HCl, filtered and the solid washed with water. The solid was dissolved in DCM, dried over MgSO₄ and the solvent removed *in vacuo*. The product was recrystallized from toluene to yield **60** as a white crystalline solid (13.01 g, 94.3 %).

¹H NMR: (CDCl₃, 400.0 MHz, CHCl₃ internal standard)
δ (ppm) = 12.61 (s, 1H, OH), 8.07 (d (*J* = 8.9 Hz), 2H, ArH), 6.94 (d (*J* = 8.9 Hz), 2H, ArH), 5.86 (ddt (*J* = 16.9 (*trans*), 10.2 (*cis*), 6.6 (*gem*) Hz), 1H, CH=CH₂), 5.08 (dd (*J* = 17.1, 1.7 Hz), 1H, CH=CHH_{*trans*}), 5.02 (dd (*J* = 10.2, 1.7 Hz), 1H, CH=CHH_{*cis*}), 4.04 (t (*J* = 6.4 Hz), 2H, CH₂O), 2.31 – 2.19 (m, 2H, CH₂), 1.98 – 1.85 (m, 2H, CH₂)

¹³C NMR: (CDCl₃, 100.4 MHz, CHCl₃ internal standard)
δ (ppm) = 172.43 (1C, COO), 163.72 (1C, ArC-O), 137.65 (1C, CH=CH₂), 132.48 (2C, ArC), 121.62 (1C, ArC), 115.56 (1C, CH=CH₂), 114.31 (2C, ArC), 67.52 (1C, CH₂O), 30.13 (1C, CH₂), 28.33 (1C, CH₂)

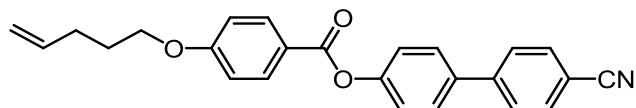
IR (cm⁻¹): 2939 (s, ArH), 1674 (vs, C=O stretch), 1604 (s, C-O stretch)

Mass (ESI):

m/z = 207.1011 (M+H)⁺, 189.09, 164.05

calculated = 207.1021 (M+H)⁺

10.3.17 4'-Cyanobiphenyl-4-yl 4-(pent-4-enyloxy)benzoate, **17**¹¹⁸



4-Hydroxy, 4'-cyanobiphenyl (6.05 g, 31 mmol), 4-(pent-4-enyloxy)benzoic acid, **60** (6.19 g, 30 mmol), EDAC (5.59 g, 36 mmol) and DMAP (0.75 g, 3 mmol) were dissolved in DCM (350 mL) and the solution stirred overnight. The solution was washed with water (3 x 250 mL), dried over MgSO₄ and the solvent removed *in*

Chapter 10: Experimental

vacuo. The product was isolated *via* flash column chromatography (flash grade silica gel, eluting with DCM, $R_f = 0.68$) yielding **17** as a white crystalline solid (10.26 g, 89.2 %).

^1H NMR: (CDCl₃, 400 MHz, CHCl₃ internal standard)

δ (ppm) = 8.16 (2H, d ($J = 8.9$ Hz), ArH), 7.74 (2H, d ($J = 8.6$ Hz), ArH), 7.68 (2H, d ($J = 8.6$ Hz), ArH), 7.64 (2H, d ($J = 8.7$ Hz), ArH), 7.33 (2H, d ($J = 8.6$ Hz), ArH), 6.99 (2H, d ($J = 9.0$ Hz), ArH), 5.87 (ddt ($J = 16.9$ (*trans*), 10.2 (*cis*), 6.7 (*gem*) Hz), 1H, CH=CH₂), 5.09 (dd ($J = 17.1$, 1.7 Hz), 1H, CH=CHH_{*trans*}), 5.03 (dd ($J = 10.2$, 1.7 Hz), 1H, CH=CHH_{*cis*}), 4.07 (2H, t ($J = 6.4$ Hz), CH₂O), 2.25 - 2.30 (2H, m, CH₂), 1.99 - 1.89 (1H, m, CH₂)

^{13}C NMR: (CDCl₃, 100.4 MHz, CHCl₃ internal standard)

δ (ppm) = 164.95 (1C, COO), 163.72 (1C, ArC), 151.68 (1C, ArC), 144.98 (1C, ArC), 137.62 (1C, CH=CH₂), 136.82 (1C, ArC), 132.78 (2C, ArC), 132.49 (2C, ArC), 128.47 (2C, ArC), 127.82 (2C, ArC), 122.70 (2C, ArC), 121.41 (1C, ArC), 119.03 (1C, ArC), 115.61 (1C, CN), 114.49 (2C, ArC), 111.09 (1C, ArC), 67.59 (1C, CH₂O), 30.13 (1C, CH₂), 28.33 (1C, CH₂)

IR (cm⁻¹): 3062 (w, ArH), 2947 (w, ArH), 2877 (w, ArH), 2222 (s, CN), 1720 (vs, C=O), 1597 (s, C-O)

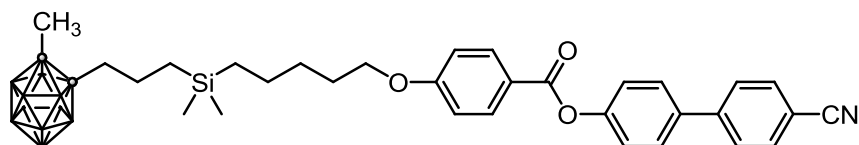
Mass (ESI):

m/z 406.1414 (M+Na)⁺, 384.16 (M+H)⁺, 252.58, 189.09, 167.01, 125.99

calculated = 406.1419 (M+Na)⁺

DSC/POM: Cr 108.0 [31.0] N 264.0 [1.2] Iso

10.3.18 1-Methyl, 2-[propyl-3-dimethylsilyl-(4'-cyanobiphenyl-4-yl 4-(pentyloxy)benzoate]dodecacarborane, 11



A solution of 1-methyl, 2-(propyl-3-dimethylsilyl)dodecacarborane, **56** (31 mg, 0.12 mmol) and 4'-cyanobiphenyl-4-yl 4-(pent-4-enyloxy)benzoate, **17** (71 mg, 0.19 mmol) in dry, low sulphur toluene (3 mL) was added to a dry Schlenk tube under Ar and purged with Ar. Karstedt's catalyst (20 μ L) was added and the solution stirred overnight. The solution was dried *in vacuo* and the residue purified *via* flash column chromatography (eluting with DCM 10 % Hexane, flash grade silica, R_f – 0.29) to yield **11** as a white crystalline solid (23.2 mg, 30.1 %).

^1H { ^{10}B } NMR: (CDCl₃, 500.0 MHz, CHCl₃ internal standard)

δ (ppm) = 8.16 (d, (J = 8.8 Hz), 2H, ArH), 7.74 (d (J = 8.4 Hz), 2H, ArH), 7.69 (d (J = 8.4 Hz), 2H, ArH), 7.64 (d (J = 8.6 Hz), 2H, ArH), 7.33 (d (J = 8.6 Hz), 2H, ArH), 6.99 (d (J = 8.9 Hz), 2H, ArH), 4.06 (t (J = 6.5 Hz), 2H, CH₂O), 2.24 (s, br, 5H, BH), 2.16 (t (J = 8.5 Hz) 2H, CH₂Cluster), 2.12 (s, br, 3H, BH), 2.10 (s, br, 2H, BH), 1.99 (s, 3H, CH₃Cluster), 1.90 – 1.78 (m, 2H, CH₂), 1.62 – 1.46 (m, 4H, CH₂), 1.46 – 1.30 (m, 2H, CH₂), 0.62 – 0.53 (m, 2H, CH₂Si), 0.54 – 0.46 (m, 2H, CH₂Si), 0.00 (s, 6H, CH₃Si)

^{13}C NMR: (CDCl₃, 100.4 MHz, CHCl₃ internal standard)

δ (ppm) = 164.97 (1C, COO), 163.78 (1C, ArC-O), 151.70 (1C, ArC-O), 145.00 (1C, ArC), 136.84 (1C, ArC), 132.79 (2C, ArC), 132.50 (2C, ArC), 128.49 (2C, ArC), 127.83 (2C, ArC), 122.70 (2C, ArC), 121.38 (1C, ArC), 119.03 (1C, ArC), 114.48 (2C, ArC), 111.11 (1C, C \equiv N), 78.22 (1C, C_{cluster}), 74.70 (1C, C_{cluster}), 68.39 (1C, CH₂O), 39.14 (1C, CH₂), 30.00 (1C, CH₂), 28.93 (1C, CH₂), 24.46 (1C, CH₂), 23.79 (1C, CH₂),

Chapter 10: Experimental

23.27 (1C, CH₂), 15.46 (1C, CH₂), 15.20 (1C, CH₃Cluster), -3.29 (2C, CH₃Si)

¹⁰B NMR: (CDCl₃, 128.0 MHz)

δ (ppm) = -5.99 (d (*J* = 168.2 Hz), 2B), -8.43 – -17.18 (m, 8B)

²⁹Si NMR: (CDCl₃, 79.0 MHz)

δ (ppm) = 3.00 (1 Si, Si(CH₃)₂)

IR (cm⁻¹): 2924 (m, ArH), 2870 (m, ArH), 2576 (s, br, BH), 2222 (m, CN), 1720 (s, C=O), 1604 (s, C-O)

Mass (ESI):

m/z = 644.4394 (M+H)⁺, 610.18, 541.12, 454.29, 413.27, 391.29, 338.34

calculated = 644.4334 (M+H)⁺

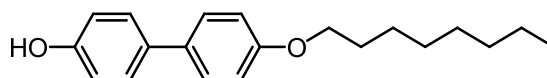
DSC/POM: Cr 102.6 [7.7] N 103.3 [1.2] Iso

Elemental Analysis:

Observed: C 62.20 %, H 7.58 %, N 1.90 %

Calculated: C 61.47 %, H 7.38 %, N 2.18 %

10.3.19 4'-(Octyloxy)-4-hydroxybiphenyl, **61**¹⁵⁰



A solution of 4,4'-biphenol (15.0 g, 80.6 mmol) and 8-bromooctane (15.56 g, 80.6 mmol) in ethanol (150 mL) was brought to reflux. A solution of KOH (4.87 g, 87.0 mmol) in water (15 mL) was added dropwise over 1 h. The solution was refluxed for a further 3 h, allowed to cool and the solvent removed *in vacuo*. The residue was purified by flash column chromatography (eluting with DCM, flash grade silica, R_f 0.29), followed by recrystallization from ethanol to yield **61** as a white crystalline solid (5.10 g, 21.2 %).

Chapter 10: Experimental

^1H NMR: (CDCl₃, 400 MHz, CHCl₃ internal standard)
 δ (ppm) = 7.45 (d (J = 8.9 Hz), 2H, ArH), 7.43 (d (J = 8.7 Hz), 2H, ArH), 6.94 (d (J = 8.7 Hz), 2H, ArH), 6.88 (d (J = 8.6 Hz), 2H, ArH), 4.74 (s, 1H, OH), 3.99 (t (J = 6.6 Hz), 2H, CH₂O), 1.89 – 1.74 (m, 2H, CH₂CH₂O), 1.55 – 1.42 (m, 2H, CH₂), 1.33 (m, 8H, CH₂), 0.90 (t (J = 6.9 Hz), 3H, CH₃)

^{13}C NMR: (CDCl₃, 100.4 MHz, CHCl₃ internal standard)
 δ (ppm) = 158.43 (1C, ArC-O), 154.66 (1C, ArC-O), 128.08 (2C, ArC), 127.81 (2C, ArC), 115.70 (2C, ArC), 114.88 (2C, ArC), 68.24 (1C, CH₂O), 31.97 (1C, CH₂), 29.53 (1C, CH₂), 29.45 (1C, CH₂), 29.41 (1C, CH₂), 26.22 (1C, CH₂), 22.82 (1C, CH₂), 14.27 (1C, CH₃)

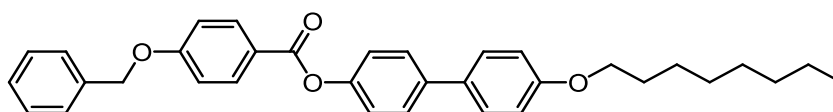
IR (cm⁻¹): 3340 (br, s, OH), 2942 (s, ArH), 2854 (m, ArH), 1604 (s, C-O stretch)

Mass (ESI):

m/z = 299.1978 (M+H)⁺, 261.11, 239.14, 226.95, 208.10, 187.08, 158.00, 144.98, 131.96, 103.96, 81.52

calculated = 299.2011 (M+H)⁺

10.3.20 4'-(Octyloxy)biphenyl-4-yl 4-(benzyloxy)benzoate, **62**



4-Benzyloxy benzoic acid (2.82 g, 12.36 mmol), 4'-(Octyloxy)-4-hydroxybiphenyl, **61** (3.69 g, 12.36 mmol), DCC (3.06 g, 14.83 mmol) and DMAP (0.62 g, 2.47 mmol) were dissolved in DCM (150 mL) and stirred over night. A white precipitate formed and was filtered and the filtrate dried *in vacuo*. The product was purified by flash column chromatography (DCM/Hexane 1:1, flash grade silica gel, R_f 0.82 in DCM) to yield **62** as a white crystalline solid (1.99 g, 31.7 %).

Chapter 10: Experimental

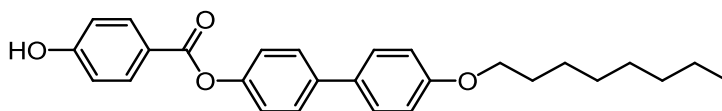
^1H NMR: (400 MHz, CDCl_3 , CDCl_3 internal standard)
 δ (ppm)= 8.18 (AA'XX' ($J = 8.9$ Hz), 2H, ArH), 7.58 (AA'XX' ($J = 8.6$ Hz), 2H, ArH), 7.51 (AA'XX' ($J = 8.7$ Hz), 2H, ArH), 7.43 (m, 5H, ArH benzyl), 7.24 (AA'XX' ($J = 8.6$ Hz), 2H, ArH), 7.07 (AA'XX' ($J = 8.9$ Hz), 2H, ArH), 6.97 (AA'XX' ($J = 8.7$ Hz), 2H, ArH), 5.17 (s, 2H, PhCH_2O), 3.99 (t ($J = 6.6$ Hz), 2H, $\text{CH}_2\text{CH}_2\text{O}$), 1.91 (m, 2H, $\text{CH}_2\text{CH}_2\text{O}$), 1.29 (m, 10H, $\text{CH}_2\text{CH}_2\text{CH}_2$), 0.89 (t ($J = 7.0$ Hz), 3H, CH_3)

^{13}C NMR: (100.4MHz, CDCl_3 , CDCl_3 internal standard)
 δ (ppm)= 164.97 (1C, COO), 163.00 (1C, Ar), 158.73 (1C, Ar), 149.91 (1C, Ar), 138.57 (1C, Ar), 136.09 (1C, Ar), 132.75 (1C, Ar), 132.32 (2C, Ar), 128.71 (2C, Ar), 128.27 (1C, Ar), 128.09 (2C, Ar), 127.68 (2C, Ar), 127.49 (2C, Ar), 122.05 (1C, Ar), 129.95 (2C, Ar), 114.77 (2C, Ar), 114.67 (2C, Ar), 70.16 (1C, CH_2O), 68.08 (1C, CH_2O), 34.90 (1C, $\text{CH}_2\text{CH}_2\text{O}$), 31.81 (1C, CH_2), 29.36 (1C, CH_2), 29.27 (1C, CH_2), 26.05 (1C, CH_2), 22.66 (1C, CH_2), 14.10 (1C, CH_3)

IR (cm^{-1}): 2924 (vs, ArH), 2113 (vs), 1720 (s, C=O), 1288 (vs), 1002 (s)

Mass (ESI): $m/z = 509.27$ (M+H)⁺

10.3.21 4'-(Octyloxy)biphenyl-4-yl 4-hydroxybenzoate, **63**¹⁵¹



4'-(Octyloxy)biphenyl-4-yl 4-(benzyloxy)benzoate, **62** (4.76 g, 9.36 mmol) was dissolved in dioxane (200 mL) and palladium (5 %) on carbon added (0.5 g). The suspension was stirred vigorously under an atmosphere of H_2 for two days. The suspension was filtered through celite, the solvent removed *in vacuo* and the product recrystallised from toluene to yield **63** as a white crystalline solid (3.38 g, 86.2 %).

Chapter 10: Experimental

^1H NMR: (400 MHz, CDCl_3 , CDCl_3 internal standard)
 δ (ppm)= 8.08 (AA'XX' ($J = 8.8$ Hz), 2H, ArH), 7.57 (AA'XX' ($J = 8.6$ Hz), 2H, ArH), 7.50 (AA'XX' ($J = 8.7$ Hz), 2H, ArH), 7.37 (s, 1H, PhOH), 7.23 (AA'XX' ($J = 8.6$ Hz), 2H, ArH), 6.96 (AA'XX' ($J = 8.8$ Hz), 2H, ArH), 6.89 (AA'XX' ($J = 8.7$ Hz), 2H, ArH), 3.98 (t ($J = 6.6$ Hz), 2H, OCH_2), 1.92 (m, 2H, $\text{CH}_2\text{CH}_2\text{O}$), 1.29 (m, 10H, CH_2), 0.88 (t ($J = 7.0$ Hz), 3H, CH_3)

^{13}C NMR: (100.4 MHz, DMSO, DMSO internal standard)
 δ (ppm)= 164.35 (1C, COO), 162.75 (1C, PhCOH), 158.28 (1C, PhCOCH₂), 149.66 (1C, PhCOCO), 137.36 (1C, PhC), 132.17 (2C, PhC), 131.52 (1C, PhC), 127.68 (2C, PhC), 127.05 (2C, PhC), 122.30 (2C, PhC), 119.15 (1C, PhC), 115.56 (2C, PhC), 114.81 (2C, PhC), 167.42 (1C, CH_2O), 31.19 (1C, $\text{CH}_2\text{CH}_2\text{O}$), 28.69 (1C, CH_2), 28.63 (2C, CH_2), 25.48 (1C, CH_2), 22.04 (1C, CH_2), 13.91 (1C, CH_3)

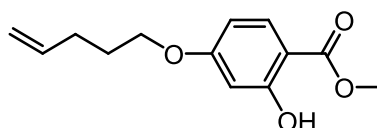
IR (cm^{-1}): 3410 (s, OH), 2924 (s, ArH), 1697 (s, C=O), 1273 (s), 1203 (vs)

Mass (ESI):

$m/z = 419.22$ (M+H)⁺

DSC/POM: Cr 173.9 [9.33] Iso

10.3.22 Methyl 2-hydroxy-4-(pent-4-enyloxy)benzoate, **64**¹¹⁹



Methyl 2,4-dihydroxybenzoate (8.40 g, 50 mmol), K_2CO_3 (27.6 g, 0.20 mol) and KI (20 mg, 0.1 mmol) were added to dry butanone (200 mL). The suspension was brought to reflux (80 °C) and 5-bromo-1-pentene (7.1 mL, 60.0 mmol) added. The solution was refluxed over night and allowed to cool. The solids were filtered and the solvent removed *in vacuo*. The product was purified by flash column

Chapter 10: Experimental

chromatography (eluting with Pet ether/diethyl ether 24/1, flash grade silica, R_f 0.35) to yield **64** as a white crystalline solid (9.36 g, 79.2 %).

^1H NMR: (CDCl₃, 400.0 MHz, CHCl₃ internal standard)
 δ (ppm)= 10.96 (s, 1H, OH), 7.70 (d (J = 9.4 Hz), 1H, ArH), 6.42 (d (J = 2.3 Hz), 1H, ArH), 6.41 (dd (J = 7.2, 2.4 Hz), 1H, ArH), 5.83 (ddt (J = 16.9 (*trans*), 10.2 (*cis*), 6.7 (*gem*) Hz), 1H, CH=CH₂), 5.05 (dd (J = 17.1, 1.7 Hz), 1H, CH=CHH_{*trans*}), 5.00 (dd (J = 10.2, 1.7 Hz), 1H, CH=CHH_{*cis*}), 3.96 (t (J = 6.5 Hz), 2H, CH₂O), 3.89 (s, 3H, CH₃O), 2.28 – 2.16 (m, 2H, CH₂), 1.94 – 1.80 (m, 2H, CH₂)

^{13}C NMR: (CDCl₃, 100.4 MHz, CHCl₃ internal standard)
 δ (ppm)= 170.47 (1C, COO), 165.16 (1C, ArC-O), 163.82 (1C, ArC-O), 137.57 (1C, CH=CH₂), 131.23 (1C, ArC), 115.47 (1C, CH₂=CH), 107.94 (1C, ArC), 105.33 (1C, ArC-COO), 101.20 (1C, ArC), 67.45 (1C, CH₂O), 52.00 (1C, CH₃O), 30.06 (1C, CH₂), 28.19 (1C, CH₂)

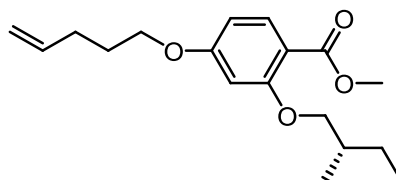
IR (cm⁻¹): 2947 (m, ArH), 1666 (s, C=O), 1620 (s, C-O)

Mass (ESI):

m/z = 237.1127 (M+H)⁺, 205.09, 158.55

calculated = 237.1127

10.3.23 (S)-Methyl 2-(2-methylbutoxy)-4-(pent-4-enyloxy)benzoate, **65**¹¹⁹



Methyl 2-hydroxy-4-(pent-4-enyloxy)benzoate, **64** (8.56 g, 36.25 mmol), K₂CO₃ (5.00 g, 120.8 mmol) and KI (10 mg, 0.06 mmol) were added to dry butanone (200 mL) and the suspension brought to reflux (80 °C). (S)-(+)-1-Bromo-2-methyl-butane

Chapter 10: Experimental

(5.00 g, 30.2 mmol) was added and the suspension stirred overnight. The suspension was allowed to cool, the solids filtered and the solvent removed *in vacuo*. The product was purified by flash column chromatography (eluting with hexane/diethyl ether 24:1, flash grade silica, R_f 0.06) yielding **65** as a colourless oil (0.75 g, 8.1%).

^1H NMR: (CDCl₃, 400.0 MHz, CHCl₃ internal standard)

δ (ppm)= 7.84 – 7.77 (m, 1H, ArH), 6.46 – 6.39 (m, 2H, ArH), 5.81 (ddt (J = 16.9 (*trans*), 10.2 (*cis*), 6.6 (*gem*) Hz), 1H, CH=CH₂), 5.04 (dd (J = 17.1, 1.7 Hz), 1H, CH=CHH_{*trans*}), 4.98 (dd (J = 10.2, 1.7 Hz), 1H, CH=CHH_{*cis*}), 3.96 (t (J = 6.4 Hz), 2H, CH₂CH₂O), 3.85 – 3.73 (m, 2H, CHCH₂O), 3.82 (s, 3H, OCH₃), 2.28 – 2.18 (m, 2H, CH₂), 1.99 – 1.81 (m, 3H, CH and CH₂), 1.58 (m, 1H, CH₂CH₃), 1.39 – 1.19 (m, 1H, CH₂CH₃), 1.04 (d, (J = 6.8 Hz), 3H, CHCH₃), 0.93 (t, (J = 7.5 Hz), 3H, CH₂CH₃)

^{13}C NMR: (CDCl₃, 100.4 MHz, CHCl₃ internal standard)

δ (ppm)= 166.42 (1C, COO), 163.63 (1C, ArC-O), 160.93 (1C, ArC-O), 137.53 (1C, CH=CH₂), 133.81 (1C, ArC), 115.36 CH₂=CH), 112.31 (1C, ArC-COO), 104.91 (1C, ArC), 100.03 (1C, ArC), 73.41 (1C, CH₂O), 67.27 (1C, CH₂O), 51.47 (1C, CH₃O), 34.77 (1C, CH), 30.01 (1C, CH₂CH=CH₂), 28.28 (1C, CH₂), 26.03 (1C, CH₂), 16.54 (1C, CH₃CH), 11.35 (1C, CH₃CH₂)

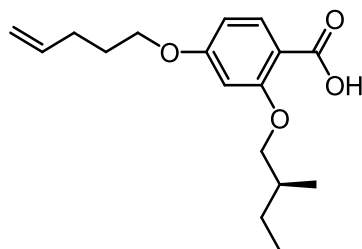
IR (cm⁻¹): 3078 (m, alkene), 2954 (s, ArH), 1666 (s, C=O), 1620 (s, C-O)

Mass (ESI):

m/z = 307.1897 (M+H)⁺, 275.16, 237.11, 214.09, 193.58

calculated = 307.1909 (M+H)⁺

10.3.24 (S)-2-(2-Methylbutoxy)-4-(pent-4-enyloxy)benzoic acid, **66¹¹⁹**



A solution of (*S*)-methyl 2-(2-methylbutoxy)-4-(pent-4-enyloxy)benzoate, **65** (4.74 g, 15.5 mmol) and NaOH (2.5 g, 61.9 mmol) in water (25 mL) and methanol (150 mL) was heated to reflux under Ar for 4 h. The solution was allowed to cool, acidified with conc. HCl and the precipitate filtered. The solid was dissolved in DCM and dried over MgSO₄. The solvent was removed *in vacuo* and the product recrystallized from petroleum ether yielding **66** as a white crystalline solid (4.11 g, 90.7 %).

¹H NMR: (CDCl₃, 400 MHz, CHCl₃ internal standard)

δ (ppm) = 8.12 (d (*J* = 8.8 Hz), 1H, Ar*H*), 6.62 (dd (*J* = 8.8, 2.2 Hz), 1H, Ar*H*), 6.51 (d (*J* = 2.2 Hz), 1H, Ar*H*), 5.84 (ddt (*J* = 16.9 (*trans*), 10.2 (*cis*), 6.7 (*gem*) Hz), 1H, CH=CH₂), 5.07 (dd (*J* = 17.1, 1.6 Hz), 1H, CH=CH*H*_{*trans*}), 5.02 (dd (*J* = 10.2, 1.1 Hz), 1H, CH=CH*H*_{*cis*}), 4.14 – 3.94 (m, 4H, 2x CH₂O), 2.24 (m, 2H, CH₂CH₂O), 1.99 (m, 1H, CHCH₂O), 1.95 – 1.81 (m, 2H, CH₂), 1.55 (m, 1H, CH₂), 1.43 – 1.26 (m, 1H, CH₂), 1.08 (d (*J* = 6.8 Hz), 3H, CH₃CH), 0.98 (t (*J* = 7.5 Hz), 3H, CH₃CH₂)

¹³C NMR: (CDCl₃, 100.4 MHz, CHCl₃)

δ (ppm) = 165.41 (1C, COO), 164.67 (1C, ArC-O), 159.23 (1C, ArC-O), 137.50 (1C, ArC), 135.64 (1C, ArC), 115.70 (1C, ArC), 110.43 (1C, ArC), 107.14 (1C, H₂C=CH), 99.93 (1C, CH=CH₂), 74.99 (1C, CH₂O), 67.82 (1C, CH₂O), 34.57 (1C, CH₂), 30.08 (1C, CH₂), 28.33 (1C, CH₂), 26.23 (1C, CH₂), 16.73 (1C, CH₃), 11.32 (1C, CH₃)

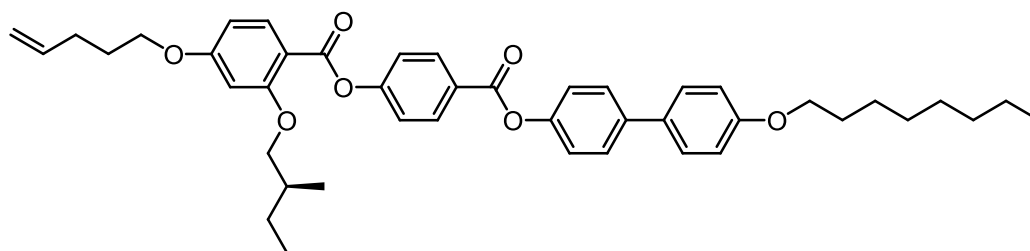
IR (cm⁻¹) 2964 (s, Ar*H*), 1680 (vs, C=O)

Mass (ESI):

m/z = 293.1747 (M+H)⁺, 275.16, 235.00, 223.10, 205.09, 186.58, 161.01,
141.96, 125.99, 84.96, 61.01

calculated = 293.1753 (M+H)⁺

**10.3.25 (S)-4-((4'-(Octyloxy)biphenyl-4-yloxy)carbonyl)phenyl
2-(2-methylbutoxy)-4-(pent-4-enyloxy)benzoate, **18**¹¹⁹**



(S)-2-(2-Methylbutoxy)-4-(pent-4-enyloxy)benzoic acid, **66** (1.05 g, 3.58 mmol), 4'-(octyloxy)biphenyl-4-yl 4-hydroxybenzoate, **63** (1.50 g, 3.58 mmol), EDAC (0.67 g, 4.29 mmol) and DMAP (0.09 g, 0.36 mmol) were dissolved in DCM (100 mL) and stirred vigorously overnight. The solution was washed with water (3x 200 mL), dried over MgSO₄, the solvent removed *in vacuo* and the residue recrystallized from petroleum ether/toluene to yield **18** as a white fluffy crystalline solid (2.04 g, 82.3%).

¹H NMR: (CDCl₃, 400 MHz, CHCl₃ internal standard)

δ (ppm) = 8.28 (d (*J* = 8.7 Hz), 2H, ArH), 8.04 (d (*J* = 8.7 Hz), 1H, ArH), 7.59 (d (*J* = 8.7 Hz), 2H, ArH), 7.51 (d (*J* = 8.7 Hz), 2H, ArH), 7.35 (d (*J* = 8.7 Hz), 2H, ArH), 7.25 (d (*J* = 8.7 Hz), 2H, ArH), 6.97 (d (*J* = 8.8 Hz), 2H, ArH), 6.61 – 6.45 (m, 2H, ArH), 5.86 (ddt (*J* = 16.9 (*trans*), 10.2 (*cis*), 6.6 (*gem*) Hz), 1H, CH=CH₂), 5.08 (dd (*J* = 17.1, 1.7 Hz), 1H, CH=CH_{trans}), 5.03 (dd (*J* = 10.1, 1.7 Hz), 1H, CH=CH_{cis}), 4.05 (t (*J* = 6.4 Hz), 2H, CH₂CH₂O), 4.00 (t (*J* = 6.6 Hz), 2H, CH₂CH₂O), 3.87 (m, 2H, CHCH₂O), 2.26 (m, 2H, CH₂CH₂O), 2.02 – 1.86 (m, 2H, CH₂CH₂O), 1.86 – 1.74 (m, 2H, CH₂CH₂O), 1.72 – 1.52 (m, 3H, CH₂ and CH), 1.52 – 1.41 (m, 2H, CH₂), 1.41 – 1.19 (m, 8H,

Chapter 10: Experimental

CH_2), 1.05 (d ($J = 6.7$ Hz), 3H, CH_3CH), 0.92 (t ($J = 7.5$ Hz), 3H, CH_3CH_2), 0.89 (t ($J = 6.8$ Hz), 3H, CH_3CH_2)

^{13}C NMR: (CDCl₃, 400 MHz, CHCl₃ internal standard)

δ (ppm) = 164.80 (1C, COO), 163.64 (1C, COO), 162.02 (1C, ArC-O), 158.92 (1C, ArC-O), 155.76 (1C, ArC-O), 149.96 (1C, ArC-O), 138.90 (1C, ArC-O), 137.63 (1C, CH=CH₂), 134.83 (1C, ArC), 132.86 (1C, ArC), 131.93 (2C, ArC), 128.25 (2C, ArC), 127.88 (2C, ArC), 126.74 (1C, ArC), 122.36 (2C, ArC), 122.04 (2C, ArC), 115.64 (1C, ArC), 114.95 (2C, ArC), 110.76 (1C, ArC), 105.41 (1C, ArC), 100.10 (1C, CH₂=CH), 73.66 (1C, CH₂O), 68.25 (1C, CH₂O), 67.61 (1C, CH₂O), 34.90 (1C, CH₂), 31.97 (1C, CH₂), 30.14 (1C, CH₂), 29.52 (1C, CH₂), 29.43 (1C, CH₂), 29.40 (1C, CH₂), 28.39 (1C, CH₂), 26.21 (1C, CH₂), 26.15 (1C, CH₂), 22.81 (1C, CH₂), 16.74 (1C, CH₃), 14.25 (1C, CH₃), 11.48 (1C, CH₃)

IR (cm⁻¹): 2924 (s, ArH), 1734 (vs, C=O), 1600 (s, C-O)

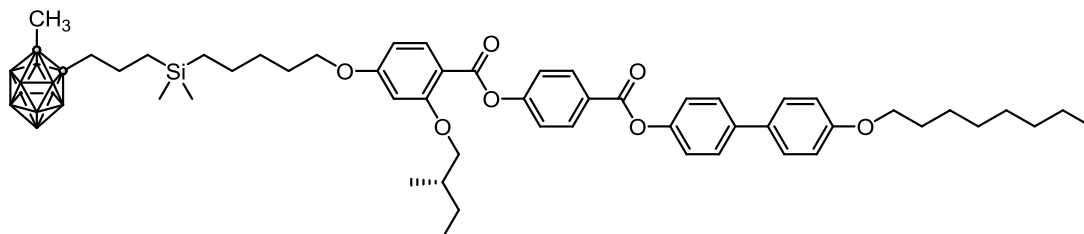
Mass (ESI):

m/z = 693.3793 (M+H)⁺, 609.24, 587.26, 554.30, 536.17, 521.19, 496.08, 448.22, 427.70

calculated = 693.3791 (M+H)⁺

DSC/POM: Cr 128.9 [45.7] N* 167.5 [1.4] Iso

10.3.26 1-Methyl, 2-[propyl-3-dimethylsilyl-((S)-4-((4'-(octyloxy)biphenyl-4-yloxy)carbonyl)phenyl 2-(2-methylbutoxy)-4-(pentyloxy)benzoate]dodecacarborane, 12



1-Methyl, 2-(propyl-3-dimethylsilane)dodecacarborane, **56** (45.1 mg, 0.173 mmol) and (S)-4-((4'-(octyloxy)biphenyl-4-yloxy)carbonyl)phenyl 2-(2-methylbutoxy)-4-(pent-4-enyloxy)benzoate, **18** (217.1 mg, 0.313 mmol) were dissolved in dry, degassed, low sulphur toluene (2 mL) in a Schlenk tube under Ar. Karstedt's catalyst (20 μ L) was added and the solution stirred over night. The solvent was removed *in vacuo* and the product isolated by flash column chromatography (eluting with DCM, flash grade silica, R_f -0.51) and then purified by recrystallizing from ethanol to yield **12** as a white fluffy crystalline solid (67.8 mg, 41.6 %).

^1H { ^{10}B } NMR: (CDCl₃, 500.0 MHz, CHCl₃ internal standard)

δ (ppm) = 8.29 (d (J = 8.6 Hz), 2H, ArH), 8.05 (d (J = 8.7 Hz), 1H, ArH), 7.60 (d (J = 8.5 Hz), 2H, ArH), 7.52 (d (J = 8.6 Hz), 2H, ArH), 7.36 (d (J = 8.6 Hz), 2H, ArH), 7.27 (d (J = 8.2 Hz), 2H, ArH), 6.98 (d (J = 8.6 Hz), 2H, ArH), 6.54 (m, 2H, ArH), 4.04 (t (J = 6.4 Hz), 2H, CH₂CH₂O), 4.01 (t J = 6.6 Hz), 2H, CH₂CH₂O), 3.96 – 3.80 (m, 2H, CHCH₂O), 2.35 – 2.05 (m, 10H, BH), 2.00 (s, 3H, CH₃cluster), 1.82 (m, 4H, CH₂CH₂O), 1.54 (m, 9H, CH₂ and CH), 1.35 (m, 10H, CH₂), 1.06 (d (J = 6.7 Hz), 3H, CH₃CH), 0.94 (t (J = 6.9 Hz), 3H, CH₃CH₂), 0.91 (t (J = 7.5 Hz), 3H, CH₃CH₂), 0.63 – 0.54 (m, 2H, CH₂Si), 0.54 – 0.47 (m, 2H, CH₂Si), 0.01 (s, 6H, CH₃Si)

^{13}C NMR: (CDCl₃, 100.4 MHz, CHCl₃ internal standard)

δ (ppm) = 164.85 (1C, COO), 164.79 (1C, COO), 163.61 (1C, ArC-O), 162.01 (1C, ArC-O), 158.90 (1C, ArC-O), 155.74 (1C, ArC-O), 149.93 (1C,

Chapter 10: Experimental

ArC-O), 138.87 (1C, ArC), 134.82 (1C, ArC), 132.82 (1C, ArC), 131.91 (2C, ArC), 128.23 (2C, ArC), 127.85 (2C, ArC), 126.72 (1C, ArC), 122.35 (2C, ArC), 122.02 (2C, ArC), 114.92 (2C, ArC), 110.66 (1C, ArC), 105.36 (1C, ArC), 100.06 (1C, ArC), 78.21 (1C, C_{cluster}), 74.70 (1C, C_{cluster}), 73.63 (1C, CH₂O), 68.39 (1C, CH₂O), 68.22 (1C, CH₂O), 39.11 (1C, CH₂CH₂O), 34.88 (1C, CHCH₂O), 31.95 (1C, CH₂), 30.01 (1C, CH₂), 29.50 (1C, CH₂), 29.41 (1C, CH₂), 29.38 (1C, CH₂), 28.96 (1C, CH₂), 26.19 (1C, CH₂), 26.12 (1C, CH₂), 24.45 (1C, CH₂), 23.79 (1C, CH₂), 23.25 (1C, CH₃), 22.80 (1C, CH₂), 16.73 (1C, CH₃), 15.43 (1C, CH₂), 15.18 (1C, CH₂), 14.25 (1C, CH₃), 11.47 (1C, CH₃cluster), -3.30 (2C, CH₃Si)

²⁹Si NMR: (CDCl₃, 79.0 MHz)

δ (ppm) = 3.02 (1Si, Si(CH₃)₂)

¹¹B NMR: (CDCl₃, 160.0 MHz)

δ (ppm) = -1.62 – -8.06 (m, 2B, B_{cluster}), -8.29 – -19.78 (m, 8B, B_{cluster})

IR (cm⁻¹): 2916 (s, ArH), 2584 (s, br, BH), 1736 (vs, C=O), 1604 (s, C-O)

Mass (ESI):

m/z = 953.6551 (M+H)⁺, 906.26, 832.24, 758.22, 707.17, 684.20, 633.15, 610.18 536.16, 457.27

calculated = 953.6526 (M+H)⁺

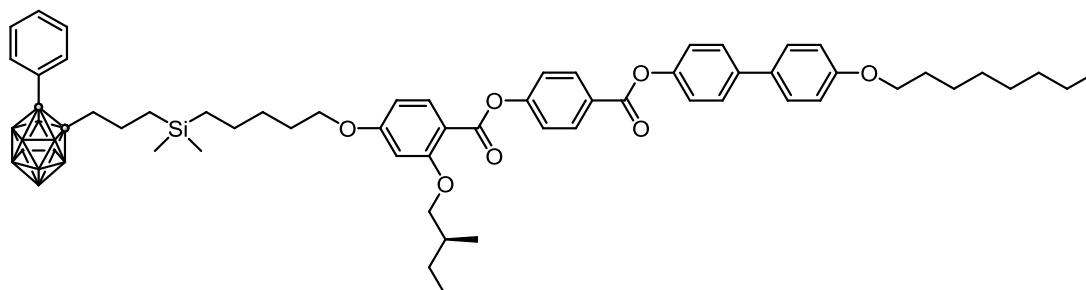
DSC/POM: Cr₁ 33.0 [-6.3] Cr₂ (87.4 [-0.6] N*) 89.0 [36.7] Iso

CHN Microanalysis:

Observed: C 63.84, H 8.20, N 0.00

Calculated: C 65.65, H 8.26, N 0.00

10.3.27 1-Phenyl, 2-(propyl-3-dimethylsilyl)-((S)-4-((4'-(octyloxy)biphenyl-4-yloxy)carbonyl)phenyl 2-(2-methylbutoxy)-4-(pentyloxy)benzoate)dodecacarborane, 13



A solution of (S)-4-((4'-(octyloxy)biphenyl-4-yloxy)carbonyl)phenyl 2-(2-methylbutoxy)-4-(pent-4-enyloxy)benzoate, **18** (129.9 mg, 0.186 mmol) and 1-phenyl, 2-(propyl-2-dimethylsilyl)dodecacarborane, **55** (50.0 mg, 0.155 mmol) in dry, low sulphur toluene (3 mL) was placed in a dry Schlenk tube, placed under Ar and degassed by purging with Ar. Next Karstedt's catalyst (50 μ L) was added and the solution stirred over night. The resultant solution was dried *in vacuo* and the product isolated by flash column chromatography (eluting with DCM, flash grade silica, R_f 0.59). The product was further purified by precipitation from DCM/ethanol yielding **13** as a white solid (26.2 mg, 16.7 %).

^1H $\{^{10}\text{B}\}$ NMR: (CDCl₃, 500.0 MHz, CHCl₃ internal standard)

δ (ppm) = 8.28 (d (J = 8.6 Hz), 2H, ArH), 8.05 (d (J = 8.7 Hz), 1H, ArH), 7.64 (d (J = 7.6 Hz), 2H, ArH), 7.60 (d (J = 8.6 Hz), 2H, ArH), 7.51 (d (J = 8.6 Hz), 2H, ArH), 7.44 (d (J = 7.6 Hz), 2H, ArH), 7.38 (m, 3H, ArH), 7.26 (d (J = 8.4 Hz), 2H, ArH), 6.98 (d (J = 8.7 Hz), 2H, ArH), 6.54 (dd (J = 8.8, 2.0 Hz), 1H, ArH), 6.51 (s, 1H, ArH), 4.02 (m, 4H, CH₂O), 3.89 (m, 2H, CHCH₂O), 2.72 (s, br, 2H, BH), 2.35 (s, br, 6H, BH), 2.24 (s, br, 2H, BH), 1.79 (m, 6H, CH₂), 1.62 (m, 1H, CH), 1.47 (m, 4H, CH₂), 1.32 (m, 14H, CH₂), 1.06 (d (J = 6.7 Hz), 3H, CHCH₃), 0.92 (m, 6H, CH₃), 0.43 (m, 2H, CH₂Si), 0.27 (m, 2H, CH₂Si), -0.13 (s, 6H, CH₃Si)

Chapter 10: Experimental

^{13}C NMR: (CDCl₃, 100.4 MHz, CHCl₃ internal standard)
 δ (ppm) = 164.84 (1C, COO), 163.66 (1C, COO), 162.04 (1C, ArC-O), 158.93 (1C, ArC-O), 155.76 (1C, ArC-O), 149.96 (1C, ArC-O), 138.91 (1C, ArC-O), 134.86 (1C, ArCH), 131.94 (2C, ArCH), 131.27 (2C, ArCH), 131.00 (1C, ArC), 130.69 (1C, ArCH), 128.98 (2C, ArCH), 128.26 (2C, ArCH), 128.06 (1C, ArC), 127.89 (2C, ArCH), 127.80 (1C, ArC), 122.37 (2C, ArCH), 122.04 (2C, ArCH), 115.70 (1C, ArC), 114.95 (2C, ArCH), 110.72 (1C, ArC), 105.37 (1C, ArCH), 100.09 (1C, ArCH), 82.50 (1C, Ccluster), 82.13 (1C, Ccluster), 73.67 (1C, CH₂O), 68.42 (1C, CH₂O), 68.26 (1C, CH₂O), 38.78 (1C, CH₂), 34.91 (1C, CH), 31.97 (1C, CH₂), 30.01 (1C, CH₂), 29.52 (1C, CH₂), 29.44 (1C, CH₂), 29.40 (1C, CH₂), 28.98 (1C, CH₂), 26.22 (1C, CH₂), 26.15 (1C, CH₂), 24.26 (1C, CH₂), 23.74 (1C, CH₂), 22.82 (1C, CH₂), 16.75 (1C, CH₃), 15.13 (2C, CH₂), 14.27 (1C, CH₃), 11.49 (1C, CH₃), -3.39 (2C, CH₃Si)

^{29}Si NMR: (CDCl₃, 79.0 MHz)
 δ (ppm) = 2.86 (1Si, Si(CH₃)₂)

^{10}B NMR: (CDCl₃, 160.0 MHz)
 δ (ppm) = -3.50 (d (J = 135.7 Hz), 4B), -8.02 – -14.48 (m, 6)

IR (cm⁻¹): 2924 (m, ArH), 2854 (w, ArH), 2584 (m, BH), 1735 (vs, C=O), 1604 (s, C-O)

Mass (ESI):
 m/z = 1014.6706 (M)⁺, 929.19, 853.17, 803.54, 775.58, 689.6699, 610.18
calculated = 1014.6604 (M)⁺

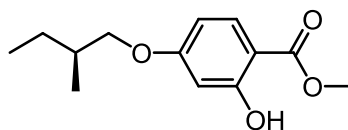
DSC/POM: Cr₁ 18.0 [-15.4] Cr₂ 36.9 [-3.1] Cr₃ (37.3[-0.3] N*) 64.0 [30.7] Iso

CHN Microanalysis:

Observed: C 66.63, H 8.57, N 0.00

Predicted: C 67.55, H 7.96, N 0.00

10.3.28 (S)-2-Hydroxy-4-(2-methyl-butoxy)-benzoic acid methyl ester, **67**



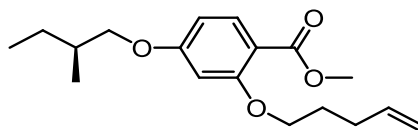
Methyl 2,4-dihydroxybenzoate (9.28 g, 55.2 mmol) and K_2CO_3 (30.5 g, 0.22 mol) were dissolved in dry butanone (200 mL). The solution was placed under Ar and then (S)-(+)-1-bromo-2-methylbutane (10.0 g, 66.2 mmol) was added. The solution was brought to reflux (80 °C) with strong stirring over night. The resulting suspension was allowed to cool and was then poured onto water (300 mL). The aqueous phase was washed with diethyl ether (2x 200 mL) and the organic phases combined. These were then washed with 5 % w/w NaOH solution (200 mL), followed by 5 % w/w NaCl solution (200 mL) and finally water (2x 200 mL). The organic phase was dried over $MgSO_4$ and the solvent removed *in vacuo*. The product was purified by flash column chromatography (DCM/Hexane 1:1, flash grade silica, R_f 0.29) to yield **67** as a pale yellow oil (4.02 g, 30.6 %).

1H NMR: (400 MHz, $CDCl_3$, $CDCl_3$ internal standard)
 δ (ppm)= 10.96 (s, 1H, OH), 7.72 (m, 1H, ArH), 6.43 (m, 2H, ArH), 3.91 (s, 3H, $COOCH_3$), 3.79 (m, 2H, CH_2O), 1.86 (m, 1H, $CHCH_2O$), 1.56 (m, 1H, CH_3CH_2), 1.26 (m, 1H, CH_3CH_2), 1.00 (d ($J = 6.7$ Hz), 3H, CH_3CH), 0.94 (t ($J = 7.4$ Hz), 3H, CH_3CH_2)

^{13}C NMR: (100.4MHz, $CDCl_3$, $CDCl_3$ internal standard)
 δ (ppm)= 170.42 (1C, COO), 165.35 (1C, Ar), 163.71 (1C, Ar), 131.09 (1C, Ar), 107.95 (1C, Ar), 105.12 (1C, Ar), 101.12 (1C, Ar), 73.01 (1C CH_2O), 51.92 (1C, CH_3OCO), 34.48 (1C, $CHCH_2O$), 26.03 (1C, CH_3CH_2), 16.43 (1C, CH_3), 11.26 (1C, CH_3)

Mass (ESI):
 m/z = 239.13 (M+H)⁺

10.3.29 (S)-4-(Methyl-butoxy)-2-pent-4-enyloxy-benzoic acid methyl ester, **68**

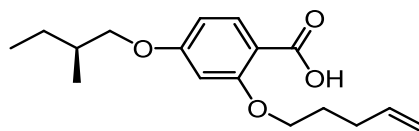


(S)-2-Hydroxy-4-(2-methyl-butoxy)-benzoic acid methyl ester, **67** (4.0 g, 16.8 mmol) K_2CO_3 (11.6 g, 83.9 mmol), KI (10 mg, 0.06 mmol) and 18-crown-6 (10 mg, 0.04 mmol) were dissolved in dry butanone (200 mL) and the solution stirred vigorously for 10 mins. Finally 5-bromopent-1-ene (2.4 mL, 20.1mmol) was added, the solution brought to reflux (80 °C) and stirred over night. The suspension was allowed to cool and was then poured onto water (200 mL). The aqueous phase was washed with diethyl ether (2x 100 mL), and the combined organic phases were washed with first 5 % w/w NaOH solution (100 mL) and then water (2x 100 mL). The solution was dried over $MgSO_4$ and the solvent removed *in vacuo*. The product was purified by flash column chromatography (DCM/Hexane 1:1, flash grade silica gel, R_f 0.06) to yield **68** as a pale yellow oil (3.92 g, 76.2 %).

1H NMR: (400 MHz, $CDCl_3$, $CDCl_3$ internal standard)
 δ (ppm)= 7.82 (d (J= 8.5 Hz), 1H, ArH), 6.47 (m, 2H, ArH), 5.87 (m, 1H, CH=CH₂), 5.04 (m, 2H, CH₂=CH), 4.02 (t (J= 6.4 Hz), 2H, CH₂CH₂O), 3.83 (s, 3H, CH₃O), 3.81 (m, 2H, CHCH₂O), 2.30 (m, 2H, CH₂CH₂O), 1.94 (m, 2H, CH₂CH=CH₂), 1.86 (m, 1H, CHCH₂O), 1.56 (m, 1H, CH₂CH₃), 1.28 (m, 1H, CH₂CH₃), 1.01 (d (J= 6.7 Hz), 3H, CH₃CH), 0.95 (t, 3H, CH₃CH₂)

^{13}C NMR: (100.4 MHz, $CDCl_3$, $CDCl_3$ internal standard)
 δ (ppm)= 166.35 (1C, COO), 163.86 (1C, Ar), 160.71 (1C, Ar), 137.79 (1C, CH=CH₂), 133.75 (1C, Ar), 115.17 (CH₂=CH), 112.19 (1C, Ar), 105.15 (1C, Ar), 100.25 (1C, Ar), 72.95 (1C, CHCH₂O), 67.93 (CH₂CH₂O), 51.53 (1C, OCH₃), 34.63 (1C, CHCH₂O), 29.98 (1C, OCH₂CH₂), 28.24 (1C, CH₂=CHCH₂), 26.04 (1C, CH₂CH₃) 16.46 (1C, CH₃), 11.28 (1C, CH₃)

Mass (ESI):

m/z = 307.19 (M+H)⁺**10.3.30 (S)-4-(2-Methylbutoxy)-2-(pent-4-enyloxy)benzoic acid,****69**

A solution of NaOH (2.04 g, 51.2 mmol) and (S)-4-(Methyl-butoxy)-2-pent-4-enyloxy-benzoic acid methyl ester **68** (3.9 g, 12.8 mmol) in MeOH and water (10:1, 50 mL) was brought to reflux (70 °C) and stirred vigorously for 2 h. The pale yellow solution was allowed to cool, diluted with water (200 mL) and acidified with conc. HCl. The white precipitate formed was washed with water, dissolved in diethyl ether and dried over MgSO₄. The solvent was removed *in vacuo* and the product recrystallised from petroleum ether yielding **69** as a white crystalline solid (3.64 g, 97.2 %).

¹H NMR: (400 MHz, CDCl₃, CDCl₃ internal standard)

δ (ppm)= 10.71 (br, 1H, OH), 8.12 (d (*J* = 8.8 Hz), 1H, ArH), 6.62 (m, 1H, ArH), 6.51 (m, 1H, ArH), 5.86 (ddt (*J* = 16.9 (*trans*), 10.2 (*cis*), 6.7 (*gem*) Hz), 1H, CH=CH₂), 5.06 (dd (*J* = 17.1, 1.8 Hz), 1H, CH=CHH_{*trans*}), 4.99 (dd (*J* = 10.2, 1.9 Hz), 1H, CH=CHH_{*cis*}), 4.23 (t (*J* = 6.4 Hz) 2H, OCH₂CH₂), 3.85 (m, 2H, OCH₂CH), 2.26 (m, 2H, CH₂CH₂O), 2.02 (m, 2H, CH₂CH=CH₂), 1.88 (m, 1H, CHCH₂O), 1.56 (m, 1H, CH₂CH₃), 1.23 (m, 1H, CH₂CH₃), 1.02 (d (*J* = 6.7 Hz), 3H, CH₃CH), 0.95 (t (*J* = 7.4 Hz), 3H, CH₃CH₂)

¹³C NMR: (100.4MHz, CDCl₃, CDCl₃ internal standard)

δ (ppm)= 165.28 (1C, COO), 164.77 (1C, Ar), 158.79 (1C, Ar), 136.47 (1C, CH=CH₂), 135.47 (1C, Ar), 116.32 (1C, CH₂=CH), 110.12 (1C, Ar), 107.11 (1C, Ar), 99.76 (1C, Ar), 73.29 (1C, CHCH₂O), 69.28 (1C, CH₂CH₂O), 34.59 (1C, CHCH₂O), 29.85 (1C, CH₂CH₂O), 27.89 (1C,

Chapter 10: Experimental

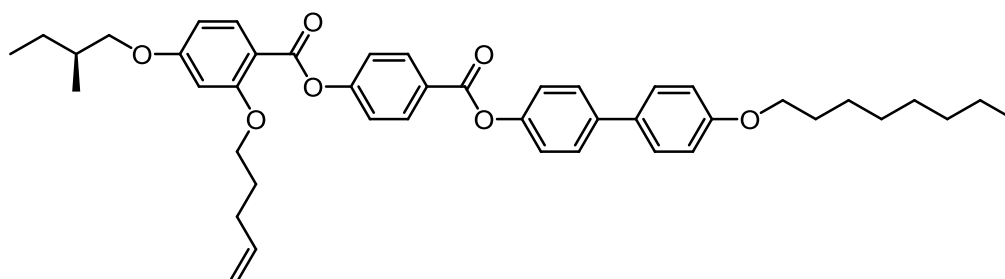
$\text{CH}_2\text{CH}=\text{CH}_2$), 25.99 (1C, CH_2CH_3), 16.44 (CH_3CH), 11.27 (1C, CH_3CH_2)

IR (cm^{-1}): 2962 (m, Ar H), 1658 (vs, C=O), 1242 (s), 1010 (vs)

Mass (ESI):

m/z = 293.18 (M+H)⁺

10.3.31 (S)-4-((4'-(Octyloxy)biphenyl-4-yloxy)carbonyl)phenyl 4-(2-methylbutoxy)-2-(pent-4-enyloxy)benzoate, **19¹²⁰**



(S)-4-(2-Methylbutoxy)-2-(pent-4-enyloxy)benzoic acid, **69** (1.05 g, 3.58 mmol), 4'-(octyloxy)biphenyl-4-yl 4-hydroxybenzoate, **63** (1.50 g, 3.58 mmol), EDAC (0.67 g, 4.30 mmol) and DMAP (90 mg, 0.36 mmol) were dissolved in DCM (150 mL) and stirred for 72 h. The solution was washed with water (3x 150 mL), dried over MgSO_4 and the solvent removed *in vacuo*. The product was then recrystallised from pet ether and a small amount of toluene to yield **19** as a fluffy white crystalline solid (2.08 g, 83.8 %).

¹H NMR: (CDCl_3 , 400 MHz, CDCl_3 internal standard)

δ (ppm)= 8.28 (AA'XX' ($J = 8.8$ Hz), 2H, ArH), 8.05 (d ($J = 8.7$ Hz), 1H, ArH), 7.59 (AA'XX' ($J = 8.7$ Hz), 2H, ArH), 7.52 (AA'XX' ($J = 8.8$ Hz), 2H, ArH), 7.36 (AA'XX' ($J = 8.8$ Hz), 2H, ArH), 7.26 (AA'XX' ($J = 8.7$ Hz), 2H, ArH), 6.98 (AA'XX' ($J = 8.8$ Hz), 2H, ArH), 6.56 (dd ($J = 2.3, 8.8$ Hz), 1H, ArH), 6.51 (d ($J = 2.2$ Hz), 1H, ArH), 5.83 (ddt ($J = 16.9$ (*trans*), 10.2 (*cis*), 6.6 (*gem*) Hz), 1H, $\text{CH}=\text{CH}_2$), 5.03 (dd ($J = 17.1, 1.8$ Hz), 1H, $\text{CH}=\text{CHH}_{\text{trans}}$), 4.98 (dd ($J = 10.2, 1.8$ Hz),

Chapter 10: Experimental

1H, CH=CH_{*cis*}), 4.06 (t (*J* = 6.3 Hz), 2H, OCH₂CH₂), 4.00 (d (*J* = 6.6 Hz), 2H, OCH₂CH₂), 3.86 (m, 2H, OCH₂CH), 2.29 (m, 2H, CH₂CH₂O), 1.96 (m, 2H, CH₂CH=CH₂), 1.89 (m, 1H, CHCH₂O), 1.81 (m, 2H, CH₂CH₂O), 1.48 (m, 2H, CH₂), 1.29 (m, 8H, CH₂), 1.05 (d (*J* = 6.7 Hz), 3H, CH₃CH), 0.97 (t (*J* = 7.5 Hz), 3H, CH₃CH₂), 0.89 (t (*J* = 7.1 Hz), 3H, CH₃CH₂)

¹³C NMR: (CDCl₃, 100.4 MHz, CDCl₃ internal standard)

δ (ppm)= 164.92 (1C, COO), 164.68 (1C, COO), 136.31 (1C, ArC-O), 161.76 (1C, ArC-O), 158.76 (1C, ArC-O), 155.56 (1C, ArC-O), 149.79 (1C, ArC-O), 138.75 (1C, ArC), 137.65 (1C, ArC), 134.59 (1C, ArC), 132.71 (1C, ArC), 131.77 (2C, ArC), 128.11 (2C, ArC), 127.73 (2C, ArC), 126.59 (1C, ArC), 122.23 (2C, ArC), 121.89 (2C, ArC), 115.32 (1C, ArC), 114.79 (2C, ArC), 110.45 (1C, ArC), 105.48 (1C, C=C), 100.12 (1C, C=C), 73.13 (1C, CH₂O), 68.09 (1C, CH₂O), 67.97 (1C, CH₂O), 34.65 (1C, CH₂CH₂O), 31.82 (1C, CH₂CH₂O), 29.99 (1C, CH₂CH₂O), 29.37 (1C, CH₂), 29.28 (1C, CH₂), 29.25 (1C, CH₂), 28.24 (1C, CH₂CH=CH₂), 26.06 (2C, CH₂), 22.66 (1C, CH₂), 16.49 (1C, CH₃CH), 14.11 (1C, CH₃CH₂), 11.32 (1C, CH₃CH₂)

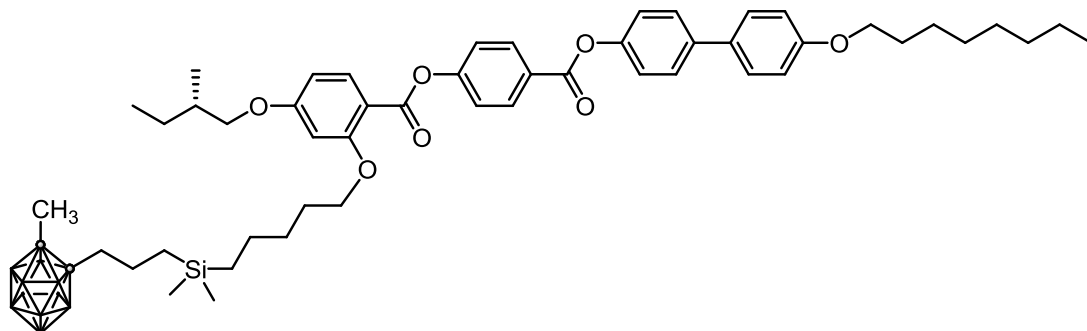
IR (cm⁻¹): 3240 (m), 2854 (m, ArH), 1736 (s, C=O), 1621 (s, C-O), 1265 (s), 1195 (vs)

Mass (ESI):

m/z = 693.38 (M+H)⁺

DSC/POM: Cr 110.3 [43.0] N* 151.4 [1.2] Iso

10.3.32 1-Methyl, 2-(propyl-3-dimethylsilyl-((S)-4-((4'-(octyloxy)biphenyl-4-yloxy)carbonyl)phenyl 4-(2-methylbutoxy)-2-(pentylloxy)benzoate)dodecacarborane, 14



A solution of (S)-4-((4'-(octyloxy)biphenyl-4-yloxy)carbonyl)phenyl 4-(2-methylbutoxy)-2-(pent-4-enyloxy)benzoate, **19** (193.0 mg, 0.28 mmol) and 1-methyl, 2-(propyl-3-dimethylsilyl)dodecacarborane, **56** (60.0 mg, 0.23 mmol) in dry, low sulphur toluene (4 mL) was placed in a dry Schlenk tube under Ar and degassed by purging with Ar. Karstedt's catalyst (40 μ L) was added and the solution stirred over night. The solvent was removed *in vacuo* and the product purified by flash column chromatography (eluting with DCM, flash grade silica gel, R_f 0.51) to yield **14** as a white crystalline solid (66.3 mg, 30.3 %).

^1H $\{^{10}\text{B}\}$ NMR: (CDCl₃, 500.0 MHz, CHCl₃ internal standard)

δ (ppm) = 8.28 (d (J = 8.6 Hz), 2H, ArH), 8.05 (d (J = 8.7 Hz), 1H, ArH), 7.60 (d (J = 8.6 Hz), 2H, ArH), 7.52 (d (J = 8.7 Hz), 2H, ArH), 7.37 (d (J = 8.6 Hz), 2H, ArH), 7.27 (d (J = 8.7 Hz), 2H, ArH), 6.98 (d (J = 8.7 Hz), 2H, ArH), 6.56 (dd (J = 8.8, 2.0 Hz), 1H, ArH), 6.54 (d (J = 9.2 Hz), 1H, ArH), 4.06 (t (J = 6.4 Hz), 2H, CH₂O), 4.01 (t (J = 6.6 Hz), 2H, CH₂O), 3.87 (m, 2H, CH₂O), 2.23 (s, br, 5H, BH), 2.14 (s, br, 2H, BH), 2.19 – 2.11 (m, 2H, CH₂Cluster), 2.10 (s, br, 2H, BH), 1.97 (s, 3H, CH₃Cluster), 1.93 – 1.76 (m, 4H, CH₂), 1.65 – 1.43 (m, 7H, CH₂), 1.44 – 1.23 (m, 12H, CH₂), 1.06 (d (J = 6.7 Hz), 3H, CH₃CH), 0.98 (t

Chapter 10: Experimental

($J = 7.5$ Hz), 3H, CH_3), 0.91 (t ($J = 6.7$ Hz), 3H, CH_3), 0.55 – 0.47 (m, 2H, CH_2Si), 0.50 – 0.43 (m, 2H, CH_2Si), -0.03 (s, 6H, CH_3Si)

^{13}C NMR: (CDCl₃, 100.4 MHz, CHCl₃ internal standard)
 δ (ppm) = 165.09 (1C, COO), 164.77 (1C, COO), 163.38 (1C, ArC-O), 162.01 (1C, ArC-O), 158.93 (1C, ArC-O), 155.74 (1C, ArC-O), 149.92 (1C, ArC-O), 138.91 (1C, ArC), 134.69 (1C, ArCH), 132.81 (1C, ArC), 131.86 (2C, ArCH), 128.23 (2C, ArCH), 127.86 (2C, ArCH), 126.71 (1C, ArC), 122.37 (2C, ArCH), 122.01 (2C, ArCH), 114.95 (2C, ArCH), 110.60 (1C, ArC), 105.57 (1C, ArCH), 100.27 (1C, ArCH), 78.26 (1C, Ccluster), 74.70 (1C, Ccluster), 73.28 (1C, CH_2O), 68.96 (1C, CH_2O), 68.23 (1C, CH_2O), 39.09 (1C, CH_2), 34.80 (1C, CH), 31.95 (1C, CH_2), 30.03 (1C, CH_2), 29.50 (1C, CH_2), 29.42 (1C, CH_2), 29.38 (1C, CH_2), 29.02 (1C, CH_2), 26.20 (2C, CH_2), 24.43 (1C, CH_2), 23.75 (1C, CH_2), 23.22 (1C, CH_3 cluster), 22.80 (1C, CH_2), 16.63 (1C, CH_3), 15.39 (1C, CH_2), 15.21 (1C, CH_2), 14.25 (1C, CH_3), 11.46 (1C, CH_3), -3.35 (2C, CH_3Si)

^{10}B NMR: (CDCl₃, 160.0 MHz)
 δ (ppm) = -5.05 (m, 2B), -9.86 (m, 8B)

^{29}Si NMR: (CDCl₃, 79.0 MHz)
 δ (ppm) = 2.94 (1 Si, $Si(CH_3)_2$)

IR (cm⁻¹): 2924 (s, ArH), 2862 (m, ArH), 2584 (s, br, BH), 1735 (vs, C=O), 1604 (s, C-O)

Mass (ESI):
m/z = 952.6591 (M)⁺, 803.54, 745.73, 689.67, 604.62
calculated = 952.6447 (M)⁺

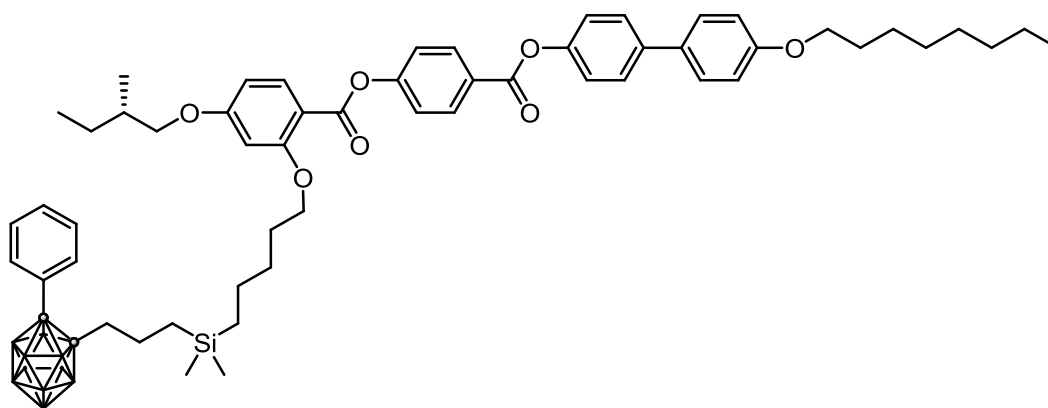
DSC/POM: Cr (38.3 [-0.2] N*) 56.2 [18.5] Iso

CHN Microanalysis:

Observed: C 63.86 %, H 8.30 %, N 0.00 %

Predicted: C 65.65%, H 8.26 %, N 0.00 %

10.3.33 1-Phenyl, 2-(propyl-3-dimethylsilyl-((S)-4-((4'-(octyloxy)biphenyl-4-yloxy)carbonyl)phenyl 4-(2-methylbutoxy)-2-(pentylloxy)benzoate)dodecacarborane, 15



A solution of (S)-4-((4'-(octyloxy)biphenyl-4-yloxy)carbonyl)phenyl 4-(2-methylbutoxy)-2-(pent-4-enyloxy)benzoate, **19** (128.9 mg, 0.186 mmol) and 1-phenyl, 2-(propyl-3-dimethylsilyl)dodecacarborane, **55** (50.0 mg, 0.155 mmol) in dry, low sulphur toluene (3 mL) was placed in a dry Schlenk tube, put under Ar and degassed via purging with Ar. Karstedt's catalyst (50 μ L) was added and the solution stirred over night, dried *in vacuo* and isolated by flash column chromatography (eluting with DCM 20 % Hexane, flash grade silica, R_f 0.61). The product was then precipitated from DCM/ethanol to yield **15** as a white solid (16.4 mg, 10.4 %).

^1H { ^{10}B } NMR: (CDCl₃, 500.0 MHz, CHCl₃ internal standard)

δ (ppm) = 8.25 (d (J = 8.6 Hz), 2H, ArH), 8.03 (d (J = 8.7 Hz), 1H, ArH), 7.59 (d (J = 7.3 Hz), 2H, ArH), 7.58 (d (J = 8.4 Hz), 2H, ArH), 7.50 (d (J = 8.6 Hz), 2H, ArH), 7.37 (m, 5H, ArH), 7.24 (d (J = 8.4 Hz), 2H, ArH), 6.96 (d (J = 8.6 Hz), 2H, ArH), 6.53 (dd (J = 8.8, 1.8 Hz), 1H, ArH), 6.50 (s, 1H, ArH), 4.02 (t (J = 6.4 Hz), 2H, CH₂O), 3.99 (t (J =

Chapter 10: Experimental

6.6 Hz), 2H, CH₂O), 3.85 (m, 2H, CHCH₂O), 2.68 (s, br, 2H, BH), 2.32 (s, br, 6H, BH), 2.21 (s, br, 2H, BH), 1.80 (m, 4H, CH₂), 1.73 (m, 2H, CH₂), 1.57 (m, 1H, CH), 1.46 (m, 4H, CH₂), 1.30 (m, 14H, CH₂), 1.03 (d (*J* = 6.7 Hz), 3H, CH₃), 0.96 (t (*J* = 7.4 Hz), 3H, CH₃), 0.88 (t (*J* = 6.4 Hz), 3H, CH₃), 0.33 (m, 2H, CH₂Si), 0.20 (m, 2H, CH₂Si), -0.19 (s, 6H, CH₃Si)

¹³C NMR: (CDCl₃, 100.4 MHz, CHCl₃ internal standard)

δ (ppm) = 165.10 (1C, COO), 162.04 (1C, COO), 158.94 (1C, ArC-O), 155.74 (1C, ArC-O), 149.94 (1C, ArC-O), 138.93 (1C, ArC-O), 137.15 (1C, ArC-O), 134.72 (1C, ArCH), 132.85 (1C, ArC), 131.88 (2C, ArCH), 131.23 (2C, ArCH), 130.96 (1C, ArC), 130.68 (1C, ArCH), 128.97 (2C, ArCH), 128.81 (1C, ArC), 128.26 (2C, ArCH), 127.89 (2C, ArCH), 126.74 (1C, ArC), 122.39 (2C, ArCH), 122.03 (2C, ArCH), 114.96 (2C, ArCH), 110.59 (1C, ArC), 105.56 (1C, ArCH), 100.30 (1C, ArCH), 83.46 (1C, Ccluster), 82.53 (1C, Ccluster), 73.30 (1C, CH₂O), 68.98 (1C, CH₂O), 68.26 (1C, CH₂O), 38.74 (1C, CH₂), 34.82 (1C, CH), 31.97 (1C, CH₂), 30.49 (1C, CH₂), 29.99 (1C, CH₂), 29.52 (1C, CH₂), 29.44 (1C, CH₂), 29.40 (1C, CH₂), 29.00 (1C, CH₂), 26.22 (1C, CH₂), 24.23 (1C, CH₂), 23.68 (1C, CH₂), 22.82 (1C, CH₂), 16.66 (1C, CH₃), 15.12 (1C, CH₂), 15.07 (1C, CH₂), 14.26 (1C, CH₃), 11.48 (1C, CH₃), -3.43 (2C, CH₃Si)

²⁹Si NMR: (CDCl₃, 79.0 MHz)

δ (ppm) = 2.79 (1Si, Si(CH₃)₂)

¹⁰B NMR: (CDCl₃, 160.0 MHz)

δ (ppm) = -3.51 (d (*J* = 153.1 Hz), 2B), -10.39 (d (*J* = 123.2 Hz), 8B)

IR (cm⁻¹): 2924 (m, ArH), 2845 (m, ArH), 2584 (w, BH), 1735 (s, C=O), 1604 (s, C-O)

Chapter 10: Experimental

Mass (ESI):

$m/z =$ 1014.6719 (M)⁺, 911.21, 856.52, 803.54, 745.73, 689.67, 658.46,
610.18, 577.12, 541.12

calculated = 1014.6604 (M)⁺

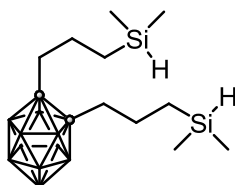
DSC/POM: Cr (35.9 [0.09] N*) 46.3 [45.9] Iso

CHN Microanalysis:

Observed: C 64.04 %, H 8.04 %, N 0.00 %

Predicted: C 67.55 %, H 7.96 %, N 0.00 %

10.3.34 1,2 Di-(3-(dimethylsilyl)propyl)dodecacarborane, **70**



1,2 Di-(prop-2-enyl)dodecacarborane (210.3 mg, 0.939 mmol) was dissolved in degassed dimethylchlorosilane (6 mL) in a Schlenk tube under Ar. Karstedt's catalyst (20 μ L) was added and the solution stirred for 4 h, the excess silane removed *in vacuo in situ*. The residue was dissolved in dry THF (10 mL) and cooled to 0 °C. Next a solution of LiAlH_4 in dry THF (13 mL, 0.23 mol dm^{-3}) was added drop-wise over 1 h. The solution was stirred over night and ethyl acetate (20 mL) added to destroy any remaining LiAlH_4 . The resulting suspension was passed through celite 3 times and the solvent removed *in vacuo*. The residue was dissolved in hexane and the remaining crystalline solid filtered. The solvent was removed *in vacuo* yielding **70** as a pale yellow oil (0.26 g, 80.7 %).

¹H NMR: (CDCl_3 , 400 MHz, CHCl_3 internal standard)

δ (ppm) = 3.86 (q ($J = 7.1$ Hz), 2H, SiH), 2.21 – 2.09 (m, 4H, CH_2 cluster), 1.58 (m, 4H, CH_2), 0.68 – 0.52 (m, 4H, CH_2Si), 0.09 (d ($J = 3.7$ Hz), 12H, CH_3Si)

Chapter 10: Experimental

^{13}C NMR: (CDCl₃, 100.4 MHz, CHCl₃ internal standard)
 δ (ppm) = 79.74 (2C, $C_{cluster}$), 38.29 (2C, CH_{2cluster}), 24.93 (2C, CH₂), 14.22 (2C, CH₂Si), -4.42 (4C, CH₃Si)

^{10}B NMR: (CDCl₃, 160.0 MHz)
 δ (ppm) = -5.81 (m, 2B), -14.07 (m, 8B)

^{29}Si NMR: (CDCl₃, 79.0 MHz)
 δ (ppm) = -12.81 (s, 2Si)

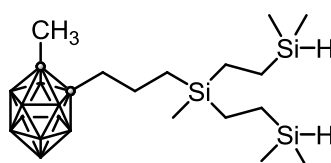
IR (cm⁻¹): 3278 (m, br, BH), 2954 (w, ArH), 2877 (w, ArH), 2576 (s, br, BH), 2113 (m, SiH)

Mass (ESI):

m/z = 360.3212 (M+OH)⁺, 337.14, 315.16, 301.14, 241.17, 171.10, 125.99, 81.53, 61.02

calculated = 3060.3443 (M+OH)⁺

10.3.35 1 Methyl, 2-(propyl-3-[silyl(methyl)bis(ethyl-2-dimethylsilane)])dodecacarborane, 71



1-Methyl, 2-(propyl-3-[silyl(methyl)bis(ethyl-2-enyl)])dodecacarborane (233 mg, 0.78 mmol) was placed in a Schlenk tube under Ar and dissolved in dimethylchlorosilane (4 mL). The solution was degassed by purging with Ar, Karstedt's catalyst (30 μL) was added and the solution stirred over night. Excess chlorosilane was removed *in vacuo in situ* and the resultant residue dissolved in dry THF (5 mL). Next LiAlH₄ in THF (1M, 4 mL) was added drop wise over 10 mins. The solution was stirred over night and dried *in vacuo*. The product was extracted into hexane, filtered through

Chapter 10: Experimental

celite and the solvent removed *in vacuo* to yield **71** as a clear mobile oil (200 mg, 67.5 %).

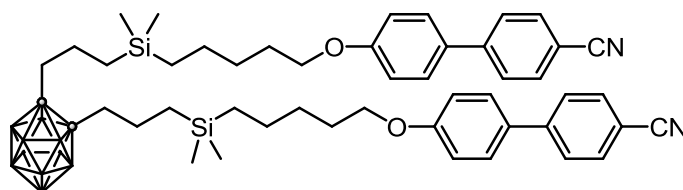
^1H NMR: (CDCl₃, 400.0 MHz, CHCl₃ internal standard)
 δ (ppm) = 3.89 – 3.79 (m, 2H, SiH), 2.23 – 2.10 (m, 2H, CH₂cluster), 2.00 (s, 3H, CH₃cluster), 1.53 (m, 2H, CH₂), 0.60 – 0.49 (m, 2H, CH₂Si), 0.46 (s, 8H, CH₂Si), 0.07 (d (J = 3.6 Hz), 12H, CH₃Si), -0.03 (s, 3H, CH₃Si)

^{13}C NMR: (CDCl₃, 100.4 MHz, CHCl₃ internal standard)
 δ (ppm) = 78.26 (1C, C_{cluster}), 74.68 (1C, C_{cluster}), 39.25 (1C, CH₂), 24.49 (1C, CH₂), 23.26 (1C, CH₂), 13.17 (1C, CH₃), 6.50 (2C, CH₂Si), 5.98 (2C, CH₂Si), -4.70 (4C, CH₃Si), -5.95 (1C, CH₃Si)

^{10}B NMR: (CDCl₃, 128.0 MHz)
 δ (ppm) = 1.52 – -8.32 (m, 2B), -8.32 – -20.09 (m, 8B)

^{29}Si NMR: (CDCl₃, 79.0 MHz)
 δ (ppm) = 6.72 (1Si), -9.44 (2Si, SiH)

10.3.36 1,2 Di-(propyl-3-[4'-(5-[dimethylsilyl]- pentyloxy)biphenyl-4-carbonitrile])-dodecacarborane, **20**



4'-(pent-4-enyloxy)biphenyl-4-carbonitrile, **5** (113.2 mg, 0.43 mmol) and 1,2 di-(3-(dimethylsilyl)propyl)dodecacarborane, **70** (60.8 mg, 0.18 mmol) were dissolved in dry low sulphur toluene (1 mL) in a Schlenk tube. The solution was degassed *via* aeration with Ar and placed under Ar. Karstedt's catalyst (20 μL) was added and the solution stirred over night. The solvent was removed *in vacuo* and the product

Chapter 10: Experimental

purified by flash column chromatography (eluting with DCM, flash grade silica, R_f 0.35) to yield **20** as a white crystalline solid (66.9 mg, 42.7 %).

^1H $\{^{10}\text{B}\}$ NMR: (CDCl₃, 500.0 MHz, CHCl₃ internal standard)

δ (ppm) = 7.68 (d (J = 8.3 Hz), 4H, ArH), 7.63 (d (J = 8.3 Hz), 4H, ArH), 7.52 (d (J = 8.7 Hz), 4H, ArH), 6.99 (d (J = 8.7 Hz), 4H, ArH), 4.00 (t (J = 6.5 Hz), 4H, CH₂O), 2.35 – 2.05 (m, 10H, BH), 2.18 – 2.11 (m, 4H, CH₂Cluster), 1.88 – 1.75 (m, 4H, CH₂CH₂O), 1.63 – 1.45 (m, 8H, CH₂), 1.38 (m, 4H, CH₂), 0.62 – 0.52 (m, 4H, CH₂Si), 0.53 – 0.44 (m, 4H, CH₂Si), 0.00 (s, 12H, CH₃Si)

^{13}C NMR: (CDCl₃, 100.4 MHz, CHCl₃ internal standard)

δ (ppm) = 159.86 (2C, ArC-O), 145.36 (2C, ArC), 132.69 (4C, ArC), 131.41 (2C, ArC), 128.46 (4C, ArC), 127.19 (4C, ArC), 119.24 (1C, ArC-CN), 115.17 (4C, ArC), 110.16 (2C, CN), 79.76 (2C, C_{cluster}), 68.18 (2C, CH₂O), 38.83 (2C, CH₂), 30.07 (2C, CH₂), 29.07 (2C, CH₂), 24.50 (2C, CH₂), 23.80 (2C, CH₂), 15.50 (2C, CH₂Si), 15.20 (2C, CH₂Si), -3.27 (4C, CH₃Si)

^{10}B NMR: (CDCl₃, 140.0 MHz)

δ (ppm) = -5.78 (s, 2B), -11.52 (s, 8B)

^{29}Si NMR: (CDCl₃, 79.0 MHz)

δ (ppm) = 2.98 (s, 2Si)

IR (cm⁻¹): 2931 (s, ArH), 2576 (s, br, BH), 2222 (m, CN), 1604 (vs, C-O)

Mass (ESI):

m/z = 873.6017 (M+H)⁺, 855.20, 832.24, 758.22, 684.20, 610.18, 577.12, 559.12, 536.16

calculated = 873.5985 (M+H)⁺

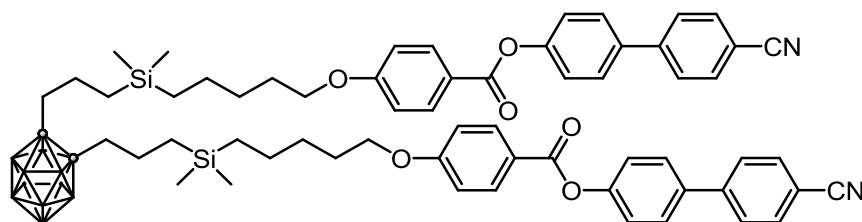
DSC/POM: Cr (15.8 [-2.3] SmA) 79.7 [31.6] Iso

CHN Microanalysis:

Observed: C 65.71 %, H 8.17 %, N 3.03 %

Predicted: C 66.16 %, H 8.10 %, N 3.21 %

10.3.37 1,2 Di-(propyl-3-dimethylsilyl-(4'-cyanobiphenyl-4-yl 4-(pentyloxy)benzoate)dodecacarborane, 21



4'-Cyanobiphenyl-4-yl 4-(pent-4-enyloxy)benzoate, **17** (133 mg, 0.35 mmol) was placed in a Schlenk tube under Ar and a solution of 1,2 di-(3-(dimethylsilyl)propyl)dodecacarborane, **70** (51 mg, 0.15 mmol) in dry, low sulphur toluene (5 mL) was added. The solution was degassed by purging with Ar, Karstedt's catalyst (30 μ L) added and stirred over night. The solvent was removed *in vacuo* and the product purified by flash column chromatography (eluting with DCM 10 % hexane, flash grade silica, R_f 0.19) to yield **21** as a white solid (112 mg, 67.4 %).

^1H { ^{10}B } NMR: (CDCl₃, 500.0 MHz, CHCl₃ internal standard)

δ (ppm): 8.16 (d (J = 8.7 Hz), 4H, ArH), 7.72 (d (J = 8.3 Hz), 4H, ArH), 7.68 (d (J = 8.2 Hz), 4H, ArH), 7.63 (d (J = 8.5 Hz), 4H, ArH), 7.32 (d (J = 8.5 Hz), 4H, ArH), 6.98 (d (J = 8.7 Hz), 4H, ArH), 4.05 (t (J = 6.3 Hz), 4H, CH₂O), 2.24 – 2.13 (m, 10H, BH), 2.18 – 2.11 (m, 4H, CH₂Cluster), 1.90 – 1.76 (m, 4H, CH₂), 1.55 – 1.51 (m, 8H, CH₂), 1.44 – 1.34 (m, 4H, CH₂), 0.63 – 0.54 (m, 4H, CH₂Si), 0.54 – 0.46 (m, 4H, CH₂Si), 0.01 (s, 12H, CH₃Si)

^{13}C NMR: (CDCl₃, 100.4 MHz, CHCl₃ internal standard)

δ (ppm) = 164.95 (2C, COO), 163.77 (2C, ArC-O), 151.68 (2C, ArC-O), 144.97 (2C, ArC), 136.83 (2C, ArC), 132.78 (4C, ArCH), 132.50 (4C, ArCH), 128.48 (4C, ArCH), 127.81 (4C, ArCH), 122.69 (4C, ArCH),

Chapter 10: Experimental

121.38 (2C, ArC), 119.02 (2C, ArC), 114.47 (4C, ArCH), 111.10 (2C, CN), 79.76 (C, C_{cluster}), 68.39 (2C, CH_2O), 38.84 (2C, CH_2), 30.02 (2C, CH_2), 28.94 (2C, CH_2), 24.50 (2C, CH_2), 23.80 (2C, CH_2), 15.50 (2C, CH_2), 15.20 (2C, CH_2), -3.27 (4C, CH_3Si)

^{10}B NMR: (CDCl₃, 160.0 MHz)
 δ (ppm) = -5.71 (s, 4B), -11.49 (s, 6B)

^{29}Si NMR: (CDCl₃, 79.0 MHz)
 δ (ppm) = 3.00 (s, 2Si)

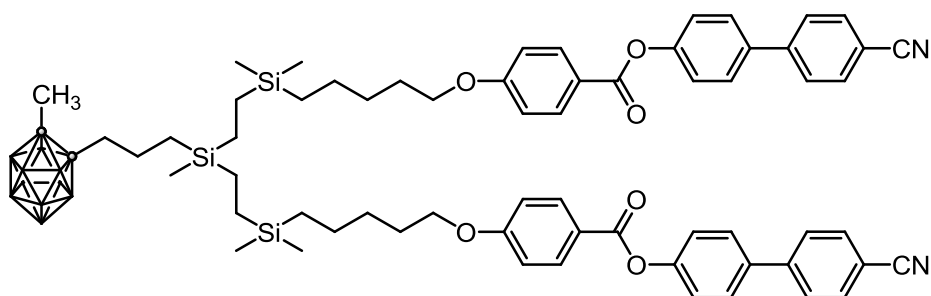
IR (cm⁻¹) 2931 (m, ArH), 2870 (w, ArH), 2576 (br, s, BH), 2222 (w, CN), 1728 (vs, C=O), 1604 (s, C-O)

Mass (LIFDI):
 m/z = 1111.56 (M+H)⁺

DSC/POM: Glass 21.9 SmA 182.8 [6.8] Iso

CHN microanalysis:
Observed: C 63.58 %, H 7.22 %, N 2.15 %
Calculated: C 66.90 %, H 7.07 %, N 2.52 %,

10.3.38 1 Methyl, 2-(propyl-3-[silyl(methyl)bis(ethyl-2-[dimethylsilyl(4'-Cyanobiphenyl-4-yl 4-(pent-4-enyloxy)benzoate])])dodecacarborane, 22



Chapter 10: Experimental

4'-Cyanobiphenyl-4-yl 4-(pent-4-enyloxy)benzoate, **17** (132 mg, 0.35 mmol) was placed in a Schlenk tube under Ar. A solution of 1 methyl, 2-(propyl-3-[silyl(methyl)bis(ethyl-2-[dimethylsilane])])dodecacarborane, **71** (60 mg, 0.14 mmol) in dry, low sulphur toluene (3 mL) was added and degassed by purging with Ar. Next Karstedt's catalyst (30 μ L) was added and the solution stirred over night. The solvent was removed *in vacuo* and the product purified by flash column chromatography (eluting with DCM, flash grade silica, R_f 0.24) to yield **22** as a white solid (100.6 mg, 60.7 %)

^1H NMR: (CDCl₃, 500.0 MHz, CHCl₃ internal standard)

δ (ppm) = 8.15 (d (J = 8.8 Hz), 4H, ArH), 7.72 (d (J = 8.3 Hz), 4H, ArH), 7.67 (d (J = 8.3 Hz), 4H, ArH), 7.63 (d (J = 8.6 Hz), 4H, ArH), 7.32 (d (J = 8.5 Hz), 4H, ArH), 6.98 (d (J = 8.8 Hz), 4H, ArH), 4.05 (t (J = 6.5 Hz), 4H, CH₂O), 2.25 (s, br, 5H, BH), 2.21 – 2.14 (m, 2H, CH₂Cluster), 2.17 (s, br, 3H, BH), 2.11 (s, br, 2H, BH), 2.00 (s, 3H, CH₃Cluster), 1.89 – 1.80 (m, 4H, CH₂), 1.55 – 1.51 (m, 6H, CH₂), 1.43 – 1.36 (m, 4H, CH₂), 0.58 – 0.52 (m, 6H, CH₂Si), 0.44 -0.35 (m, 8H, CH₂Si), -0.01 (s, 12H, CH₃Si), -0.03 (s, 3H, CH₃Si)

^{13}C NMR: (CDCl₃, 100.4 MHz, CHCl₃ internal standard)

δ (ppm) = 164.93 (2C, COO), 163.78 (2C, ArC-O), 151.66 (2C, ArC-O), 144.94 (2C, ArC), 136.79 (2C, ArC), 132.75 (4C, ArC-H), 132.46 (4C, ArC-H), 128.45 (4C, ArC-H), 127.79 (4C, ArC-H), 122.67 (4C, ArC-H), 121.31 (2C, ArC), 119.00 (2C, ArC), 114.46 (4C, ArC-H), 111.06 (2C, CN), 78.24 (1C, C_{cluster}), 74.67 (1C, C_{cluster}), 68.46 (2C, CH₂O), 39.21 (1C, CH₂), 30.07 (2C, CH₂), 28.95 (2C, CH₂), 24.54 (1C, CH₂), 23.90 (2C, CH₂), 23.24 (1C, CH₂Si), 14.77 (2C, CH₂Si), 13.04 (1C, CH₃Cluster), 7.35 (2C, CH₂Si), 5.16 (2C, CH₂Si), -3.79 (4C, CH₃Si), -5.99 (1C, CH₃Si)

^{10}B NMR: (CDCl₃, 128.0 MHz)

δ (ppm) = -6.04 (m, 2B), -11.53 (s, 8B)

Chapter 10: Experimental

^{29}Si NMR: (CDCl_3 , 79.0 MHz)

δ (ppm) = 6.77 (s, 1Si, SiCH_3), 4.54 (s, 2Si, $\text{Si}(\text{CH}_3)_2$)

IR (cm^{-1}): 2908 (s, ArH), 2576 (br, s, BH), 2222 (w, CN), 1728 (vs, C=O), 1604 (s, C-O)

Mass (ESI):

m/z = 1184.6813 (M^+), 989.62, 832.24, 812.56, 781.77

calculated = 1184.6724 (M^+)

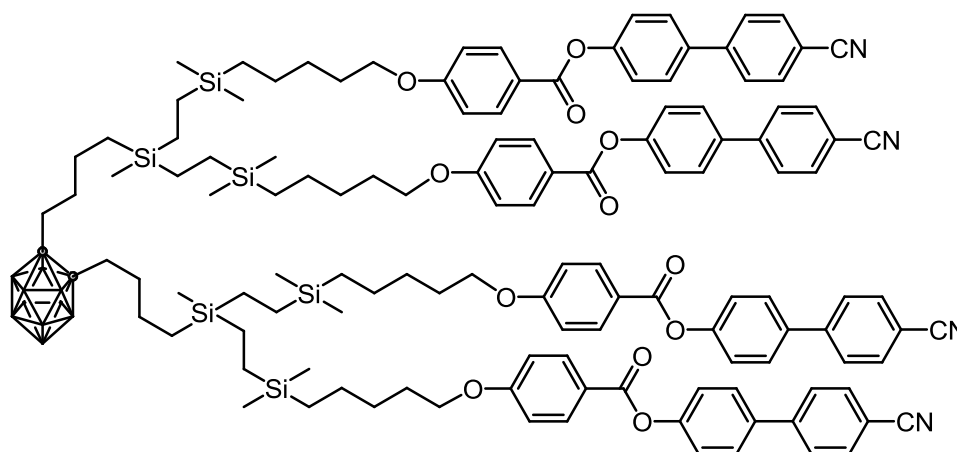
DSC/POM: Glass 18.0 SmA 180.8 [9.7] Iso

CHN microanalysis:

Observed: C 59.39 %, H 6.61 %, N 1.93 %,

Calculated: C 65.95 %, H 7.32 %, N 2.37 %,

10.3.39 Bis 1,2-(butyl-4-[silyl(methyl)bis(ethyl-2-[dimethylsilyl(4'-cyanobiphenyl-4-yl 4-(pent-4-enyloxy)benzoate])])dodecacarborane, **23**



Bis 1,2-(butyl-4-[silyl(methyl)bis(ethyl-2-[dimethylsilane])])dodecacarborane (65 mg, 0.098 mmol) and 4'-cyanobiphenyl-4-yl 4-(pent-4-enyloxy)benzoate, **17** (255 mg, 0.67 mmol) were dissolved in dry low sulphur toluene (8 mL) and the solution degassed by purging with Ar. Karstedt's catalyst (40 μL) was added and the solution

Chapter 10: Experimental

stirred overnight. The solvent was removed *in vacuo* and the product isolated by flash column chromatography (flash grade silica, eluting with hexane/DCM/ethyl acetate 3:2:1, R_f 0.83). Finally the material was purified by precipitation from DCM/MeOH yielding **23** as a white viscous fluid (23 mg, 10.6 %).

^1H NMR: (CDCl₃, 400 MHz, CHCl₃ internal standard)

δ (ppm) = 8.15 (d (J = 8.7 Hz), 8H, ArH), 7.73 (d (J = 8.2 Hz), 8H, ArH), 7.67 (d (J = 8.3 Hz), 8H, ArH), 7.63 (d (J = 8.5 Hz), 8H, ArH), 7.31 (d (J = 8.5 Hz), 8H, ArH), 6.97 (d (J = 8.7 Hz), 8H, ArH), 4.04 (t (J = 6.3 Hz), 8H, CH₂O), 2.19 – 2.07 (m, 4H, CH₂C_{cluster}), 1.89 – 1.76 (m, 4H, CH₂), 1.61 – 1.46 (m, 12H, CH₂), 1.44 – 1.18 (m, 16H, CH₂), 0.67 – 0.47 (m, 12H, CH₂Si), 0.47 – 0.27 (m, 16H, CH₂Si), 0.16 – -0.16 (m, 30H, CH₃Si)

^{13}C NMR: (CDCl₃, 100.4 MHz, CHCl₃ internal standard)

δ (ppm) = 164.94 (4C, COO), 163.79 (4C, ArC), 151.69 (4C, ArC), 144.96 (4C, ArC), 136.86 (4C, ArC), 132.79 (8C, ArC), 132.50 (8C, ArC), 128.48 (8C, ArC), 127.82 (8C, ArC), 122.69 (8C, ArC), 121.40 (4C, ArC), 119.01 (4C, CN), 114.48 (8C, ArC), 111.15 (4C, ArC), 79.95 (2C, C_{cluster}), 68.49 (4C, CH₂O), 34.96 (2C, CH₂), 33.83 (2C, CH₂), 30.11 (4C, CH₂), 29.01 (4C, CH₂), 24.05 (2C, CH₂), 23.94 (4C, CH₂), 14.82 (4C, CH₂), 12.88 (2C, CH₂), 7.37 (4C, CH₂), 5.23 (4C, CH₂), -3.75 (8C, CH₃Si), -6.00 (2C, CH₃Si)

^{11}B NMR: (CDCl₃, 128 MHz)

δ (ppm) = -5.55 (6B), -11.21 (4B)

^{29}Si NMR: (CDCl₃, 79 MHz)

δ (ppm) = 6.68 (2Si), 4.51 (4Si)

IR (cm⁻¹): 2908 (s, ArH), 2870 (s, ArH), 2584 (s, br, BH), 2222 (m, CN), 1782 (vs, C=O), 1604 (s, C-O)

Chapter 10: Experimental

Mass (MALDI):

$m/z = 2262.15208 (M+K)^+, 2246.22 (M+Na)^+$

calculated = $2262.1216 (M+K)^+$

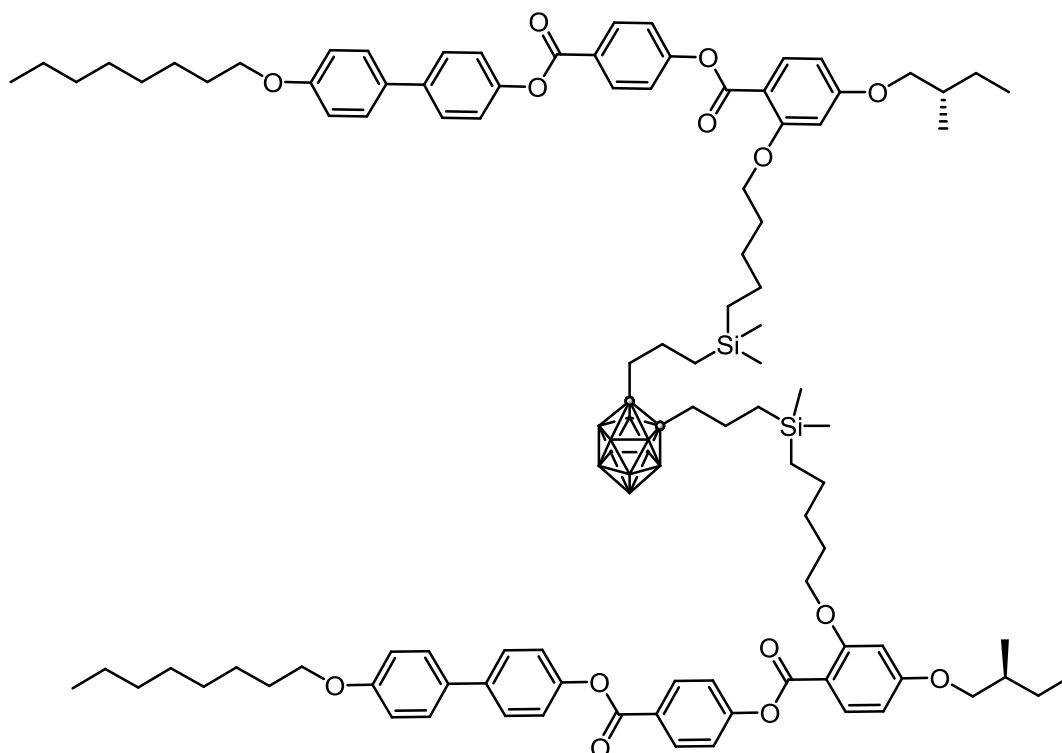
DSC/POM: Glass 21.2 SmA 164.7 [14.7] Iso

CHN microanalysis: (VO₅ combustion aid)

Observed: C 69.15 %, H 7.25 %, N 2.52 %,

Calculated: C 65.71 %, H 7.35 %, N 1.19 %,

10.3.40 Bis 1,2-(propyl-3-dimethylsilyl-((S)-4-((4'-(octyloxy)biphenyl-4-yloxy)carbonyl)phenyl 4-(2-methylbutoxy)-2-(pentyloxy)benzoate)dodecacarborane, **24**



1,2 Di-(3-(dimethylsilyl)propyl)dodecacarborane, **70** (48 mg, 0.14 mmol) and (S)-4-((4'-(octyloxy)biphenyl-4-yloxy)carbonyl)phenyl 4-(2-methylbutoxy)-2-(pent-4-enyloxy)benzoate, **19** (232 mg, 0.33 mmol) were dissolved in dry low sulphur toluene (6 mL) and the solution degassed by purging with Ar. Karstedt's catalyst (30

Chapter 10: Experimental

μL) was added and the solution stirred for 2 days. The solvent was removed *in vacuo* and the product isolated using flash column chromatography (flash grade silica, eluting with hexane/DCM/ethyl acetate 5:2:1, R_f 0.38). The product was purified by flash column chromatography (flash grade silica, pet ether/DCM/ethyl acetate 12:2:1, R_f 0.19) to yield **24** as a white crystalline solid (20 mg, 8.2 %).

^1H NMR: (500 MHz, CDCl_3 , CHCl_3 internal standard)
 δ (ppm) = 8.27 (d ($J = 8.7$ Hz), 4H, ArH), 8.05 (d ($J = 8.7$ Hz), 2H, ArH), 7.59 (d ($J = 8.6$ Hz), 4H, ArH), 7.51 (d ($J = 8.7$ Hz), 4H, ArH), 7.36 (d ($J = 8.7$ Hz), 4H, ArH), 7.26 (d ($J = 8.6$ Hz), 4H, ArH), 6.97 (d ($J = 8.7$ Hz), 4H, ArH), 6.55 (dd ($J = 8.8, 2.2$ Hz), 2H, ArH), 6.52 (d ($J = 2.2$ Hz), 2H), 4.05 (t ($J = 6.4$ Hz), 4H, CH_2O), 4.00 (t ($J = 6.6$ Hz), 4H, CH_2O), 3.86 (ddd ($J = 39.8, 9.0, 6.3$ Hz), 4H, CH_2O), 2.17 (s, 10H, BH), 2.16 – 2.03 (m, 12H, CH_2), 1.94 – 1.75 (m, 12H, CH_2), 1.63 – 1.45 (m, 12H, CH_2), 1.42 – 1.25 (m, 23H, CH_2), 1.05 (d ($J = 6.8$ Hz), 3H, CH_3), 0.97 (t ($J = 7.5$ Hz), 3H, CH_3), 0.90 (t ($J = 6.9$ Hz), 3H, CH_3), 0.55 – 0.43 (m, 8H, CH_2Si), 0.06 (s, 12H, CH_3Si)

^{13}C NMR: (101.4 MHz, CDCl_3 , CHCl_3 internal standard)
 δ (ppm) = 165.11 (2C, COO), 164.80 (2C, COO), 163.37 (2C, ArC), 162.05 (2C, ArC), 158.93 (2C, ArC), 155.75 (2C, ArC), 149.94 (2C, ArC), 138.92 (2C, ArC), 134.71 (2C, ArCH), 132.84 (2C, ArC), 131.88 (4C, ArCH), 128.25 (4C, ArCH), 127.88 (4C, ArCH), 126.73 (2C, ArC), 122.39 (4C, ArCH), 122.03 (4C, ArCH), 114.96 (4C, ArCH), 110.59 (2C, ArC), 105.58 (2C, ArCH), 100.29 (2C, ArCH), 79.83 (2C, 38.83 (2C, CH_2), 38.52 (2C, CH_2), 34.82 (2C, CH), 31.97 (2C, CH_2), 30.03 (2C, CH_2), 29.52 (2C, CH_2), 29.44 (2C, CH_2), 29.40 (2C, CH_2), 29.02 (2C, CH_2), 26.22 (2C, CH_2), 24.49 (2C, CH_2), 23.90 (2C, CH_2), 23.76 (2C, CH_2), 22.82 (2C, CH_2), 18.36 (2C, CH_2), 16.65 (2C, CH_3), 15.47 (2C, CH_2), 15.22 (2C, CH_2), 14.26 (2C, CH_3), 11.48 (2C, CH_3), 0.55 (4C, CH_3Si)

^{11}B NMR: (128 MHz, CDCl_3)
 δ (ppm) = -5.67 (s, br, 3B), -11.59 (s, br, 7B)

Chapter 10: Experimental

^{29}Si NMR: (79 MHz, CDCl_3)

δ (ppm) = 2.92 (s, 2Si)

Mass (LIFDI):

m/z = 1754.44 (M+H)⁺

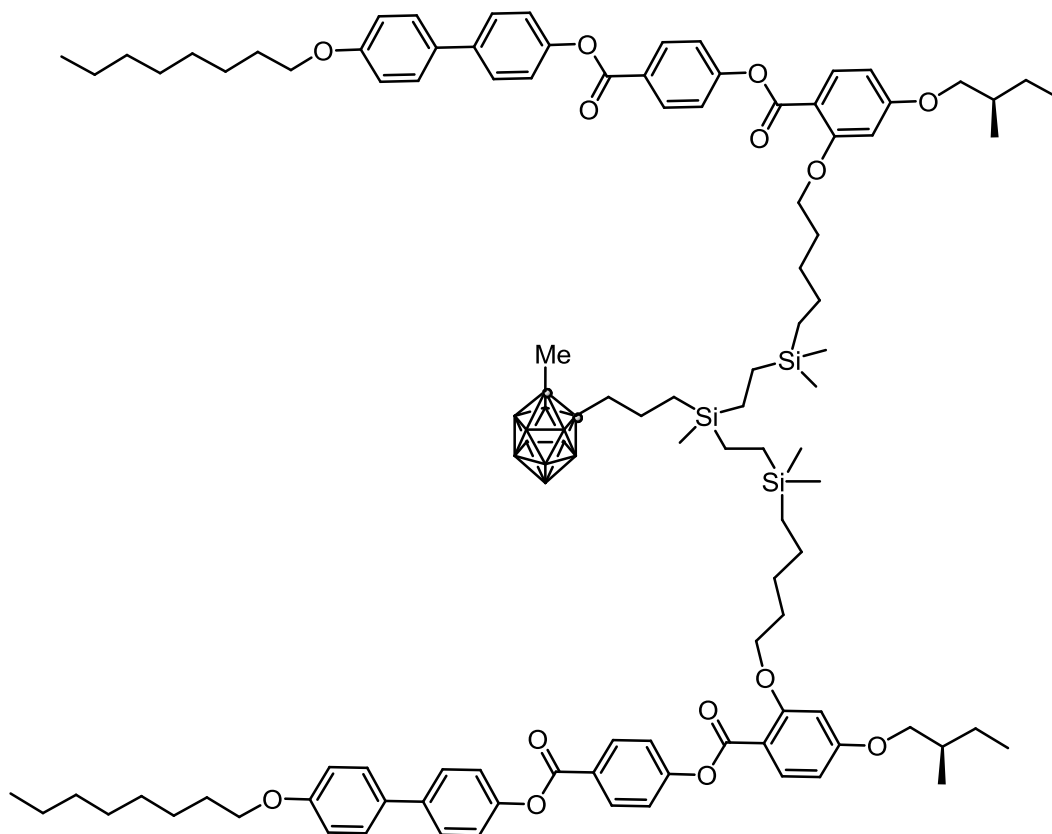
DSC/POM: Cr 48.2 [37.3] Iso

CHN microanalysis:

Observed: C 63.691 %, H 8.466 %, N 0.00 %,

Calculated: C 69.41 %, H 8.15 %, N 0.00 %

10.3.41 1 Methyl, 2-(propyl-3-[silyl(methyl)bis(ethyl-2-[dimethylsilyl-[(*S*)-4-((4'-(octyloxy)biphenyl-4-yloxy)carbonyl)phenyl 4-(2-methylbutoxy)-2-(pentyloxy)benzoate]]))]dodecacarborane, 25



1 Methyl, 2-(propyl-3-[silyl(methyl)bis(ethyl-2-[dimethylsilane]))]dodecacarborane, **71** (76.5 mg, 0.18 mmol) and (*S*)-4-((4'-(octyloxy)biphenyl-4-yloxy)carbonyl)phenyl 4-(2-methylbutoxy)-2-(pent-4-enyloxy)benzoate, **19** (305 mg, 0.44 mmol) were dissolved in dry low sulphur toluene (8 mL) and the solution degassed by purging with Ar. Karstedt's catalyst (30 μ L) was added and the solution stirred over night. The solvent was removed *in vacuo* and the product isolated *via* flash column chromatography (flash grade silica, DCM 20 % hexane, R_f 0.54). Finally the product was purified by column chromatography (flash grade silica, pet ether/DCM/ethyl acetate 12:2:1, R_f 0.38) to yield **25** as a white crystalline solid (28 mg, 8.6 %).

Chapter 10: Experimental

^1H $\{^{10}\text{B}\}$ NMR: (500 MHz, CDCl_3 , CHCl_3 internal standard)

δ (ppm) = 8.27 (d ($J = 8.6$ Hz), 4H, ArH), 8.05 (d ($J = 8.7$ Hz), 2H, ArH), 7.59 (d ($J = 8.5$ Hz), 4H, ArH), 7.51 (d ($J = 8.6$ Hz), 4H, ArH), 7.36 (d ($J = 8.6$ Hz), 4H, ArH), 7.25 (d ($J = 7.6$ Hz), 4H), 6.97 (d ($J = 8.7$ Hz), 4H, ArH), 6.54 (dd ($J = 8.8, 2.2$ Hz), 2H, ArH), 6.51 (d ($J = 2.1$ Hz), 2H, ArH), 4.04 (t ($J = 6.5$ Hz), 4H, CH_2O), 4.00 (t ($J = 6.6$ Hz), 4H, CH_2O), 3.85 (ddd ($J = 39.8, 9.0, 6.3$ Hz), 4H, CH_2O), 2.23 (s, br, 4H, BH), 2.17 – 2.12 (m, 4H, $\text{CH}_2\text{C}_{\text{cluster}}$), 2.08 (s, br, 3H, BH), 1.99 – 1.92 (m, 3H, $\text{CH}_3\text{C}_{\text{cluster}}$), 1.92 – 1.77 (m, 12H, CH_2), 1.65 – 1.42 (m, 15H, CH_x), 1.42 – 1.19 (m, 28H, CH_2), 1.04 (d ($J = 6.7$ Hz), 6H, CH_3), 0.97 (t ($J = 7.5$ Hz), 6H, CH_3), 0.90 (t ($J = 6.9$ Hz), 6H, CH_3), 0.55 – 0.43 (m, 6H, CH_2Si), 0.44 – 0.27 (m, 8H, CH_2Si), 0.04 (s, 3H, CH_3Si), -0.07 (s, 12H, CH_3Si)

^{13}C NMR: (100.4 MHz, CDCl_3 , CHCl_3 internal standard)

δ (ppm) = 165.09 (2C, COO), 164.79 (2C, COO), 163.37 (2C, ArC), 162.09 (2C, ArC), 158.93 (2C, ArC), 155.75 (2C, ArC), 149.94 (2C, ArC), 138.90 (2C, ArC), 134.69 (2C, ArCH), 132.83 (2C, ArC), 131.87 (4C, ArCH), 128.25 (4C, ArCH), 127.87 (4C, ArCH), 126.71 (2C, ArC), 122.39 (4C, ArCH), 122.03 (4C, ArCH), 114.95 (4C, ArCH), 110.56 (2C, ArC), 105.58 (2C, ArCH), 100.27 (2C, ArCH), 78.30 (1C, $\text{C}_{\text{cluster}}$), 74.70 (1C, $\text{C}_{\text{cluster}}$), 73.28 (2C, CH_2O), 69.09 (2C, CH_2O), 68.25 (2C, CH_2O), 39.22 (1C, $\text{CH}_2\text{C}_{\text{cluster}}$), 34.81 (1C, $\text{CH}_3\text{C}_{\text{cluster}}$), 31.97 (2C, CH_2), 30.10 (2C, CH_2), 29.52 (2C, CH_2), 29.44 (2C, CH_2), 29.40 (2C, CH_2), 29.04 (2C, CH_2), 26.21 (4C, CH_2), 24.54 (2C, CH_2), 23.88 (2C, CH_2), 23.23 (2C, CH), 22.81 (2C, CH_2), 16.65 (2C, CH_3), 14.78 (2C, CH_2), 14.26 (2C, CH_3), 13.00 (1C, CH_2), 11.47 (2C, CH_3), 7.34 (1C, CH_2), 5.18 (2C, CH_2), -3.81 (4C, CH_3Si), -6.02 (1C, CH_3Si)

^{11}B NMR: (128 MHz, CDCl_3)

δ (ppm) = -5.28 (1B), -6.69 (2B), -11.56 (10B)

^{29}Si NMR: (79 MHz, CDCl_3)

δ (ppm) = 6.76 (1Si), 4.48 (2Si)

Chapter 10: Experimental

IR (cm⁻¹): 2924 (s, br, BH), 2854 (m, br, BH), 2584 (m, br, BH), 1735 (vs, C=O), 1604 (s, C-O)

Mass (MALDI):

m/z = 1826.09873 (M+Na)⁺

calculated = 1826.1005 (M+Na)⁺

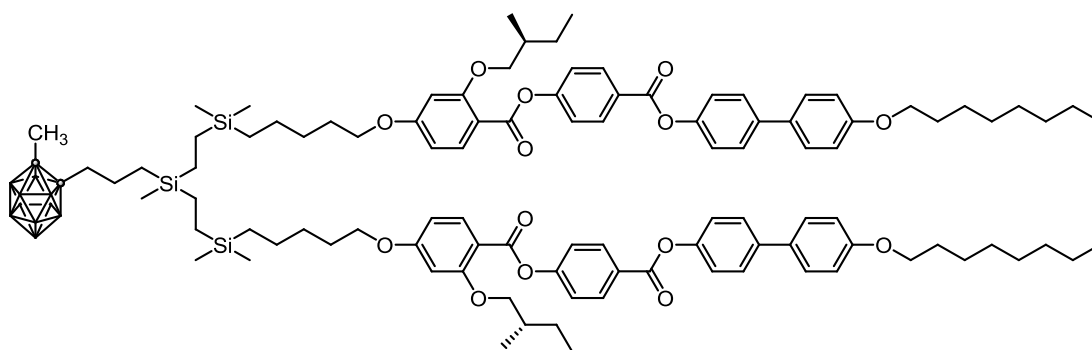
DSC/POM: Cr 54.8 [39.5] N* 61.1 [0.9] Iso

CHN microanalysis: (VO₅ combustion aid)

Observed: C 67.77 %, H 8.51 %, N 0.00 %

Calculated: C 68.63 %, H 8.28 %, N 0.00 %

10.3.42 1 Methyl, 2-(propyl-3-[silyl(methyl)bis(ethyl-2-[dimethylsilyl-[(S)-4-((4'-(octyloxy)biphenyl-4-yloxy)carbonyl)phenyl 2-(2-methylbutoxy)-4-(pentyloxy)benzoate))])])dodecacarborane, 27



1 Methyl, 2-(propyl-3-[silyl(methyl)bis(ethyl-2-[dimethylsilane])])dodecacarborane, compound **71** (60 mg, 0.14 mmol) and (S)-4-((4'-(Octyloxy)biphenyl-4-yloxy)carbonyl)phenyl 2-(2-methylbutoxy)-4-(pent-4-enyloxy)benzoate, **18** (243 mg, 0.35 mmol) were dissolved in dry low sulphur toluene (10 mL) and the solution degassed *via* purging with Ar. Karstedt's catalyst (30 μ L) was added and the solution stirred over night. The solvent was removed *in vacuo* and the product isolated *via* flash column chromatography (flash grade silica, DCM 20 % hexane, R_F 0.55). The

Chapter 10: Experimental

product was purified by flash column chromatography (flash grade silica, pet ether/DCM/ethyl acetate 4:2:1, R_f 0.74) to yield **27** white crystalline solid (31 mg, 12.3 %).

^1H $\{^{10}\text{B}\}$ NMR: (500 MHz, CDCl_3 , CHCl_3 internal standard)

δ (ppm) = 8.28 (d (J = 6.3 Hz), 4H, ArH), 8.04 (d (J = 8.7 Hz), 2H, ArH), 7.59 (d (J = 6.6 Hz), 4H, ArH), 7.51 (d (J = 7.1 Hz), 4H, ArH), 7.35 (d (J = 6.2 Hz), 4H, ArH), 7.26 (d (J = 11.0 Hz), 4H, ArH), 6.98 (d (J = 7.5 Hz), 4H, ArH), 6.54 (dd (J = 8.8, 1.7 Hz), 2H, ArH), 6.51 (d, (J = 1.7 Hz), 2H, ArH), 4.04 (t (J = 6.4 Hz), 4H, CH_2O), 4.00 (t (J = 6.6 Hz), 4H, CH_2O), 3.95 – 3.80 (m, 4H, CH_2O), 2.24 (s, br, 7H, BH), 2.20 – 2.14 (m, 3H, $\text{CH}_3\text{C}_{\text{cluster}}$), 2.11 (s, br, 3H, BH), 1.82 (m, 8H, CH_2), 1.53 (m, 16H, CH_x), 1.43 – 1.20 (m, 26H, CH_x), 1.05 (d (J = 6.7 Hz), 6H, CH_3), 0.93 (t (J = 7.6 Hz), 6H, CH_3), 0.90 (t (J = 7.1 Hz), 6H, CH_3), 0.55 (m, 6H, CH_2Si), 0.40 (m, 8H, CH_2Si), 0.12 – 0.03 (m, 3H, CH_3Si), 0.02 – -0.06 (s, 12H, CH_3Si)

^{13}C NMR: (100.4 MHz, CDCl_3 , CHCl_3 internal standard)

δ (ppm) = 164.90 (2C, COO), 164.82 (2C, COO), 163.66 (2C, ArC), 162.04 (2C, ArC), 158.93 (2C, ArC), 155.76 (2C, ArC), 149.96 (2C, ArC), 138.90 (2C, ArC), 134.83 (2C, ArCH), 132.87 (2C, ArC), 131.93 (4C, ArCH), 128.26 (4C, ArCH), 127.88 (4C, ArCH), 126.75 (2C, ArC), 122.37 (4C, ArCH), 122.04 (4C, ArCH), 114.96 (4C, ArCH), 110.69 (2C, ArC), 105.42 (2C, ArCH), 100.09 (2C, ArCH), 78.24 (1C, $\text{C}_{\text{cluster}}$), 74.69 (1C, $\text{C}_{\text{cluster}}$), 73.66 (2C, CH_2O), 68.51 (2C, CH_2O), 68.25 (2C, CH_2O), 39.26 (1C, $\text{CH}_2\text{C}_{\text{cluster}}$), 34.91 (1C, $\text{CH}_3\text{C}_{\text{cluster}}$), 31.97 (2C, CH_2), 30.14 (2C, CH_2), 29.85 (2C, CH_2), 29.52 (2C, CH_2), 29.44 (2C, CH_2), 29.40 (2C, CH_2), 29.04 (2C, CH_2), 26.21 (2C, CH_2), 26.15 (2C, CH_2), 24.57 (2C, CH_2), 23.95 (2C, CH_2), 23.28 (2C, CH_3), 22.81 (2C, CH_2), 16.75 (2C, CH_3), 14.81 (2C, CH_2), 14.26 (2C, CH_3), 13.09 (1C, CH_2), 11.48 (2C, CH), 10.44 (1C, CH_2), -3.77 (1C, CH_3Si), -5.95 (4C, CH_3Si)

Chapter 10: Experimental

^{11}B NMR: (128 MHz, CDCl_3)
 δ (ppm) = -6.65 (3B), -11.54 (7B)

^{29}Si NMR: (79 MHz, CDCl_3)
 δ (ppm) = 6.90 (1Si), 4.54 (2Si)

IR (cm^{-1}): 2924 (s, br, BH), 2854 (m, br, BH), 2584 (m, br, BH), 1735 (vs, C=O), 1604 (s, C-O)

Mass (MALDI):

m/z = 1842.08249 ($\text{M}+\text{K}$)⁺, 1826.16 ($\text{M}+\text{Na}$)⁺

calculated = 1842.0745 ($\text{M}+\text{K}$)⁺

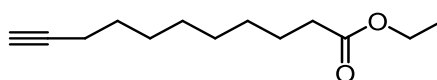
DSC/POM: Cr 63.2 [24.5] N* 63.5 [6.7] Iso

CHN microanalysis:

Observed: C 62.85 %, H 8.68 %, N 0.00 %

Calculated: C 68.63 %, H 8.28 %, N 0.00 %

10.3.43 Ethyl undec-10-ynoate, **72**



Undec-10-ynoic acid (2.00 g, 10.97 mmol) was dissolved in ethanol (100 mL) and concentrated H_2SO_4 (1 mL) was added. The resultant solution was gently refluxed for 2 h and allowed to cool to room temperature. The solution was poured onto brine (150 mL) and diethyl ether added (150 mL). The organic phase was washed with water (2 x 100 mL) dried over MgSO_4 and the solvent removed *in vacuo*. The resulting yellow oil was passed through a silica pad eluting with DCM to yield **72** as a mobile colourless oil (2.17 g, 94.1 %).

Chapter 10: Experimental

^1H NMR: (CDCl₃, 400.0 MHz, CHCl₃ internal standard)
 δ (ppm) = 4.11 (q (J = 7.1 Hz), 2H, CH₃CH₂O), 2.27 (t (J = 7.5 Hz), 2H, CH₂CH₂O), 2.16 (td (J = 7.1, 2.6 Hz), 2H, HC≡CCH₂), 1.92 (t (J = 2.6 Hz), 1H, HC≡C), 1.61 (m, 2H, CH₂), 1.51 (m, 2H, CH₂), 1.39 (m, 2H, CH₂), 1.30 (m, 4H, CH₂), 1.24 (t (J = 7.1 Hz), 3H, CH₃)

^{13}C NMR: (CDCl₃, 100.4 MHz, CHCl₃ internal standard)
 δ (ppm) = 173.97 (1C, COO), 84.81 (1C, C≡CH), 68.21 (1C, HC≡C), 60.27 (1C, CH₂O), 34.47 (1C, CH₂), 29.22 (1C, CH₂), 29.18 (1C, CH₂), 29.01 (1C, CH₂), 28.77 (1C, CH₂), 28.54 (1C, CH₂), 25.05 (1C, CH₂), 18.49 (1C, CH₂C≡CH), 14.37 (1C, CH₃)

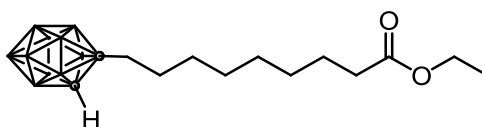
IR (cm⁻¹): 3302 (m, br, C≡C-Hh), 2931 (s, C-H), 2854 (m, C-H), 2113 (w, C≡C stretch), 1728 (vs, C=O)

Mass (ESI):

m/z = 211.1692 (M+H)⁺, 165.13, 145.57, 125.99, 81.52

calculated = 211.1698 (M+H)⁺

10.3.44 2-(Ethyl nonanoate)dodecacarborane, **73**



Decaborane(14) (510 mg, 4.17 mmol) was dissolved in dry acetonitrile (15 mL) under Ar and refluxed for 2 h. A solution of ethyl undec-10-ynoate, **72** (0.97 g, 4.59 mmol) in dry toluene (4 mL) was added and the solution stirred at reflux for 2 days. The solution was allowed to cool, the solvent removed *in vacuo* and the product extracted with hot hexane. The solution was washed with 10 % w/w NaOH in water (50 mL), dried over MgSO₄ and the solvent removed *in vacuo* to yield **73** as a pale yellow oil (1.02 g, 87.1 %).

Chapter 10: Experimental

^1H NMR: (CDCl_3 , 400.0 MHz, CHCl_3 internal standard)
 δ (ppm) = 4.09 (q ($J = 7.1$ Hz), 2H, COOCH_2), 3.58 (s, 1H, ClusterCH), 2.25 (t ($J = 7.5$ Hz), 2H, CH_2COO), 2.20 – 2.11 (m, 2H, Cluster CH_2), 1.60 – 1.56 (m, 2H, CH_2), 1.53 – 1.32 (m, 2H, CH_2), 1.32 – 1.25 (m, 8H, CH_2 , 8H), 1.23 (t ($J = 7.1$ Hz), 3H, CH_3)

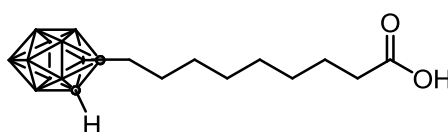
^{10}B NMR: (CDCl_3 , 128.0 MHz)
 δ (ppm) = -3.45 (s, 1B), -6.92 (s, (1B), -10.37 (s, 2B), -11.29 – -17.27 (m, 6B)

Mass (ESI):

m/z = 353.3238 ($\text{M}+\text{Na}$) $^+$, 331.34 ($\text{M}+\text{H}$) $^+$, 233.15, 211.17, 165.17, 145.54, 125.99, 110.01, 81.53

calculated = 353.3231 ($\text{M}+\text{H}$) $^+$

10.3.45 1-Hydrido, 2-(nonanoic acid)dodecacarborane, **74**



LiOH (0.43 g, 17.9 mmol) was added to a suspension of water (8 mL) and a solution of 2-(ethyl nonanoate)dodecacarborane, **73** (197.2 mg, 0.597 mmol) in THF (12 mL) and stirred at 40 °C over night. The suspension was allowed to cool, diluted with water (80 mL) and acidified with conc. HCl. The product was extracted into ethyl acetate (3 x 80 mL) and the combined organic fractions washed with brine (2 x 60 mL). The solution was dried over MgSO_4 and the solvent removed *in vacuo* to yield **74** as a pale yellow oil (173.9 mg, 96.9 %).

^1H NMR: (Methanol- D_3 , 400.0 MHz)
 δ (ppm) = 4.15 (s, 1H, ClusterCH), 2.24 (t ($J = 7.4$ Hz), 2H, CH_2COO), 2.21 – 2.15 (m, 2H, Cluster CH_2), 1.66 – 1.50 (m, 2H, CH_2), 1.51 – 1.17 (m, 10H, CH_2)

^{10}B NMR: (Methanol- D_3 , 128.0 MHz)

Chapter 10: Experimental

δ (ppm) = -3.79 (s, 1B), -7.11 (s, 1B), -10.58 (s, 2B), -11.61 – -20.46 (m, 6B)

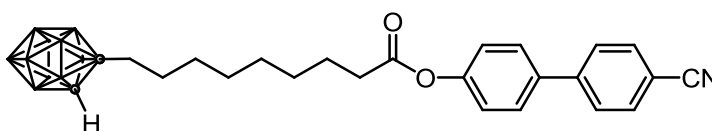
IR (cm⁻¹): 2924 (m, br, BH), 2854 (m, br, BH), 2576 (m, br, BH), 1705 (s, C=O)

Mass (ESI):

m/z = 324.2963 (M+Na)⁺, 288.92, 242.28, 226.95, 205.12, 172.09, 158.97,
125.99, 102.13

calculated = 324.2954 (M+Na)⁺

10.3.46 2-(Cyanobiphenyl nonanoate)dodecacarborane, **28**



2-(Nonanoic acid)dodecacarborane, **74** (50 mg, 0.17 mmol), cyanobiphenyl (39 mg, 0.19 mmol), DMAP (5 mg, 0.02 mmol) and EDAC (31 mg, 0.19 mmol) were dissolved in dry DCM (25 mL) and stirred for 2 days. The solvent was removed *in vacuo* and the product isolated by flash column chromatography (eluting with DCM 10 % hexane, flash grade silica, R_f 0.81). The product was then recrystallized from hexane to yield **28** as a white crystalline solid (29.7 mg, 36.6 %).

¹H {¹⁰B} NMR: (CDCl₃, 500.0 MHz, CHCl₃ internal standard)

δ (ppm) = 7.72 (d (*J* = 8.4 Hz), 2H, Ar*H*), 7.65 (d (*J* = 8.3 Hz), 2H, Ar*H*), 7.59 (d (*J* = 8.6 Hz), 2H, Ar*H*), 7.20 (d (*J* = 8.6 Hz), 2H, Ar*H*), 3.56 (s, br, 1H, Cluster*H*), 2.58 (t (*J* = 7.4 Hz), 2H, CH₂COO), 2.30 (s, br, 3H, BH), 2.19 (t (*J* = 8.4 Hz), 2H, CH₂Cluster), 2.19 (s, br, 4H, BH), 2.13 (s, br, 2H, BH), 1.82 – 1.72 (m, 2H, CH₂), 1.48 – 1.39 (m, 4H, CH₂), 1.38 – 1.19 (m, 6H, CH₂)

¹³C NMR: (CDCl₃, 100.4 MHz, CHCl₃ internal standard)

δ (ppm) = 172.27 (1C, COO), 151.26 (1C, ArC-O), 144.87 (1C, ArC), 136.91 (1C, ArC), 132.78 (2C, ArCH), 128.46 (2C, ArCH), 127.79 (2C, ArCH), 122.42 (2C, ArCH), 111.13 (1C, C≡N), 75.50 (1C, ClusterC),

Chapter 10: Experimental

68.27 (1C, ClusterC), 61.09 (1C, CH₂COO), 38.18 (1C, CH₂), 34.42 (1C, CH₂), 29.28 (1C, CH₂), 29.11 (1C, CH₂), 29.03 (1C, CH₂), 28.95 (1C, CH₂), 24.89 (1C, CH₂)

¹⁰B NMR: (CDCl₃, 128.0 MHz)
δ (ppm) = -3.40 (s, 1B), -6.86 (s, 1B), -10.33 (s, 2B), -11.46 – -15.69 (m, 6B)

IR (cm⁻¹): 3055 (w, ArH stretch), 2924 (m, br, BH), 2854 (m, br, BH), 2576 (s, br, BH), 2222 (m, CN), 1743 (vs, C=O), 1604 (m, C-O)

Mass (ESI):
m/z = 480.3669 (M+H)⁺
calculated = 480.3677 (M+H)⁺

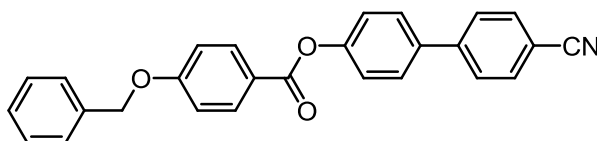
POM/DSC: Cr₁ 46.8 [-18.8] Cr₂ 88.2 [42.1] Iso

CHN microanalysis:

Observed: C 62.00 %, H 7.38 %, N 2.85 %

Calculated: C 60.35 %, H 7.39 %, N 2.93 %

10.3.47 4' –Cyanobiphenyl-4-yl 4-(benzyloxy)benzoate, **75**



4-Benzyloxy benzoic acid (2.81 g, 12.3 mmol), 4'-hydroxycyanobiphenyl (2.40 g, 12.3 mmol), DMAP (0.33 g, 1.3 mmol) and EDAC (1.94 g, 12.5 mmol) were dissolved in DCM (150 mL) and stirred for 3 days. The solvent was removed *in vacuo* and the product purified by flash column chromatography (eluting with DCM, flash grade silica, R_F 0.67) to yield **75** as a white crystalline solid (4.58 g, 91.8 %).

¹H NMR: (CDCl₃, 400.0 MHz, CHCl₃ internal standard)

Chapter 10: Experimental

δ (ppm) = 8.18 (d (J = 8.9 Hz), 2H, ArH), 7.74 (d (J = 8.6 Hz), 2H, ArH), 7.69 (d (J = 8.6 Hz), 2H, ArH), 7.64 (d (J = 8.7 Hz), 2H, ArH), 7.49 – 7.35 (m, 5H, ArH), 7.33 (d (J = 8.7 Hz), 2H, ArH), 7.08 (d (J = 8.9 Hz), 2H, ArH), 5.18 (s, 2H, CH₂O)

¹³C NMR: (CDCl₃, 100.4 MHz, CHCl₃ internal standard)

δ (ppm) = 164.90 (1C, COO), 163.33 (1C, COO), 151.67 (1C, ArC-O), 144.99 (1C, ArC-O), 136.88 (1C, ArC), 136.18 (1C, ArC), 132.79 (2C, ArCH), 132.54 (2C, ArCH), 128.88 (2C, ArCH), 128.50 (2C, ArCH), 128.45 (1C, ArCH), 127.83 (2C, ArCH), 127.64 (2C, ArCH), 122.69 (2C, ArCH), 121.86 (1C, ArC), 119.03 (1C, ArC), 114.91 (2C, ArCH), 111.13 (1C, C \equiv N), 70.35 (1C, CH₂O)

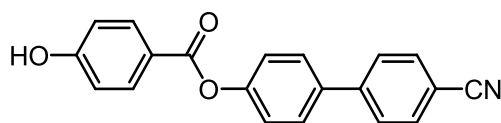
IR (cm⁻¹): 3062 (m, ArH), 2947 (w, ArH), 2885 (w, ArH), 2222 (m, CN), 1720 (vs, C=O), 1597 (s, C-O)

Mass (ESI):

m/z = 406.1426 (M+H)⁺, 325.11, 304.60, 284.09

calculated = 406.1443 (M+H)⁺

10.3.48 4'-Cyanobiphenyl-4-yl 4-hydroxybenzoate, **76**



4'-Cyanobiphenyl-4-yl 4-(benzyloxy)benzoate, **75** (2.95 g, 7.28 mmol) was dissolved in dioxane (250 mL) and Pd on activated carbon suspended in the solution. The suspension was stirred under an atmosphere of hydrogen for 1 week. The solvent was removed *in vacuo*, the product loaded onto a silica pad and washed repeatedly with DCM. The product was then eluted with DCM 10 % ethyl acetate. The solvent was removed *in vacuo* and the product suspended in DCM, stirred over night and then filtered to yield **76** as a white crystalline solid (1.57 g, 68.4 %).

Chapter 10: Experimental

^1H NMR: (DMSO- d_6 , 400.0 MHz, DMSO internal standard)

δ (ppm) = 10.58 (s, br, 1H, ArOH), 8.00 (d (J = 8.8 Hz), 2H, ArH), 7.95 (d (J = 8.8 Hz), 2H, ArH), 7.92 (d (J = 8.8 Hz), 2H, ArH), 7.84 (d (J = 8.7 Hz), 2H, ArH), 7.39 (d (J = 8.7 Hz), 2H, ArH), 6.94 (d (J = 8.8 Hz), 2H, ArH)

^{13}C NMR: (DMSO- d_6 , 100.4 MHz, DMSO internal standard)

δ (ppm) = 164.30 (1C, COO), 162.88 (1C, ArC-O), 151.35 (1C, ArC-O), 143.86 (1C, ArC), 135.78 (1C, ArC), 132.93 (2C, ArCH), 132.34 (2C, ArCH), 128.33 (2C, ArCH), 127.60 (2C, ArCH), 122.81 (2C, ArCH), 119.12 (1C, ArC), 118.90 (1C, ArC), 115.68 (2C, ArCH), 110.07 (1C, C \equiv N)

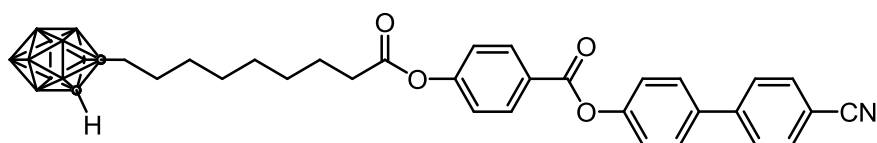
IR (cm^{-1}): 3379 (s, ArH), 2222 (m, CN), 1689 (vs, C=O), 1589 (s, C-O)

Mass (ESI):

m/z = 338.0774 ($\text{M}+\text{Na}$) $^+$, 316.10 ($\text{M}+\text{H}$) $^+$, 275.05, 247.18, 225.20, 198.04, 172.10, 121.03, 73.53, 61.01

calculated = 338.0793 ($\text{M}+\text{Na}$) $^+$

10.3.49 1-Hydrido, 2-(4'-cyanobiphenyl-4-yl 4-(nonanoyloxy)benzoate)dodecacarborane, 29



1-Hydrido, 2-(nonanoic acid)dodecacarborane, **74** (47.7 mg, 0.16 mmol), 4'-cyanobiphenyl-4-yl 4-hydroxybenzoate, **76** (64.3 mg, 0.20 mmol), DMAP (5 mg, 0.02 mmol) and EDAC (31 mg, 0.19 mmol) were dissolved in a solution of DCM (15 mL) and ethyl acetate (10 mL) and stirred for 2 days. The solvent was removed *in vacuo* and the product isolated by flash column chromatography (eluting with DCM,

Chapter 10: Experimental

flash grade silica, R_f - 0.52). The product was recrystallized from cyclohexane to yield **29** as a white crystalline solid (17.0 mg, 17.8 %).

^1H $\{^{10}\text{B}\}$ NMR: (CDCl₃, 500.0 MHz, CHCl₃ internal standard)

δ (ppm) = 8.23 (d (J = 8.6 Hz), 2H, ArH), 7.72 (d (J = 8.2 Hz), 2H, ArH), 7.67 (d (J = 8.2 Hz), 2H, ArH), 7.63 (d (J = 8.5 Hz), 2H, ArH), 7.32 (d (J = 8.5 Hz), 2H, ArH), 7.23 (d (J = 8.5 Hz), 2H, ArH), 3.54 (s, 1H, ClusterH), 2.58 (t (J = 7.4 Hz), 2H, CH₂COO), 2.28 (s, br, 3H, BH), 2.17 (t (J = 8.5 Hz), 2H, CH₂Cluster), 2.17 (s, br, 4H, BH), 2.12 (s, br, 3H, BH), 1.82 – 1.69 (m, 2H, CH₂), 1.52 – 1.37 (m, 4H, CH₂), 1.37 – 1.17 (m, 6H, CH₂)

^{13}C NMR: (100.4 MHz, CDCl₃, CHCl₃ internal standard)

δ (ppm) = 171.73 (1C, COO), 164.44 (1C, COO), 155.21 (1C, ArC), 151.44 (1C, ArC), 144.90 (1C, ArC), 137.16 (1C, ArC), 132.82 (2C, ArC), 132.00 (2C, ArC), 128.58 (2C, ArC), 127.86 (2C, ArC), 126.82 (1C, ArC), 122.58 (2C, ArC), 122.07 (2C, ArC), 119.00 (1C, ArC), 111.22 (1C, CN), 75.49 (2C, C_{cluster}), 61.10 (1C, CH₂COO), 38.21 (1C, CH₂), 34.45 (1C, CH₂), 29.29 (1C, CH₂), 29.13 (1C, CH₂), 29.05 (1C, CH₂), 28.98 (1C, CH₂), 24.83 (1C, CH₂)

^{11}B NMR: (128 MHz, CDCl₃)

δ (ppm) = -3.39 (1B), -6.88 (1B), -10.32 (2B), -12.38 (2B), -13.19 (2B), -14.13 (2B)

IR (cm⁻¹) 3062 (m, ArH), 2924 (m, ArH), 2854 (m, AH), 2569 (vs, br, BH), 2222 (w, CN), 1759 (s, C=O), 1728 (vs, C-O)

Mass (ESI):

m/z = 600.3923 (M+H)⁺, 598.40, 541.13, 380.71, 338.34, 275.17, 225.19

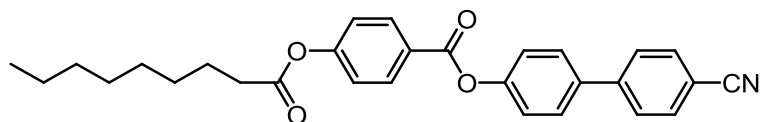
calculated = 600.3888 (M+H)⁺

DSC/POM: Cr₁ 59.4 [0.6] Cr₂ 101.8 [25.6] SmA 139.8 [0.3] N 149.0 [0.3] Iso

CHN microanalysis:

Observed: C 63.97 %, H 6.77 %, N 2.30 %

Calculated: C 62.29 %, H 6.58 %, N 2.34 %

10.3.50 4'-Cyanobiphenyl-4-yl 4-(nonanoyloxy)benzoate, 30

4'-Cyanobiphenyl-4-yl 4-hydroxybenzoate, **76** (50 mg, 0.16 mmol), undecanoic acid (32 mg, 0.20 mmol), EDAC (32 mg, 0.20 mmol) and DMAP (5 mg, 0.02 mmol) were dissolved in DCM (10 mL) and stirred for 4 day. The solvent was removed *in vacuo* and the product purified by flash column chromatography (flash grade silica, DCM, R_f 0.51) yielding **30** as a white crystalline solid (45.6 mg, 62.5 %).

¹H NMR: (400 MHz, CDCl₃, CHCl₃ internal standard)

δ (ppm) = 8.25 (d (J = 8.7 Hz), 2H, ArH), 7.74 (d (J = 8.4 Hz), 2H, ArH), 7.69 (d (J = 8.4 Hz), 2H, ArH), 7.65 (d (J = 8.6 Hz), 2H, ArH), 7.34 (d (J = 8.6 Hz), 2H, ArH), 7.26 (d (J = 8.7 Hz), 2H, ArH), 2.60 (t (J = 7.5 Hz), 2H, CH₂COO), 1.86 – 1.71 (m, 2H, CH₂), 1.50 – 1.18 (m, 10H, CH₂), 0.90 (t (J = 6.8 Hz), 3H, CH₃)

¹³C NMR: (100.4 MHz, CDCl₃, CHCl₃ internal standard)

δ (ppm) = 171.83 (1C, COO), 164.46 (1C, COO), 155.29 (1C, ArC), 151.47 (1C, ArC), 144.91 (1C, ArC), 137.14 (1C, ArC), 132.81 (2C, ArC), 131.98 (2C, ArC), 128.57 (2C, ArC), 127.86 (2C, ArC), 126.77 (1C, ArC), 122.59 (2C, ArC), 122.11 (2C, ArC), 118.99 (1C, ArC), 111.23 (1C, CN), 34.56 (1C, CH₂COO), 31.94 (1C, CH₂), 29.34 (1C, CH₂), 29.25 (1C, CH₂), 29.23 (1C, CH₂), 24.97 (1C, CH₂), 22.79 (1C, CH₂), 14.24 (1C, CH₃)

IR (cm⁻¹): 2924 (m, ArH), 2854 (m, ArH), 2229 (s, CN), 1728 (vs, C=O), 1604 (s, C-O)

Chapter 10: Experimental

Mass (ESI):

m/z = 478.1988 (M+Na)⁺, 456.22 (M+H)⁺, 362.93, 294.94, 226.95

calculated = 478.1994 (M+Na)⁺

DSC/POM: Cr₁ 68.9 [2.7] Cr₂ 83.0 [32.8] SmA 178.7* N 234.9 [0.9] Iso

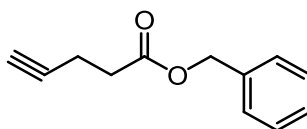
* not detectable by DSC, value given take from microscopy

CHN microanalysis:

Observed: C 75.74 %, H 6.51 %, N 3.07 %

Calculated: C 76.46 %, H 6.42 %, N 3.07 %

10.3.51 Benzyl pent-4-ynoate, **77**



Pent-5-ynoic acid (1.00 g, 10.2 mmol), benzylalcohol (1.32 g, 12.2 mmol), DMAP (0.26 g, 1.02 mmol) and EDAC (1.90 g, 12.2 mmol) were dissolved in DCM (100 mL) and stirred over night. The solvent was removed *in vacuo* and the product was isolated by flash column chromatography (eluting with DCM, flash grade silica, R_f 0.62) to yield **77** as a colourless oil (1.76 g, 91.7 %).

¹H NMR: (CDCl₃, 400.0 MHz, CHCl₃ internal standard)

δ (ppm) = 7.41 – 7.30 (m, 5H, ArH), 5.16 (s, 2H, CH₂O), 2.64 – 2.58 (m, 2H, CH₂), 2.57 – 2.49 (m, 2H, CH₂), 2.01 (t (J = 2.5 Hz), 1H, CH)

¹³C NMR: (CDCl₃, 100.4 MHz, CHCl₃ internal standard)

δ (ppm) = 171.47 (1C, COO), 135.76 (1C, ArC), 128.51 (2C, ArCH), 128.23 (1C, ArC), 128.20 (2C, ArCH), 82.40 (1C, C≡CH), 69.19 (1C, HC≡C), 66.42 (1C, CH₂O), 33.27 (1C, CH₂), 14.30 (1C, CH₂)

IR (cm⁻¹): 3294 (m, ArH), 3032 (w, ArH), 2947 (w, ArH), 2121 (w, C≡C), 1728 (vs, C=O)

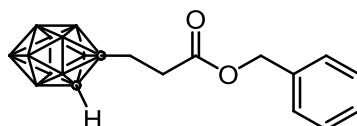
Chapter 10: Experimental

Mass (ESI):

$m/z =$ 211.0730 (M+Na)⁺, 189.09 (M+H)⁺, 129.07, 111.04, 91.05, 61.01

calculated = 211.0735 (M+Na)⁺

10.3.52 1-Hydrido, 2-(benzyl propanoate)dodecacarborane, **78**



Decaborane (1.02 g, 8.35 mmol) was dissolved in dry acetonitrile (30 mL) under Ar and refluxed for 2 h. A solution of benzyl pent-4-ynoate, **77** (1.57 g, 8.35 mmol) in dry toluene (10 mL) was added and the resultant solution refluxed for a further 2 days. The solution was allowed to cool, the solvent removed *in vacuo* and the product extracted with hot hexane (150 mL). The hexane solution was washed with sodium hydroxide in water (10% w/w 50 mL), followed by brine (50 mL x 2), dried over MgSO₄ and the solvent removed *in vacuo* to yield **78** as a white crystalline solid (0.95 g, 37.1 %).

¹H NMR: (CDCl₃, 400.0 MHz, CHCl₃ internal standard)

δ (ppm) = 7.41 – 7.30 (m, 5H, ArH), 5.16 (s, 2H, CH₂OOC), 2.64 – 2.58 (m, 2H, CH₂COO), 2.57 – 2.49 (m, 2H, CH₂Cluster), 2.01 (t ($J = 2.5$ Hz), 1H, BH)

¹³C NMR: (CDCl₃, 100.4 MHz, CHCl₃ internal standard)

δ (ppm) = 171.47 (1C, COO), 135.76 (1C, ArC), 128.51 (2C, ArCH), 128.23 (1C, ArCH), 128.20 (2C, ArCH), 82.40 (1C, ClusterC), 69.19 (1C, ClusterCH), 66.42 (1C, CH₂OOC), 33.27 (1C, CH₂COO), 14.30 (1C, CH₂Cluster)

IR (cm⁻¹): 3062 (m, br, BH), 2931 (w, br, BH), 2576 (vs, br, BH), 1720 (vs, C=O)

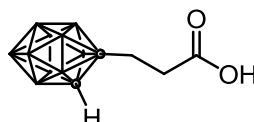
Chapter 10: Experimental

Mass (ESI):

$m/z =$ 331.2466 ($M+Na$)⁺, 305.16, 275.17, 261.13, 217.11, 158.97, 144.06,
122.0811, 102.18, 90.98, 80.95

calculated = 331.2448 ($M+Na$)⁺

10.3.53 1-Hydrido, 2-(propanoic acid)dodecacarborane, **79**



2-(Benzyl propanoate)dodecacarborane, **78** (0.95 g, 3.1 mmol) was dissolved in hexane (30 mL) and Pd on carbon (50 mg) added, the suspension stirred under an atmosphere of H₂ for 3 days. The suspension was passed through a pad of celite and the solvent removed *in vacuo*. The product was purified by flash column chromatography (flash grade silica, eluting with DCM 20 % ethyl acetate, R_f 0.13) to yield **79** as white needles (208 mg, 31.0 %).

¹H NMR: (400 MHz, CDCl₃, CHCl₃ internal standard)

δ (ppm) = 9.68 (s, br, 1H, COOH), 3.68 (s, br, 1H, CH_{cluster}), 2.67 – 2.52 (m, 4H, CH₂)

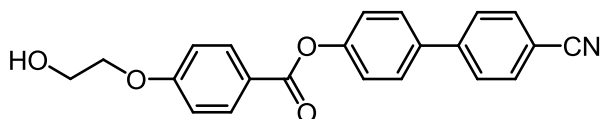
¹³C NMR: (100.4 MHz, CDCl₃, CHCl₃ internal standard)

δ (ppm) = 177.19 (1C, COO), 73.67 (1C, C_{cluster}), 61.74 (1C, CH_{cluster}), 33.28 (1C, CH₂), 32.45 (1C, CH₂)

¹¹B NMR: (128 MHz, CDCl₃)

δ (ppm) = -2.96 (1B), -6.38 (1B), -10.21(2B) , -12.65 (2B), -13.20 (2B), -13.76 (2B)

IR (cm⁻¹): 3047 (w, br, BH), 2924 (w, br, BH), 2569 (vs, br, BH), 1697 (s, C=O)

10.3.54 4'-Cyanobiphenyl-4-yl 4-(2-hydroxyethoxy)benzoate, 80

4'-Cyanobiphenyl-4-yl 4-hydroxybenzoate, **76** (567 mg, 1.8 mmol), 2-bromo-ethanol (225 mg, 1.8 mmol), K_2CO_3 (0.99 g, 7.2 mmol) and KI (50 mg, 0.3 mmol) were suspended in butanone (150 mL) and refluxed over night. The solvent was removed *in vacuo* and the product isolated by flash column chromatography (flash grade silica, DCM 10 % ethyl acetate, R_f 0.33) yielding **80** as a white crystalline solid (236 mg, 36.4 %).

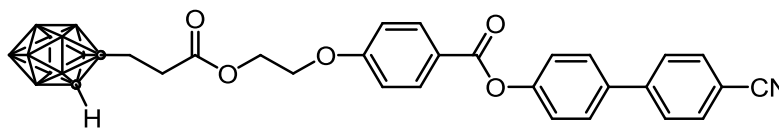
1H NMR: (400 MHz, $CDCl_3$, $CHCl_3$ internal standard)
 δ (ppm) = 7.79 (d (J = 8.6 Hz), 2H, ArH), 7.42 (d (J = 8.4 Hz), 2H, ArH), 7.39 (d (J = 8.5 Hz), 2H, ArH), 7.33 (d (J = 8.4 Hz), 2H, ArH), 6.99 (d (J = 8.5 Hz), 2H, ArH), 6.70 (d (J = 8.8 Hz), 2H, ArH), 4.26 (t (J = 5.5 Hz), 1H, OH), 3.83 (t (J = 4.8 Hz), 2H, CH_2O), 3.59 (m, 2H, CH_2O)

^{13}C NMR: (100.4 MHz, $CDCl_3$, $CHCl_3$ internal standard)
 δ (ppm) = 164.31 (1C, COO), 163.13 (1C, ArH), 151.11 (1C, ArH), 144.34 (1C, ArH), 136.19 (1C, ArH), 132.24 (2C, ArH), 131.88 (2C, ArH), 127.92 (2C, ArH), 127.30 (2C, ArH), 122.16 (2C, ArH), 120.97 (1C, ArH), 118.47 (1C, ArH), 114.13 (2C, ArH), 110.41 (1C, CN), 69.48 (1C, CH_2O), 60.03 (1C, CH_2O)

IR (cm^{-1}): 3471 (vs, br, OH), 3070 (w, ArH), 2924 (w, ArH), 2222 (m, CN), 1720 (vs, C=O), 1604 (s, C-O)

Mass (ESI):
 m/z = 382.1037 ($M+Na$)⁺, 360.12 ($M+H$)⁺, 226.95, 107.04, 90.98
 calculated = 382.1055 ($M+Na$)⁺

10.3.55 1-Hydrido, 2-(4'-cyanobiphenyl-4-yl 4-ethoxybenzoate)propionate)dodecacarborane, 31



4'-Cyanobiphenyl-4-yl 4-(2-hydroxyethoxy)benzoate, **80** (90 mg, 0.25 mmol), 1-hydrido, 2-(propanoic acid)dodecacarborane, **79** (50 mg, 0.23 mmol), EDAC (39 mg, 0.25 mmol) and DMAP (6 mg, 0.025 mmol) were dissolved in DCM (20 mL) and stirred for 4 days. The solvent was removed *in vacuo* and the product isolated by flash column chromatography (flash grade silica, DCM, R_f 0.44) yielding **31** as a white crystalline solid (48.2 mg, 37.6 %).

^1H { ^{11}B } NMR: (500 MHz, CDCl_3 , CHCl_3 internal standard)

δ (ppm) = 8.19 (d (J = 8.9 Hz), 2H, ArH), 7.73 (d (J = 8.4 Hz), 2H, ArH), 7.69 (d (J = 8.4 Hz), 2H, ArH), 7.64 (d (J = 8.6 Hz), 2H, ArH), 7.33 (d (J = 8.6 Hz), 2H, ArH), 7.01 (d (J = 8.9 Hz), 2H, ArH), 4.55 – 4.48 (m, 2H, CH_2O), 4.31 – 4.25 (m, 2H, CH_2O), 3.74 (s, br, 1H, $\text{CH}_{\text{cluster}}$), 2.61 (m, 4H, CH_2), 2.31 (s, br, 3H, BH), 2.17 (s, br, 6H)

^{13}C NMR: (100.4 MHz, CDCl_3 , CHCl_3 internal standard)

δ (ppm) = 171.40 (1C, COO), 164.75 (1C, COO), 162.81 (1C, ArH), 151.60 (1C, ArH), 144.94 (1C, ArH), 136.93 (1C, ArH), 132.78 (1C, ArH), 132.59 (1C, ArH), 128.50 (1C, ArH), 127.82 (1C, ArH), 122.65 (1C, ArH), 122.34 (1C, ArH), 119.01 (1C, ArH), 114.54 (1C, ArH), 111.14 (1C, CN), 73.96 (1C, $\text{C}_{\text{cluster}}$), 65.96 (1C, CH_2O), 63.27 (1C, CH_2O), 61.69 (1C, $\text{CH}_{\text{cluster}}$), 33.46 (1C, CH_2), 32.65 (1C, CH_2)

^{11}B NMR: (128 MHz, CDCl_3)

δ (ppm) = -3.01 (1B), -6.42 (1B), -10.31 (2B), -12.57 (2B), -13.14 (2B), -13.77 (2B)

Chapter 10: Experimental

IR (cm⁻¹): 3062 (w, ArH), 2924 (w, ArH), 2854 (w, ArH), 2576 (vs, br, BH),
2229 (m, CN), 1728 (vs, C=O), 1604 (s, C-O)

Mass (ESI):

m/z = 560.3221 (M+H)⁺, 224.01

calculated = 560.3211 (M+H)⁺

DSC/POM: Cr (48.2 [0.1] N) 122.9 [43.2] Iso

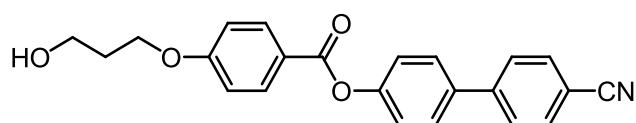
CHN microanalysis:

Observed: C 58.42 %, H 5.77 %, N 2.40 %

Calculated: C 58.15 %, H 5.60 %, N 2.51 %

10.3.56 4'-Cyanobiphenyl-4-yl 4-(3-hydroxypropoxy)benzoate,

81



4'-Cyanobiphenyl-4-yl 4-hydroxybenzoate, **76** (567 mg, 1.8 mmol), K₂CO₃ (0.99 g, 7.2 mmol) and KI (50 mg, 0.3 mmol) were suspended in butanone and brought to reflux. Next 3-bromopropan-1-ol (250 mg, 1.8 mmol) was added and the solution stirred over night. The solvent was removed *in vacuo* and the product recrystallized from toluene to yield **81** as a white crystalline solid (0.42 g, 62.5 %).

¹H NMR: (400 MHz, CDCl₃, CHCl₃ internal standard)

δ (ppm) = 8.17 (d (*J* = 8.8 Hz), 2H, ArH), 7.74 (d (*J* = 8.0 Hz), 2H, ArH), 7.69 (d (*J* = 8.4 Hz), 2H, ArH), 7.64 (d (*J* = 8.5 Hz), 2H, ArH), 7.33 (d (*J* = 8.6 Hz), 2H, ArH), 7.01 (d (*J* = 8.8 Hz), 2H, ArH), 4.23 (t (*J* = 6.0 Hz), 2H, CH₂O), 3.90 (dt (*J* = 10.7, 5.4 Hz), 2H, CH₂OH), 2.18 – 2.04 (m, 2H, CH₂)

Chapter 10: Experimental

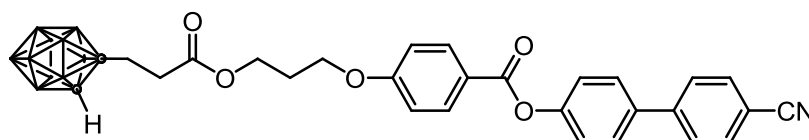
^{13}C NMR: (100.4 MHz, CDCl_3 , CHCl_3 internal standard)
 δ (ppm) = 164.93 (1C, COO), 163.49 (1C, ArC), 151.69 (1C, ArC), 145.01 (1C, ArC), 136.89 (1C, ArC), 132.80 (2C, ArC), 132.54 (2C, ArC), 128.50 (2C, ArC), 127.84 (2C, ArC), 122.70 (2C, ArC), 121.71 (1C, ArC), 119.04 (1C, ArC), 114.52 (2C, ArC), 111.13 (1C, CN), 65.77 (1C, CH_2O), 60.03 (1C, CH_2O), 32.01 (1C, CH_2)

IR (cm^{-1}): 3286 (vs, br, OH), 2924 (w, ArH), 2877 (w, ArH), 2222 (m, CN) 1720 (vs, C=O)

Mass (ESI):

m/z = 396.1207 ($\text{M}+\text{Na}$)⁺, 374.14 ($\text{M}+\text{H}$)⁺, 226.95, 158.96, 90.98
calculated = 396.1212 ($\text{M}+\text{Na}$)⁺

10.3.57 1-Hydrido, 2-(4'-cyanobiphenyl-4-yl 4-propoxybenzoate)propionate)dodecacarborane, **32**



4'-Cyanobiphenyl-4-yl 4-(3-hydroxypropoxy)benzoate, **81** (95 mg, 0.25 mmol), 1-Hydrido, 2-(propanoic acid)dodecacarborane, **79** (50 mg, 0.23 mmol), EDAC (39 mg, 0.25 mmol) and DMAP (6 mg, 0.025 mmol) were dissolved in DCM (10 mL) and stirred for 4 days. The solvent was removed *in vacuo* and the product isolated by flash column chromatography (flash grade silica, DCM, R_f 0.52) yielding **32** as a white crystalline solid (99.8 mg, 75.9 %).

^1H { ^{11}B } NMR: (500 MHz, CDCl_3 , CHCl_3 internal standard)
 δ (ppm) = 8.17 (d (J = 8.9 Hz), 2H, ArH), 7.72 (d (J = 8.4 Hz), 2H, ArH), 7.68 (d (J = 8.5 Hz), 2H, ArH), 7.63 (d (J = 8.6 Hz), 2H, ArH), 7.32 (d (J = 8.6 Hz), 2H, ArH), 6.99 (d (J = 8.9 Hz), 2H, ArH), 4.33 (t (J = 6.3 Hz), 2H, CH_2O), 4.15 (t (J = 6.0 Hz), 2H, CH_2O), 3.73 (s, br, 1H,

Chapter 10: Experimental

CH_{cluster}), 2.57 (m, 4H, CH_2), 2.30 (s, br, 3H, BH), 2.18 (m, 9H, CH_2 + BH)

^{13}C NMR: (100.4 MHz, CDCl_3 , CHCl_3 internal standard)
 δ (ppm) = 171.50 (1C, COO), 164.81 (1C, COO), 163.22 (1C, ArC), 151.60 (1C, ArC), 144.91 (1C, ArC), 136.83 (1C, ArC), 132.75 (2C, ArC), 132.52 (2C, ArC), 128.46 (2C, ArC), 127.79 (2C, ArC), 122.64 (2C, ArC), 121.84 (1C, ArC), 118.99 (1C, ArC), 114.43 (2C, ArC), 111.05 (1C, CN), 74.01 (1C, C_{cluster}), 64.58 (1C, CH_2O), 61.98 (1C, $\text{CH}_{\text{cluster}}$), 61.73 (1C, CH_2O), 33.45 (1C, CH_2), 32.65 (1C, CH_2), 28.45 (1C, CH_2)

^{11}B NMR: (128 MHz, CDCl_3)
 δ (ppm) = -3.05 (1B), -6.47 (1B), -10.33 (2B), -12.61 (2B), -13.10 (2B), -13.77 (2B)

IR (cm^{-1}): 3062 (w, ArH), 2924 (w, ArH), 2854 (w, ArH), 2584 (vs, br BH), 2222 (m, CN), 1720 (s, C=O), 1597 (m, C-O)

Mass (ESI):
 m/z = 574.3422 ($\text{M}+\text{H}$)⁺, 498.90, 430.91, 367.19, 294.94, 226.95
calculated = 574.3368 ($\text{M}+\text{H}$)⁺

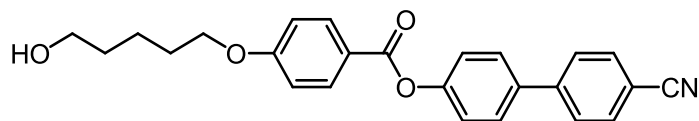
DSC/POM: Cr₁ 35.8 [-13.3] Cr₂ (76.5 [0.1] N) 94.3 [24.5] Iso

CHN microanalysis:

Observed: C 57.95 %, H 5.94 %, N 2.27 %

Calculated: C 58.83 %, H 5.82 %, N 2.45 %

10.3.58 4'-Cyanobiphenyl-4-yl 4-(3-hydroxypentoxy)benzoate, 82



4'-Cyanobiphenyl-4-yl 4-hydroxybenzoate, **76** (500 mg, 1.59 mmol), K_2CO_3 (0.88 g, 6.34 mmol) and KI (50 mg, 0.3 mmol) were suspended in butanone (150 mL) and brought to reflux. Next 5-bromo-pentan-1-ol (0.32 g, 1.9 mmol) was added and the solution refluxed for 4 h. The solvent was removed *in vacuo* and the product purified by recrystallization from toluene to yield **82** as a white crystalline solid (314 mg, 49.2 %).

1H NMR: (400 MHz, $CDCl_3$, $CHCl_3$ internal standard)
 δ (ppm) = 8.16 (d (J = 8.9 Hz), 2H, ArH), 7.74 (d (J = 8.5 Hz), 2H, ArH), 7.68 (d (J = 8.5 Hz), 2H, ArH), 7.64 (d (J = 8.6 Hz), 2H, ArH), 7.33 (d (J = 8.7 Hz), 2H, ArH), 6.98 (d (J = 8.9 Hz), 2H, ArH), 4.07 (t (J = 6.4 Hz), 2H, CH_2O), 3.70 (t (J = 6.3 Hz), 2H, CH_2), 1.93 – 1.83 (m, 2H, CH_2), 1.74 – 1.52 (m, 4H, CH_2)

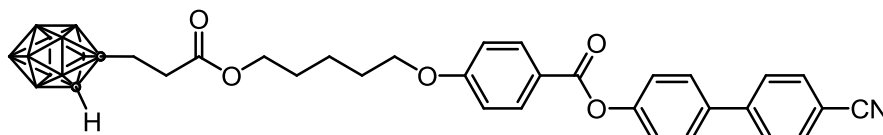
^{13}C NMR: (100.4 MHz, $CDCl_3$, $CHCl_3$ internal standard)
 δ (ppm) = 164.97 (1C, COO), 163.73 (1C, ArC), 151.70 (1C, ArC), 145.01 (1C, ArC), 136.85 (1C, ArC), 132.79 (2C, ArC), 132.51 (2C, ArC), 128.49 (2C, ArC), 127.83 (2C, ArC), 122.70 (2C, ArC), 121.43 (1C, ArC), 119.03 (1C, ArC), 114.48 (2C, ArC), 111.10 (1C, CN), 68.27 (1C, CH_2O), 62.87 (1C, CH_2O), 32.50 (1C, CH_2), 29.02 (1C, CH_2), 22.48 (1C, CH_2)

IR (cm^{-1}): 3533 (vs, br, O-H), 3062 (w, ArH), 2931 (w, ArH), 2222 (s, CN), 1782 (vs, C=O), 1597 (s, C-O)

Mass (ESI):

m/z = 424.1546 (M+Na)⁺, 402.17 (M+H)⁺, 302.62, 282.10, 226.05calculated = 424.1525 (M+Na)⁺

10.3.59 1-Hydrido, 2-(4'-cyanobiphenyl-4-yl 4-pentoxybenzoate propionate)dodecacarborane, **33**



4'-Cyanobiphenyl-4-yl 4-(3-hydroxypentoxy)benzoate, **82** (100 mg, 0.25 mmol), 1-Hydrido, 2-(propanoic acid)dodecacarborane, **79** (50 mg, 0.23 mmol), EDAC (39 mg, 0.25 mmol) and DMAP (6 mg, 0.025 mmol) were dissolved in DCM (25 mL) and stirred for 2 days. The solvent was removed *in vacuo* and the product isolated *via* flash column chromatography (flash grade silica, DCM 5 % ethyl acetate, R_f 0.48). The product was recrystallized from ethanol to yield **33** (42.5 mg, 30.8 %).

¹H {¹¹B} NMR: (500 MHz, CDCl₃, CHCl₃ internal standard)

δ (ppm) = 8.17 (d (J = 8.8 Hz), 2H, ArH), 7.74 (d (J = 8.4 Hz), 2H, ArH), 7.69 (d (J = 8.4 Hz), 2H, ArH), 7.64 (d (J = 8.6 Hz), 2H, ArH), 7.33 (d (J = 8.6 Hz), 2H, ArH), 6.99 (d (J = 8.9 Hz), 2H, ArH), 4.15 (t (J = 6.6 Hz), 2H, CH₂O), 4.08 (t (J = 6.3 Hz), 2H, CH₂O), 3.73 (s, br, 1H, CH_{cluster}), 2.56 (m, 4H, CH₂), 2.31 (s, br, 3H, BH), 2.17 (s, br, 5H, BH), 1.95 – 1.83 (m, 2H, CH₂), 1.79 – 1.69 (m, 2H, CH₂), 1.64 – 1.50 (m, 2H, CH₂)

¹³C NMR: (100.4 MHz, CDCl₃, CHCl₃ internal standard)

δ (ppm) = 171.65 (1C, COO), 164.93 (1C, COO), 163.62 (1C, ArC), 151.69 (1C, ArC), 145.00 (1C, ArC), 136.88 (1C, ArC), 132.79 (2C, ArC), 132.53 (2C, ArC), 128.50 (2C, ArC), 127.84 (2C, ArC), 122.69 (2C, ArC), 121.58 (1C, ArC), 119.03 (1C, ArC), 114.46 (2C, ArC), 111.13 (1C, CN), 74.12 (1C, C_{cluster}), 68.04 (1C, CH₂O), 65.22 (1C, CH₂O), 61.70

Chapter 10: Experimental

(1C, CH_{cluster}), 33.56 (1C, CH₂), 32.76 (1C, CH₂), 28.84 (1C, CH₂), 28.41 (1C, CH₂), 22.69 (1C, CH₂)

¹¹B NMR: (128 MHz, CDCl₃)

δ (ppm) = -3.02 (1B), -6.48 (1B), -10.34 (2B), -12.56 (2B), -13.13 (2B), -13.80 (2B)

IR (cm⁻¹): 3047 (w, ArH), 2924 (w, ArH), 2854(w, ArH), 2576 (s, br, BH), 2222 (m, CN), 1712 (vs, C=O), 1597 (m, C-O)

Mass (ESI):

m/z = 624.3532 (M+Na)⁺, 602.37 (M+H)⁺, 405.31

calculated = 624.3500 (M+Na)⁺

DSC/POM: Cr (99.6 [0.1] SmA 119.0 [0.4] N) 145.8 [42.6] Iso

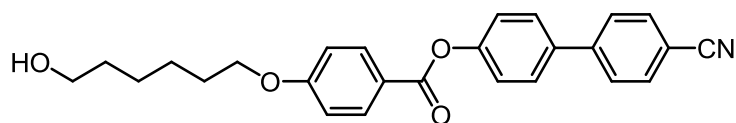
CHN microanalysis:

Observed: C 60.31 %, H 6.16 %, N 2.10 %

Calculated: C 60.08 %, H 6.22 %, N 2.34 %

10.3.60 4'-Cyanobiphenyl-4-yl 4-(6-hydroxyhexyloxy)benzoate,

83



4'-Cyanobiphenyl-4-yl 4-hydroxybenzoate, **76** (0.1 g, 0.32 mmol), K₂CO₃ (0.22 g, 1.6 mmol) and KI (50 mg, 0.3 mmol) were suspended in butanone (30 mL) and brought to reflux. Next 6-bromo-hexan-1-ol (73 mg, 0.4 mmol) was added and the solution refluxed for 6 h. The solution was allowed to cool, the solids filtered and the solvent removed *in vacuo*. The product was isolated by flash column chromatography (flash grade silica, DCM 4 % ethyl acetate, R_f 0.78) to yield **83** as a white crystalline solid (111 mg, 83.5 %).

Chapter 10: Experimental

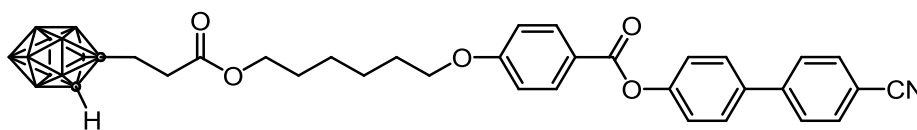
^1H NMR: (400 MHz, CDCl_3 , CHCl_3 internal standard)
 δ (ppm) = 8.15 (d (J = 8.8 Hz), 2H, ArH), 7.73 (d (J = 8.3 Hz), 2H, ArH), 7.68 (d (J = 8.4 Hz), 2H, ArH), 7.63 (d (J = 8.6 Hz), 2H, ArH), 7.32 (d (J = 8.6 Hz), 2H, ArH), 6.98 (d (J = 8.9 Hz), 2H, ArH), 4.06 (t (J = 6.5 Hz), 2H, CH_2O), 3.67 (t (J = 6.5 Hz), 2H, CH_2O), 1.91 – 1.79 (m, 2H, CH_2), 1.69 – 1.58 (m, 2H, CH_2), 1.58 – 1.39 (m, 4H, CH_2)

^{13}C NMR: (100.4 MHz, CDCl_3 , CHCl_3 internal standard)
 δ (ppm) = 164.95 (1C, COO), 163.76 (1C, ArC), 151.69 (1C, ArC), 144.98 (1C, ArC), 136.81 (1C, ArC), 132.76 (2C, ArC), 132.48 (2C, ArC), 128.46 (2C, ArC), 127.80 (2C, ArC), 122.68 (2C, ArC), 121.37 (1C, ArC), 119.00 (1C, ArC), 114.48 (2C, ArC), 111.08 (1C, CN), 68.31 (1C, CH_2O), 62.93 (1C, CH_2O), 32.74 (1C, CH_2), 29.18 (1C, CH_2), 25.95 (1C, CH_2), 25.65 (1C, CH_2)

Mass (ESI):

m/z = 438.1676 ($\text{M}+\text{Na}$)⁺, 416.19 ($\text{M}+\text{H}$)⁺, 344.19, 317.61, 297.09, 224.01
calculated = 438.1681 ($\text{M}+\text{Na}$)⁺

10.3.61 1-Hydrido, 2-(4'-cyanobiphenyl-4-yl 4-hexyloxybenzoate propionate)dodecacarborane, **34**



4'-Cyanobiphenyl-4-yl 4-(6-hydroxyhexyloxy)benzoate, **83** (69 mg, 0.166 mmol), 1-hydrido, 2-(propanoic acid)dodecacarborane, **79** (30 mg, 0.139 mmol), EDAC (30 mg, 0.194 mmol) and DMAP (4 mg, 0.019 mmol) were dissolved in DCM (15 mL) and stirred for 3 days. The solvent was removed *in vacuo* and the product isolated by flash column chromatography (flash grade silica, DCM, R_f 0.30) yielding **34** (71.8 mg, 84.2 %).

Chapter 10: Experimental

^1H { ^{11}B } NMR: (500 MHz, CDCl_3 , CHCl_3 internal standard)

δ (ppm) = 8.16 (d ($J = 8.9$ Hz), 2H, ArH), 7.74 (d ($J = 8.5$ Hz), 2H, ArH), 7.69 (d ($J = 8.6$ Hz), 2H, ArH), 7.64 (d ($J = 8.7$ Hz), 2H, ArH), 7.33 (d ($J = 8.7$ Hz), 2H, ArH), 6.98 (d ($J = 8.9$ Hz), 2H, ArH), 4.12 (t ($J = 6.7$ Hz), 2H, CH_2O), 4.06 (t ($J = 6.4$ Hz), 2H, CH_2O), 3.73 (s, br, 1H, $\text{CH}_{\text{cluster}}$), 2.65 – 2.50 (m, 4H, CH_2), 2.31 (s, br, 3H, BH), 2.17 (s, 5H, BH), 1.92 – 1.81 (m, 2H, CH_2), 1.73 – 1.65 (m, 2H, CH_2), 1.60 – 1.50 (m, 2H, CH_2), 1.50 – 1.41 (m, 2H, CH_2)

^{13}C NMR: (100.4 MHz, CDCl_3 , CHCl_3 internal standard)

δ (ppm) = 171.66 (1C, COO), 164.94 (1C, COO), 163.70 (1C, ArC), 151.68 (1C, ArC), 144.99 (1C, ArC), 136.85 (1C, ArC), 132.78 (2C, ArC), 132.51 (2C, ArC), 128.48 (2C, ArC), 127.82 (2C, ArC), 122.69 (2C, ArC), 121.47 (1C, ArC), 119.02 (1C, ArC), 114.47 (2C, ArC), 111.11 (1C, CN), 74.14 (1C, $\text{C}_{\text{cluster}}$), 68.19 (1C, CH_2O), 65.33 (1C, CH_2O), 61.68 (1C, $\text{CH}_{\text{cluster}}$), 33.56 (1C, CH_2), 32.75 (1C, CH_2), 29.10 (1C, CH_2), 28.57 (1C, CH_2), 25.81 (1C, CH_2), 25.79 (1C, CH_2)

^{11}B NMR: (128 MHz, CDCl_3)

δ (ppm) = -3.03 (1B), -6.48 (1B), -10.35 (2B), -12.55 (2B), -13.11 (2B), -13.81 (2B)

IR (cm^{-1}): 3047 (m, ArH), 2947 (m, ArH), 2854 (m, ArH), 2576 (vs, br BH), 2229 (m, CN), 1728 (vs, C=O), 1597 (s, C-O)

Mass (ESI):

m/z = 638.3754 ($\text{M}+\text{Na}$)⁺, 566.89, 498.90, 483.51, 430.92

calculated = 638.3656 ($\text{M}+\text{Na}$)⁺

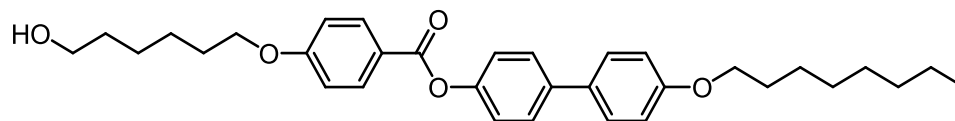
DSC/POM: Cr (92.5 SmA [0.1] 108.5 [0.2] N) 158.4 [59.8] Iso

CHN microanalysis:

Observed: C 59.97 %, H 6.37 %, N 20.1 %

Calculated: C 60.66 %, H 6.40 %, N 2.28 %

10.3.62 4'-(octyloxy)biphenyl-4-yl 4-(6-hydroxyhexyloxy)benzoate, 84



4'-(Octyloxy)biphenyl-4-yl 4-hydroxybenzoate, **63** (0.33 g, 0.788 mmol), K_2CO_3 (0.33 g, 2.36 mmol) and KI (50 mg, 0.3 mmol) were suspended in butanone (50 mL) and brought to reflux. Next 6-bromo-hexan-1-ol (0.14 g, 0.788 mmol) was added and the solution refluxed for 5 h. The solution was allowed to cool, the solids filtered and the solvent removed *in vacuo*. The product was recrystallized from ethanol to yield **84** as a white crystalline solid (284 mg, 69.5 %).

1H NMR: (400 MHz, $CDCl_3$, $CHCl_3$ internal standard)

δ (ppm) = 8.16 (d (J = 9.0 Hz), 2H, ArH), 7.58 (d (J = 8.7 Hz), 2H, ArH), 7.51 (d (J = 8.8 Hz), 2H, ArH), 7.24 (d (J = 8.7 Hz), 2H, ArH), 6.97 (dd (J = 8.9, 2.2 Hz), 4H, ArH), 4.06 (t (J = 6.5 Hz), 2H, CH_2O), 4.00 (t (J = 6.6 Hz), 2H, CH_2O), 3.68 (t (J = 6.5 Hz), 2H, CH_2O), 1.92 – 1.76 (m, 4H, CH_2), 1.69 – 1.58 (m, 2H, CH_2), 1.58 – 1.41 (m, 6H, CH_2), 1.41 – 1.21 (m, 8H, CH_2), 0.89 (t (J = 6.9 Hz), 3H, CH_3)

^{13}C NMR: (100.4 MHz, $CDCl_3$, $CHCl_3$ internal standard)

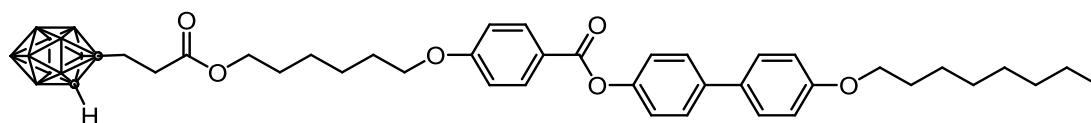
δ (ppm) = 165.21 (1C, COO), 163.60 (1C, ArC), 158.87 (1C, ArC), 150.09 (1C, ArC), 138.68 (1C, ArC), 132.91 (1C, ArC), 132.44 (2C, ArC), 128.23 (2C, ArC), 127.82 (2C, ArC), 122.12 (2C, ArC), 121.73 (1C, ArC), 114.93 (2C, ArC), 114.41 (2C, ArC), 68.27 (1C, CH_2O), 68.24 (1C, CH_2O), 63.00 (1C, CH_2O), 32.77 (1C, CH_2), 31.96 (1C, CH_2), 29.51 (1C, CH_2), 29.43 (1C, CH_2), 29.40 (1C, CH_2), 29.21 (1C, CH_2), 26.20 (1C, CH_2), 25.98 (1C, CH_2), 25.67 (1C, CH_2), 22.81 (1C, CH_2), 14.26 (1C, CH_3)

IR (cm^{-1}): 3286 (vs, br, OH), 2924 (s, ArH), 2854 (s, ArH), 1720 (vs, C=O), 1604 (s, C-O)

Mass (ESI):

m/z = 541.2906 (M+Na)⁺, 519.31 (M+H)⁺, 360.32, 321.11calculated = 541.2930 (M+Na)⁺

10.3.63 1-Hydrido, 2-(4'-(octyloxy)biphenyl-4-yl 4-(6-hydroxyhexyloxy)benzoate propionate)dodecacarborane, **35**



4'-(Octyloxy)biphenyl-4-yl 4-(6-hydroxyhexyloxy)benzoate, **84** (70 mg, 0.135 mmol), 1-hydrido, 2-(propanoic acid)dodecacarborane, **79** (35 mg, 0.165 mmol), EDAC (25 mg, 0.165 mmol) and DMAP (4 mg, 0.0165 mmol) were dissolved in DCM (10 mL) and stirred for 3 days. The solvent was removed *in vacuo* and the product was purified by flash column chromatography (flash grade silica, DCM, R_F 0.44) to yields **35** as a white waxy solid (29 mg, 30.0 %).

¹H NMR: (400 MHz, CDCl₃, CHCl₃ internal standard)

δ (ppm) = 8.16 (d (*J* = 8.9 Hz), 2H, ArH), 7.58 (d (*J* = 8.7 Hz), 2H, ArH), 7.51 (d (*J* = 8.8 Hz), 2H, ArH), 7.24 (d (*J* = 8.7 Hz), 2H, ArH), 6.97 (dd (*J* = 8.8, 1.5 Hz), 4H, ArH), 4.12 (t (*J* = 6.7 Hz), 2H, CH₂O), 4.06 (t (*J* = 6.4 Hz), 2H, CH₂O), 4.00 (t (*J* = 6.6 Hz), 2H, CH₂O), 3.73 (s, br, 1H, CH_{cluster}), 2.63 – 2.49 (m, 4H, CH₂), 1.91 – 1.75 (m, 4H, CH₂), 1.75 – 1.64 (m, 2H, CH₂), 1.57 – 1.41 (m, 6H, CH₂), 1.41 – 1.22 (m, 8H, CH₂), 0.89 (t (*J* = 6.9 Hz), 3H, CH₃)

¹³C NMR: (100.4 MHz, CDCl₃, CHCl₃ internal standard)

δ (ppm) = 171.69 (1C, COO), 165.17 (1C, COO), 163.52 (1C, ArC), 158.87 (1C, ArC), 150.07 (1C, ArC), 138.70 (1C, ArC), 132.89 (1C, ArC), 132.46 (2C, ArC), 128.23 (2C, ArC), 127.83 (2C, ArC), 122.11 (2C, ArC), 121.81 (1C, ArC), 114.92 (2C, ArC), 114.38 (2C, ArC), 74.13 (1C,

Chapter 10: Experimental

C_{cluster}), 68.23 (1C, CH_2O), 68.14 (1C, CH_2O), 65.36 (1C, CH_2O), 61.68 (1C, $\text{CH}_{\text{cluster}}$), 33.56 (1C, CH_2), 32.74 (1C, CH_2), 31.97 (1C, CH_2), 29.52 (1C, CH_2), 29.43 (1C, CH_2), 29.40 (1C, CH_2), 29.11 (1C, CH_2), 28.57 (1C, CH_2), 26.21 (1C, CH_2), 25.83 (1C, CH_2), 25.80 (1C, CH_2), 22.81 (1C, CH_2), 14.27 (1C, CH_3)

^{11}B NMR: (128 MHz, CDCl_3)
 δ (ppm) = -3.03 (1B), -6.49 (1B), -10.35 (2B), -12.54 (2B), -13.12 (2B), -13.80 (2B)

IR (cm^{-1}): 3062 (w, ArH), 2924 (s, ArH), 2854 (s, ArH), 2584 (vs, br, BH), 1728 (vs, C=O), 1604 (s, C-O)

Mass (LIFDI):

m/z = 716.51 (M^+)

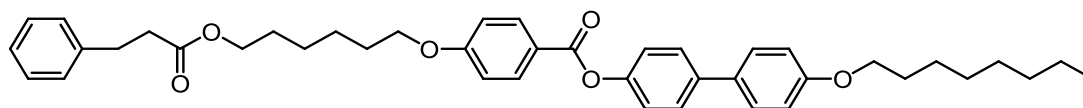
DSC/POM: Cr_1 72.2 [6.0] Cr_2 84.1 [16.3] SmA 93.0 [1.5] Iso

CHN microanalysis: (V_2O_5 combustion agent)

Observed: C 64.00 %, H 7.95 %, N 0.00 %

Calculated: C 63.66 %, H 7.87 %, N 0.00 %

10.3.64 4'-(Octyloxy)biphenyl-4-yl 4-(6-(3-phenylpropanoyloxy)hexyloxy)benzoate, **36**



4'-(Octyloxy)biphenyl-4-yl 4-(6-hydroxyhexyloxy)benzoate, **84** (70 mg, 0.135 mmol), hydrocinnamic acid (24 mg, 0.162 mmol), EDAC (25 mg, 0.162 mmol) and DMAP (4 mg, 0.016 mmol) were dissolved in DCM (10 mL) and stirred for 3 days. The solvent was removed *in vacuo* and the product isolated by flash column

Chapter 10: Experimental

chromatography (flash grade silica, DCM, R_f 0.28) to yield **36** as a waxy white solid (58 mg, 66.0 %).

^1H NMR: (400 MHz, CDCl_3 , CHCl_3 internal standard)
 δ (ppm) = 8.17 (d (J = 8.9 Hz), 2H, ArH), 7.59 (d (J = 8.6 Hz), 2H, ArH), 7.52 (d (J = 8.8 Hz), 2H, ArH), 7.35 – 7.16 (m, 7H, ArH), 6.98 (d (J = 8.9 Hz), 4H, ArH), 4.10 (t (J = 6.6 Hz), 2H, CH_2O), 4.04 (t (J = 6.4 Hz), 2H, CH_2O), 4.00 (t (J = 6.6 Hz), 2H, CH_2O), 2.96 (t (J = 7.8 Hz), 2H, CH_2), 2.65 (t (J = 7.8 Hz), 2H, CH_2), 1.90 – 1.76 (m, 4H, CH_2), 1.72 – 1.60 (m, 2H, CH_2), 1.58 – 1.45 (m, 4H, CH_2), 1.45 – 1.22 (m, 10H, CH_2), 0.90 (t (J = 6.9 Hz), 3H, CH_3)

^{13}C NMR: (100.4 MHz, CDCl_3 , CHCl_3 internal standard)
 δ (ppm) = 173.12 (1C, COO), 165.15 (1C, COO), 163.54 (1C, ArC), 158.85 (1C, ArC), 150.07 (1C, ArC), 140.63 (1C, ArC), 138.65 (1C, ArC), 132.87 (1C, ArC), 132.42 (2C, ArC), 128.60 (2C, ArC), 128.40 (2C, ArC), 128.21 (2C, ArC), 127.79 (2C, ArC), 126.37 (1C, ArC), 122.10 (2C, ArC), 121.74 (1C, ArC), 114.89 (2C, ArC), 114.37 (2C, ArC), 68.20 (1C, CH_2O), 68.17 (1C, CH_2O), 64.52 (1C, CH_2O), 36.02 (1C, CH_2), 31.95 (1C, CH_2), 31.10 (1C, CH_2), 29.50 (1C, CH_2), 29.41 (1C, CH_2), 29.38 (1C, CH_2), 29.09 (1C, CH_2), 28.65 (1C, CH_2), 26.19 (1C, CH_2), 25.80 (2C, CH_2), 22.79 (1C, CH_2), 14.25 (1C, CH_3)

IR (cm^{-1}): 2924 (s, ArH), 2854 (s, ArH), 1782 (vs, C=O), 1604 (s, C-O)

Mass (ESI):

m/z = 673.3505 ($\text{M}+\text{Na}$)⁺, 615.14, 541.12, 360.33

calculated = 673.3505 ($\text{M}+\text{Na}$)⁺

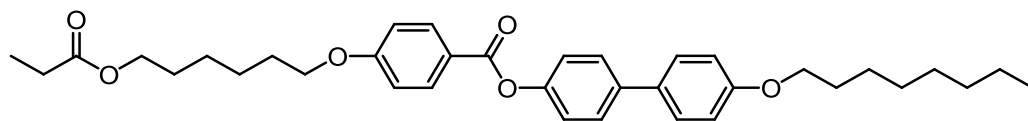
DSC/POM: Cr₁ 63.1 [16.3] Cr₂ 85.4 [24] SmC 109.9 [0.6] N 136.6 [0.7] Iso

CHN microanalysis:

Observed: C 77.149 %, 7.769 %, 0.00 %

Calculated: C 77.51 %, H 7.74 %, N 0.00 %

10.3.65 4'-(Octyloxy)biphenyl-4-yl 4-(6-(propionyloxy)hexyloxy)benzoate, 37



4'-(Octyloxy)biphenyl-4-yl 4-(6-hydroxyhexyloxy)benzoate, **84** (70 mg, 0.135 mmol), propionic acid (13 mg, 0.165 mmol), EDAC (24 mg, 0.165 mmol) and DMAP (4 mg, 0.016 mmol) were dissolved in DCM (10 mL) and stirred for 3 days. The solvent was removed *in vacuo* and the product purified by flash column chromatography (flash grade silica, DCM, R_f 0.26) to yield **37** as a white crystalline solid.

^1H NMR: (400 MHz, CDCl_3 , CHCl_3 internal standard)

δ (ppm) = 8.17 (d (J = 8.9 Hz), 2H, ArH), 7.59 (d (J = 8.6 Hz), 2H, ArH), 7.51 (d (J = 8.7 Hz), 2H, ArH), 7.25 (d (J = 8.6 Hz), 2H, ArH), 7.02 – 6.90 (m, 4H, ArH), 4.10 (t (J = 6.7 Hz), 2H, CH_2O), 4.05 (t (J = 6.4 Hz), 2H, CH_2O), 4.00 (t (J = 6.6 Hz), 2H, CH_2O), 2.34 (q (J = 7.6 Hz), 2H, CH_2COO), 1.91 – 1.76 (m, 4H, CH_2), 1.76 – 1.62 (m, 2H, CH_2), 1.60 – 1.41 (m, 6H, CH_2), 1.41 – 1.22 (m, 8H, CH_2), 1.15 (t (J = 7.6 Hz), 3H, CH_3), 0.90 (t (J = 6.8 Hz), 3H, CH_3)

^{13}C NMR: (100.4 MHz, CDCl_3 , CHCl_3 internal standard)

δ (ppm) = 174.70 (1C, COO), 165.13 (1C, COO), 163.53 (1C, ArC), 158.84 (1C, ArC), 150.06 (1C, ArC), 138.63 (1C, ArC), 132.85 (1C, ArC), 132.40 (2C, ArC), 128.19 (2C, ArC), 127.77 (2C, ArC), 122.09 (2C, ArC), 121.72 (1C, ArC), 114.88 (2C, ArC), 114.36 (2C, ArC), 68.17 (2C, CH_2O), 64.35 (1C, CH_2O), 31.94 (1C, CH_2), 29.49 (1C, CH_2), 29.40 (1C, CH_2), 29.37 (1C, CH_2), 29.10 (1C, CH_2), 28.68 (1C, CH_2), 27.71 (1C, CH_2), 26.18 (1C, CH_2), 25.83 (1C, CH_2), 25.81 (1C, CH_2), 22.78 (1C, CH_2), 14.24 (1C, CH_3), 9.28 (1C, CH_3)

Chapter 10: Experimental

IR (cm⁻¹): 2924 (s, ArH), 2854 (m, ArH), 1728 (vs, C=O), 1604 (m, C-O)

Mass (ESI):

m/z = 597.3163 (M+Na)⁺, 541.12, 519.14, 413.27

calculated = 597.3192 (M+Na)⁺

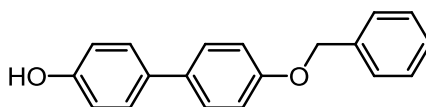
DSC/POM: Cr₁ 80.4 [1.2] Cr₂ 95.8 [24.5] SmC 142.0 [0.2] SmA 145.8 [0.3] N
168.4 [1.3] Iso

CHN microanalysis:

Observed: C 75.203 %, H 8.009 %, N 0.00 %

Calculated: C 75.23 %, H 8.07 %, N 0.00 %

10.3.66 4'-(Benzyloxy)biphenyl-4-ol, **85**



4, 4'-Biphenol (5.00 g, 26.9 mmol), K₂CO₃ (7.42 g, 53.7 mmol) and KI (50 mg, 0.3 mmol) were suspended in butanone (500 mL) and brought to reflux. Next a solution of benzyl bromide (3.09 g, 18.1 mmol) in butanone (100 mL) was added drop-wise and the solution refluxed over night. The solution was allowed to cool, the solid filtered and the solvent removed *in vacuo*. The product was isolated by flash column chromatography (flash grades silica, DCM 6 % ethyl acetate, R_f 0.58) and then purified by recrystallization from ethanol to yield **85** as a white crystalline solid (2.04 g, 40.8 %).

¹H NMR: (400 MHz, CDCl₃, CHCl₃ internal standard)

δ (ppm) = 7.34 – 7.06 (m, 9H, ArH), 6.81 (d (*J* = 8.4 Hz), 2H, ArH), 6.69 (d (*J* = 8.4 Hz), 2H, ArH), 4.90 (s, 2H, CH₂O)

¹³C NMR: (100.4 MHz, CDCl₃, CHCl₃ internal standard)

Chapter 10: Experimental

δ (ppm) = 156.05 (1C, ArC), 155.30 (1C, ArC), 135.69 (1C, ArC), 132.22 (1C, ArC), 129.87 (1C, ArC), 127.11 (2C, ArC), 126.50 (1C, ArC), 126.16 (2C, ArC), 125.99 (2C, ArC), 125.85 (2C, ArC), 114.42 (2C, ArC), 113.72 (2C, ArC), 68.32 (1C, CH₂O)

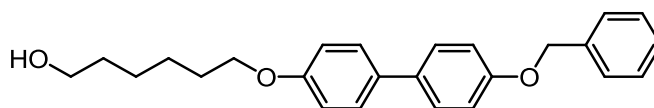
IR (cm⁻¹): 3379 (vs, br, OH), 3039 (w, ArH), 2908 (w, ArH), 2870 (w, ArH), 1604 (s, C-O)

Mass (ESI):

m/z = 299.1041 (M+Na)⁺, 277.12 (M+H)⁺, 139.07

calculated = 299.1048 (M+Na)⁺

10.3.67 6-(4'-(Benzyloxy)biphenyl-4-yloxy)hexan-1-ol, **86**



4'-(Benzyloxy)biphenyl-4-ol, **85** (1.00 g, 3.62 mmol), K₂CO₃ (1.50 g, 10.86 mmol) and KI (50 mg, 0.3 mmol) were suspended in butanone (100 mL) and brought to reflux. Next 6-bromo-hexan-1-ol (0.786 g, 4.34 mmol) was added and the solution refluxed for 1 day. The solution was allowed to cool, the solids filtered and the solvent removed *in vacuo*. The product was recrystallized twice from ethanol to yield **86** as a white crystalline solid (0.7 g, 49.2 %).

¹H NMR: (400 MHz, ACETONE-D₆, 35 °C, Acetone internal standard)

δ (ppm) = 7.57 – 7.46 (m, 6H, ArH), 7.44 – 7.28 (m, 3H, ArH), 7.08 (d (*J* = 8.8 Hz), 2H, ArH), 6.98 (d (*J* = 8.8 Hz), 2H, ArH), 5.16 (s, 2H, CH₂O), 4.03 (t (*J* = 6.5 Hz), 2H CH₂O), 3.50 (dd (*J* = 12.5, 6.2 Hz), 2H, CH₂OH), 1.86 – 1.73 (m, 2H, CH₂), 1.57 – 1.37 (m, 6H, CH₂)

¹³C NMR: (100.4 MHz, ACETONE-D₆, 35 °C, Acetone internal standard)

δ (ppm) = 159.16 (1C, ArC), 158.74 (1C, ArC), 138.33 (1C, ArC), 134.13 (1C, ArC), 133.60 (1C, ArC), 129.17 (2C, ArC), 128.48 (2C, ArC), 128.29

Chapter 10: Experimental

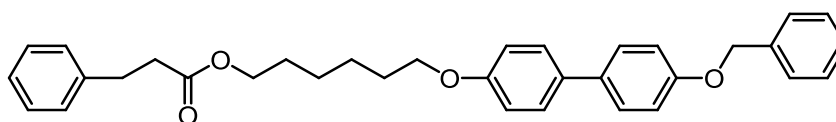
(2C, ArC), 128.14 (3C, ArC), 115.98 (2C, ArC), 115.59 (2C, ArC), 70.38 (1C, CH₂O), 68.48 (1C, CH₂O), 61.98 (1C, CH₂O), 61.85 (1C, CH₂), 33.60 (1C, CH₂), 26.52 (1C, CH₂), 26.34 (1C, CH₂)

Mass (ESI):

m/z = 399.1931 (M+Na)⁺, 377.21 (M+H)⁺, 179.02, 101.00

calculated = 399.1936 (M+Na)⁺

10.3.68 6-(4'-(Benzyloxy)biphenyl-4-yloxy)hexyl 3-phenylpropanoate, **87**



6-(4'-(Benzyloxy)biphenyl-4-yloxy)hexan-1-ol, **86** (210 mg, 0.56 mmol), hydrocinnamic acid (105 mg, 0.70 mmol), EDAC (109 mg, 0.70 mmol) and DMAP (18 mg, 0.07 mmol) were dissolved in DCM (50 mL) and stirred over night. The solvent was removed *in vacuo* and the product isolated by flash column chromatography (flash grade silica, DCM, R_f 0.38) to yield **87** as a white crystalline solid (252 mg, 88.5 %).

¹H NMR: (400 MHz, CDCl₃, CHCl₃ internal standard)

δ (ppm) = 7.58 – 7.47 (m, 6H, ArH), 7.46 – 7.42 (m, 2H, ArH), 7.39 (d (*J* = 7.2 Hz), 1H, ArH), 7.37 – 7.30 (m, 2H, ArH), 7.27 – 7.24 (m, 3H, ArH), 7.07 (d (*J* = 8.6 Hz), 2H, ArH), 6.99 (d (*J* = 8.5 Hz), 2H, ArH), 5.13 (s, 2H, CH₂O), 4.13 (t (*J* = 6.6 Hz), 2H, CH₂O), 4.02 (t (*J* = 6.4 Hz), 2H, CH₂O), 3.00 (t (*J* = 7.8 Hz), 2H, CH₂), 2.68 (t (*J* = 7.8 Hz), 2H, CH₂), 1.90 – 1.79 (m, 2H, CH₂), 1.75 – 1.63 (m, 2H, CH₂), 1.60 – 1.49 (m, 2H, CH₂), 1.49 – 1.38 (m, 2H, CH₂)

¹³C NMR: (100.4 MHz, CDCl₃, CHCl₃ internal standard)

δ (ppm) = 173.09 (1C, COO), 158.29 (1C, ArC), 157.97 (1C, ArC), 140.63 (1C, ArC), 137.13 (1C, ArC), 133.82 (1C, ArC), 133.34 (1C, ArC), 128.70

(2C, ArC), 128.58 (2C, ArC), 128.39 (2C, ArC), 128.06 (1C, ArC), 127.80 (3C, ArC), 127.58 (2C, ArC), 126.34 (2C, ArC), 115.18 (2C, ArC), 114.81 (2C, ArC), 70.15 (1C, CH₂O), 67.90 (1C, CH₂O), 64.56 (1C, CH₂O), 36.01 (1C, CH₂), 31.09 (1C, CH₂), 29.27 (1C, CH₂), 28.66 (1C, CH₂), 25.86 (1C, CH₂), 25.81 (1C, CH₂)

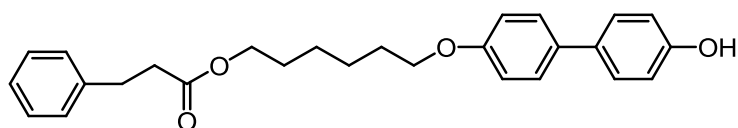
IR (cm⁻¹): 3032 (w, ArH), 2931 (m, ArH), 2862 (m, ArH), 1728 (vs, C=O), 1604 (s, C-O)

Mass (ESI):

m/z = 531.2480 (M+Na)⁺, 509.27 (M+H)⁺

calculated = 531.2511 (M+Na)⁺

10.3.69 6-(4'-Hydroxybiphenyl-4-yloxy)hexyl 3-phenylpropanoate, **88**



6-(4'-(Benzyloxy)biphenyl-4-yloxy)hexyl 3-phenylpropanoate, **87** (252 mg, 0.495 mmol) was dissolved in THF (25 mL) and Pd on carbon (50 mg) added. The suspension was stirred under an atmosphere of H₂ for 2 days. The suspension was filtered through celite and the solvent removed *in vacuo*. The product was purified by flash column chromatography (flash grade silica, DCM, R_f 0.38) to yield **88** as a white crystalline solid (185 mg, 89.3 %).

¹H NMR: (400 MHz, CDCl₃, CHCl₃ internal standard)

δ (ppm) = 7.47 (d (*J* = 8.7 Hz), 2H, ArH), 7.44 (d (*J* = 8.6 Hz), 2H, ArH), 7.36 – 7.28 (m, 2H, ArH), 7.28 – 7.19 (m, 3H, ArH), 6.96 (d (*J* = 8.7 Hz), 2H, ArH), 6.92 (d (*J* = 8.6 Hz), 2H, ArH), 4.13 (t (*J* = 6.6 Hz), 2H, CH₂O), 4.00 (t (*J* = 6.4 Hz), 2H, CH₂O), 2.99 (t (*J* = 7.8 Hz), 2H, CH₂), 2.68 (t (*J* = 7.8 Hz), 2H, CH₂), 1.90 – 1.77 (m, 2H, CH₂), 1.75 –

Chapter 10: Experimental

1.62 (m, 2H, CH_2), 1.57 – 1.46 (m, 2H, CH_2), 1.46 – 1.34 (m, 2H, CH_2)

^{13}C NMR: (100.4 MHz, $CDCl_3$, $CHCl_3$ internal standard)
 δ (ppm) = 173.68 (1C, COO), 158.16 (1C, ArC), 155.07 (1C, ArC), 140.48 (1C, ArC), 133.49 (1C, ArC), 133.43 (1C, ArC), 128.58 (2C, ArC), 128.37 (1C, ArC), 127.95 (1C, ArC), 127.74 (1C, ArC), 126.37 (1C, ArC), 115.74 (1C, ArC), 114.84 (1C, ArC), 67.96 (1C, CH_2O), 64.81 (1C, CH_2O), 36.06 (1C, CH_2), 31.07 (1C, CH_2), 29.23 (1C, CH_2), 28.59 (1C, CH_2), 25.81 (1C, CH_2), 25.76 (1C, CH_2)

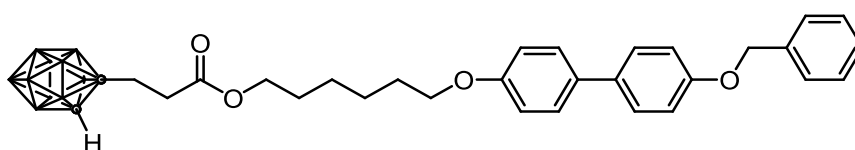
IR (cm^{-1}): 3387 (vs, br OH), 3062 (w, ArH), 2931 (m, ArH), 2862 (m, ArH), 1705 (vs, C=O), 1612 (s, C-O)

Mass (ESI):

m/z = 441.2044 ($M+Na$)⁺

calculated = 441.2042 ($M+Na$)⁺

10.3.70 1-Hydrido, 2-([6-(4'-(benzyloxy)biphenyl-4-yloxy)hexyl] propionate)dodecacarborane, **89**



6-(4'-(Benzyloxy)biphenyl-4-yloxy)hexan-1-ol, **86** (210 mg, 0.56 mmol), 1-hydrido, 2-(propanoic acid)dodecacarborane, **79** (151 mg, 0.70 mmol), EDAC (109 mg, 0.70 mmol) and DMAP (18 mg, 0.07 mmol) were dissolved in DCM (50 mL) and the solution stirred over night. The solvent was removed *in vacuo* and the product purified by flash column chromatography (flash grade silica, DCM, R_f 0.35) to yield **89** as a white crystalline solid (289 mg, 89.8 %).

Chapter 10: Experimental

^1H NMR: (400 MHz, CDCl_3 , CHCl_3 internal standard)

δ (ppm) = 7.57 – 7.47 (m, 6H, ArH), 7.45 – 7.42 (m, 2H, ArH), 7.39 – 7.35 (m, 2H, ArH), 7.07 (d ($J = 8.7$ Hz), 2H, ArH), 6.98 (d ($J = 8.7$ Hz), 2H, ArH), 5.12 (s, 2H, CH_2O), 4.14 (t ($J = 6.6$ Hz), 2H, CH_2O), 4.02 (t ($J = 6.3$ Hz), 2H, CH_2O), 3.71 (s, br, 1H, $\text{CH}_{\text{cluster}}$), 2.64 – 2.49 (m, 4H, CH_2), 1.91 – 1.79 (m, 2H, CH_2), 1.79 – 1.66 (m, 2H, CH_2), 1.64 – 1.52 (m, 2H, CH_2), 1.50 – 1.33 (m, 2H, CH_2)

^{13}C NMR: (100.4 MHz, CDCl_3 , CHCl_3 internal standard)

δ (ppm) = 171.54 (1C, COO), 158.24 (1C, ArC), 157.96 (1C, ArC), 137.09 (1C, ArC), 133.71 (1C, ArC), 133.31 (1C, ArC), 128.67 (2C, ArC), 128.05 (1C, ArC), 127.75 (3C, ArC), 127.56 (2C, ArC), 115.19 (2C, ArC), 114.80 (2C, ArC), 74.13 (1C, $\text{C}_{\text{cluster}}$), 70.12 (1C, CH_2O), 67.82 (1C, CH_2O), 65.32 (1C, CH_2O), 61.64 (1C, $\text{CH}_{\text{cluster}}$), 33.48 (1C, CH_2), 32.66 (1C, CH_2), 29.23 (1C, CH_2), 28.52 (1C, CH_2), 25.81 (1C, CH_2), 25.74 (1C, CH_2)

^{11}B NMR: (128 MHz, CDCl_3)

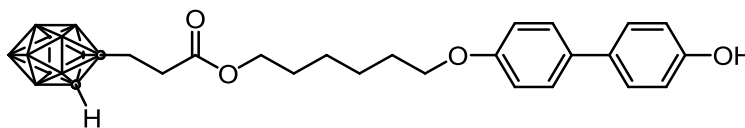
δ (ppm) = -3.03 (1B), -6.47 (1B), -10.32 (2B), -12.53 (2B), -13.15 (2B), -13.72 (2B)

IR (cm^{-1}): 3055 (m, ArH), 2939 (m, ArH), 2862 (m, ArH), 2592 (vs, br, BH), 1712 (vs, C=O), 1604 (s, C-O)

Mass (LIFDI):

$m/z = 574.42 (\text{M})^+$

10.3.71 1-Hydrido, 2-([6-(4'-Hydroxybiphenyl-4-yloxy)hexyl]propionate)dodecacarborane, **90**



1-Hydrido, 2-([6-(4'-(benzloxy)biphenyl-4-yloxy)hexyl]propionate)dodecacarborane, **89** (289 mg, 0.503 mmol) was dissolved in THF (25 mL) and Pd on carbon (50 mg) added. The solution was stirred under an atmosphere of H₂ for 2 days, filtered through celite and the solvent removed *in vacuo*. The product was isolated by flash column chromatography (flash grade silica, DCM 5 % ethyl acetate, R_f 0.40) yielding **90** as a low melting white crystalline solid (149 mg, 61.1 %).

¹H NMR: (400 MHz, CDCl₃, CHCl₃ internal standard)
 δ (ppm) = 7.46 (d (*J* = 8.7 Hz), 2H, ArH), 7.42 (d (*J* = 8.6 Hz), 2H, ArH), 6.94 (d (*J* = 8.8 Hz), 2H, ArH), 6.89 (d (*J* = 8.6 Hz), 2H, ArH), 5.73 (s, br, 1H, OH), 4.12 (t (*J* = 6.7 Hz), 2H, CH₂O), 4.00 (t (*J* = 6.4 Hz), 2H, CH₂O), 3.69 (s, br, 1H, CH_{cluster}), 2.56 – 2.52 (m, 4H, CH₂), 1.87 – 1.77 (m, 2H, CH₂), 1.74 – 1.63 (m, 2H, CH₂), 1.59 – 1.48 (m, 2H, CH₂), 1.48 – 1.37 (m, 2H, CH₂)

¹³C NMR: (100.4 MHz, CDCl₃, CHCl₃ internal standard)
 δ (ppm) = 171.83 (1C, COO), 158.19 (1C, ArC), 154.95 (1C, ArC), 133.53 (1C, ArC), 133.47 (1C, ArC), 127.98 (2C, ArC), 127.76 (2C, ArC), 115.75 (2C, ArC), 114.85 (2C, ArC), 74.08 (1C, C_{cluster}), 67.93 (1C, CH₂O), 65.48 (1C, CH₂O), 61.70 (1C, CH_{cluster}), 33.56 (1C, CH₂), 32.71 (1C, CH₂), 29.23 (1C, CH₂), 28.52 (1C, CH₂), 25.82 (1C, CH₂), 25.75 (1C, CH₂)

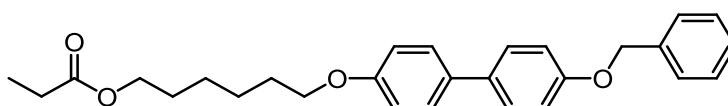
¹¹B NMR: (128 MHz, CDCl₃)
 δ (ppm) = -3.07 (1B), -6.51 (1B), -10.34 (2B), -12.59 (2B), -13.15 (2B), -13.78 (2B)

IR (cm⁻¹): 3387 (vs, br, OH), 3062 (w, ArH), 2939 (w, ArH), 2862 (w, ArH),
2576 (vs, br, BH), 1712 (s, C=O), 1604 (m, C-O)

Mass (LIFDI):

m/z = 484.35 (M)⁺

10.3.72 6-(4'-(Benzyloxy)biphenyl-4-yloxy)hexyl propionate, **91**



6-(4'-(Benzyloxy)biphenyl-4-yloxy)hexan-1-ol, **86** (205 mg, 0.54 mmol), propionic acid (52 mg, 0.70 mmol), EDAC (109 mg, 0.70 mmol) and DMAP (18 mg, 0.07 mmol) were dissolved in DCM (50 mL) and stirred over night. The solvent was removed *in vacuo* and the product isolated by flash column chromatography (flash grade silica, DCM, R_f 0.27) to yield **91** as a low melting white crystalline solid (186 mg, 79.6 %).

¹H NMR: (400 MHz, CDCl₃, CHCl₃)

δ (ppm) = 7.57 – 7.46 (m, 6H, ArH), 7.44 – 7.41 (m, 2H, ArH), 7.38 – 7.35 (m, 1H, ArH), 7.06 (d (*J* = 8.6 Hz), 2H, ArH), 6.97 (d (*J* = 8.6 Hz), 2H, ArH), 5.11 (s, 2H, CH₂O), 4.13 (t (*J* = 6.6 Hz), 2H, CH₂O), 4.01 (t (*J* = 6.4 Hz), 2H, CH₂O), 2.36 (q (*J* = 7.6 Hz), 2H, CH₂COO), 1.90 – 1.79 (m, 2H, CH₂), 1.78 – 1.65 (m, 2H, CH₂), 1.60 – 1.52 (m, 2H, CH₂), 1.51 – 1.40 (m, 2H, CH₂), 1.18 (t (*J* = 7.6 Hz), 3H, CH₃)

¹³C NMR: (100.4 MHz, CDCl₃, CHCl₃ internal standard)

δ (ppm) = 174.66 (1C, COO), 158.28 (1C, ArC), 157.95 (1C, ArC), 137.11 (1C, ArC), 133.79 (1C, ArC), 133.30 (1C, ArC), 128.67 (2C, ArC), 128.03 (1C, ArC), 127.76 (3C, ArC), 127.55 (2C, ArC), 115.16 (2C, ArC), 114.79 (2C, ArC), 70.12 (1C, CH₂O), 67.88 (1C, CH₂O), 64.38 (1C, CH₂O), 29.27 (1C, CH₂), 28.68 (1C, CH₂), 27.68 (1C, CH₂), 25.86 (1C, CH₂), 25.84 (1C, CH₂), 9.27 (1C, CH₃)

Chapter 10: Experimental

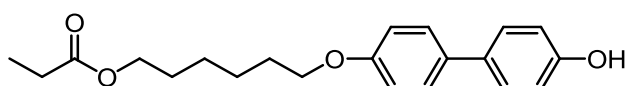
IR (cm⁻¹): 2939 (m, ArH), 2862 (m, ArH), 1743 (vs, C=O), 1604 (s, C-O)

Mass (ESI):

m/z = 455.2195 (M+Na)⁺, 433.2394 (M+H)⁺

calculated = 455.2198 (M+Na)⁺

10.3.73 6-(4'-Hydroxybiphenyl-4-yloxy)hexyl propionate, **92**



6-(4'-(Benzyloxy)biphenyl-4-yloxy)hexyl propionate, **91** (186 mg, 0.43 mmol) was dissolved in THF (25 mL) and Pd on carbon (50 mg) added. The suspension was stirred under an atmosphere of H₂ for 2 days, filtered through celite and the solvent removed *in vacuo*. The product was purified by flash column chromatography (flash grade silica, DCM 5 % ethyl acetate, R_f 0.36) to yield **92** as a white crystalline solid (147 mg, 99.8 %).

¹H NMR: (400 MHz, CDCl₃, CHCl₃ internal standard)

δ (ppm) = 7.45 (d (*J* = 8.7 Hz), 2H, ArH), 7.42 (d (*J* = 8.6 Hz), 2H, ArH), 6.94 (d (*J* = 8.7 Hz), 2H, ArH), 6.91 (d (*J* = 8.6 Hz), 2H, ArH), 6.05 (s, br, 1H, OH), 4.12 (t (*J* = 6.7 Hz), 2H, CH₂O), 3.98 (t (*J* = 6.4 Hz), 2H, CH₂O), 2.36 (q (*J* = 7.6 Hz), 2H, CH₂COO), 1.86 – 1.76 (m, 2H, CH₂), 1.74 – 1.64 (m, 2H, CH₂), 1.57 – 1.39 (m, 4H, CH₂), 1.17 (t (*J* = 7.6 Hz), 3H, CH₃)

¹³C NMR: (100.4 MHz, CDCl₃, CHCl₃ internal standard)

δ (ppm) = 175.36 (1C, COO), 158.18 (1C, ArC), 155.08 (1C, ArC), 133.49 (1C, ArC), 133.45 (1C, ArC), 127.96 (2C, ArC), 127.75 (2C, ArC), 115.74 (2C, ArC), 114.83 (2C, ArC), 67.97 (1C, CH₂O), 64.69 (1C, CH₂O), 29.27 (1C, CH₂), 28.64 (1C, CH₂), 27.80 (1C, CH₂), 25.84 (1C, CH₂), 25.82 (1C, CH₂), 9.27 (1C, CH₃)

Chapter 10: Experimental

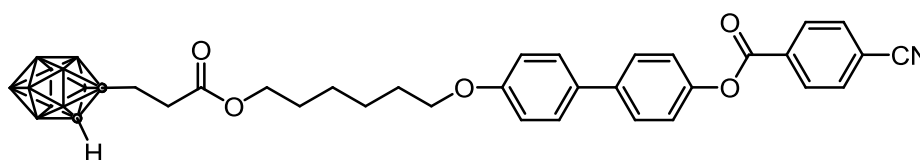
IR (cm⁻¹): 3356 (vs, br, OH), 3062 (m, ArH), 2939 (s, ArH), 2862 (s, ArH), 1735 (vs, C=O), 1681 (s, C-O)

Mass (ESI):

m/z = 365.1706 (M+Na)⁺, 343.19 (M+H)⁺, 125.99

calculated = 365.1729 (M+Na)⁺

10.3.74 1-Hydrido, 2-([6-(4'-(4-cyanobenzoyloxy)biphenyl-4-yloxy)hexyl] propionate)dodecacarborane, **38**



1-Hydrido, 2-([6-(4'-hydroxybiphenyl-4-yloxy)hexyl] propionate)dodecacarborane, **90** (50 mg, 0.103 mmol), 4-cyanobenzoic acid (18 mg, 0.124 mmol), EDAC (19 mg, 0.124 mmol) and DMAP (3 mg, 0.012 mmol) were dissolved in DCM (20 mL) and stirred over night. The solvent was removed *in vacuo* and the product isolated *via* flash column chromatography (flash grade silica, DCM 5 % ethyl acetate, R_f 0.50) and then purified by precipitation from DCM/MeOH to yield **38** as a white crystalline solid (61 mg, 96.5 %).

¹H NMR: (400 MHz, CDCl₃, CHCl₃ internal standard)

δ (ppm) = 8.32 (d (*J* = 8.5 Hz), 2H, ArH), 7.82 (d (*J* = 8.5 Hz), 2H, ArH), 7.61 (d (*J* = 8.7 Hz), 2H, ArH), 7.52 (d (*J* = 8.7 Hz), 2H, ArH), 7.26 (d (*J* = 8.6 Hz), 2H, ArH), 6.97 (d (*J* = 8.7 Hz), 2H, ArH), 4.11 (t (*J* = 6.7 Hz), 2H, CH₂O), 4.01 (t (*J* = 6.3 Hz), 2H, CH₂O), 3.73 (s, br, 1H, CH_{cluster}), 2.62 – 2.49 (m, 4H, CH₂), 1.90 – 1.78 (m, 2H, CH₂), 1.75 – 1.63 (m, 2H, CH₂), 1.62 – 1.49 (m, 2H, CH₂), 1.49 – 1.36 (m, 2H, CH₂)

Chapter 10: Experimental

^{13}C NMR: (100.4 MHz, CDCl_3 , CHCl_3 internal standard)
 δ (ppm) = 171.64 (1C, COO), 163.80 (1C, COO), 158.90 (1C, ArC), 149.54 (1C, ArC), 139.26 (1C, ArC), 133.51 (1C, ArC), 132.69 (1C, ArC), 132.53 (2C, ArC), 130.78 (2C, ArC), 128.27 (2C, ArC), 127.96 (2C, ArC), 121.77 (2C, ArC), 117.99 (1C, ArC), 117.13 (1C, CN), 114.94 (2C, ArC), 74.14 (1C, $\text{C}_{\text{cluster}}$), 67.92 (1C, CH_2O), 65.38 (1C, CH_2O), 61.67 (1C, $\text{CH}_{\text{cluster}}$), 33.55 (1C, CH_2), 32.74 (1C, CH_2), 29.26 (1C, CH_2), 28.57 (1C, CH_2), 25.87 (1C, CH_2), 25.80 (1C, CH_2)

^{11}B NMR: (128 MHz, CDCl_3)
 δ (ppm) = -3.04 (1B), -6.48 (1B), -10.35 (2B), -12.54 (2B), -13.10 (2B), -13.80 (2B)

IR (cm^{-1}): 3062 (m, ArH), 2924 (m, ArH), 2870 (m, ArH), 2576 (vs, br, BH), 2229 (w, CN), 1728 (vs, C=O), 1604 (m, C-O)

Mass (LIFDI):
 m/z = 613.39 (M^+)

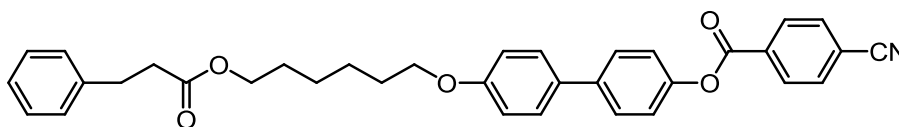
DSC/POM: Cr (89.0 [-0.3] SmA) 106.6 [33.0] N 107.9 [-0.4] Iso

CHN microanalysis: (VO_5 combustion aid)

Observed: C 60.70 %, H 6.25 %, N 2.15 %

Calculated: C 60.66 %, H 6.40 %, N 2.28 %

10.3.75 4'-(6-(3-Phenylpropanoyloxy)hexyloxy)biphenyl-4-yl 4-cyanobenzoate, **39**



6-(4'-Hydroxybiphenyl-4-yloxy)hexyl 3-phenylpropanoate, **88** (50 mg, 0.119 mmol), 4-cyanobenzoic acid (21 mg, 0.143 mmol), EDAC (22 mg, 0.143 mmol) and DAMP

Chapter 10: Experimental

(3 mg, 0.01 mmol) were dissolved in DCM (10 mL) and stirred for 2 days. The solvent was removed *in vacuo* and the product isolated by flash column chromatography (flash grade silica, DCM, R_f 0.17). The product was purified by precipitation from DCM/MeOH to yield **39** as a white crystalline solid (59 mg, 90.5 %).

^1H NMR: (400 MHz, CDCl_3 , CHCl_3 internal standard)
 δ (ppm) = 8.33 (d (J = 8.3 Hz), 2H, ArH), 7.83 (d (J = 8.3 Hz), 2H, ArH), 7.62 (d (J = 8.6 Hz), 2H, ArH), 7.52 (d (J = 8.6 Hz), 2H, ArH), 7.35 – 7.15 (m, 7H, ArH), 6.98 (d (J = 8.7 Hz), 2H, ArH), 4.10 (t (J = 6.6 Hz), 2H, CH_2O), 4.01 (t (J = 6.4 Hz), 2H, ArH), 2.97 (t (J = 7.8 Hz), 2H, CH_2), 2.65 (t (J = 7.8 Hz), 2H, , CH_2), 1.90 – 1.75 (m, 2H, , CH_2), 1.72 – 1.59 (m, 2H, , CH_2), 1.58 – 1.46 (m, 2H, , CH_2), 1.46 – 1.33 (m, 2H, , CH_2)

^{13}C NMR: (100.4 MHz, CDCl_3 , CHCl_3 internal standard)
 δ (ppm) = 173.12 (1C, COO), 163.79 (1C, COO), 158.92 (1C, ArC), 149.51 (1C, ArC), 140.64 (1C, ArC), 139.30 (1C, ArC), 133.50 (1C, ArC), 132.62 (1C, ArC), 132.52 (2C, ArC), 130.77 (2C, ArC), 128.59 (2C, ArC), 128.40 (2C, ArC), 128.25 (2C, ArC), 127.96 (2C, ArC), 126.35 (1C, ArC), 121.74 (2C, ArC), 117.98 (1C, ArC), 117.12 (1C, CN), 114.94 (2C, ArC), 67.96 (1C, CH_2O), 64.56 (1C, CH_2O), 36.03 (1C, CH_2), 31.10 (1C, CH_2), 29.25 (1C, CH_2), 28.67 (1C, CH_2), 25.86 (1C, CH_2), 25.82 (1C, CH_2)

IR (cm^{-1}): 3062 (w, ArH), 2924 (w, ArH), 2870 (w, ArH), 2229 (w, CN), 1728 (vs, C=O), 1604 (m, C-O)

Mass (ESI):

m/z = 570.2227 ($\text{M}+\text{Na}$)⁺, 548.24 ($\text{M}+\text{H}$)⁺

calculated = 570.2256 ($\text{M}+\text{Na}$)⁺

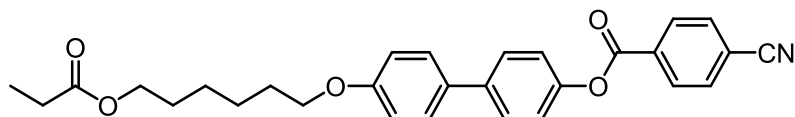
DSC/POM: Cr₁ 73.1[14.7] Cr₂ 77.6 [14.8] SmA 119.0 [0.1] N 151.7 [0.4] Iso

CHN microanalysis:

Observed: C 76.00 %, H 6.23 %, N 2.49 %

Calculated: C 76.76 %, H 6.07 %, N 2.56 %

10.3.76 4'-(6-(Propionyloxy)hexyloxy)biphenyl-4-yl 4-cyanobenzoate, 40



6-(4'-Hydroxybiphenyl-4-yloxy)hexyl propionate, **92** (50 mg, 0.146 mmol), 4-cyanobenzoic acid (26 mg, 0.175 mmol), EDAC (27 mg, 0.175 mmol) and DMAP (5 mg, 0.018 mmol) were dissolved in DCM (10 mL) and stirred over night. The solvent was removed *in vacuo* and the product isolated by flash column chromatography (flash grade silica, DCM 5 % ethyl acetate, R_f 0.41). The product was purified by precipitating from DCM/EtOH to yield **40** as a white crystalline solid (46 mg, 66.8 %).

^1H NMR: (400 MHz, CDCl_3 , CHCl_3 internal standard)

δ (ppm) = 8.32 (d (J = 8.5 Hz), 2H, ArH), 7.83 (d (J = 8.5 Hz), 2H, ArH), 7.61 (d (J = 8.6 Hz), 2H, ArH), 7.51 (d (J = 8.7 Hz), 2H, ArH), 7.26 (d (J = 8.7 Hz), 2H, ArH), 6.97 (d (J = 8.7 Hz), 2H, ArH), 4.09 (t (J = 6.7 Hz), 2H, CH_2O), 4.01 (t (J = 6.4 Hz), 2H, CH_2O), 2.33 (q (J = 7.6 Hz), 2H, CH_2COO), 1.87 – 1.78 (m, 2H, CH_2), 1.74 – 1.64 (m, 2H, CH_2), 1.60 – 1.50 (m, 2H, CH_2), 1.49 – 1.38 (m, 2H, CH_2), 1.15 (t (J = 7.6 Hz), 3H, CH_3)

^{13}C NMR: (100.4 MHz, CDCl_3 , CHCl_3 internal standard)

δ (ppm) = 174.71 (1C, COO), 163.77 (1C, COO), 158.91 (1C, ArC), 149.50 (1C, ArC), 139.28 (1C, ArC), 133.49 (1C, ArC), 132.60 (1C, ArC), 132.51 (2C, ArC), 130.75 (2C, ArC), 128.23 (2C, ArC), 127.94 (2C, ArC), 121.73 (2C, ArC), 117.97 (1C, ArC), 117.10 (1C, CN), 114.93 (2C, ArC), 67.96 (1C, CH_2O), 64.39 (1C, CH_2O), 29.26 (1C, CH_2), 28.70

Chapter 10: Experimental

(1C, CH₂), 27.71 (1C, CH₂), 25.87 (1C, CH₂), 25.85 (1C, CH₂), 9.28 (1C, CH₃)

IR (cm⁻¹): 3047 (w, ArH), 2931 (w, ArH), 2862 (w, ArH), 2237 (w, CN), 1728 (vs, C=O), 1604 (s, C-O)

Mass (ESI):

m/z = 494.1943 (M+Na)⁺, 365.17

calculated = 494.1943 (M+Na)⁺

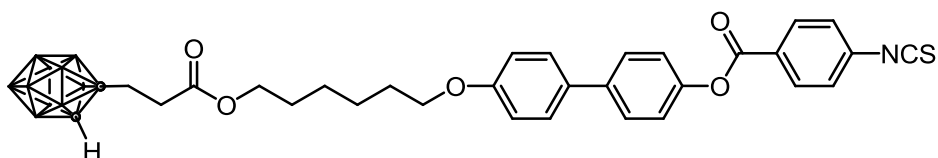
DSC/POM: Cr 92.9 [12.0] SmA 99.2 [0.2] N 187.0 [0.9] Iso

CHN microanalysis:

Observed: C 73.80 %, H 6.37 %, N 2.87 %

Calculated: C 73.87 %, H 6.20 %, N 2.97 %

10.3.77 1-Hydrido, 2-([6-(4'-(4-isothiocyanatebenzoyloxy)biphenyl-4-yloxy)hexyl] propionate)dodecacarborane, **41**



1-Hydrido, 2-([6-(4'-Hydroxybiphenyl-4-yloxy)hexyl] propionate)dodecacarborane, **90** (50 mg, 0.103 mmol), 4-isothiocyanatebenzoic acid (22 mg, 0.124 mmol), EDAC (19 mg, 0.124 mmol) and DMAP (3 mg, 0.012 mmol) were dissolved in DCM (25 mL) and stirred over night. The solvent was removed *in vacuo* and the product isolated by flash column chromatography (flash grade silica, DCM 5 % ethyl acetate, R_f 0.59). The product was purified by precipitation from DCM/MeOH to yield **41** as a white crystalline solid (58 mg, 87.2 %).

Chapter 10: Experimental

^1H NMR: (400 MHz, CDCl_3 , CHCl_3 internal standard)

δ (ppm) = 8.21 (d ($J = 8.5$ Hz), 2H, ArH), 7.59 (d ($J = 8.5$ Hz), 2H, ArH), 7.51 (d ($J = 8.6$ Hz), 2H, ArH), 7.34 (d ($J = 8.5$ Hz), 2H, ArH), 7.25 (d ($J = 8.5$ Hz), 2H, ArH), 6.97 (d ($J = 8.6$ Hz), 2H, ArH), 4.11 (t ($J = 6.6$ Hz), 2H, CH_2O), 4.01 (t ($J = 6.3$ Hz), 2H, CH_2O), 3.72 (s, br, 1H, $\text{CH}_{\text{cluster}}$), 2.65 – 2.48 (m, 4H, CH_2), 1.89 – 1.77 (m, 2H, CH_2), 1.75 – 1.63 (m, 2H, CH_2), 1.60 – 1.49 (m, 2H, CH_2), 1.49 – 1.37 (m, 2H, CH_2)

^{13}C NMR: (100.4 MHz, CDCl_3 , CHCl_3 internal standard)

δ (ppm) = 171.65 (1C, COO), 164.25 (1C, COO), 158.84 (1C, ArC), 149.76 (1C, ArC), 138.99 (1C, ArC), 138.36 (1C, NCS), 136.47 (1C, ArC), 132.83 (1C, ArC), 131.80 (2C, ArC), 128.27 (2C, ArC), 128.14 (1C, ArC), 127.90 (2C, ArC), 126.00 (2C, ArC), 121.91 (2C, ArC), 114.92 (2C, ArC), 74.14 (1C, $\text{C}_{\text{cluster}}$), 67.92 (1C, CH_2O), 65.39 (1C, CH_2O), 61.67 (1C, $\text{CH}_{\text{cluster}}$), 33.56 (1C, CH_2), 32.75 (1C, CH_2), 29.27 (1C, CH_2), 28.58 (1C, CH_2), 25.88 (1C, CH_2), 25.81 (1C, CH_2)

^{11}B NMR: (128 MHz, CDCl_3)

δ (ppm) = -3.04 (1B), -6.49 (1B), -10.35 (2B), -12.55 (2B), -13.13 (2B), -13.79 (2B)

IR (cm^{-1}): 3062 (w, ArH), 2947 (w, ArH), 2870 (w, ArH), 1728 (vs, C=O), 1604 (s, C-O)

Mass (LIFDI):

m/z = 645.37 (M)⁺, 531.22, 484.37

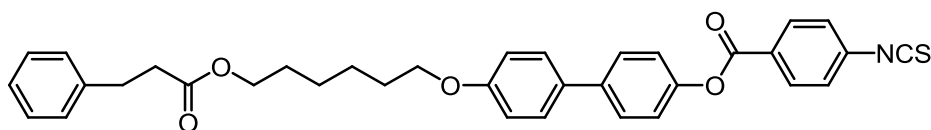
DSC/POM: Cr (55.4 [-1.3] HexB 125.8 [-1.9] SmA 127.0 [-0.5] N) 130.1 [44.4] Iso

CHN microanalysis: (VO_5 combustion aid)

Observed: C 58.23 %, H 6.07 %, N 2.09 %

Calculated: C 57.65 %, H 6.09 %, N 2.17 %

10.3.78 4'-(6-(3-Phenylpropanoyloxy)hexyloxy)biphenyl-4-yl 4-isothiocyanatobenzoate, 42



6-(4'-Hydroxybiphenyl-4-yloxy)hexyl 3-phenylpropanoate, **88** (50 mg, 0.119 mmol), 4-isothiocyanatebenzoic acid (26 mg, 0.143 mmol), EDAC (22 mg, 0.143 mmol) and DMAP (3 mg, 0.01 mmol) were dissolved in DCM (10 mL) and stirred for 2 days. The solvent was removed *in vacuo* and the product isolated by flash column chromatography (flash grade silica, DCM 4 % ethyl acetate, R_f 0.48). The product was purified by precipitation from DCM/MeOH to yield **42** as a white crystalline solid (78 mg, 97.1 %).

^1H NMR: (400 MHz, CDCl_3 , CHCl_3 internal standard)
 δ (ppm) = 8.16 (d (J = 8.6 Hz), 2H, ArH), 7.54 (d (J = 8.6 Hz), 2H, ArH), 7.46 (d (J = 8.7 Hz), 2H, ArH), 7.29 (d (J = 8.6 Hz), 2H, ArH), 7.27 – 7.12 (m, 5H, ArH), 6.92 (d (J = 8.7 Hz), 2H, ArH), 4.05 (t (J = 6.6 Hz), 2H, CH_2O), 3.95 (t (J = 6.4 Hz), 2H, CH_2O), 2.91 (t (J = 7.8 Hz), 2H, CH_2), 2.59 (t (J = 7.8 Hz), 2H, CH_2), 1.82 – 1.72 (m, 2H, CH_2), 1.67 – 1.56 (m, 2H, CH_2), 1.53 – 1.41 (m, 2H, CH_2), 1.41 – 1.31 (m, 2H, CH_2)

^{13}C NMR: (100.4 MHz, CDCl_3 , CHCl_3 internal standard)
 δ (ppm) = 173.11 (1C, COO), 164.22 (1C, COO), 158.86 (1C, ArC), 149.73 (1C, ArC), 140.65 (1C, ArC), 139.02 (1C, ArC), 138.34 (1C, NCS), 136.44 (1C, ArC), 132.76 (1C, ArC), 131.79 (2C, ArC), 128.59 (2C, ArC), 128.40 (2C, ArC), 128.24 (2C, ArC), 128.14 (1C, ArC), 127.89 (2C, ArC), 126.36 (2C, ArC), 125.98 (2C, ArC), 121.88 (2C, ArC), 114.92 (2C, ArC), 67.96 (1C, CH_2O), 64.57 (1C, CH_2O), 36.03 (1C, CH_2), 31.11 (1C, CH_2), 29.27 (1C, CH_2), 28.68 (1C, CH_2), 25.87 (1C, CH_2), 25.83 (1C, CH_2)

Chapter 10: Experimental

IR (cm⁻¹): 3062 (w, ArH), 2924 (w, ArH), 2870 (w, ArH), 2067 (vs, br, NCS), 1728 (s, C=O), 1604 (m, C-O)

Mass (ESI):

m/z = 602.1964 (M+Na)⁺

calculated = 602.1977 (M+Na)⁺

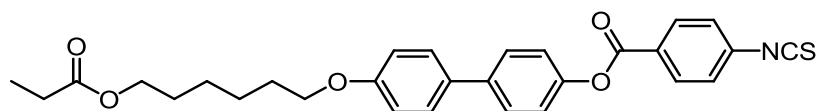
DSC/POM: Cr₁ 55.6 [10.3] Cr₂ (66.3 [-1.3] HexB) 66.9 [17.6] SmA 154.3 [1.3 N 162.0 [0.3] Iso

CHN microanalysis:

Observed: C 72.28 %, H 5.72 %, N 2.42 %

Calculated: C 72.52 %, H 5.74 %, N 2.42 %

10.3.79 4'-(6-(Propionyloxy)hexyloxy)biphenyl-4-yl 4-isothiocyanatobenzoate, **43**



6-(4'-Hydroxybiphenyl-4-yloxy)hexyl propionate, **92** (50 mg, 0.146 mmol), 4-isothiocyanatebenzoic acid (31 mg, 0.175 mmol), EDAC (27 mg, 0.175 mmol) and DMAP (5 mg, 0.018 mmol) were dissolved in DCM (10 mL) and stirred over night. The solvent was removed *in vacuo* and the product isolated by flash column chromatography (flash grade silica, DCM 5 % ethyl acetate, R_f 0.41). The product was purified by precipitation from DCM/EtOH to yield **43** as a white crystalline solid (48 mg, 65.3 %).

¹H NMR: (400 MHz, CDCl₃, CHCl₃ internal standard)

δ (ppm) = 8.20 (d (*J* = 8.6 Hz), 2H, ArH), 7.58 (d (*J* = 8.6 Hz), 2H, ArH), 7.50 (d (*J* = 8.6 Hz), 2H, ArH), 7.33 (d (*J* = 8.5 Hz), 2H, ArH), 7.24 (d (*J* = 8.7 Hz), 2H, ArH), 6.96 (d (*J* = 8.6 Hz), 2H, ArH), 4.09 (t (*J* = 6.6 Hz), 2H, CH₂O), 3.99 (t (*J* = 6.4 Hz), 2H, CH₂O), 2.33 (q (*J* = 7.6

Chapter 10: Experimental

Hz), 2H, CH_2COO), 1.89 – 1.76 (m, 2H, CH_2), 1.76 – 1.63 (m, 2H, CH_2), 1.59 – 1.37 (m, 4H, CH_2), 1.14 (t ($J = 7.6$ Hz), 3H, CH_3)

^{13}C NMR: (100.4 MHz, CDCl_3 , CHCl_3 internal standard)
 δ (ppm) = 174.75 (1C, COO), 164.25 (1C, COO), 158.87 (1C, ArC), 149.73 (1C, ArC), 139.04 (1C, ArC), 138.34 (1C, NCS), 136.45 (1C, ArC), 132.77 (1C, ArC), 131.80 (2C, ArC), 128.25 (2C, ArC), 128.15 (1C, ArC), 127.90 (2C, ArC), 125.99 (2C, ArC), 121.89 (2C, ArC), 114.92 (2C, ArC), 67.98 (1C, CH_2O), 64.43 (1C, CH_2O), 29.29 (1C, CH_2), 28.72 (1C, CH_2), 27.74 (1C, CH_2), 25.90 (1C, CH_2), 25.88 (1C, CH_2), 9.31 (1C, CH_3)

IR (cm^{-1}): 3286 (w, ArH), 2939 (w, ArH), 2529 (w, ArH), 2052 (m, NCS), 1728 (s, C=O), 1597 (m, C-O)

Mass (ESI):

m/z = 256.1651 ($\text{M}+\text{Na}$)⁺, 3060.32

calculated = 526.1664 ($\text{M}+\text{Na}$)⁺

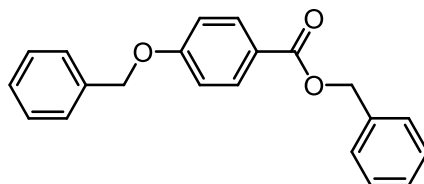
DSC/POM: Cr 62.0 [21.2] HexB 89.7 [1.7] SmA 191.2 [1.4] N 203.5 [0.5] Iso

CHN microanalysis:

Observed: C 68.25 %, H 5.99 %, N 2.59 %

Calculated: C 69.16 %, H 5.80 %, N 2.78 %

10.3.80 Benzyl 4-(benzyloxy)benzoate, 93



4-Hydroxy benzoic acid (5.18 g, 37.5 mmol), K_2CO_3 (15.55 g, 112.3 mmol) and KI (100 mg, 0.6 mmol) were suspended in butanone (250 mL) and brought to reflux.

Chapter 10: Experimental

Next benzyl bromide (7.70 g, 45.0 mmol) was added and the solution refluxed over night. The solution was allowed to cool, filtered and the solvent removed *in vacuo*. The material was loaded onto a silica pad and washed with hexane (5x 200 mL) and then eluted with chloroform to yield **93** as a white crystalline solid (9.00 g, 75.5 %).

^1H NMR: (400 MHz, CDCl_3 , CHCl_3 internal standard)

δ (ppm) = 8.04 (d ($J = 8.9$ Hz), 2H, ArH), 7.50 – 7.29 (m, 10H, ArH), 7.00 (d ($J = 8.9$ Hz), 2H, ArH), 5.34 (s, 2H, CH_2O), 5.12 (s, 2H, CH_2O)

^{13}C NMR: (100.4 MHz, CDCl_3 , CHCl_3 internal standard)

δ (ppm) = 166.22 (1C, COO), 162.66 (1C, ArC), 136.37 (1C, ArC), 136.31 (1C, ArC), 131.85 (2C, ArC), 128.77 (2C, ArC), 128.65 (2C, ArC), 128.30 (1C, ArC), 128.23 (1C, ArC), 128.19 (2C, ArC), 127.56 (2C, ArC), 122.86 (1C, ArC), 114.57 (2C, ArC), 70.19 (1C, CH_2O), 66.50 (1C, CH_2O)

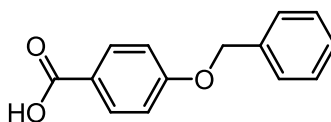
IR (cm^{-1}): 3070 (w, ArH), 2947 (w, ArH), 2877 (w, ArH), 1697 (vs, C=O), 1604 (s, C-O)

Mass (ESI):

m/z = 341.1146 ($\text{M}+\text{Na}$) $^+$, 319.13 ($\text{M}+\text{H}$) $^+$, 226.95, 158.97, 82.03

calculated = 341.1154 ($\text{M}+\text{Na}$) $^+$

10.3.81 4-(Benzyloxy)benzoic acid, **94**



Benzyl 4-(benzyloxy)benzoate, **93** (9.00 g, 28.3 mmol) was dissolved in ethanol (250 mL). Next a solution of KOH in water (50 mL) was added and the resultant solution refluxed under Ar for 3 h. The solution was allowed to cool, diluted with water (250 mL) and acidified with conc. HCl. The precipitate was filtered, washed with water

Chapter 10: Experimental

and dried in a desiccator (over CaCO_3) to yield **94** as a white crystalline solid (6.24 g, 96.7 %).

^1H NMR: (400 MHz, CDCl_3 , CHCl_3 internal standard)
 δ (ppm) = 7.90 (d ($J = 8.8$ Hz), 2H, ArH), 7.43 – 7.18 (m, 5H, ArH), 6.90 (d ($J = 8.8$ Hz), 2H, ArH), 5.03 (s, 2H, CH_2O)

^{13}C NMR: (100.4 MHz, CDCl_3 , CHCl_3 internal standard)
 δ (ppm) = 167.67 (1C, COO), 161.74 (1C, ArC), 135.79 (1C, ArC), 131.24 (2C, ArCH), 128.11 (2C, ArCH), 127.63 (1C, ArCH), 126.99 (2C, ArCH), 123.00 (1C, ArC), 113.80 (2C, ArCH), 69.48 (1C, CH_2O)

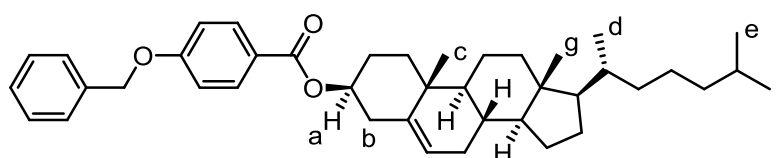
IR (cm^{-1}): 2816 (w, ArH), 2553 (w, ArH), 1681 (s, C=O), 1604 (s, C-O)

Mass (ESI):

m/z = 251.0673 ($\text{M}+\text{Na}$) $^+$, 299.09 ($\text{M}+\text{H}$) $^+$, 211.08, 158.9653, 82.03

calculated = 251.0684 ($\text{M}+\text{Na}$) $^+$

10.3.82 4-Benzyloxy cholesterol benzoate, **95**



4-Benzyloxy benzoic acid, **94** (3.01 g, 13.19 mmol), cholesterol (5.61 g, 14.5 mmol), EDAC (2.25 g, 14.51 mmol) and DMAP (0.3 g, 1.2 mmol) were dissolved in DCM (75 mL) and stirred for 3 days. The solvent was removed *in vacuo* and the product purified by flash column chromatography (flash grade silica, DCM, R_f 0.71) to yield **95** as a white crystalline solid (2.26 g, 31.2 %).

^1H NMR: (400 MHz, CDCl_3 , CHCl_3 internal standard)
 δ (ppm) = 7.99 (d ($J = 8.9$ Hz), 2H, ArH), 7.47 – 7.30 (m, 5H, ArH), 6.98 (d ($J = 8.9$ Hz), 2H, ArH), 5.41 (d ($J = 4.4$ Hz), 1H, C=CH), 5.12 (s, 2H,

Chapter 10: Experimental

CH_2O), 4.89 – 4.76 (m, 1H, CH_aOOC), 2.44 (d ($J = 7.7$ Hz), 2H, CH_{2b}), 2.06 – 1.94 (m, 3H, $alkH$), 1.94 – 1.87 (m, 1H, $alkH$), 1.87 – 1.78 (m, 1H, $alkH$), 1.78 – 1.64 (m, 1H, $alkH$), 1.64 – 1.41 (m, 8H, $alkH$), 1.41 – 1.38 (m, 3H, $alkH$), 1.28 – 1.08 (m, 6H, $alkH$), 1.06 (s, 3H, CH_{3c}), 1.04 – 0.95 (m, 3H, $alkH$), 0.92 (d ($J = 6.5$ Hz), 3H, CH_{3d}), 0.87 (d ($J = 1.8$ Hz), 3H, CH_{3e}), 0.86 (d ($J = 1.8$ Hz), 3H, CH_{3f}), 0.69 (s, 3H, CH_{3g})

^{13}C NMR: (100.4 MHz, $CDCl_3$, $CHCl_3$ internal standard)

δ (ppm) = 165.84 (1C, COO), 162.45 (1C, ArC), 139.88 (1C, C=CH), 136.42 (1C, ArC), 131.69 (2C, ArCH), 128.80 (2C, ArCH), 128.32 (1C, ArCH), 127.60 (2C, ArCH), 123.63 (1C, ArC), 122.82 (1C, C=CH), 114.49 (2C, ArCH), 74.37 (1C, CH_aO), 70.19 (1C, CH_2O), 56.82 (1C, CH), 56.26 (1C, CH), 50.17 (1C, CH), 42.45 (1C, CR_4), 39.87 (1C, CH_2), 39.65 (1C, CH_2), 38.42 (1C, CH_2), 37.18 (1C, CH_2), 36.78 (1C, CR_4), 36.32 (1C, CH_2), 35.94 (1C, CH), 32.07 (1C, CH_2), 32.01 (1C, CH), 28.38 (1C, CH_2), 28.16 (1C, CH), 28.07 (1C, CH_2), 24.43 (1C, CH_2), 23.97 (1C, CH_2), 22.98 (1C, CH_3), 22.72 (1C, CH_3), 21.18 (1C, CH_2), 19.52 (1C, CH_3), 18.86 (1C, CH_3), 12.00 (1C, CH_3)

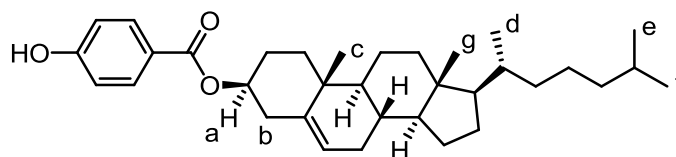
IR (cm^{-1}): 2931 (vs, ArH), 2862 (vs, ArH), 1705 (vs, C=O), 1604 (m, C-O)

Mass (ESI):

m/z = 369.33, 338.34, 262.07, 227.00, 209.03

calculated = 596.4229 (M)⁺

(No M^+ , but characteristic fragments visible)

10.3.83 4-Hydroxy cholesterol benzoate, **96**

4-Benzyloxy cholesterol benzoate, **95** (2.46 g, 4.1 mmol) was dissolved in THF (150 mL) and Pd on carbon added (50 mg). The solution was stirred under an atmosphere of H₂ for 3 days. The solution was filtered and the solvent was removed *in vacuo* to yield **96** as a white crystalline solid (2.05 g, 98.8 %).

¹H NMR: (400 MHz, CDCl₃, CHCl₃ internal standard)

δ (ppm) = 7.84 (d (*J* = 8.6 Hz), 2H, ArH), 6.80 (d (*J* = 8.6 Hz), 2H, ArH), 5.34 (d (*J* = 4.1 Hz), 1H, C=CH), 4.79 – 4.67 (m, 1H, CH_aOOC), 2.37 (d (*J* = 7.7 Hz), 2H, CH_{2b}), 2.02 – 1.72 (m, 5H, alkH), 1.71 – 1.57 (m, 1H, alkH), 1.57 – 1.35 (m, 6H, alkH), 1.35 – 1.22 (m, 4H, alkH), 1.23 – 1.02 (m, 7H, alkH), 1.00 (s, 3H, CH_{3c}), 0.99 – 0.89 (m, 3H, alkH), 0.86 (d (*J* = 6.5 Hz), 3H, CH_{3d}), 0.81 (d (*J* = 1.5 Hz), 3H, CH_{3e}), 0.80 (d (*J* = 1.4 Hz), 3H, CH_{3f}), 0.63 (s, 3H, CH_{3g})

¹³C NMR: (100.4 MHz, CDCl₃, CHCl₃ internal standard)

δ (ppm) = 166.05 (1C, COO), 159.84 (1C, ArC), 139.83 (1C, C=CH), 132.02 (2C, ArCH), 123.51 (1C, ArC), 122.90 (1C, C=CH), 115.25 (1C, ArCH), 74.57 (1C, CH_aO), 56.84 (1C, CH), 56.29 (1C, CH), 50.19 (1C, CH), 42.48 (1C, CR₄), 39.89 (1C, CH₂), 39.67 (1C, CH₂), 38.42 (1C, CH₂), 37.19 (1C, CH₂), 36.81 (1C, CR₄), 36.34 (1C, CH₂), 35.96 (1C, CH), 32.09 (1C, CH₂), 32.04 (1C, CH), 28.39 (1C, CH₂), 28.17 (1C, CH), 28.08 (1C, CH₂), 24.45 (1C, CH₂), 24.00 (1C, CH₂), 22.98 (1C, CH₃), 22.72 (1C, CH₃), 21.20 (1C, CH₂), 19.53 (1C, CH₃), 18.87 (1C, CH₃), 12.02 (1C, CH₃)

IR (cm⁻¹): 2931 (vs, ArH), 2862 (vs, ArH), 1705 (vs, C=O), 1604 (m, C-O)

Chapter 10: Experimental

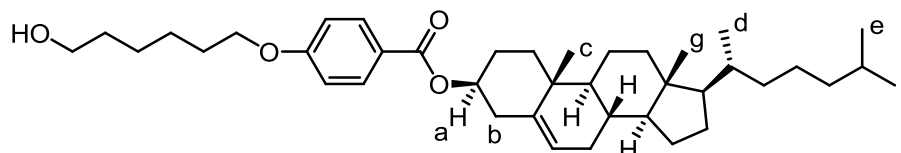
Mass (ESI):

$m/z =$ 369.36, 338.3491, 285.14

calculated = 506.3760 (M^+)

(No M^+ , but characteristic fragments visible)

10.3.84 4-(6-Hydroxyhexyloxy) cholesterol benzoate, **97**



4-Hydroxy cholesterol benzoate, **96** (0.17 g, 0.33 mmol), K_2CO_3 (0.22 g, 1.6 mmol) and KI (50 mg, 0.3 mmol) were suspended in butanone (35 mL) and brought to reflux. Next 6-bromo-hexan-1-ol (72.4 mg, 0.4 mmol) was added and the solution refluxed over night. The solution was allowed to cool, filtered and the solvent removed *in vacuo*. The product was purified by recrystallization from ethanol to yield **97** as a white crystalline solid (131 mg, 66.7 %).

1H NMR: (400 MHz, $CDCl_3$, $CHCl_3$ internal standard)

δ (ppm) = 7.97 (d ($J = 8.8$ Hz), 2H, ArH), 6.89 (d ($J = 8.9$ Hz), 2H, ArH), 5.41 (d ($J = 4.7$ Hz), 1H, C=CH), 4.81 (dd ($J = 8.1, 3.4$ Hz), 1H, CH_aOOC), 4.00 (t ($J = 6.5$ Hz), 2H, CH_2O), 3.66 (t ($J = 6.5$ Hz), 2H, CH_2), 2.44 (d ($J = 7.7$ Hz), 2H, CH_{2b}), 2.06 – 1.87 (m, 4H, alkH), 1.87 – 1.65 (m, 4H, alkH), 1.65 – 1.54 (m, 4H, alkH), 1.54 – 1.40 (m, 10H, alkH), 1.40 – 1.08 (m, 12H, alkH), 1.06 (s, 3H, CH_3c), 1.04 – 0.94 (m, 3H, alkH), 0.92 (d ($J = 6.6$ Hz), 3H, CH_3d), 0.87 (d ($J = 1.8$ Hz), 3H, CH_3e), 0.85 (d ($J = 1.8$ Hz), 3H, CH_{3f}), 0.68 (s, 3H, CH_{3g})

^{13}C NMR: (100.4 MHz, $CDCl_3$, $CHCl_3$ internal standard)

δ (ppm) = 165.92 (1C, COO), 162.86 (1C, ArC), 139.87 (1C, C=CH), 131.62 (2C, ArCH), 123.14 (1C, ArC), 122.77 (1C, C=CH), 114.05 (2C, ArC), 74.31 (1C, CH_aO), 68.11 (1C, CH_2O), 62.91 (1C, CH_2), 56.80 (1C, CH), 56.25 (1C, CH), 50.15 (1C, CH), 42.43 (1C, CR_4), 39.85

Chapter 10: Experimental

(1C, CH₂), 39.63 (1C, CH₂), 38.40 (1C, CH₂), 37.17 (1C, CH₂), 36.76 (1C, CR₄), 36.30 (1C, CH₂), 35.92 (1C, CH), 32.75 (1C, CH₂), 32.04 (1C, CH₂), 31.99 (1C, CH), 29.21 (1C, CH₂), 28.35 (1C, CH₂), 28.12 (1C, CH), 28.05 (1C, CH₂), 25.95 (1C, CH₂), 25.65 (1C, CH₂), 24.41 (1C, CH₂), 23.96 (1C, CH₂), 22.94 (1C, CH₃), 22.69 (1C, CH₃), 21.17, (1C, CH₂) 19.49 (1C, CH₃), 18.84 (1C, CH₃), 11.98 (1C, CH₃)

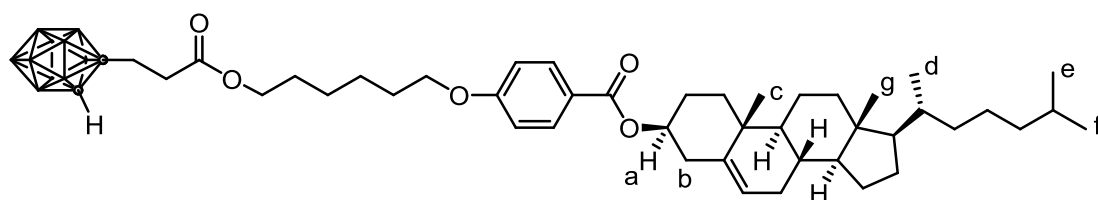
IR (cm⁻¹): 2891 (vs, ArH), 2862 (s, ArH), (1705 vs, C=O), 1604 (m, C-O)

Mass (ESI):

m/z = 607.4798 (M+H)⁺, 369.35, 338.34, 226.95, 209.05

calculated = 607.4726 (M+H)⁺

10.3.85 1-Hydrido, 2-([cholesterol phenyl-4-yl 4-(6-hexyloxy)benzoate] propionate) dodecacarborane, **44**



4-(6-Hydroxyhexyloxy) cholesterol benzoate, **97** (101 mg, 0.166 mmol), hydrido, 2-(propanoic acid)dodecacarborane, **79** (30 mg, 0.139 mmol), EDAC (30 mg, 0.194 mmol) and DMAP (4 mg, 0.019 mmol) were dissolved in DCM (15 mL) and stirred for 3 days. The solvent was removed *in vacuo* and the product isolated by flash column chromatography (flash grade silica, DCM, R_f-0.50) to yield **44** as a white crystalline solid (75.2 mg, 67.2 %).

¹H NMR: (500 MHz, CDCl₃, CHCl₃ internal standard)

δ (ppm) = 7.98 (d (*J* = 8.9 Hz), 2H, ArH), 6.89 (d (*J* = 8.9 Hz), 2H, ArH), 5.41 (d (*J* = 3.8 Hz), 1H, C=CH), 4.87 – 4.78 (m, 1H, CH_aOOC), 4.10 (t (*J* = 6.7 Hz), 2H, CH₂O), 4.01 (t (*J* = 6.4 Hz), 2H, CH₂O), 3.72 (s, br, 1H, CH_{cluster}), 2.62 – 2.49 (m, 4H, CH₂), 2.45 (d (*J* = 7.7 Hz), 2H,

Chapter 10: Experimental

CH_{2b}), 2.30 (s, br, 3H, BH), 2.16 (s, br, 6H, BH), 2.06 – 1.94 (m, 2H, alkH), 1.94 – 1.87 (m, 2H, alkH), 1.87 – 1.76 (m, 4H, alkH), 1.74 – 1.63 (m, 4H, alkH), 1.63 – 1.47 (m, 8H, alkH), 1.47 – 1.40 (m, 4H, alkH), 1.38 – 1.29 (m, 4H, alkH), 1.29 – 1.19 (m, 3H, alkH), 1.19 – 1.07 (m, 6H, alkH), 1.06 (s, 3H, CH_{3c}), 1.05 – 0.95 (m, 4H, alkH), 0.92 (d ($J = 6.5$ Hz), 3H, CH_{3d}), 0.87 (d ($J = 2.2$ Hz), 3H, CH_{3e}), 0.86 (d ($J = 2.2$ Hz), 3H, CH_{3f}), 0.69 (s, 3H, CH_{3g})

^{13}C NMR: (100.4 MHz, $CDCl_3$, $CHCl_3$ internal standard)
 δ (ppm) = 171.63 (1C, COO), 165.88 (1C, COO), 162.79 (1C, ArC), 139.88 (1C, C=CH), 131.65 (2C, ArCH), 123.25 (1C, ArC), 122.80 (1C, C=CH), 114.05 (2C, ArCH), 74.34 (1C, CH_aO), 74.13 (1C, $C_{cluster}$), 67.98 (1C, CH_2O), 65.33 (1C, CH_2O), 61.67 (1C, $CH_{cluster}$), 56.81 (1C, CH), 56.25 (1C, CH), 50.16 (1C, CH), 42.44 (1C, CR_4), 39.86 (1C, CH_2), 39.64 (1C, CH_2), 38.41 (1C, CH_2), 37.18 (1C, CH_2), 36.78 (1C, CR_4), 36.31 (1C, CH_2), 35.93 (1C, CH), 33.54 (1C, CH_2), 32.74 (1C, CH_2), 32.06 (1C, CH_2), 32.00 (1C, CH), 29.10 (1C, CH_2), 28.55 (1C, CH_2), 28.37 (1C, CH_2), 28.14 (1C, CH), 28.06 (1C, CH_2), 25.80 (1C, CH_2), 25.77 (1C, CH_2), 24.42 (1C, CH_2), 23.96 (1C, CH_2), 22.96 (1C, CH_3), 22.70 (1C, CH_3), 21.18 (1C, CH_2), 19.51 (1C, CH_3), 18.85 (1C, CH_3), 11.99 (1C, CH_3)

^{11}B NMR: (128 MHz, $CDCl_3$)
 δ (ppm) = -3.01 (1B), -6.43 (1B), -10.34 (2B), -12.53 (2B), -13.16 (2B), -13.79 (2B)

IR (cm^{-1}): 3062 (vw, ArH), 2931 (vs, ArH), 2854 (vs, ArH), 2584 (vs, br, BH), 1735 (s, C=O), 1697 (vs, C=O), 1604 (m, C-O)

Mass (ESI):
 m/z = 807.6789 (M+H)⁺, 610.19, 536.17
calculated = 807.6702 (+H)⁺

DSC/POM: Cr (113.2 [-0.6] SmA 107.3* TGB 131.7 [-0.8] N*) 143.2 [25.4] Iso

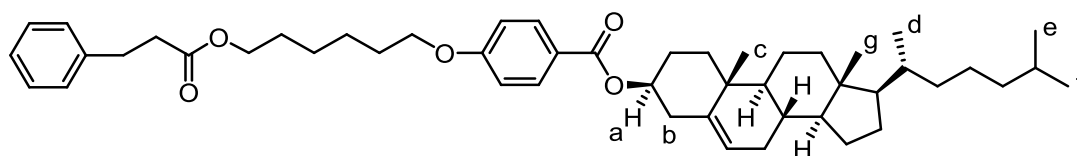
The transition temperature marked with * is only observed by POM and thus there is no measured enthalpy.

CHN microanalysis: (VO₅ combustion aid)

Observed: C 67.08 %, H 9.42 %, N 0.00 %

Calculated: C 67.12 %, H 9.51 %, N 0.00 %

10.3.86 Cholesteryl 4-(6-(3-phenylpropanoyloxy)hexyloxy)benzoate, **45**



4-(6-Hydroxyhexyloxy) cholesterol benzoate, **97** (26 mg, 0.038 mmol), hydrocinnamic acid (6.8 mg, 0.045 mmol), EDAC (6.9 mg, 0.045 mmol) and DMAP (1.3 mg, 0.005 mmol) were dissolved in DCM (10 mL) and stirred for 5 days. The solvent was removed *in vacuo* and the product purified by flash column chromatography (flash grade silica, DCM 2 % ethyl acetate, R_f 0.57) to yield **45** as a white crystalline solid (19.2 mg, 57.7 %).

¹H NMR: (400 MHz, CDCl₃, CHCl₃ internal standard)

δ (ppm) = 7.98 (d (*J* = 8.8 Hz), 2H, ArH), 7.34 – 7.27 (m, 2H, ArH), 7.22 – 7.16 (m, 3H, ArH), 6.89 (d (*J* = 8.8 Hz), 2H, ArH), 5.41 (d (*J* = 4.1 Hz), 1H, C=CH), 4.88 – 4.76 (m, 1H, CH_aOOC), 4.08 (t (*J* = 6.6 Hz), 2H, CH₂O), 3.99 (t (*J* = 6.4 Hz), 2H, CH₂O), 2.95 (t (*J* = 7.8 Hz), 2H, CH₂), 2.63 (t (*J* = 7.8 Hz), 2H, CH₂), 2.45 (d (*J* = 7.7 Hz), 2H, CH_{2b}), 2.08 – 1.94 (m, 3H, alkH), 1.94 – 1.87 (m, 1H, alkH), 1.87 – 1.70 (m, 4H, alkH), 1.68 – 1.55 (m, 6H, alkH), 1.55 – 1.44 (m, 6H, alkH), 1.44 – 1.30 (m, 6H, alkH), 1.30 – 1.09 (m, 8H, alkH), 1.06 (s, 3H, CH_{3c}), 1.05 – 0.95 (m, 3H, alkH), 0.92 (d (*J* = 6.5 Hz), 3H, CH_{3d}), 0.88 (d (*J*

Chapter 10: Experimental

= 1.7 Hz), 3H, CH_{3e}), 0.86 (d ($J = 1.7$ Hz), 3H, CH_{3f}), 0.69 (s, 3H, CH_{3g})

^{13}C NMR: (100.4 MHz, $CDCl_3$, $CHCl_3$ internal standard)
 δ (ppm) = 173.14 (1C, COO), 165.94 (1C, COO), 162.86 (1C, ArC), 140.67 (1C, ArC), 139.93 (1C, C=CH), 131.67 (2C, ArCH), 128.62 (2C, ArCH), 128.42 (2C, ArCH), 126.39 (1C, ArCH), 123.25 (1C, ArC), 122.81 (1C, C=CH), 114.08 (2C, ArCH), 74.35 (1C, CH_4O), 68.08 (1C, CH_2O), 64.55 (1C, CH_2O), 56.85 (1C, CH), 56.29 (1C, CH), 50.20 (1C, CH), 42.47 (1C, CR_4), 39.90 (1C, CH_2), 39.67 (1C, CH_2), 38.44 (1C, CH_2), 37.21 (1C, CH_2), 36.81 (1C, CR_4), 36.33 (1C, CH_2), 36.05 (1C, CH_2), 35.95 (1C, CH), 32.09 (1C, CH_2), 32.04 (1C, CH), 31.14 (1C, CH_2), 29.14 (1C, CH_2), 28.68 (1C, CH_2), 28.39 (1C, CH_2), 28.16 (1C, CH), 28.09 (1C, CH_2), 25.83 (2C, CH_2), 24.44 (1C, CH_2), 23.98 (1C, CH_2), 22.97 (1C, CH_3), 22.71 (1C, CH_3), 21.20 (1C, CH_2), 19.54 (1C, CH_3), 18.87 (1C, CH_3), 12.01 (1C, CH_3)

IR (cm^{-1}): 2924 (s, ArH), 2862 (m, ArH), 1705 (s, C=O), 1604 (m, C-O)

Mass (ESI):

m/z = 761.5143 ($M+Na$)⁺, 610.19

calculated = 761.5121 ($M+Na$)⁺

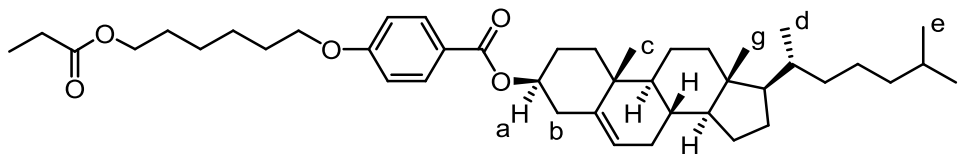
DSC/POM: Cr₁ 35.7 [3.6] Cr₂ (16.0 [-2.2] CrE) 49.2 [13.2] SmA 116.9* TGB
118.0 [0.3] N* 148.7* BP2 148.9 [0.4] Iso

The transition temperatures marked with * are only observed by POM and thus there is no measured enthalpy.

CHN microanalysis:

Observed: C 77.49 %, H 9.32 %, N 0.00 %

Calculated: C 79.63 %, H 9.55 %, N 0.00 %

10.3.87 Cholesteryl 4-(6-(propanoyloxy)hexyloxy)benzoate, **46**

4-(6-Hydroxyhexyloxy) cholesterol benzoate, **97** (100 mg, 0.165 mmol), propionic acid (15 mg, 0.198 mmol), EDAC (31 mg, 0.198 mmol) and DMAP (5 mg, 0.019 mmol) were dissolved in DCM (20 mL) and stirred over night. The solvent was removed *in vacuo* and the product purified by flash column chromatography (flash grade silica, Chloroform, R_f 0.32) to yield **46** as a white crystalline solid (34.1 mg, 31.2 %).

^1H NMR: (400 MHz, CDCl_3 , CHCl_3 internal standard)

δ (ppm) = 7.97 (d (J = 8.9 Hz), 2H, ArH), 6.88 (d (J = 9.0 Hz), 2H, ArH), 5.41 (d (J = 3.7 Hz), 1H, C=CH), 4.89 – 4.74 (m, 1H, CH_aOOC), 4.08 (t (J = 6.7 Hz), 2H, CH_2O), 4.00 (t (J = 6.4 Hz), 2H, CH_2O), 2.44 (d (J = 7.7 Hz), 2H, CH_{2b}), 2.32 (q (J = 7.6 Hz), 2H, CH_2COO), 2.06 – 1.94 (m, 3H, alkH), 1.94 – 1.86 (m, 1H, alkH), 1.86 – 1.74 (m, 3H, alkH), 1.74 – 1.61 (m, 3H, alkH), 1.61 – 1.39 (m, 9H, alkH), 1.40 – 1.28 (m, 3H, alkH), 1.28 – 1.16 (m, 6H, alkH), 1.13 (t (J = 7.6 Hz), 3H, CH_3CH_2), 1.06 (s, 3H, CH_3c), 1.05 – 0.94 (m, 3H, alkH), 0.92 (d (J = 6.6 Hz), 3H, CH_3d), 0.87 (d (J = 1.8 Hz), 3H, CH_3e), 0.85 (d (J = 1.8 Hz), 3H, CH_3f), 0.68 (s, 3H, CH_3g)

^{13}C NMR: (100.4 MHz, CDCl_3 , CHCl_3 internal standard)

δ (ppm) = 174.75 (1C, COO), 165.93 (1C, COO), 162.83 (1C, ArC), 139.89 (1C, C=CH), 131.64 (2C, ArCH), 123.18 (1C, ArC), 122.79 (1C, C=CH), 114.05 (2C, ArCH), 74.31 (1C, CH_aO), 68.05 (1C, CH_2O), 64.38 (1C, CH_2O), 56.81 (1C, CH), 56.24 (1C, CH), 50.15 (1C, CH), 42.44 (1C, CR_4), 39.86 (1C, CH_2), 39.64 (1C, CH_2), 38.41 (1C, CH_2), 37.17 (1C, CH_2), 36.78 (1C, CR_4), 36.30 (1C, CH_2), 35.93 (1C, CH), 32.06 (1C, CH_2), 32.00 (1C, CH), 29.14 (1C, CH_2), 28.69 (1C, CH_2), 28.37 (1C,

Chapter 10: Experimental

CH₂), 28.15 (1C, CH), 28.06 (1C, CH₂), 27.73 (1C, CH₂), 25.85 (1C, CH₂), 25.83 (1C, CH₂), 24.42 (1C, CH₂), 23.96 (1C, CH₂), 22.96 (1C, CH₃), 22.70 (1C, CH₃), 21.17 (1C, CH₂), 19.52 (1C, CH₃), 18.85 (1C, CH₃), 11.99 (1C, CH₃), 9.30 (1C, CH₃)

IR (cm⁻¹): 2939 (vs, ArH), 2862 (s, ArH), 1705 (vs, C=O), 1604 (m, C-O)

Mass (ESI):

m/z = 685.4765 (M+Na)⁺, 610.19, 536.17

calculated = 385.4808 (M+Na)

DSC/POM: Cr 101.4 [39.8] SmA 142.0* TGB 152.2 [0.8] N* 182.2* BP2 185.3
[1.0] Iso

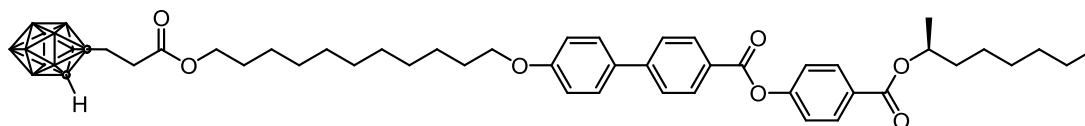
The transition temperatures marked with * are only observed by POM and thus there is no measured enthalpy.

CHN microanalysis:

Observed: C 76.70 %, H 9.82 %, N 0.00 %

Calculated: C 77.90 %, H 10.03 %, N 0.00 %

10.3.88 1-Hydrido, 2-([(S)-4-((octan-2-yloxy)carbonyl)phenyl 4'-(11-undecyloxy)biphenyl-4-carboxylate] propionate) dodecacarborane, 47



(S)-4-((octan-2-yloxy)carbonyl)phenyl 4'-(11-hydroxyundecyloxy)biphenyl-4-carboxylate (86 mg, 0.139 mmol), hydrido, 2-(propanoic acid)dodecacarborane, **79** (30 mg, 0.139 mmol), EDAC (30 mg, 0.194 mmol) and DMAP (4 mg, 0.019 mmol) were dissolved in DCM (25 mL) and stirred for 5 days. The solvent was removed *in*

Chapter 10: Experimental

vacuo and the product isolated by flash column chromatography (flash grade silica, DCM 5 % ethyl acetate, R_f 0.75) to yield **47** white crystalline solid (104 mg, 91.8 %).

^1H NMR: (500 MHz, CDCl_3 , CHCl_3 internal standard)
 δ (ppm) = 8.24 (d, (J = 8.5 Hz), 2H, ArH), 8.13 (d (J = 8.7 Hz), 2H, ArH), 7.70 (d (J = 8.5 Hz), 2H, ArH), 7.60 (d (J = 8.8 Hz), 2H, ArH), 7.31 (d (J = 8.7 Hz), 2H, ArH), 7.01 (d (J = 8.8 Hz), 2H, ArH), 5.21 – 5.12 (m, 1H, CHO), 4.09 (t (J = 6.8 Hz), 2H, CH_2O), 4.02 (t (J = 6.5 Hz), 2H, CH_2O), 3.73 (s, br, 1H, $\text{CH}_{\text{cluster}}$), 2.62 – 2.50 (m, 4H, CH_2), 2.31 (s, br, 3H, BH), 2.17 (s, br, 5H, BH), 1.88 – 1.78 (m, 2H, CH_2), 1.68 – 1.59 (m, 4H, CH_2), 1.53 – 1.43 (m, 2H, CH_2), 1.43 – 1.22 (m, 24H, alkH), 0.89 (t (J = 6.9 Hz), 3H, CH_3)

^{13}C NMR: (100.4 MHz, CDCl_3 , CHCl_3 internal standard)
 δ (ppm) = 171.66 (1C, COO), 165.61 (1C, COO), 164.78 (1C, COO), 159.76 (1C, ArC), 154.65 (1C, ArC), 146.35 (1C, ArC), 131.98 (1C, ArC), 131.27 (2C, ArCH), 130.92 (2C, ArCH), 128.65 (1C, ArC), 128.53 (2C, ArCH), 127.17 (1C, ArC), 126.76 (2C, ArCH), 121.84 (2C, ArCH), 115.13 (2C, ArCH), 74.18 (1C, $\text{C}_{\text{cluster}}$), 72.07 (1C, CHO), 68.27 (1C, CH_2O), 65.57 (1C, CH_2O), 61.65 (1C, $\text{CH}_{\text{cluster}}$), 36.20 (1C, CH_2), 33.57 (1C, CH_2), 32.76 (1C, CH_2), 31.87 (1C, CH_2), 29.66 (1C, CH_2), 29.61 (2C, CH_2), 29.51 (1C, CH_2), 29.37 (1C, CH_2), 29.32 (1C, CH_2), 29.29 (1C, CH_2), 28.62 (1C, CH_2), 26.17 (1C, CH_2), 25.98 (1C, CH_2), 25.54 (1C, CH_2), 22.72 (1C, CH_2), 20.23 (1C, CH_3CH), 14.21 (1C, CH_3CH_2)

IR (cm^{-1}): 3047 (m, ArH), 2924 (s, ArH), 2854 (s, ArH), 2576 (vs, br, BH), 1705 (vs, C=O), 1604 (s, C-O)

Mass (ESI):
 m/z = 838.5732 ($\text{M}+\text{Na}$)⁺, 466.54, 413.27, 306.32, 338.34, 316.13, 284.19
calculated = 839.5637 ($\text{M}+\text{Na}$)⁺

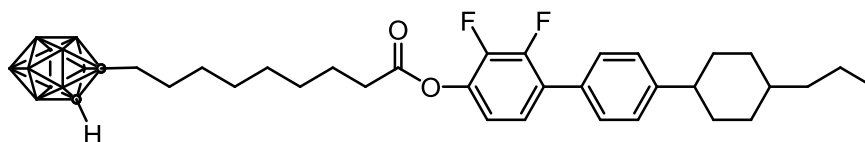
DSC/POM: Cr 101.2 [71.3] Iso

CHN microanalysis:

Observed: C 65.13 %, H 8.09 %, N 0.00 %

Calculated: C 64.84 %, H 8.16 %, N 0.00 %

10.3.89 1-Hydrido 2-(2,3-difluoro-4'-(4-propylcyclohexyl)biphenyl-4-yl nonanoate)dodecacarborane, 48



1-Hydrido, 2-(nonanoic acid)dodecacarborane, **74** (31 mg, 0.103 mmol), 2,3-difluoro-4'-(4-propylcyclohexyl)biphenyl-4-ol (41 mg, 0.124 mmol), EDAC (20 mg, 0.124 mmol) and DMAP (3 mg, 0.01 mmol) were dissolved in DCM (20 mL) and stirred over night. The solvent was removed *in vacuo* and the product isolated by flash column chromatography (flash grade silica, DCM, R_f 0.81) and then precipitated from DCM/MeOH to yield **48** (24 mg, 37.9 %).

^1H NMR: (400 MHz, CDCl_3 , CHCl_3 internal standard)

δ (ppm) = 7.44 (d (J = 8.1 Hz), 2H, ArH), 7.30 (d (J = 8.2 Hz), 2H, ArH), 7.21 – 7.14 (m, 1H, ArH), 6.98 – 6.91 (m, 1H, ArH), 3.56 (s, br, 1H, $\text{CH}_{\text{cluster}}$), 2.63 (t (J = 7.3 Hz), 2H, CH_2COO), 2.57 – 2.46 (m, 1H, CH), 2.25 – 2.13 (m, 2H, CH_2), 1.99 – 1.85 (m, 4H, CH_2), 1.82 – 1.74 (m, 2H, CH_2), 1.63 – 1.17 (m, 17H, alkH), 1.13 – 1.02 (m, 2H, alkH), 0.91 (t (J = 7.2 Hz), 3H, CH_3)

^{13}C NMR: (100.4 MHz, CDCl_3 , CHCl_3 internal standard)

δ (ppm) = 171.12 (1C, COO), 148.30 (1C, ArC), 146.20 (dd (J = 245.6, 13.4 Hz), 1C, ArCF), 142.76 – 138.08 (m, 1C, ArCF), 132.90 – 132.66 (m, 1C, ArC-O), 131.81 (1C, ArC), 128.89 (d (J = 2.6 Hz), 2C, ArCH),

Chapter 10: Experimental

127.31 (2C, ArCH), 124.12 (d ($J = 3.5$ Hz), 1C, ArC), 118.40 (1C, ArCH), 114.58 (1C, ArCH), 75.53 (1C, C_{cluster}), 61.08 (1C, $\text{CH}_{\text{cluster}}$), 44.51 (1C, CH), 39.85 (1C, CH), 38.22 (1C, CH_2), 37.14 (1C, CH_2), 34.39 (2C, CH_2), 33.92 (1C, CH_2), 33.66 (2C, CH_2), 29.29 (1C, CH_2), 29.08 (1C, CH_2), 29.02 (1C, CH_2), 28.95 (1C, CH_2), 28.91 (1C, CH_2), 24.91 (1C, CH_2), 20.18 (1C, CH_2), 14.57 (1C, CH_3)

^{11}B NMR: (128 MHz, CDCl_3)

δ (ppm) = -3.38 (1B), -6.89 (1B), -10.32 (2B), -12.36 (2B), -13.17 (2B), -14.12 (2B)

IR (cm^{-1}): 2924 (s, ArH), 2854 (m, ArH), 2576 (s, br, BH), 1766 (vs, C=O), 1735 (m, C=O), 1604 (m, C-O)

Mass (LIFDI):

m/z = 614.4650 (M^+), 73.95

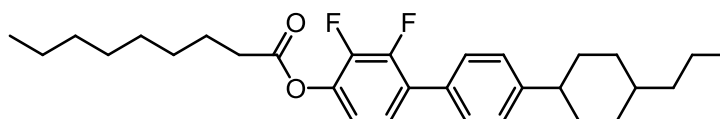
DSC/POM: Cr 123.3 [14.7] Iso

CHN microanalysis: (VO_5 combustion aid)

Observed: C 65.38 %, H 8.36 %, N 0.00 %

Calculated: C 62.71 %, H 8.22 %, N 0.00 %

10.3.90 2,3-Difluoro-4'-(4-propylcyclohexyl)biphenyl-4-yl nonanoate, **49**



2,3-Difluoro-4'-(4-propylcyclohexyl)biphenyl-4-ol (125 mg, 0.379 mmol), nonanoic acid (80 mg, 0.506 mmol), EDAC (59 mg, 0.379 mmol) and DMAP (10 mg, 0.04 mmol) were dissolved in DCM (20 mL) and stirred over night. The solvent was removed *in vacuo* and the product isolated by flash column chromatography (flash

Chapter 10: Experimental

grade silica, DCM, R_f 0.81) and purified by precipitation from DCM/MeOH to yield **49** as a white crystalline solid (105 mg, 58.9 %).

^1H NMR: (400 MHz, CDCl_3 , CHCl_3 internal standard)
 δ (ppm) = 7.45 (dd (J = 8.1, 1.3 Hz), 2H, ArH), 7.31 (d (J = 8.2 Hz), 2H, ArH), 7.22 – 7.15 (m, 1H, ArH), 7.00 – 6.93 (m, 1H, ArH), 2.64 (t (J = 7.5 Hz), 2H, CH_2COO), 2.59 – 2.47 (m, 1H, CH), 2.01 – 1.86 (m, 4H, CH_2), 1.86 – 1.73 (m, 2H, CH_2), 1.58 – 1.19 (m, 17H, alkH), 1.15 – 1.01 (m, 2H, CH_2), 0.93 (t (J = 6.8 Hz), 3H, CH_3), 0.91 (d (J = 6.9 Hz), 3H, CH_3)

^{13}C NMR: (100.4 MHz, CDCl_3 , CHCl_3 internal standard)
 δ (ppm) = 171.19 (1C COO), 148.68 (dd (J = 250.8, 11.4 Hz), 1C, ArCF), 148.22 (1C, ArC), 143.77 (dd (J = 251.0, 15.2 Hz), 1C, ArCF), 138.35 (d (J = 9.0 Hz), 1C, ArC), 131.87 (1C, ArC), 128.89 (d (J = 2.9 Hz), 2C, ArCH), 128.75 (1C, ArCH), 127.27 (2C, ArCH), 124.04 (t (J = 3.6 Hz), 1C, ArC), 118.41 (d (J = 3.9 Hz), 1C, ArCH), 44.51 (1C, CH), 39.85 (1C, CH), 37.15 (1C, CH_2), 34.44 (2C, CH_2), 34.00 (1C, CH_2), 33.66 (2C, CH_2), 31.94 (1C, CH_2), 29.33 (1C, CH_2), 29.25 (1C, CH_2), 29.14 (1C, CH_2), 25.03 (1C, CH_2), 22.79 (1C, CH_2), 20.18 (1C, CH_2), 14.55 (1C, CH_3), 14.23 (1C, CH_3)

IR (cm^{-1}): 2916 (s, ArH), 2854 (s, ArH), 1766 (vs, C=O), 1604 (w, C-O)

Mass (ESI):

m/z = 493.2883 ($\text{M}+\text{Na}$)⁺, 471.31 ($\text{M}+\text{H}$)⁺

calculated = 493.2894 ($\text{M}+\text{Na}$)⁺

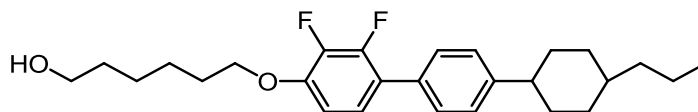
DSC/POM: Cr 92.9 [28.4] N 138.7 [0.6] Iso

CHN microanalysis:

Observed: C 76.57 %, H 8.56 %, N 0.00 %

Calculated: C 76.56 %, H 8.57 %, N 0.00 %

10.3.91 6-(2,3-Difluoro-4'-(4-propylcyclohexyl)biphenyl-4-yloxy)hexan-1-ol, 98



2,3-Difluoro-4'-(4-propylcyclohexyl)biphenyl-4-ol (150 mg, 0.454 mmol), K_2CO_3 (188 mg, 1.302 mmol) and KI (50 mg, 0.3 mmol) were suspended in butanone (25 mL) and brought to reflux. Next 6-bromo-hexan-1-ol (99 mg, 0.545 mmol) was added and the solution refluxed over night. The solution was allowed to cool, filtered and the solvent removed *in vacuo*. The product was dissolved in DCM (30 mL) and passed through a silica pad eluting with DCM and then recrystallized from acetonitrile to yield **98** as a white crystalline solid (109 mg, 55.8 %).

1H NMR: (400 MHz, $CDCl_3$, $CHCl_3$ internal standard)
 δ (ppm) = 7.43 (d ($J = 6.9$ Hz), 2H, ArH), 7.28 (d ($J = 8.2$ Hz), 2H, ArH), 7.09 (td ($J = 8.5, 2.1$ Hz), 1H, ArH), 6.83 – 6.73 (m, 1H, ArH), 4.07 (t ($J = 6.5$ Hz), 2H, CH_2O), 3.67 (t ($J = 6.5$ Hz), 2H, CH_2), 2.59 – 2.45 (m, 1H, CH), 2.01 – 1.78 (m, 6H, alkH), 1.70 – 1.57 (m, 3H, alkH), 1.57 – 1.41 (m, 5H, alkH), 1.41 – 1.28 (m, 3H, alkH), 1.28 – 1.16 (m, 2H, CH_2), 1.16 – 0.99 (m, 2H, CH_2), 0.92 (t ($J = 7.2$ Hz), 3H, CH_3)

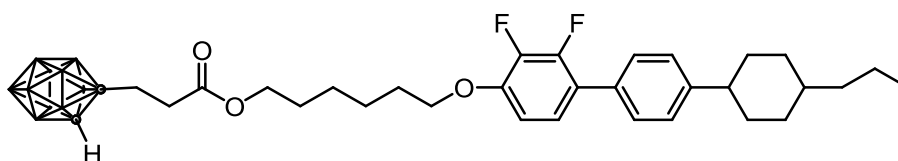
^{13}C NMR: (100.4 MHz, $CDCl_3$, $CHCl_3$ internal standard)
 δ (ppm) = 148.95 (dd ($J = 247.0, 9.4$ Hz), 1C, ArCF), 147.67 – 147.37 (m, 1C, ArCH), 147.51 (1C, ArC), 141.89 (dd ($J = 246.9, 15.1$ Hz), 1C, ArCF), 132.43 (1C, ArC), 128.69 (d ($J = 2.8$ Hz), 2C, ArCH), 127.15 (2C, ArCH), 123.61 (t ($J = 4.1$ Hz) 1C, ArCH), 123.14 (d ($J = 11.0$ Hz), 1C, ArC), 109.59 (1C, ArC), 69.81 (1C, CH_2O), 62.92 (1C, CH_2O), 44.44 (1C, CH), 39.83 (1C, CH), 37.12 (1C, CH_2), 34.39 (2C, CH_2), 33.65 (2C, CH_2), 32.73 (1C, CH_2), 29.24 (1C, CH_2), 25.85 (1C, CH_2), 25.60 (1C, CH_2), 20.15 (1C, CH_2), 14.54 (1C, CH_3)

IR (cm^{-1}): 3302 (vs, br, OH), 2916 (s, ArH), 2854 (s, ArH), 1635 (m, C-O)

Mass (ESI):

m/z = 453.2583 (M+Na)⁺, 431.28 (M+H)⁺calculated = 453.2581 (M+Na)⁺

10.3.92 1-Hydrido, 2-([6-(2,3-difluoro-4'-(4-propylcyclohexyl)biphenyl-4-yloxy)hexoyloxy] propionate) dodecacarborane, 50



6-(2,3-Difluoro-4'-(4-propylcyclohexyl)biphenyl-4-yloxy)hexan-1-ol, **98** (38 mg, 0.088 mmol), hydrido, 2-(propanoic acid)dodecacarborane, **79** (22 mg, 0.1 mmol), EDAC (16 mg, 0.1 mmol) and DMAP (3 mg, 0.012 mmol) were dissolved in DCM (10 mL) and stirred for 3 days. The solution was passed through a silica pad eluting with DCM to yield **50** as a white low melting solid (40 mg, 77.3 %).

¹H NMR: (400 MHz, CDCl₃, CHCl₃ internal standard)

δ (ppm) = 7.43 (dd (*J* = 8.1, 1.3 Hz), 2H, ArH), 7.28 (d (*J* = 8.2 Hz), 2H, ArH), 7.09 (td (*J* = 8.5, 2.3 Hz), 1H, ArH), 6.83 – 6.72 (m, 1H, ArH), 4.11 (t (*J* = 6.7 Hz), 2H, CH₂O), 4.08 (t (*J* = 6.9 Hz), 2H, CH₂O), 3.73 (s, br, 1H, CH_{cluster}), 2.64 – 2.46 (m, 4H, CH₂), 2.02 – 1.79 (m, 6H, alkH), 1.74 – 1.63 (m, 2H, alkH), 1.62 – 1.41 (m, 6H, alkH), 1.41 – 1.30 (m, 3H, alkH), 1.30 – 1.16 (m, 3H, alkH), 1.15 – 1.00 (m, 2H, alkH), 0.91 (t (*J* = 7.2 Hz), 3H, CH₃)

¹³C NMR: (100.4 MHz, CDCl₃, CHCl₃ internal standard)

δ (ppm) = 171.66 (1C, COO), 148.97 (dd (*J* = 248.7, 11.1 Hz), 1C, ArCF), 147.61 (1C, ArC), 147.58 – 147.47 (m, 1C, ArCH), 141.93 (dd (*J* = 246.8, 15.4 Hz), 1C, ArCF), 132.42 (1C, ArC), 128.72 (d (*J* = 2.8 Hz), 2C, ArCH), 127.20 (2C, ArCH), 123.68 (t (*J* = 4.1 Hz), 1C, ArC), 123.28 (d (*J* = 10.9 Hz), 1C, ArCH), 109.64 (1C, ArC), 74.17

Chapter 10: Experimental

(1C, C_{cluster}), 69.76 (1C, CH₂O), 65.38 (1C, CH₂O), 61.67 (1C, CH_{cluster}), 44.48 (1C, CH), 39.85 (1C, CH), 37.15 (1C, CH₂), 34.42 (2C, CH₂), 33.68 (2C, CH₂), 33.56 (1C, CH₂), 32.76 (1C, CH₂), 29.16 (1C, CH₂), 28.56 (1C, CH₂), 25.80 (1C, CH₂), 25.78 (1C, CH₂), 20.17 (1C, CH₂), 14.56 (1C, CH₃)

¹¹B NMR: (128 MHz, CDCl₃)
δ (ppm) = -3.06 (1B), -6.50 (1B), -10.36 (2B), -12.55 (2B), -13.11 (2B), -13.81 (2B)

IR (cm⁻¹): 3055 (w, ArH), 2924 (s, ArH), 2854 (m, ArH), 2584 (vs, br, BH), 1720 (s, C=O), 1627 (w, C-O)

Mass (LIFDI):

m/z = 628.43 (M)⁺

DSC/POM: Cr₁ 78.4 [6.5] Cr₂ (20.1* SmA) 97.9 [35.3] Iso

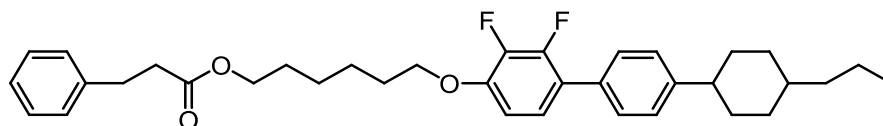
The transition temperature marked with * is only observed by POM and thus there is no measured enthalpy.

CHN microanalysis: (VO₅ combustion aid)

Observed: C 60.67 %, H 8.12 %, N 0.00 %

Calculated: C 61.12 %, H 8.01 %, N 0.00 %

10.3.93 6-(2,3-Difluoro-4'-(4-propylcyclohexyl)biphenyl-4-yloxy)hexyl 3-phenylpropanoate, 51



6-(2,3-Difluoro-4'-(4-propylcyclohexyl)biphenyl-4-yloxy)hexan-1-ol, **98** (34.5 mg, 0.08 mmol), hydrocinnamic acid (15 mg, 0.1 mmol), EDAC (16 mg, 0.10 mmol) and DMAP (2 mg, 0.008 mmol) were dissolved in DCM (10 mL) and stirred for 3 days.

Chapter 10: Experimental

The solution was passed through a silica pad eluting with DCM to yield **51** as a low melting white solid (43 mg, 95.5 %).

^1H NMR: (400 MHz, CDCl_3 , CHCl_3 internal standard)
 δ (ppm) = 7.44 (dd ($J = 8.1, 1.4$ Hz), 2H, ArH), 7.33 – 7.27 (m, 4H, ArH), 7.25 – 7.17 (m, 3H, ArH), 7.09 (td ($J = 8.5, 2.3$ Hz), 1H, ArH), 6.83 – 6.74 (m, 1H, ArH), 4.10 (t ($J = 5.8$ Hz), 2H, CH_2O), 4.07 (t ($J = 5.6$ Hz), 2H, CH_2O), 2.97 (t ($J = 7.8$ Hz), 2H, CH_2), 2.65 (t ($J = 7.8$ Hz), 2H, CH_2), 2.57 – 2.46 (m, 1H, CH), 2.03 – 1.78 (m, 6H, alkH), 1.71 – 1.60 (m, 2H, alkH), 1.59 – 1.47 (m, 3H, alkH), 1.47 – 1.17 (m, 8H, alkH), 1.17 – 1.01 (m, 2H, alkH), 0.92 (t ($J = 7.2$ Hz), 3H, CH_3)

^{13}C NMR: (100.4 MHz, CDCl_3 , CHCl_3 internal standard)
 δ (ppm) = 173.15 (1C, COO), 148.98 (dd ($J = 248.8, 11.0$ Hz), 1C, ArCF), 147.56 (1C, ArC), 145.40 (dd ($J = 448.5, 10.2$ Hz), 1C, ArCF), 140.66 (1C, ArC), 140.55 (d ($J = 46.1$ Hz), 1C, ArCH), 132.46 (1C, ArC), 128.73 (d ($J = 2.6$ Hz), 2C, ArCH), 128.60 (2C, ArCH), 128.41 (2C, ArCH), 127.18 (2C, ArCH), 126.36 (1C, ArCH), 123.63 (1C, ArC), 123.23 (d ($J = 10.8$ Hz), 1C, ArCH), 109.62 (1C, ArC), 69.78 (1C, CH_2O), 64.56 (1C, CH_2O), 44.47 (1C, CH), 39.85 (1C, CH), 37.14 (1C, CH_2), 36.03 (1C, CH_2), 34.42 (2C, CH_2), 33.68 (2C, CH_2), 31.12 (1C, CH_2), 29.18 (1C, CH_2), 28.67 (1C, CH_2), 25.81 (1C, CH_2), 25.74 (1C, CH_2), 20.17 (1C, CH_2), 14.56 (1C, CH_3)

IR (cm^{-1}): 2924 (s, ArH), 2854 (s, ArH), 1728 (vs, C=O), 1627 (m, C-O)

Mass (ESI):

m/z = 585.3143 ($\text{M}+\text{Na}$)⁺, 563.33 ($\text{M}+\text{H}$)⁺

calculated = 585.3156($\text{M}+\text{Na}$)⁺

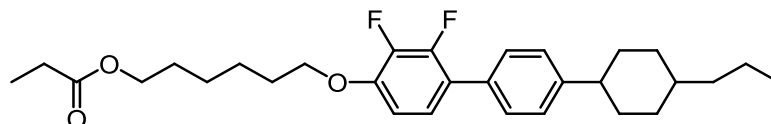
DSC/POM: Glass -28.0 SmA 34.8 [0.3] N 46.9 [0.3] Iso

CHN microanalysis:

Observed: C 76.22 %, H 7.99 %, N 0.00 %

Calculated: C 76.84 %, H 7.88 %, N 0.00 %

10.3.94 6-(2,3-Difluoro-4'-(4-propylcyclohexyl)biphenyl-4-yloxy)hexyl propionate, **52**



6-(2,3-Difluoro-4'-(4-propylcyclohexyl)biphenyl-4-yloxy)hexan-1-ol, **98** (35 mg, 0.08 mmol), propionic acid (8 mg, 0.1 mmol), EDAC (16 mg, 0.1 mmol) and DMAP (2 mg, 0.008 mmol) were dissolved in DCM (10 mL) and stirred for 3 days. The solution was passed through a silica pad eluting with DCM and the solvent removed *in vacuo* to yields **52** as a low melting white solid (38 mg, 97.6 %).

¹H NMR: (400 MHz, CDCl₃, CHCl₃ internal standard)

δ (ppm) = 7.43 (dd (*J* = 8.2, 1.5 Hz), 2H, ArC), 7.28 (d (*J* = 8.2 Hz), 2H, ArH), 7.08 (td (*J* = 8.5, 2.3 Hz), 1H, ArH), 6.81 – 6.73 (m 1H, ArH), 4.09 (t (*J* = 6.7 Hz), 2H, CH₂O), 4.07 (t (*J* = 6.5 Hz), 2H, CH₂O), 2.57 – 2.46 (m, 1H, CH), 2.33 (q (*J* = 7.6 Hz), 2H, CH₂COO), 1.98 – 1.80 (m, 6H, alkH), 1.74 – 1.63 (m, 2H, alkH), 1.58 – 1.42 (m, 6H, alkH), 1.42 – 1.29 (m, 3H, alkH), 1.29 – 1.18 (m, 3H, alkH), 1.15 (t (*J* = 7.6 Hz), 3H, CH₃), 1.11 – 0.99 (m, 2H, alkH), 0.91 (t (*J* = 7.3 Hz), 3H)

¹³C NMR: (100.4 MHz, CDCl₃ internal standard)

δ (ppm) = 174.75 (1C, COO), 148.98 (dd (*J* = 248.5, 11.1 Hz), 1C, ArCF), 147.56 (1C, ArC), 145.40 (dd (*J* = 449.3, 10.0 Hz), 1C, ArCF), 140.71 (d (*J* = 15.1 Hz), 1C, ArC), 132.47 (1C, ArC), 128.73 (d (*J* = 2.7 Hz), 2C, ArCH), 127.18 (2C, ArCH), 123.63 (t (*J* = 4.1 Hz), 1C, ArC), 123.22 (d (*J* = 10.9 Hz), 1C, ArC), 109.64 (d (*J* = 2.5 Hz), 1C, ArC), 69.79 (1C, CH₂O), 64.40 (1C, CH₂O), 44.48 (1C, CH), 39.85 (1C, CH), 37.15 (s), 34.42 (2C, CH₂), 33.68 (2C, CH₂), 29.20 (1C,

Chapter 10: Experimental

CH_2), 28.71 (1C, CH_2), 27.74 (1C, CH_2), 25.85 (1C, CH_2), 25.76 (1C, CH_2), 20.17 (1C, CH_2), 14.55 (1C, CH_3), 9.30 (1C, CH_3)

IR (cm^{-1}): 2924 (s, ArH), 2854 (s, ArH), 1735 (vs, C=O), 1627 (m, C-O)

Mass (ESI):

m/z = 509.2816 (M+Na)⁺, 478.31 (M+H)⁺

calculated = 509.2843 (M+Na)⁺

DSC/POM: Cr₁ 7.8 [1.1] Cr₂ 28.9 [24.3] SmA 55.0 [0.2] N 94.6 [0.5] Iso

CHN microanalysis:

Observed: C 74.24 %, H 8.48 %, N 0.00 %

Calculated: C 74.04 %, H 8.29 %, N 0.00 %

Appendix: List of Final Compounds

Appendix: List of Final Compounds

1	
2	
3	
4	
8	
9	

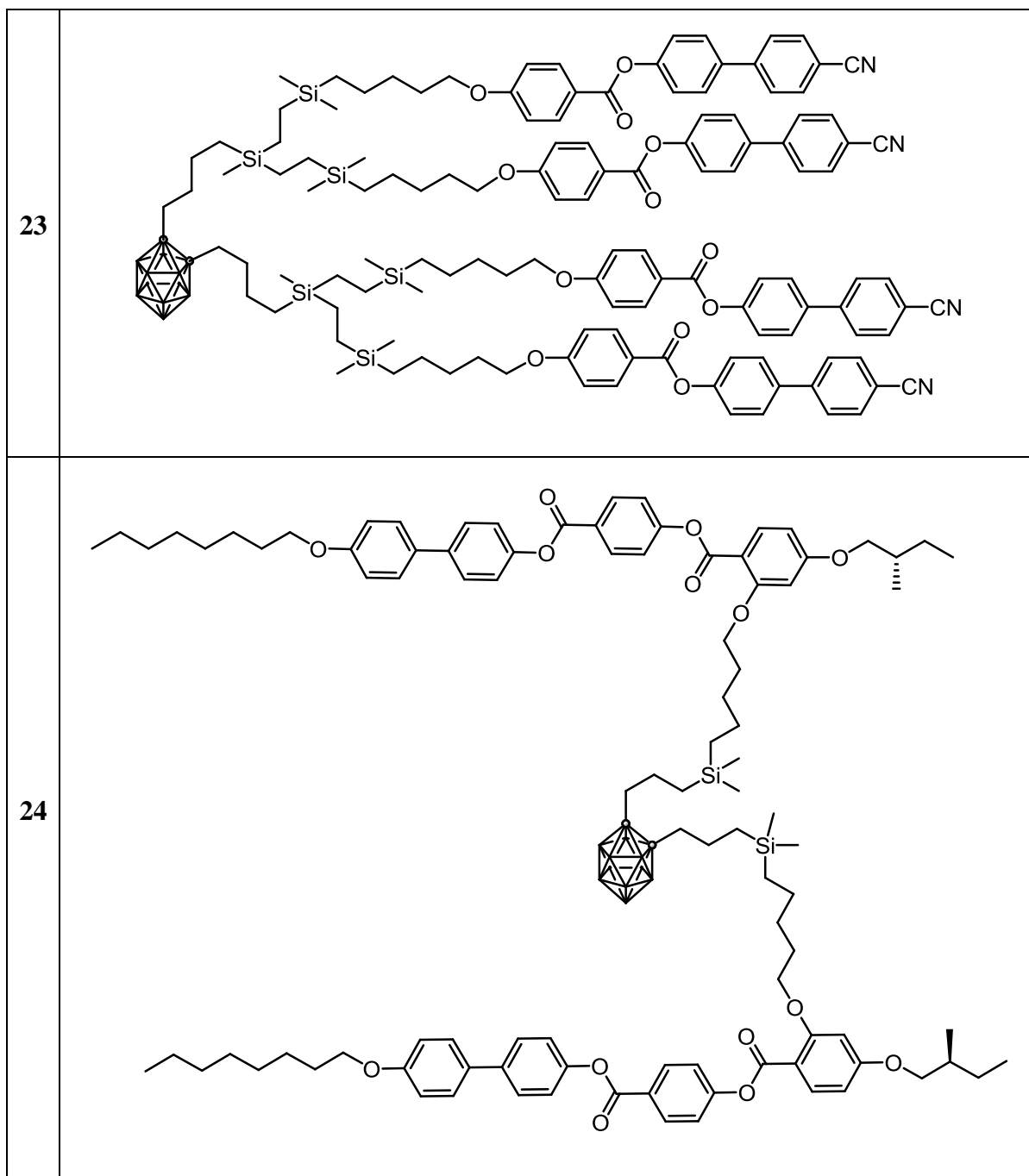
Appendix: List of Final Compounds

10	
11	
12	
13	
14	

Appendix: List of Final Compounds

15	
20	
21	
22	

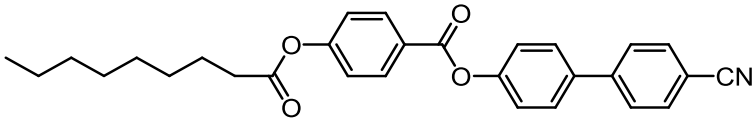
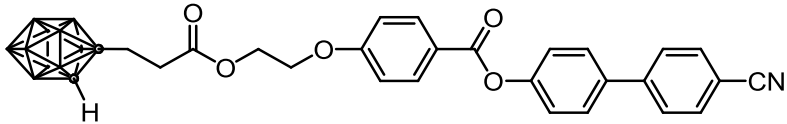
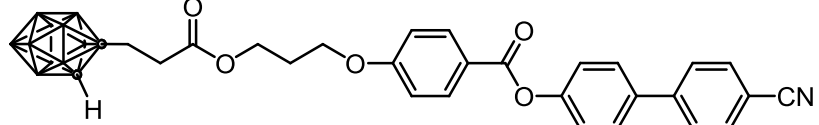
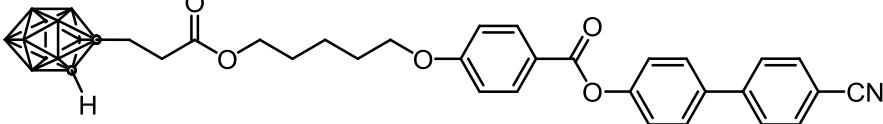
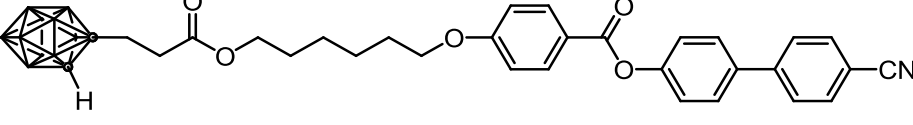
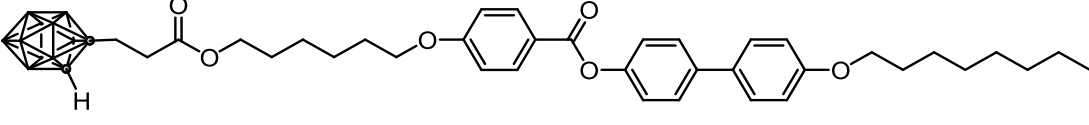
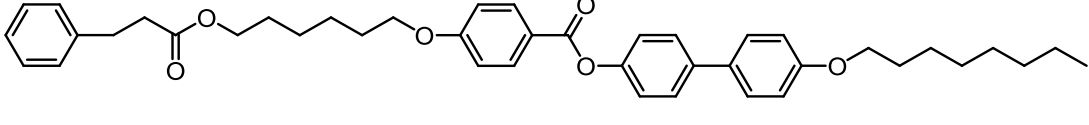
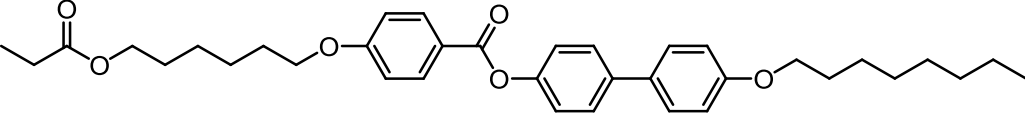
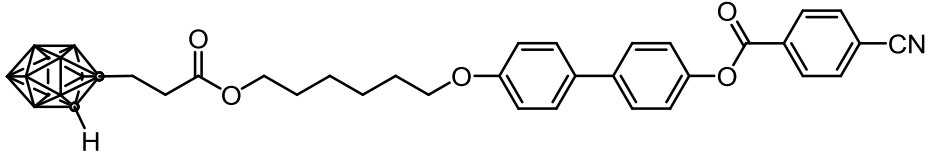
Appendix: List of Final Compounds



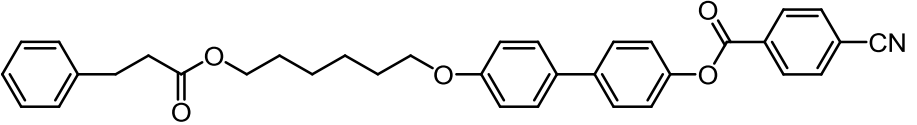
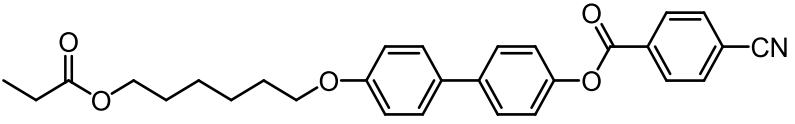
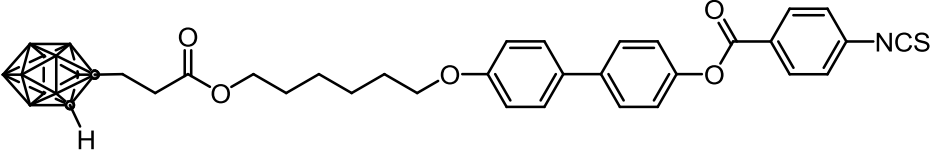
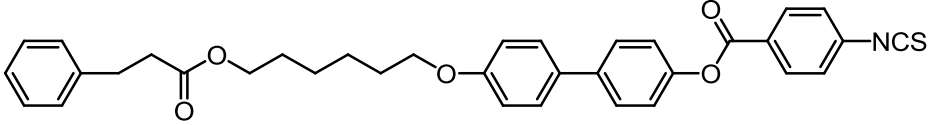
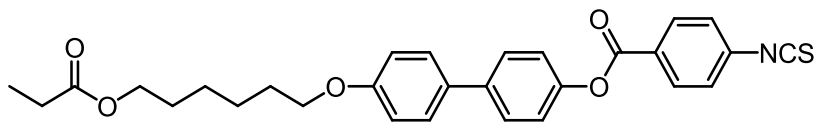
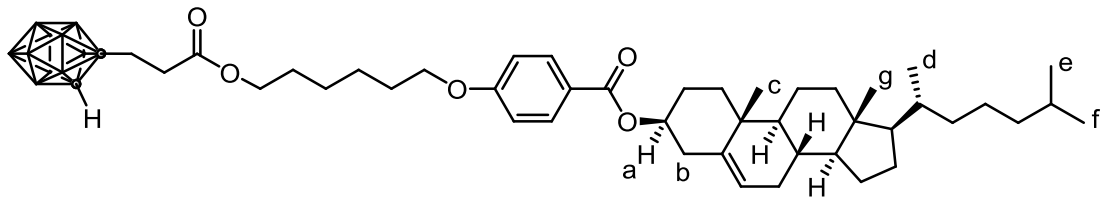
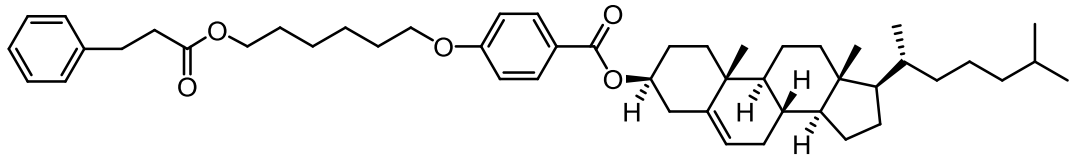
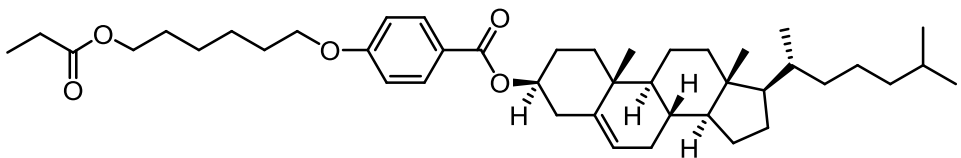
Appendix: List of Final Compounds

25	
27	
28	
29	

Appendix: List of Final Compounds

30	
31	
32	
33	
34	
35	
36	
37	
38	

Appendix: List of Final Compounds

39	
40	
41	
42	
43	
44	
45	
46	

Appendix: List of Final Compounds

47	
48	
49	
50	
51	
52	

Abbreviations

Abbreviations

LC	Liquid crystal
N	Nematic
SmA	Smectic A
SmC	Smectic C
SmB	Smectic B
N*	Chiral nematic
\hat{n}	Director
SMM	Single-molecule magnets
CB	Cyanobiphenyl
2D	Two-dimensional
3D	Three-dimensional
POSS	Polyhedral octasilsesquioxane
POM	Polarised optical microscopy
DSC	Differential scanning calorimetry
Iso	Isotropic
z	Layer normal
HexB	Hexatic B
SCLCP	Side-chain liquid crystal polymer
MCLCP	Main-chain liquid crystal polymer
3D	Three-dimensional
MO	Molecular orbital
2D	Two-dimensional
TGB	Twist grain boundary
BP2	Blue phase II
CrE	Crystal E
SmC*	Chiral smectic C
EDAC	<i>N</i> -(3-nimethylaminopropyl)- <i>N'</i> -ethylcarbodiimide hydrochloride
TLC	Thin layer chromatography
NMR	Nuclear magnetic resonance
s	Singlet
d	Doublet
t	Triplet
q	Quartet
dd	Double doublet

Abbreviations

ddd	Double double doublet
dt	Double triplet
ddt	Double double triplet
m	Multiplet
MS	Mass spectrometry
ESI	electrospray ionization
LIFDI	liquid introduction field desorption ionization
MALDI	Matrix assisted laser desorption ionization
IR	Infra-red spectroscopy
CHN	Carbon, hydrogen and nitrogen microanalysis
DMF	Dimethylformamide
DCC	N,N-Dicyclohexylcarboiimide
DMAP	4-Dimethylaminopyridine
THF	Tetrahydrofuran
ppm	Parts per million
DCM	Dichloromethane
Hex	Hexane
w/w	weight for weight
SmA ₂	Smectic A bilayer
SmA _d	Interdigitated smectic A
SmA ₁	Smectic A monolayer
SmA*	Chiral smectic A
RT	Room temperature
XRD	X-ray diffraction
Iso liq.	Isotropic liquid
Pd/C	Palladium on carbon

References

1. P. J. Collings and M. Hird, *Introduction to Liquid Crystals: Chemistry and Physics, Chapter 7*, Taylor and Francis, London, 1997.
2. P. J. Collings and M. Hird, *Introduction to Liquid Crystals: Chemistry and Physics, Chapter 3*, Taylor and Francis, London, 1997.
3. S. Chandrasekhar, *Liquid Crystals, Chapter 2*, Cambridge University Press, Cambridge, 1977.
4. P. J. Collings and M. Hird, *Introduction to Liquid Crystals: Chemistry and Physics, Chapter 1*, Taylor and Francis, London, 1997.
5. G. W. Gray and J. W. Goodby, *Smectic Liquid Crystals: Textures and structures, Chapter 1*, Leonard Hill, Glasgow, 1984.
6. G. W. Gray and J. W. Goodby, *Smectic Liquid Crystals: Textures and Structures, Chapter 2*, Leonard Hill, Glasgow, 1984.
7. A. Wulf, *Phys. Rev. A: At. Mol. Opt. Phys.*, 1975, **11**, 365.
8. W. L. McMillan, *Phys. Rev. A: At. Mol. Opt. Phys.*, 1973, **8**, 1921.
9. G. W. Gray and J. W. Goodby, *Smectic Liquid Crystals: Textures and Structures, Chapter 10*, Leonard Hill, Glasgow, 1984.
10. P. J. Collings and M. Hird, *Introduction to Liquid Crystals: Chemistry and Physics, Chapter 6*, Taylor and Francis, London, 1997.
11. T. Harada and P. Crooker, *Mol. Cryst. Liq. Cryst.*, 1975, **30**, 79-86.
12. C. Tschierske, *Isr. J. Chem.*, 2012, **52**, 935-959.
13. K. Borisch, S. Diele, P. Goring, H. Muller and C. Tschierske, *Liq. Cryst.*, 1997, **22**, 427-443.
14. B. M. Rosen, C. J. Wilson, D. A. Wilson, M. Peterca, M. R. Imam and V. Percec, *Chem. Rev.*, 2009, **109**, 6275-6540.
15. D. Lose, S. Diele, G. Pelzl, E. Dietzmann and W. Weissflog, *Liq. Cryst.*, 1998, **24**, 707-717.
16. J. Y. Jang and Y. W. Park, *Liq. Cryst.*, 2013, **40**, 511-515.
17. J. Newton, H. Coles, P. Hodge and J. Hannington, *J. Mater. Chem.*, 1994, **4**, 869-874.
18. C. Meyer, Y. Nastishin and M. Kleman, *Mol. Cryst. Liq. Cryst.*, 2007, **477**, 43/[537]-553/[547].
19. C. T. Imrie and P. A. Henderson, *Chem. Soc. Rev.*, 2007, **36**, 2096-2124.
20. W. S. Bae, J. W. Lee and J. I. Jin, *Liq. Cryst.*, 2001, **28**, 59-67.
21. C. T. Imrie and P. A. Henderson, *Curr. Opin. Colloid Interface Sci.*, 2002, **7**, 298-311.
22. C. B. McArdle, *Side Chain Liquid Crystal Polymers*, Springer, 1989.
23. A. Greiner, H.-W. Schmidt, D. Demus, J. Goodby, G. W. Gray, H. W. Spiess and V. Vill, *Handbook of Liquid Crystals: Part IV*, Wiley-VCH Verlag GmbH, 2008.
24. P. J. Collings, *Liquid Crystals: Natures Delicate Phase of Matter*, 2nd edn., Princeton University Press, Princeton, 2001.
25. P. J. Collings and M. Hird, *Introduction to Liquid Crystals: Chemistry and Physics, Chapter 5*, Taylor and Francis, London, 1997.
26. I. M. Saez and J. W. Goodby, *J. Mater. Chem.*, 2005, **15**, 26-40.
27. I. M. Saez and J. W. Goodby, *Supramolecular Soft Matter Chapter 15*, John Wiley & Sons, Inc., 2011.

References

28. C. Tschierske, *J. Mater. Chem.*, 1998, **8**, 1485-1508.
29. G. R. Newkome, C. N. Moorefield and F. Vögtle, *Denrimers and Dendrons: Concepts, Syntheses and Applications*, Wiley, Germany, 2001.
30. V. S. K. Balagurusamy, G. Ungar, V. Percec and G. Johansson, *J. Am. Chem. Soc.*, 1997, **119**, 1539-1555.
31. B. Donnio, S. Buathong, I. Bury and D. Guillon, *Chem. Soc. Rev.*, 2007, **36**, 1495-1513.
32. J. W. Goodby, G. H. Mehl, I. M. Saez, R. P. Tuffin, G. Mackenzie, R. Auzely-Velty, T. Benvegna and D. Plusquellec, *Chem. Commun.*, 1998, 2057-2070.
33. V. Percec, M. R. Imam, M. Peterca, W. D. Cho and P. A. Heiney, *Isr. J. Chem.*, 2009, **49**, 55-70.
34. C. Schlenk and H. Frey, *Monatsh. Chem.*, 1999, **130**, 3-14.
35. K. Lorenz, D. Holter, B. Stuhn, R. Mulhaupt and H. Frey, *Adv. Mater.*, 1996, **8**, 414-&.
36. Y. Molard, F. Dorson, V. Circu, T. Roisnel, F. Artzner and S. Cordier, *Angew. Chem.-Int. Edit.*, 2010, **49**, 3351-3355.
37. W. Li, W. F. Bu, H. L. Li, L. X. Wu and M. Li, *Chem. Commun.*, 2005, 3785-3787.
38. E. Terazzi, C. Bourgogne, R. Welter, J. L. Gallani, D. Guillon, G. Rogez and B. Donnio, *Angew. Chem.-Int. Edit.*, 2008, **47**, 490-495.
39. V. Percec, W. D. Cho and G. Ungar, *J. Am. Chem. Soc.*, 2000, **122**, 10273-10281.
40. B. Kosata, G. M. Tamba, U. Baumeister, K. Pelz, S. Diele, G. Pelzl, G. Galli, S. Samaritani, E. V. Agina, N. I. Boiko, V. P. Shibaev and W. Weissflog, *Chem. Mater.*, 2006, **18**, 691-701.
41. B. Donnio and D. Guillon, *Supramolecular Polymers Polymeric Betains Oligomers*, Springer-Verlag Berlin, Berlin, 2006.
42. S. K. Ahn, M. Gopinadhan, P. Deshmukh, R. K. Lakhman, C. O. Osuji and R. M. Kasi, *Soft Matter*, 2012, **8**, 3185-3191.
43. T. Narumi, Y. Miura, T. Ashina and A. Yoshizawa, *Liq. Cryst.*, 2011, **38**, 639-648.
44. A. Yoshizawa, *J. Mater. Chem.*, 2008, **18**, 2877-2889.
45. T. Kato, *Science*, 2002, **295**, 2414-2418.
46. S. Campidelli, P. Bourgun, B. Guintchin, J. Furrer, H. Stoeckli-Evans, I. M. Saez, J. W. Goodby and R. Deschenaux, *J. Am. Chem. Soc.*, 2010, **132**, 3574-3581.
47. N. Tirelli, F. Cardullo, T. Habicher, U. W. Suter and F. Diederich, *J. Chem. Soc.-Perkin Trans. 2*, 2000, 193-198.
48. I. M. Saez and J. W. Goodby, *Liq. Cryst.*, 1999, **26**, 1101-1105.
49. C. Noel and P. Navard, *Prog. Polym. Sci.*, 1991, **16**, 55-110.
50. D. Felder-Flesch, L. Rupnicki, C. Bourgogne, B. Donnio and D. Guillon, *J. Mater. Chem.*, 2006, **16**, 304-309.
51. J. M. Rueff, J. Barbera, B. Donnio, D. Guillon, M. Marcos and J. L. Serrano, *Macromolecules*, 2003, **36**, 8368-8375.
52. I. M. Saez and J. W. Goodby, *Chem. Eur. J.*, 2003, **9**, 4869-4877.
53. A. H. W. A.M. Donald, S. Hanna, *Liquid Crystalline Polymers*, 2 edn., Cambridge University Press, Cambridge, 2006.
54. M. R. Wilson, L. M. Stimson and J. M. Ilnytskyi, *Liq. Cryst.*, 2006, **33**, 1167-1175.

References

55. I. M. Saez, J. W. Goodby and R. M. Richardson, *Chem.Eur. J.*, 2001, **7**, 2758-2764.
56. K. Wade, *Chem. Br.*, 1975, **11**, 177-183.
57. K. Wade, *Adv. Inorg. Chem. Radiochem.*, 1976, **18**.
58. R. B. King, *Chem. Rev.*, 2001, **101**, 1119-1152.
59. E. Hückel, *Z. Physik*, 1931, **70**, 204-286.
60. K. Wade, *Advances in Inorganic Chemistry and Radiochemistry*, Academic Press, 1976.
61. J. Aihara, *J. Am. Chem. Soc.*, 1978, **100**, 3339-3342.
62. R. N. Grimes, *Carboranes*, Academic Press, New York, 1970.
63. V. I. Bregadze, *Chem. Rev.*, 1992, **92**, 209 - 223.
64. R. Maruca, H. Schroeder and A. W. Laubengayer, *Inorg. Chem.*, 1967, **6**, 572-574.
65. E. J. Houser and T. M. Keller, *J. Polym. Sci. Pol. Chem.*, 1998, **36**, 1969-1972.
66. C. D. Entwistle and T. B. Marder, *Angew. Chem.-Int. Edit.*, 2002, **41**, 2927-2931.
67. S. Peper, Y. Qin, P. Almond, M. McKee, M. Telting-Diaz, T. Albrecht-Schmitt and E. Bakker, *Anal. Chem.*, 2003, **75**, 2131-2139.
68. S. V. Vinogradova, P. M. Valetskii and Y. A. Kabachii, *Usp. Khim.*, 1995, **64**, 390-413.
69. O. A. Melnik, A. A. Sakharova and T. M. Frunze, *Usp. Khim.*, 1988, **57**, 1529-1545.
70. M. K. Kolel-Veetil, D. D. Dominguez and T. M. Keller, *J. Polym. Sci. Pol. Chem.*, 2008, **46**, 2581-2587.
71. K. M. Galie, A. Mollard and I. Zharov, *Inorg. Chem.*, 2006, **45**, 7815-7820.
72. C. H. Lai, Y. C. Lin, F. I. Chou, C. F. Liang, E. W. Lin, Y. J. Chuang and C. C. Lin, *Chem. Commun.*, 2012, **48**, 612-614.
73. F. Lerouge, C. Viñas, F. Teixidor, R. Nuñez, A. Abreu, E. Xochitiotzi, R. Santillán and N. Farfán, *Dalton Trans.*, 2007, 1898-1903.
74. E. J. Juárez-Pérez, C. Vinas, F. Teixidor, R. Santillán, N. Farfán, A. Abreu, R. Yepéz and R. Nuñez, *Macromolecules*, 2010, **43**, 150-159.
75. M. C. Parrott, E. B. Marchington, J. F. Valliant and A. Adronov, *J. Am. Chem. Soc.*, 2005, **127**, 12081-12089.
76. M. C. Parrott, J. F. Valliant and A. Adronov, *Langmuir*, 2006, **22**, 5251-5255.
77. Y. Haba, A. Harada, T. Takagishi and K. Kono, *J. Am. Chem. Soc.*, 2004, **126**, 12760-12761.
78. S. Nozary, H. Modarress and A. Eliassi, *J. Appl. Polym. Sci.*, 2003, **89**, 1983-1990.
79. M. Ataman, *Colloid & Polymer Science*, 1987, **265**, 19-25.
80. A. González-Campo, C. Viñas, F. Teixidor, R. Nuñez, R. Sillanpää and R. Kivekäs, *Macromolecules*, 2007, **40**, 5644-5652.
81. A. n. González-Campo, E. J. Juárez-Pérez, C. Viñas, B. Boury, R. Sillanpää, R. Kivekäs and R. Nuñez, *Macromolecules*, 2008, **41**, 8458-8466.
82. E. J. Juárez-Pérez, C. Viñas, F. Teixidor and R. Nuñez, *Organometallics*, 2009, **28**, 5550-5559.
83. A. G. Douglass, K. Czuprynski, N. Mierzwa and P. Kaszynski, *Chem. Mater.*, 1998, **10**, 2399-2402.
84. A. Jankowiak, P. Kaszynski, W. R. Tilford, K. Ohta, A. Januszko, T. Nagamine and Y. Endo, *Beilstein J. Org. Chem.*, 2009, **5**.

References

85. K. Czuprynski and P. Kaszynski, *Liq. Cryst.*, 1999, **26**, 775-778.
86. P. Kaszynski, S. Pakhomov and K. F. Tesh, *Inorg. Chem.*, 2001, **40**, 6622-6631.
87. P. Kaszynski and A. G. Douglass, *J. Organomet. Chem.*, 1999, **581**, 28-38.
88. M. J. S. Dewar and R. S. Goldberg, *J. Am. Chem. Soc.*, 1970, **92**, 1582-&.
89. T. Nagamine, A. Januszko, P. Kaszynski, K. Ohta and Y. Endo, *J. Mater. Chem.*, 2006, **16**, 3836-3843.
90. A. Januszko, K. L. Glab and P. Kaszynski, *Liq. Cryst.*, 2008, **35**, 549-553.
91. B. Ringstrand, J. Vroman, D. Jensen, A. Januszko, P. Kaszynski, J. Dziaduszek and W. Drzewinski, *Liq. Cryst.*, 2005, **32**, 1061-1070.
92. A. Januszko, P. Kaszynski, M. D. Wand, K. M. More, S. Pakhomov and M. O'Neill, *J. Mater. Chem.*, 2004, **14**, 1544-1553.
93. K. Czuprynski, A. G. Douglass, P. Kaszynski and W. Drzewinski, *Liq. Cryst.*, 1999, **26**, 261-269.
94. A. G. Douglass, K. Czuprynski, M. Mierzwa and P. Kaszynski, *J. Mater. Chem.*, 1998, **8**, 2391-2398.
95. M. Hird and K. J. Toyne, *Mol. Cryst. Liq. Cryst.*, 1998, **323**, 1-67.
96. D. Pocięcha, K. Ohta, A. Januszko, P. Kaszynski and Y. Endo, *J. Mater. Chem.*, 2008, **18**, 2978-2982.
97. I. M. Saez and J. W. Goodby, *J. Mater. Chem.*, 2003, **13**, 2727-2739.
98. K. J. Shepperson, T. Meyer and G. H. Mehl, *Mol. Cryst. Liq. Cryst.*, 2004, **411**, 1227-1233.
99. J. G. Bogdan Marciniec, Włodzimierz Urbaniak and Zygmunt W. Kornetka, in *Comprehensive Handbook of Hydrosilylation* ed. B. Marciniec, Pergamon Press, Oxford, Editon edn., 1992, pp. 8 - 94.
100. G. G. W., H. K. and N. J., *Liquid Crystals and Order Fluids*, 1974, **2**, 617 - 643.
101. S. J. Cowling, A. W. Hall and J. W. Goodby, *Liq. Cryst.*, 2005, **32**, 1483-1498.
102. G. H. Mehl and J. W. Goodby, *Chem. Ber.*, 1996, **129**, 521-525.
103. G. H. Mehl and J. W. Goodby, *Angew. Chem.-Int. Edit. Engl.*, 1996, **35**, 2641-2643.
104. M. Ibnelhaj, H. J. Coles, D. Guillon and A. Skoulios, *J. Phys. II*, 1993, **3**, 1807-1817.
105. A. Yoshizawa and A. Yamaguchi, *Chem. Commun.*, 2002, 2060-2061.
106. G. S. Attard and A. G. Douglass, *Liq. Cryst.*, 1997, **22**, 349-358.
107. S. A. Ponomarenko, N. I. Boiko, V. P. Shibaev, R. M. Richardson, I. J. Whitehouse, E. A. Rebrov and A. M. Muzafarov, *Macromolecules*, 2000, **33**, 5549-5558.
108. E. Terazzi, G. Rogez, J.-L. Gallani and B. Donnio, *J. Am. Chem. Soc.*, 2013, **135**, 2708-2722.
109. A. J. Leadbetter, J. C. Frost, J. P. Gaughan, G. W. Gray and A. Mosley, *Journal De Physique*, 1979, **40**, 375-380.
110. R. Deschenaux, B. Donnio and D. Guillon, *New J. Chem.*, 2007, **31**, 1064-1073.
111. R. Nuñez, A. González-Campo, A. Laromaine, F. Teixidor, R. Sillanpää, R. Kivekäs and C. Viñas, *Org. Lett.*, 2006, **8**, 4549-4552.
112. B. Dardel, D. Guillon, B. Heinrich and R. Deschenaux, *J. Mater. Chem.*, 2001, **11**, 2814-2831.

References

113. J. Lenoble, S. Campidelli, N. Maringa, B. Donnio, D. Guillon, N. Yevlampieva and R. Deschenaux, *J. Am. Chem. Soc.*, 2007, **129**, 9941-9952.
114. S. Nakanishi and M. Ueda, *Chem. Lett.*, 2007, **36**, 452-453.
115. T. B. Jensen, E. Terazzi, K.-L. Buchwalder, L. Guénée, H. Nozary, K. Schenk, B. t. Heinrich, B. Donnio, D. Guillon and C. Piguet, *Inorg. Chem.*, 2010, **49**, 8601-8619.
116. E. Terazzi, B. Bocquet, S. Campidelli, B. Donnio, D. Guillon, R. Deschenaux and C. Piguet, *Chem. Commun.*, 2006, 2922-2924.
117. W. Clegg, S. J. Coles, I. A. Fallis, P. M. Griffiths and S. J. Teat, *Acta Crystallographica Section C*, 1998, **54**, 882-885.
118. Y. W. Zhou, M. Jaroniec, G. L. Hann and R. K. Gilpin, *Anal. Chem.*, 1994, **66**, 1454-1458.
119. I. M. Saez, *unpublished results*.
120. R. A. Lewthwaite, J. W. Goodby and K. J. Toyne, *J. Mater. Chem.*, 1993, **3**, 241-245.
121. P. A. a. J. d. Paula, in *Atkins' Physical Chemistry*, Oxford University Press, Oxford, Editon edn., 2006, pp. 150 - 153.
122. J. W. Goodby, I. M. Saez, S. J. Cowling, J. S. Gasowska, R. A. MacDonald, S. Sia, P. Watson, K. J. Toyne, M. Hird, R. A. Lewis, S. E. Lee and V. Vaschenko, *Liq. Cryst.*, 2009, **36**, 567-605.
123. P. Keller, D. L. Thomsen and M. H. Li, *Macromolecules*, 2001, **35**, 581-584.
124. E. J. Davis, University of York, 2013.
125. I. M. Saez and J. W. Goodby, *J. Mater. Chem.*, 2001, **11**, 2845-2851.
126. R. M. Laine, C. X. Zhang, A. Sellinger and L. Viculis, *Appl. Organomet. Chem.*, 1998, **12**, 715-723.
127. A. Yamaguchi, M. Watanabe and A. Yoshizawa, *Liq. Cryst.*, 2007, **34**, 633-639.
128. M. Loseva, N. Chernova, V. Vorflusev, L. Beresnev, R. Hiller and W. Haase, *Mol. Cryst. Liq. Cryst. Sci. Technol. Sect. A*, 1995, **260**, 261-267.
129. A. Yamaguchi, Y. Maeda, H. Yokoyama and A. Yoshizawa, *Chem. Mater.*, 2006, **18**, 5704-5710.
130. B. Neises and W. Steglich, *Angew. Chem. Int. Ed. Engl.*, 1978, **17**, 522-524.
131. M. M. Fein, J. Bobinski, N. Mayes, N. Schwartz and M. S. Cohen, *Inorg. Chem.*, 1963, **2**, 1111-1115.
132. R. Schaeffer, *J. Am. Chem. Soc.*, 1957, **79**, 1006-1007.
133. H. W. Heine and W. Siegfried, *J. Am. Chem. Soc.*, 1954, **76**, 489-490.
134. K. J. Toyne, in *Thermotropic Liquid Crystals- Critical Reports on Applied Chemistry*, ed. G. W. Gray, Biddles Ltd, Guildford, Editon edn., 1987, vol. 22, pp. 28-63.
135. J. Jadzyn, R. Dabrowski, T. Lech and G. Czechowski, *J. Chem. Eng. Data*, 2001, **46**, 110-112.
136. G. W. Gray, *Mol. Cryst. Liq. Cryst.*, 1981, **63**, 3-17.
137. D. Coates and G. W. Gray, *J. Chem. Soc.-Perkin Trans. 2*, 1976, 863-868.
138. N. Carr, G. W. Gray and D. G. McDonnell, *Mol. Cryst. Liq. Cryst.*, 1983, **97**, 13-28.
139. M. F. Daniel, O. C. Lettington and S. M. Small, *Mol. Cryst. Liq. Cryst.*, 1983, **96**, 373-385.
140. J. Constant and E. P. Raynes, *Mol. Cryst. Liq. Cryst.*, 1980, **62**, 115-123.
141. D. Johnson and A. Saupe, *Physical Review A*, 1977, **15**, 2079-2085.
142. A. W. Laubengayer and W. R. Rysz, *Inorg. Chem.*, 1965, **4**, 1513-1514.

References

143. R. Dabrowski and E. Zytyński, *Mol. Cryst. Liq. Cryst.*, 1982, **87**, 109-135.
144. G. W. Gray and J. W. Goodby, *Smectic Liquid Crystals: Textures and Structures, Chapter 5*, Leonard Hill, Glasgow, 1984.
145. J. S. Gasowska, S. J. Cowling, M. C. R. Cockett, M. Hird, R. A. Lewis, E. P. Raynes and J. W. Goodby, *J. Mater. Chem.*, 2010, **20**, 299-307.
146. W. C. Still, M. Kahn and A. Mitra, *The Journal of Organic Chemistry*, 1978, **43**, 2923-2925.
147. R. Nuñez, A. González-Campo, C. Viñas, F. Teixidor, R. Sillanpää and R. Kivekäs, *Organometallics*, 2005, **24**, 6351-6357.
148. D. L. Thomsen, P. Keller, J. Naciri, R. Pink, H. Jeon, D. Shenoy and B. R. Ratna, *Macromolecules*, 2001, **34**, 5868-5875.
149. K. J. Shepperson, T. Meyer and G. H. Mehl, *Mol. Cryst. Liq. Cryst.*, 2004, **411**, 185-191.
150. T. Kunitake, Y. Okahata, M. Shimomura, S. Yasunami and K. Takarabe, *J. Am. Chem. Soc.*, 1981, **103**, 5401-5413.
151. H. Takeda, Y. Sakurai, S. Takenaka, H. Miyake, T. Doi and S. Kusabayashi, *Chem. Lett.*, 1989, 1335-1338.